

## *Editors' Note*

### **Thematic Issue on Determination of Absolute Configuration**

In the past, *Chirality* has published a few review articles focused on some methods useful for determination of absolute configuration. However, in view of the rapid progress in the field, and in particular, of the recent advancement of computational methods, we found it appropriate to summarize the recent developments in the most important methods for determination of absolute configuration in a single Thematic Issue, which is the first one to provide a comprehensive coverage.

We hope that this Thematic Issue of *Chirality* will serve its purpose to give a good overview of the present status of the field and of the progress that has recently been made. We also hope that it will promote a further development of this highly important field. Finally, we are grateful to all the distinguished scientists who have agreed to contribute with either review or research articles from their respective areas of expertise.

**Professor Emeritus Stig Allenmark**

Guest Editor

Department of Chemistry  
Göteborg University, Sweden

**Professor Jacek Gawronski**

Guest Editor

Department of Chemistry  
A. Mickiewicz University  
Poznan, Poland

**Professor Nina Berova**

Editor

Department of Chemistry  
Columbia University, New York

## Review Article

# Determination of Absolute Configuration—an Overview Related to This Special Issue

STIG ALLENMARK<sup>1\*</sup> AND JACEK GAWRONSKI<sup>2</sup>

<sup>1</sup>Department of Chemistry, Göteborg University, Göteborg, Sweden

<sup>2</sup>Department of Chemistry, A. Mickiewicz University, Poznan, Poland

**ABSTRACT** Rapid progress in asymmetric synthesis stimulated a further development of methods and techniques for the determination of absolute configuration of chiral molecules. In recent years the direct methods, *i.e.* X-ray diffraction analysis, circular dichroism (vibrational and electronic), Raman optical activity, optical rotation measurements, as well as indirect methods for relative configuration assignment with the use of NMR spectroscopy or enzymatic transformations, are receiving increasing attention not only by specialists in the field but also by synthetic and structural chemists alike. This paper provides a short overview of the methods currently used, as well as references to contributions collected in this Thematic Issue of Chirality. *Chirality* 20:606–608, 2008. © 2008 Wiley-Liss, Inc.

**KEY WORDS:** circular dichroism (ECD, VCD); *ab initio* computational (TD DFT) methods; X-ray crystallography; NMR anisotropy effects; enzymatic methods; crystal growth; helical cholesteric phases

## INTRODUCTION

Ever since the suggestion in 1874 by van't Hoff and LeBel that individual molecules possess a three-dimensional structure that may give rise to dissymmetry,<sup>1,2</sup> the exact orientation of the atoms in space, *i.e.* the absolute configuration (AC) has been an intriguing problem to be solved. In 1938, however, Kuhn suggested an absolute configuration assignment of the two enantiomers of 2-butanol, based on their different interaction with right and left circularly polarized light,<sup>3</sup> which later turned out to be correct. The definite solution came in 1951, when yet another Dutch scientific achievement was announced by Bijvoet et al. who had discovered that in X-ray crystallography an anomalous dispersion effect, recognizable from a heavy atom in a crystal of an optically active compound, could be used to determine its absolute three-dimensional structure.<sup>4</sup> Fortunately, it then turned out that all configurations that had been established based on Fischer's arbitrarily assigned (+)-L-tartaric acid<sup>5</sup> and D-glyceraldehyde were in fact correct and did not need to be reversed. More recently, thanks to the development of computerized *ab initio* quantum mechanical calculations of chiroptical data [electronic (ECD) and vibrational (VCD) circular dichroism spectra as well as optical rotation (OR)], particularly within the framework of density functional theory (TD DFT), a big step forward has been taken, soon probably making direct AC determination an uncomplicated matter. Below, a brief tutorial introduction to the basic features of the methods presented in this Special Issue of the journal is given.

## CHIROPTICAL METHODS

All chiroptical methods depend on the different interaction of an optically active compound with left- and right-handed circularly polarized light (CPL). Plane polarized, monochromatic light can be treated as composed of a left and right circularly polarized vector component. If these components interact differently with a chiral medium (such as a solution of a chiral compound), the medium is said to be optically active. This can be manifested in different ways: (a) Because of a *difference in velocity* through the medium, a *circular birefringence* or anisotropic refraction is obtained, *i.e.*  $(n_L - n_R) \neq 0$ , observed as a rotation of the plane of polarization. (b) Because of a *difference in absorption* by the medium, a *circular dichroic effect* or anisotropic absorption can also be registered, *i.e.*  $(A_L - A_R) \neq 0$ , hence  $\Delta\epsilon \neq 0$ .

The first of these phenomena has been utilized for a very long time in the form of polarimetry, *i.e.* determination of optical rotation at a specific wavelength (often at 589 nm, the sodium D-line). The limited value of polarimetry in conjunction with determination of AC and the necessity to measure the optical rotation at shorter wavelengths, led to instruments for recording the optical rotatory dispersion (ORD) over the available UV-VIS region, giving infor-

\*Correspondence to: Dr. Stig Allenmark, Department of Chemistry, Göteborg University, Göteborg, Sweden. E-mail: allen@chem.gu.se  
Received for publication 16 October 2007; Accepted 6 November 2007  
DOI: 10.1002/chir.20524  
Published online 16 January 2008 in Wiley InterScience (www.interscience.wiley.com).

mation about the change in sign of the rotation on passage of the absorption band, the Cotton effect (CE). The octant rule, used for the determination of AC in the steroid field, is a result from the pioneering work of Djerassi and collaborators<sup>6</sup> in the 1950's. While of increasing interest in combination with *ab initio* methods for calculation of optical rotation,<sup>7</sup> ORD has largely been replaced by ECD as an experimental technique. In this issue the application of ECD combined with OR calculation for the determination of absolute configuration of simple arene metabolites is presented by Kwit, Sharma, Boyd, and Gawronski.

Chmielewski, Cierpucha, Kowalska, Kwit, and Frelek use the calculated ECD spectra for structural correlations within the clavam antibiotic family. Quantum chemical ECD calculations can be combined with on-line HPLC-ECD measurements for assignment of the absolute configuration of natural products, as described in this issue by Bringmann, Gulder, Reichert and Gulder.

In CD the absorption band is either positive (+CE) or negative (−CE), except when the compound contains two or more chromophores suitable to interact with each other through space (coupled oscillators). Such interaction leading to a split CD band (couplet) represents the basis of the exciton chirality approach, first introduced by Harada and Nakanishi as the dibenzoate chirality method in the early 1970's.<sup>8</sup> In the past few decades the CD exciton chirality method has undergone a further development and has established itself as one of the most versatile methodologies for determination of AC of natural products<sup>9</sup> and other chiral molecules.<sup>10</sup>

In the absence of conformational ambiguity, the sign of the couplet can be directly correlated with the mutual orientation of the chromophores and thereby the AC. Accounts on basic principles and various applications of exciton chirality can be found in several review articles and monographs,<sup>8,11–13</sup> including the excellent book from 2000 on the various CD methods available and their use.<sup>11</sup>

Vibrational CD (VCD) makes use of CPL in the infrared region<sup>14,15</sup> and has become a very powerful technique since the introduction of the first commercially available instrument. The large number of diagnostically useful bands in a VCD spectrum, and the relative ease by which a spectrum can be calculated, represent two advantages over electronic CD. A review of the use of VCD spectroscopy for the determination of the absolute configurations is presented in this issue by Stephens, Devlin, and Pa. Polavarapu discusses the importance of simultaneous use of more than one chiroptical spectroscopic method for determination of the structures of chiral molecules. Freedman, Cao, Luz, Zimmerman, Poupko, and Nafie present the application of VCD spectroscopy for determining the absolute configuration of cyclotrimeratrylene derivatives.

### X-RAY CRYSTALLOGRAPHIC METHODS

The direct method, introduced by Bijvoet and relying on the anomalous scattering effect produced by a heavy atom, is still regarded as the most reliable method; provided only that a suitable single crystal can be obtained and that the intensity difference between the Bijvoet pairs obtained

is large enough. Rigorous differentiation of enantiomers by the X-ray diffraction method is now possible through the use of the Flack parameter.<sup>16</sup> In this issue Flack and Bernardinelli provide in-depth review of X-ray crystallography for absolute configuration determination.

In many cases, though, it may be necessary to perform a derivatization of the compound to get a crystalline product. If a chiral reagent is used for this purpose, a second stereogenic center of known AC is introduced and the X-ray structure obtained is then unambiguous and gives the AC of the first compound. A number of such indirect methods have been developed and successfully applied.<sup>17,18</sup>

### NMR METHODS

By the use of chiral derivatization techniques similar to those mentioned above, the difference in NMR anisotropy effects between two diastereomers can be used to deduce the absolute configuration. The method requires knowledge of the most stable solution conformations of the respective diastereomer for an interpretation of the chemical shift difference observed due to the difference in anisotropy effects.<sup>19</sup> So far, it has been used mainly for AC determination of monofunctional compounds, like alcohols, amines and carboxylic acids, and of bifunctional species such as diols and amino alcohols. Several chiral reagents for this purpose have been developed from the initially used Mosher's acid ( $\alpha$ -methoxy- $\alpha$ -(trifluoromethyl)phenylacetic acid, MTPA). In all these reagents an aromatic moiety (phenyl-, naphthyl-) is essential as a producer of the necessary anisotropy effect. Naturally, the complexity of the system studied in the NMR increases in polyfunctional compounds and the procedure may require a multistep operation to give safely interpretable data. Highly instructive reviews of the field have been published<sup>20,21</sup> and a monograph by Wenzel appeared quite recently.<sup>22</sup> In this issue the method is addressed by Harada.

### ENZYMATIC METHODS

Since most enzymes are highly stereoselective and often used for kinetic resolution of racemates, it is not surprising that studies in this field have led to empirical rules used for the determination of absolute configuration. Such methods were used quite early for the determination of the absolute configuration of some simple compounds (e.g. acetates) which were chiral only by virtue of isotopic (<sup>2</sup>H, <sup>3</sup>H) substitution.<sup>23</sup> With the computational facilities available today, modeling of an enzyme's active site combined with docking experiments have opened up new possibilities for rationalization and even prediction of the outcome of enzyme-catalyzed stereoselective reactions.<sup>24</sup> In this issue Kazlauskas and Jing review the determination of absolute configuration of secondary alcohols using lipase-catalyzed kinetic resolutions.

### OTHER METHODS, TECHNIQUES, AND APPLICATIONS

Studies of crystal growth in three dimensions and particularly the inhibition of growth has enabled a method of direct determination of absolute configuration.<sup>25</sup> The

method is reviewed in this issue by its co-inventors, Weissbuch, Leiserowitz, and Lahav. Another interesting technique is based on the formation of a helical cholesteric phase when a chiral solute is dissolved in an achiral liquid crystalline nematic phase, followed by observation of the sign of the induced CE in a CD spectrum of the helical phase.<sup>26,27</sup> The method is reviewed here by Ferrarini, Pieraccini, and Spada.

Methods other than those mentioned above have been used for AC determination and the interested reader should consult the superb monograph by Eliel and Wilen.<sup>28</sup>

### SOME FINAL COMMENTS

Of course, all methods have their limitations and the reliability of the results is entirely dependent on the quality of the data produced. Thus, while in chiroptical methods the conformer distribution of the compound must be known, in X-ray crystallography the solid state eliminates this problem. On the other hand, non-crystalline compounds can be used directly in chiroptical methods, but have to be derivatized or otherwise modified to be applicable to X-ray methods. Also, ECD spectroscopy requires a suitable chromophore in the compound,<sup>29</sup> while this is irrelevant with VCD and ROA (Raman optical activity) techniques. On the other hand, an ECD spectrum can be obtained from sub- $\mu$ g amounts, while the methods based on vibrational optical activity require much larger amounts.

To cover the field completely, we have thought it is appropriate not to exclude methods for AC determination that are not *direct*, but requiring a chiral auxiliary (such as a chiral derivatizing agent, CDA) or reference of known AC. Consequently, a number of important methods that may be classified as *indirect* have been included. These methods, strictly speaking, deliver *relative configuration*, since the configuration of CDA or reagent (enzyme) is *a priori* known. Such methodologies include NMR anisotropy methods with the use of an internal source of chirality, enzymatic methods as mentioned above and chemical correlation methods. The latter, however, even though of tremendous importance for the establishment of configurational relationships since the days of Fischer, have not been incorporated. Their significance for the AC determination of compounds with axial and planar chirality<sup>30</sup> should be kept in mind, however.

### LITERATURE CITED

- van't Hoff JH. Voorstel tot uitbreiding der teegenwoordig in de scher-kunde gebruikte structuur-formules in de ruimte. Greven, Utrecht; 1874.
- Le Bel JA. Sur les relations qui existent entre les formules atomiques des corps organiques, et le pouvoir rotatoire de leurs dissolutions. Bull Soc Chim Paris 1874;22:227.
- Kuhn W. Das Problem der absoluten Konfiguration optisch aktiver Stoffe. Naturwiss 1938;26:305–310.
- Bijvoet JM, Peerdeman AF, van Bommel AJ. Determination of the absolute configuration of optically active compounds by means of X-rays. Nature (Lond) 1951;168:271–272.
- Fischer E. Configuration der Weinsäure. Ber Deutsch Chem Ges 1896;29:1377–1383.
- Djerassi C. Optical rotatory dispersion. New York: McGraw-Hill; 1960. p 293.
- Stephens PJ, Devlin FJ, Cheeseman JR, Frisch MJ. Calculation of optical rotation using density functional theory. J Phys Chem A 2001;105:5356–5371.
- Harada N, Nakanishi K. Circular dichroic spectroscopy—exciton coupling in organic stereochemistry. Mill Valley, CA: University Science Books; 1983. p 460.
- Allenmark S. Chiroptical methods in the stereochemical analysis of natural products. Nat Prod Rep 2000;17:145–155.
- Gawronski J. Determination of absolute and relative configuration by chiroptical methods. In: Helmchen G, Hoffmann RW, Mulzer J, Schumann E, editors. Houben-Weyl methods of organic chemistry, 4th ed.; Vol E21a; Stuttgart: Georg Thieme; 1995. p 499–533.
- Berova N, Nakanishi K, Woody RW, editors. Circular dichroism: principles and applications, 2nd ed. New York: Wiley-VCH; 2000. p 877.
- Superchi S, Giorgio E, Rosini C. Structural determination by circular dichroism spectral analysis using coupled oscillator methods: an update of the application of the DeVoe polarizability model. Chirality 2004;16:422–451.
- Berova N, Di Bari L, Pescitelli G. Application of electronic circular dichroism in configurational and conformational analysis of organic compounds. Chem Soc Rev 2007;36:914–931.
- Nafie LA. Circular polarization spectroscopy of chiral molecules. J Mol Spectrosc 1995;347:83–100.
- Freedman TB, Xiaolin C, Dukor RK, Nafie LA. Absolute configuration determination of chiral molecules in the solution state using vibrational circular dichroism. Chirality 2003;15:743–758.
- Flack HD, Bernardinelli G. Absolute structure and absolute configuration. Acta Crystallogr A 1999;55:908–915.
- Kosaka M, Watanabe M, Harada N. Enantioresolution by the chiral phthalic acid method: absolute configurations of substituted benzylic alcohols. Chirality 2000;12:362–365.
- Harada N. Chiral auxiliaries powerful for both enantiomer resolution and determination of absolute configuration by X-ray crystallography. Top Stereochem 2006;25:177–203.
- Kasai Y, Tajiri H, Fujita T, Yamamoto Y, Akagi M, Sugio A, Kuwahara S, Watanabe M, Harada N, Ichikawa A, Schurig V. M $\alpha$ NP Acid, a powerful chiral molecular tool for preparation of enantiopure alcohols by resolution and determination of their absolute configurations by the <sup>1</sup>H NMR anisotropy method. Chirality 2004;16:569–585.
- Seco JM, Quiñoá E, Riguera R. The assignment of absolute configuration by NMR. Chem Rev 2004;104:17–117.
- Wenzel TJ, Wilcox JD. Chiral reagents for the determination of enantiomeric excess and absolute configuration using NMR spectroscopy. Chirality 2003;15:256–270.
- Wenzel TJ. Discrimination of chiral compounds using NMR spectroscopy. New York: Wiley; 2007. p 549.
- Bentley R. The use of biochemical methods for determination of configuration. In: Jones JB, Sih CJ, Perlman D, editors. Applications of biochemical systems in organic chemistry, Part I. New York: Wiley-Interscience; 1976. p 403–477.
- Kazlauskas R. Molecular modeling and biocatalysis: explanations, predictions, limitations, and opportunities. Curr Opin Chem Biol 2000;4:81–88.
- Addadi L, Berkovitch-Yellin Z, Weissbuch I, Lahav M, Leiserowitz L. A link between macroscopic phenomena and molecular chirality: crystals as probes for the direct assignment of absolute configuration of chiral molecules. Top Stereochem 1986;16:1–85.
- Gottarelli G, Spada GP, Solladié G. Some stereochemical applications of induced cholesteric liquid crystals. Nouv J Chim 1986;10:691–696.
- Gottarelli G, Spada GP. Some correlations between molecular and cholesteric handedness. Top Stereochem 2003;24:425–455.
- Eliel EL, Wilen SH. Stereochemistry of organic compounds. New York: Wiley; 1994. p 1267.
- Gawronski J, Skowronek P. New chromophores for organic stereochemical analysis by exciton-coupled circular dichroism. Curr Org Chem 2004;8:65–82.
- Krow G. The determination of absolute configuration of planar and axially dissymmetric molecules. Top Stereochem 1970;5:31–68.





# Determination of Absolute Configuration of Conformationally Flexible *cis*-Dihydrodiol Metabolites: Effect of Diene Substitution Pattern on the Circular Dichroism Spectra and Optical Rotations

MARCIN KWIT,<sup>1</sup> NARAIN D. SHARMA,<sup>2,3</sup> DEREK R. BOYD,<sup>2,3\*</sup> AND JACEK GAWRONSKI<sup>1\*</sup>

<sup>1</sup>Department of Chemistry, A. Mickiewicz University, Poznań, Poland

<sup>2</sup>School of Chemistry and Chemical Engineering, The Queen's University of Belfast, Belfast, United Kingdom

<sup>3</sup>QUESTOR Centre, The Queen's University of Belfast, Belfast, United Kingdom

**ABSTRACT** Absolute configurations of a number of *cis*-dihydrodiols (*cis*-1,2-dihydroxy-3,5-cyclohexadienes), synthetically useful products of TDO-catalyzed dihydroxylations of 1,2- and 1,3-disubstituted benzene derivatives, have been determined by a comparison of calculated and experimental CD spectra and optical rotations and by methods involving X-ray crystallography, <sup>1</sup>H NMR spectra of diastereoisomeric derivatives, and by stereochemical correlations. The computations disclosed a significant effect of the substituents on conformational equilibria of *cis*-dihydrodiols and chiroptical properties of individual conformers. The assigned absolute configurations of *cis*-dihydrodiols have allowed the validity of a simple predictive model for TDO-catalyzed arene dihydroxylations to be extended. *Chirality* 20:609–620, 2008. © 2007 Wiley-Liss, Inc.

**KEY WORDS:** absolute configuration; conformation; *cis*-diene; *cis*-dihydrodiol; TDDFT; fluorine effect; circular dichroism; optical rotation

## INTRODUCTION

Experimental determination of absolute and relative configuration of organic as well as inorganic molecules currently relies on techniques such as X-ray crystallography, circular dichroism,<sup>1</sup> analysis of NMR spectra of diastereoisomeric derivatives,<sup>2</sup> and stereochemical correlation.<sup>3</sup> In principle, absolute configuration (AC) of a chiral molecule can be deduced from its optical rotation (OR) and/or its electronic circular dichroism (ECD) data. In practice, this requires the use of reliable methodologies for calculation of OR and/or ECD, followed by comparison with the corresponding experimental data.

Many successful assignments of AC of chiral molecules have been reported during the past decade by comparison of experimental and theoretical ECD spectra.<sup>4–7</sup> This methodology allows not only the determination of the AC but also the preferred conformations of investigated molecules (absolute stereochemistry) in the same calculation process. Recently, Diedrich and Grimme systematically investigated and critically reviewed the applications of modern quantum chemical methods for predicting ECD spectra.<sup>8</sup>

In recent years, advances in the field of theoretical chemistry have led to development of new computational approaches for calculating OR at various levels of accuracy<sup>9–13</sup> and allow direct assignment of AC. In many cases, the accordance of experimental and theoretical data was found satisfactory.<sup>14</sup>

The calculations of OR, as well as ECD, are very sensitive to inaccuracy in determining the equilibrium of participating conformers. Thus, carefully carried out confor-

mational analysis of the molecule is the first and the most important step of the calculations. For rigid molecules, which were investigated in the pioneering years of the studies, this step could be neglected, but for floppy molecules the relative energies of participating conformers should be calculated with the highest available accuracy.<sup>15–18</sup> It has been shown that even minor changes in molecule conformation can result in a change of sign and/or magnitude of calculated OR.<sup>19–21</sup>

Recently, TDDFT calculations of both OR and ECD are being increasingly used for determining ACs.<sup>22,23</sup> The essence of such an approach has been summarized by Stephens et al. as providing higher reliability of the AC determination. If the use of OR and CD confrontation yields opposite ACs, the AC determination using either phenomenon is ambiguous.<sup>23</sup> Such methodology has been used quite recently for the stereochemical characterization of cytotoxic natural products<sup>24</sup> and chiral rigid and flexible alkenes with satisfactory results.<sup>25</sup>

Contract grant sponsor: Ministry of Science (Poland); Contract grant number: PBZ KBN 126/T09/10.

Contract grant sponsor: Science Foundation Ireland; Contract grant numbers: 04/IN3/B581.

Contract grant sponsor: CenTACat.

\*Correspondence to: Derek R. Boyd, School of Chemistry and Chemical Engineering and QUESTOR Centre, The Queen's University of Belfast, Belfast BT9 5AG, United Kingdom. E-mail: derekrboyd@ntlworld.com or Jacek Gawronski, Department of Chemistry, A. Mickiewicz University, 60780 Poznań, Poland. E-mail: gawronsk@amu.edu.pl

Received for publication 5 June 2007; Accepted 31 July 2007

DOI: 10.1002/chir.20471

Published online 8 October 2007 in Wiley InterScience (www.interscience.wiley.com).

The method we use in this study relies on comparison of experimental and calculated electronic CD spectra and ORs of conformationally flexible chiral molecules. In cases where full agreement (ECD and OR) is not achieved, analysis of conformer population and/or chiroptical properties of contributing conformers allows identification of one of the two properties (ECD or OR) with which the assignment of AC is considered conclusive.<sup>26</sup>

Experimental and calculated ECD and OR measurements have been successfully applied to a series of chiral *cis*-dihydrodiol metabolites (**B/B'**,  $Y = H$  or  $X \neq Y \neq H$ ) obtained from the corresponding substituted benzene substrates (**A**,  $Y = H$  or  $X \neq Y \neq H$ ; Scheme 1).<sup>26–28</sup> Thus, using whole cells of the bacterium *Pseudomonas putida* UV4 (a source of toluene dioxygenase, TDO), asymmetric dihydroxylation of monosubstituted benzene substrates **A** ( $Y = H$ ) yielded mainly enantiopure (>98% ee) *cis*-dihydrodiols **B** ( $Y = H$ ).<sup>26,29</sup> Only the *cis*-dihydrodiol from fluorobenzene (**A**,  $X = F$ ,  $Y = H$ ) showed evidence of the other enantiomer **B'** ( $Y = H$ ,  $X = F$ , 60–70% ee). By contrast, biotransformation of 1,4-disubstituted benzene *cis*-dihydrodiols (**A**,  $X \neq Y \neq H$ ) often yielded both enantiomers (**B/B'**,  $X \neq Y \neq H$ ), particularly when substituents  $X$  and  $Y$  were of similar size.<sup>27,28,30</sup> All of these *cis*-diol metabolites (**B/B'**,  $Y = H$  or  $X \neq Y \neq H$ ) resulted from asymmetric dihydroxylation exclusively at the unsubstituted 2,3-bond of both monosubstituted (**A**,  $Y = H$ ) and 1,4-disubstituted benzene substrates (**A**,  $X \neq Y \neq H$ ).

Under similar biotransformation conditions in the present study, the *cis*-dihydroxylation of 1,2- (**A**,  $X$  and  $Y \neq H$ ) and 1,3-disubstituted benzene (**A**,  $X$  and  $Y \neq H$ ) substrates could in principle occur at either of the two unsubstituted bonds to yield *cis*-dihydrodiols of types **C/C'** or **D/D'** ( $X$  and  $Y \neq H$  from 1,2-disubstituted benzenes) and

**E/E'** or **F/F'** ( $X$  and  $Y \neq H$  from 1,3-disubstituted benzenes). In this context, the application of CD spectroscopy and OR measurements (involving matching of experimental and computational results) has been used: (i) to assign or confirm the ACs of *cis*-dihydrodiols derived from 1,2- (**C/C'**,  $X$  and  $Y \neq H$ ) and 1,3-disubstituted benzenes (**E/E'**,  $X$  and  $Y \neq H$ )<sup>31–33</sup> and (ii) to extend the validity of an earlier predictive model for the determination of ACs during the TDO-catalyzed asymmetric dihydroxylation to 1,2- and 1,3-disubstituted benzene substrates.<sup>28,30,32,33</sup>

## EXPERIMENTAL

### Computational Methods

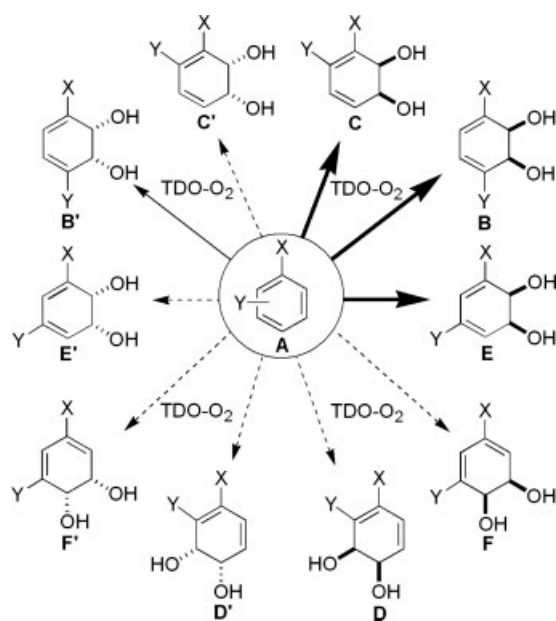
In our computations, all excited-state calculations have been performed, based upon the ground state geometries of single molecules, with the use of a Gaussian program package.<sup>34</sup> Rotatory strengths were calculated using both length and velocity representations. In the present study, the differences between the length and velocity of calculated values of rotatory strengths were quite small, and for this reason only length representations were taken into account. The CD spectra were simulated by overlapping Gaussian functions for each transition according to the procedure described by Diedrich and Grimme.<sup>8</sup>

Conformational analyses of all the benzene *cis*-dihydrodiols **1a–1d**, **2a–2d**, and **3a–3d** were carried out by a systematic conformational search with the use of a B3LYP hybrid functional and a 6-31+g(D,P) basis set, starting from the structure optimized by the B3LYP/6-31+g(D,P) method. To find the relationship between the energy of the molecule and conformations of the hydroxy substituents the torsion angles  $H-O-C^*-H$  were rotated at 30° steps to give 144 different structures for each molecule. Then the structure optimizations were performed for each structure and this allowed the construction of the potential energy surface (PES) for **1a–1d**, **2a–2d**, and **3a–3d**. The conformers which were found as energy minima on the PES were fully reoptimized at the B3LYP/6-311++g(D,P) level of theory. For optimized structures, frequency calculations were carried out at the B3LYP/6-311++g(D,P) level of theory to confirm that the conformations are stable.

For all conformations having relative energies ranging from 0.0 to 2.0 kcal mol<sup>−1</sup>, percentage populations were calculated for each compound on the basis of the  $\Delta E$  and  $\Delta G$  values, using Boltzmann statistics and  $T = 298$  K. Due to their similarity, only  $\Delta E$  values were taken into further consideration.

To test which combination of functional/basis set performs better in the case of calculations of CD spectra and OR of substituted benzene *cis*-dihydrodiols, two different functionals: mPW1PW91 and B3LYP have been employed in combination with 6-311++g(2D,2P) basis set. For selected cases, additional calculations at the B3LYP/Aug-cc-pVTZ level have been performed.

The computed oscillator strengths and rotational strengths were converted to the UV and CD spectra by broadening to Gaussian shape absorption curves. The



**Scheme 1.** Possible *cis*-dihydrodiol regio- and stereoisomers from *cis*-dihydroxylation of substituted benzenes ( $X > Y$ ).

calculated spectra were red-shifted by ca. 10 nm in relation to the experimental ones regardless the method used. Although each experimental spectrum was reproduced well by either B3LYP or mPW1PW91 hybrid functionals in conjunction with the basis sets augmented with diffuse functions, still better overall agreement was obtained with the use of mPW1PW91 hybrid functional and 6-311++g(2D,2P) basis set. It is well known that the mPW1PW91 hybrid functional generally provides results which are close to, or even better than, those obtained with the widely used B3LYP method, both for the ground as well as for the excited states.<sup>35,36</sup>

The ORs were calculated at the B3LYP/6-311++g(2D,2P) level and B3LYP/Aug-cc-pVTZ level for selected *cis*-dihydrodiols. Due to similar values of the calculated ORs and because of longer calculations time with the use of B3LYP/Aug-cc-pVTZ method, the ORs were calculated only at B3LYP/6-311++g(2D,2P) level for other *cis*-dihydrodiol molecules.

No correlation for the medium dielectric constant was implemented. For a detailed discussion see Refs. 26 and 27.

### General Information

<sup>1</sup>H NMR spectra were recorded at 300 MHz (Bruker Avance DPX-500) and at 500 MHz (Bruker Avance DRX-500) in CDCl<sub>3</sub> solvent unless stated otherwise. Chemical shifts ( $\delta$ ) are reported in ppm relative to SiMe<sub>4</sub> and coupling constants ( $J$ ) are given in Hz. Mass spectra were recorded at 70 eV on a VG Autospec Mass Spectrometer, using a heated inlet system. Accurate molecular weights were determined by the peak matching method with perfluorokerosene as standard. Elemental microanalyses were obtained on a Perkin-Elmer 2400 CHN microanalyser. CSPHPLC was carried out using a Shimadzu LC-6A liquid chromatograph connected to Hewlett Packard diode array detector. The disubstituted benzene substrates and reagents used in the formation of *cis*-dihydrodiol derivatives were obtained commercially.

The enantiomeric excess (ee) values of the *cis*-dihydrodiols were determined by CSPHPLC using Daicel columns (method i)<sup>28</sup> However, as the majority of *cis*-dihydrodiols were single enantiomers (>98% ee), an alternative method was adopted. It involved the formation of cycloadducts of the *cis*-dihydrodiols by reaction with Cookson's reagent (4-phenyl-1,2,4-triazoline-3,5-dione), followed by reaction with the acid chloride derivatives of (*R*)- and (*S*)- $\alpha$ -methoxy- $\alpha$ -(trifluoromethyl)phenyl acetic acid (MTPA) to yield the corresponding di-MTPA esters and NMR analyses (method ii).<sup>28</sup> The formation of the corresponding diastereoisomeric boronate esters, using (*R*)- and (*S*)-2-(1-methoxyethyl) benzeneboronic acid, followed by <sup>1</sup>H NMR analysis of the diastereoisomeric composition, provided another simple approach (method iii).<sup>28</sup> <sup>1</sup>H NMR analyses of the di-MTPA (method ii) and boronate (method iii) esters also provided an empirical method to determine the ACs of the parent diols. Unequivocal methods used include X-ray crystallography and stereochemical correlation.

Shake flask biotransformations were carried out on ca. 0.5 g scale, using *Ps. putida* UV4, under reported conditions. The *cis*-dihydrodiols obtained after bioconversion of the corresponding arene substrates were separated and purified by PLC (silica gel, 50% EtOAc in hexane). The minor regioisomer formed in some of the biotransformations was detected by <sup>1</sup>H NMR, GC-MS, and CSPHPLC analyses.

**(1*S*,2*S*)-1a.** (0.478 g, 80%), mp 115–118°C (from CH<sub>2</sub>Cl<sub>2</sub>/hexane); [ $\alpha$ ]<sub>D</sub> + 6 (*c* 1.24, MeOH); Found: C, 33.9; H, 2.6. C<sub>6</sub>H<sub>6</sub>O<sub>2</sub>BrF requires C, 34.5; H, 2.9%;  $\delta$ <sub>H</sub> (500 MHz, CDCl<sub>3</sub>) 4.38 (1 H, m, 2-H), 4.61 (1 H, m, 1-H), 5.90 (1 H, m, 6-H), 6.04 (1 H, m, 5-H); *m/z* (EI) 210 (M<sup>+</sup>, 41%), 208 (43), 192 (11), 190 (11), 164 (22), 83 (100); UV (MeOH)  $\lambda$  268 nm ( $\epsilon$  5800); CD  $\lambda$  284 nm ( $\Delta\epsilon$  + 8.0),  $\lambda$  245 nm ( $\Delta\epsilon$  + 6.2),  $\lambda$  214 nm ( $\Delta\epsilon$  – 6.1); >98% ee and AC (method ii, confirmation by X-ray crystallography); ca. 5% regioisomer **D'** (X = F, Y = Br).

**(1*S*,2*S*)-1b.** (0.136 g, 21%), mp 80–81°C (from CH<sub>2</sub>Cl<sub>2</sub>/hexane), [ $\alpha$ ]<sub>D</sub> – 92 (*c* 1.05, MeOH); Found: C, 49.0; H, 4.1. C<sub>6</sub>H<sub>6</sub>O<sub>2</sub>F<sub>2</sub> requires C, 48.7; H, 4.1%;  $\delta$ <sub>H</sub> (500 MHz, CDCl<sub>3</sub>) 4.40 (1 H, m, 2-H), 4.62 (1 H, m, 1-H), 5.76 (1 H, m, 6-H), 5.88 (1 H, m, 5-H); *m/z* (EI) 148 (M<sup>+</sup>, 68%), 130 (63), 119 (40); UV (MeOH)  $\lambda$  257 nm ( $\epsilon$  3150); CD  $\lambda$  255 nm ( $\Delta\epsilon$  – 5.4),  $\lambda$  204 nm ( $\Delta\epsilon$  + 5.5); 85% ee and AC (method ii).

**(1*S*,2*R*)-1c.** (0.422 g, 70%), mp 98–101°C (from CH<sub>2</sub>Cl<sub>2</sub>/hexane); [ $\alpha$ ]<sub>D</sub> – 65 (*c* 1.1, MeOH); Found: M<sup>+</sup>, 198.0304. C<sub>7</sub>H<sub>6</sub>O<sub>2</sub>F<sub>4</sub> requires 198.0304;  $\delta$ <sub>H</sub> (500 MHz, CDCl<sub>3</sub>) 4.46 (1 H, m, 2-H), 4.60 (1 H, m, 1-H), 5.92 (1 H, m, 6-H), 6.23 (1 H, m, 5-H); *m/z* (EI) 198 (M<sup>+</sup>, 79%), 180 (11), 158 (64), 101 (100); UV (MeOH)  $\lambda$  258 nm ( $\epsilon$  3300); CD  $\lambda$  257 nm ( $\Delta\epsilon$  – 1.9),  $\lambda$  214 nm ( $\Delta\epsilon$  – 3.9); >98% ee and AC (method ii).

**(1*S*,2*R*)-1d.** (0.380 g, 58%), mp 78–80°C (from CH<sub>2</sub>Cl<sub>2</sub>/hexane); [ $\alpha$ ]<sub>D</sub> – 32 (*c* 1.3, CHCl<sub>3</sub>); Found: C, 58.1; H, 6.3. C<sub>7</sub>H<sub>9</sub>O<sub>2</sub>F requires C, 58.3; H, 6.3%;  $\delta$ <sub>H</sub> (500 MHz, CDCl<sub>3</sub>) 1.85 (3 H, s, Me), 4.06 (1 H, dd, *J*<sub>2,1</sub> = *J*<sub>2,1</sub> 6.0, 2-H), 4.43 (1 H, m, 2-H), 5.85 (2 H, m, 5-H and 6-H); *m/z* (EI) 144 (M<sup>+</sup>, 61%), 126 (84), 97 (100); UV (MeOH)  $\lambda$  264 nm ( $\epsilon$  3500); CD  $\lambda$  257 nm ( $\Delta\epsilon$  – 2.0),  $\lambda$  206 nm ( $\Delta\epsilon$  + 6.4); >98% ee and AC (method ii, confirmation by X-ray crystallography); ca. 5–10% regioisomer **D'** (X = F, Y = CH<sub>3</sub>).

**(1*S*,2*S*)-2a.** (0.240 g, 40%), mp 97–100°C (from CHCl<sub>3</sub>/hexane); [ $\alpha$ ]<sub>D</sub> + 61 (*c* 0.29, MeOH); Found: C, 34.5; H, 2.6. C<sub>6</sub>H<sub>6</sub>O<sub>2</sub>BrF requires C, 34.5; H, 2.9%;  $\delta$ <sub>H</sub> (500 MHz, CDCl<sub>3</sub>) 4.40 (1 H, dd, *J*<sub>2,1</sub> 5.7, *J*<sub>2,4</sub> 1.5, 2-H), 4.48 (1 H, dd, *J*<sub>1,2</sub> 5.7, *J*<sub>1,6</sub> 11.2, 1-H), 5.52 (1 H, m, 6-H), 6.33 (1 H, m, 4-H); *m/z* (EI) 208 (M<sup>+</sup>, 16%), 190 (7), 129 (24), 83 (100); UV (MeOH)  $\lambda$  272 nm ( $\epsilon$  4800); CD  $\lambda$  271 nm ( $\Delta\epsilon$  + 2.4),  $\lambda$  203 nm ( $\Delta\epsilon$  – 5.9); >98% ee method (i); <3% regioisomer **F'** (X = F, Y = Br).

**(1*S*,2*S*)-2b.** (0.130 g, 21%), mp 63–65°C (from CH<sub>2</sub>Cl<sub>2</sub>/hexane); [ $\alpha$ ]<sub>D</sub> + 25 (*c* 1.25, MeOH); Found: M<sup>+</sup> 148.0338 C<sub>6</sub>H<sub>6</sub>O<sub>2</sub>F<sub>2</sub> requires 148.0324;  $\delta$ <sub>H</sub> (500 MHz, CDCl<sub>3</sub>) 2.47 (2 H, bs, OH), 4.46 (2 H, m, 1-H and 2-H),

5.31 (1 H, m, 6-H), 5.88 (1 H, m, 1-H);  $m/z$  (EI) 148 ( $M^+$ , 57%), 130 (90), 114 (72), 101 (100); UV (MeOH)  $\lambda$  259 nm ( $\epsilon$  2700); CD  $\lambda$  254 nm ( $\Delta\epsilon$  + 1.0),  $\lambda$  204 nm ( $\Delta\epsilon$  - 1.6); 56% ee and AC (method ii).

**(1S,2R)-2c.** (0.150 g, 25%); mp 60–62°C (from  $\text{CHCl}_3$ /hexane);  $[\alpha]_D$  - 26 ( $c$  0.33, MeOH); Found:  $M^+$  198.0312.  $\text{C}_7\text{H}_6\text{O}_2\text{F}_4$  requires 198.0304;  $\delta_H$  (500 MHz,  $\text{CDCl}_3$ ) 4.45 (1 H, d,  $J_{2,1}$  5.9, 2-H), 4.56 (1 H, m, 1-H), 5.60 (1 H, m, 6-H), 6.47 (1 H, m, 4-H);  $m/z$  (EI) 198 ( $M^+$ , 77%), 180 (10), 152 (70), 101(100); UV (MeOH)  $\lambda$  263 nm ( $\epsilon$  3300); CD  $\lambda$  255 nm ( $\Delta\epsilon$  + 6.1),  $\lambda$  226 nm ( $\Delta\epsilon$  - 2.4),  $\lambda$  205 nm ( $\Delta\epsilon$  - 1.0); >98% ee; <3% regioisomer **F'** ( $X = \text{F}$ ,  $Y = \text{CF}_3$ ).

**(1S,2R)-2d.** (0.09 g, 34%); mp 95–98°C;  $[\alpha]_D$  + 118 ( $c$  0.31, MeOH); Found:  $M^+$  144.0586.  $\text{C}_7\text{H}_9\text{O}_2\text{F}$  requires 144.0587;  $\delta_H$  (300 MHz,  $\text{CDCl}_3$ ) 1.96 (3 H, s, Me), 4.23 (1 H, m, 2-H), 4.31 (1 H, m, 1-H), 5.36 (1 H, m, 6-H), 5.65 (1 H, m, 4-H);  $m/z$  (EI) 144 ( $M^+$ , 54%), 126 (61), 125 (30), 97(100); UV (MeOH)  $\lambda$  263 nm ( $\epsilon$  3300); CD  $\lambda$  261 nm ( $\Delta\epsilon$  + 2.6),  $\lambda$  207 nm ( $\Delta\epsilon$  - 2.3); 98% ee and AC method (ii).

**(1S,2S)-2e.** (0.195 g, 31%); mp 80–82°C;  $[\alpha]_D$  + 61 ( $c$  0.36, MeOH); Found:  $M^+$  164.0046.  $\text{C}_6\text{H}_6\text{O}_2\text{ClF}$  requires 164.0040;  $\delta_H$  (500 MHz,  $\text{CDCl}_3$ ) 4.37 (1 H, m, 2-H), 4.48 (1 H, m, 1-H), 5.47 (1 H, m, 6-H), 6.09 (1 H, m, 4-H);  $m/z$  (EI) 164 ( $M^+$ , 100%), 146 (38), 118 (89), 83 (88); CD  $\lambda$  271 nm ( $\Delta\epsilon$  + 2.4),  $\lambda$  203 nm ( $\Delta\epsilon$  - 5.9); >98% ee (method i); <3% regioisomer **F'** ( $X = \text{F}$ ,  $Y = \text{Cl}$ ).

**(1S,2S)-2f.** (0.265 g, 46%); mp 98–101°C (from  $\text{CHCl}_3$ /hexane);  $[\alpha]_D$  + 74 ( $c$  0.48, MeOH); Found: C, 28.2; H, 2.1.  $\text{C}_6\text{H}_6\text{O}_2\text{IF}$  requires C, 28.1; H, 2.3%;  $\delta_H$  (300 MHz,  $\text{CDCl}_3$ ) 4.33 (1 H, d,  $J_{2,1}$  5.9, 2-H), 4.43 (1 H, m, 1-H), 5.58 (1 H, m, 6-H), 6.63 (1 H, m, 4-H);  $m/z$  (EI) 256 ( $M^+$ , 58%), 129 (67), 83 (100); CD  $\lambda$  272 nm ( $\Delta\epsilon$  + 1.3),  $\lambda$  238 nm ( $\Delta\epsilon$  - 2.2),  $\lambda$  202 nm ( $\Delta\epsilon$  - 3.3); >98% ee and AC (method ii).

**(1S,2R)-2g.**<sup>33</sup>  $[\alpha]_D$  + 99 ( $c$  0.4, MeOH); CD  $\lambda$  212 nm ( $\Delta\epsilon$  - 4.2),  $\lambda$  279 nm ( $\Delta\epsilon$  + 0.9); >98% ee and AC (method ii).

**(1S,2R)-3a.**<sup>33</sup>  $[\alpha]_D$  + 26 ( $c$  0.79, MeOH); CD  $\lambda$  228 nm ( $\Delta\epsilon$  + 3.4),  $\lambda$  260 nm ( $\Delta\epsilon$  - 0.6); >98% ee and AC (method iv).

**(1S,2R)-3b.**<sup>33</sup>  $[\alpha]_D$  - 101 ( $c$  0.50, MeOH); CD  $\lambda$  254 nm ( $\Delta\epsilon$  - 2.5),  $\lambda$  211 nm ( $\Delta\epsilon$  - 0.7); >98% ee and AC (method iv).

**(1S,2R)-3d.**<sup>33</sup>  $[\alpha]_D$  - 16 ( $c$  0.36, MeOH); CD  $\lambda$  194 nm ( $\Delta\epsilon$  - 2.8),  $\lambda$  210 nm ( $\Delta\epsilon$  + 2.1),  $\lambda$  255 nm ( $\Delta\epsilon$  - 1.25); >98% ee and AC (method iv).

**(1S,2R)-3e.**<sup>33</sup>  $[\alpha]_D$  + 20 ( $c$  0.83 MeOH); CD  $\lambda$  227 nm ( $\Delta\epsilon$  + 2.25),  $\lambda$  260 nm ( $\Delta\epsilon$  - 0.8); >98% ee and AC (method iv).

**(1S,2R)-3f.**<sup>33</sup>  $[\alpha]_D$  + 43 ( $c$  0.77, MeOH); CD  $\lambda$  212 nm ( $\Delta\epsilon$  - 3.1),  $\lambda$  242 nm ( $\Delta\epsilon$  + 4.9),  $\lambda$  305 nm ( $\Delta\epsilon$  - 0.35); >98% ee and AC (method iv).

Chirality DOI 10.1002/chir

**(1S,2S)-5a.** (0.410 g, 65%); mp 112–115°C (from  $\text{CH}_2\text{Cl}_2$ /hexane);  $[\alpha]_D$  - 13 ( $c$  0.4, MeOH); Found: C, 43.7; H, 3.2.  $\text{C}_6\text{H}_6\text{O}_2\text{FCl}$  requires C, 43.8; H 3.7%;  $\delta_H$  (500 MHz,  $\text{CDCl}_3$ ) 4.32 (1 H, dd,  $J_{2,\text{F}}$  6.0,  $J_{2,1}$  6.0, 2-H), 4.62 (1 H, m, 1-H), 5.93 (1 H, m, 6-H), 5.98 (1 H, m, 5-H);  $m/z$  (EI) 164 ( $M^+$ , 66%), 146 (21), 118 (80), 83(100); CD  $\lambda$  292 nm ( $\Delta\epsilon$  + 2.6),  $\lambda$  256 nm ( $\Delta\epsilon$  + 1.1),  $\lambda$  235 nm ( $\Delta\epsilon$  - 4.4); >98% ee and AC (method ii); ca. 5–10% regioisomer **D'** ( $X = \text{Cl}$ ,  $Y = \text{F}$ ).

**(1S,2S)-5b.** (0.248 g, 43%); mp 86–89°C (from  $\text{CH}_2\text{Cl}_2$ /hexane);  $[\alpha]_D$  + 20 ( $c$  0.68, MeOH); Found: C, 28.3; H 2.3.  $\text{C}_6\text{H}_6\text{O}_2\text{FI}$  requires C, 28.1; H 2.3%;  $\delta_H$  (500 MHz,  $\text{CDCl}_3$ ) 4.40 (1 H, d,  $J_{2,1}$  6.3, 2-H), 4.58 (1 H, m, 1-H), 5.86 (1 H, m, 6-H), 6.09 (1 H, m, 5-H);  $m/z$  (EI) 256 ( $M^+$ , 51%), 238 (67), 129 (38), 83 (100); CD  $\lambda$  278 nm ( $\Delta\epsilon$  + 2.3),  $\lambda$  226 nm ( $\Delta\epsilon$  - 8.3); >98% ee and AC (method ii).

**(1S,2S)-5c.** (0.368 g, 58%); mp 107–108 °C (from  $\text{CHCl}_3$ );  $[\alpha]_D$  + 38 ( $c$  1.8, MeOH); Found: C, 52.3; H, 5.5.  $\text{C}_7\text{H}_9\text{O}_2\text{Cl}$  requires C, 52.3; H, 5.6%;  $\delta_H$  (500 MHz,  $\text{CDCl}_3$ ) 1.91 (3 H, s, Me), 4.17 (1 H, d,  $J_{1,2}$  6.2, 1-H), 4.51 (1 H, d,  $J_{2,1}$  6.2, 2-H), 5.84 (2 H, m, 5-H and 6-H);  $m/z$  (EI) 160 ( $M^+$ , 31%), 142 (40), 79 (100); CD  $\lambda$  284 nm ( $\Delta\epsilon$  + 5.4),  $\lambda$  225 nm ( $\Delta\epsilon$  - 7.2); >98% ee and AC (method ii); 20% regioisomer **D'** ( $X = \text{Cl}$ ,  $Y = \text{Me}$ ).

**(1S,2S)-5d.** (0.34 g, 56%); mp 110–111°C (from  $\text{CHCl}_3$ /hexane);  $[\alpha]_D$  + 25 ( $c$  2.1, MeOH); Found: C, 41.0; H 4.0.  $\text{C}_7\text{H}_9\text{O}_2\text{Br}$  requires C, 41.0; H 4.4%;  $\delta_H$  (300 MHz,  $\text{CDCl}_3$ ) 1.92 (3 H, s, Me), 4.26 (1 H, m, 1-H), 4.49 (1 H, m, 2-H), 5.82 (1 H, dd,  $J_{5,6}$  9.6,  $J_{5,1}$  1.5, 5-H), 5.90 (1 H, dd,  $J_{6,5}$  9.6,  $J_{6,1}$  2.7, 6-H);  $m/z$  (EI) 204 ( $M^+$ , 29%), 206 (28), 188 (11), 186 (12), 79 (100); CD  $\lambda$  281 nm ( $\Delta\epsilon$  + 1.6),  $\lambda$  222 nm ( $\Delta\epsilon$  - 4.9),  $\lambda$  210 nm ( $\Delta\epsilon$  - 2.6); >98% ee and AC (method ii).

**(1S,2S)-5e.** (0.300 g, 52%); mp 98–100°C (from  $\text{CHCl}_3$ /hexane);  $[\alpha]_D$  + 48 ( $c$  1.63, MeOH); Found:  $M^+$ , 251.9644.  $\text{C}_7\text{H}_9\text{O}_2\text{I}$  requires 251.9647;  $\delta_H$  (300 MHz,  $\text{CDCl}_3$ ) 1.97 (3 H, s, Me), 4.29 (1 H, d,  $J_{2,1}$  6.0, 2-H), 4.47 (1 H, m, 1-H), 5.81 (1 H, dd,  $J_{5,6}$  9.7,  $J_{5,1}$  1.3, 5-H), 5.94 (1 H, dd,  $J_{6,5}$  9.7,  $J_{6,1}$  3.0, 6-H);  $m/z$  (EI) 252 ( $M^+$ , 43%), 234 (100); CD  $\lambda$  285 nm ( $\Delta\epsilon$  + 2.5),  $\lambda$  234 nm ( $\Delta\epsilon$  - 7.4),  $\lambda$  214 nm ( $\Delta\epsilon$  + 4.6); >98% ee and AC (method ii, confirmation by X-ray crystallography).

**(1S,2R)-5f.**<sup>33</sup>  $[\alpha]_D$  - 6 ( $c$  0.45, MeOH); CD  $\lambda$  206 nm ( $\Delta\epsilon$  0.5),  $\lambda$  258 nm ( $\Delta\epsilon$  - 0.9); >98% ee and AC (method iii).

## RESULTS AND DISCUSSION

Relative substituent size was found to be an important factor during TDO-catalyzed *cis*-dihydroxylation of mono- (**A**,  $Y = \text{H}$ ) or 1,4-disubstituted benzene substrates (**A**,  $X \neq Y \neq \text{H}$ ) with only one enantiomer being produced when substituent **X** was significantly larger than **Y**.<sup>26–28,30</sup> A preliminary study of *cis*-dihydrodiols (**C/C'** and **E/E'**, **X** and **Y**  $\neq \text{H}$ ) derived from the corresponding 1,2- and 1,3-disubstituted benzene substrates (**A**, **X** and **Y**  $\neq \text{H}$ )<sup>31,32</sup> suggested that substituent size (based on the sequence



$\text{CF}_3 > \text{I} > \text{Br} > \text{Cl} > \text{Me} > \text{F} > \text{H}$ ) could also be an important factor in the determination of both their regio- and stereoselectivity during TDO-catalyzed *cis*-dihydroxylation. Thus *cis*-dihydrodiols of type **C/C'** (**1a–1d**, **5a–5f**) and **E/E'** (**2a–2g**) having  $\text{X} > \text{Y}$  were obtained without any evidence of the alternative regioisomers (**D/D'** and **F/F'**). However, when substituent sizes are relatively similar, then alternative types of *cis*-dihydrodiol regioisomers from both 1,2-(**D/D'**) and 1,3-disubstituted benzenes (**F/F'**) are detectable by  $^1\text{H}$  NMR and HPLC analysis. Fortunately, the minor proportions of the latter regioisomers **1d** (5–10%), **5a** (5–10%), **5c** (20%), and **2a–2g** (<3%) were removed by chromatography and fractional recrystallization before experimental CD spectra and OR measurements were obtained on the major type **C/C'** and **E/E'** *cis*-dihydrodiols (**1a–1d**, **5a–5f**, and **2a–2g**).

Enantiopurity (% ee) values of the *cis*-dihydrodiols were determined by methods reported earlier and references therein.<sup>27,28,30</sup> These included chiral stationary phase HPLC (**2a**, **2c**, and **2e**, DAICEL columns, method i),  $^1\text{H}$  NMR analysis of both (*R*)- and (*S*)-di MTPA esters formed from cycloadducts with 4-phenyl-1,2,4-triazoline-3,5-dione (**1a–1d**, **2b**, **2d**, **2f**, and **5a–5e**, method ii) and of boronate esters formed from (*R*)- and (*S*)-2-(1-methoxyethyl) benzenboronic acids (**1b**, **2b**, **2g**, and **5f**, method iii). The other % ee values were determined by stereochemical correlation during their chemoenzymatic synthesis (**3a–3f**, method iv).<sup>37</sup>

X-ray crystallography of the cycloadduct diMTPA esters (from **1a**, **1d**, and **5e**) and stereochemical correlation (**3a–3f**, method iv) provided unequivocal AC determination methods. Tentative ACs were determined by method ii (**1b**, **1c**, **2b**, **2d**, **2f**, and **5a–5e**) and method iii (**1b**, **2b**, **2g**, and **5f**). The assignment of ACs of *cis*-dihydrodiols **2a**, **2c**, and **2e** relied totally on CD spectroscopy (see later).

With the series of *cis*-dihydrodiols (**1a–1d**, **2a–2g**, **3a**, **3b**, **3d–3f**, **5a–5f**) having diverse substituents attached

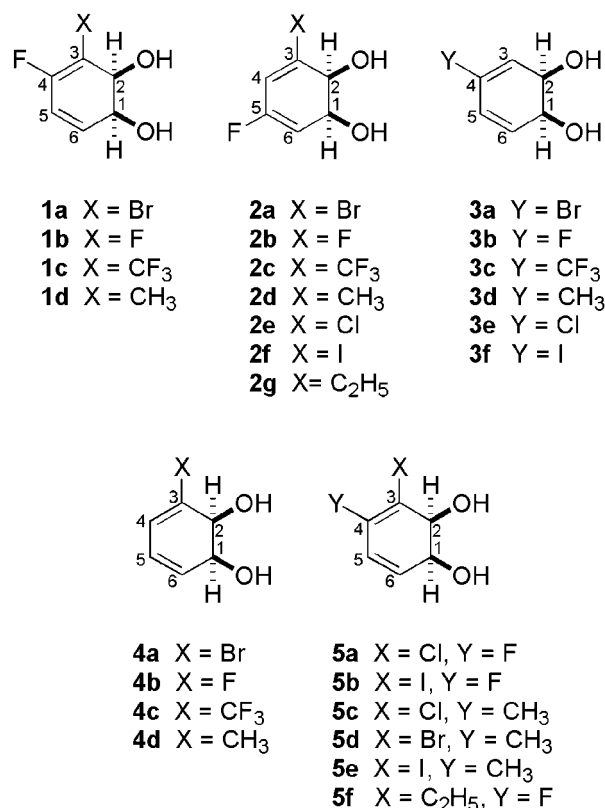
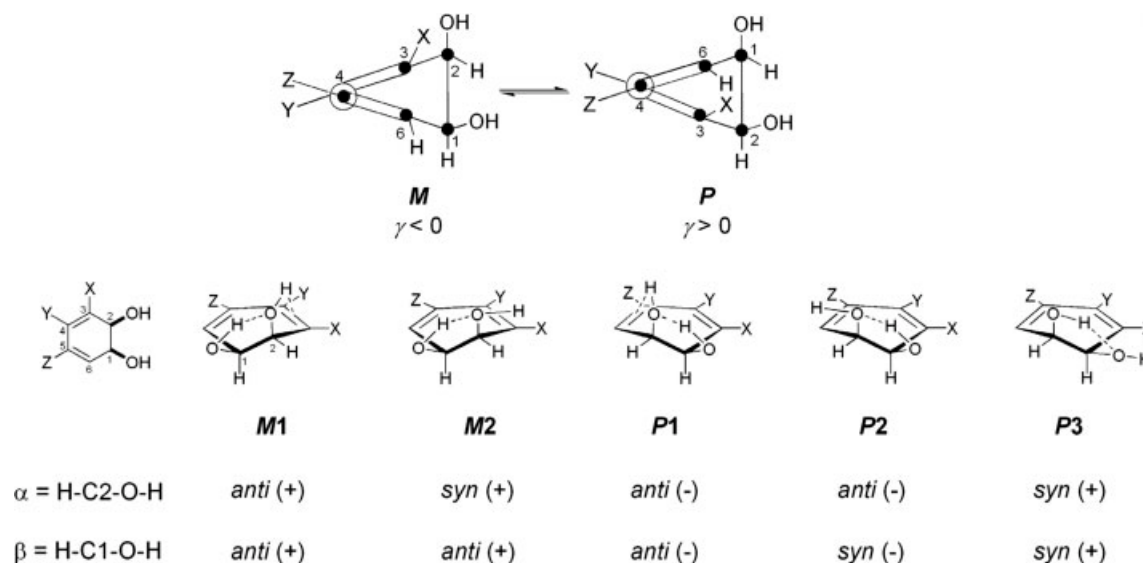


Chart 1.

to the diene chromophore available, a major objective is to study their effect on both the conformation and the chiroptical properties of these biotransformation products (Chart 1).

Conformational analysis of the dihydrodiols **1a–1d**, **2a–2d**, and **3a–3d** has been carried out using the DFT-based



**Scheme 2.** Diastereoisomeric *P* and *M* conformers of *cis*-dihydrodiols, torsion angles  $\alpha$  ( $\text{H-C2-O-H}$ ),  $\beta$  ( $\text{H-C1-O-H}$ ), and typical hydrogen-bond patterns between the hydroxy groups in conformers **M1**, **M2**, **P1**, **P2**, and **P3**.

**TABLE 1.** Calculated at the B3LYP/6-311++G(D,P) level relative energies ( $\Delta E$ ,  $\Delta G$ ), populations, and structural parameters ( $\alpha$ ,  $\beta$ ,  $\gamma$ ) for the low-energy conformers of *cis*-dihydrodiols 1a–1d, 2a–2d, and 3a–3d

Dihydrodiol	Conformer	$\Delta E$ (population) (kcal mol <sup>−1</sup> )	$\Delta G$ (population) (kcal mol <sup>−1</sup> )	$\alpha$ (°)	$\beta$ (°)	$\gamma$ (°)
1a	<b>M1</b>	0.08 (44) <sup>a</sup>	0.29 (37)	157.7	153.3	−10.9
	<b>M2</b>	0.00 (52)	0.00 (60)	55.2	159.1	−9.7
	<b>P1</b>	1.42 (4)	1.74 (3)	−155.7	−159.1	9.6
1b	<b>M1</b>	0.00 (53)	0.16 (42)	158.7	152.6	−10.2
	<b>M2</b>	0.15 (41)	0.00 (55)	49.1	159.0	−9.1
	<b>P1</b>	1.25 (6)	1.58 (3)	−153.7	−156	9.0
1c	<b>M1</b>	0.84 (19)	0.67 (24)	158.0	151.7	−10.4
	<b>M2</b>	0.00 (81)	0.00 (76)	55.3	158.4	−11.5
1d	<b>M1</b>	0.00 (70)	0.00 (66)	162.1	152.8	−11.5
	<b>M2</b>	1.86 (3)	1.20 (9)	48.3	159.4	−11.1
	<b>P1</b>	0.54 (27)	0.56 (25)	−150.7	−159.5	9.7
2a	<b>M1</b>	0.76 (16)	0.66 (16)	162.7	154.6	−10.8
	<b>M2</b>	0.89 (13)	0.47 (20)	50.8	161.1	−9.5
	<b>P1</b>	0.00 (58)	0.00 (46)	−154.6	−155.1	9.9
2b	<b>P3</b>	0.89 (13)	0.54 (18)	78.8	70.5	10.3
	<b>M1</b>	0.91 (16)	0.77 (17)	163.1	154.2	−10.4
	<b>M2</b>	1.21 (9)	0.67 (20)	45.2	161.1	−9.2
2c	<b>P1</b>	0.00 (74)	0.00 (62)	−153.3	−151.6	9.5
	<b>M1</b>	0.84 (15)	0.73 (18)	159.8	154.3	−12.0
	<b>M2</b>	0.00 (63)	0.00 (64)	53.9	160.4	−10.4
2d	<b>P1</b>	0.74 (17)	1.02 (11)	−155.0	−158.3	10.6
	<b>P2</b>	1.93 (2)	1.58 (4)	−162.0	−56.2	10.7
	<b>P3</b>	1.84 (3)	1.92 (3)	54.9	67.5	11.7
3a	<b>M1</b>	1.45 (8)	1.45 (8)	165.8	154.6	−11.0
	<b>P1</b>	0.00 (92)	0.00 (92)	−149.4	−156.6	9.8
	<b>M2</b>	0.00 (52)	0.00 (50)	158.7	152.5	−11.4
3b	<b>P1</b>	1.48 (4)	1.22 (6)	62.1	159.7	−11.4
	<b>P2</b>	0.13 (42)	0.17 (37)	−153.2	−159.4	11.2
	<b>P3</b>	1.82 (2)	1.20 (7)	−160.1	−59.6	11.3
3c	<b>M1</b>	0.00 (80)	0.00 (61)	156.5	151.6	−10.5
	<b>M2</b>	1.46 (7)	0.44 (29)	70.5	159.2	−10.5
	<b>P1</b>	1.06 (13)	1.07 (10)	−153.1	−160.6	10.1
3d	<b>M1</b>	0.69 (22)	0.61 (21)	161.7	153.1	−11.4
	<b>M2</b>	2.02 (0)	1.36 (6)	51.5	160.4	−11.1
	<b>P1</b>	0.00 (72)	0.00 (59)	−151.9	−157.4	11.0
3d	<b>P2</b>	1.45 (6)	0.84 (14)	−159.1	59.9	11.3
	<b>M1</b>	0.00 (70)	0.00 (67)	157.7	152.2	−11.7
	<b>P1</b>	0.50 (30)	0.54 (27)	−152.8	−160.4	11.7
	<b>P2</b>	2.37 (0)	1.36 (6)	−160.3	−65.3	11.8

<sup>a</sup>Values within parentheses are percentages.

protocol described in our previous publications.<sup>26,27</sup> In brief, this method uses the B3LYP hybrid functional and searches the PES arising from the rotation of the hydroxyl groups at C(1) and C(2). As it was found previously,<sup>26,27</sup> the energy of conformers of *P* and *M* helicity is strongly dependent on the pattern of intramolecular hydrogen bonding and distinct conformers can be envisioned, differing in diene helicity (*P* or *M*, characterized by torsion angle  $\gamma$ ) and H—C—O—H torsion angles  $\alpha$  and  $\beta$  (Scheme 2).

Thus, the conformers which are within an arbitrarily chosen 2 kcal mol<sup>−1</sup> window, belong to either of the stereoisomeric type, **M1**, **M2**, **P1**, and **P2** (for the assumed AC). Furthermore, in two cases (**2a**, **2c**) the **P3** conformer, having both torsion angles  $\alpha$  and  $\beta$  synperiplanar, was found to contribute to the conformational equilibrium to a small extent. The calculated conformer relative ener-

gies and populations (both in  $\Delta E$  and in  $\Delta G$  formalism) are given in Table 1.

The structures of the conformers are rigorously characterized by the torsion angles  $\alpha$ ,  $\beta$ , and  $\gamma$  (Table 1) and intramolecular hydrogen bond distances (the numerical data are available on request). Thus, for the anti and syn conformation of the H—C—O—H bonds the values  $\alpha$  and  $\beta$  are in the range 149–166° and 45–78°, with the signs either positive for **M1** and **M2** or negative for **P1** and **P2** conformers. The calculated diene torsion angle  $\gamma$  is in the range  $\pm$ (9–12°). Intramolecular O—H...O bonds are formed by equatorial H donor and axial acceptor groups and their length is calculated at 2.12–2.20 Å. In **M2** conformers, one of the O—H bonds (*syn* H—O—C<sub>2</sub>—H) is parallel to the C—X bond, providing a further stabilization of the conformer, if X is an electronegative substituent. Since this interaction is absent in **P2** conformers, **M2**

conformers are of lower energy, when X is Br (**1a**, **2a**), F (**1b**, **2b**), or CF<sub>3</sub> (**1c**, **2c**). In some of the cases (**1a**–**1c**, **2c**) the **M2** conformer is of the lowest energy and in several cases the **P2** conformer energy is beyond the 2 kcal mol<sup>−1</sup> window (therefore not listed in Table 1). This conformational preference (**M2** over **P2**) was previously observed for “parent” *cis*-dihydrodiols **4a**, **4b**, and **4c**.<sup>26</sup> If X is the methyl group, the **M2** conformer is of high energy (**1d**, **2d**, **3d** as well as **4d**<sup>26</sup>). Overall, *cis*-diene conformers of *M* helicity strongly prevail for **1a**–**1d**, **2c**, **3b**, and **3d**, regardless of the calculation formalism used ( $\Delta E$  or  $\Delta G$ ). Dihydrodiol **3a** does not show a strong preference towards either an *M* or *P* conformation, whereas **2a**, **2b**, **2d**, and **3c** exist preferably in a **P1** conformation. Axial donor hydroxy groups are found in **P3** conformers and the hydrogen bond in these conformers is longer, making these species less stable.

The anomalous behavior of substituted benzene is seen in substrates bearing only fluorine atoms, where TDO-catalyzed *cis*-dihydroxylation can produce both the expected *cis*-dihydrodiols **B** (X = F, Y = H, **4b**), **C** (X = Y = F, **1b**), **E** (X = Y = F, **2b**) and minor amounts of the corresponding enantiomers **B'** (X = F, Y = H, **4b'**), **C'** (X = Y = F, **1b'**), **E'** (X = Y = F, **2b'**). This can be rationalized in terms of the small steric requirements of a fluorine atom and greater mobility of substrate in the active site of TDO. Conformational differences clearly demonstrate a further effect of the fluorine substituent attached to the diene chromophore in **1a**, **1b**, **1d**, and **2a**, **2b**, **2d**. Regioisomeric *cis*-dihydrodiols show opposite conformational preferences, i.e., **M1** dominates over **P1** in **1a**, **1b**, **1d**, whereas **P1** is the most stable conformer of **2a**, **2b**, and **2d**. The effect of a fluorine substituent is readily explained by the strength of the hydrogen bond O–H... $\pi$  in conformers **M1** and **P1**. The fluorine-substituted C=C bond is apparently a more electron-rich and a better acceptor of the hydrogen bond, thus conformer **M1** is more stable when Y = F and X = Br, F, or CH<sub>3</sub>, whereas **P1** is more stable when Z = F, X = Br, F, or CH<sub>3</sub> (Scheme 2). Support for the electron-donating effect of a fluorine atom on an alkene group (trigonal carbon atoms) was evident from the upfield <sup>1</sup>H  $\delta$  values of vinyl fluoride groups in intermediates involved in the synthesis of **3b**.<sup>37</sup> The case of trifluoromethyl-substituted *cis*-dihydrodiols **1c** and **2c** is exceptional. As found previously for **4c**,<sup>26</sup> when X = CF<sub>3</sub> conformer **M2** is the most stable one due to the strong intramolecular hydrogen bond O–H...F<sub>3</sub>C.

The *cis*-dihydrodiols **3a**, **3b**, **3d**, obtained from **4a**, **4b** and **4d**, respectively, by chemoenzymatic synthesis (and **3c**),<sup>37</sup> deserve special mention, since the substituent Y cannot directly interact with the hydroxy groups, as does the X group in other *cis*-dihydrodiols. This is reflected in the observation that neither **M2** nor **P2** contribute significantly to the pool of low-energy conformers. Conformer **M1** is obviously the most stable when Y = F (**3b**), as discussed earlier. This is in contrast to Y = Br (**3a**); in this case the calculated population of **M1** and **P1** conformers does not differ to a great extent. Contrasting behavior is shown by compounds **3c** (Y = CF<sub>3</sub>) and **3d** (Y = CH<sub>3</sub>) where **P1** is the lowest energy conformer in the former,

**TABLE 2.** Calculated (mPW1PW91/6-311++G(2D,2P) level) transition energies, rotational strengths (*R*), and oscillator strengths (*f*) of individual conformers of *cis*-dihydrodiols **1a**–**1d**, **2a**–**2d**, and **3a**–**3d**

Dihydrodiol	Conformer	Transition energy (nm)	<i>R</i> ( $\times 10^{-40}$ erg esu cm gauss <sup>−1</sup> )	<i>f</i>
<b>1a</b>	<b>M1</b>	288	0.9	0.145
	<b>M2</b>	284	−6.3	0.151
	<b>P1</b>	294	22.1	0.168
<b>1b</b>	<b>M1</b>	275	−31.2	0.084
	<b>M2</b>	274	−34.8	0.087
	<b>P1</b>	281	25.9	0.094
<b>1c</b>	<b>M1</b>	274	−10.1	0.102
	<b>M2</b>	271	−14.0	0.115
<b>1d</b>	<b>M1</b>	276	−18.4	0.117
	<b>M2</b>	277	−24.7	0.114
	<b>P1</b>	283	33.5	0.130
<b>2a</b>	<b>M1</b>	293	8.9	0.145
	<b>M2</b>	291	−0.3	0.148
	<b>P1</b>	284	24.8	0.181
	<b>P2</b>	278	11.1	0.169
<b>2b</b>	<b>M1</b>	277	−16.5	0.076
	<b>M2</b>	277	−21.9	0.078
	<b>P1</b>	269	36.3	0.092
<b>2c</b>	<b>M1</b>	286	−4.8	0.096
	<b>M2</b>	286	−11.8	0.112
	<b>P1</b>	274	5.6	0.098
	<b>P2</b>	277	13.8	0.109
<b>2d</b>	<b>P3</b>	270	−3.1	0.127
	<b>M1</b>	279	−10.6	0.112
	<b>P1</b>	272	45.1	0.138
<b>3a</b>	<b>M1</b>	279	−16.5	0.058
	<b>M2</b>	283	−21.2	0.063
	<b>P1</b>	286	14.8	0.051
	<b>P2</b>	289	19.5	0.052
<b>3b</b>	<b>M1</b>	270	−28.3	0.084
	<b>M2</b>	274	−33.7	0.087
	<b>P1</b>	277	20.8	0.081
<b>3c</b>	<b>M1</b>	275	−13.4	0.064
	<b>P1</b>	270	20.4	0.064
	<b>P2</b>	272	31.6	0.072
<b>3d</b>	<b>M1</b>	273	−25.0	0.075
	<b>P1</b>	278	20.2	0.072

whereas **M2** dominates in the latter case. This appears to indicate that, in contrast to a fluorine substituent, a trifluoromethyl group lowers the electron density and acceptor ability of the C=C bond for hydrogen bond formation with the hydroxy group.

Helicity of the diene chromophore is not the only factor determining chiroptical behavior of a given conformer. These and previous<sup>26,27</sup> calculations show that CD spectra and OR of *cis*-dihydrodiols are dependent on diene helicity, conformation of the hydroxy groups, and the nature of the substituents attached to the cyclohexadiene chromophore (X, Y, Z in Scheme 2).

Whereas there are several electronic transitions which contribute to the UV absorption and CD spectra of cyclohexadienes above 200 nm, the longest-wavelength transition located at above 250 nm is taken as the most suitable

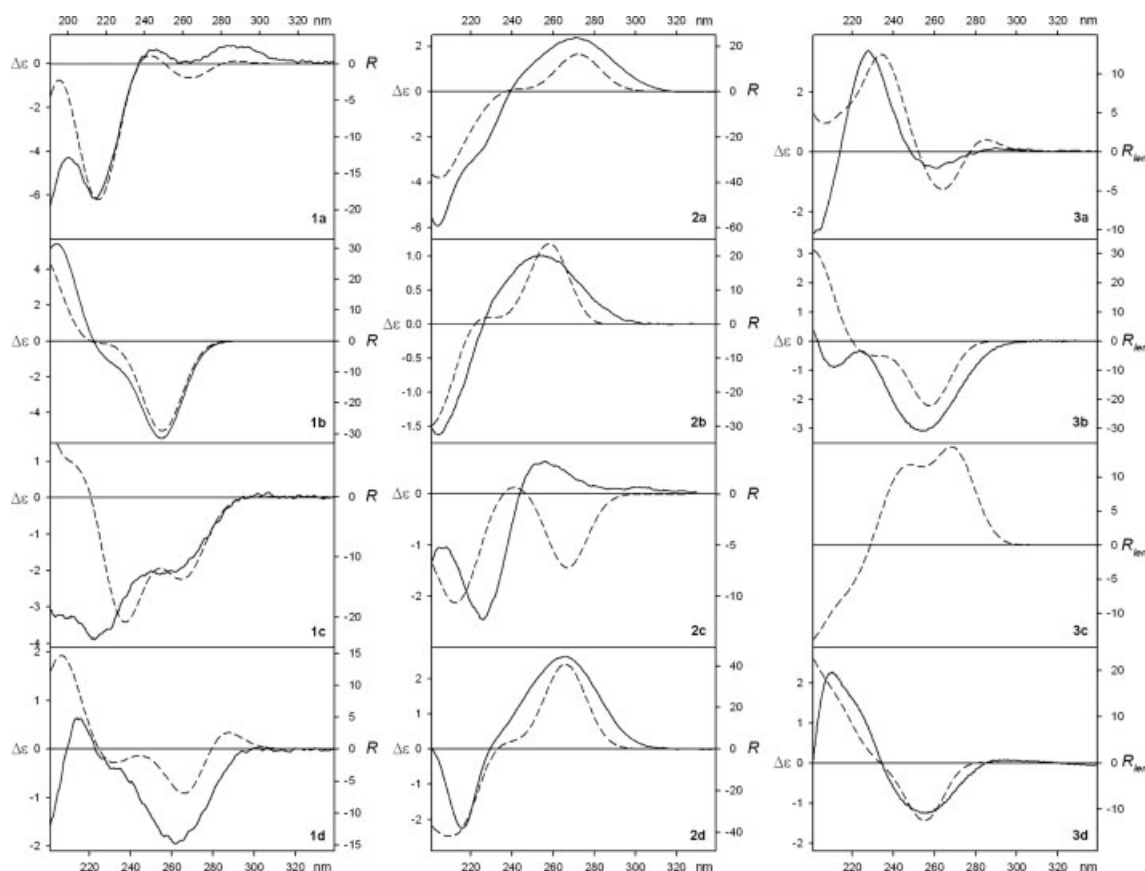


**Fig. 1.** Experimental CD spectra in methanol solution (solid line) and calculated Boltzmann averaged CD spectra (dashed line) for *cis*-dihydrodiols **1a–1d**, **2a–2d**, and **3a–3d**. The rotational strengths  $R$  were calculated at mPW1PW91/6-311++G(2D,2P) level of theory in dipole length representation. The calculated CD spectra were wavelength corrected (blue shifted by 12 nm – **1b**, **2c**; 10 nm – **3d**; 8 nm – **1a**, **2a**, **3a**, and **3b**; 6 nm – **2c**; 4 nm – **1c**, **1d**, and **2d**) to match the experimental long-wavelength  $\lambda_{\text{max}}$  values in the UV spectra.

for comparison between different *cis*-dihydrodiols and their conformers. This transition is of purely HOMO–LUMO  $\pi$ – $\pi^*$  type, in most cases well separated from higher energy electronic transitions.

In the present case, the calculated rotational strengths ( $R$ ) of the lowest energy diene  $\pi$ – $\pi^*$  transitions generally differ for conformers having  $P$  and  $M$  helicity (Table 2). Previous studies have shown that 1,3-cyclohexadiene and 1,2-*cis*-dihydrodiol conformers contribute rotational strength in accordance with the sign of diene torsion angle  $\gamma$ .<sup>26,38</sup> The presence of a bromine (e.g., **4a**) or a cyano substituent at C(3) may reverse the relationship.

Closer inspection of the data of Table 2 reveals that indeed this pattern is maintained in all the cases, except **M2** and **P1** conformers of 3-bromo-substituted *cis*-dihydrodiols of **1a** and **2a**. Thus, opposite sign rotational strengths are observed for **M1** and **M2** conformers of **1a** and **2a**, as well as for **P1/P2** and **P3** of **2c**. This is quite significant, considering the fact that these conformers differ only in the orientation of the O–H bond(s) within the molecule. Using calculated rotational strengths of *cis*-dihydrodiols and  $\Delta E$  based Boltzmann distribution of conformers, the CD spectra and OR at 589 nm were obtained, as shown in Figure 1 and Table 3, correspondingly.

Chirality DOI 10.1002/chir

Figure 1 also shows the experimental CD spectra of dihydrodiols **1a–1d**, **2a–2d**, and **3a**, **3b**, **3d** (the data are not available for **3c**). In general, good agreement between the shapes of the calculated and experimental CD spectra is observed, except in the case of *cis*-dihydrodiol **2c**. Whereas the experimental CD spectrum features a positive Cotton effect at 251 nm, the calculated one shows a negative Cotton effect at 267 nm. The two CD curves of **2c** (Fig. 1) do not have an object–mirror image relationship, therefore the assignment of AC is in this case inconclusive. While there are five conformers of **2c** contributing to the CD spectrum, the two most populated, **M2** (63%) and **P1** (17%), appear to have a decisive role in shaping the CD curve. Figure 2 shows calculated CD spectra of these two conformers. A comparison with the experimental CD spectrum leads to a conclusion that the calculation underestimates the contribution of **P1** conformer, with its strong positive sign rotational strength transition at 250 nm, in comparison to **M2**. It should be noted that the experimental CD data (Fig. 1) were taken in methanol solution. Unlike the calculated CD spectra, the effect of intramolecular hydrogen bonding on the stability of participating conformers will be diminished in methanol solution, possibly leading to the observed differences between the



**TABLE 3.** Calculated at the B3LYP/6-311++g(2d,2p) level and measured optical rotations for *cis*-dihydrodiols **1a–1d**, **2a–2d**, and **3a–3d**

Dihydrodiol	Conformer	Calcd. $[\alpha]_D$	Averaged calcd. $[\alpha]_D^a$	Exptl. $[\alpha]_D^b$
<b>1a</b>	<b>M1</b>	+53	+4	+6
	<b>M2</b>	−54		
	<b>P1</b>	+164		
<b>1b</b>	<b>M1</b>	−75	−97	−108
	<b>M2</b>	−166		
	<b>P1</b>	+180		
<b>1c</b>	<b>M1</b>	−38	−58	−65
	<b>M2</b>	−93		
<b>1d</b>	<b>M1</b>	−5	+65	−32 <sup>c</sup>
	<b>M2</b>	−134		
	<b>P1</b>	+256		
<b>2a</b>	<b>M1</b>	+9	+62	+61
	<b>M2</b>	−83		
	<b>P1</b>	+115		
<b>2b</b>	<b>M1</b>	−120	+66	+45
	<b>M2</b>	−200		
	<b>P1</b>	+140		
<b>2c</b>	<b>M1</b>	−50	−63	−26
	<b>M2</b>	−105		
	<b>P1</b>	+52		
	<b>P2</b>	+134		
<b>2d</b>	<b>M1</b>	−79	+169	+118
	<b>P1</b>	+191		
	<b>M2</b>	−66		
<b>3a</b>	<b>M1</b>	+61	+66	+28
	<b>M2</b>	−66		
	<b>P1</b>	+86		
<b>3b</b>	<b>M1</b>	−77	−56	−101
	<b>M2</b>	−235		
	<b>P1</b>	+169		
<b>3c</b>	<b>M1</b>	−41	+55	d
	<b>P1</b>	+75		
	<b>P2</b>	+176		
<b>3d</b>	<b>M1</b>	−2	+33	−16
	<b>P1</b>	+116		

<sup>a</sup>ΔE Boltzmann averaged.<sup>b</sup>In MeOH, corrected to 100% ee.<sup>c</sup>In CHCl<sub>3</sub>.<sup>d</sup>Data not available.

calculated and experimental CD spectra. Therefore the configurational assignment for **2c** based on the CD should be considered as tentative.

Considering now the calculated OR of individual conformers of *cis*-dihydrodiols, we note that the sign of OR in general corresponds to the helicity of the diene chromophore, i.e., it is negative for *M* and positive for *P* conformers. Exceptions to this relationship are the **M1** conformers of **1a**, **2a**, and **3a** for which the calculated ORs are positive. Since **M2** conformers of these dihydrodiols show a negative OR, this is an additional indication of the powerful effect of the hydroxy group conformation on the chiroptical properties of *cis*-dihydrodiols.

Table 3 shows the calculated (Boltzmann averaged) and experimental ORs of *cis*-dihydrodiols **1a–1d**, **2a–2d**, and **3a–3d**. The signs of ORs are identical (and magnitudes of ORs are often similar) for the ACs assumed in calculations, thus allowing the establishment of the configuration of *cis*-dihydrodiols, with the exception of **1d** and **3d**. In these two cases, the signs of calculated and experimental ORs are opposite due to the very low calculated ORs of the most-populated (70%) conformer **M1**. The calculated rotation of the next conformer **P1** (27–30%) is ca. 50 times higher. This imbalance makes the assignment of AC of **1d** and **3d** inconclusive, based on OR values. In these two cases, the AC assignment based on the CD spectra is conclusive, since the calculated rotational strengths *R* of the two conformers, shown in Table 2, are of comparable magnitude. In addition, the assignment of AC of **1d** is in agreement with the assumed structure, based on the X-ray diffraction data (see Experimental section).

A summary of AC determinations of the *cis*-dihydrodiols discussed herein is presented in Table 4.

Note that the AC determination presented in this study is the only one carried out for *cis*-dihydrodiols **2a** and **2c**. Using the chiroptical data for dihydrodiols listed in Table 4 and elsewhere,<sup>38</sup> we can additionally predict the ACs of other halogenated *cis*-dihydrodiols **2e–2g**, **3e**, **3f**, and **5a–5f**. As in our previous publication,<sup>27</sup> we used the analogy between the properties of Cl, Br, and I, as well as between Me and Et substituted *cis*-dihydrodiols. In one case we also assumed that substitution of a C(4) hydrogen atom (in **4a**) by the methyl group would not alter significantly the conformational and chiroptical properties of the homologue **5d**, since the properties of the dihydrodiol molecule are dominated by the bromine substituent at C(3) (Table 5).

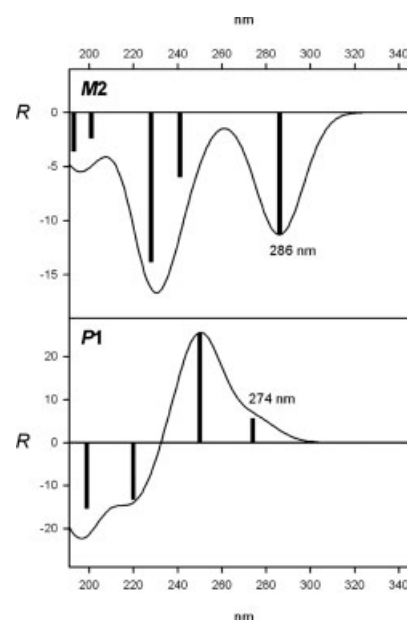


**Fig. 2.** Calculated CD spectra of **M2** and **P1** conformers of **2c**. Bars indicate the rotational strengths of conformer individual electronic transitions.

**TABLE 4.** Summary of absolute configuration determinations of *cis*-dihydrodiols **1a–1d**, **2a–2d**, **3a**, **3b**, **3d** by different methods (yes, conclusive result; no, inconclusive result)

Dihydrodiol	CD (exptl. vs. calcd.)	$[\alpha]_D$ (exptl. vs. calcd.)	NMR of derivatives <sup>a</sup>	X-ray <sup>a</sup>
<b>1a</b>	Yes	Yes	Yes	Yes
<b>1b</b>	Yes	Yes	Yes	
<b>1c</b>	Yes	Yes	Yes	
<b>1d</b>	Yes	No		Yes
<b>2a</b>	Yes	Yes		
<b>2b</b>	Yes	Yes	Yes	
<b>2c</b>	No	Yes		
<b>2d</b>	Yes	Yes	Yes	
<b>3a</b>	Yes	Yes		
<b>3b</b>	Yes	Yes		
<b>3d</b>	Yes	No		

<sup>a</sup>See Experimental section.

In this way we are able to use the CD and OR methods to assign ACs to *cis*-dihydrodiols **2a**, **2c**, and **2e**, to confirm the previous tentative assignments made by <sup>1</sup>H NMR spectroscopy (**1a–1d**, **2b**, **2d**, **2f**, **2g**, **5a–5f**), and to concur with unequivocal assignments made by X-ray crystallography (**1a**, **1d**, and **5e**) and stereochemical correlation (**3a**, **3b**, **3d–3f**).

Based on the confirmed ACs now available from this study, it is possible to extend the general applicability of an active site model which had been used earlier for predicting the preferred AC of *cis*-dihydrodiol products from TDO-catalyzed asymmetric dihydroxylation of mono- and 1,4-disubstituted benzene substrates (Scheme 3).<sup>28,30,32,33</sup> Thus, when substituent X is much larger than substituents Y<sub>3</sub> (Y<sub>1</sub> = Y<sub>2</sub> = H), Y<sub>1</sub> (Y<sub>2</sub> = Y<sub>3</sub> = H), and Y<sub>2</sub> (Y<sub>1</sub> = Y<sub>3</sub> = H) then the preferred major regioisomer and enantiomer will be that shown in Scheme 3.

**TABLE 5.** CD and OR data and absolute configurations for related halogenated dihydrodiols

Dihydrodiol	$\Delta\epsilon^a$	$[\alpha]_D^b$	Reference dihydrodiol
<b>2e</b>	+2.4 (271) <sup>c</sup>	+61	<b>2a</b>
<b>2f</b>	+1.3 (272)	+74	<b>2a</b>
<b>2g</b>	+1.2 (271)	+99 <sup>d</sup>	<b>2d</b>
<b>3e</b>	−0.8 (260)	+20	<b>3a</b>
<b>3f</b>	−0.4 (305)	+43	<b>3a</b>
<b>5a</b>	+2.6 (292)	−13	<b>1a</b> , <b>1b</b>
<b>5b</b>	+2.3 (277)	+20	<b>1a</b>
<b>5c</b>	+5.4 (284)	+38	<b>5d</b>
<b>5d</b>	+1.6 (281)	+25	<b>4a</b>
<b>5e</b>	+2.5 (285)	+48 <sup>e</sup>	<b>5d</b>
<b>5f</b>	−0.9 (258)	−6 <sup>d</sup>	<b>1d</b>

<sup>a</sup>In acetonitrile, ee > 98%.

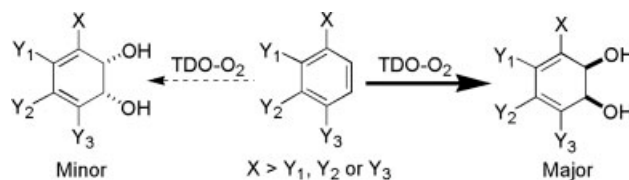
<sup>b</sup>In methanol, ee > 98%.

<sup>c</sup>Values within parentheses are wavelength (λ) in nanometers.

<sup>d</sup>Data from Ref. 33.

<sup>e</sup>In chloroform, ee > 98%.

Chirality DOI 10.1002/chir



**Scheme 3.** Predictive model for the preferred AC of *cis*-dihydrodiols resulting from TDO-catalyzed dihydroxylation of mono-, 1,2-, 1,3-, and 1,4-disubstituted benzenes.

## CONCLUSIONS

This study shows that the use of the method based on comparison of experimental and calculated CD and/or OR data allows the determination of ACs of flexible organic molecules, even those with many contributing conformers, as is the case of *cis*-dihydrodiol metabolites. In most cases, both CD and OR data lead to a conclusive assignment. Analysis of the calculated CD and OR data allows the property (either CD or OR) with which the assignment of AC would be inconclusive, to be discounted. As a result, the present study led to the first AC assignments of several *cis*-dihydrodiols and matched the previous configurational assignments made by either <sup>1</sup>H NMR spectroscopy (diastereoisomer derivatives) or X-ray diffraction.

The study revealed a significant effect of the substituents attached to the cyclohexadiene chromophore on conformational equilibria of *cis*-dihydrodiols. Despite its small size, which can account for the presence of the other enantiomeric forms of diols **4b**, **1b**, and **2b**, a fluorine substituent at C(4) or C(5) also changes the stability of *M* and *P* conformers by modulation of intramolecular O—H... $\pi$  hydrogen bonds.

The sign of calculated rotational strength of a dihydrodiol long-wavelength transition is distinctly dependent on the diene substitution pattern (Table 6).

Thus, 3-bromo-substituted dihydrodiols show rotational strengths of the same sign, regardless of the diene conformation and the presence of an additional fluorine substituent. For 3-methyl- and 3-trifluoromethyl-substituted *cis*-dihydrodiols, the rotational strength is of opposite sign for *M* and *P* conformers, again regardless of the presence of an additional fluorine substituent. Finally, in the case of 3-fluoro-substituted *cis*-dihydrodiols, the sign of rotational

**TABLE 6.** Sign of rotational strength (*R*) of the long-wavelength  $\pi$ – $\pi^*$  transition for *M1*(*M2*)/*P1* conformers of *cis*-dihydrodiols with different substitution pattern

Substituent	3-Br	3-F	3-CF <sub>3</sub>	3-CH <sub>3</sub>
	<i>M1/P1</i>	<i>M1/P1</i>	<i>M2/P1</i>	<i>M1/P1</i>
None <sup>a</sup>	+/+	+/-	-/+	-/+
4-F	+/+	-/+	-/+	-/+
5-F	+/+	-/+	-/+	-/+
6-F <sup>b</sup>	+/+	<sup>c</sup>	-/+	-/+

<sup>a</sup>Data from Ref. 26.

<sup>b</sup>Data from Refs. 27, 28, and 30.

<sup>c</sup>Achiral structure.

strength changes from positive to negative depending on the diene conformation and the presence of an additional fluorine substituent. By contrast, the calculated rotational strength of **P1** conformers of 4-substituted benzene *cis*-dihydrodiols **3a–3d** is uniformly positive, and for diastereoisomeric **M1** conformers, it is negative.

These observations are expected to be useful in further applications of CD spectra for AC determinations of many other *cis*-dihydrodiol metabolites. Furthermore, the ACs obtained for these *cis*-dihydrodiols have allowed the validity of a simple predictive model for TDO-catalyzed arene dihydroxylations to be extended.

### ACKNOWLEDGMENTS

The authors thank Dr. J.F. Malone for the X-ray crystallographic analysis and Drs. N.A. Kerley, M.R. Grocock, N.I. Bowers, and P. Gray for assistance with the biotransformations and bioproduct analyses. All calculations were performed at Poznan Supercomputing Center, Poland.

### LITERATURE CITED

1. Nakanishi K, Berova N, Woody RW. Circular dichroism—principles and applications. New York: VCD Publishers; 1994.
2. Dale JA, Mosher HS. Nuclear magnetic resonance enantiomer reagents. Configurational correlations via nuclear magnetic resonance chemical shifts of diastereomeric mandelate, *O*-methylmandelate, and  $\alpha$ -methoxy- $\alpha$ -trifluoromethylphenylacetate (MTPA) esters. *J Am Chem Soc* 1973;95:512–519.
3. Eliel EL, Wilen SH, Mander LN. Stereochemistry of organic compounds. New York: Wiley; 1994.
4. Bauernschmitt R, Ahlrichs R. Treatment of electronic excitations within the adiabatic approximation of time dependent density functional theory. *Chem Phys Lett* 1996;256:454–464.
5. Furche F, Ahlrichs R, Wachsmann C, Weber E, Sobanski A, Vögtle F, Grimme S. Circular dichroism of helicenes investigated by time-dependent density functional theory. *J Am Chem Soc* 2000;122:1717–1724.
6. Autschbach J, Ziegler T, Gisbergen van SJA, Baerends EJ. Chiroptical properties from time-dependent density functional theory. Circular dichroism spectra of organic molecules. *J Chem Phys* 2002;116:6930–6940.
7. Crawford TD. Ab initio calculation of molecular chiroptical properties. *Theor Chem Acc* 2006;115:227–245.
8. Diedrich C, Grimme S. Systematic investigation of modern quantum chemical methods to predict electronic circular dichroism spectra. *J Phys Chem A* 2003;107:2524–2539.
9. Polavarapu PL. Molecular optical rotations and structures. *Tetrahedron: Asymmetry* 1997;8:3397–3401.
10. Kondru RK, Wipf P, Beratan DN. Theory-assisted determination of absolute stereochemistry for complex natural products via computation of molar rotation angles. *J Am Chem Soc* 1998;120:2204–2205.
11. Goldsmith MR, Jayasuriya N, Beratan DN, Wipf P. Optical rotation of noncovalent aggregates. *J Am Chem Soc* 2003;125:15696–15697.
12. McCann DM, Stephens PJ, Cheeseman JR. Determination of absolute configuration using density functional theory calculation of optical rotation: Chiral alkanes. *J Org Chem* 2004;69:8709–8717.
13. Polavarapu PL. Protocols for the analysis of theoretical optical rotations. *Chirality* 2006;18:348–356.
14. Stephens PJ, McCann DM, Cheeseman JR, Frisch MJ. Determination of absolute configurations of chiral molecules using ab initio time-dependent density functional theory of optical rotation: How reliable are absolute configurations obtained for molecules with small rotations. *Chirality* 2005;17:S52–S64.
15. Specht KM, Nam J, Ho DM, Berova N, Kondru RK, Beratan DN, Wipf P, Pascal RA Jr, Kahne D. Determining absolute configuration in flexible molecules: A case study. *J Am Chem Soc* 2001;123:8961–8966.
16. Marchesan D, Coriani S, Forzato C, Nitti P, Pitacco G, Ruud K. Optical rotation calculation of a highly flexible molecule: The case of paracetic acid. *J Phys Chem A* 2005;109:1449–1453.
17. Wiberg KB, Vaccaro PH, Cheeseman JR. Conformational effects on optical rotation. 3-Substituted 1-butenes. *J Am Chem Soc* 2003;125:1888–1896.
18. Pecul M, Ruud K, Rizzo A, Helgaker T. Conformational effects on the optical rotation of alanine and proline. *J Phys Chem A* 2004;108:4269–4276.
19. Pecul M. Conformational structures and optical rotation of serine and cysteine. *Chem Phys Lett* 2006;418:1–10.
20. Kundrat MD, Autschbach J. Time dependent density functional theory modeling of chiroptical properties of small amino acids in solution. *J Phys Chem A* 2006;110:4115–4123.
21. Kundrat MD, Autschbach J. Time dependent density functional theory modeling of specific rotation and optical rotatory dispersion of the aromatic amino acids in solution. *J Phys Chem A* 2006;110:12908–12917.
22. Stephens PJ, McCann DM, Butkus E, Stončius S, Cheeseman JR, Frisch MJ. Determination of absolute configuration using concerted ab initio dft calculations of electronic circular dichroism and optical rotation: Bicyclo[3.3.1]nonane diones. *J Org Chem* 2004;69:1948–1958.
23. Stephens PJ, McCann DM, Devlin FJ, Cheeseman JR, Frisch MJ. Determination of the absolute configuration of [3<sub>2</sub>](1,4)barrelenophanedicarbonitrile using concerted time-dependent density functional theory calculations of optical rotation and electronic circular dichroism. *J Am Chem Soc* 2004;126:7514–7521.
24. Stephens PJ, McCann DM, Devlin FJ, Smith AB III. Determination of the absolute configurations of natural products via density functional theory calculations of optical rotation, electronic circular dichroism, and vibrational circular dichroism: The cytotoxic sesquiterpene natural products quadron, suberosenone, suberosanone, and suberosenol A acetate. *J Nat Prod* 2006;69:1055–1064.
25. McCann DM, Stephens PJ. Determination of absolute configuration using density functional theory calculations of optical rotation and electronic circular dichroism: chiral alkenes. *J Org Chem* 2006;71:6074–6098.
26. Gawronski J, Kwit M, Boyd DR, Sharma ND, Malone JF, Drake AF. Absolute configuration, conformation, and circular dichroism of monocyclic arene dihydrodiol metabolites: it is all due to the heteroatom substituents. *J Am Chem Soc* 2005;127:4308–4319.
27. Kwit M, Sharma ND, Boyd DR, Gawronski J. Absolute configuration of conformationally flexible *cis*-dihydrodiol metabolites by the method of confrontation of experimental and calculated electronic CD spectra and optical rotations. *Chem Eur J* 2007;13:5812–5821.
28. Boyd DR, Sharma ND, Coen GN, Gray P, Malone JF, Gawronski J. Enzyme-catalysed synthesis and absolute configuration assignments of *cis*-dihydrodiol metabolites from 1,4-disubstituted benzenes. *Chem Eur J* 2007;13:5804–5811.
29. Hand MV, Malone JF, Sheldrake GN, Blacker J, Dalton H. Enzymatic and chemoenzymatic synthesis and stereochemical assignment of *cis*-dihydrodiol derivatives of monosubstituted benzenes. *J Chem Soc Perkin Trans* 1998;1:1935–1943.
30. Boyd DR, Sharma ND, Hand MV, Grocock MR, Kerley NA, Dalton H, Chima J, Sheldrake GN. Stereodirecting substituent effects during enzyme-catalysed synthesis of *cis*-dihydrodiol metabolites of 1,4-disubstituted benzene substrates. *J Chem Soc Chem Commun* 1993;974–976.
31. Boyd DR, Sharma ND, Barr SA, Dalton H, Chima J, Whited GM, Seemayer R. Chemoenzymatic synthesis of enantiomeric pairs of the 2,3- and 3,4-*cis*-dihydrodiols of monosubstituted benzenes. *J Am Chem Soc* 1994;116:1147–1148.
32. Boyd DR, Sheldrake GN. The dioxygenase-catalysed formation of *vicinal cis*-diols. *Nat Product Rep* 1998;15:309–324.
33. Boyd DR, Sharma ND, Bowers NI, Dalton H, Garrett MD, Harrison JS, Sheldrake GN. Dioxygenase-catalysed oxidation of disubstituted

- benzene substrates: Benzylic monohydroxylation *versus* aryl *cis*-dihydroxylation and the *meta* effect. *Org Biomol Chem* 2006;4:3343–3349.
34. Frisch MJ, Trucks GW, Schlegel HB, Scuseria GE, Robb MA, Cheeseman JR, Zakrzewski VG, Montgomery JA Jr, Stratmann RE, Burant JC, Dapprich S, Millam JM, Daniels AD, Kudin KN, Strain MC, Farkas O, Tomasi J, Barone V, Cossi M, Cammi R, Mennucci B, Pomelli C, Adamo C, Clifford S, Ochterski J, Petersson GA, Ayala PY, Cui Q, Morokuma K, Salvador P, Dannenberg JJ, Malick DK, Rabuck AD, Raghavachari K, Foresman JB, Cioslowski J, Ortiz JV, Baboul AG, Stefanov BB, Liu G, Liashenko A, Piskorz P, Komaromi I, Gomperts R, Martin RL, Fox DJ, Keith T, Al-Laham MA, Peng CY, Nanayakkara A, Challacombe M, Gill PMW, Johnson B, Chen W, Wong MW, Andres JL, Gonzalez C, Head-Gordon M, Replogle ES, Pople JA. Gaussian 03. Pittsburgh PA: Gaussian, Inc.; 2001.
35. Adamo C, Matteo di A, Barone V. From classical density functionals to adiabatic connection methods. The state of the art. In: Löwdin PO, editor. *Advances in quantum chemistry*, Vol. 36. New York: Academic Press; 1999. p 45–75.
36. Adamo C, Barone V. Exchange functionals with improved long-range behavior and adiabatic connection methods without adjustable parameters: The *m*PW and *m*PW1PW models. *J Chem Phys* 1998;108:664–675.
37. Boyd DR, Sharma ND, Llamas NM, O'Dowd CR, Allen CCR. *syn*-Benzene dioxides: Chemoenzymatic synthesis from *cis*-2,3-dihydrodiol derivatives of monosubstituted benzenes and their application in the synthesis of regioisomeric 1,2- and 3,4-*cis*-dihydrodiols and 1,4-dioxocins. *Org Biomol Chem* 2007;5:2267–2273.
38. Lightner DA, Bouman TD, Gawronski JK, Gawronska K, Chappuis JL, Crist BV, Hansen AE. Dissymmetric chromophores. On the optical activity of conjugated cisoid dienes: an experimental-theoretical study of 5-alkyl-1,3-cyclohexadienes. *J Am Chem Soc* 1981;103:5314–5327.



# Structure–Chiroptical Properties Relationship in Clavams: An Experimental and Theoretical Study

MAREK CHMIELEWSKI,<sup>1</sup> MACIEJ CIERPUCHA,<sup>1</sup> PATRYCJA KOWALSKA,<sup>1</sup> MARCIN KWIT,<sup>2</sup> AND JADWIGA FRELEK<sup>1\*</sup>

<sup>1</sup>*Institute of Organic Chemistry of the Polish Academy of Sciences, Warsaw, Poland*

<sup>2</sup>*Faculty of Chemistry, Adam Mickiewicz University, Poznan, Poland*

**ABSTRACT** It is well known that the biological activity of clavams depends strongly on the absolute configuration at the ring junction carbon atom. Therefore, development of the efficient stereo-controlled synthetic methods for the new oxygen analogs of penams, and the structure–activity relationship studies call for a reliable determination of the absolute stereochemistry of newly synthesized compounds. Recently, we proposed an empirical helicity rule relating the configuration of the bridgehead carbon atom to the sign of the 240 nm band observed in the electronic circular dichroism (ECD) spectrum of clavams. In the present work, we investigate the validity of this structure–property relationship for several enantiomeric pairs of model compounds possessing an additional, interfering chromophore in the molecule. For this purpose a combination of the ECD spectroscopy and the time-dependent density functional theory (TD-DFT) is used. A comparison of the ECD spectra with the theoretical ones obtained by the TD-DFT calculations gives a reasonable interpretation of the Cotton effects observed in the 250–220 nm spectral range. Moreover, the calculations confirm validity of the helicity rule for systems studied here and demonstrate that ECD spectroscopy may be used as a highly sensitive probe of the three-dimensional molecular structure of clavams. *Chirality* 20:621–627, 2008. © 2007 Wiley-Liss, Inc.

**KEY WORDS:** Clavams; ECD; TD-DFT; absolute configuration; Cotton effect

## INTRODUCTION

The family of  $\beta$ -lactams constitutes one of the largest, most versatile and commercially valuable classes of antibiotics. Amongst them the clavams, which are the oxygen analogues of penicillins, constitute an important group because they display interesting therapeutic properties in both (5*R*) and (5*S*) configurational forms. It is well known that clavams with the (5*S*)-configuration at the ring junction are antifungal agents but alanylclavam, valclavam, and hydroxyethylclavam with the same (5*S*)-configuration are both bacteriostatic and fungistatic.<sup>1</sup> On the other hand, clavams with the (5*R*)-configuration exhibit the  $\beta$ -lactamase inhibition and a weak antibacterial activity.<sup>1–3</sup> The most important representative of clavams with the  $\beta$ -lactamase inhibitory activity is clavulanic acid, belonging to the (5*R*)-clavams family.  $\beta$ -Lactamases, which catalyse hydrolysis of the  $\beta$ -lactam ring, are responsible for the antibiotic resistance and some  $\beta$ -lactams, including clavulanic acid, were explicitly developed as  $\beta$ -lactamase antagonists. The very strong  $\beta$ -lactamase inhibitory activity of clavulanic acid is related to its unique (2*R*,5*R*) stereochemistry. The clavaminic acid, a biosynthetic precursor of clavulanic acid with the opposite stereochemistry, i.e., (2*S*,5*S*), exhibits a poor inhibitory activity.<sup>4</sup> This means that the (5*R*) stereochemistry is required for this kind of activity. The  $\beta$ -lactamase mediated resistance, however, still constitutes one of

the more prevalent problems. The clinical significance of this fact originally prompted, and still continues to stimulate considerable efforts toward the discovery of alternative structures with a similar or improved  $\beta$ -lactamase inhibitory as well as other pharmacological and toxicological properties. In this context, an access to the practical method that allows for the unequivocal and reliable determination of the absolute stereochemistry of such bioactive compounds is vital for further enhancement of their bioactivity by the rational synthetic modifications.

The electronic circular dichroism spectroscopy is a convenient and sensitive technique to probe the stereochemistry of azetidinones and their polycyclic derivatives.<sup>5–7</sup> Recently, we reported a correlation between the stereostructure of 5-dethia-5-oxacephams and their respective circular dichroism.<sup>8</sup> As a result, a simple helicity rule was proposed, which permits the assignment of absolute con-

Contract grant sponsor: Poznań Supercomputing Centre (PCSS), Poland.  
Contract grant sponsor: Polish State Committee for Scientific Research (KBN); Contract grant number: PBZ-KBN-126/T09/2004.

\*Correspondence to: Jadwiga Frelek, Institute of Organic Chemistry of the Polish Academy of Sciences, Kasprzaka 44, 01-224 Warsaw, Poland.

E-mail: frelek@icho.edu.pl

Received for publication 1 June 2007; Accepted 27 August 2007

DOI: 10.1002/chir.20484

Published online 8 October 2007 in Wiley InterScience (www.interscience.wiley.com).

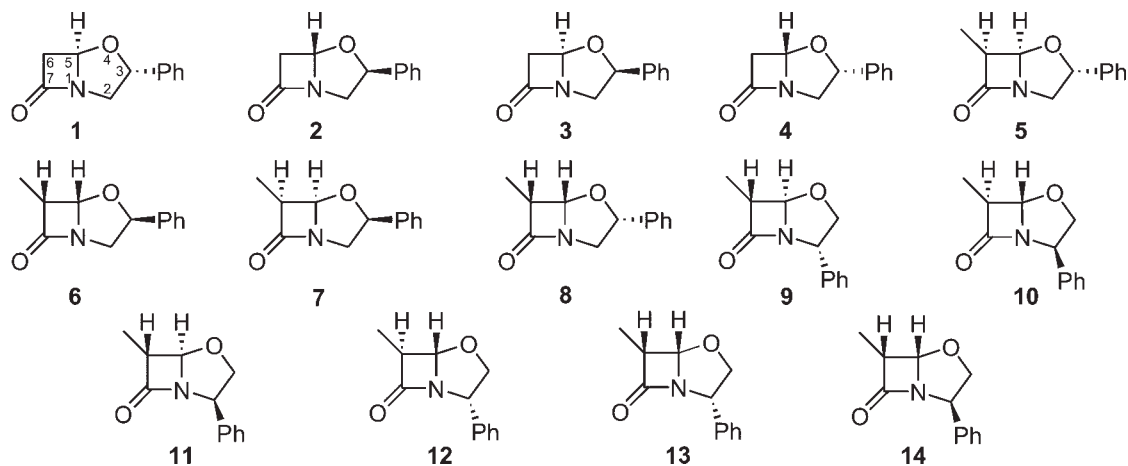


Chart 1. Investigated compounds.

figuration at the ring junction carbon atom based on the sign of the ECD band at around 220 nm. According to this rule, a positive sign of the 220-nm Cotton effect (CE) corresponds to the (*R*) absolute configuration at the bridge-head carbon atom whereas a negative sign of the same CE indicates the (*6S*) absolute configuration. The rule was demonstrated experimentally to be correct for a variety of oxacephams.<sup>8,9</sup> It was also found that the same rule is valid for clavams.<sup>10,11</sup> This helicity rule for both oxacephams and clavams was established empirically on the basis of X-ray structures and the tentative assignment of the electronic transition at ~220 (oxacephams) and 240 nm (clavams) to an  $n\pi^*$  amide transition in the azetidinone system.<sup>8,10</sup> The rule was established under the assumption of the conformational rigidity of the bicyclic system and a realization that most of the molecular excitations are localized within the amide chromophore. Since the CD spectroscopy is very sensitive to the details of geometric and electronic structure of investigated molecules, it is obvious that the successful application of the CD method calls for an accurate theoretical treatment. The comparison of the experimental and simulated CD spectra should allow an assignment of the absolute configuration with higher confidence. Very recently, such a combined treatment of the ECD spectroscopy and the time-dependent density functional theory was used to investigate the structure–chiroptical properties relationship of carba- and oxacephams.<sup>12</sup> The obtained results pointed to a surprisingly high sensitivity of the CD to the molecular conformation. Nevertheless, the helicity rule may provide a good first guess of the absolute configuration of cepham analogues. For a more definite assignment of the absolute configuration, however, the good corroboration of the predictions made by the helicity rule by the computational results was strongly recommended.

In this work we intend to apply the same combined treatment of experimental and theoretical analysis of ECD to the clavams. Since clavams are composed of a five-membered ring fused to a four-membered  $\beta$ -lactam ring, the bicyclic system of clavams is expected to be conformationally more constrained than that of cephams. The X-ray

structure studies revealed that this assumption is indeed valid.<sup>4,10</sup> Thus, the presence of different conformers should not significantly affect the ECD as it was observed in the case of carba- and oxacephams. However, substitution of the fused ring with an additional, chromophoric substituent may substantially perturb the electronic structure of the system and therefore significantly influence the ECD spectra. We decided therefore to find a theoretical model that correlates the observed spectrum to the three-dimensional molecular structure to validate the helicity rule in context of the substituted clavams. As model compounds for this study, the group of several enantiomeric pairs of clavams shown in Chart 1 was chosen.

## MATERIALS AND METHODS

The synthesis, biological activity, and spectral characterization of compounds **1–8** was published before.<sup>11</sup>

Compounds **9–14** were obtained from the (*R*)- and (*S*)-phenyl-glycol by a known sequence of reactions,<sup>11</sup> involving the formation of terminal vinyl ether, [2 + 2]cycloaddition with chlorosulfonyl isocyanate, and the intramolecular alkylation of  $\beta$ -lactam nitrogen atom followed by the separation of diastereomers. The detailed procedures will be published elsewhere. Among the clavams **1–14** only two (compounds **9** and **10**) formed crystals suitable for the X-ray diffraction analysis.

### (2*S*,5*R*,6*S*)-6-Methyl-2-phenyl-4-oxa-1-azabicyclo[3.2.0]heptan-7-one (**9**)

$[\alpha]_D^{22} -20$  (c 0.3,  $\text{CH}_2\text{Cl}_2$ );  $^1\text{H}$  NMR (500 MHz;  $\text{CDCl}_3$ ) 1.45 (d,  $J = 7.7$  Hz, 3H), 3.18 (q,  $J = 7.7$  Hz, 1H), 4.02 (dd,  $J = 8.7$ , 5.9 Hz, 1H); 4.61 (dd,  $J = 8.7$ , 7.0 Hz, 1H), 5.09–5.13 (m, 2H), 7.28–7.34 (m, 3H), 7.36–7.41 (m, 2H); HRMS (LSIMS)  $m/z$  ( $M + \text{Na}$ )<sup>+</sup> calcd for  $\text{C}_{12}\text{H}_{13}\text{NO}_2\text{NaSi}$ : calcd 226.08385, found 226.08451.

### (2*R*,5*S*,6*S*)-6-Methyl-2-phenyl-4-oxa-1-azabicyclo[3.2.0]heptan-7-one (**10**)

m.p. 43–45°C (methanol);  $[\alpha]_D^{22} +22$  (c 0.2,  $\text{CH}_2\text{Cl}_2$ ); enantiomer of **9**.

**(2R,5R,6R)-6-Methyl-2-phenyl-4-oxa-1-azabicyclo[3.2.0]heptan-7-one (11)**

$[\alpha]_D^{22} + 79$  (c 0.2, CH<sub>2</sub>Cl<sub>2</sub>); <sup>1</sup>H NMR (500 MHz; CDCl<sub>3</sub>) 1.33 (d, *J* = 7.6 Hz, 3H), 3.17 (q, *J* = 7.6 Hz, 1H), 4.27 (dd, *J* = 8.4, 4.7 Hz, 1H), 4.39–4.46 (m, 2H), 4.96 (s, 1H), 7.30–7.39 (m, 5H); <sup>13</sup>C NMR (125 MHz; CDCl<sub>3</sub>) 11.47, 52.39, 64.02, 77.48, 91.35, 128.32, 128.59, 128.65, 134.97, 176.04; HRMS (LSIMS) *m/z* (M + Na)<sup>+</sup> calcd for C<sub>12</sub>H<sub>13</sub>NO<sub>2</sub>NaSi: calcd 226.08385, found 226.08351.

**(2S,5S,6S)-6-Methyl-2-phenyl-4-oxa-1-azabicyclo[3.2.0]heptan-7-one (12)**

$[\alpha]_D^{22} - 56$  (c 0.3, CH<sub>2</sub>Cl<sub>2</sub>); enantiomer of **11**.

**(2S,5S,6R)-6-Methyl-2-phenyl-4-oxa-1-azabicyclo[3.2.0]heptan-7-one (13)**

$[\alpha]_D^{22} - 177$  (c 1.5, CH<sub>2</sub>Cl<sub>2</sub>); <sup>1</sup>H NMR (500 MHz; CDCl<sub>3</sub>) 1.26 (d, *J* = 7.8 Hz, 3H), 3.34 (qd, *J* = 7.6, 3.2 Hz, 1H), 4.20 (dd5 *J* = 8.0, 5.5 Hz, 1H), 4.42–4.48 (m, 2H), 5.25 (d, *J* = 3.2 Hz, 1H), 7.32–7.39 (m, 5H); <sup>13</sup>C NMR (125 MHz; CDCl<sub>3</sub>) 7.70, 47.86, 63.77, 76.44, 87.82, 128.39, 128.47, 128.59, 134.06, 178.10; HRMS (LSIMS) *m/z* (M + Na)<sup>+</sup> calcd for C<sub>12</sub>H<sub>13</sub>NO<sub>2</sub>NaSi: calcd 226.08385, found 226.08376.

**(2R,5S,6R)-6-Methyl-2-phenyl-4-oxa-1-azabicyclo[3.2.0]heptan-7-one (14)**

$[\alpha]_D^{22} - 16$  (c 0.1, CH<sub>2</sub>Cl<sub>2</sub>); <sup>1</sup>H NMR (500 MHz; CDCl<sub>3</sub>) 1.20 (d, *J* = 7.6 Hz, 3H), 3.50 (qd, *J* = 7.6, 3.2 Hz, 1H), 4.02 (dd, *J* = 8.6, 5.6 Hz, 1H), 4.53 (dd, *J* = 8.6, 7.0 Hz, 1H), 5.04 (t, *J* = 6.3 Hz, 1H), 5.36 (d, *J* = 3.2 Hz, 1H), 7.26–7.31 (m, 3H), 7.33–7.37 (m, 2H); <sup>13</sup>C NMR (125 MHz; CDCl<sub>3</sub>) 7.72, 48.28, 60.80, 77.66, 87.93, 126.02, 127.75, 128.78, 138.92, 182.41; HRMS (LSIMS) *m/z* (M + Na)<sup>+</sup> calcd for C<sub>12</sub>H<sub>13</sub>NO<sub>2</sub>NaSi: calcd 226.08385, found 226.08355.

The UV spectra were measured using Cary 100 spectrophotometer in acetonitrile solutions. The CD spectra were recorded between 185 and 300 nm at room temperature with a JASCO J-715 spectropolarimeter in acetonitrile solutions. The solutions with concentrations in the range of  $0.8 \times 10^{-4}$  to  $1.2 \times 10^{-3}$  mol dm<sup>-3</sup> were examined in cells with the path length of 0.1 or 1 cm.

**X-ray Analysis of Compound 9**

The data collection for compound **9** was performed at room temperature on the MACH3 diffractometer, Cu Kα radiation, and ω-θ scanning mode were used. The structure was solved by the direct methods using SHELXS97 program<sup>13</sup> and refined against F<sup>2</sup> with the SHELXL97 program.<sup>14</sup> The hydrogen atoms were added geometrically and refined with the riding model<sup>†</sup>.

<sup>†</sup> The crystallographic data for structures **9** and **10** have been deposited with the Cambridge Crystallographic Data Centre as supplementary publications No CCDC 647860 and CCDC 648134 respectively. The data can be obtained free of charge at <http://www.ccdc.cam.ac.uk> or from the Cambridge Crystallographic Data Centre, 12 Union Road, Cambridge CB2 1EZ, UK.

**X-ray Analysis of Compound 10**

The data collection for compound **10** was carried out with the Bruker KappaCCD diffractometer using graphite-monochromated MoKα radiation ( $\lambda = 0.71073$  Å). The structure was solved by the direct methods<sup>13</sup> and refined by a full-matrix least-squares on *F*<sup>2</sup>.<sup>14</sup> All the hydrogen atoms were placed in the calculated positions and refined using the riding model. The structure contains two symmetrically independent molecules in the unit cell.

**Computational Method**

The theoretical calculations of CD spectra were done for the selected clavams, namely compounds **1–4**, and **10–11**. At first we determined the lowest-energy conformations for each investigated compound. These conformations were found by the MM3 force field and CONFLEX<sup>15</sup> software and were subsequently reoptimized at B3LYP/6-311++G(D,P) level.<sup>16</sup> All the DFT-optimized structures converged to only one stable conformer in each case. To confirm the stability of calculated structures, the frequency calculations were performed at B3LYP/6-311++G(D,P) level. For the stable structures, the rotational strengths were calculated at the B3LYP/6-311++G(2D,2P) level. The rotatory strengths were calculated using both the length and the velocity representations. The differences between the length and the velocity calculated values of the rotatory strengths were quite small and for this reason only the velocity rotatory strengths were taken into further consideration. The CD and UV spectra were simulated by overlapping Gaussian functions for each transition according to the procedure described by Diedrich and Grimme.<sup>17</sup> No correlation for the medium dielectric constant was implemented. The conformational analysis has been performed with the use of CaChe program package.<sup>15</sup>

**RESULTS AND DISCUSSION****Experimental UV and ECD Spectra of Clavams 1–14**

The electronic absorption and chiroptical data for compounds **1–14** is presented in Table 1. The considerably lower intensity of the ECD bands observed for clavams **9–14** (except clavam **13**) in comparison with clavams substituted at the C(3) position (**1–8**) is due to the lower optical purity caused by problems with the separation of diastereomers.

As evident from the Table 1, three bands are present in the ECD spectra of investigated compounds in the spectral range 200–250 nm. For the purpose of our studies only the lowest energy band occurring at around 240 nm is of a particular interest because this band is the subject of the helicity rule. This band can be attributed to the amide *n*(O)→*π*<sup>\*</sup> transition and its corresponding electronic absorption is hidden by the neighboring absorption bands (see Table 1). Most probably, however, the CD band represents a sum of contributions from the amide and benzene (<sup>1</sup>L<sub>b</sub>) chromophores present in these molecules. In the respective UV spectra, the electronic absorption of

TABLE 1. UV and ECD data of clavams 1–14 measured in acetonitrile in the range of 200–300 nm

Comp.	UV $\epsilon$ ( $\lambda_{\text{max}}$ ); [mol <sup>-1</sup> dm <sup>3</sup> cm <sup>-1</sup> (nm)]			CD $\Delta\epsilon$ ( $\lambda_{\text{max}}$ ); [mol <sup>-1</sup> dm <sup>3</sup> cm <sup>-1</sup> (nm)]		
1	14600 (208 <sup>sh</sup> )	12800 (214 <sup>sh</sup> )	370 (256)	-10.3 (212.5)	+17.8 (226.0 <sup>sh</sup> )	+23.7 (236.5)
2	11600 (208 <sup>sh</sup> )	11000 (215 <sup>sh</sup> )	350 (256)	+8.7 (213.0)	-14.5 (225.0 <sup>sh</sup> )	-21.4 (236.5)
3	9750 (208 <sup>sh</sup> )	8300 (215 <sup>sh</sup> )	240 (257)	-8.5 (200.5)	+16.2 (220.5)	+15.8 (233.0)
4	7600 (209 <sup>sh</sup> )	6800 (215 <sup>sh</sup> )	220 (257)	+7.6 (200.5)	-14.8 (220.0)	-13.8 (233.0)
5	11100 (209 <sup>sh</sup> )	10000 (215 <sup>sh</sup> )	340 (257)	-9.6 (214.0)	+11.6 (227.0 <sup>sh</sup> )	+18.7 (240.2)
6	11800 (208 <sup>sh</sup> )	10900 (215 <sup>sh</sup> )	410 (257)	+10.6 (213.0)	-11.0 (226.0 <sup>sh</sup> )	-19.8 (240.2)
7	8700 (209 <sup>sh</sup> )	7800 (214 <sup>sh</sup> )	230 (257)	-6.8 (201.5)	+13.2 (220.0)	+14.2 (236.0)
8	9300 (208 <sup>sh</sup> )	8070 (214 <sup>sh</sup> )	260 (257)	+6.8 (201.0)	-13.7 (219.0)	-14.6 (236.0)
9	13000 (208 <sup>sh</sup> )	6000 (215 <sup>sh</sup> )	360 (256)	-4.2 (201.0)	+1.7 (218.0)	+5.0 (239.5)
10	13750 (206 <sup>sh</sup> )	6250 (215 <sup>sh</sup> )	375 (257)	+4.4 (201.0)	-2.4 (218.5)	-7.0 (240.0)
11	11000 (205 <sup>sh</sup> )	7000 (215 <sup>sh</sup> )	500 (257)	-2.9 (203.5)	-3.0 (216.5)	+3.2 (240.0)
12	10750 (205 <sup>sh</sup> )	6750 (215 <sup>sh</sup> )	375 (257)	+1.2 (216.0)	+1.2 (216.0)	-1.1 (240.5)
13	11150 (205 <sup>sh</sup> )	7800 (215 <sup>sh</sup> )	400 (257)	+9.2 (204.0)	+9.2 (216.0)	-15.1 (241.0)
14	15000 (206 <sup>sh</sup> )	7250 (215 <sup>sh</sup> )	500 (257)	+6.9 (200.0)	-3.8 (217.5)	-9.2 (238.0)

phenyl group is clearly visible at *ca.* 257 nm and possesses characteristic fine structure (Table 1).

Regarding the long-wavelength CD band occurring at  $\sim 240$  nm, the investigated compounds fall under two different classes. In the first class, consisting of compounds **1**, **3**, **5**, **7**, **9**, and **11**, the sign of the 240 nm CD band is positive, whereas in the second class, represented by compounds **2**, **4**, **6**, **8**, **10**, **12–14**, the sign of this band is negative. According to the helicity rule, compounds from the first group, which show a positive 240 nm CE, should have the (*R*)-configuration at the ring junction, whereas the negative sign of this CE for the second group would indicate the (*S*)-configuration at C(5).<sup>7</sup> This prediction has been confirmed by the X-ray structure analysis for clavams **9** and **10** (Fig. 1). In addition, the X-ray data for clavams **9** and **10** demonstrate the pyramidal nature of the  $\beta$ -lactam nitrogen atom as evidenced by the distance 51.0 pm of the nitrogen atom from the least-squares plane containing C(2), C(5), and C(7) atoms (Table 2). The signs of the O=C–N–C $_{\alpha}$  torsional angles for **9** and **10** are negative and positive, respectively, and, accordingly, the signs of the long-wavelength CE at about 240 nm are positive and negative, respectively (Table 1). Thus, it can be concluded that for clavams **9** and **10** the helicity rule works well and correlates the negative/positive sign of the O=C–N–C $_{\alpha}$  torsional angles with a positive/negative sign of the long-wavelength CD band at around 240 nm.

To prove whether the helicity rule correctly predicts the absolute configuration at C(5) for clavams, which do not

form crystals suitable for the X-ray analysis, the TDDFT calculations were performed for the selected clavams. First, we sought the validation of our calculation methodology by the direct comparison of the geometry-related data obtained from the X-ray studies and from the molecular modeling of clavam **10**. The results demonstrate a good conformity between the calculated and the solid-state values (Table 2). The calculated data show a nonplanarity of chromophores in all clavams. Consequently, they allow to apply the helicity rule to correlate the structure and respective chiroptical properties. Thus, it can be stated that among clavams **1–14** the ones with a negative long-wavelength CE possess the (*5S*)-configuration whereas clavams exhibiting a positive sign of this CE have the (*5R*) configuration. The data from Tables 1 and 2 demonstrates that clavams **1–14** conform to the above prediction and follow the helicity rule.<sup>7</sup>

Concerning the second band occurring between 220 and 227 nm for the 3-phenyl substituted clavams **1–8**, originating most likely from the <sup>1</sup>L<sub>a</sub> phenyl transition, the shape of this band varies depending on the relative configuration at carbons C(3) and C(5). So, for the clavams **1**, **2**, **5**, and **6** with syn-oriented both the hydrogen atom at C(5) and the phenyl group at C(3), this band is not developed to a distinct maximum and is visible only as a positive or negative inflection point on the short-wavelength part of the 240 nm CD band. The sign of the inflection point is the same as the sign for the main 240 nm band. On the contrary, in isomeric clavams **3**, **4**, **7**, and **8** with

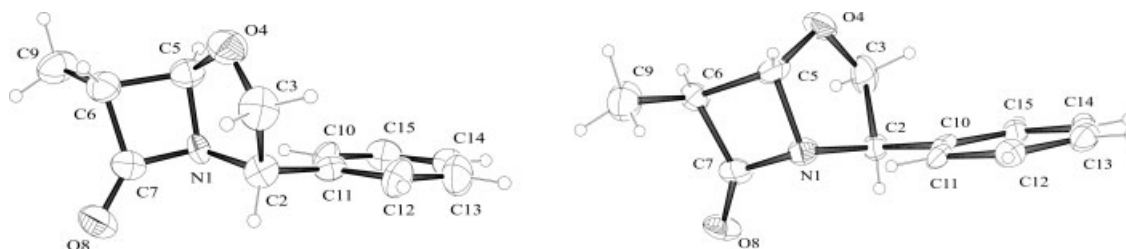


Fig. 1. ORTEP diagrams of compounds **9** (left) and **10** (right). Thermal ellipsoids are shown at 50% probability level.



**TABLE 2.** Selected torsional angles in deg (°) and pyramid height for the N-atom in pm determined by the X-ray diffraction and calculated by DFT/B3LYP/6-311++G(D,P) methods

Comp.	Conf. at C(5)	240 nm obser.	CE sign pred.		6-7-1-5	8-7-1-2	8-7-1-5	6-7-1-2	Pyr. height
<b>1</b>	( <i>R</i> )	(+)	(+)	calc.	+8.2	−54.3	−168.5	+122.4	−50.2
<b>2</b>	( <i>S</i> )	(−)	(−)	calc.	−8.2	+54.4	+168.6	−122.4	+50.1
<b>3</b>	( <i>R</i> )	(+)	(+)	calc.	+10.2	−50.9	−166.6	+125.8	−48.6
<b>4</b>	( <i>S</i> )	(−)	(−)	calc.	−10.2	+50.9	+166.5	−125.8	+48.7
<b>9</b>	( <i>R</i> )	(+)	(+)	X-ray	+9.5	−56.4	−170.4	+123.6	−51.0
<b>10</b>	( <i>S</i> )	(−)	(−)	X-ray	−8.9	+57.0	+169.9	−121.8	+51.0
				calc.	−6.7	+54.4	+170.6	−123.0	+48.6
<b>11</b>	( <i>R</i> )	(+)	(+)	calc.	+7.9	−55.3	−171.1	+123.6	−45.3

the anti-directed substituents, this band is well developed and is clearly visible as a maximum or minimum (Fig. 2).

The shape of the ECD spectra of the 2-phenyl substituted clavams **9–14** also varies depending upon the relative configuration at carbons C(2) and C(5). If the proton at the C(5) and the phenyl at C(2) are syn-directed, such as it is in compounds **9**, **10**, and **14**, the 220-nm CD band is well-developed and possesses the same sign as the 240 nm band. In the case of the anti-relationship of the proton and phenyl at C(5) and C(2) carbon atoms, respectively (clavams **11–13**), the 220 and the 240 nm CD bands differ in sign. An additional inflection point occurring in these compounds approximately at 230 nm possesses the same sign as the 240 nm band. Accordingly, based on that observation we may infer a further conclusion regarding the relative configuration of phenyl substituent in the five-membered ring.

#### Calculated ECD Spectra of Clavams 1–4 and 10–11

To corroborate the conclusions made on the basis of the experimental data, the ECD spectra of the selected clavams were calculated. A fundamental prerequisite for the computational calculation of CD spectra is the knowledge of all CD-relevant conformational species of the respective molecule. In our case, the conformational analysis of clavams **1–4** and **10–11** revealed only one stable conformer in each case (see Computational Method in Materials and Methods). In the light of this result it can be asserted that the investigated clavams are conformation-

ally rigid since in the range of 10 kcal mol<sup>−1</sup> no other stable conformer is found.

The calculated and experimental ECD spectra of compounds **1–4** and **10–11** are shown in Figure 3. For clarity, the clavams are divided into three groups, namely compounds **1** and **4**, **2** and **3**, and **10** and **11**. The members of each group differ in the absolute configuration at the ring junction carbon atom, while the absolute configuration at the carbon atom bearing the phenyl substituent is the same. In general, the TD DFT singlet state calculations excellently reproduce the experimental data in the region between 260 and 215 nm, although the excitation energies are typically underestimated by about 5 nm. The higher energy regions are well reproduced in the cases of clavams **1**, **2**, and **10**, whereas for their respective isomers **4**, **3**, and **11** the calculated higher-energy rotational strengths are of opposite signs. Since our attention is limited to the analysis of the long-wavelength Cotton effects, the short-wavelength spectral region lies outside of the scope of present work.

The analysis of spectra shows that the long-wavelength Cotton effects in each pair are of opposite signs. So, in the case of clavams **1** and **4** the sign is positive for **1** and negative for **4**. The opposite pattern of signs appears in the second and third pairs where a negative sign of the same Cotton effect is observed for clavams **2** and **10**, whilst a positive one for clavams **3** and **11**. In the cases of compounds **3**, **4**, and **10**, the 220-nm Cotton effect exhibits the same sign as the lowest-energy Cotton effect at 240 nm. The best fit for the 215–260 nm spectral range is

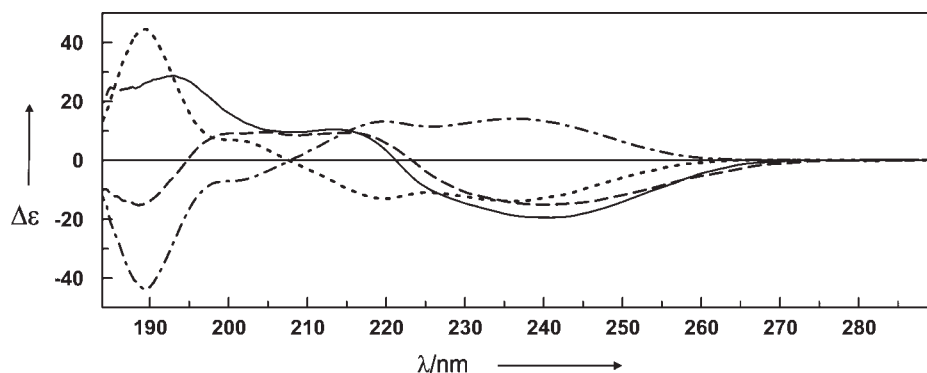


**Fig. 2.** CD spectra of clavams **6** (—), **7** (— · — · —), **8** (· · · · ·), and **13** (— — —) recorded in acetonitrile. [Color figure can be viewed in the online issue, which is available at [www.interscience.wiley.com](http://www.interscience.wiley.com).]

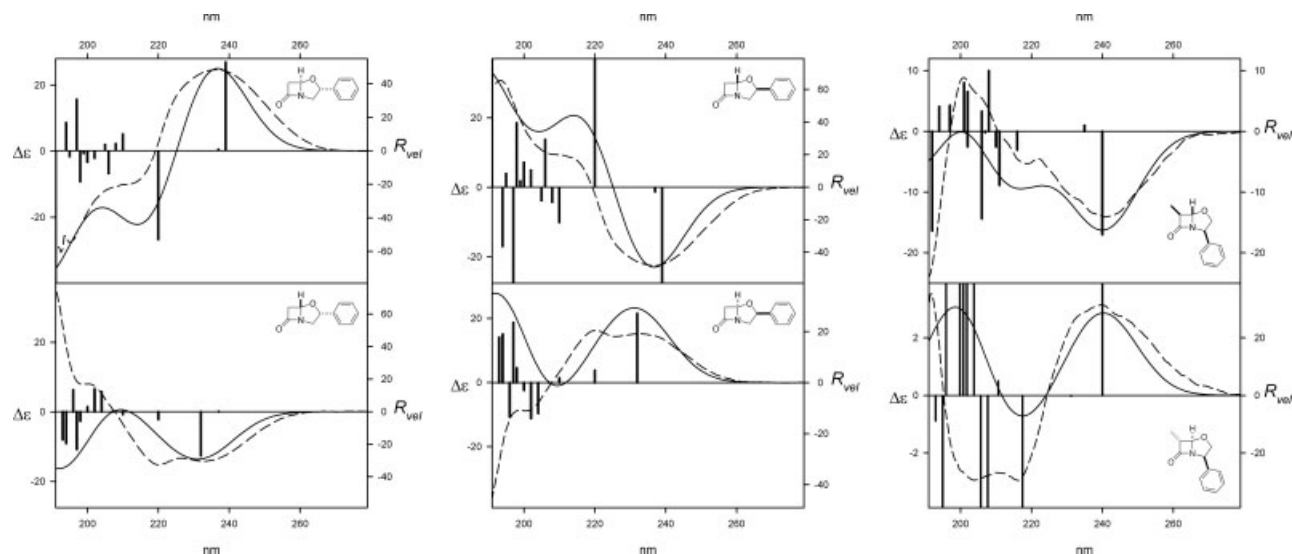


**Fig. 3.** Experimental CD spectra in acetonitrile solution (dashed line) and calculated CD spectra (solid line) for: left - clavams **1** (upper panel) and **4** (lower panel); middle - clavams **2** (upper panel) and **3** (lower panel); right - clavams **10** (upper panel) and **11** (lower panel). The vertical bars represent calculated at B3LYP/6-311++G(2D,2P) level rotatory strengths.

obtained for clavam **10**, whereas in the case of clavams **3** and **4**, the rotatory strengths calculated at ca. 220 nm are underestimated. However, the location of this underestimated rotatory strength in both clavams **3** and **4** is in a perfect agreement with the location of the ECD band in the experimental spectrum (Fig. 3).

In the cases of **1**, **2**, and **11** both the experimental and the calculated spectra show bisignate sequence of Cotton effects observed at around 240 and 220 nm. The sequences of effects are as follows: positive/negative for **1** and **11** and negative/positive for **2**.

In addition, each of the investigated pairs has two long-wavelength transitions with one large and the second one with very small rotatory strengths. In the case of clavam **1** the calculated first long-wavelength electronic transition, originating mainly from the  $\pi-\pi^*$  electronic transition in phenyl ring and the  $n(\text{O})\rightarrow\pi^*$  transition in amide chromophore, is located at 239 nm. The second transition at 237 nm involves the HOMO(-1), HOMO(-2) and the LUMO(+1) and LUMO(+2) orbitals, but its very small rotational strength does not affect the calculated overall long-wavelength CE. The same is observed in the case of clavam **2**, for which both transitions are calculated at 239 and at 237 nm, respectively. In the case of clavams **3** and **4** the two long-wavelength electronic transitions are calculated at 237 and 232 nm. These rotatory strengths generated by the transitions at 237 and 232 nm are of the opposite signs. The rotatory strengths at 237 nm have very small magnitudes and their influence on the overall long-wavelength Cotton effects is negligible.

In compounds **1–4** the third electronic transitions calculated at 220 nm originates mostly from the HOMO(-1), HOMO(-2) and the LUMO, LUMO(+1) transitions of phenyl chromophore. According to our results, the signs of rotatory strengths generated by these electronic transitions reflect the chirality on the C(3) carbon atoms. The same

situation is observed in clavams **10** and **11** for the electronic transitions calculated at around 220 nm. The most intense lowest-energy electronic transitions in both clavams are calculated again at around 240 nm. They represent a mixture of the degenerated  $\pi-\pi^*$  electronic transition in phenyl ring and the  $n(\text{O})\rightarrow\pi^*$  transition in amide chromophore. Because of the low intensity of the second low-energy electronic transition calculated at about 235 and 231 nm, respectively, only the transitions calculated at around 240 nm affect the calculated (and observed) respective Cotton effects.

## CONCLUSIONS

The relationship between the molecular structure and the chiroptical properties of clavams **1–14** was investigated by means of the X-ray diffraction analysis, the electronic circular dichroism spectroscopy and the time-dependent density functional theory. The agreement between the simulated and the experimental ECD spectra is very satisfactory, and confirms the absolute configuration of compounds **1–14**. The computed  $\text{O}=\text{C}-\text{N}-\text{C}_\alpha$  torsion angles for compounds **1–4** and **10–11** provide corroborating evidence for the nonplanarity of amide chromophore. The band at 240 nm has mainly the character of an amide  $n(\text{O})\rightarrow\pi^*$  transition. Its positive or negative sign, depending upon the (5*R*) or (5*S*) absolute configuration, respectively, is predicted by both the helicity rule and the TDDFT calculations. Thus, we can conclude that the helicity rule is valid for the investigated clavams. The presented data allows to infer a supplementary conclusion concerned with the relative configuration of phenyl substituent located at the C(2) and C(3) in the five-membered ring.

The present work demonstrates that the helicity rule can successfully be applied for the absolute configura-

tional assignment of both unsubstituted and substituted clavams.

### LITERATURE CITED

1. Liras P, Rodríguez-García A. Clavulanic acid, a  $\beta$ -lactamase inhibitor: Biosynthesis and molecular genetics. *Appl Microbiol Biotechnol* 2000;54:467–475.
2. Mueller J-C, Toome V, Pruess DL. Ro 22-5417, a new clavam antibiotic from *Streptomyces Clavuligerus* III. Absolute stereochemistry. *J Antibiot* 1983;36:217–225.
3. Liras P, Martin JF. Gene clusters for  $\beta$ -lactam antibiotics and control of their expression: why have clusters evolved, and from where did they originate? *Int Microbiol* 2006;9:9–19.
4. Baggaley KH, Brown AG, Schofield CJ. Chemistry and biosynthesis of clavulanic acid and other clavams. *Nat Prod Rep* 1997;107:309–333.
5. Ogura H, Takayanagi H, Kubo K, Furuhashi K. Conformation of (–)-menthone lactam and *N*-methylmenthone lactam. *J Am Chem Soc* 1973;95:8056–8059.
6. Boyd DB, Riehl JP, Richardson FS. Chiroptical properties of 1-carbapenam and orbital mixing in nonplanar amides. *Tetrahedron* 1979;35:1499–1508.
7. Tomme V, Wegrzynski B, Reymond G. Chiroptical properties of fluorescamine condensation compounds with  $\alpha$ -amino acids in situ. *Biochem Biophys Res Commun* 1976;69:206–211.
8. Lysek R, Borsuk K, Chmielewski K, Kaluza Z, Urbanczyk-Lipkowska Z, Klimek A, Frelek J. 5-Dethia-5-oxacephams: towards correlation of absolute configuration and chiroptical properties. *J Org Chem* 2002;67:1472–1479.
9. Danh TT, Bocian W, Kozerski L, Szczukiewicz P, Frelek J, Chmielewski M. Stereochemistry of [2+2]cycloaddition of chlorosulfonyl isocyanate to chiral alkoxyallenes derived from 1,3-alkylidene L-erythritol and D-threitol. *Eur J Org Chem* 2005;429–440.
10. Frelek J, Lysek R, Borsuk K, Jagodzinski J, Furman B, Klimek A, Chmielewski M. Structure-chiroptical properties relationship in oxabicyclic  $\beta$ -lactam derivatives. *Enantiomer* 2002;7:107–114.
11. Cierpucha M, Solecka J, Frelek J, Szczukiewicz P, Chmielewski M. Synthesis, biological and optical activity of 3-phenyl-clavams. *Biorg Med Chem* 2004;12:405–416.
12. Frelek J, Kowalska P, Masnyk M, Kazimierski A, Korda A, Woznica M, Chmielewski M, Furche F. Circular dichroism and conformational dynamics of cepams and their carba- and oxanalogues. *Chem Eur J* 2007;13:6732–6744.
13. Sheldrick GM. SHELXS-97 Program for crystal structure solution. Göttingen: University of Göttingen, Germany; 1979.
14. Sheldrick GM. SHELXL97 Program for the refinement of crystal structures. Göttingen: University of Göttingen, Germany; 1997.
15. CaChe. Ws Pro 5.0, Fujitsu Ltd.
16. Frisch MJ, Trucks GW, Schlegel HB, Scuseria GE, Robb MA, Cheeseman JR, Zakrzewski VG, Montgomery JAJ, Stratmann RE, Burant JC, Dapprich S, Millam JM, Daniels AD, Kudin KN, Strain MC, Farkas O, Tomasi J, Barone V, Cossi M, Cammi R, Mennucci B, Pomelli C, Adamo C, Clifford S, Ochterski J, Petersson GA, Ayala PY, Cui Q, Morokuma K, Salvador P, Dannenberg JJ, Malick DK, Rabuck AD, Raghavachari K, Foresman JB, Cioslowski J, Ortiz JV, Baboul AG, Stefanov BB, Liu G, Liashenko A, Piskorz P, Komaromi I, Gomperts R, Martin RL, Fox DJ, Keith T, Al-Laham MA, Peng CY, Nanayakkara A, Challacombe M, Gill PMW, Johnson B, Chen W, Wong MW, Andres JL, Gonzalez C, Head-Gordon M, Replogle ES, Pople. Gaussian 03. Pittsburgh, PA: Gaussian; 2003.
17. Diedrich C, Grimme S. Systematic investigation of modern quantum chemical methods to predict electronic circular dichroism spectra. *J Phys Chem A* 2003;107:2524–2539.



## Review Article

# The Online Assignment of the Absolute Configuration of Natural Products: HPLC-CD in Combination with Quantum Chemical CD Calculations

GERHARD BRINGMANN,\* TOBIAS A.M. GULDER, MATTHIAS REICHERT, AND TANJA GULDER

*Institute of Organic Chemistry, University of Würzburg, Am Hubland, D-97074 Würzburg, Germany*

**ABSTRACT** The application of modern online methods, e.g., HPLC-MS/MS and HPLC-NMR, allows the elucidation of constitutions and relative configurations of new natural products directly from crude extracts. To additionally establish the full absolute configurations of such secondary metabolites without the necessity of first isolating the compounds, we have introduced HPLC-CD coupling (CD = circular dichroism) into natural product analysis, taking advantage of the different chiroptical properties of stereoisomers, in particular of enantiomers. In combination with quantum chemical CD calculations this method allows the stereochemical characterization of (even structurally unprecedented) chiral molecules, thus avoiding the—often risky—merely empirical assignment by comparison with the CD spectra of related compounds with known absolute stereostructures, or by other methods such as, e.g., the exciton chirality approach. This review presents the experimental requirements for the hyphenation and the theoretical background of the calculation of UV and CD spectra, which is then exemplified by some recent HPLC-CD applications to the elucidation of absolute configurations of most diverse compounds of mainly natural origin. *Chirality* 20:628–642, 2008. © 2008 Wiley-Liss, Inc.

**KEY WORDS:** resolution of enantiomers; separation of diastereomers; online CD measurements; axial chirality; centrochirality; Boltzmann weighting; force field calculation; semiempirical calculations; molecular dynamics; density functional theory

## INTRODUCTION

The isolation and structural elucidation of new natural products, e.g., from plants or microorganisms, is a rewarding—but often time-consuming—task, since it is a major effort to isolate each compound in a pure form, even the known ones. Furthermore, to obtain the required milligram quantities of all metabolites, even in the case of minor substances, one may need large amounts of the sometimes rare biological material and of expensive tools and supplies, e.g., adsorbents and eluents. Another problem, in particular when dealing with unstable compounds, is that they may decompose already during the preparative separation and thus may escape the analysis. For this reason, there is increasing demand for methods to rapidly identify known and structurally characterize new metabolites.

The hyphenation of high-performance liquid chromatography (HPLC) with spectroscopic methods such as NMR spectroscopy (HPLC-NMR)<sup>1–4</sup> and tandem mass spectrometry (HPLC-MS/MS)<sup>3,5</sup> has led to new strategies that do not only permit to differentiate between known and unknown compounds, but can even establish full constitutions and relative configurations of new natural products directly from the crude extract with a minimum amount of material. But with these methods alone, no information concerning the absolute configuration of the metabolites

can usually be acquired—unless, e.g., by chromatography on a chiral phase, which, however, requires the availability of both enantiomers, their successful chromatographic resolution, and their secure stereochemical assignment.

A clue to the solution of this problem are the chiroptical properties of the chiral analytes, in particular their circular dichroism (CD) data, since two enantiomers are unambiguously characterized by their fully opposite CD spectra. Although the hyphenation of CD measurements with HPLC techniques has been known for several years,<sup>6–9</sup> applications are still rare and mainly concern the measurement of isomerization barriers of configurationally unstable known compounds or the determination of the elution order of enantiomers of given (known) chiral substances on a chiral phase, e.g., of drugs.<sup>10</sup> So the introduction of this methodology for the determination of the absolute

Contract grant sponsors: DFG, the German Bundesministerium für Bildung, Wissenschaft und Forschung (BMBF), the Free State of Bavaria, the University of Würzburg.

\*Correspondence to: Prof. Dr. G. Bringmann, Institute of Organic Chemistry, University of Würzburg, Am Hubland, D-97074 Würzburg, Germany. E-mail: bringman@chemie.uni-wuerzburg.de

Received for publication 25 September 2007; Accepted 1 February 2008  
DOI: 10.1002/chir.20557

Published online 26 March 2008 in Wiley InterScience  
(www.interscience.wiley.com).



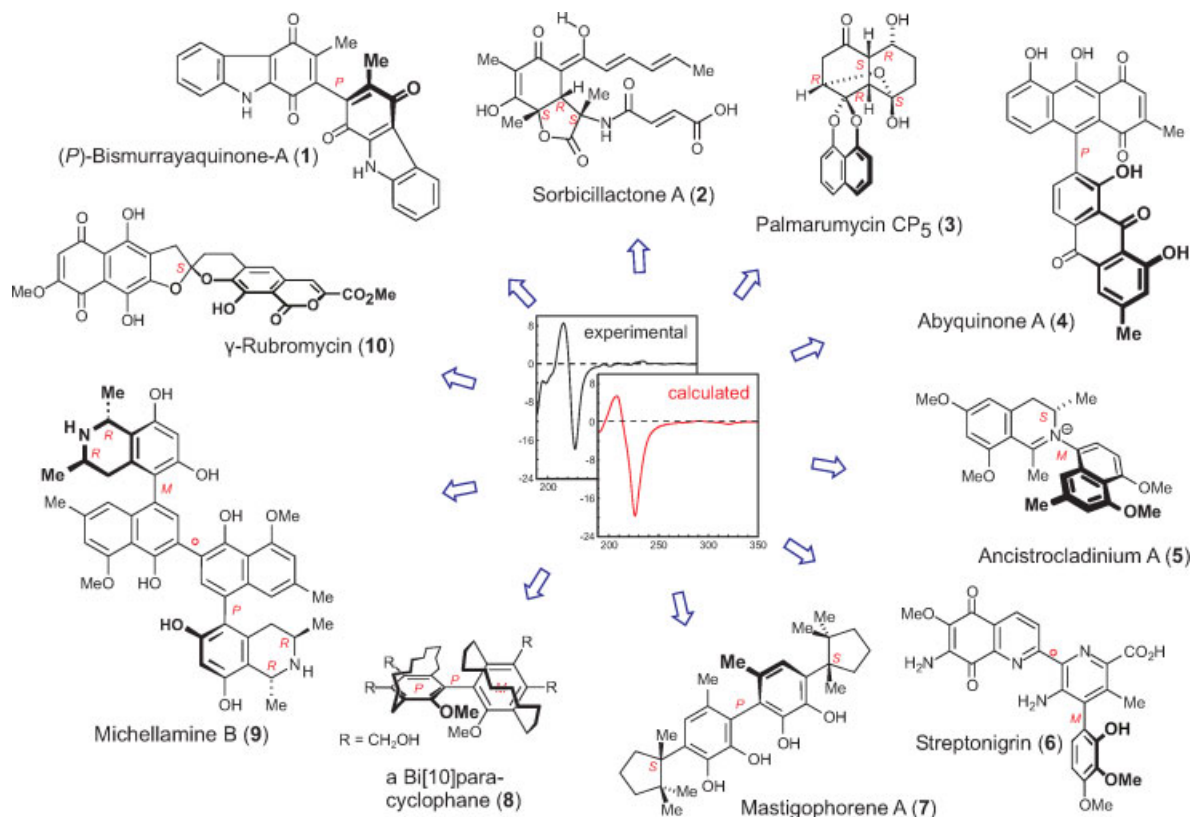


Fig. 1. Selection of structurally interesting compounds—in many cases isolated by other groups—which were stereochemically characterized by quantum chemical CD calculations in our group.<sup>57–66</sup>

configuration of new compounds—and not only natural ones—directly from a crude mixture is a rewarding goal.<sup>11–13</sup> From the CD spectrum, whether taken online or offline, the absolute configuration of the respective stereoisomers can then easily be established—if experimental data from structurally related compounds of known absolute configurations are available or if the structure fits into semiempirical CD rules, e.g., the octant rule.<sup>14–16</sup> Today the most common classical approach for the determination of the absolute configuration of natural products is the electronic circular dichroism (ECD),<sup>15–19</sup> which has recently been improved, e.g., by the development of new CD reporter groups<sup>15</sup> like metalloporphyrins.<sup>20,21</sup> Nevertheless, these ECD methods may suffer from a lack of suitable chromophores, which additionally have to be attached by chemical derivatization procedures, e.g., by formation of dibenzoates.<sup>22</sup> But if the preconditions for these methods are not fulfilled, the interpretation of CD spectra may become difficult or even impossible.

Thus, especially for novel-type structures, a most efficient alternative for the interpretation of CD spectra is the quantum chemical simulation of the curves for both enantiomers, and their comparison with the experimental one.<sup>23–27</sup> This procedure has become a most valuable tool for assigning absolute configurations to a broad variety of chiral compounds of synthetic and natural origin, involving all kinds of chirality, not only stereogenic centers, but also axial and/or planar chirality.<sup>28–56</sup> The chiral structures 1–10 in Figure 1 represent a small selection of compounds

whose absolute configuration had as yet been unknown, but were clearly assigned by theoretical CD investigations in our group.<sup>57–66</sup> For further selected examples, see references 24–52.

## THEORETICAL CONCEPT

CD investigations can normally only distinguish between stereoisomers with a sufficient chiroptical differentiation, i.e., usually between enantiomers, whose CD curves are fully opposite. This means that in the case of more than one stereogenic element, the relative configuration has to be known beforehand by other methods (e.g., by NMR or X-ray diffraction). It can also imply that in molecules equipped with multiple stereogenic elements, some may have larger contributions than others on the overall CD spectrum appearance. This is frequently the case, e.g., in axially chiral biaryls with additional stereogenic centers, where usually only the axial, not the central chirality can be assigned, due to the predominance of the biaryl chromophore.<sup>67</sup> Thus atropo-diastereomers will usually give near-opposite CD spectra, irrespective of the absolute configuration at the stereogenic center(s). Thus, only in very few cases even two stereogenic elements, biaryl axes and stereogenic centers, could be independently assigned by CD calculations, usually requiring higher-level calculations. For the opposite case, i.e. the chiroptical prevalence of stereogenic centers (which are, in this case, part of an extended enone chromophore) over the axis, see Reference 68.



Because the CD spectrum strongly depends on the molecular flexibility of the chromophors, more than for any other spectroscopic method, a detailed investigation of the conformational space is indispensable and forms the first step en route to the simulated CD curve. For the screening of the respective potential energy surface, different approaches are in use.

### THE BOLTZMANN APPROACH

Starting with an arbitrarily chosen enantiomer of the chiral compound, a set of reasonable starting structures of the molecular framework is generated manually by taking into account the most relevant conformational freedom degrees of flexible substituents. These are then subjected to a refinement by investigating the corresponding rotations, usually at a semiempirical level (AM1,<sup>69</sup> PM3<sup>70,71</sup>), in order to find all minimum geometries that are significantly populated at ambient temperature. This applies for all those structures that range energetically within 3 kcal/mol above the global minimum found. With neglect of all geometries possessing a higher energy concerning the aforementioned cut-off criterion, the remaining minima are, in most of the cases, submitted to at least one further optimization step, now by means of density-functional theory (DFT), using predominantly the B3LYP<sup>72,73</sup> hybrid functional and a split-valence double-zeta basis set, e.g., 6-31G\*.<sup>74</sup>

### THE MOLECULAR DYNAMICS APPROACH

In particular for highly flexible molecules, the molecular dynamics (MD) procedure is a time-saving alternative for the investigation of the conformational space. Within this approach, the stereoisomer is exposed to a force field, usually to the one provided by Tripos (SYBYL, Tripos, Inc., St. Louis, MO)<sup>75</sup> or to the MM3<sup>76–79</sup> one, for a certain span of time. During that period, the Newton equations of motion are permanently solved and single geometries are extracted in particular intervals. Usually, a simulation time of 500 ps is chosen, while every 0.5 ps a molecular structure is extracted from the trajectory of motion. The corresponding Newton equations are solved every 2 fs. Heat is used to surmount potential energy barriers and, thus, to find all conformations of the corresponding molecule. The chosen temperature is controlled and kept constant by coupling to a virtual thermal bath.<sup>80</sup>

At this point, a connection to the Boltzmann approach can be established, namely if the force-field generated conformers are submitted to further optimization steps, based on either *ab initio* or DFT procedures.

### CALCULATION OF ELECTRONIC TRANSITIONS

The second step of the computations comprises the calculation of the electronic transitions from the ground state to (selected) excited states. Simulating the molecular CD, the decisive quantity is the rotatory strength  $R$ ,<sup>81</sup> which is defined as the imaginary part of the scalar product of electric and magnetic transition dipole moments between the two states,  $\Psi_0$  and  $\Psi_k(1)$ .

Chirality DOI 10.1002/chir

$$R_{0k} = \Im\{\langle\Psi_0|\hat{\mu}_{0k}|\Psi_k\rangle \cdot \langle\Psi_k|\hat{m}_{0k}|\Psi_0\rangle\} \quad (1)$$

Since experimentally the molecular CD is usually measured in units of  $\Delta\epsilon$ , i.e., the difference of the extinction coefficients for left- and right-circularly polarized light, the computed rotatory strengths  $R_{0k}$  are accordingly transformed and superimposed with Gaussian functions (2),<sup>82</sup> centered at the respective wavelengths  $\lambda_k$  of the electronic transitions, to give the calculated single CD spectrum.

$$\Delta\epsilon(\lambda) = \frac{16\pi^2\beta N_A\lambda}{6909\hbar c} \cdot \sum_k R_{0k} \frac{e^{-\left(\frac{\lambda-\lambda_k}{\Gamma_k}\right)^2}}{\Gamma_k\sqrt{\pi}} \quad (2)$$

In this equation,  $\beta$  means the Lorentz correction, which considers the perturbation of the external field by the local one of the chromophore (usually, the local field is ignored, i.e.,  $\beta$  is equated to unity),  $N_A$  is the Avogadro constant, and  $\Gamma_k$  is the exponential half-width (width of the band at 1/e height). In parallel to the simulation of the CD spectrum the UV curve is calculated, because the electric transition dipole moments are integral part of both. In the case of the UV spectrum, the basic quantity is the electric dipole strength  $D$ , which is just the square of the absolute value of the respective electric dipole moment. However, more familiar is the oscillator strength  $f$ , which is easily obtainable from  $D$  (3).

$$f_{0k} = \frac{4\pi m_e c}{3\hbar e^2 \lambda_k} D_{0k} \quad (3)$$

To get a UV curve comparable with the experimental one, the calculated oscillator strengths  $f_{0k}$  have to be converted into units of  $\epsilon$ , the extinction coefficient, and again, as in the case of CD, overlaid with Gaussian functions (4).

$$\epsilon(\lambda) = \frac{4\pi^2\beta N_A\lambda}{6909\hbar c} \cdot \sum_k D_{0k} \frac{e^{-\left(\frac{\lambda-\lambda_k}{\Gamma_k}\right)^2}}{\Gamma_k\sqrt{\pi}} \quad (4)$$

Having followed the MD approach, the single UV and CD curves of all conformers as obtained according to the above procedure, are superposed to give the total simulated UV spectrum and the CD curve, respectively, whereas in the case of the Boltzmann procedure they are summed energetically weighted, i.e., with respect to the heats of formation of the corresponding minimum geometries. When calculating electronic transitions, the major challenge is a reliable consideration of (dynamic) electron correlation. To receive trustable wave functions for the ground state and the excited ones, together with the corresponding energies, several methodologies are applicable.<sup>83</sup> The most common one is the configuration interaction (CI) approach,<sup>84</sup> where the overall electronic wavefunction  $\Psi_{CI}$  is constructed as a linear combination of weighted single determinants (5) with the Hartree-Fock (HF) determinant as the reference.

$$\Psi_{CI} = a_0\Psi_{HF} + \sum_S a_S\Psi_S + \sum_D a_D\Psi_D + \sum_T a_T\Psi_T + \cdots \quad (5)$$

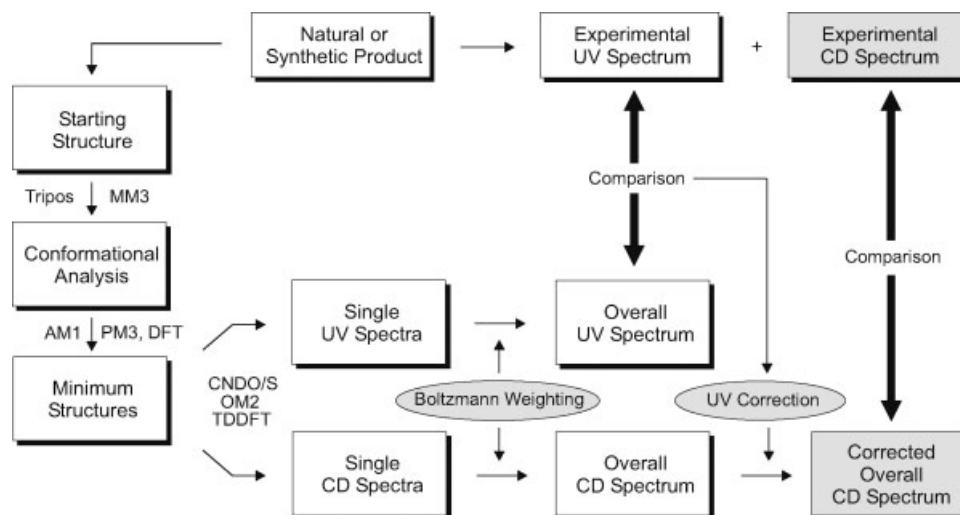


**Fig. 2.** Overview of the Boltzmann-based approach to determine the absolute configuration of a chiral compound by CD calculations. The MD based procedure is in principle the same, except for the fact that conformers instead of minimum structures are obtained, the exclusive applicability of CNDO/S or OM2 for the calculation of the excited states, and the simple superposition of the obtained single spectra without an energetical weighting.

On the basis of this approach, the authors' group has frequently applied the semiempirical CNDO/S<sup>85–87</sup> and OM2<sup>88</sup> Hamiltonians in the past with a CI expansion that covers single excitations ( $\Psi_S$ ). However, to account for the aforementioned dynamic electron correlation, at least the double excitations ( $\Psi_D$ ) have to be included in the CI progression, since the mere single ones ( $\Psi_S$ ) do not interact with the ground state wave function, according to Brillouin's theorem.<sup>89</sup> This is accounted for by likewise performing OM2-CISD calculations. Unfortunately, the software used for CNDO/S calculations is only able to treat CIS. Another technique to compute electronic transitions uses the propagator method, which applies a time-dependent (TD) perturbation to the system, generated by a fluctuating linear electric field. A Fourier transformation to the frequency domain delivers an expression for the frequency-dependent polarizability  $\alpha(\omega)$  of the molecule (6), whose numerator corresponds to the electric transition dipole moments, whereas the denominator consists of the frequency of the electric field and of the energies of the ground state and the excited states.

$$\alpha(\omega) = \sum_{k>0} \frac{|\langle \Psi_0 | \hat{\mu}_{0k} | \Psi_k \rangle|^2}{\omega - (E_k - E_0)} \quad (6)$$

This approach has been applied to both, the HF and the DFT method, while the latter one, TDDFT (TD),<sup>90</sup> is undoubtedly superior and nowadays frequently used.<sup>91</sup> Thus, solving the TD Kohn-Sham equations is equivalent to finding the poles of the frequency-dependent polarizability, which deliver the respective excitation energies in conjunction with the transition moments. Besides the aforementioned semiempirical techniques, we also use TDDFT by default, adopting the B3LYP hybrid functional or BLYP,<sup>73,92</sup> the latter one together with the resolution-of-the-identity<sup>93</sup> approximation, each with a triple-zeta valence polarized basis set (TZVP).<sup>94</sup>

## UV CORRECTION

Before simulated and experimental CD curves are compared in order to attribute the respective absolute configuration, a correction step is performed that is able to compensate systematic computational errors. For that purpose the overall UV spectrum calculated by the same conformational analysis is compared with the measured UV curve and the shift necessary to match the peaks of the two graphs is determined.<sup>27</sup> This wavelength scaling by UV matching ("UV correction") is easier and more unequivocal than for the CD spectra because of the usually larger number of—positive and negative—peaks of the latter. The general proceeding is schematically displayed in Figure 2.

## EXPERIMENTAL SETUP

The technical equipment for the measurement of online CD spectra consists of a standard HPLC system with a degassing unit and an "external" UV detector, coupled to an additional spectrometer that simultaneously measures the CD and UV profile of the analyte in the flow cell at a single wavelength. The application of two independently operating detectors provides the opportunity to use two different wavelengths for a most sensitive detection of the analyte at both, its UV ("external" detector) and its CD maxima (CD spectrometer), in a single run. The hyphenation of the chromatographic system to the spectrometer is achieved by using a motor valve, permitting to stop the solvent flow through the measurement cell at the maximum concentration of the analyte (stopped-flow mode) by redirecting the eluent from the HPLC pump directly into a waste flask. When using a solvent gradient for the resolution of a complex compound mixture, the current eluent composition is, in addition, automatically kept constant upon bypassing the column and the spectrometer, thus offering the advantage of subsequently proceeding with

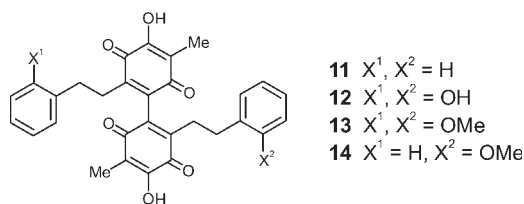


**Fig. 3.** Constitutions of parvestimins A-D (**11–14**) from *Stemona parviflora* Wright.

the analysis of further substances within the same run. The measurement of the actual full CD spectrum of a chiral analyte is accomplished in the stopped-flow mode.

In most cases, the resolution of a mixture of enantiomers is achieved by application of a column with a suitable chiral normal-phase adsorbant, because the diversity of the respective materials, and thus of different chromatographical selectivities, is much larger when compared with the smaller number of reversed-phase chiral systems. The resolution of diastereomeric compounds, by contrast, is mostly achieved by reversed-phase chromatography, which is usually superior in the case of achiral material. In many cases the quality of the separation can be decisively improved by optimizing the temperature of the chromatographic system by using a column oven. The application of different HPLC phases and chromatographic conditions for the online analysis of chiral natural products is exemplified in the following section.

## EXPERIMENTAL EXAMPLES

In the following section, the broad applicability of the LC-CD methodology in combination with quantum chemical CD calculations to the determination of the absolute configuration of chiral substances will be demonstrated. This will be exemplified for most diverse classes of natural and unnatural structures and reference is made to further selected examples.

### Parvestimins—Constitutionally Symmetric Bisbenzoquinones

An example of the elucidation of the absolute configuration of a natural product with only one element of chirality by HPLC-CD, is the assignment of the atropo-enantiomers of the parvestimins A-D (**11–14**).<sup>95</sup> These dimeric phenylethyl benzoquinones were isolated from the aerial parts of *Stemona parviflora* Wright,<sup>95</sup> a plant distributed in the Chinese Hainan province,<sup>96</sup> where it is used in traditional medicine to treat respiratory disorders.<sup>97,98</sup> The constitutions of **11–14** were elucidated by NMR spectroscopy (see Fig. 3). All parvestimins are equipped with a biaryl-like quinone-quinone axis, which is fourfold *ortho*-substituted and should thus be configurationally stable. Still, these natural products did not exhibit any optical rotation,<sup>95</sup> and thus might be racemic in nature, like quite a few other chiral natural biaryls.<sup>99–101</sup>

To investigate the existence of possible atropo-enantiomers of **11–14** and to determine their natural ratio, a method for the enantiomeric resolution by HPLC on a chiral phase was developed, starting with parvestimin A (**11**) as the “parent compound.” The best results were achieved with a Chiralcel OD-H column (Daicel) and *n*-hexane/*i*-propanol (97.5/2.5) as the eluent at elevated temperatures (55°C), providing a perfect baseline separation. That the two LC-UV peaks observed (Fig. 4a) indeed corresponded to the respective atropo-enantiomers of **11**, was verified by online CD analysis, giving a negative and a positive peak at 260 nm (Fig. 4b). Integration of the LC-UV peaks

ral phase was developed, starting with parvestimin A (**11**) as the “parent compound.” The best results were achieved with a Chiralcel OD-H column (Daicel) and *n*-hexane/*i*-propanol (97.5/2.5) as the eluent at elevated temperatures (55°C), providing a perfect baseline separation. That the two LC-UV peaks observed (Fig. 4a) indeed corresponded to the respective atropo-enantiomers of **11**, was verified by online CD analysis, giving a negative and a positive peak at 260 nm (Fig. 4b). Integration of the LC-UV peaks

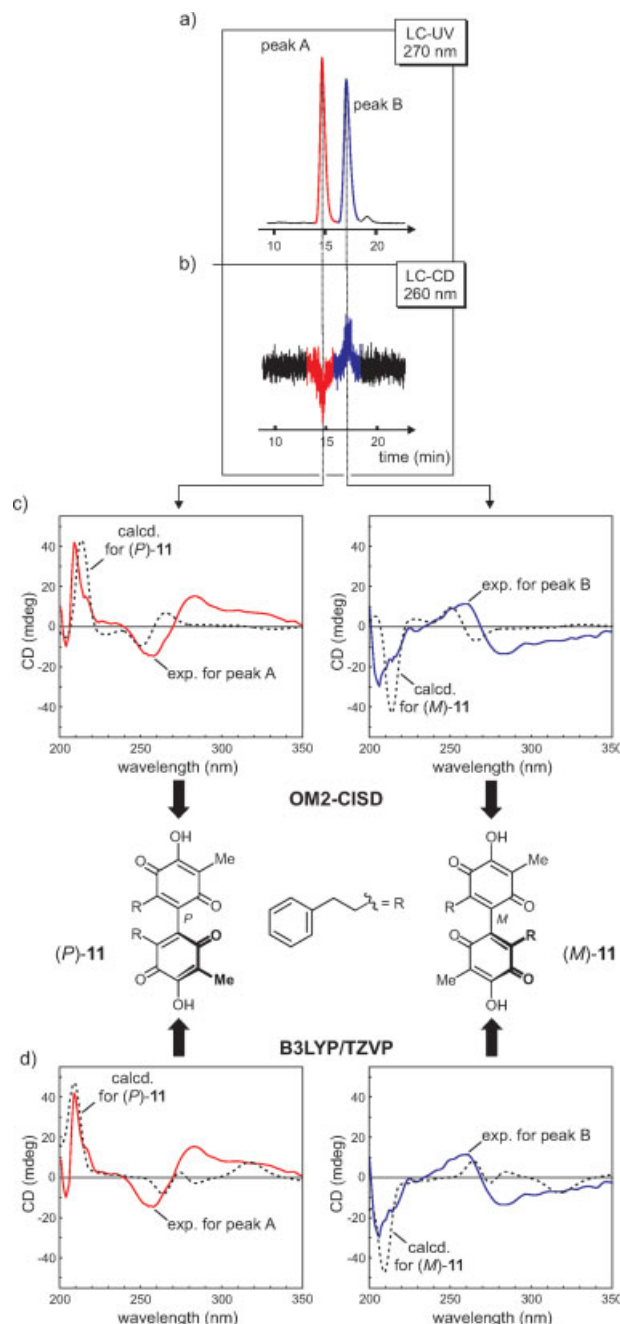


**Fig. 4.** Stereochemical assignment of the two enantiomers of parvestimin A (**11**), by LC-CD coupling and quantum chemical CD calculations using OM2-CISD and TDDFT (B3LYP/TZVP).



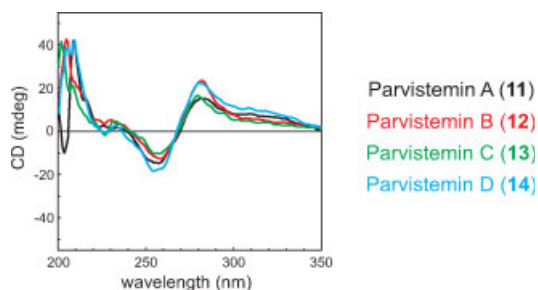


Fig. 5. Comparison of the LC-CD spectra of the faster eluting atropo-enantiomers of the parvestemins A-D (11-14).

showed a 1:1 ratio, evidencing the fully racemic character of naturally occurring **11**.

For a complete stereochemical attribution of the two atropo-enantiomers of **11**, full LC-CD spectra were recorded in the stopped-flow mode, resulting in almost mirror-shaped CD curves. To attribute the respective absolute configuration to the corresponding atropisomer of **11**, the CD spectra of the (*P*)- and the (*M*)-enantiomers were quantum chemically calculated and compared with the experimental curves.

Arbitrarily starting with (*P*)-**11**, the conformational space was scanned using at first the PM3 method. The resulting 40 minimum structures were further optimized by means of DFT calculations (BLYP/6-31G\*), converging to only two relevant conformers, which were then submitted to CD calculations using the semiempirical OM2 Hamiltonian in combination with CI computations, including single and double excitations. The single spectra obtained were added up according to the Boltzmann statistics, resulting in the overall simulated CD curve, which was UV corrected and then compared with the experimental spectra of the faster atropo-enantiomer of **11** (peak A) and the more slowly (peak B) eluting one. These comparisons revealed good agreements between (*P*)-**11** and peak A (Fig. 4c, left) on the one hand, and between (*M*)-**11** and peak B (Fig. 4c, right) on the other, thus permitting assignment of the absolute configurations to the respective enantiomers.

To prove these attributions, more accurate CD computations were carried out. By using TDDFT (B3LYP/TZVP) the first 100 excitations were calculated. The CD spectra resulting for (*P*)- and (*M*)-**11** again showed good agreements between peak A (Fig. 4d, left) and peak B (Fig. 4d, right), respectively, thus fully confirming the above-deduced assignment.

For a complete stereochemical attribution of the other parvestemins B-D (**12–14**), which are likewise new natural products, the above described separation method for **11** had to be individually adjusted to these metabolites by slightly changing the solvent composition (*n*-hexane/*i*-propanol in a 90/10 ratio for **12** and **13**, and in a 95/5 ratio for **14**) and the temperature (40°C). Under these modified conditions, baseline separations were achieved in all cases, thus permitting determination of the racemic nature of all parvestemins by integration of the LC-UV signals. Compari-

son of the online CD spectra of the respective faster eluting peaks of the parvestemins B-D (**12–14**) with the one in the enantio-separation of **11** expectedly revealed a high similarity of all these CD curves (see Fig. 5), clearly evidencing all faster eluting peaks to correspond to the (*P*)-configured products.

### Isoplagiochin C—A Macrocycle with Strain-induced Chirality

An example of a stereochemically much more complex group of natural products successfully analyzed by HPLC-CD coupling are the macrocyclic bisbibenzyls, e.g., isoplagiochin C (**15**) from bryophytes (Fig. 6).<sup>102,103</sup> Biosynthetically, these compounds originate from two units of the natural diphenylethane lunularin joined together by twofold phenol-oxidative *C,C*-coupling.<sup>104</sup> The resulting biaryl axes, however, appear to be configurationally unstable at first sight. Therefore, it was not unexpected that **15**, e.g., when isolated from the liverwort *Plagiochila fruticosa*, was initially obtained in an optically inactive form.<sup>105</sup> More recently, however, **15** was found to have significant optical rotatory powers, with  $[\alpha]_D$  values of +42.5 (*c* 0.2, MeOH) when isolated from *Lepidozia incurvata*<sup>106</sup> and +74.8 (*c* 0.2, MeOH) when derived from *Herbertus sakuraii*.<sup>107</sup> Although CD spectra were recorded in the latter case, suggesting the presence of atropisomers, the absolute configurations could not be established.<sup>108</sup>

By computational methods we were able to show that the reason for the chirality exhibited by **15** is the molecular helicity of the entire compound, whose ring strain makes the molecule rigid overall, with (formally) four stereogenic elements (two biaryl axes, one helical stilbene unit, and a helical 1,2-diarylethane unit).<sup>109,110</sup> Still, as shown by calculating the respective rotational barriers, only one of the biaryl axes (the “upper” one) has a fully stable configuration, leading to four interconverting diastereomers, yet without racemization at room temperature.

Given the different  $[\alpha]_D$  values for **15** in the literature, ranging from strongly dextrorotatory in some cases<sup>105</sup> (see above) to zero in others,<sup>106,107,109</sup> and, in addition, the laevorotatory form of **15** in our hands ( $[\alpha]_D = -49^\circ$ ) as isolated from *Plagiochila deflexa*, the enantiomeric ratio of the natural product was investigated by developing a method for the resolution of its atropo-enantiomers on a chiral HPLC phase using racemic synthetic material.<sup>109</sup> This succeeded on a chiral OD-H column with an *n*-hexane/*i*-PrOH gradient, resulting in a nice baseline separa-

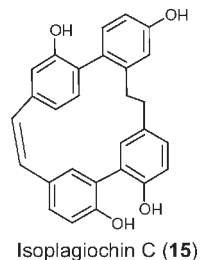
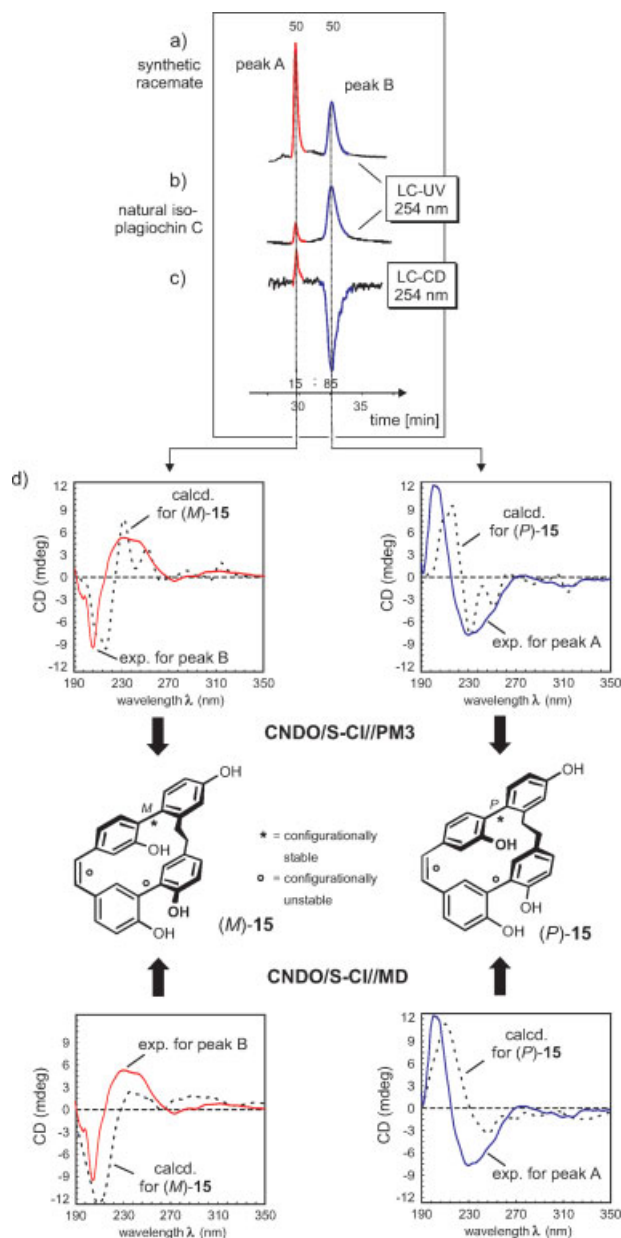


Fig. 6. Constitution of the macrocyclic bisbibenzyl isoplagiochin C (**15**).



**Fig. 7.** Resolution (a) of the two enantiomeric components of synthetic material of racemic isoplagiochin C (*rac*-**15**) and (b) of the natural product from *P. deflexa* on a chiral Chiralcel OD-H phase; HPLC-CD coupling (c) monitoring one wavelength (254 nm) and (d) with measurement of full online CD spectra.

tion of the two atropo-enantiomers of the optically inactive sample (Fig. 7a). Application of the method to the analysis of natural **15** allowed to determine the enantiomeric ratio by integration of the LC-UV peaks (Fig. 7b) to be 85:15 for the slower and the faster peaks, respectively, and likewise permitted the first measurement of the two mirror-imaged CD spectra of both pure enantiomers of isoplagiochin C (**15**) from a single sample. Furthermore, the separation method facilitated kinetic studies for the determination of the racemization rates of **15**, giving an experimental activation energy of 23.8 kcal/mol, which was in rough

accordance with the calculated value of 24.2 kcal/mol—and sufficiently high to prevent racemization at room temperature.

The configurations of the atropo-enantiomers of **15** were again assigned by quantum chemical CD calculations, exemplarily for (*P*)-**15**. This time, the conformational analysis was performed by means of the AM1 method. For each of the relevant 30 minimum structures, the particular CD spectrum was computed by applying the semiempirical CNDO/S approach. The resulting single curves were then summed weighted according to the Boltzmann statistics, to give the overall calculated CD spectra, which were then UV-corrected. Comparison of these computed CD spectra with the experimental ones showed a good agreement between the data predicted for (*P*)-**15** and the online spectrum of the more slowly eluting stereoisomer (Fig. 7d, right), and, vice versa between (*M*)-**15** and the faster atropo-enantiomer (Fig. 7d, left), thus permitting their stereochemical assignment.

To verify this configurational attribution, MD simulations were carried out, of which the run at a virtual temperature of 1200 K appeared to be reliable with respect to the observed conformational behavior and was therefore chosen as a basis for the following CD calculations. At this virtual temperature, all barriers were found to be surmounted, except for that of the “upper” axis **A**, as the “stereochemical anchor,” thus guaranteeing chiral stability of **15** during the simulation process—just as found experimentally at room temperature, and computationally, by the conformational analysis. For the 1000 structures collected during the simulation, single CD spectra were computed, again using CNDO/S, and averaged arithmetically to yield the overall theoretical CD spectra, which now showed an even excellent agreement between (*P*)-**15** and peak B (Fig. 7e, right) and between (*M*)-**15** and peak A (Fig. 7e, left), thus confirming the results of the conformational analysis approach.

### *Ancisheynine, the First N,C-Coupled Naphthylisoquinoline—A Positively Charged Hetero Biaryl from Nature!*

Another, stereochemically likewise highly demanding type of natural products, are the naphthylisoquinoline alkaloids, as intensely investigated in the authors' group.<sup>111,112</sup> These secondary metabolites constitute a rapidly growing class of structurally, biosynthetically, and pharmacologically unique naturally occurring biaryls with about 120 characterized representatives so far, all of them from plants belonging to the Ancistrocladaceae and Dioncophyllaceae,<sup>99</sup> thus likewise serving as a phytochemical marker for these two closely related tropical plant families. In contrast to most other alkaloids of this type, which are based on a configurationally more or less stable biaryl system, i.e., with a C,C axis connecting the isoquinoline and naphthalene portions, ancisheynine (**16**) as recently been isolated by Butler et al.,<sup>113</sup> is the first N,C-coupled naphthylisoquinoline alkaloid. In that original article,<sup>113</sup> the stereochemical properties of **16**, however, were not investigated. As in the case of the parvistemins A-D, (**11–14**) ancisheynine (**16**) was likewise reported to be optically



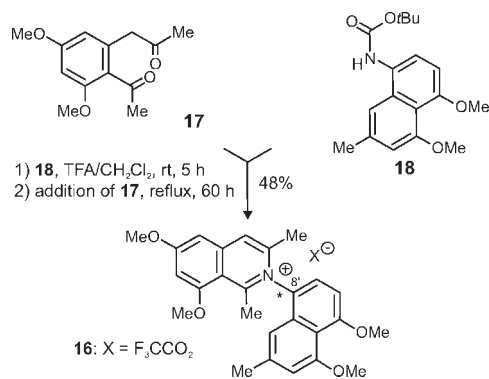


Fig. 8. Key steps in the first total synthesis of ancisheynine (**16**).

inactive, thus raising the question why it is racemic: Is it produced by the plant in a racemic form straightaway, i.e., without any enantioselectivity, or is it possibly configurationally unstable or semistable at the hetero-biaryl axis? After all, ancisheynine (**16**) has only three *ortho*-substituents next to the axis, in contrast to, e.g., **11–14**, with their four-fold *ortho*-substituted biaryl systems.

To answer this question, sufficient quantities of **16** in both enantiomeric forms (or as a racemate) were required for the development of a method for its online HPLC-CD analysis. In fresh plant material of *Ancistrocladus heyneanus* from our botanical garden, ancisheynine (**16**) was present only in traces, so that we developed a first total synthetic access to this compound in a racemic form (see Fig. 8).<sup>114</sup> The key steps of this convergent synthesis were the in-situ deprotection of the *N*-Boc protected naphthalene **17** and its cyclocondensation with the diketone **18** to give (racemic) ancisheynine (**16**) in 48% yield.

The stable axial chirality of **16** was evidenced by the resolution of its atropo-enantiomers by HPLC on a chiral OD-RH column at 5°C with acetonitrile/water (30/70) as the eluent (Fig. 9a), expectedly resulting in two peaks with opposite-signed single-wavelength LC-CD signals (Fig. 9b) and mirror-imaged full LC-CD spectra recorded in the stopped-flow mode. Still, a merely empirical assignment of the absolute configuration at the hetero-biaryl axis of **16** was impossible due to its novel-type structure, again making quantum chemical CD calculations the method of choice.

Starting with (*M*)-**16**, the conformational space was screened by means of PM3, resulting in six minima within an energetical array of 0.6 kcal/mol. These structures were submitted to CD calculations, using the OM2 Hamiltonian in conjunction with CISD. The single spectra received were added up following the Boltzmann statistics.

The predicted overall CD curves thus obtained were UV-corrected and compared with the experimental online CD spectra of the faster (peak A) and the more slowly (peak B) eluting atropo-enantiomers of **16**. This comparison revealed quite good agreements between (*M*)-**16** and peak A (Fig. 9c, left), and between (*P*)-**16** and peak B (Fig. 9c, right), thus permitting to assign the absolute configurations to the corresponding atropo-enantiomers.

Since the calculated spectra failed to match the experimental curves at wavelengths higher than 280 nm, a con-

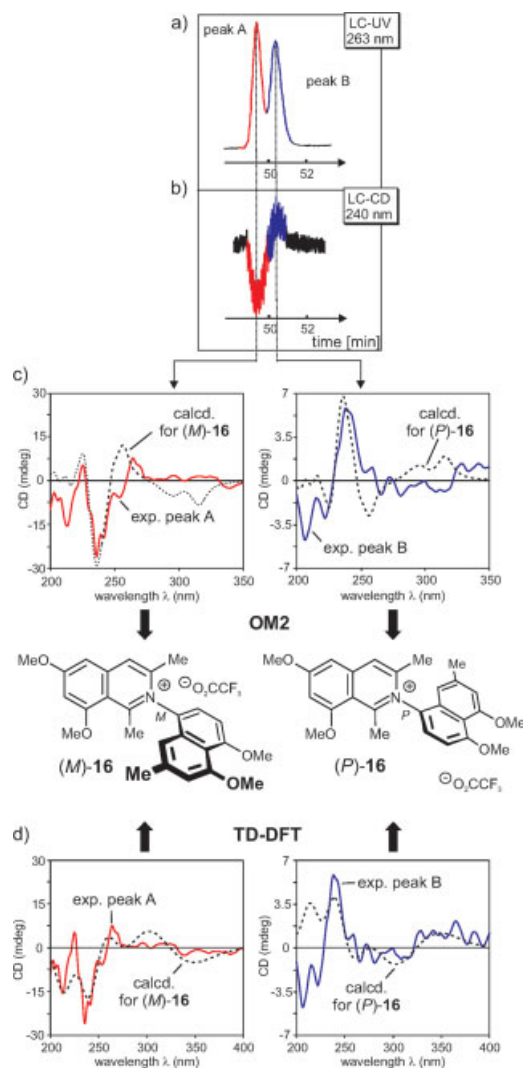


Fig. 9. Stereochemical assignment of the two enantiomers of ancisheynine (**16**), by LC-CD coupling combined with quantum chemical CD calculations.

firmation of the results seemed desirable. Therefore, the six minimum structures found with PM3 were further optimized using DFT (B3LYP/6-31G\*), thus converging to only two minima. For these, CD calculations applying TDDFT (B3LYP/TZVP) were carried out taking the first 100 excitations into account. The resulting CD curves for (*M*)-**16** and (*P*)-**16** again showed a good agreement with the measured spectra of peaks A (Fig. 9d, left) and B (Fig. 9d, right), respectively, but now over the complete range

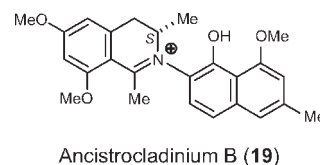
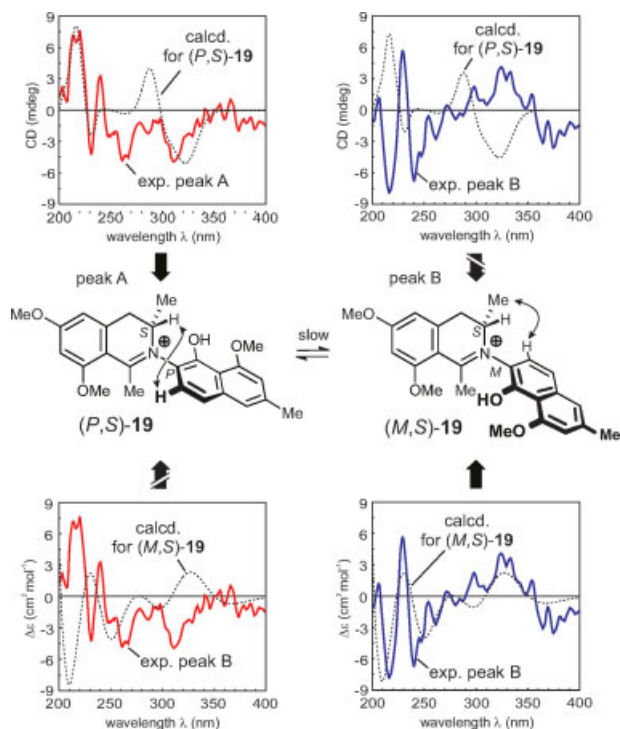


Fig. 10. Constitution of ancistrocladinium B (**19**).



**Fig. 11.** Assignment of the relative and the absolute axial configurations to ancistrocladinium B [(*P,S*)-**19**] and its atropo-diastereomer, (*M,S*)-**19**, by specific NOE interactions (center, double arrows) and by comparison of the experimental LC-CD spectra (stopped-flow mode) of peak A (left) and B (right) with the spectra calculated for (*P,S*)-**19** and (*M,S*)-**16**, by using TDDFT (B3LYP/TZVP).

of wavelength investigated, thus fully confirming the semi-empirical results described earlier.

The rotational stability of ancisheynine (**16**) was evidenced by applying the aforementioned separation method at a semi-preparative level and re-injecting the enantio-enriched samples thus obtained, showing their constant enantiomeric ratio over time. Thus, the reason for the natural occurrence of ancisheynine (**16**) in a racemic form is not its imaginable configurational instability, but must be the lack of enantioselectivity of the biosynthetic system. That the formation of **16** really takes place in vivo and not in a non-enzymatic (and therefore non-enantioselective) step, was proven by online analysis of fresh samples in our laboratory, again showing a 50:50 ratio of the two enantiomers according to LC-CD.

#### *Ancistrocladinium B—Chirality Involving a Rotationally Hindered *N*-iminium-*C*<sub>aryl</sub> Axis and a Stereogenic Center!*

The approach to determine absolute stereostructures by quantum chemical CD calculations is of course not restricted to the assignment of axial configurations alone, but can also be applied to the efficient stereoanalysis of molecules bearing stereogenic centers or both, axes and centers, e.g., in the case of *N,C*-coupled naphthyldihydroisoquinoline alkaloids. The authors' group has recently discovered the first representatives of this type, ancistrocladinium A (**5**, Fig. 1) and B (**19**, Fig. 10), from a Congolese *Ancistrocladus* species with an as yet unprecedented rotationally hindered iminium-aryl axis in nature and, in addition, equipped with a stereogenic center at C-3, thus

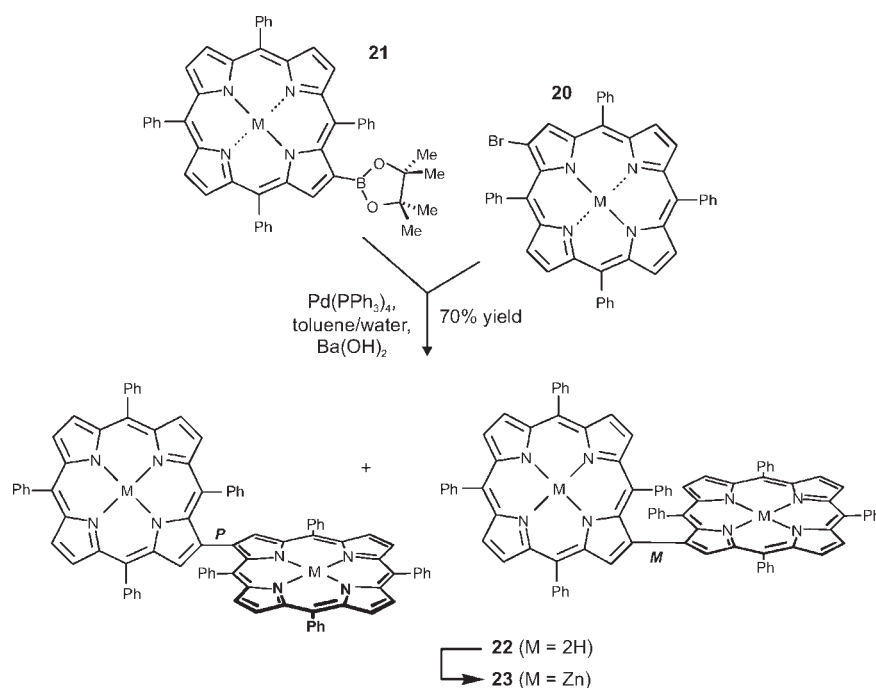


**Fig. 12.** Synthesis of the first intrinsically axially chiral bisporphyrin derivatives **22** and **23** in a racemic form.

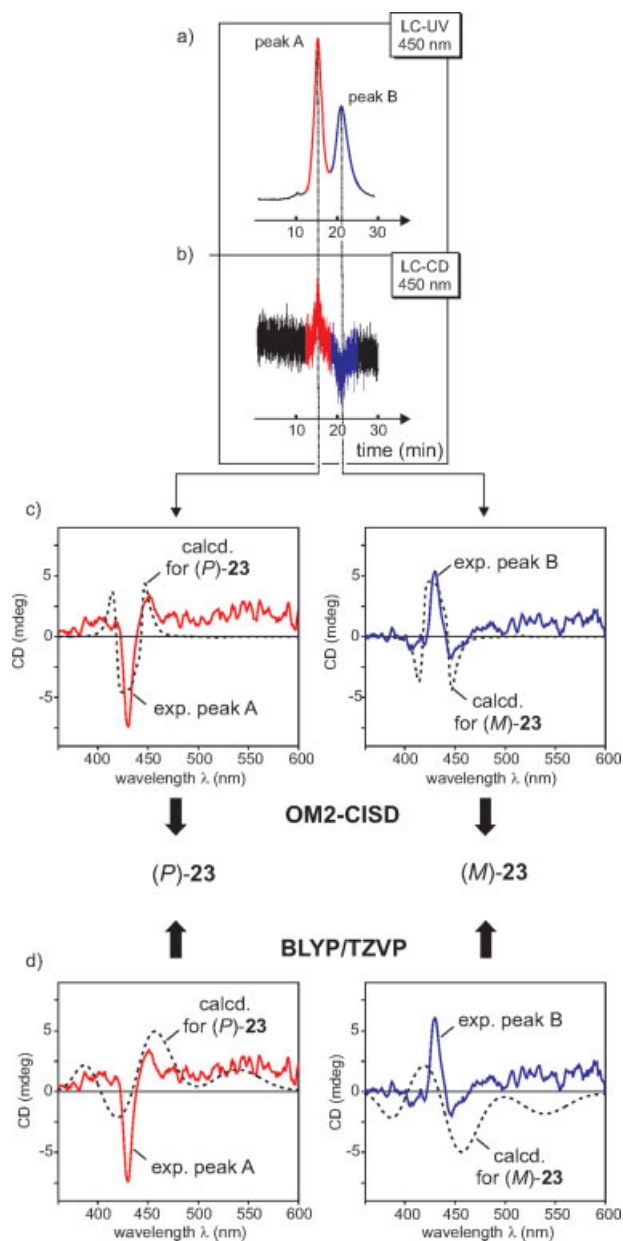


**Fig. 13.** Stereochemical assignment of the two atropo-enantiomers of **23**, by resolution on a Chiracel OD-H column with LC-CD coupling and quantum chemical CD calculations (performed on **22** as the metal-free analog).

giving rise to atropo-diastereomers, not -enantiomers as in the case of ancisheynine (**16**).<sup>115</sup>

According to our stereoanalysis, ancistrocladinium A (**5**), whose central axis is configurationally stable, occurs as a 10:1 mixture of its two atropo-diastereomers, so that offline-CD measurements were feasible (not shown). This was, however, not possible in the case of ancistrocladinium B, (**19**) whose axial configuration is only semi-stable, causing a slow interconversion of its atropo-diastereomers at room temperature; the CD analysis of **19** was therefore performed online, in direct hyphenation with the

HPLC separation of its two rotational isomers.<sup>115</sup> Although these are diastereomers, their CD spectra, as recorded in the stopped-flow mode, were found to be virtually opposite, due to the fact that the hetero-biaryl system, with its dihedral angle between the chromophores at the axis, strongly dominates the CD curves, like also in the case of conventional, *C,C*-coupled naphthylisoquinoline alkaloids.<sup>116,117</sup> Still, the presence of the new coupling type in **19**—now even with a positive charge as part of the chiroptically dominant element of axial chirality—prohibited a configurational assignment of the two atropisomers by a merely empirical comparison of their experimental CD spectra with that of a configurationally known similar alkaloid. The attribution of the two peaks to the atropo-diastereomers of **19** was thus again achieved by quantum chemical CD calculations.

Since the configuration of the centers (C-3) relative to the axes for each of the two atropo-diastereomers was deducible from specific NOE interactions of H-7' of the naphthalene molecular portion with either H-3 in the more rapidly eluting isomer of **19** (peak A) or with 3-CH<sub>3</sub> in the slower diastereomer (peak B, Fig. 12), the computational efforts concentrated on the assignment of the absolute configurations of the chiral axis. Starting with the (*S*)-isomers at C-3, independent conformational analyses at the semiempirical PM3 level for the two atropo-diastereomers, (*P,3S*)-**19** and (*M,3S*)-**19**, resulted in five and six minimum structures, respectively. These geometries were further optimized using DFT (B3LYP/6-31G\*). In both cases, only four relevant conformers remained, which were submitted to CD calculations by means of TDDFT (B3LYP/TZVP) considering the first 100 excitations. The overall spectra thus obtained were subsequently UV-corrected and compared with the measured CD curves of the atropo-diastereomers of **19** (see Fig. 11).

The experimental CD spectra of peaks A and B fitted well to the ones simulated for (*P,3S*)-**19** (Fig. 11, top left) and (*M,3S*)-**19** (Fig. 11, bottom right), respectively, which thus permitted unambiguous attribution of the absolute configurations of the two atropo-diastereomers. This assignment was further confirmed by the subsequent independent determination of the absolute configuration at the stereogenic center at C-3 as *S* by ruthenium-mediated oxidative degradation<sup>118</sup> directly on the atropisomeric mixture of pure **19**, which afforded the *S*-enantiomer of 3-aminobutyric acid, exclusively.<sup>115</sup>

#### *A Synthetic Example: the First $\beta,\beta$ -Coupled Bisporphyrin with Intrinsic Axial Chirality*

The utility of the online CD analysis in combination with quantum chemical CD calculations for the fast configurational assignment of chiral compounds of natural, but also synthetic origin is also evident from its recent application in the stereochemical characterization of the first intrinsically axially chiral  $\beta,\beta'$ -coupled bisporphyrin system.<sup>119</sup> The decisive step in the synthesis of these stereochemically highly congested compounds was the cross coupling of the bromide **20** of TPP (tetraphenyl porphyrin) with the borylated derivative **21** using Pd(PPh<sub>3</sub>)<sub>4</sub> as the catalyst and Ba(OH)<sub>2</sub> as the base in toluene.



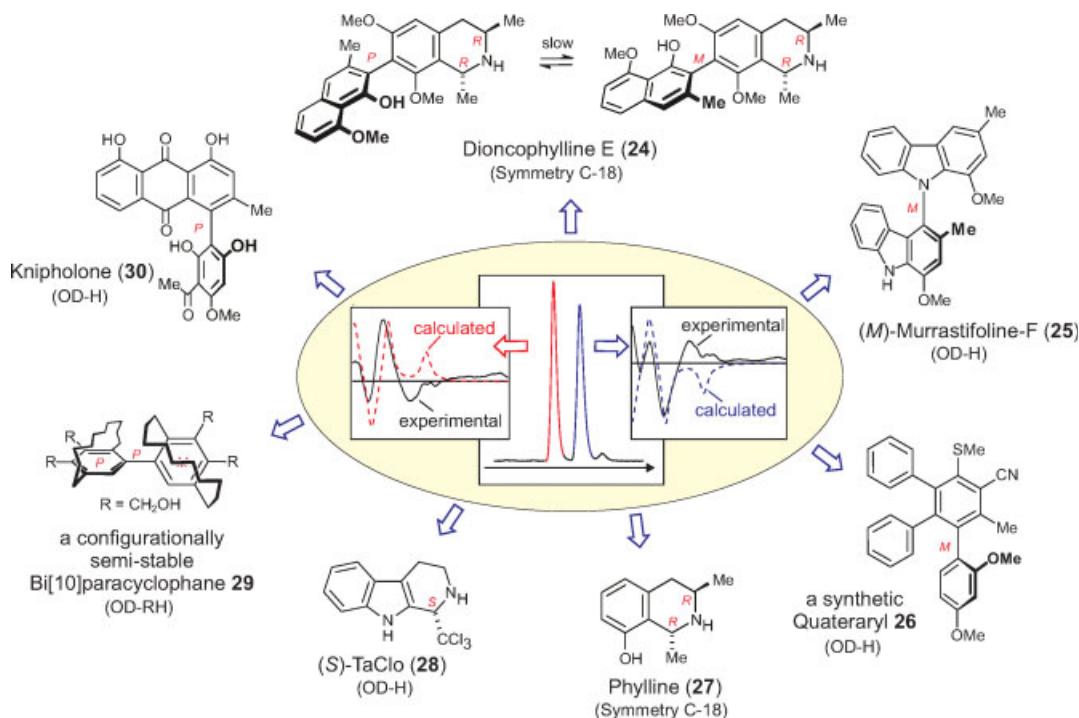


**Fig. 14.** Further selected examples of stereochemical assignments by LC-CD coupling (chiral phases used for the respective separations shown in parantheses) combined with quantum chemical CD calculations.

uene/water furnishing the racemic bisporphyrin **22** in 70% yield (see Fig. 12).<sup>119</sup>

Although the racemic free bisporphyrin **22** could not be resolved on a variety of different HPLC phases under various conditions, its bis-zinc complex **23** (see Fig. 14) gave a clear baseline separation of its two atropo-enantiomers at room temperature when using a Chirex 3010 column (*n*-hexane/*i*-propanol = 60/40).

The online CD spectra recorded in the stopped-flow mode showed a positive first Cotton effect around 450 nm for the faster (peak A) and a negative one for the more slowly (peak B) eluting enantiomer. Because of the identity of the two coupled porphyrin chromophores of **23**, the exciton chirality approach was applicable for a first configurational assignment. Accordingly, peak A was attributed the (*P*)-assignment, and peak B should be (*M*)-configured (see Fig. 13).

This ECD result was further corroborated by quantum chemical CD calculations. Because of the large size of the bisporphyrin system and the required additional computational demand for the inserted Zn atoms, and because no major influence of the CD spectrum from these two Zn atoms was expected, the calculations were carried out with the transition-metal free parent compound **22**. Starting with (*M*)-**22**, the conformational space was investigated by means of PM3, resulting in 32 minimum structures, which differed only in the dihedral angles of the peripheral phenyl substituents.

Since these phenyl groups should not significantly influence the molecular CD, only the global minimum was further optimized using DFT (B3LYP/3-21G) and then sub-

mitted to CD calculations by means of OM2-CISD and TDDFT (BLYP/TZVP), considering the first 100 excitations in the second approach. The computed CD curves thus obtained for the two enantiomers were both UV-corrected and compared with the experimental spectra of the faster (peak A) and the more slowly eluting (peak B) atropo-enantiomer of **22**. This comparison revealed good agreements between (*P*)-**21** and peak A (Figs. 13c and 13d, left) on the one hand and between (*M*)-**21** and peak B (Figs. 13c and 13d, right) on the other, thus permitting to assign the corresponding absolute configurations to the respective atropo-enantiomers, in full accordance with the above predictions based on the Exciton Chirality method.

### Further Selected Examples

Further stereochemically intriguing examples from most different classes of compounds, with stereogenic centers or elements of axial or planar chirality, whose absolute configurations have been established by LC-CD in combination with quantum chemical CD calculations, are shown in Figure 14.<sup>11,101,120–125</sup>

## CONCLUSIONS

In summary, HPLC-CD coupling in combination with modern, high-level quantum chemical CD calculations is a most valuable tool for the stereochemical assignment of chiral compounds, in particular when possessing novel-type molecular structures. It is also the method of choice in the case of compounds whose chemical or configurational instability would not permit the classical isolation

with separate—i.e., offline—CD investigations. By application of this methodology together with complementary other online techniques, e.g., HPLC-MS/MS and HPLC-NMR, it is even possible to assign full absolute 3D structures of novel natural products directly from crude extracts. This approach is not only useful for a fast dereplication of known secondary metabolites from a complex compound mixture in natural product chemistry, but also applicable to other fields of chemical research dealing with structurally novel chiral substances, e.g., for the fast analysis of the stereochemical outcome of asymmetric syntheses.

### ACKNOWLEDGMENTS

The experimental work described in this article was supported by the DFG (SFB 630 'Recognition, Preparation, and Functional Analysis of Agents against Infectious Diseases', SFB 251 'Ecology, Physiology, and Biochemistry of Plants and Animals under Stress', SPP 1152 'Evolution of Metabolic Diversity', Individual Grant 'Molecular Phylogeny and Chemotaxonomy of the Family Ancistrocladaceae', and the Individual Grant 'Enantioselective Synthesis of Bisbibenzyl Natural Products of the Isoplagiochin Type Combining Axial and Helical Chirality', the Fonds der Chemischen Industrie (supplies to G.B. and fellowship to T.G.), the German Bundesministerium für Bildung, Wissenschaft und Forschung (BMBF; research networks *BIOTECmarin* 'Molecular Biotechnology and Bioactive Compounds of Marine Sponges and Sponge-Associated Micro-Organisms' and 'Neurotoxins and Neuroprotection: Importance of Radical Mechanisms and of the Inhibition of the Respiratory Chain for the Etiology of the Parkinsonian Syndrome, of Neurodegenerative, and Aging Processes'), the Free State of Bavaria, and the University of Würzburg. The authors thank Dr. Torsten Bruhn for useful suggestions. Thank is due to all members of our group in particular to J. Mühlbacher, K. Maksimenka, M. Dreyer, I. Kajahn, F. Meyer, S.E.H. Pedersen, J.H. Faber, S. Rüdener, D.C.G. Götz, and to our external partners Prof. Y. Ye (Shanghai Institute of Materia Medica), PD Dr. A. Speicher (Universität des Saarland) who were involved in the work presented in this review.

### LITERATURE CITED

1. Lindon JC, Nicholson JK, Wilson ID. Direct coupling of chromatographic separations to NMR spectroscopy. *Prog NMR Spectrosc* 1996;29:1–49.
2. Wolfender J-L, Hostettmann K. LC/NMR in natural product chemistry. *Curr Org Chem* 1998;2:575–596.
3. Vogler B, Klaiber I, Roos G, Walter CU, Hiller W, Sandor P, Kraus W. Combination of LC-MS and LC-NMR as a tool for the structure determination of natural products. *J Nat Prod* 1998;61:175–178.
4. Bringmann G, Günther C, Schlauer J, Rückert M. HPLC-NMR online coupling including the ROESY technique: direct characterization of naphthylisoquinoline Alkaloids in crude plant extracts. *Anal Chem* 1998;70:2805–2811.
5. Bringmann G, Rückert M, Schlauer J, Herderich M. Acetogenic isoquinoline alkaloids. CXII. Separation and identification of dimeric naphthylisoquinoline alkaloids by liquid chromatography coupled to electrospray ionization mass spectrometry. *J Chromatogr A* 1998; 810:231–236.
6. Mannschreck A. Chiroptical detection during liquid chromatography, Part 4: Applications to stereoanalysis and stereodynamics. *Chirality* 1992;4:163–169.
7. Brandl G, Kastner F, Fritsch R, Zinner H, Mannschreck A. Chiroptical detection during liquid chromatography, Part 5: On-line measurement of circular dichroism spectra during stops of chromatographic flow. *Monatsh Chem* 1992;123:1059–1069.
8. Mannschreck A. On-line measurement of circular dichroism spectra during enantioselective liquid chromatography. *Trends Anal Chem* 1993;12:220–225.
9. Salvadori P, Di Bari L, Pescitelli G. HPLC-CD: Stereochemical analysis at work. In: Nakanishi K, Berova N, Woody RW, editors. *Circular dichroism: principles and application*. New York: VCH Publishers; 2000. p 797–817.
10. McConell O, Bach A II, Balibar C, Byrne N, Cai Y, Carter G, Chlenov M, Di L, Fan K, Goljer I, He Y, Herold D, Kagan M, Kerns E, Koehn F, Kraml C, Marathias V, Marquez B, McDonald L, Nogle L, Petucci C, Schlingmann G, Tawa G, Tischler M, Williamson RT, Sutherland A, Watts W, Young M, Zhang M-Y, Zhang Y, Zhou D, Ho D. Enantiomeric separation and determination of absolute stereochemistry of asymmetric molecules in drug discovery—building chiral technology toolboxes. *Chirality* 2007;19:658–682.
11. Bringmann G, Messer K, Wohlfarth M, Kraus J, Dumbuya K, Rückert M. HPLC-CD on-line coupling in combination with HPLC-NMR and HPLC-MS/MS for the determination of the full absolute stereostructure of new metabolites in plant extracts. *Anal Chem* 1999;71: 2678–2686.
12. Bringmann G, Wohlfarth M, Rischer H, Heubes M, Saeb W, Diem S, Herderich M, Schlauer J. A photometric screening method for dimeric naphthylisoquinoline alkaloids and complete on-line structural elucidation of a dimer in crude plant extracts, by the LC-MS/LC-NMR/LC-CD triad. *Anal Chem* 2001;73:2571–2577.
13. Bringmann G, Lang G. Full absolute novel marine natural products: stereostructures of natural product directly from crude extracts: the HPLC-MS/MS-NMR-CD 'Triad'. In: Müller WEG, editor. *Sponges (Porifera)*. Berlin, Heidelberg: Springer Verlag; 2003. p 89–116.
14. Lightner DA, Gurst JE. *Organic conformational analysis and stereochemistry from circular dichroism spectroscopy*. New York: Wiley-VCH; 2000.
15. Lightner DA. The octant rule. In: Nakanishi K, Berova N, Woody RW, editors. *Circular Dichroism: principles and application*. New York: VCH Publishers; 2000. p 261–304.
16. Berova N, Di Bari L, Pescitelli G. Application of electronic circular dichroism in configurational and conformational analysis of organic compounds. *Chem Soc Rev* 2007;36:914–931.
17. Harada N, Nakanishi K. The exciton chirality method and its application to configurational and conformational studies of natural products. *Acc Chem Res* 1972;5:257–263.
18. Harada N, Nakanishi K. *Circular dichroic spectroscopy—exciton coupling in organic stereochemistry*. Oxford: Oxford University Press; 1983.
19. Berova N, Nakanishi K. Exciton chirality method: principles and applications. In: Nakanishi K, Berova N, Woody RW, editors. *Circular dichroism: principles and applications*. New York: VCH Publishers; 2000. p 337–382.
20. Huang X, Nakanishi K, Berova N. Porphyrins and metalloporphyrins: versatile circular dichroic reporter groups for structural studies. *Chirality* 2000;12:237–255.
21. Huang X, Fujioka N, Pescitelli G, Koehn FE, Williamson RT, Nakanishi K, Berova N. Absolute configurational assignment of secondary amines by cd-sensitive dimeric zinc porphyrin host. *J Am Chem Soc* 2002;124:10320–10335.
22. Harada N, Nakanishi K. *Circular dichroic spectroscopy exciton coupling in organic synthesis*. Mill Valley: University Science Books; 1983.
23. Stephens PJ, McCann DM, Devlin FJ, Smith AB III. Determination of the absolute configuration of natural products via density functional theory calculations of optical rotation, electronic circular dichroism, and vibrational circular dichroism: the cytotoxic sesquiterpene natural products quadrone, suberosenone, subero-



- sanone, and suberosenol A acetate. *J Nat Prod* 2006;69:1055–1064.
24. Enders D, Milovanovic M, Voloshina E, Raabe G, Fleischhauer J. First asymmetric synthesis and determination of the absolute configuration of a lignan isolated from *Virola sebifera*. *Eur J Org Chem* 2005;1984–1990.
25. Diedrich C, Grimme S. Systematic investigation of modern quantum chemical methods to predict electronic circular dichroism spectra. *J Phys Chem A* 2003;107:2524–2539.
26. Sandström J. Determination of absolute configurations and conformations of organic compounds by theoretical calculations of CD spectra. *Chirality* 2000;12:162–171.
27. Bringmann G, Busemann S. The quantum chemical calculation of cd spectra: the absolute configuration of chiral compounds from natural or synthetic origin. In: Schreier P, Herderich M, Humpf HU, Schwab W, editors. *Natural product analysis*. Braunschweig: Vieweg; 1998. p 195–212.
28. Kozłowski M, Dugan EC, DiVirgilio ES, Maksimenka K, Bringmann G. Asymmetric total synthesis of nigerone and *ent*-nigerone: enantioselective oxidative biaryl coupling of highly hindered naphthols. *Adv Synth Cat* 2007;349:583–594.
29. Osswald P, Reichert M, Bringmann G, Würthner F. Perylene Bismide Atropisomers: synthesis, resolution, and stereochemical assignment. *J Org Chem* 2007;72:3403–3411.
30. Xu M, Gessner G, Groth I, Lange C, Christner A, Bruhn T, Deng Z, Li X, Heinemann SH, Grabley S, Bringmann G, Sattler I, Lin W. Shearinines D-K. New indole triterpenoids from an endophytic *Penicillium* sp. (strain HKI0459) with blocking activity on large-conductance calcium-activated potassium channels. *Tetrahedron* 2006;63:435–444.
31. Hölscher D, Reichert M, Görls H, Ohlenschläger O, Bringmann G, Schneider B. Monolaterol, the first configurationally assigned phenylphenalenone derivative with a stereogenic center at C-9, from *Monochoria elata*. *J Nat Prod* 2006;69:1614–1617.
32. Bringmann G, Scharl H, Maksimenka K, Radacki K, Braunschweig H, Wich P, Schmuck C. Atropodistereoselective cleavage of configurationally unstable biaryl lactones with amino acid esters. *Eur J Org Chem* 2006;4349–4361.
33. Ishida K, Maksimenka K, Fritzsche K, Scherlach K, Bringmann G, Hertweck C. The boat-shaped polyketide resistoflavin results from re-facial central hydroxylation of the discoid metabolite resistomycin. *J Am Chem Soc* 2006;128:14619–14624.
34. Sontag B, Rütt M, Spittler P, Arnold N, Steglich W, Reichert M, Bringmann G. Chromogenic meroterpenoids from the mushrooms *Russula ochroleuca* and *R. viscida*. *Eur J Org Chem* 2006;1023–1033.
35. Müller M, Lamottke K, Steglich W, Busemann S, Reichert M, Bringmann G, Spittler P. Biosynthesis and stereochemistry of phlegmacin-type fungal pigments. *Eur J Org Chem* 2004;4850–4855.
36. Hiort J, Maksimenka K, Reichert M, Perović-Ottstadt S, Lin WH, Wray V, Steube K, Schaumann K, Weber H, Proksch P, Ebel R, Müller WEG, Bringmann G. New natural products from the sponge-derived fungus *Aspergillus niger*. *J Nat Prod* 2004;67:1532–1543.
37. Bringmann G, Mühlbacher J, Messer K, Dreyer M, Ebel R, Nugroho BW, Wray V, Proksch P. Cyclorocaglamide, the first bridged cyclopentatetrahydrobenzofuran, and a related “open chain” Rocaglamide derivative from *Aglaia oligophylla*. *J Nat Prod* 2003;66:80–85.
38. Edrada R, Heubes M, Brauers G, Wray V, Berg A, Gräfe U, Wohlfarth M, Mühlbacher J, Schaumann K, Sudarsono S, Bringmann G, Proksch P. Online analysis of xestodecalactones A-C, novel bioactive metabolites from the fungus *Penicillium cf. montanense* and their subsequent isolation from the sponge *Xestospongia exigua*. *J Nat Prod* 2002;65:1598–1604.
39. Meyring M, Mühlbacher J, Messer K, Kastner-Pustet N, Bringmann G, Mannschreck A, Blaschke G. In vitro biotransformation of (*R*)- and (*S*)-thalidomide: application of circular dichroism spectroscopy to the stereochemical characterization of the hydroxylated metabolites. *Anal Chem* 2002;74:3726–3735.
40. Bringmann G, Hinrichs J, Henschel P, Kraus J, Peters K, Peters E-M. Atropo-enantioselective synthesis of the natural bicoumarin (+)-isokotanin A via a configurationally stable biaryl lactone. *Eur J Org Chem* 2002;1096–1106.
41. Feling R, Polborn K, Steglich W, Mühlbacher J, Bringmann G. The absolute configuration of the mushroom metabolites involutin and chamonixin. *Tetrahedron* 2001;57:7857–7863.
42. Bringmann G, Mühlbacher J, Repges C, Fleischhauer J. MD-based CD calculations for the assignment of the absolute axial configuration of the naphthylisoquinoline alkaloid dioncophylline A. *J Comp Chem* 2001;22:1273–1278.
43. Bringmann G, Hamm A, Kraus J, Ochse M, Noureldeen A, Jumbam DN. Gardenamide A from *Rothmannia urcelliformis* (Rubiaceae)—isolation, absolute stereostructure, and biomimetic synthesis from genipin. *Eur J Org Chem* 2001;1983–1987.
44. Dreyer M, Nugroho BW, Bohnenstengel FI, Ebel R, Wray V, Witte L, Bringmann G, Mühlbacher J, Herold M, Hung PD, Kiet LC, Proksch P. New insecticidal rocaglamide derivatives and related compounds from *Aglaia oligophylla*. *J Nat Prod* 2001;64:415–420.
45. Bringmann G, Saeb W, Kraus J, Brun R, François G, Jozimine B, a constitutionally unsymmetric, antiplasmodial “dimer” of the naphthylisoquinoline alkaloid ancistrocladine. *Tetrahedron* 2000;56:3523–3531.
46. Brauers G, Edrada RA, Ebel R, Proksch P, Wray V, Berg A, Gräfe U, Schächtele C, Totzke F, Finkenzeller G, Marne D, Kraus J, Münchbach M, Michel M, Bringmann G, Schaumann K. Anthraquinones and betanone derivatives from the sponge-associated fungus *Microsphaeropsis* species: novel inhibitors of protein kinases. *J Nat Prod* 2000;63:739–745.
47. Buske A, Busemann S, Mühlbacher J, Schmidt J, Porzel A, Bringmann G, Adam G. Revised structure of antidesmone, an unusual alkaloid from tropical Antidesma plants (Euphorbiaceae). *Tetrahedron* 2000;56:3691–3695.
48. Bringmann G, Günther C, Mühlbacher J, Lalith MD, Gunathilake P, Wickramasinghe A. Tropane alkaloids from *Erythroxylum zeylanicum* O.E. Schulz (Erythroxylaceae). *Phytochemistry* 2000;53:409–416.
49. Fleischhauer J, Kosłowski A, Repges C, Gulden K-P, Bringmann G. The absolute configuration of isoancistrocladine and isohamatine by quantum-chemical CD calculations. *Z Naturforschung A* 1998;53:993–996.
50. Tóth G, Simon A, Linker T, Rebień F, Kraus J, Bringmann G. Elucidation of the conformations and absolute configurations of enantiomerically pure tetralin derivatives. *Magn Reson Chem* 1999;37:53–59.
51. Linker T, Rebień F, Tóth G, Simon A, Kraus J, Bringmann G. Convenient catalytic synthesis and assignment of the absolute configuration of enantiomerically pure dihydronaphthalenes and their corresponding epoxides. *Chem Eur J* 1998;4:1944–1951.
52. Bringmann G, Günther C, Busemann S, Schäffer M, Olowokudejo JD, Alo BI. Ancistroguineines A and B as well as ancistrotectorine-naphthylisoquinoline alkaloids from *Ancistrocladus guineensis*. *Phytochemistry* 1997;47:37–43.
53. Hallock YF, Caredellina JH II, Schäffer M, Stahl M, Bringmann G, François G, Boyd MR. Yaoundamines A and B, new antimalarial naphthylisoquinoline alkaloids from *Ancistrocladus korupensis*. *Tetrahedron* 1997;53:8121–8128.
54. Bringmann G, Stahl M, Gulden K-P. Circular dichroism of naphthyl-dihydroisoquinoline alkaloids: determination of the axial configuration of yaoundamine A. *Tetrahedron* 1997;53:2817–2822.
55. Bringmann G, Gulden K-P, Busse H, Fleischhauer J, Kramer B, Zobel E. Circular dichroism of naphthyltetrahydroisoquinoline alkaloids: calculation of CD spectra by semiempirical methods. *Tetrahedron* 1993;49:3305–3312.
56. Fleischhauer J, Kosłowski A, Kramer B, Zobel E, Bringmann G, Gulden K-P, Ortmann T, Peter B. Detection and calculation of the CD spectra from the biaryl alkaloids ancistrocladine and dioncophylline A. *Z Naturforschung B* 1993;48:140–148.
57. Bringmann G, Kajahn I, Reichert M, Pedersen SEH, Faber JH, Gulder T, Brun R, Christensen SB, Ponte-Sucre A, Moll H, Heubl G, Mudogo V. Ancistrocladinium A und B, the first *N,C*-coupled naphthyl-dihydroisoquinoline alkaloids from a congolese *Ancistrocladus* species. *J Org Chem* 2006;71:9348–9356.

58. Bringmann G, Reichert M, Hemberger Y. The absolute configuration of streptonigrin. *Tetrahedron* 2008;64:515–521.
59. Bringmann G, Pabst T, Henschel P, Kraus J, Peters K, Peters E-M, Rycroft DS, Connolly JD. Nondynamic and dynamic kinetic resolution of lactones with stereogenic centers and axes: stereoselective total synthesis of herbertenediol and mastigophorenes A and B. *J Am Chem Soc* 2000;122:9127–9133.
60. Tochtermann W, Kuckling D, Meints C, Kraus J, Bringmann G. Synthesis and absolute configuration of a Bi[10]paracyclophane with two chiral planes and one chiral axis. *Tetrahedron: Asymm* 1999; 10:21–24.
61. Bringmann G, Gulden K-P, Hallock YF, Manfredi KP, Cardellina J II, Boyd MR, Kramer B, Fleischhauer J. Acetogenic isoquinoline alkaloids 63. Circular dichroism of michellamines: independent assignment of axial chirality by calculated and experimental CD spectra. *Tetrahedron* 1994;50:7807–7814.
62. Bringmann G, Kraus J, Schmitt U, Puder C, Zeek A. Determination of the absolute configuration of  $\gamma$ -rubromycin and related spiro compounds by quantum chemical CD calculations. *Eur J Org Chem* 2000;2729–2734.
63. Bringmann G, Ledermann A, Stahl M, Gulden K-P. Novel concepts in directed biaryl synthesis. 53. Bismurrayquinone A: synthesis, chromatographic enantiomer resolution, and stereoanalysis by computational and experimental CD investigations. *Tetrahedron* 1995;51: 9353–9360.
64. Krohn K, Beckmann K, Flörke U, Aust H-J, Dräger S, Schulz B, Busemann S, Bringmann G. Biologically active metabolites from fungi. 9. New palmarumycins CP4a and CP5 from *Coniothyrium palmarum*: structure elucidation, crystal structure analysis and determination of the absolute configuration by CD calculations. *Tetrahedron* 1997;53:3101–3110.
65. Bringmann G, Lang G, Gulder TAM, Tsuruta H, Mühlbacher J, Maksimenka K, Steffens S, Schaumann K, Stöhr R, Wiese J, Imhoff JF, Perovic-Ottstadt S, Boreiko O, Müller WEG. The first sorbicillinoid alkaloids, the antileukemic sorbicillactones A and B, from a sponge-derived *Penicillium chrysogenum* strain. *Tetrahedron* 2005;61:7252–7265.
66. Wanjohi JM, Yenesew A, Midiwo JO, Heydenreich M, Peter MG, Dreyer M, Reichert M, Bringmann G. Three dimeric anthracene derivatives from the fruits of *Bulbine abyssinica*. *Tetrahedron* 2005;61:2667–2674.
67. Govindachari TR, Nagarayan K, Parthasarathy PC, Rajagopalan TG, Desai HK, Chen SL, Nakanishi KJ. Absolute stereochemistry of ancistrocladine and ancistrocladinine. *J Chem Soc Perkin Transl* 1974;12:1413–1417.
68. Bracher F, Eisenreich WJ, Mühlbacher J, Dreyer M, Bringmann G. Saludimerines A and B, novel-type dimeric alkaloids with stereogenic centers and configurationally semistable biaryl axes. *J Org Chem* 2004;69:8602–8608.
69. Dewar MJS, Zebisch EG, Healy EF, Stewart JJP. AM1: a new general purpose quantum mechanical molecular model. *J Am Chem Soc* 1985;107:3902–3909.
70. Stewart JJP. Optimization of parameters for semiempirical methods I. Method J. *Comput Chem* 1989;10:209–220.
71. Stewart JJP. Optimization of parameters for semiempirical methods II. Applications. *J Comput Chem* 1989;10:221–264.
72. Becke AD. Density-functional thermochemistry. III. The role of exact exchange. *J Chem Phys* 1993;98:5648–5652.
73. Lee C, Yang W, Parr RG. Development of the Colle-Salvetti correlation-energy formula into a functional of the electron density. *Phys Rev B* 1988;37:785–789.
74. Hariharan PC, Pople JA. The influence of polarization functions on molecular orbital hydrogenation energies. *Theor Chim Acta* 1973;28: 213–222.
75. Clark M, Crammer RD III, Van Opdenbosch M. Validation of the general purpose Tripos 5.2 force field. *J Comput Chem* 1989;10:982–1012.
76. Allinger NL, Yuh YH, Lii J-H. Molecular mechanics. The MM3 force field for hydrocarbons 1. *J Am Chem Soc* 1989;111:8551–8566.
77. Lii J-H, Allinger NL. Molecular mechanics. The MM3 force field for hydrocarbons. 2. Vibrational frequencies and thermodynamics. *J Am Chem Soc* 1989;111:8566–8575.
78. Lii J-H, Allinger NL. Molecular mechanics. The MM3 force field for hydrocarbons. 3. The van der Waals' potentials and crystal data for aliphatic and aromatic hydrocarbons. *J Am Chem Soc* 1989;111: 8576–8582.
79. Cui W, Li F, Allinger NL. Simulation of conformational dynamics with the MM3 force field: the pseudorotation of cyclopentane. *J Am Chem Soc* 1993;115:2943–2951.
80. Berendsen HJC, Postma JPM, van Gunsteren WF, DiNola A, Haak JR. Molecular dynamics with coupling to an external bath. *J Chem Phys* 1984;81:3684–3690.
81. Condon EU, Altar W, Eyring H. One-electron rotatory power. *J Chem Phys* 1937;5:753–775.
82. Schellman JA. Circular dichroism and optical rotation. *Chem Rev* 1975;75:323–331.
83. Grimme S. Calculation of the electronic spectra of large molecules. In: Lipkowitz KB, Larter R, Cundari TR, editors. *Rev Comput Chem*. New York: Wiley-VCH; 2004. p 153–218.
84. Sherrill CD, Schaefer HF III. The configuration interaction method: advances in highly correlated approaches. In: Löwdin P-O, Sabin JR, Zerner MC, Brändas E, editors. *Adv Quant Chem San Diego*: Academic Press; 1999. p 143–270.
85. Del Bene J, Jaffé HH. Use of the CNDO method in spectroscopy. I. Benzene, pyridine, and the diazines. *J Chem Phys* 1968;48:1807–1813.
86. Del Bene J, Jaffé HH. Use of the CNDO method in spectroscopy. II. Five-membered rings. *J Chem Phys* 1968;48:4050–4055. (c) Ellis RL, Kuehnlenz G, Jaffé HH. Use of the CNDO method in spectroscopy. VI. Further  $n\pi^*$  transitions. *Theor Chim Acta* 1972;26:131–140.
87. Ellis RL, Kuehnlenz G, Jaffé HH. Use of the CNDO method in spectroscopy. VI. Further  $n\pi^*$  transitions. *Theor Chim Acta* 1972;26: 131–140.
88. Weber W, Thiel W. Orthogonalization corrections for semiempirical methods. *Theor Chem Acc* 2000;103:495–506.
89. Levy B, Berthier G. Generalized brillouin theorem for multiconfigurational SCF theories. *Int J Quantum Chem* 1968;2:307–319.
90. Gross EKV, Dobson JF, Petersilka M. Density functional theory of time-dependent phenomena. In: Nalewajski RF, editor. *Top Curr Chem Berlin*: Springer; 1996. p 81–172.
91. Dreuw A, Head-Gordon M. Single-reference ab initio methods for the calculation of excited states of large molecules. *Chem Rev* 2005;105:4009–4037.
92. Becke AD. Density-functional exchange-energy approximation with correct asymptotic behavior. *Phys Rev A* 1988;38:3098–3100.
93. Vahtras O, Almlöf J, Feyereisen MW. Integral approximation for LCAO-SCF calculations. *Chem Phys Lett* 1993;213:514–518.
94. Schäfer A, Huber C, Ahlrichs R. Fully optimized contracted Gaussian basis sets of triple zeta valence quality for atoms Li to Kr. *J Chem Phys* 1994;100:5829–5835.
95. Xinzhou Y, Gulder TAM, Reichert M, Chunping T, Changqiang K, Yang Y. Parvestimins A-D, novel dimeric phenylethyl benzoquinones from *Stemona parviflora* Wright. *Tetrahedron* 2007;63:4688–4694.
96. Guangdong Institute of Botany. *Flora of Hainan*. Beijing (P. R. China): Sciences Press; 1977. p 148.
97. Jiangsu New Medical College. *The Dictionary of Traditional Chinese Medicine*, Shanghai (P. R. China): Science and Technology Press; 1986. p 860.
98. Xu GJ, He HX, Xu LS, Jin RY. *The Chinese materia medica (Zhonghua Bencao)*. Beijing (P. R. China): Chinese Medicinal Science and Technology Publishing House; 1996. p 467–472.
99. Bringmann G, Günther C, Ochse M, Schupp O, Tasler S. Biaryls in nature: a multi-faceted class of stereochemically, biosynthetically, and pharmacologically intriguing secondary metabolites. In: Herz W, Falk H, Kirby GW, Moore RE, editors. *Progr Chem Org Nat Prod Wien*: Springer; 2001. p 1–249.
100. Cass QB, Tiritan E, Matlin SA, Freire EC, Gossypol enantiomer ratios in cotton seeds. *Phytochemistry* 1991;30:2655–2657.

101. Bringmann G, Tasler S, Endress H, Kraus J, Messer K, Wohlfarth M, Lobin W. Murrastifoline-F: first total synthesis, Atropo-enantiomer resolution, and stereoanalysis of an axially chiral *N,C*-coupled biaryl alkaloid. *J Am Chem Soc* 2001;123:2703–2711.
102. Zinsmeister HD, Becker H, Eicher T. Bryophytes, a source of biologically active, naturally occurring material? *Angew Chem Int Ed Engl* 1991;30:130–147.
103. Asakawa Y. Chemosystematics of the hepaticae. *Phytochemistry* 2004;65:623–669.
104. Geserü GM, Nógrádi M. The chemistry of macrocyclic bis(bibenzyls). *Nat Prod Rep* 1995;12:69–75.
105. Hashimoto T, Kanayama S, Kan Y, Tori M, Asakawa Y. Isoplagiochins C and D, new type of macrocyclic bis(bibenzyls), having two biphenyl linkages from the liverwort *Plagiochila fruticosa*. *Chem Lett* 1996;741–742.
106. Scher JM, Zapp J, Schmidt A, Becker H, Bazzanins L-R, chlorinated macrocyclic bisbibenzyls from the liverwort *Lepidozia incurvata*. *Phytochemistry* 2003;64:791–796.
107. Hashimoto T, Irita H, Takaoka S, Tanaka M, Asakawa Y. New chlorinated cyclic bis(bibenzyls) from the liverworts *Herbertus sakuraii* and *Mastigophora diclados*. *Tetrahedron* 2000;56:3153–3159.
108. Asakawa Y, Toyota M, Tori M, Hashimoto T. Chemical structures of macrocyclic bis(bibenzyls) isolated from liverworts (Hepaticae). *Spectroscopy* 2000;14:149–175.
109. Bringmann G, Mühlbacher J, Reichert M, Dreyer M, Kolz J, Speicher A. Stereochemistry of isoplagiochin c, a macrocyclic bisbibenzyl from liverworts. *J Am Chem Soc* 2004;126:9283–9290.
110. Scher JM, Zapp J, Becker H, Kather N, Kolz J, Speicher A, Dreyer M, Maksimenka K, Bringmann G. Optically active bisbibenzyls from *Bazzania trilobata*: isolation and stereochemical analysis by chromatographic, chiroptical, and computational methods. *Tetrahedron* 2004;60:9877–9881.
111. Bringmann G, Pokorny F. The naphthylisoquinoline alkaloids. In: Cordell GA, editor. *The alkaloids*. New York: Academic Press; 1995. p 127–271.
112. Bringmann G, François G, Aké Assi L, Schlauer J. The alkaloids of *Triphyophyllum peltatum*. *Chimia* 1998;52:18–28.
113. Yang LK, Glover R, Yoganathan K, Sarnaik JP, Godbole AJ, Soejarto DD, Buss AD, Butler MS. Ancisheynine, a novel naphthylisoquinolinium alkaloid from *Ancistrocladus heyneanus*. *Tetrahedron Lett* 2003;44:5827–5829.
114. Bringmann G, Gulder T, Reichert M, Meyer F. Ancisheynine, the first *N,C*-coupled naphthylisoquinoline alkaloid: total synthesis and stereochemical analysis. *Org Lett* 2006;8:1037–1040.
115. Bringmann G, Kajahn I, Reichert M, Pedersen SEH, Faber JH, Gulder T, Brun R, Christensen SB, Ponte-Sucre A, Moll H, Heubl G, Mudogo V. Ancistrocladinium A and B, the first *N,C*-coupled naphthylidihydroisoquinoline alkaloids, from a congolese *Ancistrocladus* species. *J Org Chem* 2006;71:9348–9356.
116. Bringmann G, Teltschik F, Michel M, Busemann S, Rückert M, Haller R, Bär S, Robertson A, Kaminsky R. Ancistrobertsonines B, C, and D as well as 1,2-didehydroancistrobertsonine D from *Ancistrocladus robertsoniorum*. *Phytochemistry* 1999;52:321–332.
117. Bringmann G, Gulden KP, Hallock YF, Manfredi KP, Cardellina JH II, Boyd MR, Kramer B, Fleischhauer J. Circular dichroism of michellamines: independent assignment of axial chirality by calculated and experimental CD spectra. *Tetrahedron* 1994;50:7807–7813.
118. Bringmann G, God R, Schäffer M. An improved degradation procedure for determination of the absolute configuration in chiral isoquinoline and  $\beta$ -carboline derivatives. *Phytochemistry* 1996;43:1393–1403.
119. Bringmann G, Rüdener S, Götz DCG, Gulder TAM, Reichert M. Axially chiral directly  $\beta,\beta$ -linked bisporphyrins: synthesis and stereostructure. *Org Lett* 2006;8:4743–4746.
120. Bringmann G, Messer K, Wolf K, Mühlbacher J, Grüne M, Brun R, Louis AM. Dioncophylline E from *Dioncophyllum thollonii*, the first 7,3'-coupled dioncophyllaceous naphthylisoquinoline alkaloid. *Phytochemistry* 2002;60:389–397.
121. Bringmann G, Feineis D, God R, Maksimenka K, Mühlbacher J, Messer K, Münchbach M, Gulden K-P, Peters E-M, Peters K. Resolution and chiroptical properties of the neurotoxin 1-trichloromethyl-1,2,3,4-tetrahydro- $\beta$ -carboline (TaClo) and related compounds: quantum chemical CD calculations and X-ray diffraction analysis. *Tetrahedron* 2004;60:8143–8151.
122. Goel A, Singh FV, Kumar V, Reichert M, Gulder TAM, Bringmann G. Synthesis, optical resolution, and configurational assignment of novel axially chiral quateraryls. *J Org Chem* 2007;72:7765–7768.
123. Bringmann G, Gulder TAM, Maksimenka K, Kuckling D, Tochtermann W. A borderline case between *meso* and stable C1: an axially chiral, yet configurationally semi-stable biphenyl with two oppositely configured [10]paracyclophane portions. *Tetrahedron* 2005;61:7241–7246.
124. Bringmann G, Kraus J, Menche D, Messer K. Elucidation of the absolute configuration of knipholone and knipholone anthrone by quantum chemical CD calculations. *Tetrahedron* 1999;55:7563–7572.
125. Bringmann G, Maksimenka K, Mutanyatta-Comar J, Knauer M, Bruhn T. The absolute axial configurations of knipholone and knipholone anthrone by TDDFT and DFT/MRCI CD calculations: a revision. *Tetrahedron* 2007;63:9810–9824.



## Review Article

# The Determination of the Absolute Configurations of Chiral Molecules Using Vibrational Circular Dichroism (VCD) Spectroscopy

PHILIP J. STEPHENS,\* FRANK J. DEVLIN, AND JIAN-JUNG PAN

*Department of Chemistry, University of Southern California, Los Angeles, CA 90089-0482*

**ABSTRACT** The vibrational circular dichroism (VCD) spectra of the two enantiomers of a chiral molecule are of equal magnitude and opposite sign: i.e. mirror-image enantiomers give mirror-image VCD spectra. In principle, the absolute configuration (AC) of a chiral molecule can therefore be determined from its VCD spectrum. In practice, the determination of the AC of a chiral molecule from its experimental VCD spectrum requires a methodology which reliably predicts the VCD spectra of its enantiomers. The only reliable methodology developed to date uses the Stephens quantum-mechanical theory of the rotational strengths of fundamental vibrational transitions, developed in the early 1980s, implemented using *ab initio* density functional theory in the GAUSSIAN program in the mid 1990s. This methodology has by now been widely used in determining ACs from experimental VCD spectra. In this article we discuss the protocol for determining the ACs of chiral molecules with optimum reliability and its implementation for a variety of molecules, including the  $D_3$  symmetry perhydrotriphenylene, a thiazino-oxadiazolone recently shown to be a highly active calcium entry channel blocker, the alkaloid natural products schizogyne, iso-schizogaline, and iso-schizogamine, and the iridoid natural products plumericin, iso-plumericin, and prismatomerin. The power of VCD spectroscopy in determining ACs, even for large organic molecules and for substantially conformationally-flexible organic molecules is clearly documented. *Chirality* 20:643–663, 2008. © 2007 Wiley-Liss, Inc.

**KEY WORDS:** absolute configuration; density functional theory; vibrational circular dichroism

## INTRODUCTION

Chiral organic molecules are currently of widespread interest to organic chemists and pharmaceutical chemists. Chiral drugs—e.g., omeprazole—are of increasing importance in the pharmaceutical industry. Since the two enantiomers of a chiral drug generally possess different pharmaceutical activities, the resolution and clinical testing of both enantiomers is prerequisite to the development of the optimum drug. The increasing importance of chiral drugs has stimulated the development of improved techniques, especially chromatographic, for the resolution of racemic mixtures of chiral molecules, and of new asymmetric synthesis methods. In addition to synthetic chiral molecules, naturally occurring molecules (“natural products”), which are invariably chiral and generally enantiomerically enriched, are of increasing interest as drugs, or leads for new drugs. Many natural products have been used in folk medicine for centuries and such molecules are now receiving increasing attention.

As a consequence of the increasing attention to chiral organic molecules, methods for the structural characterization of chiral molecules are of increasing importance. The

absolute configuration (AC) and conformations of a chiral molecule are important factors in determining its pharmaceutical activity. While X-ray crystallography and NMR spectroscopy are powerful techniques for structural determination, their application to the determination of ACs and to conformational analysis is limited. The Bijvoet method for determining ACs using X-ray crystallography requires the presence of a “heavy” atom. NMR spectra are not enantiomerically sensitive and cannot be used to determine ACs. As a consequence, chiroptical spectroscopy is widely used by organic chemists in determining ACs and for conformational analysis.

The famous chirality-sensitive optical properties of chiral molecules are optical rotation (OR) and circular dichroism

Contract grant sponsor: National Science Foundation (NSF); Contract grant numbers: CHE-0209957, CHE-0614577.

\*Correspondence to: P. J. Stephens, Department of Chemistry, University of Southern California, University Park Campus, Los Angeles, CA 90089-0482, USA.

E-mail: pstephen@usc.edu

Received for publication 22 June 2007; Accepted 8 August 2007

DOI: 10.1002/chir.20477

Published online 22 October 2007 in Wiley InterScience (www.interscience.wiley.com).



(CD).<sup>1-4</sup> OR originates in the difference in the refractive indices of left- and right-circularly polarized light ( $n_L$  and  $n_R$ ). CD is the differential absorption of left- and right-circularly polarized light:  $\Delta A = A_L - A_R$ . First measured by Cotton in 1895, CD is often referred to as the Cotton effect (CE). Both the OR and CD of a chiral molecule are frequency-dependent; measurement of OR and CD over a range of frequencies gives optical rotatory dispersion (ORD) and CD spectra. The ORD and CD spectra of the two enantiomers of a chiral molecule are of equal magnitude and opposite sign: i.e., mirror-image enantiomers give mirror-image ORD and CD spectra. Consequently, the AC of a chiral molecule can in principle be determined from its ORD and/or CD spectrum.

The use of ORD and CD for the characterization of the stereochemistries of chiral organic molecules expanded rapidly after World War II as a result of the development of improved instrumentation for the measurement of ORD and CD spectra<sup>1,2,5</sup> and of "Sector Rules" correlating the signs of ORD and CD spectra with ACs. The most famous sector Rule was the "Octant Rule", which predicts the sign of the ORD and CD of the  $n \rightarrow \pi^*$  electronic excitations of carbonyl groups.<sup>6</sup>

Historically, the applications of ORD and CD spectroscopies have been predominantly in the visible-ultraviolet spectral region. ORD and CD in this region originate in electronic excitations. In the 1970s, the question arose: Can ORD and CD, originating in vibrational excitations, be measured in the infrared (IR) spectral region? The measurement of IR ORD was first attempted, but was unsuccessful.<sup>7,8</sup> At USC, in the late 1960s, we had built a CD instrument operating in the visible-near-IR spectral region (down to  $\sim 3300 \text{ cm}^{-1}$ ), whose principal purpose was the measurement of electronic magnetic CD spectra.<sup>9</sup> In 1973 extension of the frequency limit of this instrument to lower frequencies led to our first measurements of VCD spectra.<sup>10-14</sup> Key to this breakthrough was our construction of a new photoelastic modulator with a ZnSe optical element, transmitting down to  $\sim 650 \text{ cm}^{-1}$ .<sup>15</sup> Since then, VCD instrumentation has developed in both frequency range and sensitivity. Currently, Fourier transform (FT) VCD instruments are commercially available (FT VCD instruments are currently manufactured by Bomem, Bruker, Jasco, and Varian).

After it was shown that VCD spectra could be measured, the utilization of VCD spectroscopy by organic chemists for the stereochemical characterization of chiral molecules required the development of a methodology permitting the relationship between the structure of a molecule and its VCD spectrum to be predicted. The intensity of the CD of the vibrational transition  $i \rightarrow f$  is determined by its rotational strength:

$$R(i \rightarrow f) = \text{Im} \left[ \langle i | \bar{\mu}_{\text{el}} | f \rangle \cdot \langle f | \bar{\mu}_{\text{mag}} | i \rangle \right] \quad (1)$$

where  $\bar{\mu}_{\text{el}}$  and  $\bar{\mu}_{\text{mag}}$  are the electric dipole and magnetic dipole operators respectively. The electric dipole transition moment,  $\langle i | \bar{\mu}_{\text{el}} | f \rangle$  simultaneously determines the dipole strength of the transition:

Chirality DOI 10.1002/chir

$$D(i \rightarrow f) = \left| \langle i | \bar{\mu}_{\text{el}} | f \rangle \right|^2 \quad (2)$$

which determines the unpolarized absorption intensity of the transition (i.e., its intensity in the standard IR spectrum). Within the Born-Oppenheimer approximation for the electronic and vibrational wave functions and the harmonic approximation for the vibrational motion,  $\langle i | \bar{\mu}_{\text{el}} | f \rangle$  for the fundamental transition of the  $i$ th normal mode is given by

$$\langle 0 | (\mu_{\text{el}})_{\beta} | 1 \rangle_i = \left( \frac{\hbar}{4\pi v_i} \right)^{1/2} \sum_{\lambda\alpha} S_{\lambda\alpha,i} P_{\alpha\beta}^{\lambda} \quad (3)$$

where  $v_i$  is the harmonic frequency of the  $i$ th mode, the  $S_{\lambda\alpha,i}$  matrix defines the relationship between its normal coordinate  $Q_i$  and the Cartesian displacement coordinates,  $X_{\lambda\alpha}$  ( $\lambda$  = nucleus;  $\alpha$  =  $x, y, z$ ):

$$X_{\lambda\alpha} = \sum_i S_{\lambda\alpha,i} Q_i \quad (4)$$

and  $P_{\alpha\beta}^{\lambda}$  is the atomic polar tensor (APT), given by

$$P_{\alpha\beta}^{\lambda} = \left( \frac{\partial (\mu_{\text{el}}^G)_{\beta}}{\partial X_{\lambda\alpha}} \right)_0 \quad (5)$$

where  $\bar{\mu}_{\text{el}}^G$  is the electric dipole moment of the ground electronic state,  $G$ , and  $\left( \frac{\partial (\mu_{\text{el}}^G)_{\beta}}{\partial X_{\lambda\alpha}} \right)_0$  is its derivative with respect to  $X_{\lambda\alpha}$  at the equilibrium geometry  $\bar{R}_0$ .  $P_{\alpha\beta}^{\lambda}$  is the sum of electronic and nuclear contributions,  $E_{\alpha\beta}^{\lambda}$  and  $N_{\alpha\beta}^{\lambda}$ :

$$\begin{aligned} P_{\alpha\beta}^{\lambda} &= E_{\alpha\beta}^{\lambda} + N_{\alpha\beta}^{\lambda} \\ E_{\alpha\beta}^{\lambda} &= 2 \left\langle \left( \frac{\partial \psi_G}{\partial X_{\lambda\alpha}} \right)_0 \left| (\mu_{\text{el}}^e)_{\beta} \right| \psi_G^0 \right\rangle \\ N_{\alpha\beta}^{\lambda} &= (Z_{\lambda} e) \delta_{\alpha\beta} \end{aligned} \quad (6)$$

where  $(\partial \psi_G / \partial X_{\lambda\alpha})_0$  is the derivative of the ground state electronic wave function with respect to  $X_{\lambda\alpha}$  at  $\bar{R}_0$  and  $\bar{\mu}_{\text{el}}^e$  is the electronic contribution to the electric dipole moment operator. Prediction of vibrational dipole strengths and IR spectra thus requires the calculation of the frequencies and normal coordinates of the  $3N - 6$  ( $N$  = number of nuclei) normal modes and of the APTs.

To predict vibrational rotational strengths and VCD spectra, the magnetic dipole transition moments must also be calculated. At the time of the earliest VCD measurements, no quantum-mechanical equation for magnetic dipole vibrational transition moments existed, and quantum-mechanically rigorous calculations of vibrational rotational strengths were impossible. Fortunately for the development of VCD spectroscopy, such an equation was soon developed by Stephens.<sup>16-18</sup> The Stephens equation for the magnetic dipole transition moment of the fundamental transition of the  $i$ th normal mode within the harmonic approximation is:

$$\langle 0 | (\mu_{\text{mag}})_{\beta} | 1 \rangle_i = \left( 4\pi \hbar^3 v_i \right)^{1/2} \sum_{\lambda\alpha} S_{\lambda\alpha,i} M_{\alpha\beta}^{\lambda} \quad (7)$$



where  $M_{\alpha\beta}^{\lambda}$  are atomic tensors, termed atomic axial tensors by Stephens, and given by:

$$\begin{aligned} M_{\alpha\beta}^{\lambda} &= I_{\alpha\beta}^{\lambda} + J_{\alpha\beta}^{\lambda} \\ I_{\alpha\beta}^{\lambda} &= \left\langle \left( \frac{\partial \psi_G}{\partial X_{\lambda\alpha}} \right)_0 \left| \left( \frac{\partial \psi_G}{\partial H_{\beta}} \right)_0 \right. \right\rangle \\ J_{\alpha\beta}^{\lambda} &= \frac{i}{4\hbar c} \sum_{\gamma} (Z_{\lambda} e) R_{\lambda\gamma}^0 \epsilon_{\alpha\beta\gamma} \end{aligned} \quad (8)$$

where  $I_{\alpha\beta}^{\lambda}$  and  $J_{\alpha\beta}^{\lambda}$  are the electronic and nuclear contributions to  $M_{\alpha\beta}^{\lambda}$ , and  $(\partial \psi_G / \partial H_{\beta})_0$  is the derivative of the ground state electronic wave function of the molecule in the presence of the external magnetic field perturbation  $\sum_{\beta} -(\mu_{\text{mag}}^e)_{\beta} H_{\beta}$  with respect to  $H_{\beta}$ , where  $\mu_{\text{mag}}^e$  is the electronic magnetic dipole moment operator. Compared to the calculation of APTs, the calculation of AATs requires simply the additional calculation of the magnetic field derivatives  $(\partial \psi_G / \partial H_{\beta})_0$ . Combining eqs 1, 3, and 7 gives the Stephens equation for the vibrational rotational strength of the fundamental transition,  $0 \rightarrow 1$ , of the  $i$ th normal mode:

$$R(0 \rightarrow 1)_i = \hbar^2 \sum_{\beta} \sum_{\lambda\alpha, \lambda'\alpha'} (S_{\lambda\alpha, i} P_{\alpha\beta}^{\lambda}) (S_{\lambda'\alpha', i} M_{\alpha'\beta}^{\lambda'}) \quad (9)$$

At the time of the development of the Stephens equation for vibrational rotational strengths, the most accurate predictions of IR spectra were being made using ab initio methods for the prediction of vibrational force fields, frequencies and normal coordinates and of APTs. It was therefore clear that the most accurate predictions of VCD spectra would require ab initio vibrational force fields, frequencies and normal coordinates, and APTs and AATs. From the beginning, therefore, the implementation of the Stephens equation has been carried out using ab initio methods. The first implementations used the Hartree-Fock (HF)/self-consistent field (SCF) methodology, within the ab initio programs GAUSSIAN and CADPAC.<sup>17,19–23</sup> Over the next decade it became clear that considerable improvement in the accuracy of VCD spectra, calculated using ab initio methods, would result from the use of methods more accurate than the HF/SCF method.<sup>24–30</sup> In 1996, this expectation led to the application of density functional theory (DFT) to the calculation of AATs, using GIAOs (in order to give origin-independent rotational strengths) by Drs. J.R. Cheeseman and M.J. Frisch at Gaussian, Inc., within the GAUSSIAN program.<sup>31,32</sup> Together with the calculation of vibrational force fields and APTs using DFT, and thence vibrational dipole strengths and IR spectra, which had been available since 1992, this development permitted the prediction of vibrational rotational strengths and VCD spectra using DFT. Comparison of DFT and HF/SCF VCD spectra for molecules whose experimental VCD spectra were available showed clearly that the DFT VCD spectra were much more accurate, as long as state-of-the-art density functionals were used for the DFT calculations.<sup>31–36</sup> As a result, the DFT method has become the basis for all calculations of VCD spectra, using the Stephens equation for vibrational rotational strengths.

In order to reliably determine the AC of a chiral molecule by comparison of its experimental VCD spectrum to the VCD spectra of the two enantiomers, calculated using the Stephens equation and DFT, a basis set giving minimal basis set error and a density functional as close to the exact functional in accuracy as possible are required. The relative accuracies of different basis sets and functionals in predicting VCD spectra have been evaluated using a number of conformationally-rigid molecules, including methyl-oxirane, camphor, fenchone, and  $\alpha$ -pinene.<sup>33–35,37</sup> It has been shown that the basis sets TZ2P and cc-pVTZ are close to the complete basis set limit, while much smaller basis sets such as 6-31G\* are substantially less accurate. In addition, it has been shown that Becke-hybrid density functionals, such as B3PW91 and B3LYP, give much more accurate VCD spectra than local and gradient-corrected pure functionals, such as LSDA and BLYP. Consequently, optimum choices of basis set and functional are TZ2P/cc-pVTZ and B3PW91/B3LYP. These basis sets and functionals have been used in the determinations of the ACs of chiral organic molecules discussed in the following section.

Organic molecules are frequently conformationally-flexible: i.e., at room temperature, the temperature at which experimental VCD spectra are measured, multiple conformations are present in equilibrium. In the case of a conformationally-flexible molecule, prediction of the VCD spectrum requires conformational analysis to be carried out: i.e., the prediction of the geometries, relative free energies and equilibrium populations of the populated conformations. The VCD spectra of the populated conformations are then calculated and weighted by the conformational populations and summed to predict the “conformationally-averaged VCD spectrum”. The reliability of this spectrum is dependent on the accuracy of the conformational analysis; if the number of populated conformations is incorrectly predicted and if the relative free energies and equilibrium populations are inaccurately predicted, the predicted VCD spectrum is less accurate than that of a conformationally-rigid molecule. At the present time, the optimum conformational analysis procedure for large flexible organic molecules is the following: (1) a molecular mechanics force field (MMFF) is used to identify the stable conformations of the molecule with energies within at least 20 kcal/mol of the global minimum conformation; (2) the MMFF conformations are then optimized using DFT (with the same basis sets and functionals to be used for VCD calculations), and their harmonic frequencies calculated to prove that the conformations are stable and to permit the calculation of their free energies. This protocol has been utilized in the determinations of the ACs of conformationally-flexible chiral organic molecules discussed in the following sections.

## HOW TO DETERMINE THE AC OF A CHIRAL ORGANIC MOLECULE USING VCD SPECTROSCOPY

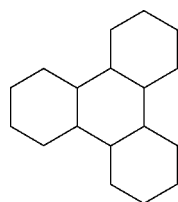
First, the experimental VCD spectrum of a solution of an enantiomer of the molecule of known OR is measured in the mid-IR spectral region, together with the corresponding IR spectrum, using a solution of sufficiently dilute concentration that Beer’s law is obeyed, guaranteeing

the absence of contributions to the IR and VCD spectra from molecular aggregates. Second, conformational analysis of the molecule is carried out to determine the number, structures, relative free-energies, and populations of the conformations in equilibrium at room temperature (the temperature at which the experimental IR and VCD spectra are measured). Third, the harmonic vibrational frequencies, dipole strengths, and rotational strengths of the fundamental transitions of all significantly-populated conformations are predicted using DFT, and the IR and VCD spectra obtained thence, using Lorentzian band shapes (since the band shapes of vibrational transitions of molecules in liquid solutions are Lorentzian). The IR and VCD spectra of each conformation are then weighted by its predicted equilibrium population and the population-weighted spectra of all conformations summed, giving the “conformationally-averaged” IR and VCD spectra. Fourth, the predicted IR spectrum is used to assign the experimental IR spectrum, automatically leading to the assignment of the experimental VCD spectrum (since the IR and VCD of each fundamental transition occur at identical frequencies). Fifth, the predicted VCD spectra of the two enantiomers are compared to the experimental VCD spectrum. The VCD spectrum of the enantiomer with the same AC as the experimental enantiomer should be in excellent agreement with the experimental VCD spectrum and the VCD spectrum of the enantiomer with opposite AC should exhibit zero agreement. The comparison of the calculated and experimental VCD spectra thus defines the AC of the experimental enantiomer. Sixth, to define the quantitative agreement of the calculated and experimental VCD spectra, the calculated and experimental rotational strengths of the transitions whose VCD is observed are compared. The experimental rotational strengths are obtained by Lorentzian fitting of the experimental VCD spectrum (in solutions obeying Beer’s law vibrational band shapes are Lorentzian). The reliability of the AC deduced from the VCD spectrum is quantitatively established by comparison of the quantitative agreement of the calculated rotational strengths of the two enantiomers with the experimental rotational strengths.

To illustrate this procedure, we discuss the determination of the ACs of the chiral alkane anti-trans-anti-trans-anti-trans perhydrotriphenylene, **1**, and the chiral thiazino-oxadiazol-3-one, **2**.

### Perhydrotriphenylene, **1**

The perhydroderivative of triphenylene, **1**, has  $D_3$  symmetry and is therefore chiral.



**1**

Optically-active **1** was first synthesized by Farina and Audisio<sup>38,39</sup> and its AC assigned as  $R(-)/S(+)$  by calculation of its  $[\alpha]_D$ , and by conversion to a keto-derivative whose AC was determined using its CE and the octant rule. Very recently, gas chromatography was applied by Schürch et al. to the resolution of PHTP.<sup>40</sup> We have redetermined the AC of PHTP using VCD spectroscopy, using a sample of (+)-**1** with ee 93.5%, obtained using gas chromatography by Schürch and Hulliger.<sup>41</sup> The mid-IR and VCD spectra of a  $CCl_4$  solution of (+)-**1** are shown in Figure 1.

Conformational analysis of **1** using the MMFF94 force field finds four conformations **a–d**; in the lowest energy conformation, **a**, all cyclohexane rings have a chair conformation; in each of the higher energy conformations, one of the peripheral cyclohexane rings has a twisted-boat conformation. B3LYP/6-31G\* DFT reoptimization of the MMFF94 conformations **a–d**, followed by harmonic frequency calculations, leads to the relative energies and free-energies of the four conformations and, thence, using Boltzmann statistics, to their room-temperature equilibrium populations. Conformation **a** is predicted to be >99% of the equilibrium mixture; thus, **1** is predicted to be effectively a conformationally-rigid molecule.

DFT calculations of the IR and VCD spectra of conformation **a** of **1** have been carried out using the B3LYP and

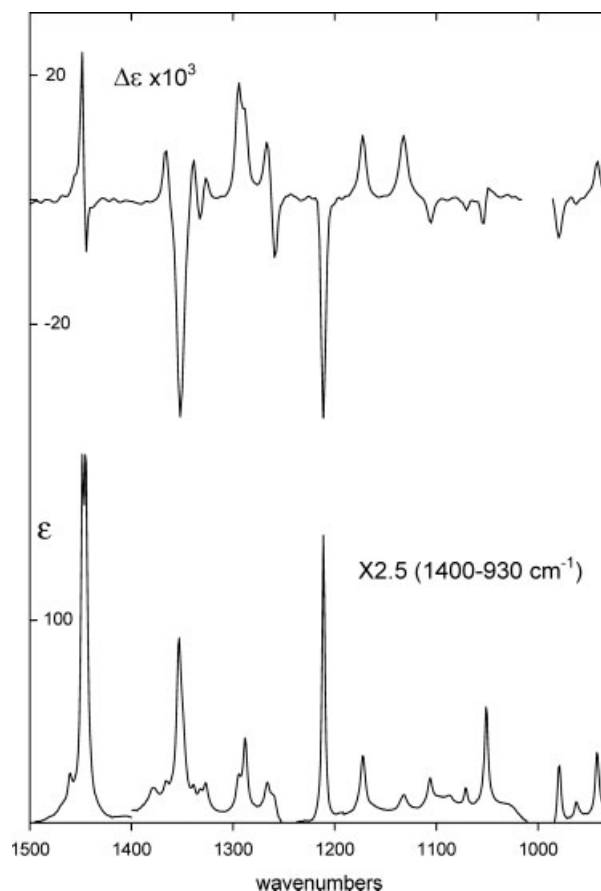


**Fig. 1.** The experimental IR and VCD spectra of (+)-**1** in  $CCl_4$  solution (0.0765 M). The VCD spectrum is normalized to 100% ee.

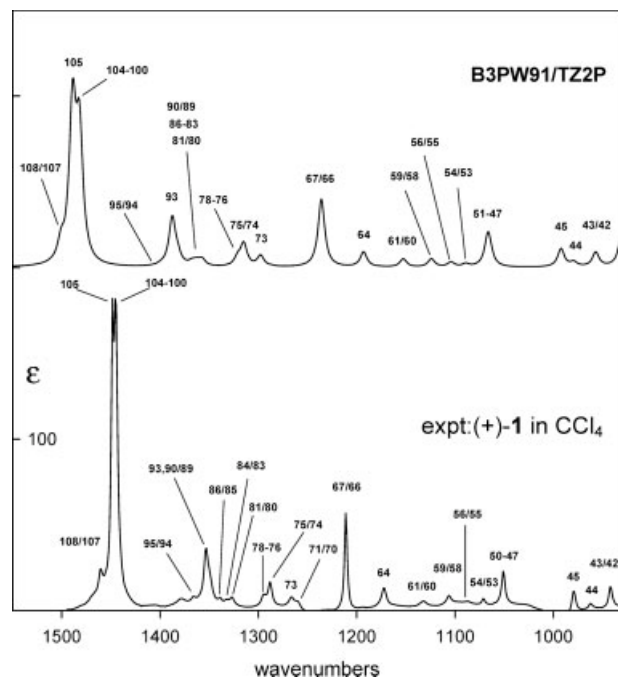
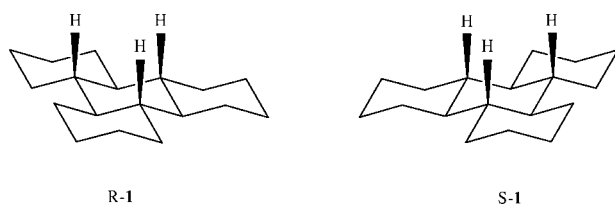


**Fig. 2.** Comparison of the B3PW91/TZ2P and experimental IR spectra of **1**. The band shapes of the calculated spectra are Lorentzian ( $\gamma = 4.0 \text{ cm}^{-1}$ ). The numbers define the fundamental modes of **1** contributing to the spectral bands.

B3PW91 functionals and the 6-31G\* and TZ2P basis sets. Comparison of the predicted IR spectra to the experimental IR spectrum showed that the best agreement with experiment was produced by the combination of B3PW91 and TZ2P. The B3PW91/TZ2P IR spectrum is compared to the experimental IR spectrum in Figure 2 and leads to unequivocal assignment of the experimental spectrum, as detailed in Figure 2. (Note that the calculated frequencies are higher by a few percent than the experimental frequencies, due to the neglect of anharmonicity in the calculations.) This, in turn, leads to the assignment of all of the bands in the VCD spectrum with frequencies identical to bands in the IR spectrum. Comparison of the B3PW91/TZ2P VCD spectra of the two enantiomers of conformation **a** of **1**,



to the experimental VCD spectrum of (+)-**1**, shown in Figure 3, leads unambiguously to the conclusion that *S* is the AC of (+)-**1**. The detailed assignment of the experimental VCD spectrum, based on the B3PW91/TZ2P assignment of the IR spectrum and the B3PW91/TZ2P VCD spectrum is shown in Figure 3. The rotational strengths of the observed VCD bands are then determined by Lorentzian fitting of the experimental VCD spectrum. Comparison to

the sums of the B3PW91/TZ2P rotational strengths of *R*-**1** and *S*-**1** for the fundamental transitions assigned to the experimental VCD bands is shown in Figure 4. The agreement of the *S*-**1** rotational strengths with the experimental rotational strengths of (+)-**1** is nearly perfect, while the agreement of the *R*-**1** rotational strengths is as bad as can be. This comparison thus definitively establishes that the AC of (+)-**1** is *S*. In addition, it supports the prediction that only conformation **a** is significantly populated, and proves that the B3PW91 functional is a very accurate functional and that the TZ2P basis set is an excellent approximation to the complete basis set. The importance of the use of a basis set leading to rotational strengths with little basis set error is emphasized by comparison of the rotational strengths of *S*-**1** predicted by B3PW91 with the 6-31G\* basis set to the experimental rotational strengths of (+)-**1**, shown in Figure 5.

The AC of (+)-**1**, determined using VCD, is the same as that assigned by Farina and Audisio.<sup>38,39</sup> At this time, there is no longer any uncertainty in the AC of **1**.

**8-(4-Br-phenyl), 8-ethoxy, 5-methyl,  
8*H*-[1,4]thiazino-[3,4-*c*][1,2,4] oxadiazol-3-one, 2**

A range of thiazino-oxadiazolones were recently synthesized by Budriesi et al., and their activities as calcium

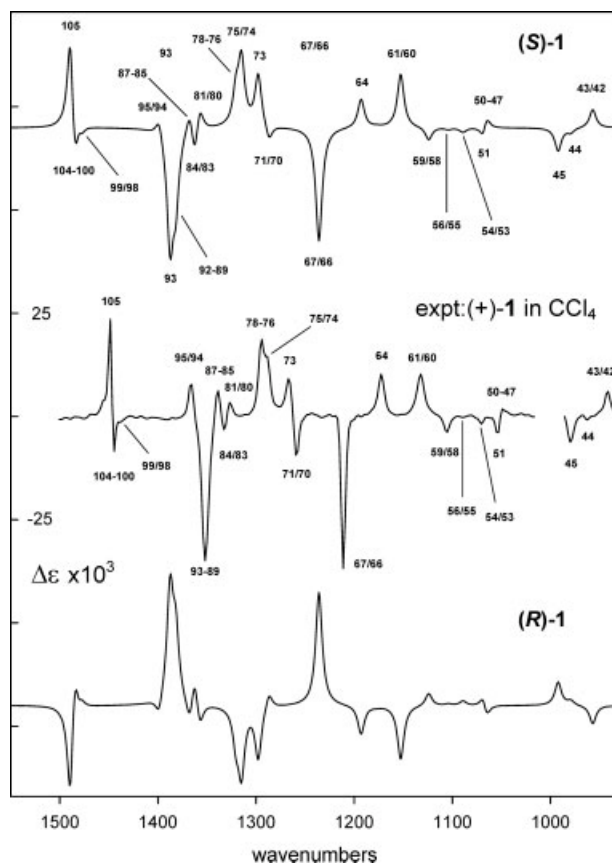


**Fig. 3.** Comparison of the B3PW91/TZ2P spectra of *S*-**1** and *R*-**1** to the experimental VCD spectrum of (+)-**1**. The band shapes of the calculated spectra are Lorentzian ( $\gamma = 4.0 \text{ cm}^{-1}$ ). The numbers define the fundamental modes of **1** contributing to the spectral bands.

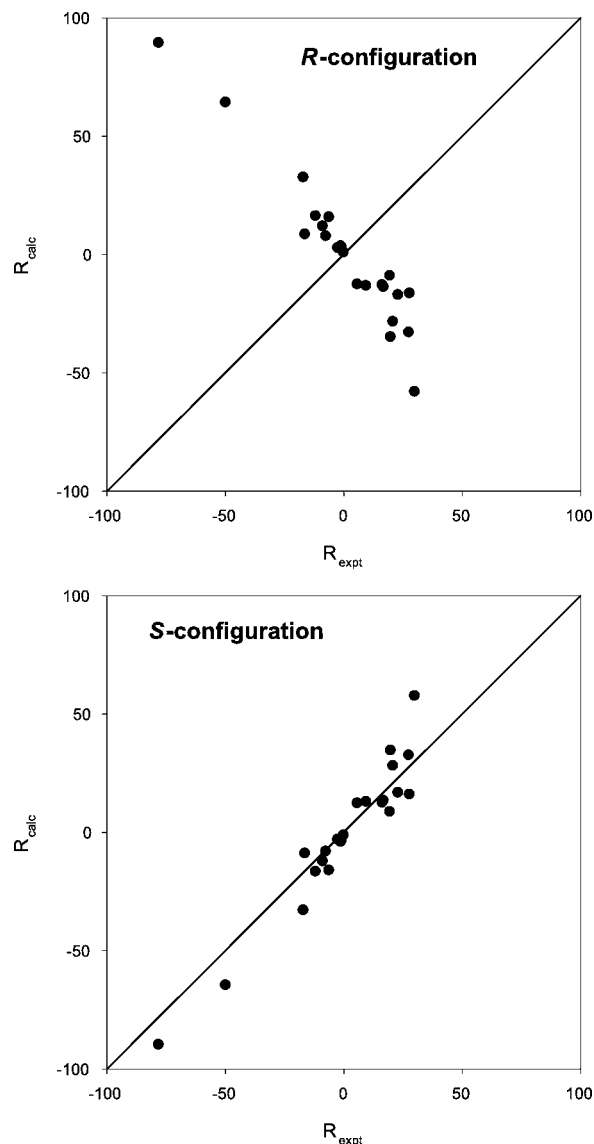
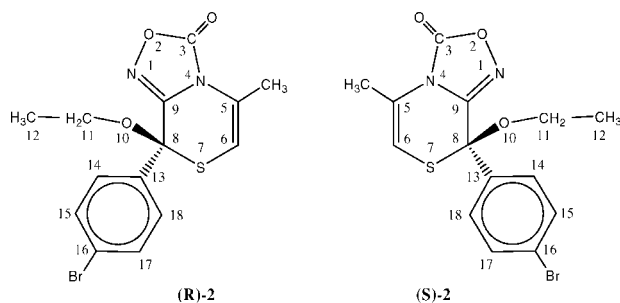


**Fig. 4.** Comparison of calculated rotational strengths for (*R*)-**1** and (*S*)-**1** to the experimental rotational strengths of (+)-**1**. Rotational strengths are in  $10^{-44}$  esu<sup>2</sup> cm<sup>2</sup>. The straight lines of slope +1 are the “lines of perfect agreement.”

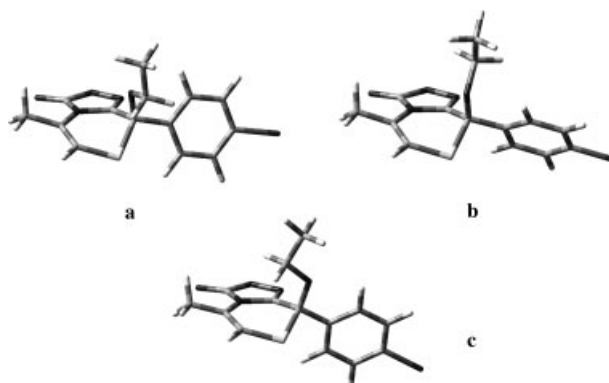
entry channel blockers assayed.<sup>42</sup> The most active compound synthesized was **2**; its activity was 20 times greater than that of diltiazem, a widely-used L-type calcium entry channel blocker. **2** contains a stereogenic C atom, C8, and is therefore chiral, the enantiomers being:



Budriesi et al. synthesized and assayed racemic **2**. To determine the enantioselectivity of the calcium entry channel blocker activity of **2**, racemic **2** was subsequently resolved using chiral HPLC by Gasparrini<sup>43</sup> and the activities of the two enantiomers assayed. (–)-**2** exhibited higher activity than did (+)-**2**.<sup>43</sup>

In order to better understand the mechanism of the calcium entry channel blocker activity of **2**, we have determined its AC using VCD,<sup>44</sup> using samples of (+)-**2** and (–)-**2** resolved by Gasparrini using HPLC. The mid-IR IR and VCD spectra of CDCl<sub>3</sub> solutions of (±)-**2** and (+)-**2**, respectively, are shown in Figure 6.

**2** is a very conformationally-flexible molecule: the six-membered thiazine ring is expected to be nonplanar and have more than one conformation; the phenyl group can rotate around the C8–C13 bond; the ethoxy group can rotate around the C8–O10 and O10–C11 bonds. As expected, conformational analysis using the MMFF94 force field finds a large number of conformations. B3LYP/6-31G\* DFT reoptimization of these conformations leads to 13 stable conformations with relative energies and free-energies within 8 kcal/mol. Luckily, only the three lowest-energy conformations, **a–c**, are predicted to have room-temperature equilibrium populations >2%:



In each of these three conformations the thiazine ring has the same conformation, but the conformation of the 8-ethoxy group is different.

DFT calculations of the IR and VCD spectra of conformations **a–c** of **2** have been carried out using B3LYP and B3PW91 functionals and the 6-31G\* and TZ2P basis sets. Comparison of the conformationally-averaged IR spectrum of **2** to the experimental IR spectrum showed that the best agreement with experiment was provided by the combination of B3PW91 and TZ2P. The B3PW91/TZ2P IR spectrum is compared to the experimental IR spectrum in Figure 7 and leads to the assignment of the experimental spectrum detailed in Figure 7. It is important to note that in the calculated spectrum, for some fundamentals the bands of the conformations **a–c** are sufficiently different in frequency that they are resolved. In these cases, the conformational splittings are also observed in the experimental spectrum, providing support for the conformational analysis of **2**. The assignment of the experimental IR spectrum leads to assignment of the bands in the VCD



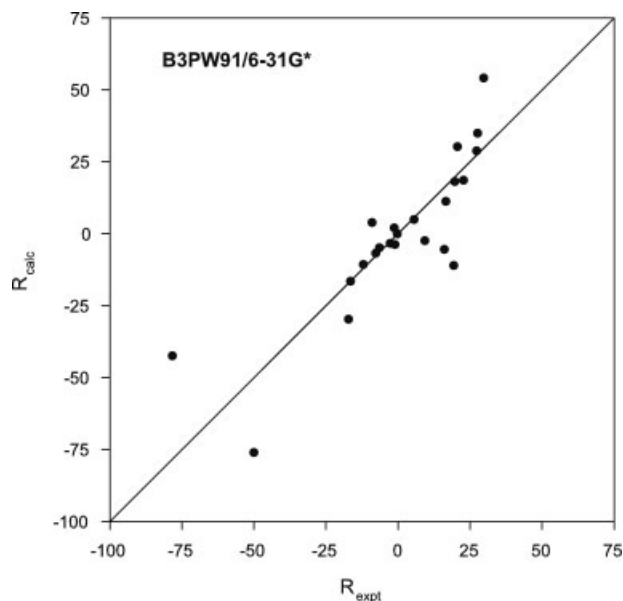


**Fig. 5.** Comparison of the B3PW91/6-31G\* rotational strengths of S-1 and the experimental rotational strengths of (+)-1. Rotational strengths are in  $10^{-44}$  esu<sup>2</sup> cm<sup>2</sup>.

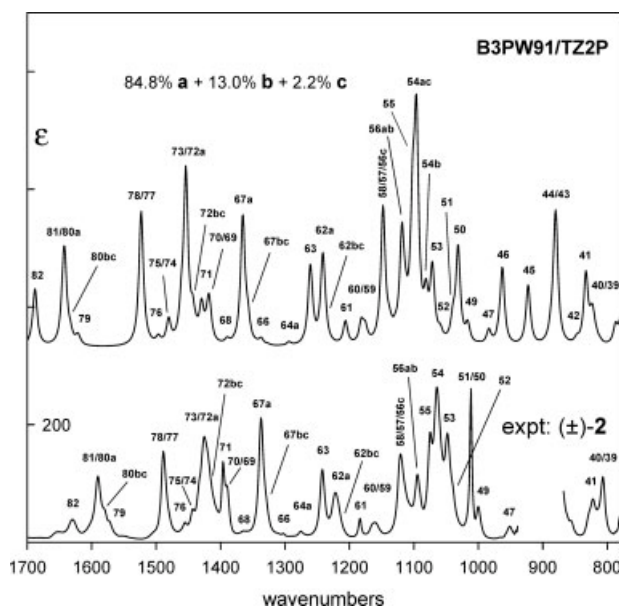


**Fig. 7.** Comparison of the conformationally averaged B3PW91/TZ2P IR spectrum of **2** to the experimental IR spectrum of (+)-**2**. The numbers are those of the fundamentals. When no conformation is specified the fundamentals of **a**, **b** and **c** are unresolved.

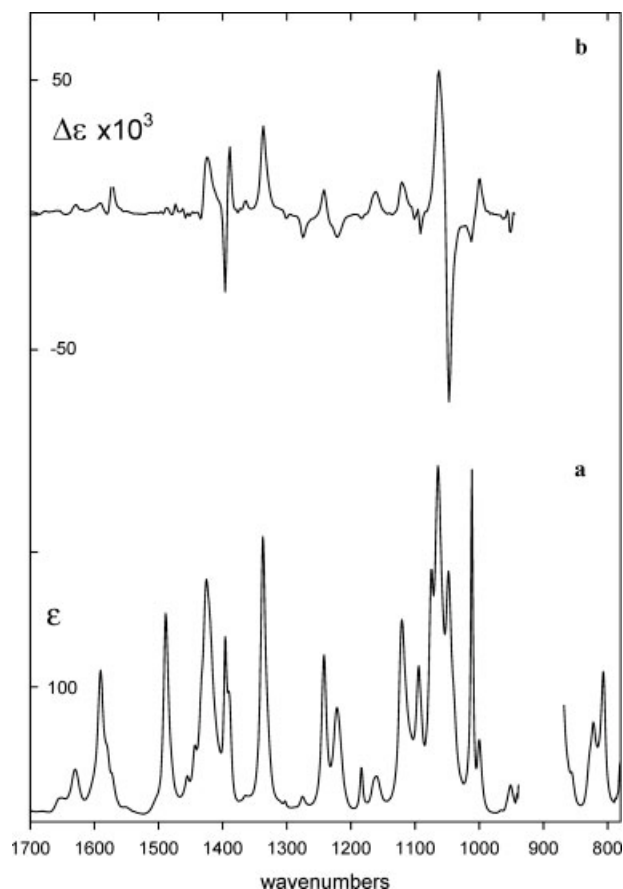


**Fig. 6.** **a:** IR spectrum of (+)-**2**; **b:** VCD spectrum of (+)-**2**. The gap at  $\sim 900$  cm<sup>-1</sup> is due to strong absorption of the CDCl<sub>3</sub> solvent.

spectrum with frequencies identical to bands in the IR spectrum. Comparison of the B3PW91/TZ2P conformationally-averaged VCD spectrum of the two enantiomers of **2** to the experimental VCD spectrum of (+)-**2**, shown in Figure 8, leads unambiguously to the conclusion that the AC of (+)-**2** is S. The detailed assignment of the experimental VCD spectrum, based on the B3PW91/TZ2P assignment of the IR spectrum and the B3PW91/TZ2P VCD spectrum, is shown in Figure 8. Again, as with the IR spectrum, resolution of the contributions of different conformations to the VCD spectra of several modes is clearly observed, further supporting the conformational analysis of **2**. The rotational strengths of the observed VCD bands are then determined by Lorentzian fitting of the experimental VCD spectrum. The B3PW91/TZ2P rotational strengths of each observed VCD band are then calculated by summing the population-weighted rotational strengths of the fundamentals assigned to the band. Comparison of these calculated rotational strengths for the two enantiomers of **2** to the experimental rotational strengths of (+)-**2** is shown in Figure 9. The agreement of the S-**2** rotational strengths with the experimental rotational strengths of (+)-**2** is excellent (except for modes 52–54), while the agreement of the R-**2** rotational strengths is terribly bad. This comparison thus definitively establishes that the AC of (+)-**2** is S. In addition, it further confirms the excellent accuracies of the B3PW91 functional and the TZ2P basis set in predicting vibrational rotational strengths.

The AC of **2**, determined using VCD, shows that the enantiomer of **2**, (–)-**2**, having the higher calcium entry channel blocker activity has the AC R. If **2** eventually becomes a commercial pharmaceutical, it will probably be the R-(–) enantiomer which is used.

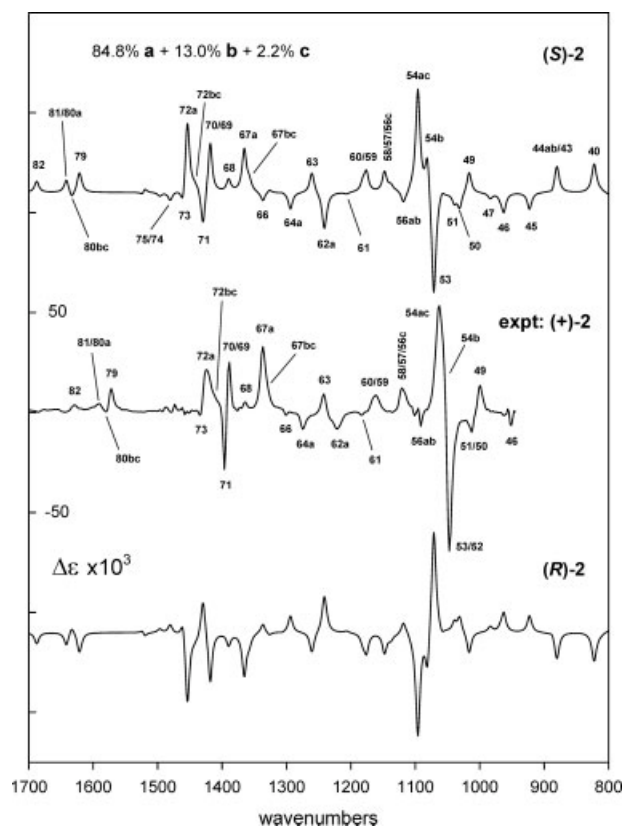


**Fig. 8.** Comparison of the conformationally averaged B3PW91/TZ2P VCD spectra of (S)-2 and (R)-2 to the experimental VCD spectrum of (+)-2. The numbers are those of the fundamentals. When no conformation is specified the fundamentals of **a**, **b** and **c** are unresolved.

#### APPLICATIONS OF VCD SPECTROSCOPY TO THE DETERMINATION OF ACs OF CHIRAL ORGANIC MOLECULES, USING THE STEPHENS EQUATION FOR VIBRATIONAL ROTATIONAL STRENGTHS AND DFT

Since the application of DFT to the calculation of vibrational rotational strengths in the GAUSSIAN program, in addition to molecules **1** and **2**, we have analyzed the VCD spectra of many chiral organic molecules using DFT. Molecules whose studies have been published are shown in Figure 10. In some cases, e.g., the monoterpenes, camphor **7**, fenchone **8**, and  $\alpha$ -pinene **9**, the ACs had previously been unambiguously determined, and the studies focused primarily on the relative accuracies of DFT calculations using different combinations of functionals and basis sets.<sup>33–35</sup> In some other cases, for example Tröger's Base, **13**, and the chromenone, **25**, while their ACs had been previously assigned, the reliability of these ACs was questionable. Our VCD studies of these molecules focused primarily on establishing their ACs definitively. In the case of Tröger's base, **13**, its AC had been assigned to be *R,R*(+) by Mason et al.<sup>45</sup> using its electronic CD (ECD) spectrum together with the Coupled Oscillator theory of electronic rotational strengths. Our VCD study of Tröger's base<sup>46,47</sup> showed that its AC is in fact *R,R*(-)/*S,S*(+), the

*Chirality* DOI 10.1002/chir

opposite of that assigned by Mason et al. In the case of **25**, its AC had been assigned to be *R*(-)/*S*(+) by Besse et al.<sup>48</sup> using the Bijvoet X-ray crystallography method. Our VCD study of the acetate derivative of **25**<sup>49</sup> showed that the AC of **25** is in fact *R*(+)/*S*(-), the opposite of that assigned by Besse et al. Our studies of **13** and **25** demonstrated the greater power of VCD spectroscopy in determining ACs compared to the coupled oscillator ECD method and the Bijvoet X-ray crystallography method when applied to molecules not having a "heavy atom."

Several of our VCD studies have been motivated by the need to understand the mechanisms of asymmetric synthesis reactions. For example, the mechanism of the asymmetric synthesis of chiral sulfoxides by reaction of

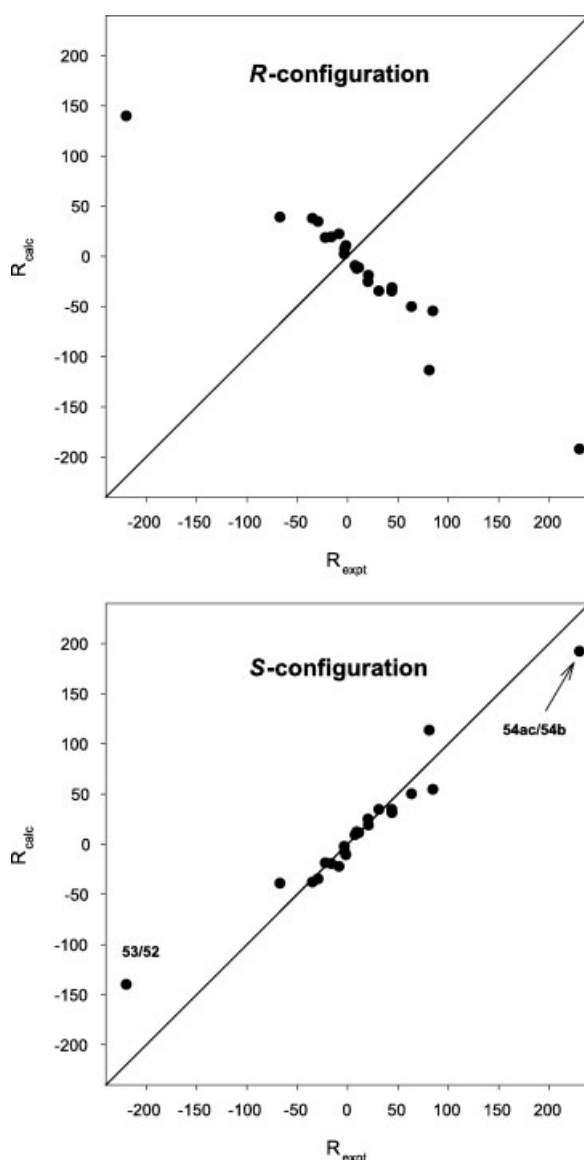


**Fig. 9.** Comparison of calculated rotational strengths for (R)-2 and (S)-2 to the experimental rotational strengths of (+)-2. Rotational strengths are in  $10^{-44}$  esu<sup>2</sup> cm<sup>2</sup>.

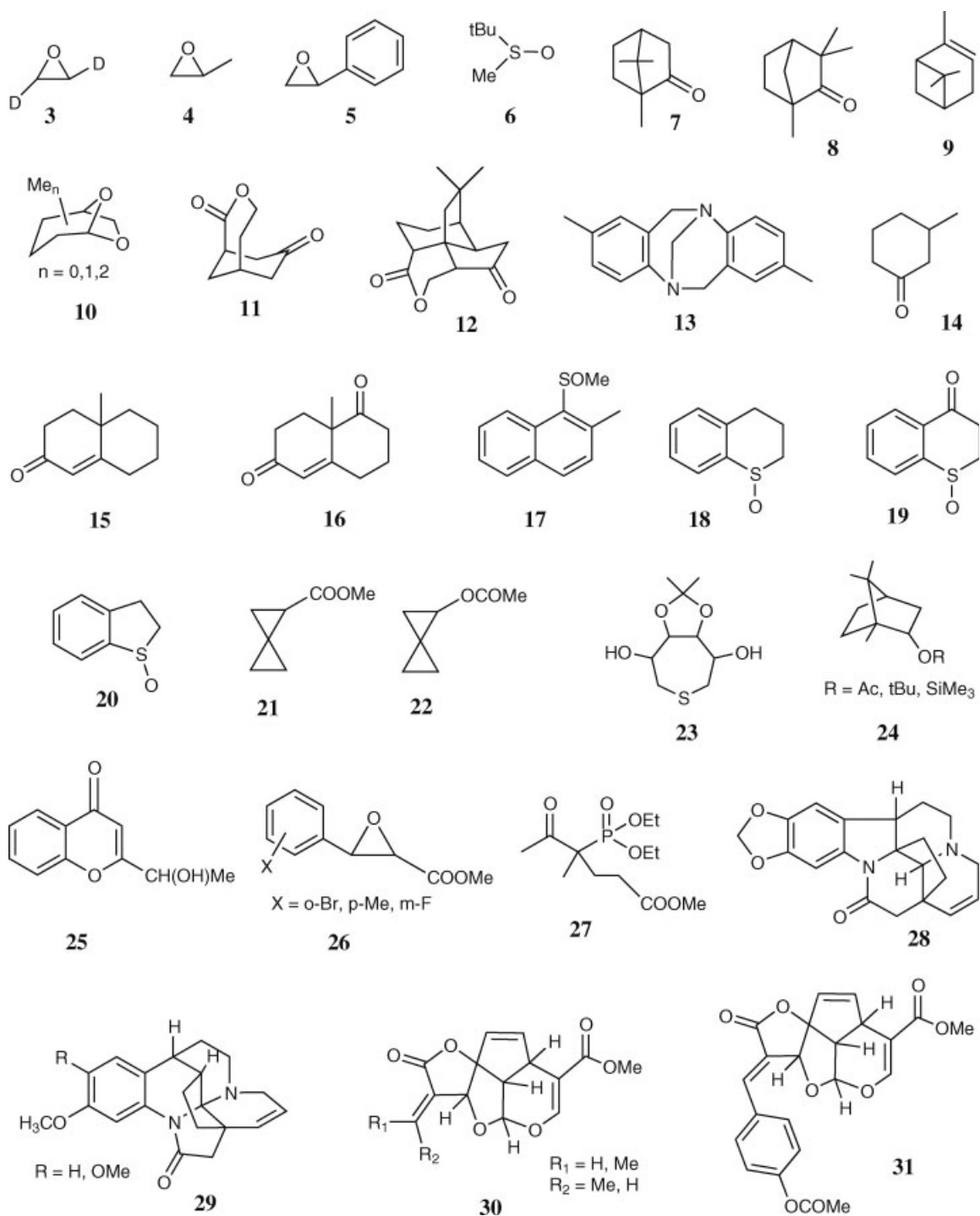
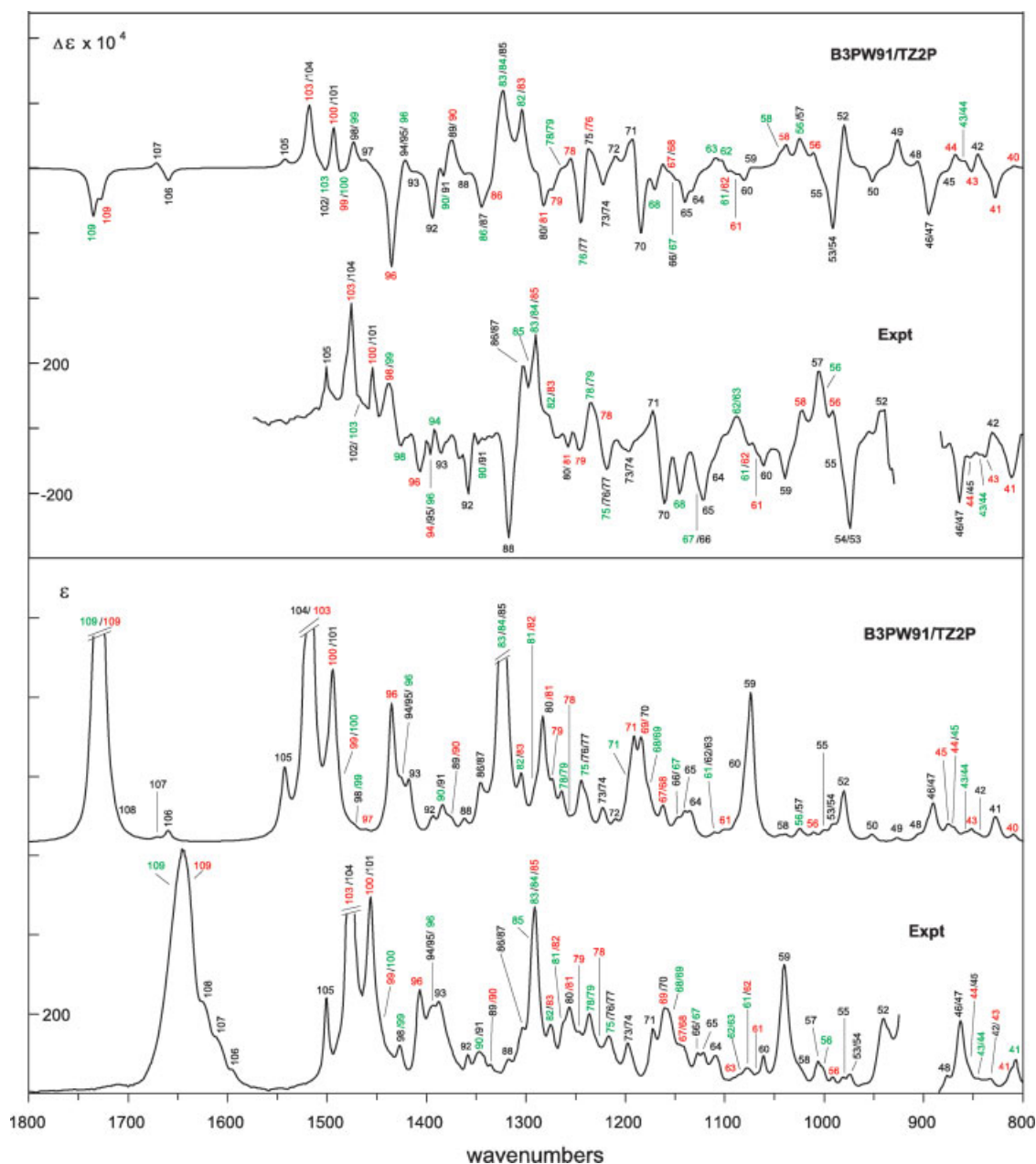


Fig. 10. Molecules whose VCD have been studied using DFT.

the corresponding sulfides with *tert*-butyl-hydroperoxide, together with  $\text{Ti}(\text{iso-PrO})_4$  and optically-active 1,2-diphenyl-ethane-1,2-diol was investigated in collaboration with Rosini by determination of the ACs of 1-Me-2-Me-naphthyl-sulfoxide, **17**,<sup>50</sup> 1-thiochroman-sulfoxide, **18**,<sup>51</sup> and 1-thiochromanone-sulfoxide, **19**.<sup>52</sup> The mechanism of the asymmetric synthesis of chiral phenyl-glycidic-acid derivatives via asymmetric epoxidation of *trans*-cinnamic acid

derivatives using oxone and a keto-bile-acid was investigated in collaboration with Bortolini by determination of the ACs of the *o*-Br, *m*-F, and *p*-CH<sub>3</sub> derivatives of phenyl glycidic acid, **26**.<sup>53</sup> The mechanism of the Baeyer-Villiger oxidation of a chiral bicyclo[3.3.1]nonane-2,7-dione, giving the chiral keto-lactone, **11**, was investigated in collaboration with Butkus by determination of the AC of **11**.<sup>54</sup> The mechanism of the asymmetric synthesis of spiropentylcar-



**Fig. 11.** Comparison of experimental and conformationally averaged B3PW91/TZ2P IR and VCD spectra of **32** for the range 800–1800  $\text{cm}^{-1}$ . Fundamentals are numbered. Red and green numbers indicate bands of conformations **a/a'** and **b/b'** respectively. Black numbers indicate superpositions of bands of conformations **a**, **a'**, **b** and **b'**. Band shapes of the calculated spectra are Lorentzian ( $\gamma = 4.0 \text{ cm}^{-1}$ ).

boxylic acid via deamination of spiropentylamine was investigated in collaboration with Wiberg by determination of the ACs of the methyl ester of spiropentylcarboxylic acid, **21**, and spiropentyl acetate, **22**.<sup>55</sup>

Another focus of our studies has been the determination of the ACs of natural products. Since our early studies of the natural products camphor, fenchone, and  $\alpha$ -pinene, it has been clear that this could become a major application of VCD spectroscopy. In 1998 we studied the natural product frontalinal, **10**,<sup>56</sup> an insect pheromone. Recently, we have returned to this area, studying the cytotoxic sesquiterpene quadron, **12**,<sup>57</sup> the alkaloids schizozigine, **28**,  
*Chirality* DOI 10.1002/chir

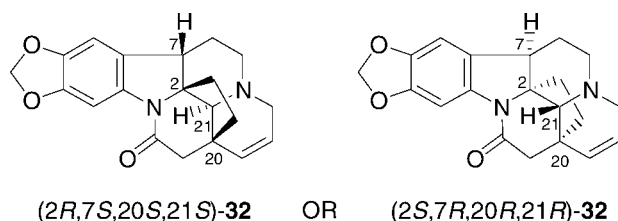
iso-schizogaline and iso-schizogamine, **29**,<sup>58,59</sup> and the iridoids plumericin and iso-plumericin, **30**, and prismatomerin **31**.<sup>60–62</sup> The studies of the alkaloids and iridoids have demonstrated the power of DFT-based VCD spectroscopy in determining the ACs of very large natural product molecules. We expect that this area of application of VCD will grow rapidly in the near future, as a result, and significantly impact the elucidation of the stereochemistries of natural products, especially those of potential pharmaceutical interest. For this reason, in the following section, we discuss our studies of the alkaloids and iridoids **28–31**.



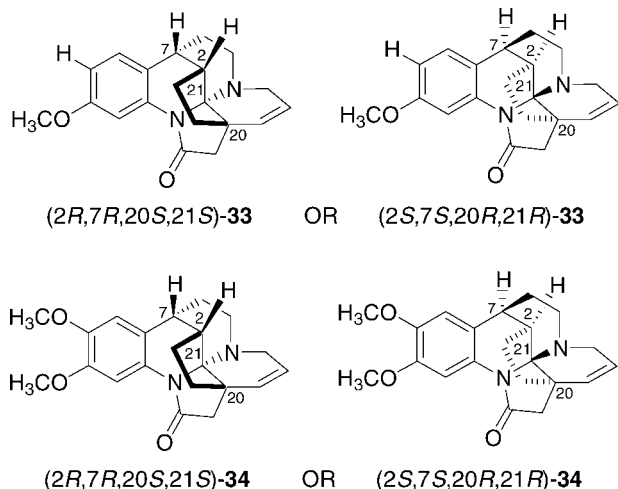
# APPLICATIONS OF VCD SPECTROSCOPY TO THE DETERMINATION OF THE ACs OF NATURAL PRODUCTS

## The Alkaloids *Schizogyne*, *Iso-schizogaline* and *Iso-schizogamine*

The alkaloids schizogyne, iso-schizogaline, and iso-schizogamine were isolated from the East African plant, *Schizogygia caffaeoides*, extracts of which have been used in traditional medicine in Kenya for the treatment of skin diseases. The spectroscopic properties and chemical reactions of schizogyne led Renner et al.<sup>63–65</sup> to the conclusion that the structure is:



The structures of iso-schizogaline and iso-schizogamine have been recently shown by NMR<sup>66,67</sup> to be:



The relative configurations of **32–34** result from their NMR studies. Until very recently, however, no determination of the ACs of these natural products had been reported. In 2006, in collaboration with Urbanová and Hájíček, we determined the ACs of these three alkaloids, using VCD.<sup>58,59</sup>

**Schizogyne**<sup>58</sup>. Naturally occurring **32** exhibits a positive  $[\alpha]_D$  value. The IR and VCD spectra of (+)-**32** were measured using  $\text{CDCl}_3$  solutions. Conformational analysis of **32** identified four conformations with B3LYP/6-31G\* energies within a range of 0.4 kcal/mol. The relative free energies, room-temperature equilibrium populations, IR and VCD spectra of these four conformations were predicted using the functionals B3LYP and B3PW91 and the basis set TZ2P. Comparison of the conformationally-averaged IR spectra to the experimental spectrum led to the conclusion that the B3PW91/TZ2P spectrum gave

the best agreement with experiment. The B3PW91/TZ2P IR spectrum is compared to the experimental spectrum in Figure 11, leading to the assignment of the experimental IR spectrum, also shown in Figure 11. The assignment of the experimental IR spectrum simultaneously leads to the assignment of the experimental VCD spectrum, as also shown in Figure 11. Comparison of the B3PW91/TZ2P VCD spectrum of (2*R*,7*S*,20*S*,21*S*)-**32** to the experimental VCD spectrum of (+)-**32** shows that the agreement is excellent, and that the AC of **32** is therefore (2*R*,7*S*,20*S*,21*S*)-(+). Quantitative comparison of the calculated rotational strengths for both enantiomers of **32** and the experimental rotational strengths, obtained by Lorentzian fitting, is shown in Figure 12. Unquestion-

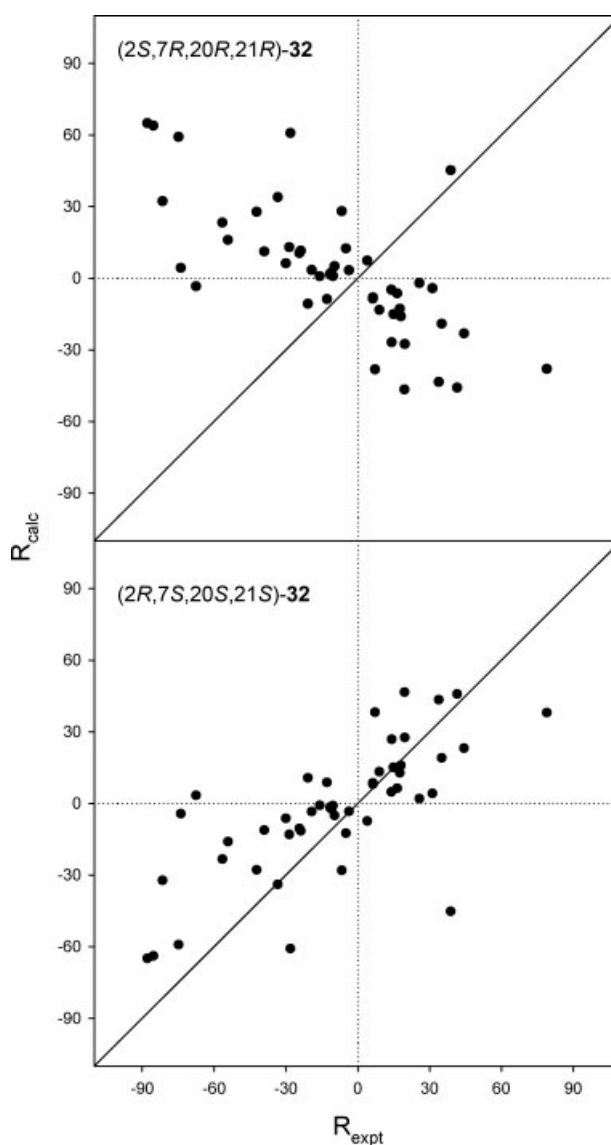


**Fig. 12.** Comparison of experimental and B3PW91/TZ2P rotational strengths of **32**. Calculated rotational strengths are for (2*R*,7*S*,20*S*,21*S*)- and (2*S*,7*R*,20*R*,21*R*)-**32**. Experimental rotational strengths are for (+)-**32**. Calculated rotational strengths are population-weighted averages. Rotational strengths are in  $10^{-44} \text{ esu}^2 \text{ cm}^2$ .

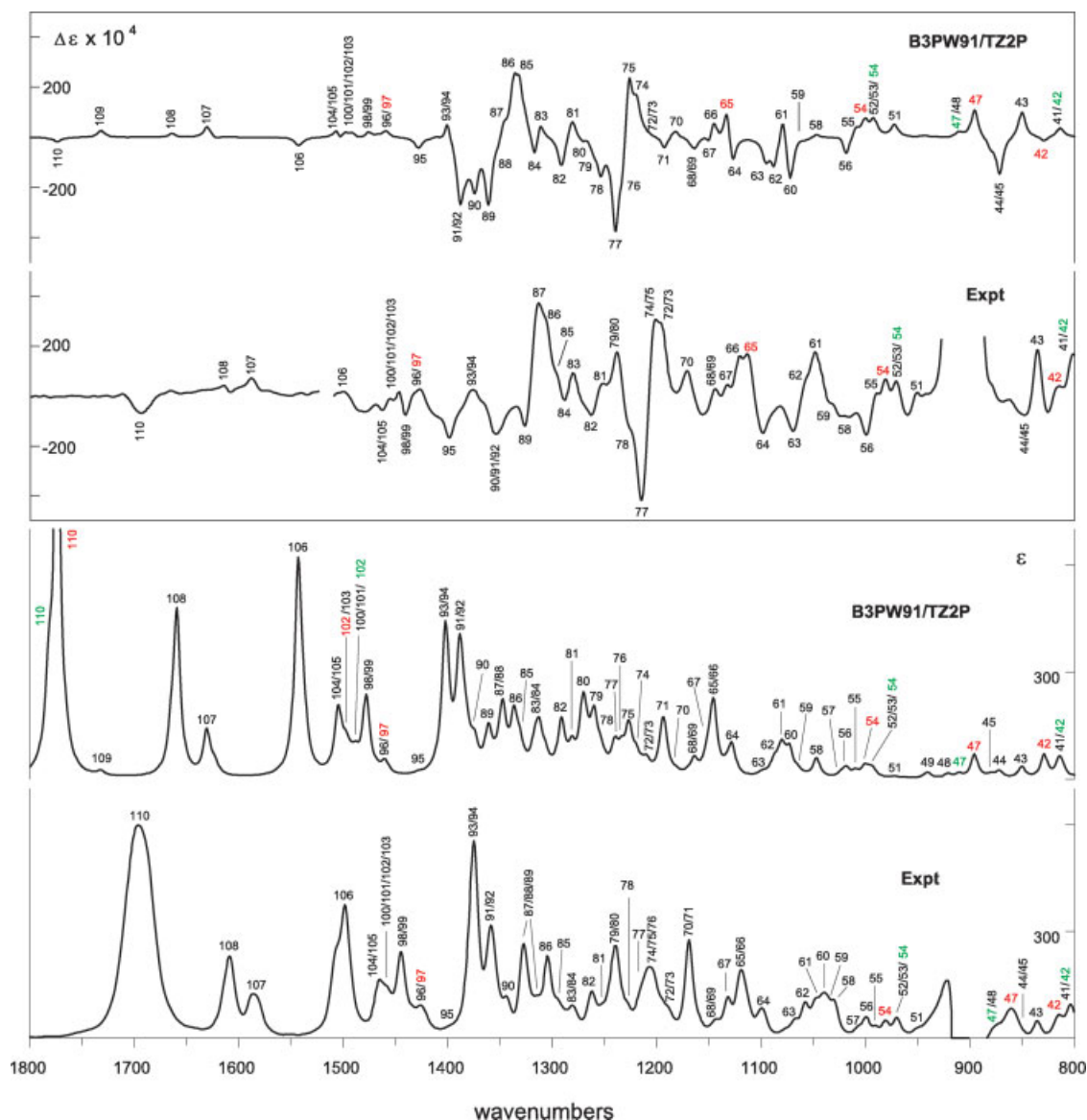


**Fig. 13.** Comparison of the experimental and B3PW91/TZ2P IR and VCD spectra of **33** for the range 800–1800  $\text{cm}^{-1}$ . The numbers define the fundamentals contributing to resolved bands. Red and green numbers refer to fundamentals of **1a** and **1b** respectively. Black numbers are used when the bands of **1a** and **1b** are not resolved. Band shapes of the calculated spectra are Lorentzian ( $\gamma = 4.0 \text{ cm}^{-1}$ ).

ably, the calculated rotational strengths for (2*R*,7*S*,20*S*,21*S*)-**32** are in far superior agreement with the experimental rotational strengths for (+)-**32** than are the calculated rotational strengths for (2*S*,7*R*,20*R*,21*R*)-**32**. The AC of (+)-**32** is unambiguously shown to be 2*R*,7*S*,20*S*,21*S*.

**Iso-schizogaline and Iso-schizogamine**<sup>59</sup>. Naturally occurring **33** and **34** both exhibit negative  $[\alpha]_D$  values. The IR and VCD spectra of (–)-**33** and (–)-**34** were measured in  $\text{CDCl}_3$  solutions. Analysis of the IR and VCD spectra followed the same protocol as used for **32**. Again, the B3PW91/TZ2P conformationally-averaged IR spectra of **33** and **34** were in the best agreement with the experi-

mental spectra. These spectra and the resulting assignments of the experimental IR and VCD spectra are shown in Figures 13 and 14. The B3PW91/TZ2P VCD spectra of (2*R*,7*R*,20*S*,21*S*)-**33** and (2*R*,7*R*,20*S*,21*S*)-**34**, also shown in Figures 13 and 14, are in excellent agreement with the experimental VCD spectra of (–)-**33** and (–)-**34**, leading to the conclusion that the ACs of both are (2*R*,7*R*,20*S*,21*S*)-(–). Quantitative comparisons of calculated rotational strengths for both enantiomers of **33** and **34** to the experimental rotational strengths of (–)-**33** and (–)-**34**, shown in Figures 15 and 16, definitively confirm that the ACs of both (–)-**33** and (–)-**34** are 2*R*,7*R*,20*S*,21*S*.

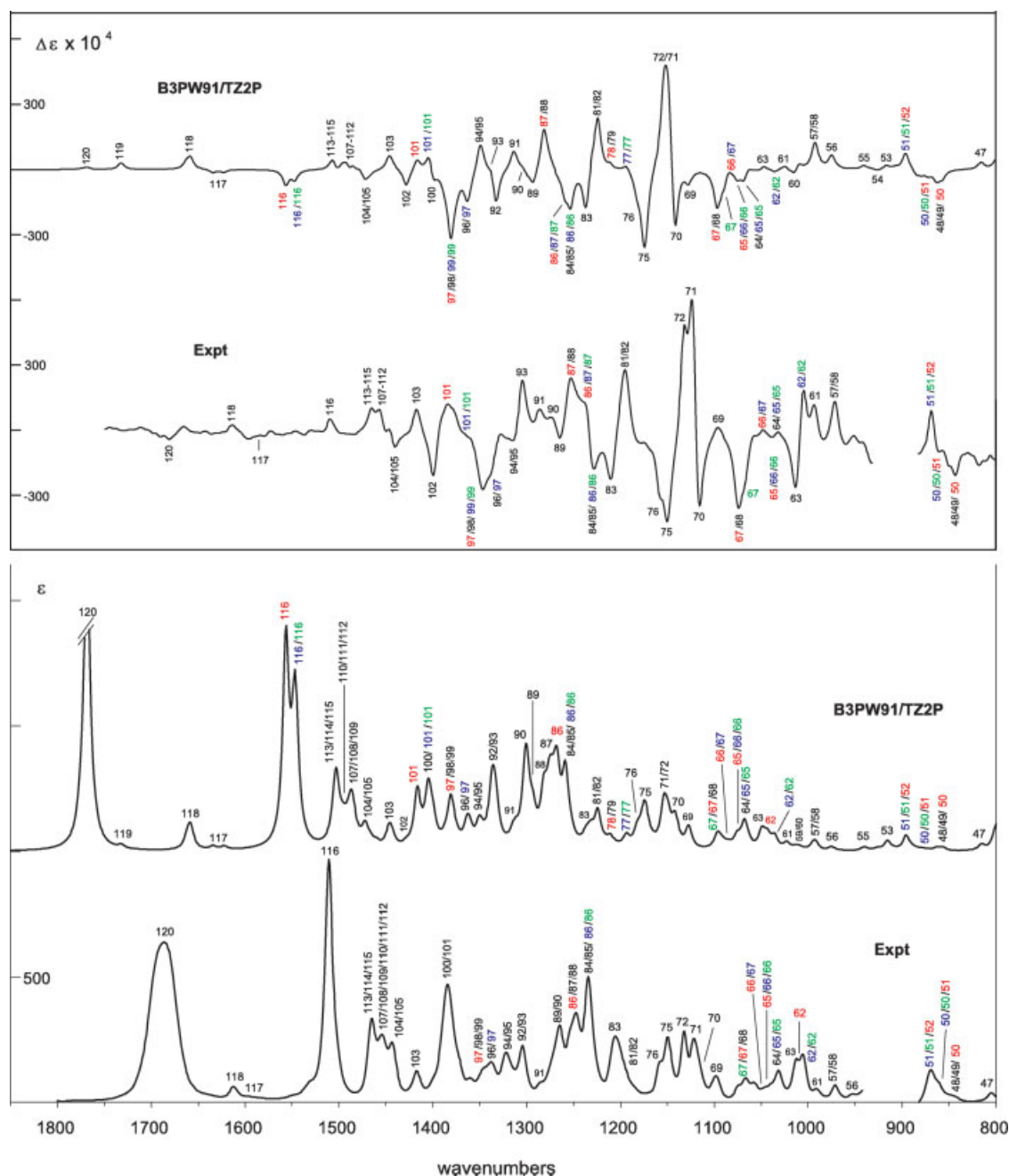
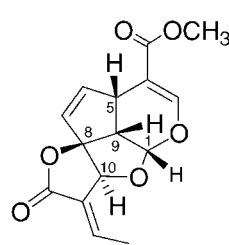


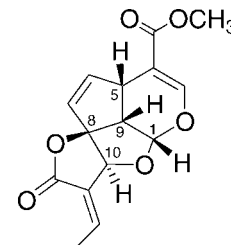
**Fig. 14.** Comparison of the experimental and B3PW91/TZ2P IR and VCD spectra of **34** for the range 800–1850  $\text{cm}^{-1}$ . The numbers define the fundamentals contributing to resolved bands. Red, green and blue numbers refer to fundamentals of **1a**, **1b** and **1c** respectively. Black numbers are used when the bands of **1a**, **1b** and **1c** are not resolved. Band shapes of the calculated spectra are Lorentzian ( $\gamma = 4.0 \text{ cm}^{-1}$ ).

**The Iridoids Plumericin, Iso-plumericin, and Prismatomerin<sup>60–62</sup>**

The iridoid natural product plumericin, **35**, was first isolated from the plant *Plumeria multiflora* by Little and Johnstone<sup>68</sup> and shown to exhibit antifungal and antibacterial activity. Later, Albers-Schönberg and Schmid<sup>69,70</sup> isolated **35** and its isomer, iso-plumericin, **36**, from *Plumeria rubra* var. *alba* and, on the basis of chemical and spectroscopic studies, assigned their structures and ACs as:



(1R,5S,8S,9S,10S)-**35**



(1R,5S,8S,9S,10S)-**36**

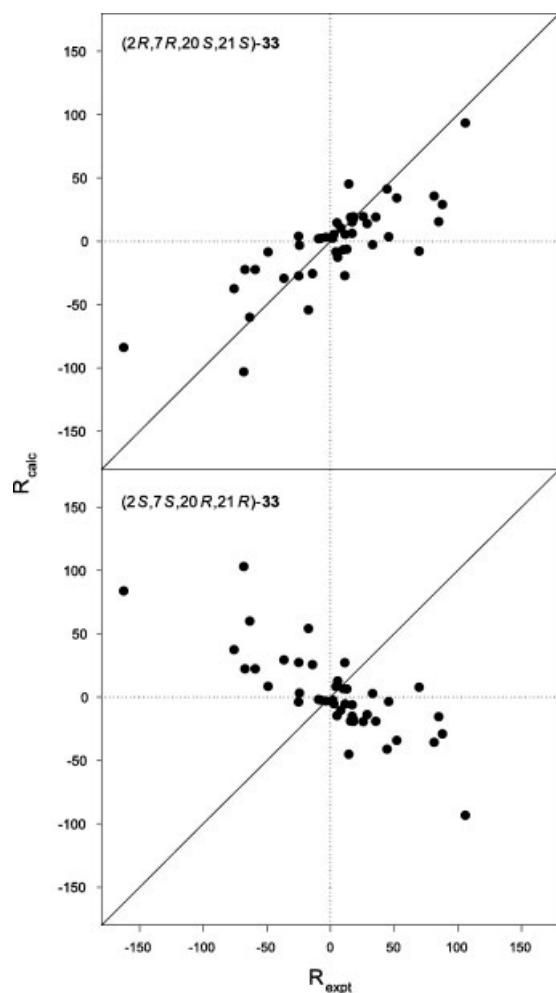
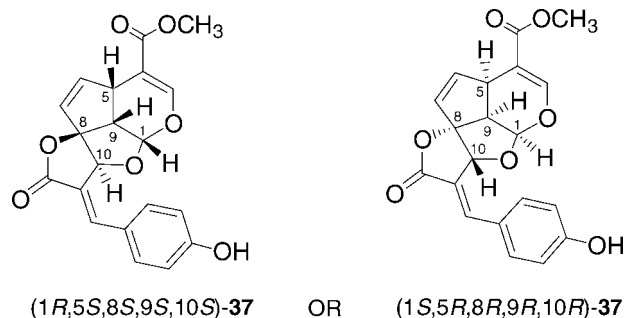


**Fig. 15.** Comparison of experimental and B3PW91/TZ2P rotational strengths of **33**. Experimental rotational strengths are for (–)-**33**. Calculated rotational strengths are for (2*R*,7*R*,20*S*,21*S*)- and (2*S*,7*S*,20*R*,21*R*)-**33**. Calculated rotational strengths are population-weighted averages of conformations **1a**, **1b** and **11a**. Rotational strengths are in  $10^{-44}$  esu<sup>2</sup> cm<sup>2</sup>.

Total syntheses of racemic **35** and **36**<sup>71–73</sup> and X-ray crystal structure determinations of the natural products (+)-**35** and (+)-**36**<sup>74</sup> have confirmed these structures, but have not confirmed or disproved the ACs. Very recently, Elsässer et al.<sup>74</sup> concluded, from comparison of the ECD spectra of (+)-**35** and (+)-**36** to ECD spectra calculated using semiempirical MO theory, that the ACs assigned by Albers-Schönberg and Schmid were incorrect. In 2006, in collaboration with Krohn and Kurtán, we redetermined the ACs of these two iridoids, using VCD,<sup>60</sup> with the results discussed below.

Very recently, a new, highly cytotoxic, iridoid has been isolated from *Prismatomeris tetrandra*, and named prismatomerin.<sup>61</sup> Chemical and spectroscopic studies identified the structure of prismatomerin, **37**, as:

*Chirality* DOI 10.1002/chir



differing from **35** and **36** simply by the substitution of a methyl group by a *para*-phenol group. The specific rotation,  $[\alpha]_D$ , of **37** is  $-136$ , similar in magnitude but opposite in sign to the  $[\alpha]_D$  of **35**,  $+204$ , raising the possibility that the AC of **37** might be opposite to that of **35**. To evaluate this conclusion, the AC of **37** was determined using the VCD of its acetate derivative, **38**<sup>61,62</sup>

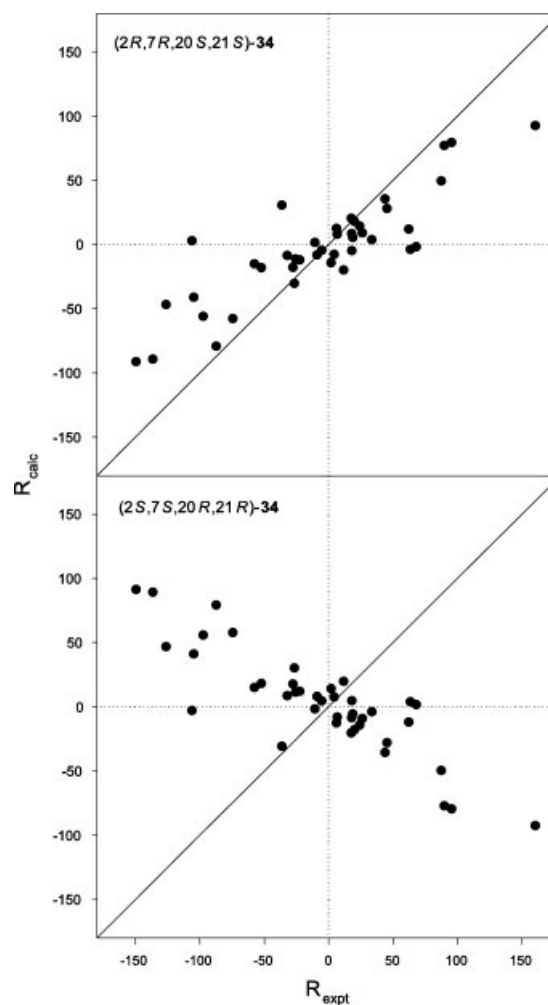


**Fig. 16.** Comparison of experimental and B3PW91/TZ2P rotational strengths of **34**. Experimental rotational strengths are for (–)-**34**. Calculated rotational strengths are for (2*R*,7*R*,20*S*,21*S*)- and (2*S*,7*S*,20*R*,21*R*)-**34**. Calculated rotational strengths are population-weighted averages of conformations **1a–1e** and **11a**. Rotational strengths are in  $10^{-44}$  esu<sup>2</sup> cm<sup>2</sup>.



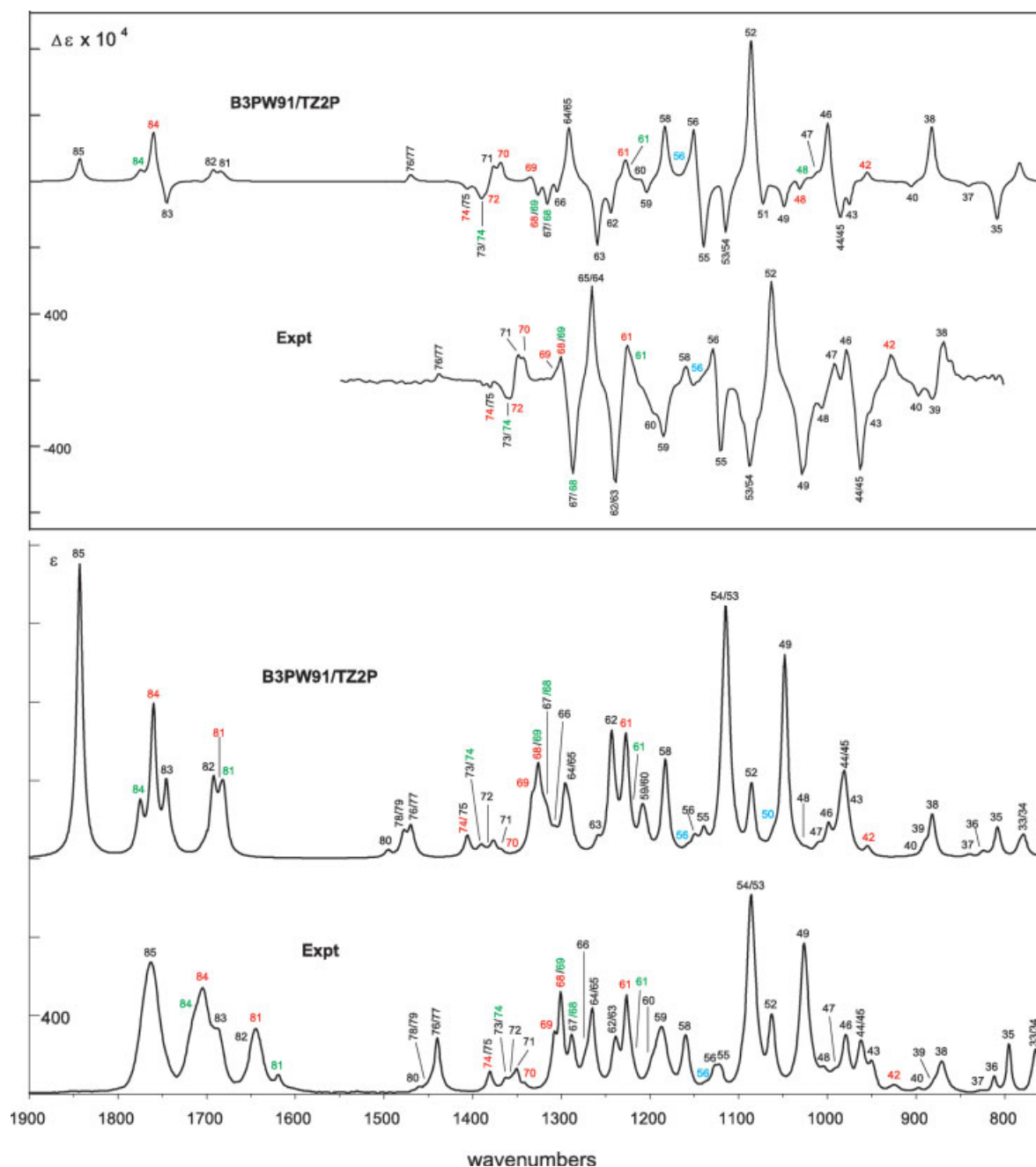
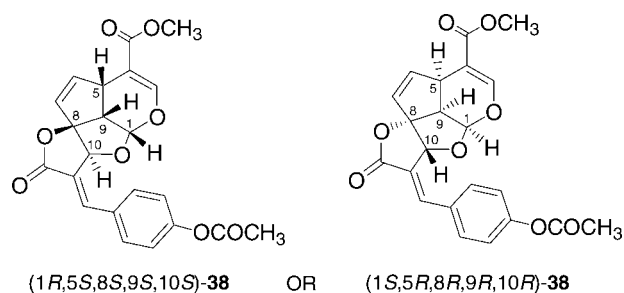


**Fig. 17.** Comparison of the experimental and B3PW91/TZ2P IR and VCD spectra of **35** for the range 750–1900  $\text{cm}^{-1}$ . The numbers define the fundamentals contributing to resolved bands. Red, green and cyan numbers refer to fundamentals of **a**, **b** and **c/d** respectively. Black numbers are used when the bands of **a** and **b** are not resolved. Band shapes of the calculated spectra are Lorentzian ( $\gamma = 4.0 \text{ cm}^{-1}$ ).



(in order to minimize intermolecular hydrogen-bonding), with the result discussed below.

**Plumericin and Iso-plumericin**<sup>60</sup>. Naturally-occurring **35** and **36** exhibit positive  $[\alpha]_D$  values. The IR and VCD spectra of (+)-**35** and (+)-**36** were measured using  $\text{CDCl}_3$  solutions. Conformational analysis of **35** and **36** identified four conformations with B3LYP/6-31G\* energies within a range of 2.0 kcal/mol. Analysis of the experimental IR and VCD spectra of (+)-**35** and (+)-**36** followed

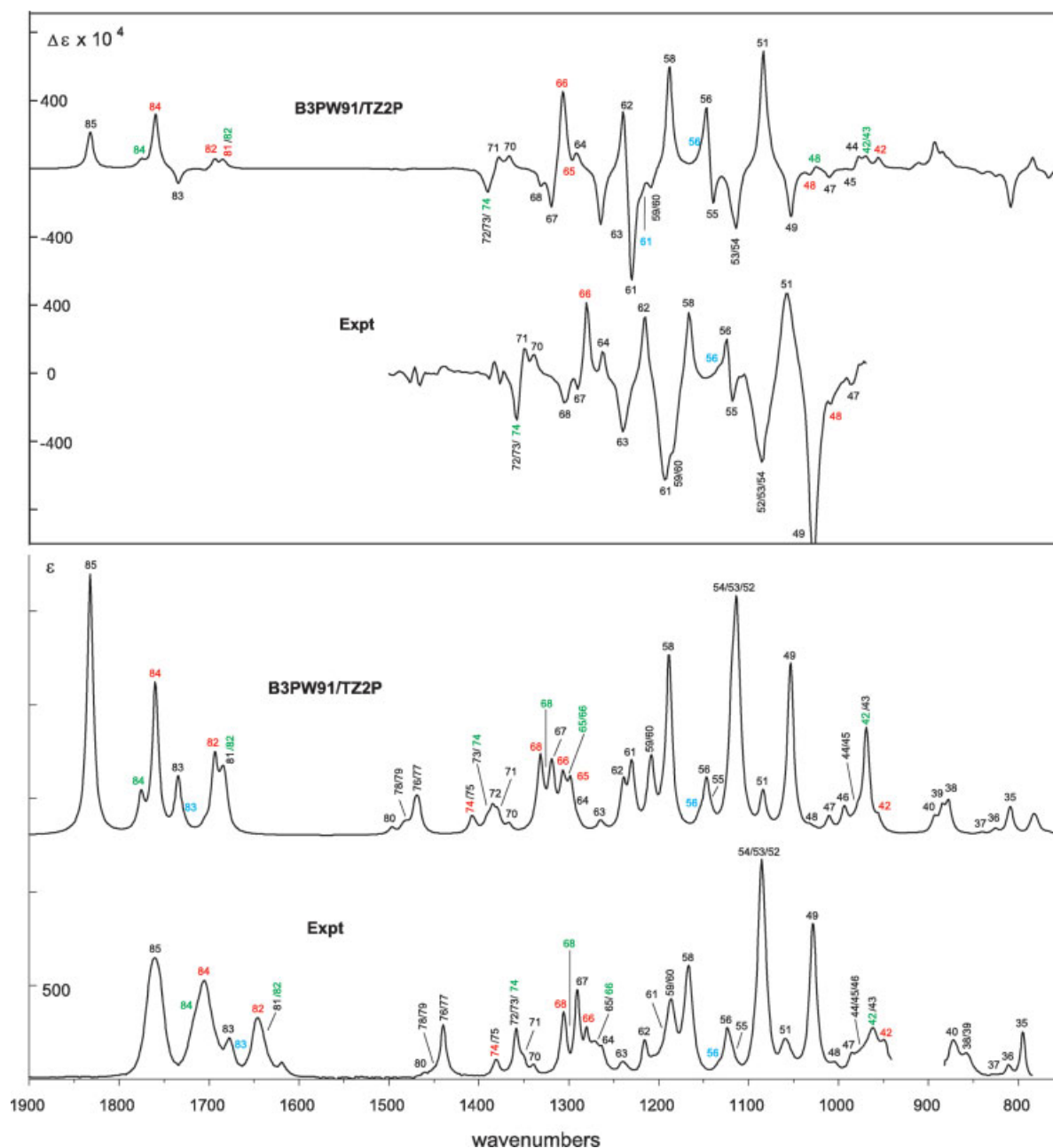


**Fig. 18.** Comparison of the experimental and B3PW91/TZ2P IR and VCD spectra of **36** for the range 750–1900  $\text{cm}^{-1}$ . The numbers define the fundamentals contributing to resolved bands. Red, green and cyan numbers refer to fundamentals of **a**, **b** and **c/d** respectively. Black numbers are used when the bands of **a** and **b** are not resolved. Band shapes of the calculated spectra are Lorentzian ( $\gamma = 4.0 \text{ cm}^{-1}$ ).

the same protocol as discussed above in the case of **32**. Again, the B3PW91/TZ2P conformationally-averaged IR and VCD spectra of (1*R*,5*S*,8*S*,9*S*,10*S*)-**35** and (1*R*,5*S*,8*S*,9*S*,10*S*)-**36** were in the best agreement with the experimental spectra. These spectra and the resulting assignments of the experimental spectra are shown in Figures 17 and 18. The B3PW91/TZ2P VCD spectra of (1*R*,5*S*,8*S*,9*S*,10*S*)-**35** and (1*R*,5*S*,8*S*,9*S*,10*S*)-**36** are in excellent agreement with the experimental VCD spectra (+)-**35** and (+)-**36**, showing that the ACs of both are (1*R*,5*S*,8*S*,9*S*,10*S*)-(+). Quantitative comparisons of calcu-

lated rotational strengths for both enantiomers of **35** and **36** to the experimental rotational strengths of (+)-**35** and (+)-**36**, shown in Figures 19 and 20, definitively confirm that the ACs of both (+)-**35** and (+)-**36** are 1*R*,5*S*,8*S*,9*S*,10*S*.

**Prismatomerin**<sup>61,62</sup>. Naturally-occurring **37** exhibits a negative  $[\alpha]_D$  value. The  $[\alpha]_D$  of the acetate derivative of **37**, **38**, is also negative. The IR and VCD spectra of (–)-**38** were measured using a  $\text{CDCl}_3$  solution. The B3PW91/TZ2P conformationally-averaged IR and VCD spectra of

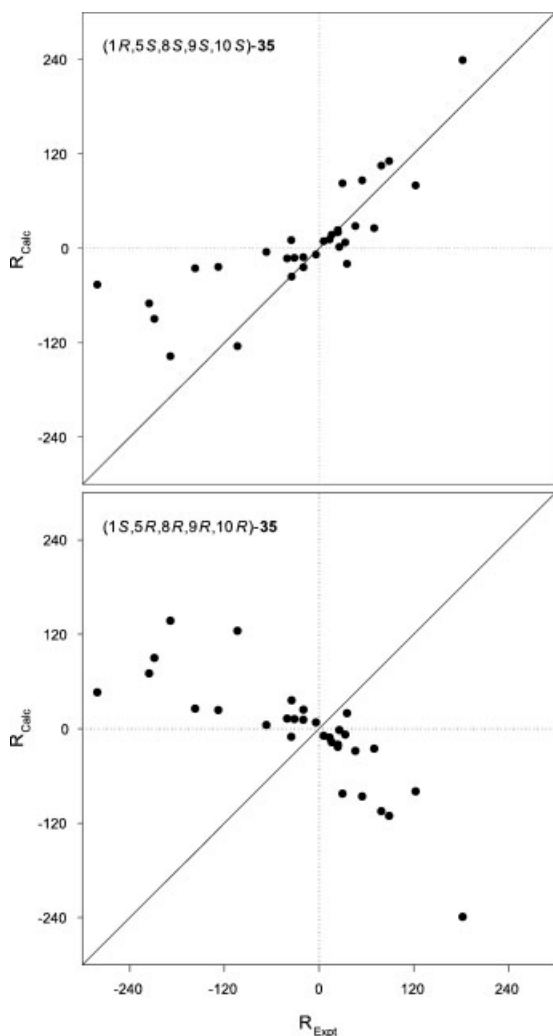


**Fig. 19.** Comparison of B3PW91/TZ2P calculated and experimental rotational strengths of **35**. Experimental rotational strengths are for (+)-**35**. Calculated rotational strengths are for (1*R*,5*S*,8*S*,9*S*,10*S*)- and (1*S*,5*R*,8*R*,9*R*,10*R*)-**35**. Calculated rotational strengths are population-weighted averages. Rotational strengths are in  $10^{-44} \text{ esu}^2 \text{ cm}^2$ .

(1*R*,5*S*,8*S*,9*S*,10*S*)-**38** are compared to the experimental IR and VCD spectra in Figure 21, leading to the assignments of the experimental IR and VCD spectra also shown in Figure 21. Comparison of calculated and experimental rotational strengths, the former for both enantiomers of **38**, is shown in Figure 22. The good agreement of the calculated VCD spectrum of (1*R*,5*S*,8*S*,9*S*,10*S*)-**38** and the experimental VCD spectrum of (–)-**38**, together with the superior agreement of the calculated rotational strengths for (1*R*,5*S*,8*S*,9*S*,10*S*)-**38**, compared to those for (1*S*,5*R*,8*R*,9*R*,10*R*)-**38**, with the experimental rotational strengths lead to the conclusion that the AC of (–)-**38** is 1*R*,5*S*,8*S*,9*S*,10*S*. It follows that the AC of (–)-**37** is also 1*R*,5*S*,8*S*,9*S*,10*S*.

The ACs of **37** and **35** are thus identical. The conclusion that they are opposite, derived from the signs of their  $[\alpha]_D$  values, is thus wrong.

## CONCLUSION

We have demonstrated that the prediction of the VCD spectra of the enantiomers of a chiral molecule using the Stephens equation for vibrational rotational strengths and the DFT methodology, together with optimally chosen basis sets and density functionals, is of sufficient reliability to permit the unambiguous determination of the ACs of organic molecules. In the cases of conformationally-rigid molecules, for example perhydrotriphenylene, **1**, predicted rotational strengths are in excellent quantitative agreement with experimental rotational strengths. The minor differences can be attributed to both experimental errors and theoretical errors. The accuracies of experimental VCD spectra depend on the magnitudes of artifact signals generated by the spectrometer used, due to imperfections in optics. The accuracies of the predicted VCD spectra depend on the accuracies of the basis set and den-

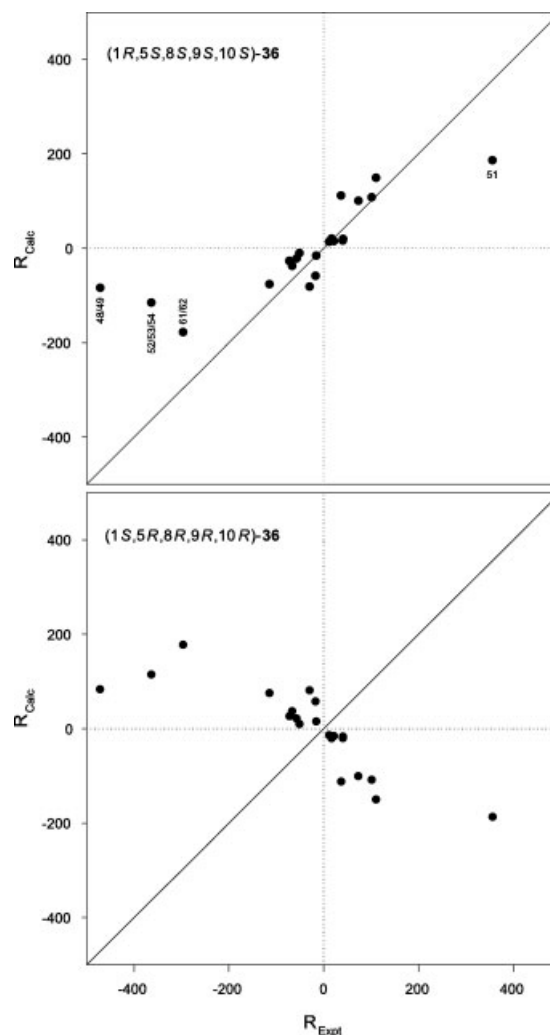


**Fig. 20.** Comparison of B3PW91/TZ2P calculated and experimental rotational strengths of **36**. Experimental rotational strengths are for (+)-**36**. Calculated rotational strengths are for (1*R*,5*S*,8*S*,9*S*,10*S*)- and (1*S*,5*R*,8*R*,9*R*,10*R*)-**36**. Calculated rotational strengths are population-weighted averages. Rotational strengths are in  $10^{-44} \text{ esu}^2 \text{ cm}^2$ .

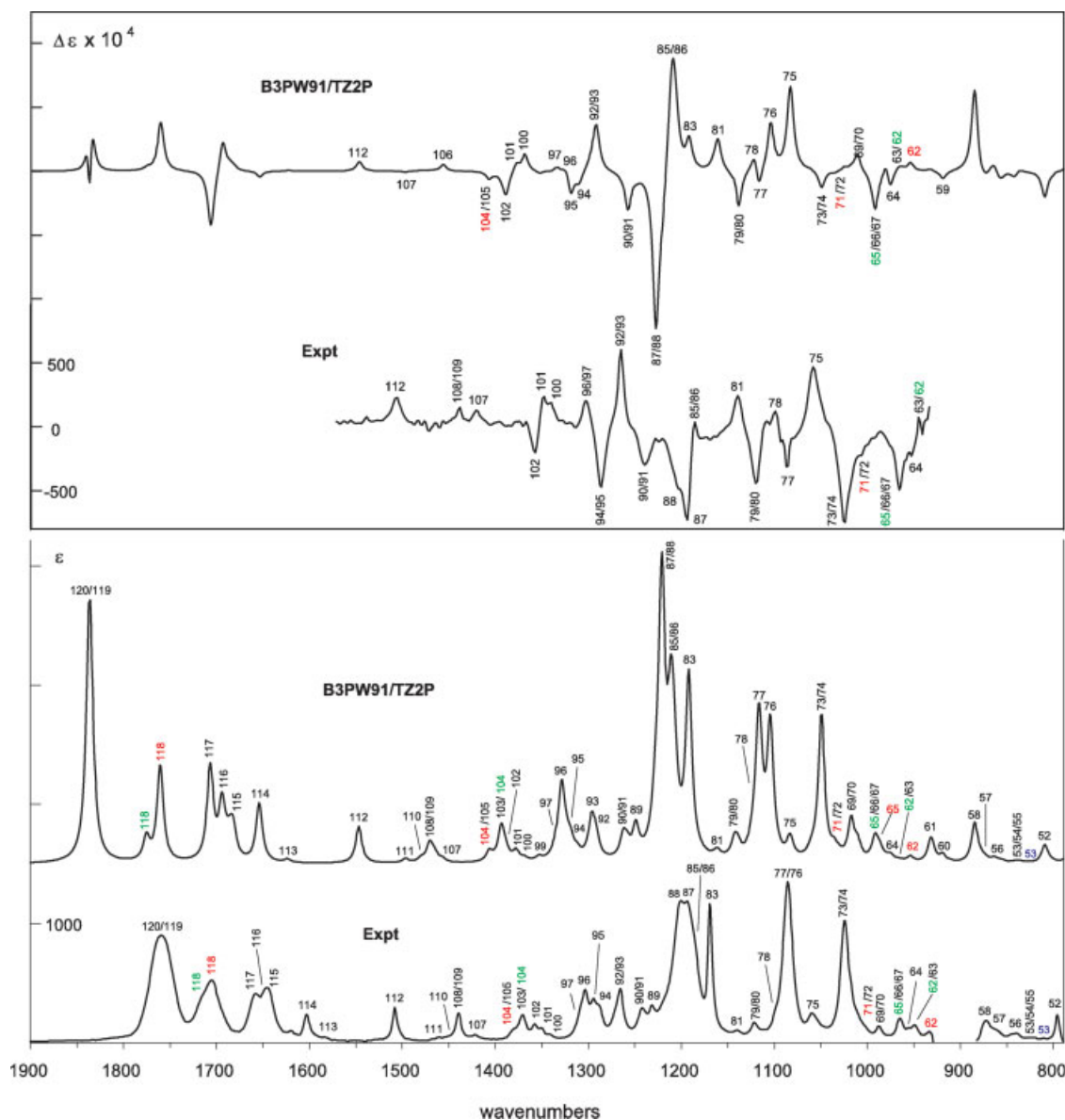


**Fig. 21.** Comparison of experimental and B3PW91/TZ2P IR and VCD spectra of **38** for the range 790–1900  $\text{cm}^{-1}$ . The calculated spectra are conformationally-averaged and simulated using Lorentzian band shapes ( $\gamma = 4.0 \text{ cm}^{-1}$ ). The red, green and blue numbers indicate bands from conformations **Aa-d**, **Ba-d** and **Ca-d** respectively; the black numbers indicate bands from conformations **Aa-d** and **Ba-d**.

sity functional used (as discussed above) and, also, on the magnitudes of contributions to the vibrational rotational strengths due to vibrational anharmonicity and solvent effects, which are not included in the predicted spectra. Except when Fermi resonance is significant, as is always the case for the C–H stretching modes of organic molecules, anharmonicity clearly causes very small contributions to the rotational strengths of vibrational transitions in the mid-IR ( $\lesssim 2000 \text{ cm}^{-1}$ ), the region universally used in determining ACs. As long as the solvent chosen for the measurement of the experimental VCD spectrum interacts weakly with the solute molecule, solvent effects clearly cause very small contributions to vibrational rotational strengths. The most commonly used solvents are  $\text{CCl}_4$ ,  $\text{CHCl}_3$ ,  $\text{CDCl}_3$ , and  $\text{CS}_2$ , because they absorb minimally in the mid-IR spectral region and interact minimally with the majority of organic molecules.

$\text{CHCl}_3$ ,  $\text{CDCl}_3$ , and  $\text{CS}_2$ , because they absorb minimally in the mid-IR spectral region and interact minimally with the majority of organic molecules.

In the cases of conformationally-flexible molecules, for example the thiazino-oxadiazolone **2** and the alkaloids and iridoids **32–37**, there is an additional source of error in the predicted VCD spectra: errors in the predicted conformational relative free energies and equilibrium populations. For some conformationally-flexible molecules, calculated and experimental rotational strengths agree less well than is the case for conformationally-rigid molecules, most likely due to errors in predicted conformational populations. Examples of molecules where this is observed are the alkaloid and iridoid molecules **32–37** (see Figs. 11–22).



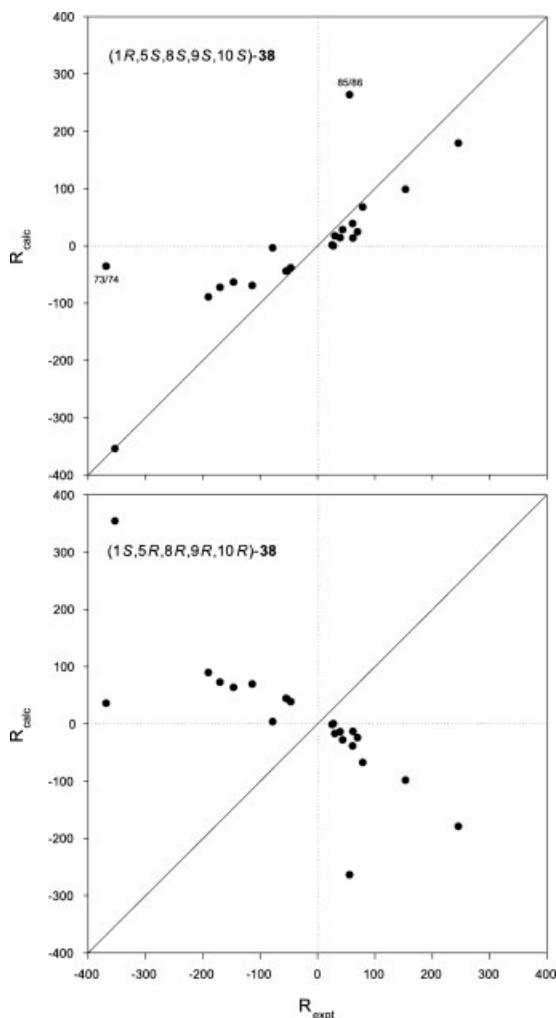


**Fig. 22.** Comparison of B3PW91/TZ2P calculated and experimental rotational strengths of **38**. Experimental rotational strengths are for (–)-**38**. Calculated rotational strengths are for (1*R*,5*S*,8*S*,9*S*,10*S*)- and (1*S*,5*R*,8*R*,9*R*,10*R*)-**38**. Calculated rotational strengths are population-weighted averages. Rotational strengths are in  $10^{-44}$  esu<sup>2</sup> cm<sup>2</sup>. The numbers indicate the fundamentals of the points.

The prediction of vibrational rotational strengths and VCD spectra will therefore be improved in accuracy in the future by the following developments: (1) the development of more accurate density functionals; (2) the inclusion of anharmonicity; (3) the inclusion of solvent effects; (4) improvement in the prediction of the equilibrium populations of conformationally-flexible molecules. Such advances will increase the reliability of the ACs of organic molecules determined using VCD spectroscopy.

The analysis of VCD spectra is substantially easier and more reliable than the analysis of ECD spectra, for two reasons. First, vibrational transitions have much smaller bandwidths than electronic transitions and, as a result, VCD spectra are much more highly resolved than are ECD spectra. Second, vibrational rotational strengths only depend on the wave function of the ground electronic state, while electronic rotational strengths depend on the wave functions of both ground and excited electronic

states. The calculation of the ground electronic state wave function is more accurate than the calculation of excited electronic state wave functions, so vibrational rotational strengths are more accurately predicted than electronic rotational strengths. The comparison of calculated and experimental electronic rotational strengths is therefore more difficult and less accurate than the comparison of calculated and experimental vibrational rotational strengths. Consequently, ACs are more easily and reliably determined using VCD, compared to ECD.

What are the limitations of VCD in determining ACs? If the molecule is enormously large, DFT calculations are impractical. At this time, therefore, bioorganic molecules such as proteins and nucleic acids cannot be analyzed. If the molecule is enormously flexible, and the number of populated conformations is enormously large, the prediction of its VCD spectrum becomes very time-consuming and less reliable. For these reasons, VCD is not universally applicable to the determination of ACs. Nevertheless, for the majority of medium-sized organic molecules VCD is a practical technique. Undoubtedly, many more applications will be carried out in the future.

#### ACKNOWLEDGMENTS

We thank the USC High Performance Computing and Communication (HPCC) facility for computer time, Hewlett-Packard Inc. for the use of a Alpha Server SC (ES45) HP computer, and Dr. J. R. Cheeseman of Gaussian Inc. for his continual assistance and advice.

#### LITERATURE CITED

1. Djerassi C. Optical rotatory dispersion: applications to organic chemistry. McGraw-Hill; 1960.
2. Crabbé P. Optical rotatory dispersion and circular dichroism in organic chemistry. Holden-Day; 1965.
3. Charney E. The molecular basis of optical activity: optical rotatory dispersion and circular dichroism. Wiley; 1979.
4. Berova N, Nakanishi K, Woody RW, editors. Circular dichroism: principles and applications. Wiley; 2000.
5. Velluz L, LeGrand M, Grosjean M. Optical circular dichroism: principles, measurements and applications. Verlag Chemie, GMBH; 1965.
6. Lightner DA. In: Berova N, Nakanishi K, Woody RW, editors. Circular dichroism: principles and applications. Wiley; 2000; Chapter 10, p. 261–303.
7. Wyss HR, Günthard HH. Optical activity of 6,7-diphenyldinaphtho[2',1';1,2:1'',2'';3,4]-5,8-diazacyclooctatetraene and 3',6'-dimethyldibenzo[1,2:3,4]-1,3-cycloheptadien-6-one in the infrared. *Helv Chim Acta* 1966;49:660–663.
8. Wyss HR, Günthard HH. Finite slit-width effect in spectropolarimeters. *J Opt Soc Am* 1966;56:888–889.
9. Osborne GA, Cheng JC, Stephens PJ. A near-infrared circular dichroism and magnetic circular dichroism instrument. *Rev Sci Instrum* 1973;44:10–15.
10. Nafie LA, Cheng JC, Stephens PJ. Vibrational circular dichroism of 2,2,2-trifluoro-1-phenylethanol. *J Am Chem Soc* 1975;97:3842–3843.
11. Nafie LA, Keiderling TA, Stephens PJ. Vibrational circular dichroism. *J Am Chem Soc* 1976;98:2715–2723.
12. Keiderling TA, Stephens PJ. Vibrational circular dichroism of overtone and combination bands. *Chem Phys Lett* 1976;41:46–48.
13. Keiderling TA, Stephens PJ. Vibrational circular dichroism of dimethyl tartrate. A coupled oscillator. *J Am Chem Soc* 1977;99:8061–8062.

14. Stephens PJ, Clark R. Vibrational circular dichroism: the experimental viewpoint. In: Mason SF, editor. Optical activity and chiral discrimination. D. Reidel; 1979. p 263–287.
15. Cheng JC, Nafie LA, Allen SD, Braunstein AI. Photoelastic modulator for the 0.55–13  $\mu\text{m}$  range. Appl Optics 1976;15:1960–1965.
16. Stephens PJ. Theory of vibrational circular dichroism. J Phys Chem 1985;89:748–752.
17. Stephens PJ, Lowe MA. Vibrational circular dichroism. Ann Rev Phys Chem 1985;36:213–241.
18. Stephens PJ. Gauge dependence of vibrational magnetic dipole transition moments and rotational strengths. J Phys Chem 1987;91:1712–1715.
19. Lowe MA, Stephens PJ, Segal GA. The theory of vibrational circular dichroism: trans-1,2-dideuteriocyclobutane and propylene oxide. Chem Phys Lett 1986;123:108–116.
20. Lowe MA, Segal GA, Stephens PJ. The theory of vibrational circular dichroism: trans-1,2-dideuteriocyclopropane. J Am Chem Soc 1986;108:248–256.
21. Amos RD, Handy NC, Jalkanen KJ, Stephens PJ. Efficient calculation of vibrational magnetic dipole transition moments and rotational strengths. Chem Phys Lett 1987;133:21–26.
22. Jalkanen KJ, Stephens PJ, Amos RD, Handy NC. Theory of vibrational circular dichroism: trans-1(S), 2(S)-dicyanocyclopropane. J Am Chem Soc 1987;109:7193–7194.
23. Jalkanen KJ, Stephens PJ, Amos RD, Handy NC. Basis set dependence of *ab initio* predictions of vibrational rotational strengths: NHD1. Chem Phys Lett 1987;142:153–158.
24. Stephens PJ, Jalkanen KJ, Devlin FJ, Chabalowski CF. *Ab initio* calculation of vibrational circular dichroism spectra using accurate post-self-consistent-field force fields: trans-2,3-dideuterio-oxirane. J Phys Chem 1993;97:6107–6110.
25. Devlin FJ, Stephens PJ. *Ab initio* calculation of vibrational circular dichroism spectra of chiral natural products using MP2 force fields: camphor. J Am Chem Soc 1994;116:5003–5004.
26. Stephens PJ, Chabalowski CF, Devlin FJ, Jalkanen KJ. *Ab initio* calculation of vibrational circular dichroism spectra using large basis set MP2 force fields. Chem Phys Lett 1994;225:247–257.
27. Stephens PJ, Devlin FJ, Chabalowski CF, Frisch MJ. *Ab initio* calculation of vibrational absorption and circular dichroism spectra using density functional force fields. J Phys Chem 1994;98:11623–11627.
28. Stephens PJ, Devlin FJ, Ashvar CS, Chabalowski CF, Frisch MJ. Theoretical calculation of vibrational circular dichroism spectra. Faraday Discuss 1994;99:103–119.
29. Devlin FJ, Finley JW, Stephens PJ, Frisch MJ. *Ab initio* calculation of vibrational absorption and circular dichroism spectra using density functional force fields: a comparison of local, non-local and hybrid density functionals. J Phys Chem 1995;99:16883–16902.
30. Stephens PJ, Devlin FJ, Ashvar CS, Bak KL, Taylor PR, Frisch MJ. Comparison of local, non-local and hybrid density functionals using vibrational absorption and circular dichroism spectroscopy. In: Laird BB, Ross RB, Ziegler T, editors. Chemical applications of density-functional theory. ACS Symposium Series, Vol. 629. 1996. p 105–113.
31. Cheeseman JR, Frisch MJ, Devlin FJ, Stephens PJ. *Ab initio* calculation of atomic axial tensors and vibrational rotational strengths using density functional theory. Chem Phys Lett 1996;252:211–220.
32. Stephens PJ, Ashvar CS, Devlin FJ, Cheeseman JR, Frisch MJ. *Ab initio* calculation of atomic axial tensors and vibrational rotational strengths using density functional theory. Mol Phys 1996;89:579–594.
33. Devlin FJ, Stephens PJ, Cheeseman JR, Frisch MJ. Prediction of vibrational circular dichroism spectra using density functional theory: camphor and fenchone. J Am Chem Soc 1996;118:6327–6328.
34. Devlin FJ, Stephens PJ, Cheeseman JR, Frisch MJ. *Ab initio* prediction of vibrational absorption and circular dichroism spectra of chiral natural products using density functional theory: camphor and fenchone. J Phys Chem 1997;101:6322–6333.
35. Devlin FJ, Stephens PJ, Cheeseman JR, Frisch MJ. *Ab initio* prediction of vibrational absorption and circular dichroism spectra of chiral natural products using density functional theory:  $\alpha$ -Pinene. J Phys Chem 1997;101:9912–9924.
36. Ashvar CS, Devlin FJ, Stephens PJ, Bak KL, Eggimann T, Wieser H. Vibrational absorption and circular dichroism of mono- and di-methyl derivatives of 6,8-dioxabicyclo[3.2.1] octane. J Phys Chem A 1998;102:6842–6857.
37. Stephens PJ, Devlin FJ, Aamouche A. Determination of the structures of chiral molecules using vibrational circular dichroism spectroscopy. In: Hicks JM, editor. Chirality: physical chemistry. ACS Symposium Series, Vol. 810. 2002. Chapter 2, p 18–33.
38. Farina M, Audisio G. Optically active perhydrotriphenylene: the first resolution of a  $\text{D}_3$  organic molecule. Tetrahedron Lett 1967;8:1285–1288.
39. Farina M, Audisio G. Stereochemistry of perhydrotriphenylene-II: absolute rotation and configuration of optically active anti-trans-anti-trans-anti-trans-perhydrotriphenylene. Tetrahedron 1970;26:1839–1844.
40. Schürch S, Saxer A, Claude S, Tabacchi R, Trusch B, Hulliger J. Semi-preparative gas chromatographic separation of all-trans-perhydrotriphenylene enantiomers on a chiral cyclodextrin stationary phase. J Chromatogr A 2001;905:175–182.
41. Stephens PJ, Devlin FJ, Schürch S, Hulliger J. Determination of the absolute configuration of chiral molecules via density functional theory calculations of vibrational circular dichroism and optical rotation: the chiral alkane  $\text{D}_3$ -anti-trans-anti-trans-anti-trans-perhydrotriphenylene. Theor Chem Acc DOI: 10.1007/s00214-006-0245-7.
42. Budriesi R, Carosati E, Chirini A, Cosimelli B, Cruciani G, Ioan P, Spinelli D, Spisani R. A new class of selective myocardial calcium channel modulators: 2. Role of the acetal chain in oxadiazol-3-one derivatives. J Med Chem 2005;48:2445–2456.
43. Carosati E, Cruciani G, Chiarini A, Budriesi R, Ioan P, Spisani R, Spinelli D, Cosimelli B, Fusi F, Frosini M, Matucci R, Gasparini F, Ciogli A, Stephens PJ, Devlin FJ. Calcium channel antagonists discovered by a multidisciplinary approach. J Med Chem 2006;49:5206–5216.
44. Stephens PJ, Devlin FJ, Gasparini F, Corosati E. Determination of the absolute configuration of an oxadiazol-3-one calcium channel blocker, via density functional theory calculations of its vibrational circular dichroism, electronic circular dichroism and optical rotation. J Org Chem 2007;72:4707–4715.
45. Mason SF, Vane GW, Schofield K, Wells RJ, Whitehurst JS. The circular dichroism and absolute configuration of Tröger's Base. J Chem Soc B 1967;553–556.
46. Aamouche A, Devlin FJ, Stephens PJ. Determination of absolute configuration using circular dichroism: Tröger's base revisited using vibrational circular dichroism. J Chem Soc Chem Comm 1999;361–362.
47. Aamouche A, Devlin FJ, Stephens PJ. Structure, vibrational absorption and circular dichroism spectra and absolute configuration of Tröger's base. J Am Chem Soc 2000;122:2346–2354.
48. Besse P, Baziard-Mouysset G, Boubekur K, Palvadeau P, Veschambre H, Payard M, Mousset G. Microbiological reductions of chromen-4-one derivatives. Tetrahedron Asymm 1999;10:4745–4754.
49. Devlin FJ, Stephens PJ, Besse P. Are the absolute configurations of 2-(1-hydroxyethyl)-chromen-4-one and its 6-bromo derivative determined by X-ray crystallography correct? A vibrational circular dichroism (VCD) study of their acetate derivatives. Tetrahedron Asymm 2005;16:1557–1566.
50. Stephens PJ, Aamouche A, Devlin FJ, Superchi S, Donnoli MI, Rosini C. Determination of absolute configuration using vibrational circular dichroism spectroscopy: the chiral sulfoxide 1-(2-methylnaphthyl) methyl sulfoxide. J Org Chem 2001;66:3671–3677.
51. Devlin FJ, Stephens PJ, Scafato P, Superchi S, Rosini C. Determination of absolute configuration using vibrational circular dichroism spectroscopy: the chiral sulfoxide 1-thiochroman S-oxide. Tetrahedron Asymm 2001;12:1551–1558.
52. Devlin FJ, Stephens PJ, Scafato P, Superchi S, Rosini C. Determination of absolute configuration using vibrational circular dichroism spectroscopy: the chiral sulfoxide 1-thiochromanone S-oxide. Chirality 2002;14:400–406.

53. Devlin FJ, Stephens PJ, Bortolini O. Determination of absolute configuration using vibrational circular dichroism spectroscopy: phenyl glycidic acid derivatives obtained via asymmetric epoxidation using oxone and a keto bile acid. *Tetrahedron Asymm* 2005;16:2653–2663.
54. Stephens PJ, McCann DM, Devlin FJ, Flood TC, Butkus E, Stoncius S, Cheeseman JR. Determination of molecular structure using vibrational circular dichroism (VCD) spectroscopy: the keto-lactone product of Baeyer–Villiger oxidation of (+)-(1*R*,5*S*)-bicyclo[3.3.1]nonane-2,7-dione. *J Org Chem* 2005;70:3903–3913.
55. Devlin FJ, Stephens PJ, Oesterle C, Wiberg KB, Cheeseman JR, Frisch MJ. Configurational and conformational analysis of chiral molecules using IR and VCD spectroscopies: spiropentylcarboxylic acid methyl ester and spiropentyl acetate. *J Org Chem* 2002;67:8090–8096.
56. Ashvar CS, Stephens PJ, Eggimann T, Wieser H. Vibrational circular dichroism spectroscopy of chiral pheromones: frontalin (1,5-dimethyl-6,8-dioxabicyclo [3.2.1] octane). *Tetrahedron Asymm* 1998;9:1107–1110.
57. Stephens PJ, McCann DM, Devlin FJ, Smith III AB. Determination of the absolute configurations of natural products via density functional theory calculations of optical rotation, electronic circular dichroism and vibrational circular dichroism: the cytotoxic sesquiterpene natural products quadrone, suberosenone, suberosanone and suberosenol A acetate. *J Nat Prod* 2006;69:1055–1064.
58. Stephens PJ, Pan JJ, Devlin FJ, Urbanová M, Hájiček J. Determination of the absolute configurations of natural products via density functional theory calculations of vibrational circular dichroism, electronic circular dichroism and optical rotation: the schizozygane alkaloid schizozygine. *J Org Chem* 2007;72:2508–2524.
59. Stephens PJ, Pan JJ, Devlin FJ, Urbanová M, Julínek O, Hájiček J. Determination of the absolute configurations of natural products via density functional theory calculations of circular dichroism, electronic circular dichroism and optical rotation: the iso-schizozygane alkaloids iso-schizogaline and iso-schizogamine. *Chirality* DOI: 10.1002/chir.20466.
60. Stephens PJ, Pan JJ, Devlin FJ, Krohn K, Kurtán T. Determination of the absolute configurations of natural products via density functional theory calculations of vibrational circular dichroism, electronic circular dichroism and optical rotation: the iridoids plumericin and iso-plumericin. *J Org Chem* 2007;72:3521–3536.
61. Krohn K, Sohrab MH, Gehle D, Dey SK, Nahar N, Mosihuzzaman M, Sultana N, Sohrab MH, Stephens PJ, Pan JJ, Sasse F. Prismatomerin, a new iridoid from *Prismatomeris tetrandra* (Rubiaceae). Structure elucidation, determination of absolute configuration and cytotoxicity. *J Nat Prod* 2007;70:1339–1343.
62. Stephens PJ, Pan JJ, Krohn K. Determination of the absolute configurations of pharmacologically active natural products via density functional theory calculations of vibrational circular dichroism: the new, cytotoxic, iridoid prismatomerin. *J Org Chem* 2007;72:7641–7649.
63. Renner U. Alkaloide aus *Schizozygia coffaeoides*. III. Strukturelle Beziehungen zwischen Schizozygine und einigen Nebenalkaloiden. *Lloydia* 1964;27:406–415.
64. Renner U, Fritz H. Alkaloide aus *Schizozygia coffaeoides* (Boj.) Baill. II. Die Struktur des Schizozygins. *Helv Chim Acta* 1965;48:308–317.
65. Hesse M, Renner U. 223. Die Massenspektren von Schizozygine und dessen Derivaten. *Helv Chim Acta* 1966;49:1875–1899.
66. Hájiček J, Taimr J, Budesinsky M. Revised structure of isoschizogamine. *Tetrahedron Lett* 1998;39:505–508.
67. Kariba RM, Houghton PJ, Yenesew A. Antimicrobial activities of a new schizozygane indoline alkaloid from *Schizozygia coffaeoides* and the revisited structure of isoschizogaline. *J Nat Prod* 2002;65:566–569.
68. Little JE, Johnstone DB. Plumericin: an antimicrobial agent from *Plumeria multiflora*. *Arch Biochem* 1951;30:445–452.
69. Albers-Schönberg G, Schmid H. Die Struktur des Plumericins und verwandter Verbindungen. *Chimia* 1960;14:127–128.
70. Albers-Schönberg G, Schmid H. Über die Struktur von Plumericin, isoplumericin,  $\beta$ -dihydroplumericin und der  $\beta$ -dihydroplumericinsäure. *Helv Chim Acta* 1961;44:1447–1473.
71. Trost BM, Balkovec JM, Mao MKT. Biomimetic approach to plumericin. *J Am Chem Soc* 1983;105:6755–6757.
72. Trost BM, Mao MKT, Balkovec JM, Buhlmyer P. A total synthesis of plumericin, allamcin and allamandin. Part 1. Basic strategy. *J Am Chem Soc* 1986;108:4965–4973.
73. Trost BM, Balkovec JM, Mao MKT. A total synthesis of plumericin, allamcin and allamandin. Part 2. A biomimetic strategy. *J Am Chem Soc* 1986;108:4974–4983.
74. Elsässer B, Krohn K, Akhtar MN, Flörke U, Kouam SF, Kuigoua MG, Ngadjui BT, Abegaz BM, Antus S, Kurtán T. Revision of the absolute configuration of plumericin and isoplumericin from *Plumeria rubra*. *Chem Biodiversity* 2005;2:799–808.



## Review Article

# Why is it Important to Simultaneously Use More Than One Chiroptical Spectroscopic Method for Determining the Structures of Chiral Molecules?

PRASAD L. POLAVARAPU\*

Department of Chemistry, Vanderbilt University, Nashville, Tennessee

**ABSTRACT** In recent years, four different chiroptical spectroscopic methods, namely vibrational circular dichroism, vibrational Raman optical activity, electronic circular dichroism, and optical rotatory dispersion, have become popular for establishing the absolute configuration and predominant conformations of chiral molecules in solution state. Many individual laboratories normally utilize only one of these methods to derive the molecular structural information. Although that approach may be satisfactory for most of the molecules studied, it is to be noted that in some instances a single method can give ambiguous conclusions or may not give complete structural information. This article summarizes the situations where simultaneous use of more than one chiroptical spectroscopic method is required to obtain molecular structural information and recommends the routine application of more than one chiroptical spectroscopic method for any given molecule. *Chirality* 20:664–672, 2008. © 2007 Wiley-Liss, Inc.

**KEY WORDS:** vibrational circular dichroism; vibrational Raman optical activity; electronic circular dichroism; optical rotatory dispersion; absolute configuration; chiral molecules

## INTRODUCTION

In recent years, there has been a renaissance<sup>1</sup> in the use of chiroptical spectroscopic methods for determining the molecular stereochemistry of chiral molecules. These spectroscopic methods include vibrational circular dichroism (VCD),<sup>2–4</sup> vibrational Raman optical activity (VROA),<sup>2–4</sup> electronic circular dichroism (ECD)<sup>5–8</sup> and optical rotatory dispersion (ORD).<sup>9,10</sup> The increased confidence in the use of these methods results from remarkable developments that were advanced by younger generation of quantum chemists for reliably predicting VCD, VROA, ECD, and ORD using quantum mechanical methods. These developments included quantum mechanical methods as well as implementation of these methods in quantum mechanical software programs that can be used with ease by newcomers to these areas.

Although numerous theories have been explored (see Ref. 3 for a summary) for VCD predictions, two related theories, namely vibronic theory<sup>11</sup> and magnetic field perturbation theory,<sup>12,13</sup> were advanced in 1983. The use of ground state electronic wave functions perturbed separately by nuclear displacements and external magnetic field, to calculate the vibrational rotational strengths, formed the basis of magnetic field perturbation theory and was first suggested in the PhD thesis of Galvas<sup>12</sup> and published a few years later.<sup>13</sup> A similar procedure was independently reported<sup>14</sup> by Stephens. The implementation of

magnetic field perturbation theory for VCD calculations with density functionals<sup>15</sup> has provided reliable predictions<sup>16–18</sup> of VCD.

A formalism to calculate electric dipole–magnetic dipole polarizability in the static limit,<sup>19</sup> as implemented at that time in the CADPAC program,<sup>20</sup> lead to the realization<sup>21</sup> by this author that VROA can be predicted quantum mechanically using numerical derivatives of polarizability tensors. Then the development of methods for calculating frequency dependent polarizabilities<sup>22</sup> made it possible to predict frequency dependent VROA for nonresonant excitation wavelengths. Later, implementation of density functional theory for VROA calculations<sup>23</sup> has lead to reliable VROA predictions. However, the numerical procedure used for obtaining the nuclear displacement derivatives of polarizabilities restricted the size of molecules that can be investigated. The development of analytic methods<sup>24,25</sup> for frequency dependent derivatives of electric dipole–electric dipole and electric dipole–electric quadrupole polarizabilities marked a significant advance. Nevertheless a similar

\*Correspondence to: P.L. Polavarapu, Department of Chemistry, Vanderbilt University, Nashville, Tennessee.

E-mail: prasad.L.polavarapu@vanderbilt.edu

Received for publication 21 June 2007; Accepted 3 August 2007

DOI: 10.1002/chir.20475

Published online 8 October 2007 in Wiley InterScience (www.interscience.wiley.com).



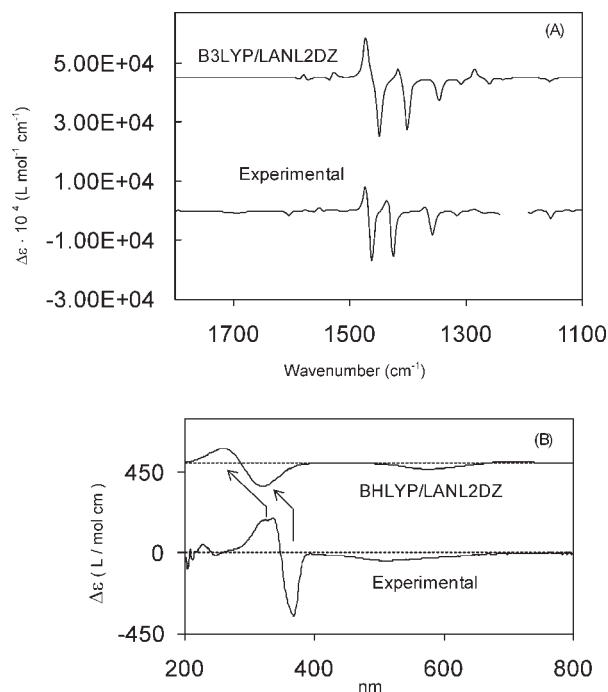


**Fig. 1.** Comparison of experimental and predicted VCD (top panel, A) and ECD (bottom panel, B) spectra for  $\text{Ni}_3[(\text{C}_5\text{H}_5\text{N})_2\text{N}]_4\text{Cl}_2$ . The experimental spectra were obtained for (–)-enantiomer and predicted spectra were obtained for *P*-enantiomer. The predicted spectra are shifted upwards for clarity. Excellent agreement between experimental and predicted spectra leads to the assignment of absolute configuration for  $\text{Ni}_3[(\text{C}_5\text{H}_5\text{N})_2\text{N}]_4\text{Cl}_2$  as (–)-*P*.

analytic method for frequency dependent derivatives of electric dipole–magnetic dipole polarizability has not yet been realized.

The first quantum mechanical calculation of optical rotation was reported<sup>26</sup> by this author in 1997 using the static limit<sup>19</sup> electric dipole–magnetic dipole polarizability. Since then remarkable advances have occurred<sup>27–35</sup> in predicting the optical rotation reliably. Simultaneous advances have taken place in the prediction of ECD as well.<sup>36–40</sup> It should be noted that ORD and ECD are not truly independent methods and theoretical ORD and ECD spectra can be obtained in a single quantum mechanical calculation using complex polarization propagator approach.<sup>1,41–43</sup>

There are now numerous applications demonstrating the reliability of each of the abovementioned chiroptical spectroscopic methods in investigating the structures of individual chiral molecules. In most typical cases it may turn out that a given chiroptical spectroscopic method may have provided satisfactory structural solution to a given molecule and that the use of a different chiroptical spectroscopic method may not have provided any additional information. As an example, for a tri-nickel complex,<sup>44</sup>  $\text{Ni}_3[(\text{C}_5\text{H}_5\text{N})_2\text{N}]_4\text{Cl}_2$ , comparison of experimental VCD spectrum with B3LYP/LANL2DZ predicted VCD spectrum indicates (see Fig. 1) that the absolute configuration of this complex is (–)-*P*. The same conclusion is reached<sup>44</sup> for this complex from the comparison of its experimental

ECD spectrum with B3LYP/LANL2DZ predicted ECD spectrum. On the basis of this example, and several other similar cases in the literature, it might appear that multiple chiroptical spectroscopic methods are likely to give redundant information and that it might be unnecessary to use more than one chiroptical spectroscopic method for structural determination. However, instead of viewing these methods as redundant, one should view them as providing independent verifications of molecular structures.

Regardless of the viewpoint preferred in such cases, one should be aware of the possibility that a given chiroptical spectroscopic method may give ambiguous, or may not give complete, and entirely correct, structural information for a given molecule. In such cases the simultaneous use of more than one chiroptical spectroscopic method may provide missing information or a solution to ambiguous conclusions. The present manuscript summarizes such cases, uncovered during the investigations in the author's laboratory, where simultaneous use of more than one chiroptical spectroscopic method is warranted to obtain reliable molecular structural information. These examples demonstrate that the routine use of more than one chiroptical spectroscopic method should be practiced for any given molecule.

## COMPARATIVE LIMITATIONS OF CHIROPTICAL SPECTROSCOPIC METHODS

*Electronic transitions and vibrational transitions need not probe the same structural aspects of chiral molecules. As a result, the information “seen” via ECD/ORD spectroscopy may not be apparent via VCD and/or VROA spectroscopy and vice versa.* In discussing this point, the context should be clarified first. For molecules which are optically active by virtue of isotopic substitution, VCD or VROA spectroscopy provides richer information<sup>45–48</sup> than ECD<sup>49</sup> and ORD<sup>50</sup> spectroscopies. However, such molecules, where chirality is solely due to isotopic substitution, are not the focus here. The main point under discussion here became evident during the investigation<sup>51</sup> of a polyguanidine (Fig. 2A). The bands in ECD spectra of polyguanidine in chloroform (Fig. 2B) and toluene (Fig. 2C) are totally different and have opposite signs, but the bands in VCD spectra of polyguanidine in these solvents have same signs and are identical (see Fig. 2D). When polyguanidine dissolved in toluene is subjected to thermal cycling in the temperature range of 25–60°C, the ECD spectra and UV–visible spectra of polyguanidine are reversibly switched<sup>51</sup>; that is, a positive ECD band present for polyguanidine at 382.0 nm at 25°C, becomes negative ECD band at 382.0 nm at 60°C. Accompanying electronic absorption band position of polyguanidine also switches<sup>51</sup> from 384.4 nm at 25°C to 382.4 nm at 60°C. The sign of measured optical rotation also changed<sup>51</sup> between 31 and 40°C. But no such temperature dependent sign reversals were seen in the VCD spectra.

The VCD spectrum of polyguanidine exhibits (see Fig. 2D) a large positive bisignate couplet (positive VCD lobe on the lower frequency side and negative VCD lobe on the higher frequency side of absorption band) at 1641  $\text{cm}^{-1}$  in

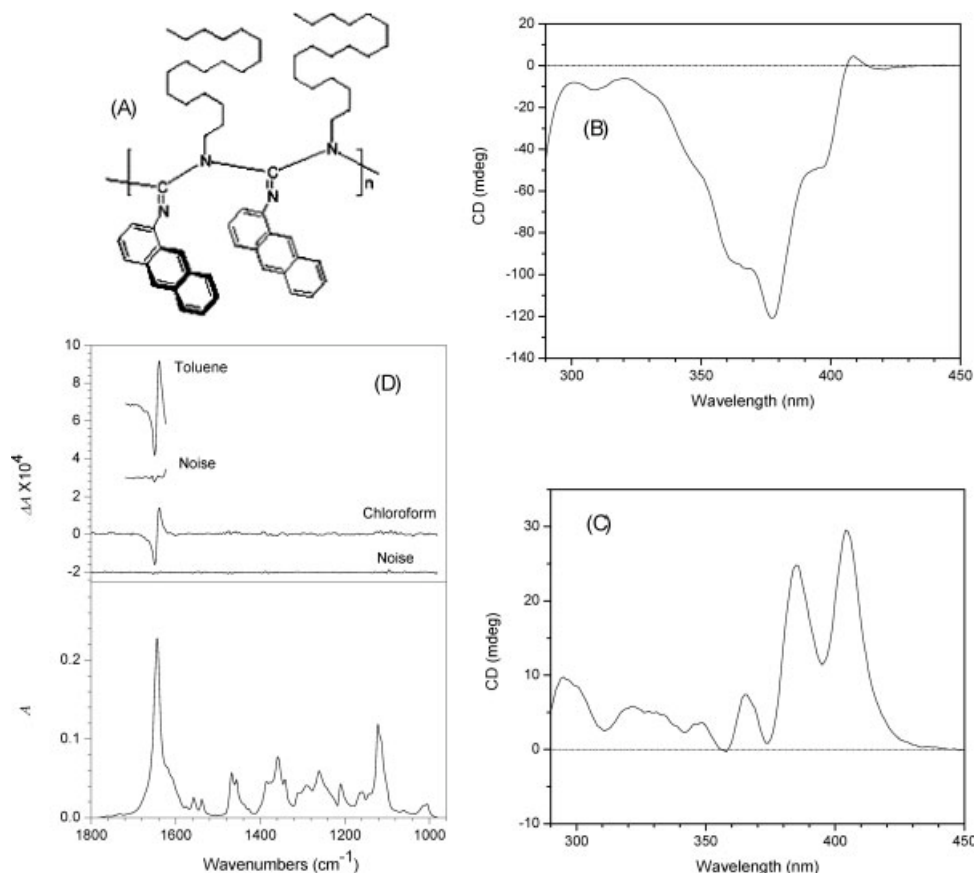


**Fig. 2.** (A) Structural drawing of polyguanidine; (B) ECD spectrum of polyguanidine in chloroform ( $c = 25.0$  mg/ml, path length = 0.1 mm); (C) ECD spectrum of polyguanidine in toluene ( $c = 20.0$  mg/ml, path length = 0.1 mm); (D) The vibrational absorbance spectrum (bottom panel, in  $\text{CDCl}_3$ ,  $c = 10.0$  mg/ml, path length = 300  $\mu\text{m}$ ) and VCD spectra (top panel, in  $\text{CDCl}_3$ ,  $c = 10.0$  mg/ml, path length = 300  $\mu\text{m}$ , and toluene  $c = 20.1$  mg/ml, path length = 200  $\mu\text{m}$ ) of polyguanidine. Spectra in  $\text{CDCl}_3$  at a concentration of 20 mg/ml are similar to those shown here. The traces labelled “noise” represent reproducibility level in the VCD spectra. VCD spectrum in toluene (shifted upwards for clarity) is not shown below  $\sim 1600$   $\text{cm}^{-1}$  due to excessive absorbance of the solvent.

both the polar solvent chloroform and the less polar solvent toluene, and is associated with the imine stretching vibration in the polyguanidine backbone. This VCD couplet remained independent in shape at various temperatures in the range of 25–60°C except for slight variation in intensity, unlike those in the ECD spectra. The handedness of polyguanidine could be established by comparing its experimental VCD spectrum with that predicted for the repeating unit of polyguanidine with *P*-handed structure using B3LYP density functional and the 6-31G\* basis set. The predicted VCD spectrum was found<sup>51</sup> to be in excellent agreement with the experimentally observed VCD spectrum of polyguanidine, establishing that investigated polyguanidine has *P*-handedness.

The two contradictory observations, namely switching of ECD and optical rotation properties with temperature and solvent polarity, and lack of such switching of VCD property, can only be reconciled if the anthracene rings are considered to synchronously wag around the N–C(Ar) bonds (thereby acting like a shutter). In this wagging motion, the orientation of anthracene rings relative to the position of lone pair electrons on nitrogen atoms changes which in turn changes the lone pair– $\pi$ -electron interactions

and hence ECD and optical rotation properties, but the chirality sensed by the vibrations of C=N bonds are not affected.

This example<sup>51</sup> illustrates that if investigations on polyguanidine were carried out only with ECD, the temperature dependent switching of ECD property could have been presumed to arise from helical inversion, while VCD studies alone would not have recognized the temperature dependent molecular motion. Combined ECD and VCD investigations, on the other hand, lead to the discovery that polyguanidine acts like a molecular shutter.

Since 3N-6 vibrational transitions encompass the entire molecule and are better resolved and widely separated, compared with the limited number of experimentally accessible electronic transitions, additional conformations may be “seen” in VCD/VROA spectral studies that may not be “seen” via ECD/ORD spectral studies. This point became transparent in the investigation of dialkyltartrates,<sup>52</sup> which can exist in three different conformations (trans-COOR, trans-OH, and trans-H) around the central C–C bond. In the carbonyl stretching region (1850–1600  $\text{cm}^{-1}$ ), vibrational spectra of dialkyl tartrates in  $\text{CCl}_4$ , show one absorption band (see Fig. 3A) and a bisignate VCD couplet (see Fig.

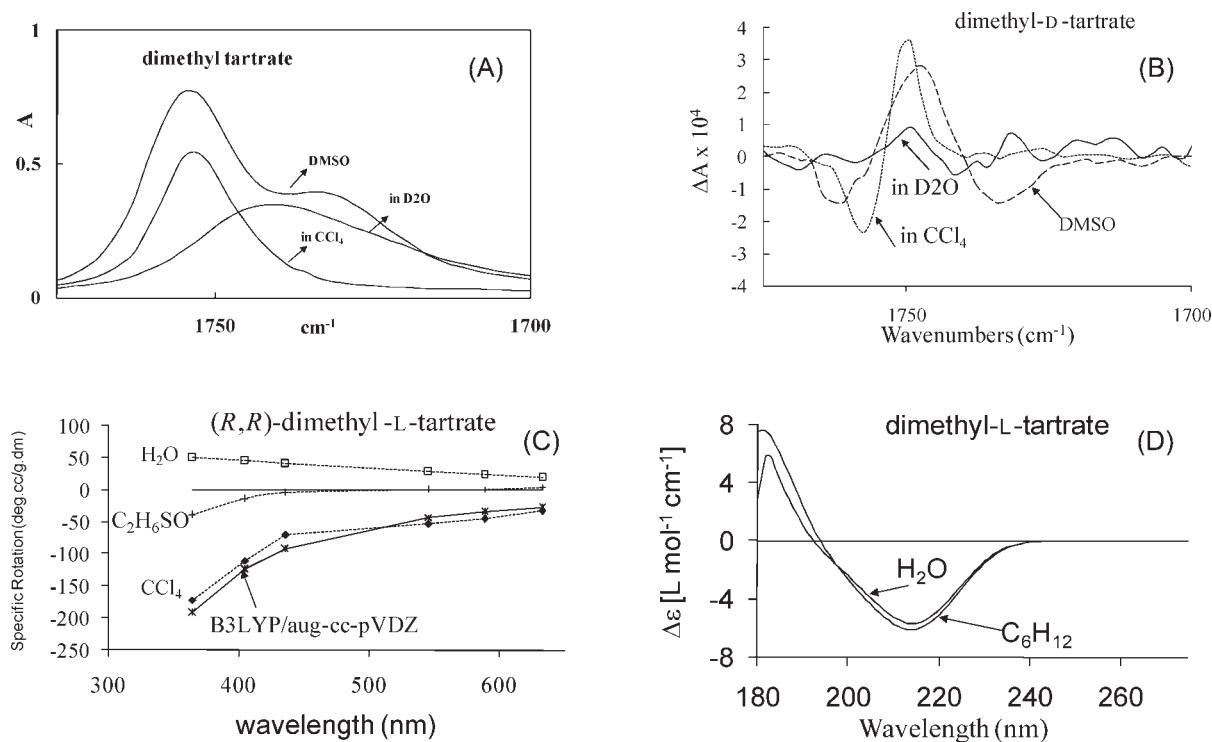


**Fig. 3.** (A) Experimental vibrational absorption spectra of dimethyl tartrate in CCl<sub>4</sub>, DMSO-d<sub>6</sub>, and D<sub>2</sub>O solvents. (B) Experimental VCD spectra of dimethyl-D-tartrate in CCl<sub>4</sub>, DMSO-d<sub>6</sub>, and D<sub>2</sub>O solvents. (C) Experimental ORD spectra of (R,R)-dimethyl-L-tartrate in CCl<sub>4</sub>, DMSO (C<sub>2</sub>H<sub>6</sub>SO) and H<sub>2</sub>O solvents and the B3LYP/aug-cc-pVDZ predicted ORD spectrum; (D) Experimental ECD spectra of (R,R)-dimethyl-L-tartrate in C<sub>6</sub>H<sub>12</sub>, and H<sub>2</sub>O solvents.

3B; negative at higher wavenumber and positive at lower wavenumber for D-enantiomer) in CCl<sub>4</sub>. The B3LYP/aug-cc-pVDZ predicted absorption and VCD spectra for the predominant conformer (trans-COOCH<sub>3</sub>-1) of isolated dimethyl-(S,S)-tartrate have good correspondence<sup>52</sup> with the corresponding experimental spectra of dialkyl tartrates in CCl<sub>4</sub>. This observation indicated that in CCl<sub>4</sub>, dialkyltartrates exist in one predominant conformation.

For a given tartrate, the absorption and VCD spectral bands are affected significantly when the solvent is changed from CCl<sub>4</sub> to dimethyl sulfoxide-d<sub>6</sub> (DMSO-d<sub>6</sub>). In the C=O stretching region two absorption bands and three VCD bands (negative–positive–negative triplet for D enantiomer) are seen (Figs. 3A and 3B) in DMSO-d<sub>6</sub>. These spectra lead to the conclusion that at least two conformers must be present for dialkyl tartrates in DMSO-d<sub>6</sub>. The absorption and VCD signals of dialkyl tartrates are also affected significantly when the solvent is changed to D<sub>2</sub>O. In the C=O stretching region one broader absorption band and no significant VCD bands are found (Figs. 3A and 3B) in D<sub>2</sub>O, suggesting further conformational changes in D<sub>2</sub>O. Thus solvent dependent conformational changes are clearly apparent through vibrational absorption and VCD spectra (Figs. 3A and 3B). A hint for such conformational change is also evident in the ORD spectra (Fig. 3C) of dimethyl tartrate in CCl<sub>4</sub>, DMSO, and H<sub>2</sub>O. While the experimental ORD of dimethyl-L-tartrate in CCl<sub>4</sub> is monosignate and negative, that in DMSO is bisignate with weak positive values at longer wavelengths and a change of sign near 546 nm. Furthermore the experimen-

tal ORD of dimethyl-L-tartrate in H<sub>2</sub>O is monosignate and positive. These solvent dependent changes in the pattern of ORD may also indicate some conformational variation in different solvents, but do not reveal the details of conformations responsible for these observations (unlike VA and VCD spectra in DMSO-d<sub>6</sub>). In contrast to VCD and ORD spectral observations, ECD spectra in the 180–300 nm region taken in nonpolar solvent C<sub>6</sub>H<sub>12</sub> and polar solvent H<sub>2</sub>O appeared quite similar (Fig. 3D). ECD spectra could not be measured in DMSO due to the solvent absorption interference. Thus ECD spectra of dialkyl tartrates in the 180–300 nm region do not reveal the presence of different conformers in different solvents. It is possible that the ECD spectra in the far-UV region (below 180 nm), if measured, may have revealed solvent dependent variations, but ECD spectra in the UV–vis region alone did not.

This example<sup>52</sup> illustrates that based on the experimental investigations of ECD spectra alone, solvent dependent conformational changes for dialkyl tartrates could not be detected. On the other hand, experimental ORD spectral studies alone would give a hint for solvent dependent conformational changes in dialkyl tartrates, but the details of conformational changes may not be obvious. The experimental vibrational absorption and VCD studies could clearly show the existence of one conformer in CCl<sub>4</sub> and at least two different conformers in DMSO. Furthermore, based on quantum mechanical predictions<sup>52</sup> of VCD, the predominant conformer of dialkyl tartrates in CCl<sub>4</sub> solvent is determined to be trans-COOR. The quantum mechanical predictions of VCD of dialkyl tartrates in DMSO solvent

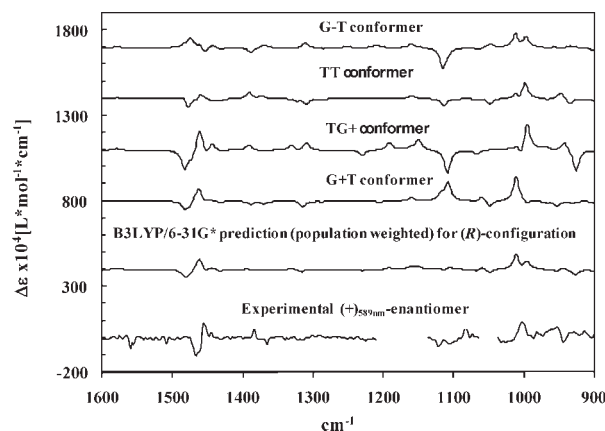


**Fig. 4.** Experimental VCD spectrum of (+)-1,1-dimethyl-2-phenylethyl phenyl sulfoxide and its comparison to B3LYP/6-31G\* predicted VCD spectra of individual conformers and population weighted predicted VCD spectrum of (R)-1,1-dimethyl-2-phenylethyl phenyl sulfoxide. Note that significant cancellation occurs for the VCD bands of different conformers at  $\sim 1100\text{ cm}^{-1}$ . The predicted spectra are shifted upwards for clarity.

suggested<sup>52</sup> the same conformer to be dominant along with a significant amount of trans-H conformer. The situation for predominant conformers of dialkyl tartrates in  $\text{H}_2\text{O}$  has not yet been resolved, and requires the investigation of water clustering<sup>53,54</sup> effects for dialkyltartrates in water.

Despite the presence of a large number of vibrational transitions, many of them for some molecules may not exhibit significant measurable VCD and/or VROA spectral intensities. In such cases the advantages of VCD and/or VROA spectra may not be realized and other chiroptical spectroscopic methods may turn out to be more useful. VCD and VROA spectroscopies have an underscoring advantage because of the rich spectral content that is expected and observed for most rigid chiral molecules. However, when a given chiral molecule has conformational freedom, the net VCD or VROA spectrum resulting from different conformers may not be rich any more due to cancellation of oppositely signed bands from different conformers. Alternately, the nature of a molecule may be such that no one conformation may exhibit significant VCD or VROA band intensities. As an example,<sup>55</sup> 1,1-dimethyl-2-phenylethyl phenyl sulfoxide in principle can exist in 81 different conformations, but based on quantum mechanical calculations four of these conformations were determined<sup>55</sup> to have significant populations. 1,1-Dimethyl-2-phenylethyl phenyl sulfoxide exhibits only a few and weak VCD bands in the experimental VCD spectrum (Fig. 4). The only characterizing VCD signature for this molecule is a weak negative–positive VCD couplet seen in the experimental spectrum in the  $1466\text{--}1454\text{ cm}^{-1}$  region. The predicted VCD spectrum with conformer population weighting also shows a limited number of weak bands and shows a couplet in the  $1480\text{--}1461\text{ cm}^{-1}$  region, corresponding to that seen in the experimental spectrum. While this correspondence may be used to suggest the molecular structure of 1,1-dimethyl-2-phenylethyl phenyl sulfoxide, because of the limited number of VCD bands associated with this molecule, it is nec-

Chirality DOI 10.1002/chir

essary to verify the conclusions resulting from experimental and predicted VCD spectra with that from other chiroptical spectroscopic methods. ECD and ORD spectral studies on 1,1-dimethyl-2-phenylethyl phenyl sulfoxide were found<sup>55</sup> to be useful to provide additional verifications of the conclusions obtained from VCD.

ORD and ECD are normally measured at much lower concentrations (some times by a factor of 1000) than those used for VCD and VROA. As a result intermolecular interactions seen via VCD and VROA may not be seen via ORD and ECD. When nonpolar, inert solvents are used for chiroptical spectroscopic measurements in solution, the nature of solvent can result in the absence of significant solute–solvent intermolecular interactions, but intermolecular hydrogen bonding can take place between two different molecules of solute leading to the formation of dimers. In such cases, the monomer–dimer equilibrium in solution needs to be considered.<sup>56,57</sup> One example [Petrovic et al. Crystallographic and chiroptical spectroscopic determination of the absolute configuration and conformations of *t*-butylphenylphosphinoamidate (in preparation)], where such monomer–dimer equilibrium exists is *t*-butylphenylphosphinoamidate (Fig. 5). The infrared absorption spectra measured at five different concentrations in the  $0.84\text{--}0.05\text{ M}$  range indicated that the monomer–dimer equilibrium constant for *t*-butylphenylphosphinoamidate is 0.34. At the concentration used for VCD studies ( $0.17\text{ M}$ ), this equilibrium constant corresponds to 90% monomer and 10% dimer populations. But at the lower concentrations used for ECD ( $0.027\text{ M}$ ) the dimer population ( $\sim 2\%$ ) is negligible. For ORD studies, where specific rotations are extrapolated to zero concentration, the dimer population can be considered to be absent. Thus the analysis of experimental VCD spectra requires the consideration of dimers, while those of ECD or ORD spectra do not. Looking at this difference from a positive viewpoint, higher concentrations normally used for VCD and VROA studies provide information on molecular dimers while lower concentrations used for ECD or ORD will not. Of course, the same observation can be viewed in an opposite sense; that is, one does not have to worry about the analysis of dimers when using ECD or ORD spectroscopy, but analysis of dimers must be undertaken when using VCD and/or VROA spectroscopy.

Because of the large number of vibrational transitions probed in VCD and VROA, it is unlikely that a change in conformation of a chiral molecule can result in oppositely signed bands in the entire VCD or VROA spectrum. However, because of the limited UV–visible wavelength region probed in ECD/ORD spectra, a change in conformation may lead to oppositely signed ECD bands and/or ORD pattern in that limited wavelength region, which may in turn be incorrectly interpreted with opposite absolute configuration. Thus the chances for incorrect assignment of absolute configuration are less with VCD and VROA spectra. This point became transparent in the investigation of *t*-butylphenylphosphinoamidate [Petrovic et al. Crystallographic and chiroptical spectroscopic determination of the absolute configuration and conformations of *t*-butylphenylphosphinoamidate (in preparation)] and *t*-butane sulfinamide.<sup>58</sup> These two mole-



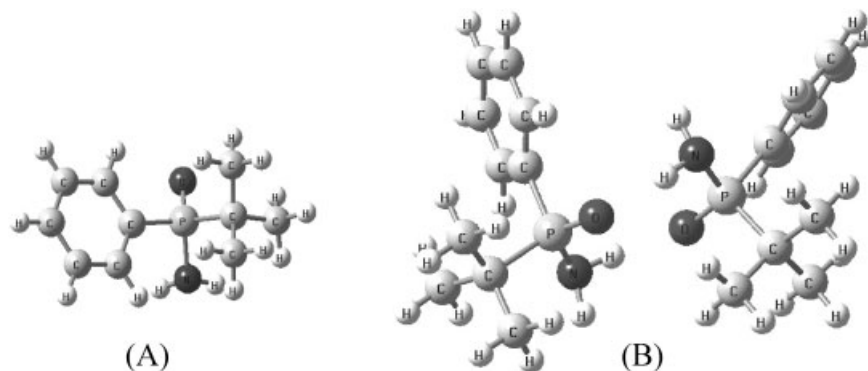


Fig. 5. Monomer (A) and dimer (B) structures of *t*-butylphenylphosphinoamidate.

cules may each exist in two different conformations (labelled as conformers 1 and 2). The calculated energy differences between different conformers of an isolated molecule may not pertain to those in solution where solute-solvent interactions may change the energy order of conformers. In the absence of any additional evidence for predominance of one conformer over the other in solution state, it is necessary to evaluate both conformers of *t*-butylphenylphosphinoamidate and *t*-butane sulfinamide.

The B3LYP/6-31G\* predicted VCD spectra for both conformers of *t*-butylphenylphosphinoamidate exhibit (Fig. 6A) the same signs for most of the vibrational bands, except for two bands near  $\sim 1600\text{ cm}^{-1}$ . Thus irrespective of the predominant conformer, B3LYP/6-31G\* VCD

results, when compared [Petrovic et al. Crystallographic and chiroptical spectroscopic determination of the absolute configuration and conformations of *t*-butylphenylphosphinoamidate (in preparation)] with corresponding experimental VCD results, will result in only one conclusion about the absolute configuration of *t*-butylphenylphosphinoamidate. On the other hand, B3LYP/6-31G\* predicted ECD spectra exhibit (Fig. 6B) opposite signs for ECD bands of the same two conformers in the UV-vis region. The same sign reversal can also be seen (Fig. 6C) in the B3LYP/6-31G\* predicted ORD spectra for the same two conformers of *t*-butylphenylphosphinoamidate. Thus depending on the presumed predominance of one of the two conformers, B3LYP/6-31G\* predicted ECD and ORD

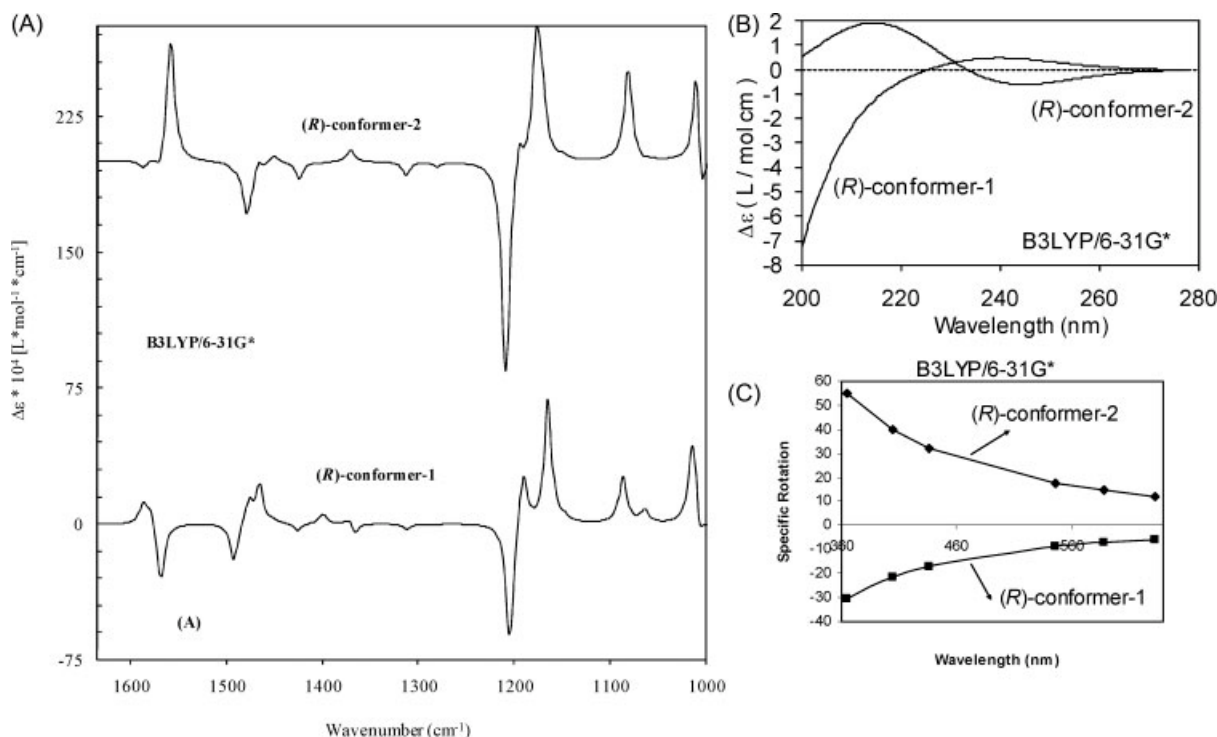
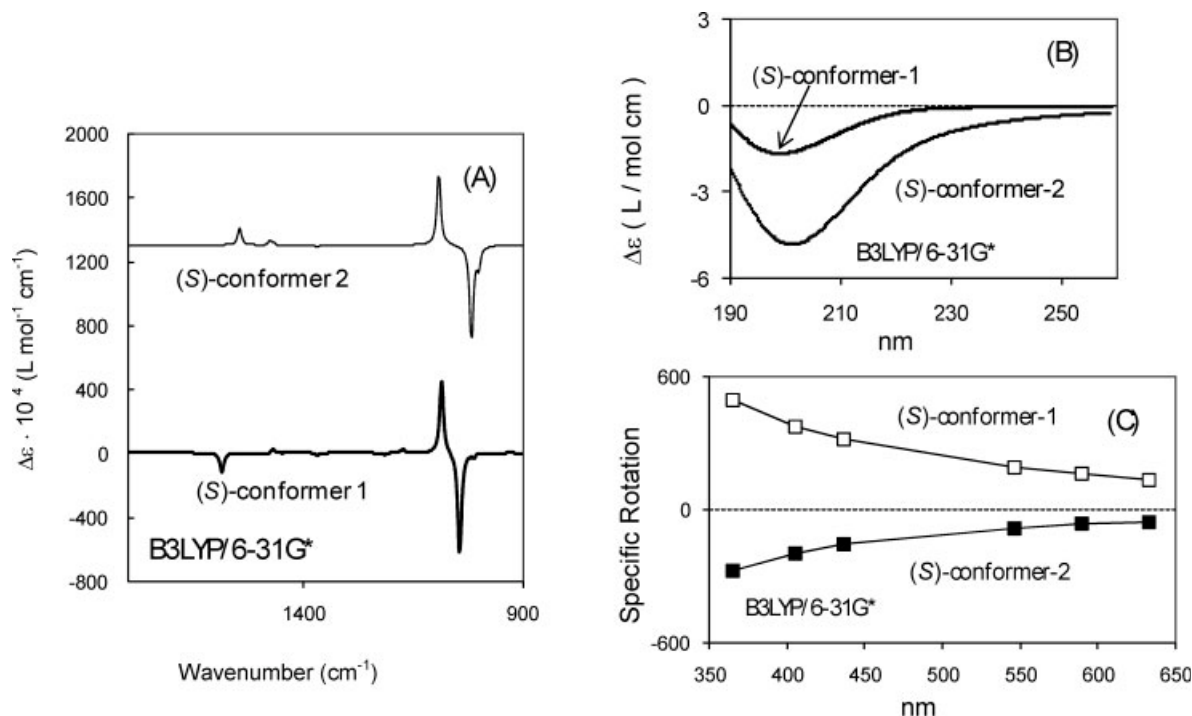


Fig. 6. (A) B3LYP/6-31G\* predicted VCD spectra for two low energy conformers of monomeric (*R*)-*t*-butylphenylphosphinoamidate; the spectrum of conformer 2 is shifted upwards for clarity. (B) B3LYP/6-31G\* predicted ECD spectra for the same two conformers of monomeric (*R*)-*t*-butylphenylphosphinoamidate; (C) B3LYP/6-31G\* predicted ORD spectra for the same two conformers of monomeric (*R*)-*t*-butylphenylphosphinoamidate.



**Fig. 7.** (A) B3LYP/6-31G\* predicted VCD spectra for two low energy conformers of monomeric (S)-*t*-butane sulfinamide; the spectrum of conformer 2 is shifted upwards for clarity. (B) B3LYP/6-31G\* predicted ECD spectra for the same two conformers of monomeric (S)-*t*-butane sulfinamide; (C). B3LYP/6-31G\* predicted ORD spectra for the same two conformers of monomeric (S)-*t*-butane sulfinamide.

spectra, when compared with corresponding experimental spectra, will result in opposite conclusions for the absolute configuration.

A similar situation appears also for *t*-butane sulfinamide.<sup>58</sup> The B3LYP/6-31G\* predicted VCD spectra for the two low energy conformers of *t*-butane sulfinamide appear similar (Fig. 7A), except for a weak band at  $\sim 1570 \text{ cm}^{-1}$ . In particular, the sign order of major VCD couplet at  $\sim 1070 \text{ cm}^{-1}$  is the same for both conformers. On the basis of this strong VCD couplet, a comparison with experimental VCD spectrum would result in the assignment of the same configuration regardless of the dominance of either of the two conformers. The same conclusion can be reached from B3LYP/6-31G\* predicted ECD spectra (Fig. 7B) because both conformers of *t*-butane sulfinamide are predicted to have negative ECD. On the other hand, the B3LYP/6-31G\* predicted ORD patterns for the same two conformers of (S)-*t*-butane sulfinamide have opposite signs (Fig. 7C) which, when compared with experimental ORD, will result in opposite conclusions for the absolute configuration depending on which one of the two conformers is considered to be predominant.

When the structural conclusions derived from different chiroptical spectroscopic methods, upon comparison of the experimental and predicted spectra, are not the same one must look for inadequacies in the predicted properties or in the experimental measurements. In the case of *t*-butylphenylphosphinoamidate [Petrovic et al. Crystallographic and chiroptical spectroscopic determination of the absolute configuration and conformations of *t*-butylphenylphosphinoamidate (in preparation)]<sup>58</sup> and *t*-butane sulfinamide, the discrepancies noted above result from the inadequacy of B3LYP/6-31G\* method for predicting ECD and ORD. When higher level B3LYP/aug-cc-pVDZ method is used the earlier mentioned discrepancies disappear.

These examples [Petrovic et al. Crystallographic and chiroptical spectroscopic determination of the absolute configuration and conformations of *t*-butylphenylphosphinoamidate (in preparation)]<sup>58</sup> illustrate the point that for different conformers of a given chiral molecule with the same absolute configuration, it is very unlikely to predict all oppositely signed VCD/VROA bands. This can be understood from the presence of both local (such as isolated stretching) as well as nonlocal (such as coupled bending or torsion) vibrations, whose optical activity need not be influenced in the same way for a given change in conformation. But for the same conformers it is possible to predict oppositely signed ECD and/or ORD spectra in the limited wavelength region accessible to experimental measurements, which can lead to incorrect absolute configurational assignment.

In the UV-visible spectral region, experimental ECD spectrum may show only a limited number of bands. But ORD in the UV-visible region can be influenced by ECD bands in the vacuum ultraviolet spectral region where experimental ECD measurements may not be feasible. Then a combination of experimental ECD and ORD spectral investigations can lead, in favorable cases, to the identification of some of ECD bands that could not be experimentally measured. It should be noted that ECD and ORD spectroscopies are not independent techniques, as they are dependent on each other through the Kramers–Kronig transform.<sup>59</sup> Furthermore

both ECD and ORD spectra can be predicted through a single quantum mechanical calculation.<sup>1,41–43</sup> If the analyses of ECD and ORD results lead to inconsistent conclusions, then that is an indication of one, or both, of two possibilities; (a) some ECD bands present in the experimentally inaccessible region are significant; (b) the level of theory used for ECD and ORD predictions is inadequate. These statements do not obviate the need to investigate both ECD and ORD spectra for a given molecule. First, both ECD and ORD spectra are needed to evaluate the needed consistency among themselves, as discussed earlier. Furthermore, since experimentally observed ORD pattern in the visible wavelength region depends also on the CD associated with electronic transitions in the short wavelength region, combined experimental investigation of ECD and ORD spectra can yield, in favorable cases, information on ECD bands present in the experimentally inaccessible short wavelength region. One such useful application for simultaneous use of ECD and ORD has been reported<sup>60</sup> for dimethyl tartrate.

From the examples given earlier, the simultaneous use of more than one chiroptical spectroscopic method for studying a given chiral molecule is useful for three different reasons. (a) Independent verification of the structural conclusions obtained with a given method, and extra confidence for those conclusions, can be obtained when the same conclusions are obtained with a different method. This was the situation for  $\text{Ni}_3[(\text{C}_5\text{H}_5\text{N})_2\text{N}]_4\text{Cl}_2$ . (b) When the analysis with a particular method is uncertain or additional evidence is preferred for the conclusions reached, those issues may be resolved by using a different method, as was suggested for 1,1-dimethyl-2-phenylethyl phenyl sulfoxide. (c) Even in the absence of obvious uncertainties in the analysis with a particular method, it is useful to explore a different method because one may not recognize that information obtained with one method is incomplete, or incorrect, until a different method has been used. This was the situation for polyguanidine, dimethyltartrate, *t*-butylphenylphosphinoamidate, and *t*-butane sulfinamide. Most of the literature investigations, that used more than one chiroptical spectroscopic method, belong to the situation (a) and/or (b); those that addressed the situation (c) are limited in number.

When multiple chiroptical spectroscopic methods are simultaneously used for each chiral molecule, it may become possible to generalize the limitations of a given method for certain type of molecules. On a practical note, most laboratories may not have access to all, or more than one, of experimental ECD, VCD, and ROA measurements, as they involve expensive instrumentation. In situations where access to more than one chiroptical spectroscopic method is not available, the present conclusions encourage collaborative efforts between different laboratories that have access to different methods.

## CONCLUSIONS

For some molecules different chiroptical spectroscopic methods may give the same or redundant information.

However instead of viewing such methods as redundant, one should view them as providing independent verifications. Regardless of the view point preferred in such cases, it should be noted that there certainly are molecules where a single chiroptical spectroscopic method may not provide complete structural information. The examples presented in this review emphasized such molecules and indicated that it is essential to simultaneously use more than one chiroptical spectroscopic method for determining the structures of chiral molecules.

## ACKNOWLEDGMENTS

Collaborations with Professor Bruce Novak and Dr. Hong-Zhi Tang, on polyguanidine research and with Dr. Jozef Drabowicz on *t*-butylphenylphosphinoamidate research are greatly appreciated. Special thanks are due to my students, Dr. Jiangtao He, Dr. Peng Zhang, and Dr. Ana G. Petrovic who carried out most of the work presented in this paper.

## LITERATURE CITED

1. Polavarapu PL. Renaissance in chiroptical spectroscopic methods for molecular structure determination. *Chem Rec* 2007;7:125–136.
2. Barron LD. Molecular light scattering and optical activity, 2nd ed. Cambridge Univ Press; 2004.
3. Polavarapu PL. Vibrational spectra: principles and applications with emphasis on optical activity. New York: Elsevier; 1998.
4. Diem M. Introduction to modern vibrational spectroscopy. New York: Wiley; 1993.
5. Berova N, Nakanishi K, Woody RW. Circular dichroism: principles and applications. New York: Wiley; 2000.
6. Harada N, Nakanishi K. Circular dichroic spectroscopy: excitation coupling in organic stereochemistry. Mill Valley: University Science Books; 1983.
7. Woody RW. Theory of circular dichroism of proteins. In: Fasman GD, editor. Circular dichroism and the conformational analysis of biomolecules. New York: Plenum; 1996.
8. Lightner DA, Gurst JE. Organic conformational analysis and stereochemistry from circular dichroism spectroscopy. New York: Wiley; 2000.
9. Lowry TM. Optical rotatory power. New York: Dover; 1964.
10. Djerassi C. Optical rotatory dispersion. New York: McGraw Hill; 1960.
11. Nafie LA, Freedman TB. Vibronic coupling theory of infrared vibrational intensities. *J Chem Phys* 1983;78:7108–7116.
12. Galwas PA. On the distribution of optical polarization in molecules. Ph.D. thesis. University of Cambridge, Cambridge; 1983.
13. Buckingham AD, Fowler PW, Galwas PA. Velocity dependent property surfaces and the theory of vibrational circular dichroism. *Chem Phys* 1987;112:1–14.
14. Stephens PJ. Theory of vibrational circular dichroism. *J Phys Chem* 1985;89:748–752.
15. Cheeseman JR, Frisch MJ, Devlin FJ, Stephens PJ. Ab initio calculation of atomic axial tensors and vibrational rotational strengths using density functional theory. *Chem Phys Lett* 1996;252:211–220.
16. Polavarapu PL, He J. Chiral analysis using circular dichroism spectroscopy in the mid-infrared. *Anal Chem* 2004;76:61A–67A.
17. Freedman TB, Cao X, Dukor RK, Nafie LA. Absolute configuration determination of chiral molecules in the solution state using vibrational circular dichroism. *Chirality* 2003;15:743–758.
18. Stephens PJ, Devlin FJ. Determination of the structure of chiral molecules using ab initio vibrational circular dichroism spectroscopy. *Chirality* 2000;12:172–179.
19. Amos RD. Electric and magnetic properties of CO, HF, HCl, and CH<sub>3</sub>F. *Chem Phys Lett* 1982;87:23–26.

20. Amos RD, Rice JE. CADPAC: The Cambridge Analytic Derivatives Package. Issue 4.0, Cambridge, 1987.
21. Polavarapu PL. Ab initio Raman and Raman optical activity spectra. *J Phys Chem* 1990;94:8106–8112.
22. Helgaker T, Ruud K, Bak KL, Jorgensen P, Olsen J. Vibrational Raman optical activity calculations using London atomic orbitals. *J Faraday Discuss* 1994;99:165–180.
23. Ruud K, Helgaker T, Bour P. Gauge-origin independent density-functional theory calculations of vibrational Raman optical activity. *J Phys Chem A* 2002;106:7448–7455.
24. Quinet O, Champagne B. Time-dependent Hartree-Fock schemes for analytical evaluation of the Raman intensities. *J Chem Phys* 2001;115:6293–6299.
25. Quinet O, Liegeois V, Champagne B. TDHF evaluation of the dipole-quadrupole polarizability and its geometrical derivatives. *J Chem Theory Comput* 2005;1:444–452.
26. Polavarapu PL. Ab initio molecular optical rotations and absolute configurations. *Mol Phys* 1997;91:551–554.
27. Polavarapu PL. Optical rotation: recent advances in determining the absolute configuration. *Chirality* 2002;14:768–781; see erratum 2003;15:284–285.
28. Crawford TD. Ab initio calculation of molecular chiroptical properties. *Theor Chem Acc* 2006;115:227–245.
29. Ruud K, Helgaker T. Optical rotation studied by density-functional and coupled-cluster methods. *Chem Phys Lett* 2002;352:533–539.
30. Grimme S. Calculation of frequency dependent optical rotation using density functional response theory. *Chem Phys Lett* 2001;339:380–388.
31. Pedersen TB, Koch H, Boman L, Sanchez de Meras AMJ. Origin invariant calculation of optical rotation without recourse to London Orbitals. *Chem Phys Lett* 2004;393:319–326.
32. Autschbach J, Jensen L, Schatz GC, Electra Tse YC, Krykunov M. Time dependent density functional calculations of optical rotatory dispersion including resonance wavelengths as a potentially useful tool for determining absolute configuration of chiral molecules. *J Phys Chem A* 2006;110:2461–2473.
33. Stephens PJ, Devlin FJ, Cheeseman JR, Frisch MJ. Calculation of optical rotation using density functional theory. *J Phys Chem A* 2001;105:5356–5371.
34. Wiberg KB, Wang Y, Murphy MJ, Vaccaro PK. Temperature dependence of optical rotation:  $\alpha$ -pinene,  $\beta$ -pinene, pinane, camphene, camphor and fenchone. *J Phys Chem A* 2004;108:5559–5563.
35. Zuber G, Goldsmith M, Beratan DN, Wipf P. Assignment of the absolute configuration of  $[n]$ -Ladderanes by TD-DFT optical rotation calculations. *Chirality* 2005;17:507–510.
36. Pedersen TB, Koch H, Ruud K. Coupled cluster response calculation of natural chiroptical spectra. *J Chem Phys* 1999;110:2883–2892.
37. Autschbach J, Ziegler T, van Gisbergen SJA, Baerends EJ. Chiroptical properties from time-dependent density functional theory. I. Circular dichroism spectra of organic molecules. *J Chem Phys* 2002;116:6930–6940.
38. Diedrich C, Grimme S. Systematic investigation of modern quantum chemical methods to predict electronic circular dichroism spectra. *J Phys Chem A* 2003;107:2524–2539.
39. Pecul M, Ruud K, Helgaker T. Density functional theory calculation of electronic circular dichroism using London orbitals. *Chem Phys Lett* 2004;388:110–119.
40. Stephens PJ, McCann DM, Devlin FJ, Cheeseman JR, Frisch MJ. Determination of the absolute configuration of  $[3(2)](1,4)$  barrelenophanedicarbonitrile using concerted time-dependent density functional theory calculations of optical rotation and electronic circular dichroism. *J Am Chem Soc* 2004;126:7514–7521.
41. Norman P, Ruud K, Helgaker T. Density-functional theory calculations of optical rotatory dispersion in the nonresonant and resonant frequency regions. *J Chem Phys* 2004;120:5027–5035.
42. Krykunov M, Kundrat MD, Autschbach J. Calculation of CD spectra from optical rotatory dispersion, and vice versa, as complementary tools for theoretical studies of optical activity using time-dependent density functional theory. *J Chem Phys* 2006;125:194110.
43. Jiemchoorj A, Norman P. Electronic circular dichroism spectra from the complex polarization propagator. *J Chem Phys* 2007;126:134102–134102-7.
44. Armstrong DW, Cotton FA, Petrovic AG, Polavarapu PL, Warnke MM. Resolution of enantiomers in solution and determination of the chirality of extended metal atom chains. *Inorg Chem* 2007;46:1535–1537.
45. Barron LD. Raman optical activity due to isotopic substitution:  $[\alpha\text{-}^2\text{H}]$  benzylalcohol. *J Chem Soc Chem Commun* 1977;9:305–306.
46. Polavarapu PL, Nafie LA, Benner SA, Morton TH. Optical activity due to isotopic substitution. vibrational circular dichroism and the absolute configuration of  $\alpha$ -deuterated cyclohexanones. *J Am Chem Soc* 1981;103:5349–5359.
47. Shaw RA, Wieser H, Dutler R, Rauk A. Vibrational optical activity of (S)-1-*d*-ethanol. *J Am Chem Soc* 1990;112:5401–5410.
48. Haesler J, Schindelholz I, Riguet E, Bochet CG, Hug W. Absolute configuration of chirally deuterated neopentane. *Nature* 2007;446:526–529.
49. Barth G, Djerassi C. Circular dichroism of molecules with isotopically engendered chirality. *Tetrahedron* 1981;37:4123–4142.
50. Brown HC, Groot C. Studies in stereochemistry: The preparation of *d*-1-deutero-2-methylbutane and the study of its optical rotation. *J Am Chem Soc* 1942;64:2563–2566.
51. Tang H-Z, Novak BM, He J, Polavarapu PL. A thermal and solvocontrollable cylindrical nanoshutter based on a single screw-sense helical polyguanidine. *Angew Chem Int Ed* 2005;44:7298–7301.
52. Zhang P, Polavarapu PL. Spectroscopic investigation of the structures of dialkyl tartrates and their cyclodextrin complexes. *J Phys Chem A* 2007;111:858–871.
53. Mukhopadhyay P, Zuber G, Goldsmith M-R, Wipf P, Beratan DN. Solvent effect on optical rotation: a case study of methyloxirane in water. *Chem Phys Chem* 2006;7:2483–2496.
54. Sadej J, Dobrowolski JC, Rode JE, Jamroz MH. DFT study of vibrational circular dichroism of D-lactic acid-water complex. *Phys Chem Chem Phys* 2006;8:101–113.
55. Petrovic AG, He J, Polavarapu PL, Xiao LS, Armstrong DW. Absolute configuration and predominant conformations of 1,1-dimethyl-2-phenylethyl phenyl sulfoxide. *Org Biomol Chem* 2005;3:1977–1981.
56. Goldsmith M-R, Jayasuriya N, Beratan DN, Wipf P. Optical rotation of noncovalent aggregates. *J Am Chem Soc* 2003;125:15696–15697.
57. Kuppens T, Herrebout W, van der Veken B, Bultinck P. Intermolecular association of tetrahydrofuran-2-carboxylic acid in solution: a vibrational circular dichroism study. *J Phys Chem A* 2006;110:10191–10200.
58. Petrovic AG, Polavarapu PL. Chiroptical spectroscopic determination of molecular structures of chiral sunfinamides: *tert*-butanesulfinamide. *J Phys Chem* (submitted).
59. Polavarapu PL. Kramers-Kronig transformation for optical rotatory dispersion studies. *J Phys Chem A* 2005;109:7013–7023.
60. Polavarapu PL, Petrovic AG, Zhang P. Kramers-Kronig transformation of experimental electronic circular dichroism: application to the analysis of optical rotatory dispersion in dimethyl tartrate. *Chirality* 2006;18:723–732.





# Isotopic Difference Spectra as an Aide in Determining Absolute Configuration Using Vibrational Optical Activity: Vibrational Circular Dichroism of $^{13}\text{C}$ - and $^2\text{H}$ -Labelled Nonamethoxy Cyclotrimeratrylene

TERESA B. FREEDMAN,<sup>1</sup> XIAOLIN CAO,<sup>1</sup> ZEEV LUZ,<sup>2</sup> HERBERT ZIMMERMANN,<sup>3</sup> RAPHY POUPKO,<sup>2</sup>  
AND LAURENCE A. NAFIE<sup>1\*</sup>

<sup>1</sup>Department of Chemistry, Syracuse University, Syracuse, New York 13244, USA

<sup>2</sup>Weizmann Institute of Science, Rehovot 76100, Israel

<sup>3</sup>Max-Planck-Institute for Medical Research, Jahnstrasse 29, 69120 Heidelberg, Germany

**ABSTRACT** The use of isotopic difference spectra in vibrational optical activity is demonstrated as a supplemental aide in determining the absolute configuration of chiral molecules. It is shown that IR and VCD difference spectra associated with isotopic substitution observed in experimental spectra can be accurately reproduced by density functional theory calculations when the IR and VCD spectra of the original isotopomer are calculated to reasonable accuracy. Results for isotopically substituted nonamethoxy cyclotrimeratrylene are presented to illustrate the degree of agreement between measured and calculated IR and VCD difference spectra for several isotopomers of this molecule. These findings highlight the utility of isotopic substitution as an aide to verifying the determination of absolute configuration using vibrational optical activity. *Chirality* 20:673–680, 2008. © 2008 Wiley-Liss, Inc.

**KEY WORDS:** vibrational optical activity; isotopic spectral shifts; absolute configuration determination; VCD; nonamethoxy cyclotrimeratrylene

## INTRODUCTION

Vibrational optical activity (VOA)<sup>1–5</sup> is comprised of two fundamentally distinct areas of spectroscopy, vibrational circular dichroism (VCD)<sup>6</sup> and vibrational Raman optical activity (ROA).<sup>7,8</sup> Both involve a difference in spectroscopic intensity with respect to left and right circularly polarized radiation for a chiral molecule undergoing a vibrational transition. VCD is observed in the mid-IR and near-IR spectral regions,<sup>9</sup> whereas ROA is observed in the visible region of the spectrum, except for a recent report using near-IR laser excitation.<sup>10</sup>

VCD has been shown to provide a powerful new approach to the determination of absolute configuration (AC) in small to medium sized chiral molecules.<sup>11–14</sup> In recent years, the application of VCD to the determination of AC has increased in diversity, complexity, and extent.<sup>15–40</sup> In addition, *a priori* calculations of ROA spectra have also been recently explored<sup>41–49</sup> and the determination of AC using ROA has been demonstrated in two high-profile examples.<sup>50,51</sup> These highlight the power of VOA to assign AC in cases that are beyond that of more traditional methods.

The determination of AC by VOA is conceptually simple, although its application, in the case of flexible molecules with multiple conformations in solution, can be challenging. One measures the solution-state infrared (IR) absorption or Raman scattering spectrum and the corresponding

VCD or ROA spectrum, and then compares these spectra to *a priori* quantum mechanical calculations of the corresponding spectra using typically density function theory (DFT). Instrumentation for the measurement of VCD and ROA is widely available from commercial sources as are computer programs from various sources for VCD and ROA calculations.

VOA has a number of advantages over classical forms of optical activity, optical rotation (OR) and electronic circular dichroism (ECD), as well as some disadvantages. The main advantages of VOA are the plethora of resolved transitions that can be measured for a given molecule and the fact that transitions occur only within the *ground* electronic state of the molecule. This makes VOA, and in particular VCD, relatively easy to calculate and compare to experiment. Furthermore, these transitions are particularly sensitive to the masses of individual nuclei, which by comparison have relatively little effect in the typical low-resolution measurement of electronic optical activity. The disadvantages are the higher concentrations of sample required for

\*Correspondence to: Laurence A. Nafie, Department of Chemistry, Syracuse University, Syracuse, New York, 13244.

E-mail: lnafie@syr.edu, lanafie@aol.com

Received for publication 13 August 2007; Accepted 26 October 2007

DOI: 10.1002/chir.20514

Published online 16 January 2008 in Wiley InterScience (www.interscience.wiley.com).

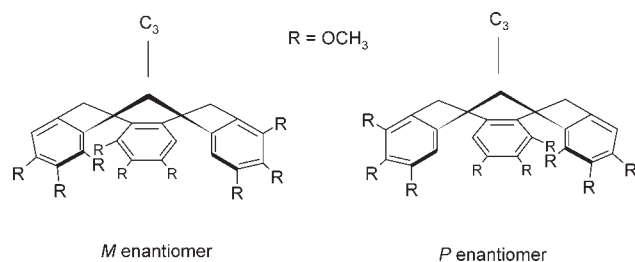


**Fig. 1.** Assignment of the absolute stereochemistry of nonamethoxy cyclotrivenatrylene.

VOA compared to ECD and the increased sophistication of instrumentation needed for VOA compared to that needed for OR.

This sensitivity to the masses of atomic nuclei has been highlighted in a number of papers over the years where VOA has been shown to exhibit normal-sized intensities for molecules that are chiral only by virtue of isotopic substitution. Particular examples are deuterio- $\alpha$ -benzyl alcohol,<sup>52</sup> dideutero- $\alpha$ -adamantanone,<sup>53</sup>  $\alpha$ -deuterated

cyclohexanones,<sup>54</sup> *trans* dideutero-oxirane,<sup>55,56</sup> deuterium and carbon-13 substituted cyclopropanes,<sup>56–60</sup> and most recently neopentane with differing degrees of deuterium substitution on its four constituent methyl groups.<sup>51</sup>

In this article, we address a different use of isotopic substitution in VOA, namely the measurement and calculation of isotopic VCD difference spectra in an inherently chiral molecule. We show that the fidelity of agreement between measurement and computation is maintained under selective isotopic substitution. This opens a new avenue for reinforcing the determination of AC by VOA where an initial AC has already been carried out without the use of isotopic substitution.

## EXPERIMENTAL

The structure of the functionalized cyclotrivenatrylene is shown Figure 1 along with its assignment of axial chirality by standard IUPAC conventions. The synthesis and resolution of functionalized cyclotrivenatrylene has been reported recently.<sup>61</sup> The parent nonamethoxy cyclotrivenatrylene without isotopic substitution, following previous

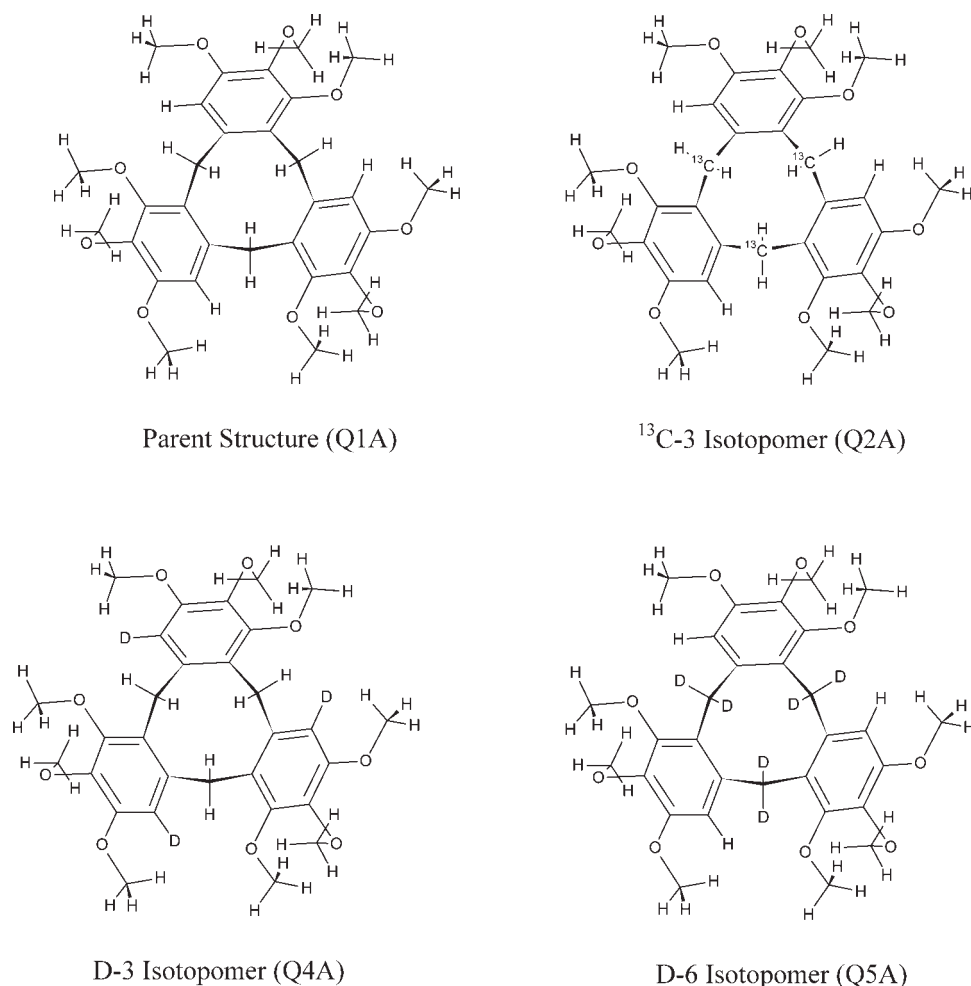


**Fig. 2.** Structure and isotopic labeling of the parent Q1A and three isotopomers Q2A, Q4A, and Q5A.

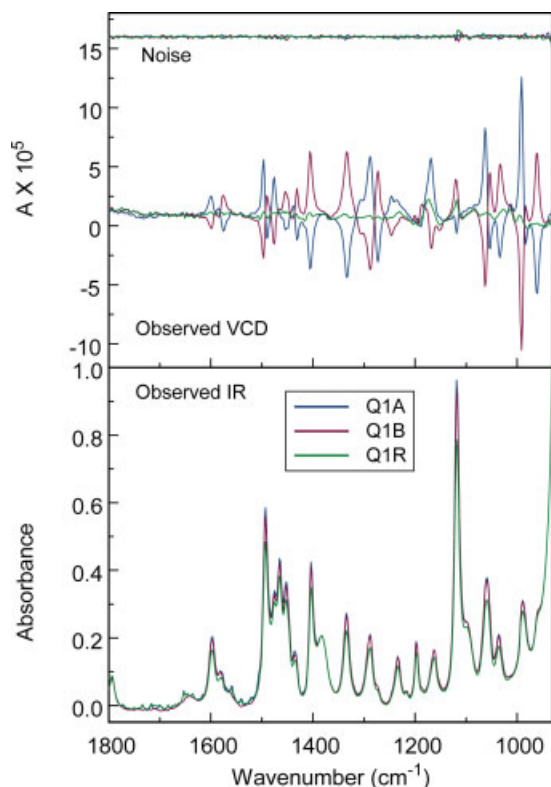


**Fig. 3.** IR (lower frame) and VCD (upper frame) spectra of Q1A, Q1B, and Q1R (4 mg/120  $\mu$ l  $\text{CDCl}_3$ ), 4  $\text{cm}^{-1}$  resolution, 5-h collection, instrument optimized at 1400  $\text{cm}^{-1}$ . Uppermost traces are VCD noise. IR spectra are solvent subtracted. [Color figure can be viewed in the online issue, which is available at [www.interscience.wiley.com](http://www.interscience.wiley.com).]

notation for this molecule, is designated Q1. The absolute configuration of the first eluted HPLC fraction Q1A has been established by VCD as the *P*-enantiomer and the second eluting fraction Q1B as the *M*-enantiomer.<sup>61</sup> Samples of Q1 in racemic (Q1R) and resolved (Q1A and Q1B) forms were provided in the crown conformation for VCD measurement. Isotopomers illustrated in Figure 2 with la-

beled carbon-13 (99%) at the three ring methylenes (designated  $^{13}\text{C}$ -3) were provided (Q2A, Q2B and Q2R), as were deuterium-substituted isotopomers (D-3) at the three aromatic hydrogen (Q4A, Q4B and Q4R) and (D-6) at the six bridge methylene hydrogen positions (Q5A, Q5B and Q5R). Solutions in  $\text{CDCl}_3$  were prepared at concentrations of approximately 4 mg per 120  $\mu$ l. Samples were placed in a 0.10-mm IR cell with  $\text{BaF}_2$  windows, and IR and VCD spectra were recorded with a modified Dual-PEM ChiralIR<sup>TM</sup> FT-VCD spectrometer (BioTools, Jupiter, FL) using 4- $\text{cm}^{-1}$  resolution, 5-h collection, and the optimum retardation of the two ZnSe photoelastic modulators (PEMs) set at 1400  $\text{cm}^{-1}$ . The observed IR, VCD, and VCD noise spectra are presented in Figure 3 for the parent crown isomer. The small baseline artifacts in the VCD spectra between 1000 and 1100  $\text{cm}^{-1}$  as seen in the VCD spectra of the racemic samples are also observed for the pure solvent (not shown), and arise from the cell used. These artifacts can be eliminated by subtraction of the solvent or racemic VCD spectrum, or by taking the difference of the two enantiomer VCD spectra and dividing by two. The last method was used to obtain the final VCD spectra of samples Q1A, Q2A, Q4A, and Q5A for comparison to calculation.

The *P*-enantiomer of the crown conformation was constructed with HyperChem software (Hypercube, Gainsville, FL). Calculations of the optimized geometry, vibrational frequencies and IR and VCD intensities were carried out on a Pentium IV PC using DFT, a 6-31G(d) basis set and B3LYP functionals with Gaussian 03W<sup>62</sup> (Gaussian, Inc., Wallingford, CT). The calculated frequencies were uniformly scaled by 0.97 and the calculated intensities were converted to Lorentzian bands with 6- $\text{cm}^{-1}$  half-width and summed over all transitions for comparison to experiment. Top and bottom views of the *P*-enantiomer along the  $\text{C}_3$ -axis for the optimized geometry are shown in Figure 4. The initial structure with all methoxy substituents in the plane of the aromatic rings optimized to a structure with one methoxy group in the plane, one above, and one below, for each phenyl group. Since the methoxy

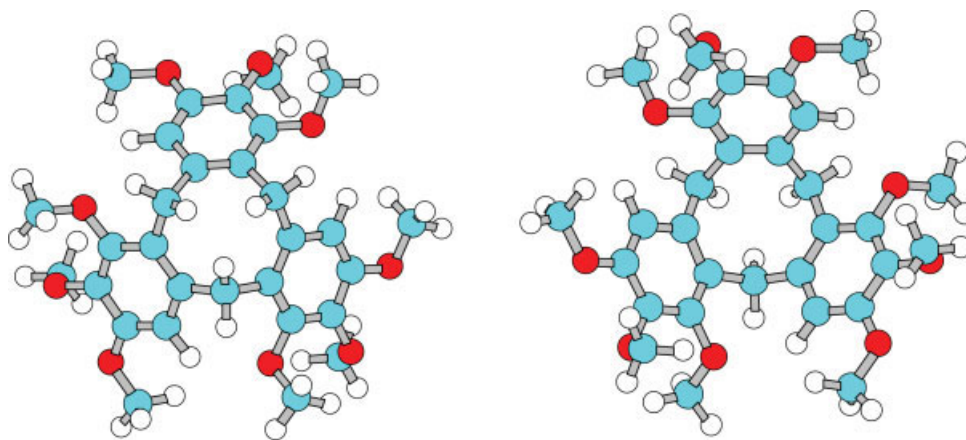


**Fig. 4.** Optimized geometry of the *P*-enantiomer of nonamethoxy cyclotrimeratrylene viewed from above (left) and below (right) along the  $\text{C}_3$ -axis. [Color figure can be viewed in the online issue, which is available at [www.interscience.wiley.com](http://www.interscience.wiley.com).]

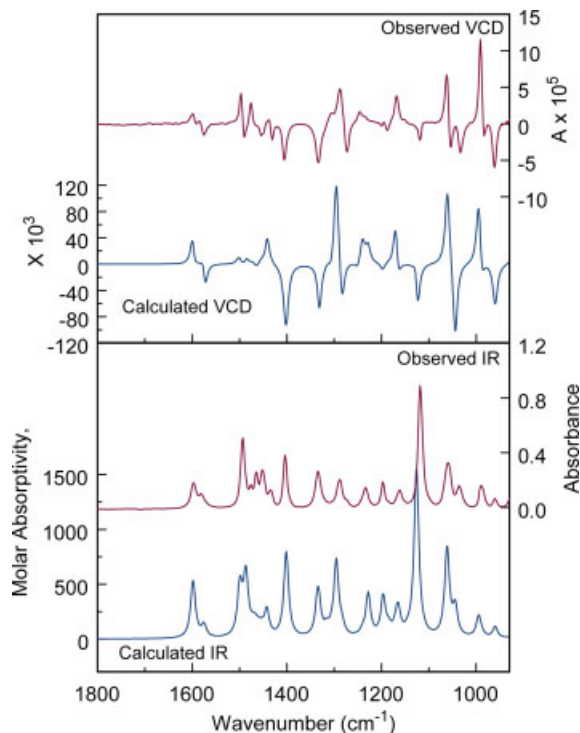


**Fig. 5.** IR (lower frame) and VCD (upper frame) observed for Q1A (right axes) compared to the calculation for the *P*-enantiomer in the conformation shown in Figures 1 and 4 (left axes). [Color figure can be viewed in the online issue, which is available at [www.interscience.wiley.com](http://www.interscience.wiley.com).]

groups all have the same relative structure on each aromatic ring, the molecule maintains  $C_3$ -symmetry.

## RESULTS AND DISCUSSION

Comparison of the observed VCD and IR spectra for samples Q1A and Q2A with calculated spectra for the *P*-enantiomer of these molecules are displayed in Figures 5 and 6, respectively. The close agreement between observed and calculated spectra establishes the absolute configurations of Q1A and Q2A as *P*, and those of Q1B and Q2B as *M*. The close similarity of the observed and calculated spectra suggests that the single conformation calculated (Fig. 4) is dominant. Carbon-13 isotopic substitution at the ring methylenes has a small but distinct effect on the vibrational spectra. Overlays of the observed and calculated spectra of these two isotopomers are shown in Figure 7. The observed IR and VCD difference spectra for the samples Q1A minus Q2A are compared to the calculated difference spectra for the  $^{12}\text{C}$ -isotopomer minus the  $^{13}\text{C}$ -isotopomer in Figure 8. The calculations reproduce virtually all the changes observed for the IR and VCD spectra of the two isotopomers, with excellent agreement for largest changes below  $1300\text{ cm}^{-1}$ . Comparing the intensity scales for the  $^{13}\text{C}$ -difference spectra relative to those of the parent structures reveals an intensity difference of approximately four times smaller for both the IR and VCD difference spectra. The agreement between both IR and VCD

*Chirality* DOI 10.1002/chir

difference spectra determined for the measurements and the calculations further supports the presence of a single dominant conformer and the assignment of the AC of these molecules. Examination of the calculated structure indicates that rotation of the out-of-plane methoxy groups to the opposite side of the aromatic plane would introduce unfavorable steric overlap with the in-plane methoxy group on the adjacent aromatic ring.

Analogous difference spectra for the two deuterium isotopomers Q4A, D-3 and Q5A, D-6 are shown in Figures 9 and 10, respectively. Again, both the match between calculated and observed IR and VCD as well as their respective isotopic difference spectra is very close. The effect of the selective isotopic substitution on the IR and VCD spectra is somewhat larger for deuterium substitution than it is for  $^{13}\text{C}$  substitution, although overall relatively minor changes are observed compared to the IR and VCD of the parent isotopomer. For the deuterium difference spectra, the intensity scales are only a factor of two to four smaller relative to those for the parent isotopomer. The degree of agreement for the deuterium substitution is qualitatively as good as that observed for the  $^{13}\text{C}$ -substitution.

It is interesting to note that small intensity shifts in nearly identical-looking IR and VCD spectra of the Q1 and Q2 isotopomers, as shown in Figure 7, give rise to relatively robust and computationally reproducible spectra, as shown in Figure 8. Furthermore, the number of positive and negative peaks nearly doubles giving the impression

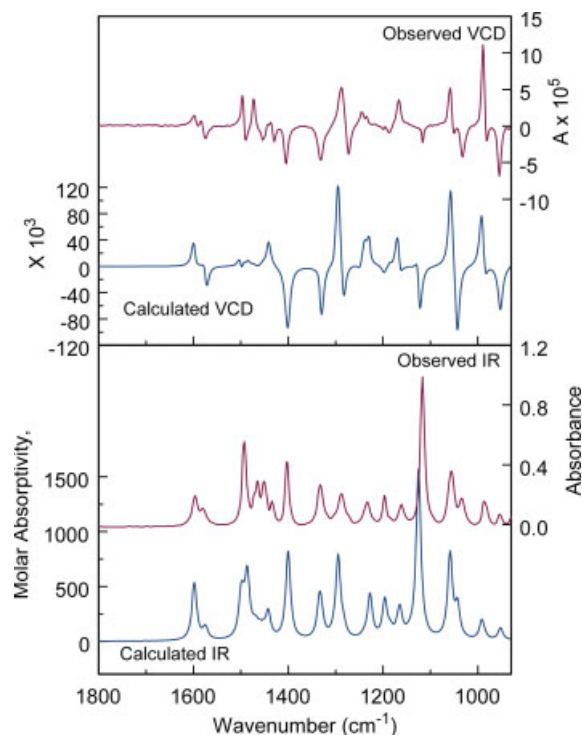


**Fig. 6.** IR (lower frame) and VCD (upper frame) observed for Q2A compared to the calculation for the *P*-enantiomer with  $^{13}\text{C}$  at three ring methylenes ( $^{13}\text{C}$ -3), in the conformation shown in Figures 1 and 4. [Color figure can be viewed in the online issue, which is available at [www.interscience.wiley.com](http://www.interscience.wiley.com).]



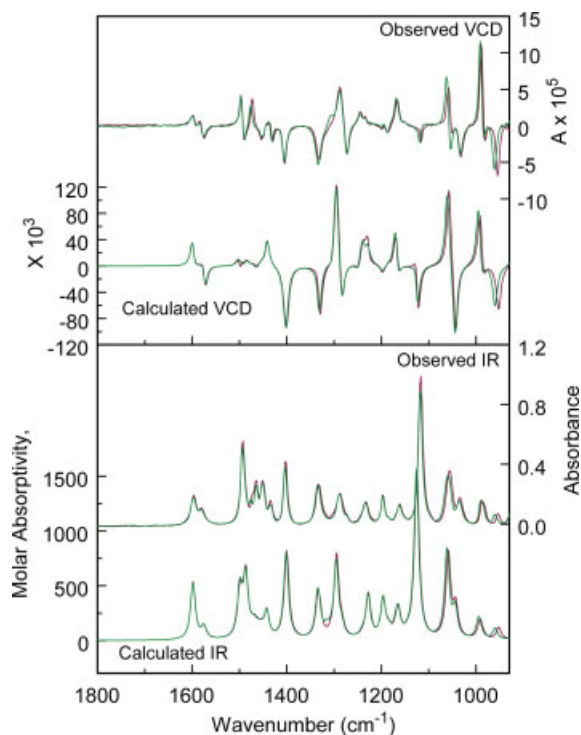


**Fig. 7.** Overlay of IR (lower frame) and VCD (upper frame) observed for Q1A (green) and Q2A (red) compared to calculations for the parent and  $^{13}\text{C}$ -3 isotopomers of the *P*-enantiomers in the conformation shown in Figures 1 and 4. [Color figure can be viewed in the online issue, which is available at [www.interscience.wiley.com](http://www.interscience.wiley.com).]

of much higher resolved spectra for the difference IR and VCD spectra. This occurs because each band that undergoes a small frequency shift in the VCD or IR spectrum becomes a derivative band with a positive and a negative peak in the corresponding difference spectrum. To maintain close correspondence between measured and calculated IR and VCD difference spectra, the direction and approximate magnitude of the isotopic frequency shift for each band must be correct. It stands to reason the isotopic difference spectrum will not be reproduced if a good force field and the correct vibrational mode ordering are accurately calculated. Thus, isotopic shift IR and VCD spectra provide a stringent test for the correctness of a proposed fit between observed and calculated VCD for the assignment of AC of a chiral molecule. This statement is as yet untested in the cases of molecules with high conformational flexibility and multiple conformers present in solution. It may be that an unambiguous fit between calculated and measured VCD spectra can be obtained for such molecules where the isotopic VCD difference spectra do not show a good fit. However, in the case of rigid molecules, computational reproduction of the isotopic VCD difference spectra does appear to provide a demanding test of the quality and correctness of the fit between experimental and calculated VCD spectra.

In the case of the isotopomers of nonamethoxy cyclotri-*veratrylene* presented here, the chirality is distributed widely over the entire molecule for two reasons. There are

no chiral centers, and the three-fold symmetry leads to vibrational coupling between each set of three corresponding structural elements in the molecule about the three-fold symmetry axis. The extensive vibrational coupling is most likely responsible for the rich and extensive pattern of IR and VCD difference intensities for all three substituted isotopomers.

For a molecule with a single chiral carbon center, one might expect to see significant difference bands only for the vibrational modes that couple significantly with structure in the vicinity of the chiral center. If this chiral carbon were isotopically substituted, one would expect a set of IR and VCD difference spectra that would be much simpler than the original IR and VCD of the parent chiral molecule. This might be particularly useful when making an AC assignment for a molecule with conformational flexibility or extensive structure far removed from the chiral center or centers. The fact that relatively large spectral features can be generated for only small changes in the parent IR and VCD spectra supports the consideration of isotopic substitution as aide to making or confirming the AC determination of a chiral molecule.

## CONCLUSIONS

The first comparison of measured and calculated isotopic VCD difference spectra of a chiral molecule are presented. Even though the frequency shifts and intensity changes of the isotopic spectra in the case of  $^{13}\text{C}$  substitu-

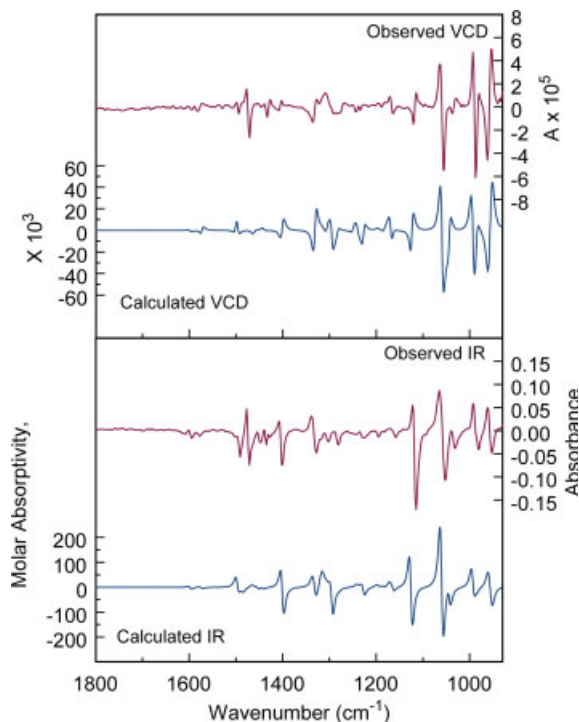


**Fig. 8.** Comparison of difference spectra of IR (lower frame) and VCD (upper frame) observed for (Q1A minus Q2A) compared to calculations of the *P*-enantiomers (parent minus  $^{13}\text{C}$ -3 isotopomer) in the conformation shown in Figures 1 and 4. [Color figure can be viewed in the online issue, which is available at [www.interscience.wiley.com](http://www.interscience.wiley.com).]

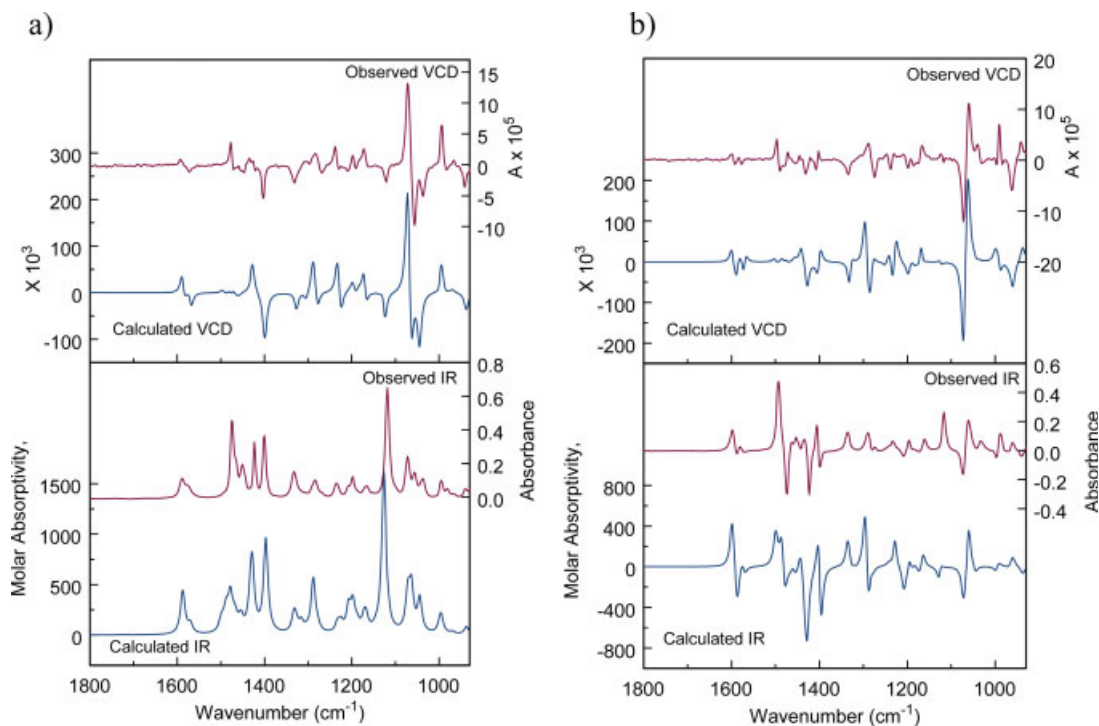


**Fig. 9.** (a) IR (lower frame) and VCD (upper frame) observed for Q4A compared to the calculation for the *P*-enantiomer of the D-3 isotopomer, and (b) Comparison of difference spectra of IR (lower frame) and VCD (upper frame) observed for (Q1A minus Q4A) compared to calculations for *P*-enantiomers for the parent minus the D-3 isotopomer. [Color figure can be viewed in the online issue, which is available at [www.interscience.wiley.com](http://www.interscience.wiley.com).]

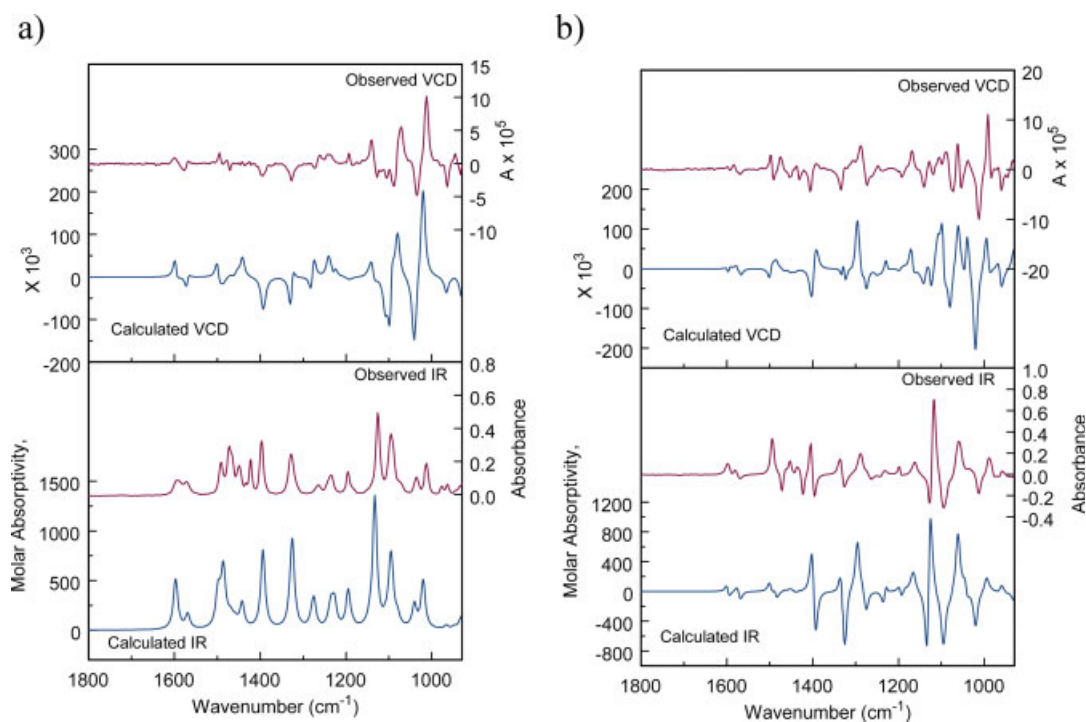


**Fig. 10.** (a) IR (lower frame) and VCD (upper frame) observed for Q5A compared to the calculation for the *P*-enantiomer of the D-6 isotopomer, and (b) Comparison of difference spectra of IR (lower frame) and VCD (upper frame) observed for (Q1A minus Q5A) compared to calculations for the *P*-enantiomers for the parent minus the D-6 isotopomer. [Color figure can be viewed in the online issue, which is available at [www.interscience.wiley.com](http://www.interscience.wiley.com).]

tion are small, the difference IR and VCD spectra are robust and appear to be calculated as accurately as the IR and VCD of the parent isotopomers. In the case of isotopic substitution with  $^{13}\text{C}$  at chiral centers, not presented here, enhanced selectivity is expected for IR and VCD difference spectra from vibrational modes that are structurally associated with the chiral center or centers of the molecule. The potential is therefore high for the productive use of isotopic labeling as an aide to the assignment of AC in vibrational optical activity, both for VCD and ROA.

## LITERATURE CITED

- Barron LD. Molecular light scattering and optical activity, 2nd ed. Cambridge: Cambridge University Press; 2004.
- Nafie LA. Infrared and raman vibrational optical activity: theoretical and experimental aspects. *Annu Rev Phys Chem* 1997;48:357–386.
- Nafie LA, Freedman TB. Vibrational optical activity theory. In: Berova N, Nakanishi K, Woody RW, editors. *Circular dichroism*, 2nd ed. New York: Wiley; 2000. p 97–131.
- Nafie LA, Dukor RK. Vibrational optical activity in chiral analysis. In: Busch KW, Busch MA, editors. *Chiral analysis*: Elsevier; 2006. p 505–544.
- Nafie LA, Dukor RK. Pharmaceutical applications of vibrational optical activity. In: Pivonka D, Griffiths PR, Chalmers JM, editors. *Applications of vibrational spectroscopy in pharmaceutical research and development*. Chichester: Wiley; 2007.
- Nafie LA, Dukor RK, Freedman TB. Vibrational circular dichroism. In: Chalmers JM, Griffiths PR, editors. *Handbook of vibrational spectroscopy*. Chichester: Wiley; 2002. p 731–744.
- Barron LD, Hecht L, McColl IH, Blanch EW. Raman optical activity comes of age. *Mol Phys* 2004;102:731–744.
- Barron LD, Zhu F, Hecht L, Tranter GE, Isaacs NW. Raman optical activity: an incisive probe of molecular chirality and biomolecular structure. *J Mol Struct* 2007;834–836:7–16.
- Guo C, Shah RD, Dukor RK, Freedman TB, Cao X, Nafie LA. Fourier transform vibrational circular dichroism from 800 to 10,000 $\text{cm}^{-1}$ : near-IR-VCD spectral standards for terpenes and related molecules. *Vibrational Spectrosc* 2006;42:254–272.
- Nafie LA, Brinson BE, Cao X, Rice DA, Rahim OM, Dukor RK, Halas NJ. Near-infrared excited raman optical activity. *Appl Spectrosc* 2007; 61:1103–1106.
- Stephens PJ, Devlin FJ. Determination of the structure of chiral molecules using ab initio vibrational circular dichroism spectroscopy. *Chirality* 2000;12:172–179.
- Freedman TB, Cao X, Dukor RK, Nafie LA. Absolute configuration determination of chiral molecules in the solution state using vibrational circular dichroism. *Chirality* 2003;15:743–758.
- Polavarapu PL, He J. Chiral analysis using mid-IR vibrational CD spectroscopy. *Anal Chem* 2004;76:61A–67A.
- Kellenbach ER, Dukor RK, Nafie LA. Vibrational circular dichroism: absolute configuration determination in solution. *Spectrosc Europe* 2007;19:14–19.
- Lassen PR, Skytte DM, Hemmingsen L, Nielsen SF, Freedman TB, Nafie LA, Christensen SB. Structure and absolute configuration of niasol and hinokiresinol via synthesis and vibrational circular dichroism spectroscopy. *J Nat Prod* 2005;68:1603–1609.
- Kuppens T, Vandyck K, Van der Eycken J, Herrebout W, van der Veken BJ, Bultinck P. Determination of the absolute configuration of three as-hydrindacene compounds by vibrational circular dichroism. *J Org Chem* 2005;70:9103–9114.
- He J, Wang F, Polavarapu PL. Absolute configurations of chiral herbicides determined from vibrational circular dichroism. *Chirality* 2005;17(Suppl):S1–S8.
- He J, Polavarapu PL. Determination of the absolute configuration of chiral  $\alpha$ -aryloxypropanoic acids using vibrational circular dichroism studies: 2-(2-chlorophenoxy) propanoic acid and 2-(3-chlorophenoxy) propanoic acid. *Spectrochim Acta A Mol Biomol Spectrosc* 2005;61: 1327–1334.
- Freedman TB, Cao X, Nafie LA, Kalbermatter M, Linden A, Rippert AJ. Determination of the atropisomeric stability and solution conformation of asymmetrically substituted biphenyls by means of vibrational circular dichroism (VCD). *Helvetica Chimica Acta* 2005;88: 2302–2314.
- Dunmire D, Freedman TB, Nafie LA, Aeschlimann C, Gerber JG, Gal J. Determination of the absolute configuration and solution conformation of the antifungal agents ketoconazole, itraconazole, and miconazole with vibrational circular dichroism. *Chirality* 2005;17(Suppl): S101–S108.
- Devlin FJ, Stephens PJ, Bortolini O. Determination of absolute configuration using vibrational circular dichroism spectroscopy: phenyl glycidic acid derivatives obtained via asymmetric epoxidation using oxone and a keto bile acid. *Tetrahedron: Asymmetry* 2005;16:2653–2663.
- Devlin FJ, Stephens PJ, Besse P. Conformational rigidification via derivatization facilitates the determination of absolute configuration using chiroptical spectroscopy: a case study of the chiral alcohol endo-Borneol. *J Org Chem* 2005;70:2980–2993.
- Devlin FJ, Stephens PJ, Besse P. Are the absolute configurations of 2-(1-hydroxyethyl)-chromen-4-one and its 6-bromo derivative determined by X-ray crystallography correct? A vibrational circular dichroism study of their acetate derivatives. *Tetrahedron: Asymmetry* 2005;16:1557–1566.
- Petrovic AG, Polavarapu PL, Drabowicz J, Zhang Y, McConnell OJ, Duddeck H. Absolute configuration of C2-symmetric spiroseleuran: 3,3,3',3'-tetramethyl-1,1'-spiro[3 H,2,1]benzoxaselenole. *Chem A Eur J* 2005;11:4257–4262.
- Petrovic AG, He J, Polavarapu PL, Xiao LS, Armstrong DW. Absolute configuration and predominant conformations of 1,1-dimethyl-2-phenylethyl phenyl sulfoxide. *Org Biomol Chem* 2005;3:1977–1981.
- Urbanova M, Setnicka V, Devlin FJ, Stephens PJ. Determination of molecular structure in solution using vibrational circular dichroism spectroscopy: the supramolecular tetramer of S-2,2'-dimethyl-biphenyl-6,6'-dicarboxylic Acid. *J Am Chem Soc* 2005;127:6700–6711.
- Stephens PJ, McCann DM, Devlin FJ, Flood TC, Butkus E, Stoncius S, Cheeseman JR. Determination of molecular structure using vibrational circular dichroism spectroscopy: the keto-lactone product of Baeyer-Villiger oxidation of (+)-(1R,5S)-Bicyclo[3.3.1]nonane-2,7-dione. *J Org Chem* 2005;70:3903–3913.
- Furo T, Mori T, Origane Y, Wada T, Izumi H, Inoue Y. Absolute configuration determination of donor-acceptor [2.2]paracyclophanes by comparison of theoretical and experimental vibrational circular dichroism spectra. *Chirality* 2006;18:205–211.
- Munoz MA, Munoz O, Joseph-Nathan P. Absolute configuration of natural diastereoisomers of 6b-hydroxyhyoscyamine by vibrational circular dichroism. *J Nat Prod* 2006;69:1335–1340.
- Morita HE, Kodama TS, Tanaka T. Chirality of camphor derivatives by density functional theory. *Chirality* 2006;18:783–789.
- Monde K, Taniguchi T, Miura N, Vairappan CS, Suzuki M. Absolute configurations of endoperoxides determined by vibrational circular dichroism (VCD). *Tetrahedron Lett* 2006;47:4389–4392.
- Monde K, Taniguchi T, Miura N, Vairappan CS, Suzuki M. Absolute configurations of brominated sesquiterpenes determined by vibrational circular dichroism. *Chirality* 2006;18:335–339.
- Soulard P, Asselin P, Cuisset A, Aviles Moreno JR, Huet TR, Petitprez D, Demaison J, Freedman TB, Cao X, Nafie LA, Crassous J. Chlorofluoroiodomethane as a potential candidate for parity violation measurements. *Phys Chem Chem Phys* 2006;8:79–92.
- Ducasse L, Castet F, Fritsch A, Huc I, Buffeteau T. Density functional theory calculations and vibrational circular dichroism of aromatic foldamers. *J Phys Chem A* 2007;111:5092–5098.
- Debie E, Kuppens T, Vandyck K, Van der Eycken J, Van Der Veken B, Herrebout W, Bultinck P. Vibrational circular dichroism DFT study on bicyclo[3.3.0]octane derivatives. *Tetrahedron: Asymmetry* 2007; 17:3203–3218.



36. Buffeteau T, Cavagnat D, Bouchet A, Brotin T. Vibrational absorption and circular dichroism studies of (–)-camphanic acid. *J Phys Chem A* 2007;111:1045–1051.
37. Kuppens T, Vandyck K, Van der Eycken J, Herrebout W, Van der Veken B, Bultinck P. A DFT conformational analysis and VCD study on methyl tetrahydrofuran-2-carboxylate. *Spectrochim Acta A Mol Biomol Spectrosc* 2007;67:402–411.
38. Stephens PJ, Pan JJ, Devlin FJ, Urbanova M, Hajicek J. Determination of the absolute configurations of natural products via density functional theory calculations of vibrational circular dichroism, electronic circular dichroism and optical rotation: the schizogyane alkaloid schizogyne. *J Org Chem* 2007;72:2508–2524.
39. Stephens PJ, Pan JJ, Devlin FJ, Krohn K, Kurtan T. Determination of the absolute configurations of natural products via density functional theory calculations of vibrational circular dichroism, electronic circular dichroism, and optical rotation: the iridoids plumericin and isoplumericin. *J Org Chem* 2007;72:3521–3536.
40. Stephens PJ, Devlin FJ, Gasparri F, Ciogli A, Spinelli D, Cosimelli B. Determination of the absolute configuration of a chiral oxadiazol-3-one calcium channel blocker, resolved using chiral chromatography, via concerted density functional theory calculations of its vibrational circular dichroism, electronic circular dichroism, and optical rotation. *J Org Chem* 2007;72:4707–4715.
41. Crawford TD. Ab initio calculation of molecular chiroptical properties. *Theor Chem Acc* 2006;115:227–245.
42. Zuber G, Hug W. Computational interpretation of vibrational optical activity: the ROA spectra of (4S)-4-methylisochromane and the (4S)-isomers of Galaxolide. *Helvetica Chimica Acta* 2004;87:2208–2234.
43. Zuber G, Hug W. Rarefied basis sets for the calculation of optical tensors. I. the importance of gradients on hydrogen atoms for the raman scattering tensor. *J Phys Chem A* 2004;108:2108–2118.
44. Hug W, Haesler J. Is the vibrational optical activity of (R)-[2H<sub>1</sub>,2H<sub>2</sub>,2H<sub>3</sub>]-neopentane measurable? *Int J Quantum Chem* 2005;104:695–715.
45. Pecul M, Ruud K. Ab initio calculation of vibrational Raman optical activity. *Int J Quantum Chem* 2005;104:816–829.
46. Liegeois V, Quinet O, Champagne B. Vibrational Raman optical activity as a mean for revealing the helicity of oligosilanes: a quantum chemical investigation. *J Chem Phys* 2005;122:214304/1–214304/8.
47. Reiher M, Liegeois V, Ruud K. Basis set and density functional dependence of vibrational raman optical activity calculations. *J Phys Chem A* 2005;109:7567–7574.
48. Zuber G, Goldsmith M-R, Beratan DN, Wipf P. Towards Raman optical activity calculations of large molecules. *Chemphyschem* 2005;6:595–597.
49. Liegeois V, Quinet O, Champagne B, Haesler J, Zuber G, Hug W. Analysis of the VROA signals of helical heptasilanes using an atomistic approach. *Vibrational Spectrosc* 2006;42:309–316.
50. Polavarapu PL. The absolute configuration of bromochlorofluoromethane. *Angew Chem Int Ed Engl* 2002;41:4544–4546.
51. Haesler J, Schindelholz I, Riguet E, Bochet CG, Hug W. Absolute configuration of chirally deuterated neopentane. *Nature* 2007;446:526–529.
52. Barron LD. Raman optical activity due to isotopic substitution: [ $\alpha$ -2H]benzyl alcohol. *J Chem Soc Chem Commun* 1977:305–306.
53. Barron LD, Numan H, Wynberg H. Raman optical activity due to isotopic substitution: (1S)-4,4-dideuterioadamantan-2-one. *J Chem Soc Chem Commun* 1978:259–260.
54. Polavarapu PL, Nafie LA, Benner SA, Morton TH. Optical activity due to isotopic substitution. Vibrational circular dichroism and the absolute configurations of  $\alpha$ -deuterated cyclohexanones. *J Am Chem Soc* 1981;103:5349–5354.
55. Freedman TB, Paterlini MG, Lee NS, Nafie LA, Schwab JM, Ray T. Vibrational circular dichroism in the carbon-hydrogen and carbon-deuterium stretching modes of (S,S)-[2,3-2H<sub>2</sub>]oxirane. *J Am Chem Soc* 1987;109:4727–4728.
56. Freedman TB, Spencer KM, Ragunathan N, Nafie LA, Moore JA, Schwab JM. Vibrational circular dichroism of (S,S)-[2,3-2H<sub>2</sub>]oxirane in the gas phase and in solution. *Can J Chem* 1991;69:1619–1629.
57. Freedman TB, Cianciosi SJ, Ragunathan N, Baldwin JE, Nafie LA. Optical activity arising from carbon-13 substitution: vibrational circular dichroism study of (2S,3S)-cyclopropane-1-13C,2H,2,3-2H<sub>2</sub>. *J Am Chem Soc* 1991;113:8298–8305.
58. Cianciosi SJ, Ragunathan N, Freedman TB, Nafie LA, Lewis DK, Glenar DA, Baldwin JE. Racemization and geometrical isomerization of (2S,3S)-cyclopropane-1-13C-1,2,3-d<sub>3</sub> at 407°C: kinetically competitive one-center and two-center thermal epimerizations in an isotopically substituted cyclopropane. *J Am Chem Soc* 1991;113:1864–1866.
59. Cianciosi SJ, Ragunathan N, Freedman TB, Nafie LA, Baldwin JE. Racemization and geometrical isomerization of (–)-(R,R)-cyclopropane-1,2-2H<sub>2</sub>. *J Am Chem Soc* 1990;112:8204–8206.
60. Cianciosi SJ, Spencer KM, Freedman TB, Nafie LA, Baldwin JE. Synthesis and gas-phase vibrational circular dichroism of (+)-(S,S)-cyclopropane-1,2-2H<sub>2</sub>. *J Am Chem Soc* 1989;111:1913–1915.
61. Luz Z, Poupko R, Wachtel EJ, Zheng H, Friedman N, Cao X, Freedman TB, Nafie LA, Zimmermann H. The structural and optical isomers of nonamethoxy cyclotrimeratrylene—separation and physical characterization. *J Phys Chem A* 2007;111:10507–10516.
62. Frisch MJ, Trucks GW, Schlegel HB, Scuseria GE, Robb MA, Cheeseman JR, Montgomery JAJ, Vreven T, Kudin KN, Burant JC, Millam JM, Iyengar SS, Tomasi J, Barone V, Mennucci B, Cossi M, Scalmani G, Rega N, Petersson GA, Nakatsuji H, Hada M, Ehara M, Toyota K, Fukuda R, Hasegawa J, Ishida M, Nakajima T, Honda Y, Kitao O, Nakai H, Klene M, Li X, Knox JE, Hratchian HP, Cross JB, Adamo C, Jaramillo J, Gomperts R, Stratmann RE, Yazyev O, Austin AJ, Cammi R, Pomelli C, Ochterski JW, Ayala PY, Morokuma K, Voth GA, Salvador P, Dannenberg JJ, Zakrzewski VG, Dapprich S, Daniels AD, Strain MC, Farkas O, Malick DK, Rabuck AD, Raghavachari K, Foresman JB, Ortiz JV, Cui Q, Baboul AG, Clifford S, Cioslowski J, Stefanov BB, Liu G, Liashenko A, Piskorz P, Komaromi I, Martin RL, Fox DJ, Keith T, Al-Laham MA, Peng CY, Nanayakkara A, Challacombe M, Gill PMW, Johnson B, Chen W, Wong MW, Gonzalez C, Pople JA. Gaussian 03. Revision B.03. Pittsburgh, PA: Gaussian, Inc.; 2003.



## Review Article

# The Use of X-ray Crystallography to Determine Absolute Configuration

H. D. FLACK\* AND G. BERNARDINELLI

*Laboratoire de Cristallographie, University of Geneva, Switzerland*

**ABSTRACT** Essential background on the determination of absolute configuration by way of single-crystal X-ray diffraction (XRD) is presented. The use and limitations of an internal chiral reference are described. The physical model underlying the Flack parameter is explained. Absolute structure and absolute configuration are defined and their similarities and differences are highlighted. The necessary conditions on the Flack parameter for satisfactory absolute-structure determination are detailed. The symmetry and purity conditions for absolute-configuration determination are discussed. The physical basis of resonant scattering is briefly presented and the insights obtained from a complete derivation of a Bijvoet intensity ratio by way of the mean-square Friedel difference are exposed. The requirements on least-squares refinement are emphasized. The topics of right-handed axes, XRD intensity measurement, software, crystal-structure evaluation, errors in crystal structures, and compatibility of data in their relation to absolute-configuration determination are described. Characterization of the compounds and crystals by the physicochemical measurement of optical rotation, CD spectra, and enantioselective chromatography are presented. Some simple and some complex examples of absolute-configuration determination using combined XRD and CD measurements, using XRD and enantioselective chromatography, and in multiply-twinned crystals clarify the technique. The review concludes with comments on absolute-configuration determination from light-atom structures. *Chirality* 20:681–690, 2008. © 2007 Wiley-Liss, Inc.

**KEY WORDS:** absolute structure; crystal structure; resonant scattering

## INTRODUCTION

X-ray diffraction (XRD) of single crystals has the capacity to distinguish between the enantiomorphs of a chiral crystal structure and the enantiomers of a chiral molecule. The technique may be applied to compounds of a vast range of chemical composition. Essential chemical information such as the molecular geometry, bond distances and angles, and the packing of the molecules in the crystal are part and parcel of the results of the analysis. However there are limitations. Absolute-configuration determination is a fine detail of crystal-structure determination, which depends on being able to identify small diffraction intensity differences between two crystal-structure models of opposite chirality. With compounds containing only light atoms a significant difference is not guaranteed. The physical reason that these differences are small is described in the section *Resonant scattering and its effect on the diffraction intensities*.

Clearly it makes no sense to claim that an absolute configuration has been determined unless the gross features of the structure and its determination, such as intensity measurements, symmetry, atomic positions, interatomic distances, and atomic displacement parameters have been evaluated and shown not to be in error. This review is writ-

ten for the person who has sufficient knowledge of X-ray crystallography to accomplish this essential step.

Of particular relevance in absolute-configuration determination are the following questions:

- Does the model crystal structure properly represent the crystal structure inside the crystal(s) that have been measured? Is the crystal structure chiral? Is the model that of the real crystal structure and not its enantiomorph? Is the compound enantiomerically pure? Is the assumed space-group symmetry neither too low nor too high?
- Does the model crystal structure properly represent the bulk product from which the crystal was grown?
- Have the bulk and the measured single crystal been sufficiently characterized or fingerprinted to enable another experimentalist to correctly identify the material studied?

\*Correspondence to: H. D. Flack, Laboratoire de Cristallographie, 24 quai Ernest-Ansermet, CH-1211 Genève 4, Switzerland.

E-mail: howard.flack@unige.ch

Received for publication 14 May 2007; Accepted 16 July 2007

DOI: 10.1002/chir.20473

Published online 8 October 2007 in Wiley InterScience (www.interscience.wiley.com).

In a presentation of the way that absolute-configuration determination is undertaken by single-crystal XRD, the review provides essential background information and highlights those aspects which are the cause of confusion and error. Techniques to improve the capacity of single-crystal XRD to determine absolute configuration are reviewed, along with a few examples of other more complex cases. The all-important topic of characterization of bulk and individual single crystals is treated and the concluding remarks contain comments on some current technical limitations. The current review does not go into any detail concerning the phase diagrams of enantiomeric mixtures as we have recently contributed detailed information on the absolute-configuration determination from binary enantiomeric mixtures<sup>1</sup> which are neither enantiomerically pure nor racemates (scalemates).

### SINGLE-CRYSTAL XRD TECHNIQUES USING AN INTERNAL CHIRAL REFERENCE

The presence in a crystal structure of enantiomerically pure chiral molecules, groups, or chiral centers of known absolute configuration leads directly to the determination of the absolute configuration of the other constituents of the crystal by making the image of the atomic arrangement correspond to that of the chiral molecules whose absolute configuration is known. The chiral molecules (or groups or centers) thus act as an internal reference. These may be introduced as part of the compound by chemical reaction or as part of the crystal by cocrystallization using an enantiomerically pure sample of the reference substance. It is important to stress that the correctness of absolute-configuration determination using an internal chiral reference depends crucially on the knowledge of the enantiomeric purity of the reference material and its indicated absolute configuration. It is not sufficient to assume that chemical reaction, crystallization, or operations of mechanochemistry (i.e., grinding) will necessarily conserve the chirality of the reference material.

### SINGLE-CRYSTAL XRD TECHNIQUES EXPLOITING RESONANT SCATTERING

#### *The Flack Parameter*

The distinction by single-crystal XRD of inversion-related models of a noncentrosymmetric crystal structure relies on the phenomenon of resonant scattering (see section *Resonant scattering and its effect on the diffraction intensities*) and is measured by the Flack parameter.<sup>2</sup> The physical model underlying the Flack parameter is that of a crystal twinned by inversion and composed of distinguishable domains, all of these being real phenomena well established in the fields of mineralogy, crystal growth, crystal physics, and solid-state physics.<sup>3</sup> The macroscopic crystal is formed of two types of homogeneous and perfectly-oriented domains, the relationship between the two domain types being that of inversion. A simple way of picturing the crystal twinned by inversion is to imagine a racemic conglomerate in which the crystals have stuck together at

growth in a perfectly oriented manner giving diffraction patterns that look like those of a single crystal. For a nice illustrative example see.<sup>4</sup> Let  $X$  represent the model crystal structure as given by its cell dimensions, space group, and atomic coordinates and  $\bar{X}$  its image inverted through a point. The macroscopic crystal may be represented as  $C = (1 - x)X + x\bar{X}$  for which the Flack parameter  $x$  measures respectively the mole fractions  $(1-x)$  and  $x$  of the two types of domain  $X$  and  $\bar{X}$ . When  $x = 0$ , there is only one domain in the crystal which is that of the model  $X$ . When  $x = 1$ , there is only one domain in the crystal which is that of the inverted model  $\bar{X}$ . When  $x = 0.3$  both types of domain are present in the crystal in the proportion 70% of  $X$  to 30% of  $\bar{X}$ . The physically meaningful values of  $x$  are  $0 \leq x \leq 1$ , but due to statistical fluctuations and systematic errors, experimental values may lie a little outside of this range by a few standard uncertainties. A crystal of an enantiomerically pure compound in the correct absolute configuration has a value of the Flack parameter of zero. In crystallographic jargon one says that the Flack parameter measures the absolute structure of a noncentrosymmetric crystal and from this one may deduce the absolute configuration of the chiral molecules forming the crystal.

#### *What are Absolute Structure and Absolute Configuration?*

For convenience, the formal definitions of these quantities are reproduced<sup>5</sup> in the glossary to this review. Absolute structure is a crystallographer's term and applies to noncentrosymmetric crystal structures. Absolute configuration is a chemist's term and refers to chiral molecules. Note particularly that both the entity under consideration, viz. crystal structure versus molecule, and the symmetry restrictions, viz. noncentrosymmetric versus lack of mirror reflection, inversion through a point, and rotoinversions, are different. Both terms concern the complete specification of the spatial arrangement of atoms with respect to inversion and require that the sample under investigation be characterized by some other physical measurement.

#### *Absolute-Structure Determination*

There are conditions under which one may say that the absolute structure of the crystal has been determined satisfactorily.<sup>6</sup> Firstly one wants to know whether the absolute-structure determination is sufficiently precise by looking to see whether the standard uncertainty  $u$  of the Flack parameter  $x(u)$  is sufficiently small: in general  $u$  should be less than 0.04 but this value may be relaxed to 0.10 for a compound proven by other means to be enantiomerically pure. Secondly the value of the Flack parameter itself should be close to zero within a region of three standard uncertainties i.e.  $u < 0.04$  (or  $u < 0.10$  for a chemically proven enantiomeric excess of 100%) and  $|x|/u < 3.0$ . Moreover the crystal and bulk need to be characterized. The above criteria have been established by way of statistical reasoning<sup>6</sup> to ensure that the structure analyst, by an examination of  $x(u)$  alone, does not claim an absolute-structure determination where none is valid. An unfortunate consequence of such a conservative or safe approach is that some borderline but valid absolute-structure deter-

minations are deemed to be unacceptable. Some of the above criteria may be relaxed somewhat by taking account of a broader spectrum of knowledge over a class of compounds in conjunction with other nondiffraction data or accumulated knowledge of a particular instrument but this needs exceedingly careful, individual and expert evaluation.

#### ***Absolute-Configuration Determination***

Once the absolute structure has been determined satisfactorily, it is only then the moment to see whether something can be said about the absolute configuration of its constituent molecules, as not all valid determinations of absolute structure can necessarily lead to the assignment of an absolute configuration. Although the following description of restrictions<sup>7</sup> is self-sufficient, it has to be admitted that more background knowledge on chiral and achiral crystal structures<sup>5</sup> helps in its understanding. The weakest and most easily-applicable restriction is given first and the strongest one is given last. In fact the third restriction is sufficient in itself, the other two not so.

**Space-group restriction.** The simplest restriction is one of space-group symmetry. If the space group contains symmetry operations of the second kind (i.e., rotoinversions or roto reflections, glide reflections), it must occur that these operate either intramolecularly, forcing the individual molecules to be achiral, or intermolecularly, forcing an arrangement of pairs of opposite enantiomers. Thus, in the first case, the molecules are achiral and in the second a racemate is present. Consequently it is only in crystals displaying space groups containing exclusively symmetry operations of the first kind (i.e., pure or proper rotations, screw rotations) that the determination of absolute configuration is possible (geometric crystal classes: 1, 2, 222, 4, 422, 3, 32, 6, 622, 23, and 432).

**Chiral molecular entity restriction.** To comply with the definition of absolute configuration,<sup>5</sup> one needs to identify a chiral molecular entity and its spatial arrangement in the crystal structure. For example, in a couple of alkali tartrate salts,<sup>8,9</sup> the absolute configuration of the tartrate anion (a chiral molecule) was established but correctly no claims to have done so for the sodium or rubidium atoms were made as these are achiral cations and not molecules. The symmetry group of an achiral molecule contains rotoinversion or roto reflection operations, and these may or may not be part of the space-group symmetry of the crystal. So one must always examine the spatial arrangement of a candidate molecule for noncrystallographic rotoinversion or roto reflection symmetry operations and if any are found, the molecule is achiral and its absolute configuration cannot be determined. For example any planar molecule has mirror symmetry and is achiral whether the mirror plane is part of the space-group symmetry or not.

**Solid-state enantiomeric purity restriction.** One needs to verify that all occurrences of the chiral molecular entity in the crystal structure are the same enantiomer for an absolute-configuration assignment to be valid. This is of

particular concern when the asymmetric unit contains more than one occurrence of the chiral molecule ( $Z' > 1$ ).

Some of the above criteria may be relaxed, but such studies need exceedingly careful, individual and expert evaluation as described in the section *Absolute-configuration determination from a bulk racemate by combined CD and XRD*.<sup>10</sup> Bulk samples which are mixtures of diastereoisomers may give rise to crystals which contain several of the diastereoisomers either in an ordered or disordered arrangement. The crystal structure may clearly and distinctly show the configuration of some of the elements of chirality common to all of the diastereoisomers whereas those elements which vary amongst the diastereoisomers may be in doubt due to disordered atomic positions arising from the superposition of more than one diastereoisomer.

The space-group restriction mentioned earlier implies that absolute configuration may only be undertaken from chiral crystal structures. The latter are necessarily noncentrosymmetric, but not all noncentrosymmetric crystal structures are chiral. Achiral noncentrosymmetric crystal structures exist and the absolute structure of their crystals may be determined. However, it is not possible to deduce the absolute configuration of their constituent molecules for the reasons given above. As we have explained previously,<sup>5</sup> chiral crystal structures are found formed either of enantiomerically pure (chiral) molecules, or of chiral molecules as a racemate, or of achiral molecules. Achiral crystal structures, which may be either centrosymmetric or noncentrosymmetric, are found formed either of chiral molecules as a racemate or of achiral molecules. Enantiomerically pure compounds are found to crystallize exclusively in chiral crystal structures.

#### ***Resonant Scattering and Its Effect on the Diffraction Intensities***

Optical systems working with visible light distinguish objects of opposite chirality without difficulty i.e., one can easily see the difference between one's own right and left hand. The major difference in the diffraction pattern of the right and left hand occurs in the phases of the inversion-related reflections whereas their amplitudes are identical in the absence of any resonant effects. Differences in intensities of the latter occur only if a resonant frequency of the diffracting object is near to that of the incident electromagnetic radiation. Therein lies the essential difficulty for chirality distinction using X-rays. As no lens exists for focusing X-rays, one has to rely only on the intensity of the reflections in the Fraunhofer diffraction pattern. Moreover, if the frequency of the incident X-rays is close to that of some of the atomic electrons which cause diffraction, it will be only a small proportion of these electrons which are resonant, and the intensity difference between inversion-related reflections (Friedel opposites in crystallographic jargon) is small. A further complication is that the resonant frequencies of light atoms occur at long X-ray wavelengths which are very difficult to access experimentally. It helps to remember that resonant scattering is no more or no less than the response of a forced damped harmonic oscillator of which there are numerous examples in nature. There is nothing anomalous about resonant scat-



tering (apart perhaps from the commonly-used names anomalous dispersion and anomalous scattering).

An important tool<sup>11</sup> in understanding resonant-scattering effects in XRD and of use in the planning of experimentation and the evaluation of results has been provided very recently in an analytical expression for the mean-square Friedel intensity difference for a noncentrosymmetric crystal structure with a centrosymmetric substructure. A related Bijvoet intensity ratio  $\chi$  gives a measure of Friedel differences relative to the average intensity of Friedel opposites. A spreadsheet application available with the publication<sup>11</sup> undertakes the necessary calculations from the elemental composition of the compound for some common X-ray wavelengths. Values of  $10^4 \chi$  called Friedif<sup>11</sup> are calculated both for the case of all atoms arranged noncentrosymmetrically and also allowing for atoms arranged on a centrosymmetric substructure if it is possible to identify these. We now rapidly pass in review some of the principal insights that this work has provided:

- The Bijvoet ratio is largest when all atoms are arranged noncentrosymmetrically and zero when all atoms are arranged centrosymmetrically.
- The Bijvoet ratio is zero when all atoms are of the same chemical element regardless of whether the structure is noncentrosymmetric or centrosymmetric. Such is the case, in the spherical atom approximation, for the chiral crystal structure of elemental Se in the form of a helix.<sup>12</sup>
- The Bijvoet ratio quantifies a contrast and needs both resonant and nonresonant atoms to attain large values.
- Rather surprisingly the presence in an otherwise noncentrosymmetric structure of a centrosymmetric arrangement of resonant atoms of one (heavy) chemical element does not diminish the value of the Bijvoet intensity ratio, an observation which had already been confirmed experimentally.<sup>13,14</sup>
- The analytical form of the Bijvoet ratio shows that there are no classes of Bragg reflections having particularly large or small values. Consequently, in the absence of a model of the crystal structure, no particular reflections nor any specific regions of reciprocal space on average are established as showing large Friedel differences.

Calculation of the Bijvoet ratio at different wavelengths enables an optimal choice of X-ray wavelength to be made prior to experimentation. Further it allows the molecular composition of the crystal to be optimized. Suppose for example that a compound is found to have a Bijvoet ratio that is too small for absolute-configuration determination. One may envisage the synthesis of a suitable derivative or the fabrication of a solvate or cocrystal of the compound having a higher Bijvoet ratio. As has been shown above it is unimportant if the solvent or cocrystal molecule takes an essentially centrosymmetric arrangement in the crystal as this does not tend to diminish the Bijvoet ratio. Moreover we have found,<sup>14</sup> using an approximate form of the Bijvoet ratio<sup>15</sup> and a small set of pseudocentrosymmetric structures, a relationship between the Bijvoet ratio and the standard uncertainty on the Flack parameter. This relation-

ship allows a priori estimates of the standard uncertainty of the Flack parameter. Work is currently in progress to establish the corresponding relationship between the full Bijvoet ratio and the standard uncertainty on the Flack parameter for a much larger set of non-pseudosymmetric structures. Unfortunately as this review goes to press, we have not yet completed the data analysis to determine the values of Friedif corresponding to our limiting values of  $u$  of 0.04 and 0.10, and to investigate in more detail the influence of pseudosymmetry.

### *Least-Squares Refinement*

Early results<sup>16,17</sup> and subsequent experience from many crystal-structure determinations have shown that the Flack parameter is robust and converges in only a few cycles to its final value during least-squares refinement. However, as the Flack parameter is one of many parameters of the physical model of a crystal structure, the values of which are to be found by optimization based on some general criterion, it is essential in the final cycles of optimization that all parameters be varied jointly and simultaneously. If this prescription is not followed, two effects may occur separately or together: (a) the value of the Flack parameter may not correspond to the best value for the optimization criterion and (b) its standard uncertainty may be incorrectly estimated, most frequently underestimated. In the case of least-squares minimization, the final refinement needs to be undertaken by full-matrix least-squares (all parameters varied jointly and simultaneously) and needs to have converged.

Another important aspect of least-squares minimization which needs some words of explanation is that of stabilization and damping.<sup>18</sup> To avoid a least-squares refinement becoming unstable and failing to converge, certain numerical techniques, grouped together under the general term *damping*, are often applied automatically or manually. A side effect of these techniques is that stabilized parameters stay close to their starting or target values with standard uncertainties that are systematically underestimated. Biased (wrong) parameter estimates and underestimated standard uncertainties are the result.

### *Inverting a Model Structure*

It sometimes happens that a model crystal structure yields a value of the Flack parameter larger than 0.5. To represent the majority component in the crystal, the model needs to be inverted so the Flack parameter takes a value less than 0.5. In general this inversion is obtained by inversion in the origin by just changing all atomic coordinates  $x, y, z$  into  $-x, -y, -z$  or some point symmetry-equivalent to it. However, for the chiral crystal structures which are necessary for absolute-configuration determination, there are some cases where this simple change of coordinates is insufficient or inappropriate. So in the case of a space group belonging to one of the 11 pairs of enantiomorphic space groups ( $P4_1-P4_3$ ;  $P4_122-P4_322$ ;  $P4_12_12-P4_32_12$ ;  $P3_1-P3_2$ ;  $P3_121-P3_221$ ;  $P3_112-P3_212$ ;  $P6_1-P6_5$ ;  $P6_2-P6_4$ ;  $P6_122-P6_522$ ;  $P6_222-P6_422$ ;  $P4_132-P4_332$ ), the space group should also be changed into the other member of the pair. As they occur in enantiomorphic pairs, these 22 space groups



are the only ones that are correctly described as being chiral.<sup>5</sup> Moreover, there are cases where for the standard setting of the space group<sup>19</sup> that the coordinates need to be inverted in some point other than the origin. The coordinates of the appropriate inversion point can be found in the columns *Inversion through a centre at* of the tables of Euclidean normalizers of space groups.<sup>20</sup> For nonstandard settings an algorithmic solution to this problem has been provided.<sup>16</sup>

## CHARACTERIZATION OF COMPOUNDS AND CRYSTALS

The phase diagrams of enantiomeric mixtures can be complicated,<sup>21,22</sup> giving rise to solid and liquid phases of different composition. Also kinetic effects play an important role in crystallization. It is for these reasons that for absolute-configuration determination, some characterization or measurement of the enantiomeric purity not only of the bulk but also of the single crystal used for the diffraction studies is recommended. There are three principal methods of characterization:

OR: The specific rotation of the optical activity in solution.

As the measurement of specific rotation is a single-wavelength technique, the presence and effect of impurities can easily go undetected. Moreover, OR can not be applied to microgram quantities (i.e., a single crystal used for diffraction studies). Also OR can only provide a measure of enantiomeric excess if the specific rotation of the enantiomerically pure compound is sufficiently strong and has been determined previously.

CD: The visible and near-UV circular dichroism spectrum in solution. The presence and effect of impurities may be readily recognized in a CD spectrum. In favorable circumstances, CD may be applied to the single crystal used for the diffraction measurements taken into solution. For compounds that racemize rapidly in solution, solid-state CD in a KBr disk may be applied to the bulk compound and perhaps even to a powdered single crystal.<sup>23–25</sup> One may expect vibrational CD, either IR or Raman, to be used increasingly in the future.

Enantioselective chromatography (EC): This sensitive technique is applicable to microgram quantities and provides estimates of the enantiomeric excess. It is of course necessary to establish that under the chosen experimental conditions that the two enantiomers are clearly separated. The retention times provide a satisfactory characterization of the two enantiomers.

Regrettably little use is made of differential scanning calorimetry (DSC) by synthetic chemists and structure analysts. Nevertheless, the measurement of melting temperatures and enthalpies is a valuable technique for establishing a phase diagram. DSC measurements may be applied to the bulk.

In passing, we also mention that powder diffraction can be useful. The simple expedient of comparing the X-ray powder diffraction pattern of the bulk product with that

simulated from the results of a single-crystal study allows the presence in the bulk of polymorphs and crystalline diastereoisomers to be revealed. Clearly although this technique is of no help for detecting racemic conglomerates, it is very helpful for other solid mixtures.<sup>26</sup> As the presence of diastereoisomers has the capability of invalidating the determination of absolute configuration, any method which establishes the number and relative concentration of these isomers should be used to characterize the bulk compound and if possible the single crystal used for the diffraction studies.

## EXPERIMENTATION AND ANALYSIS NEEDS IMPECCABLE TECHNIQUE

### *Right-Handed Axes*

As emphasized and discussed previously,<sup>27</sup> right-handed sets of axes must be used at every stage of an analysis of absolute structure. Of particular danger for the structure analyst are basis transformations performed to bring the unit cell into a standard setting. To maintain right-handed axes, any basis transformation matrix must have a positive determinant. A transformation matrix with a negative determinant will transform a right-handed set of axes into a left-handed set of axes, and conversely. The sign of the determinant cannot be spotted simply by counting the number of positive and negative elements in the transformation matrix. The orientation matrix (UB) of the crystal on the diffractometer must have a positive determinant. It is standard practice in our laboratory to calibrate every diffractometer after a hardware or software modification with a well-defined reference material of a chiral crystal structure and containing a sufficient amount of resonant scattering. We use enantiomerically pure potassium hydrogen (2*R*, 3*R*) tartrate. With such a test material, structure solution must give a Flack parameter very close to zero for the (2*R*, 3*R*) configuration of the acid tartrate anion.

### *XRD Intensity Measurements*

It has been established,<sup>13,14</sup> under certain particular conditions, which it is not necessary to detail here, that unless intensity measurements of both members, *hkl* and  $\bar{h}\bar{k}\bar{l}$  of each pair of Friedel opposites are made and used separately in the least-squares refinement, false values of the Flack parameter may result. It hence seems prudent, whether these particular conditions apply or not, to always measure both members of each Friedel pair. Fortunately, with modern-day equipment using area detectors this criterion is easy to achieve and is often the default mode of operation. At the data-reduction stage it is essential for absolute-configuration determination not to average the intensities of Friedel opposites,<sup>6</sup> to transform reflection indices only according to the symmetry operations of the crystal point group<sup>6</sup> and not to use any semiempirical absorption correction which applies a different correction to the intensities of *hkl* and  $\bar{h}\bar{k}\bar{l}$ .<sup>1</sup>

In writing about pairs of Friedel opposites in this review,  $\bar{h}\bar{k}\bar{l}$  should be taken in a general sense to mean  $\bar{h}\bar{k}\bar{l}$  or any Bragg reflection symmetry-equivalent to it under the

point group of the crystal. For a noncentrosymmetric crystal  $hkl$  and  $\bar{h}\bar{k}\bar{l}$  are not symmetry-equivalent under the point group of the crystal. Later on in this review the term Friedel coverage is also used. If in the intensity data, for each reflection  $hkl$  the reflection  $\bar{h}\bar{k}\bar{l}$ , or one symmetry-equivalent to it, has been measured then the Friedel coverage is 100%. If for each  $hkl$ ,  $\bar{h}\bar{k}\bar{l}$  or one symmetry-equivalent to it has not been measured then the Friedel coverage is 0%.

### *Getting the Best Out of Your Software*

In the section *Least-squares refinement* above it was pointed out that full-matrix simultaneous refinement of all variables should be used in the final cycles to obtain reliable results. One widely-used least-squares refinement programme, SHELXL93/97,<sup>28</sup> uses by default a sparse-matrix technique,<sup>6</sup> called *hole-in-one*, for the refinement of the Flack parameter. SHELXL may nevertheless be coaxed into doing the appropriate full-matrix calculation.<sup>13,29</sup>

One may make one or two simple checks of any refinement software. The first is to invert the structure and check that a value of the Flack parameter of  $1 - x$  with the same standard uncertainty is obtained. A second check is to undertake the refinement using a different starting value of the Flack parameter which should lead to exactly the same value of  $x(u)$ .

### *Crystal-Structure Evaluation*

The results of a crystal-structure determination are transmitted nowadays by means of computer-readable files viz. a Crystallographic Information Framework<sup>30</sup> (CIF) file which may be used for display, analysis, evaluation, and archiving. A great deal may be achieved by the automated evaluation of the information contained in a CIF file concerning the data measurements and the crystal-structure determination. Systems can be designed to make use of a considerable amount of general and specific crystallographic knowledge and know-how in the evaluation of a structure determination, and to alert the structure analyst to ambiguities, contradictions, and shortcomings in the information encapsulated in a CIF file. With the aid of these alerts, the data-measurement and structure-refinement procedures may be improved, completed and justified. An essential element is the examination of a graphical representation of the atomic displacement parameters.<sup>31</sup> The most elaborate system currently in operation for the evaluation of crystal-structure determinations is the free-of-charge online checkCIF/PLATON<sup>32,33</sup> operated by the International Union of Crystallography.

### *Erroneous Crystal Structures*

One should bear in mind that a structure analysis may be erroneous. An error with which one should be familiar is the one in which the symmetry of a crystal structure has been incorrectly assigned to a noncentrosymmetric space group whereas the crystal structure itself is really centrosymmetric. In an erroneous noncentrosymmetric description of a crystal structure, the conditions for absolute-configuration determination may apparently be achieved which do not of course apply in the true centrosymmetric description.

<sup>13,14</sup> The measurement of a whole sphere of reflection intensities (see section XRD *intensity measurements*) is a prudent approach to help avoiding falling into this trap. Of equal relevance to absolute-configuration determination are those cases of analysis in which an achiral crystal structure of a racemate (often disordered) with a space group containing rotoinversion operations has erroneously been assigned to a crystal which has in fact a chiral crystal structure of an enantiomerically pure compound with a space group containing only rotation and screw rotation operations. This latter case may arise when a bulk racemate crystallizes by spontaneous resolution and the structure analyst force-feeds the structure solution with a racemate. The possibility of undertaking an absolute-configuration is hence lost.

From an analysis of the atomic coordinates and cell parameters, checkCIF/PLATON may provide an alert that a space group of too low symmetry has been chosen. The most common situation is that it may be possible to add a center of symmetry to the chosen space group. This proposition should be rejected if there is strong evidence to show that the compound is enantiomerically pure in the crystalline state.

Partial-polar ambiguities<sup>34</sup> have the capacity to falsify an absolute-configuration determination. In a crystal-structure solution suffering from a partial-polar ambiguity, some of the atoms are correctly located but the others are images of the real atoms inverted in a point. One may be able to recognize this type of error by a study of interatomic distances and angles.

### *Compatibility of Chemical and Crystallographic Data*

In our recent study<sup>1</sup> of 135 published crystal structures of metallacycles an appalling 26% had incompatible chemical and crystallographic data. In general, for these incompatible crystal structures, the chemical evidence was adequate to convince us that the bulk products had a composition close to an enantiomeric excess of 100%. The crystal structures were determined as being chiral but with values of the Flack parameter close to 0.5, with a low standard uncertainty, indicative of a crystal twinned by inversion with an overall composition near to that of the racemate, in contradiction to the chemical evidence. We hypothesized that for the incompatible crystal-structure determinations that either the data-reduction software had averaged Friedel opposites or that an empirical absorption correction procedure had tended to eliminate intensity differences between Friedel opposites. Other considerations have also been highlighted.<sup>14</sup>

## **SOME EXAMPLES TO STRETCH ONE'S UNDERSTANDING**

### *Experimental Values of the Flack Parameter*

We owe a debt of gratitude to the referees of this article for suggesting the inclusion of this section giving the interpretation of some typical values of the Flack parameter. We cannot stress sufficiently yet again that a necessary step, prior to examining and interpreting the Flack parameter, is to scrutinize the output of a system such as check-

CIF/PLATON<sup>31–33</sup> to ensure the overall validity of the structure determination. For absolute-configuration determination one pays particular attention to any indications of pseudosymmetry, incorrect space group, and insufficient number of intensity measurements of Friedel opposites. Moreover, the noncrystallographic chemical evidence concerning the enantiopurity both of the bulk and of the individual single crystal used for the diffraction studies needs to be reviewed.

$x(u) = 0.05(2)$ , space group  $P2_1/c$ : This report is complete rubbish as a crystal structure with this space group is centrosymmetric implying that both absolute structure and the Flack parameter are meaningless. If there are chiral molecules in this structure, they are present as the racemate.

$x(u) = 0.05(2)$ , space group  $Pna2_1$ : Absolute-configuration determination is not possible as this space group contains rotoinversion operations in the form of the glide reflections  $n$  and  $a$ . The crystal structure is noncentrosymmetric and achiral. If there are chiral molecules in this structure, they are present as the racemate. Absolute-structure determination, but not absolute-configuration determination, may have been possible in this case.

$x(u) = 0.05(2)$ , space group  $C2$ , good Friedel coverage, enantiomerically-pure bulk compound: The standard uncertainty on the Flack parameter is less than 0.10, and the Flack parameter itself is within three standard uncertainties of zero. Absolute-structure determination has been achieved. Moreover, as the space group contains only pure rotations and screw rotations, the crystal structure is noncentrosymmetric and chiral. The enantiopurity of the bulk compound ensures the enantiopurity of the single crystal used for the diffraction studies and consequently absolute-configuration determination has been achieved. Characterization of the bulk compound by OR, CD or enantioselective chromatography is necessary to make the absolute-configuration determination complete.

$x(u) = 0.05(2)$ , space group  $C2$ , good Friedel coverage, racemic bulk compound: Similar to the case immediately above but the compound has crystallized by spontaneous resolution. For measurements on a series of crystals all refined using the same structure model, about 50% of the crystals would give  $x(u) \approx 0.05(2)$  and the other 50% would give  $x(u) \approx 0.95(2)$ . Absolute configuration is achieved if it is possible to characterize by either CD or enantioselective chromatography the single crystal used for the diffraction study.

$x(u) = -0.1(2)$ : The value 0.2 of the standard uncertainty is larger than either of the limiting values 0.04 or 0.1, and consequently absolute-structure and absolute-configuration determination are not possible from the experimental intensity measurements. The negative value of the Flack parameter is within three standard uncertainties of zero and entirely compatible with the statistical fluctuations inherent in the experimental measurements. Possible remedies to achieve a smaller standard uncertainty on the Flack parameter are more accurate intensity measurements, measurement at a lower temperature, accurate measurement of a selected set of Bragg reflections having the largest model Friedel intensity differences, use of a

radiation of different wavelength, synthesis of a derivative containing resonant-scattering atoms, and synthesis of a cocrystal or solvate containing resonant scatterers.

$x(u) = 0.00$ : No standard uncertainty on the Flack parameter has been reported and the Flack parameter may not even have been refined. As it is hence impossible to assess the accuracy of the Flack parameter, absolute-structure and absolute-configuration determination have not been achieved.

$x(u) = 0.0(3)$ : This is a situation similar to that of  $x(u) = -0.1(2)$  but with an even greater uncertainty.

$x(u) = 0.81(12)$ : For values of the Flack parameter greater than 0.5, the structure model should be inverted and the refinement restarted.

$x(u) = 0.19(12)$ : When using SHELXL<sup>28</sup> there is the danger that positive values of the Flack parameter noticeably different from zero may not have converged. One must use the TWIN/BASF commands<sup>13,29</sup> and report the value of BASF1 for the Flack parameter. If this has been done in the present case and there is good Friedel coverage, the crystal is probably twinned by inversion containing 81% of the model and 19% of the inverted model. See the section *Absolute-configuration determination from a bulk racemate by combined CD and XRD*. However  $x(u) = 0.19(12)$  is also rather typical of structure solutions suffering from a partial-polar ambiguity.<sup>34</sup>

$x(u) = 0.49(2)$ , good Friedel coverage, enantiomerically pure bulk compound: The chemical and the crystallographic evidence are contradictory. One needs to examine both very critically. A similar situation pertains when a centrosymmetric crystal structure is obtained for an enantiomerically pure bulk compound. The chemists' curse is the opposite enantiomer as impurity in a binary system for which the melting temperature of the racemic compound is much higher than that of the enantiomerically pure compounds. The crystallographers' curse is bad software implementing inappropriate averaging algorithms or absorption corrections. No absolute-configuration determination is possible. Watch out as well for disordered racemates which may be enantiomerically-pure crystals produced by spontaneous resolution.

$x(u) = 0.042(8)$ , poor Friedel coverage, indications from checkCIF/PLATON that a center of symmetry needs to be added to the space group, no chemical data indicating that the compound is enantiomerically pure: Due to insufficient intensity data, the refinement of the Flack parameter has probably stuck at its starting value of zero<sup>13,14</sup> for this centrosymmetric structure refined as noncentrosymmetric. The analyst should undertake refinement in the appropriate centrosymmetric space group. No absolute-configuration determination is possible.

$x(u) = 0.042(8)$ , good Friedel coverage, indications from checkCIF/PLATON that a center of symmetry needs to be added to the space group, strong chemical evidence that the compound is enantiomerically pure: This is a very nice absolute-configuration determination.

$x(u) = 0.49(2)$ , good Friedel coverage, bulk compound is either a racemate or achiral: If there are indications from checkCIF/PLATON that a center of symmetry needs to be added to the space group, this is most likely the



case. If there are no such indications, the crystal is most likely a 50:50 inversion twin. No absolute-configuration determination is possible.

#### ***Absolute-Configuration Determination from a Bulk Racemate by Combined CD and XRD***

A chiral chromium complex<sup>35</sup> was synthesized, and crystals were grown from a solution of the racemate. The crystal structure is chiral displaying the space group  $P2_12_12_1$ . One would suspect thus that the crystallization had proceeded by spontaneous resolution giving rise to a racemic conglomerate. Two different crystals were measured by XRD and gave values for the Flack parameter<sup>2</sup>  $x$  of 0.36(4) [ $ee$  (i.e., enantiomeric excess) = 28(8)%] and 0.90(3) [ $ee$  = -80(6)%]. Both crystals are thus twinned by inversion, being in effect oriented agglomerates of enantiomerically pure domains containing molecules of opposite chirality in the manner of hexahelicene.<sup>4</sup> Moreover, the second crystal shows a higher enantiomeric excess than the first but contains a majority of the enantiomer opposite to that present as majority component in the first crystal. The two crystals were put into separate solutions and the CD-spectra of these were measured and normalized to equal crystal volume. The CD-spectrum of the solution from crystal 1 is indeed weaker and in form the mirror image of that from crystal 2. The ratio of the enantiomeric excesses from the XRD gives a value of -0.35(10) whereas the ratio of the normalized peak heights at 350 nm of the CD spectra is -0.42. The agreement is very good indeed. So long as a CD spectrum of a solution of the crystal used for the diffraction experiment is published with the results of the structure analysis, it will be justifiable to claim that the absolute configuration has been determined. This is very satisfactory considering that one is working from a racemate in solution.

#### ***Absolute-Configuration Determination Relying on Enantioselective Chromatography***

The synthesis of an *N*-sulphonated aziridine, resulted in an enantiomeric mixture which was found to have an enantiomeric excess of 43% of the (1*R*, 3*R*, 6*S*) enantiomer.<sup>36,37</sup> The enantiomers were separated by semipreparative HPLC on Chiracel OD H using hexane/isopropanol 9:1 at 0.5 ml/min giving retention times of 15.3 and 16.3 min. The product from the minority component (retention time 15.3 min) was used to make crystals. Their crystal structure is chiral displaying space group  $P2_1$  giving a Flack parameter<sup>2</sup>  $x(u) = -0.03(12)$ . Although the standard uncertainty on  $x$ , 0.12, is very slightly larger than our upper safe limit of 0.10, the conditions of experimentation, experience with other similar compounds, the small value of  $x$  convince us that absolute-structure determination has been achieved. The absolute configuration was determined to be (1*S*, 3*S*, 6*R*). The retention time and experimental conditions provide a sufficient characterization of the enantiomer in the absolute-configuration determination. In this case, it would not have been possible to use optical activity or CD as these effects are far too weak:  $[\alpha_D] = 0.7^\circ$  for  $ee = 43\%$  and the CD spectrum is flat.

Chirality DOI 10.1002/chir

#### ***Determination of Absolute Configuration from Multiply-Twinned Crystals***

A twinned crystal may be viewed as a solid-state agglomerated mixture of rotated and/or inverted copies of the untwinned crystal structure. Each component in this mixture is specified by two attributes.

1. The volume fraction  $x_i$  of the  $i$ th component in the macroscopic crystal. This value may be established during structure refinement.
2. The isometry relating the orientation of the component to that of the basic one. This twin symmetry operation may be established by arguments of symmetry<sup>3,38,39</sup> and is not unique. It comes from a group  $G$  of isometries which leave the crystal lattice invariant but not necessarily the crystal structure. The crystal point group  $P$  is a subgroup of  $G$ ,  $G \supseteq P$ .

As we are dealing here solely with cases in which the crystal structure is chiral, so that  $P$  is one of the point groups containing only rotations (geometric crystal classes: 1, 2, 222, 4, 422, 3, 32, 6, 622, 23, 432). So long as the criteria given in the subsection *absolute-configuration determination* are obeyed, it is still possible to proceed to the determination of absolute configuration for the multiply-twinned crystal. Full details of the group-theoretical analysis with the related restrictions to its application are given in<sup>7</sup> but here it suffices to point out that twin-symmetry operations that have a determinant of +1 are pure rotations and do not change the chirality of the molecules in the crystalline domain upon which they act. On the other hand twin-symmetry operations that have a determinant of -1 are rotoinversions and change the chirality of the molecules. For the purposes of the analysis of absolute configuration, the total amount of rotated-only structure,  $x^+$ , may be deduced by summing the volume fractions corresponding to twin laws of determinant +1,  $x^+ = \sum x_i^+$ , and that of rotated-and-inverted structure,  $x^-$ , may be deduced by summing the volume fractions corresponding to twin laws of determinant -1,  $x^- = \sum x_i^-$ .  $x^-$  is the equivalent of the Flack  $x$  parameter for multiply-twinned crystals possessing a chiral crystal structure. Let us make this clear from an example.<sup>40</sup> The space group is  $P3_1$  which belongs to geometric crystal class 3 and thus the crystal structure is chiral. The structure was refined as a four-component twin:  $k_2 = 0.064(13)$  for matrix 010,100,00-1,  $k_3 = 0.038(17)$  for matrix -100,0-10,00-1, and  $k_4 = 0.329(13)$  for matrix 0-10,-100,001.<sup>40</sup>  $k_1$  may be obtained from the relationship  $k_1 = 1 - k_2 - k_3 - k_4$  to give  $k_1 = 0.569(14)$  for matrix 100,010,001. The twin symmetry operations are of determinant +1 for matrices 1 and 2, and -1 for matrices 3 and 4. In the nomenclature of the current analysis, one has  $x_1^+ (=k_1) = 0.569(14)$ ,  $x_2^+ (=k_2) = 0.064(13)$ ,  $x_1^- (=k_3) = 0.038(17)$ , and  $x_2^- (=k_4) = 0.329(13)$ , giving  $x^+ (=x_1^+ + x_2^+) = 0.633(17)$  and  $x^- (=x_1^- + x_2^-) = 0.367(17)$ .  $x^-$  is equivalent to the Flack  $x$  parameter for this multiply-twinned crystal. Its standard uncertainty is low and hence the value of the Flack parameter is significant. The experiment clearly shows that 63% of the crystalline sample contains



the structure as determined in space group  $P3_1$  and 37% contains the inverted structure in space group  $P3_2$  making the enantiomeric excess of the crystalline sample 26%. From these measurements, it is clearly not possible to establish the absolute configuration for this compound.

### CONCLUDING REMARKS

Compounds composed only of light atoms, i.e., those having a low value of Friedel,<sup>11</sup> give rise to standard uncertainties on the Flack parameter which are too large for absolute-configuration determination. On the experimental side it may help to measure at a longer wavelength although synchrotron radiation does not seem to provide the easy answer that one might at first imagine.<sup>14</sup> Higher precision intensity measurements on a small set of Bragg reflections selected from the crystal-structure model as having large Friedel differences may be undertaken.<sup>41</sup> In various published<sup>41</sup> and unpublished works, improvement of the uncertainty of the absolute-configuration determination has been attempted by way of alternative statistical procedures to that of least squares. In our view, all the procedures we have examined suffer from the same problem as sparse-matrix least squares by assuming invariance of parameters of the model which should be variable. It is perfectly correct that the average of Friedel opposites<sup>11</sup> calculated from the crystal-structure model is independent of the Flack parameter or the absolute structure. However, the corresponding difference of Friedel opposites (of the model) depends both on the Flack parameter and all the other atomic parameters of the model. It is the latter dependence which is assumed to be invariant in the procedures we have studied. Only the procedure of Parsons<sup>42</sup> escapes from this pitfall but needs further development.

### GLOSSARY<sup>5</sup>

**Absolute configuration<sup>5</sup>:** The spatial arrangement of the atoms of a physically identified chiral molecular entity (or group) and its stereochemical description (e.g., (*R*) or (*S*), (*P*) or (*M*), D or L, etc).

**Absolute structure<sup>5</sup>:** The spatial arrangement of the atoms of a physically identified noncentrosymmetric crystal and its description by way of unit-cell dimensions, space group, and representative coordinates of all atoms.

**Flack parameter<sup>5</sup>:** The Flack parameter<sup>2</sup> is the molar fraction  $x$  in the defining equation  $C = (1 - x) X + x \bar{X}$ , where  $C$  represents an oriented two-domain-structure crystal, twinned by inversion, consisting of an oriented domain structure  $X$  and an oriented inverted domain structure  $\bar{X}$ . In reciprocal space, the Flack parameter<sup>2</sup>  $x$  is defined by the structure-amplitude equation  $G^2(h, k, l, x) = (1 - x) |\mathbf{F}(hkl)|^2 + x |\mathbf{F}(\bar{h} \bar{k} \bar{l})|^2$ . For a multidomain-structure twin of a chiral crystal structure, an equivalent Flack parameter may be calculated according to the method of Flack and Bernardinelli.<sup>7</sup>

### LITERATURE CITED

1. Djukic JP, Hijazi A, Flack HD, Bernardinelli G. Non-racemic (scalene) planar-chiral five-membered metallacycles: routes, means, and pitfalls in their synthesis and characterization. *Chem Soc Rev* 2007; DOI: 10.1039/B618557F.
2. Flack HD. On enantiomorph-polarity estimation. *Acta Cryst A* 1983; 39:876–881.
3. Hahn Th, Janovec V, Klapper H, Privratska J. Twinning and domain structures. In: Authier A, editor. *International tables for crystallography, volume D: physical properties of crystals*. Dordrecht: International Union of Crystallography and Kluwer Academic Publishers; 2003. p 377–505.
4. Green BS, Knossow M. Lamellar twinning explains the nearly racemic composition of chiral, single crystals of hexahelicene. *Science* 1981; 214:795–797.
5. Flack HD. Chiral and achiral crystal structures. *Helv Chim Acta* 2003;86:905–921.
6. Flack HD, Bernardinelli G. Reporting and evaluating absolute-structure and absolute-configuration determinations. *J Appl Cryst* 2000; 33:1143–1148.
7. Flack HD, Bernardinelli G. Absolute structure and absolute configuration. *Acta Cryst B* 1999;55:908–915.
8. Bijvoet JM. Phase determination in direct Fourier-synthesis of crystal structures. *Proc K Ned Akad Wet Ser B* 1949;52:313–314.
9. Peerdeman AF, van Bommel AJ, Bijvoet JM. Determination of absolute configuration of optical active compounds by means of X-rays. *Proc K Ned Akad Wet Ser B* 1951;54:16–19.
10. Flack HD, Bernardinelli G. The Mirror of Galadriel: looking at chiral and achiral crystal structures. *Cryst Eng* 2003;6:213–223.
11. Flack HD, Shmueli U. The mean-square Friedel intensity difference in  $P1$  with a centrosymmetric substructure. *Acta Cryst A* 2007;63:257–265.
12. McIntyre G. A prediction of Bijvoet intensity differences in the non-centrosymmetric structures of selenium and tellurium. *Acta Cryst A* 1978;34:936–939.
13. Flack HD, Bernardinelli G. Centrosymmetric crystal structures described as non-centrosymmetric; an analysis of reports in *Inorganica Chimica Acta*. *Inorg Chim Acta* 2006;359:383–387.
14. Flack HD, Bernardinelli G, Clemente DA, Linden A, Spek AL. Centrosymmetric and pseudo-centrosymmetric structures refined as non-centrosymmetric. *Acta Cryst B* 2006;62:695–701.
15. Girard E, Stelter M, Vicat J, Kahn R. A new class of lanthanide complexes to obtain high-phasing-power heavy-atom derivatives for macromolecular crystallography. *Acta Cryst D* 2003;59:1914–1922.
16. Bernardinelli G, Flack HD. Least-squares absolute-structure refinement. Practical experience and ancillary calculations. *Acta Cryst A* 1985;41:500–511.
17. Bernardinelli G, Flack HD. Least-squares absolute-structure refinement. A case study of the effect of absorption correction, data region, stability constant and neglect of light atoms. *Acta Cryst A* 1987;43:75–78.
18. Schwarzenbach D, Flack HD. High energy spectroscopy: structure refinement (solid state diffraction). In: Lindon J, Tranter G, John Holmes J, editors. *Encyclopedia of spectroscopy and spectrometry*. London: Academic Press; 1999. p 2271–2278.
19. Hahn Th, editor. *International tables for crystallography, volume A: space-group symmetry*. Dordrecht: International Union of Crystallography and Kluwer Academic Publishers; 2002.
20. Koch E, Fischer W, Müller U. Normalizers of space groups and their use in crystallography. In: Hahn Th, editor. *International tables for crystallography, volume A: space-group symmetry*. Dordrecht: International Union of Crystallography and Kluwer Academic Publishers; 2002. Tables 15.2.1.3 and 15.2.1.4, p 883–898.
21. Jacques J, Collet A, Wilen S. *Enantiomers, racemates and resolutions*. New York: Wiley; 1981.
22. Coquerel G. Review on the heterogeneous equilibria between condensed phases in binary systems of enantiomers. *Enantiomer* 2000; 5:481–498.

23. Johansson A, Hakansson M, Jagner S. Total spontaneous resolution of chiral covalent networks from stereochemically labile metal complexes. *Chem Eur J* 2005;11:5311–5318.
24. Minguet M, Amabilino DB, Wurst K, Veciana J. Circular dichroism studies of crystalline chiral and achiral  $\alpha$ -nitronyl nitroxide radicals in a KBr matrix. *J Chem Soc Perkin Trans 2*. 2001;670–676.
25. Kuroda R, Honma T. CD Spectra of solid-state samples. *Chirality* 2000;12:269–277.
26. Hutin M, Cramer CJ, Gagliardi L, Shahi ARM, Bernardinelli G, Cerny R, Nitschke JR. Self-sorting chiral subcomponent rearrangement during crystallization. *J Am Chem Soc* 2007;129:8774–8780.
27. Rogers D. Some fundamental problems of relating tensorial properties to the chirality or polarity of crystals. In: Ramaseshan S, Abrahams SC, editors. *Anomalous scattering*. Copenhagen: Munksgaard; 1975. p 231–250.
28. Sheldrick GM. SHELXL93/97. Program for the refinement of crystal structures. (1993/1997). University of Göttingen, Germany.
29. Clegg W. Some guidelines for publishing SHELXL-generated CIF results in *Acta Crystallographica*. *Acta Cryst E* 2003;59:e2–e5.
30. Hall SR, McMahon B, editors. *International tables for crystallography, volume G: Definition and exchange of crystallographic data*. Dordrecht: International Union of Crystallography and Kluwer Academic Publishers; 2006.
31. Harlow RL. Troublesome crystal structures: Prevention, detection, and resolution. *J Res NIST* 1996;101:327–339.
32. checkCIF/PLATON service of the International Union of Crystallography. Available at <http://journals.iucr.org/services/cif/checking/checkform.html>.
33. Spek AL. Single-crystal structure validation with the program PLATON. *J Appl Cryst* 2003;36:7–13.
34. Kuchta MC, Parkin G. Incorrect atom connectivity in X-ray structure solutions associated with a 'partial polar ambiguity': a non-macrocyclic structure for the macrocyclic lead complex,  $[\eta^4\text{-Me}_8\text{taa}] \text{Pb}$ . *New J Chem* 1998;22:523–530.
35. Kündig EP, Bernardinelli G, Kondratenko M, Robieux F, Romanens P. New chromium enolates. *Helv Chim Acta* 2003;86:4169–4184.
36. Müller P, Riegert D, Bernardinelli G. Desymmetrization of N-sulfonated aziridines by alkyllithium reagents in the presence of chiral ligands. *Helv Chim Acta* 2004;87:227–239.
37. Müller P, Nury P. Desymmetrization of meso-N-sulfonylaziridines with chiral nonracemic nucleophiles and bases. *Helv Chim Acta* 2001;84:662–677.
38. Janovec V. Group analysis of domains and domain pairs. *Czech J Phys B* 1972;22:974–994.
39. Flack HD. The derivation of twin laws for (pseudo-)merohedry by coset decomposition. *Acta Cryst A* 1987;43:564–568.
40. Herbst-Irmer R, Sheldrick GM. Refinement of twinned structures with SHELXL97. *Acta Cryst B* 1998;54:443–449.
41. Le Page Y, Gabe EJ, Gainsford GJ. A robust alternative to [eta] refinement for assessing the hand of chiral compounds. *J Appl Cryst* 1990; 23:406–411.
42. Parsons S. Contribution E0043 to the American Crystallographic Association Meeting, San Antonio, Texas, 25th–30th May 2002.

## Review Article

# Determination of Absolute Configurations by X-ray Crystallography and $^1\text{H}$ NMR Anisotropy

NOBUYUKI HARADA\*

Department of Chemistry, Columbia University, New York

**ABSTRACT** To determine the absolute configurations of chiral compounds, many spectroscopic and diffraction methods have been developed. Among them, X-ray crystallographic Bijvoet method, CD exciton chirality method, and the combination of vibrational circular dichroism and quantum mechanical calculations are of nonempirical nature. On the other hand, X-ray crystallography using a chiral internal reference, and  $^1\text{H}$  NMR spectroscopy using chiral anisotropy reagents are relative and/or empirical methods. In addition to absolute configurational determinations, preparations of enantiopure compounds are strongly desired. As chiral reagents useful for both the preparation of enantiopure compounds by HPLC separation and the simultaneous determination of their absolute configurations, we have developed camphorsultam dichlorophthalic acid (CSDP acid) for X-ray crystallography and 2-methoxy-2-(1-naphthyl)propionic acid (M $\alpha$ NP acid) for  $^1\text{H}$  NMR spectroscopy. In this review, the principles and applications of these X-ray and NMR methods are explained using mostly our own data. *Chirality* 20:691–723, 2008. © 2007 Wiley-Liss, Inc.

**KEY WORDS:** absolute configuration; X-ray crystallography; internal reference; chiral X-ray reference reagents (CXR); camphorsultam dichlorophthalic acid (CSDP acid);  $^1\text{H}$  NMR anisotropy; chiral  $^1\text{H}$  NMR anisotropy reagents (CAR); 2-methoxy-2-(1-naphthyl)propionic acid; M $\alpha$ NP acid; diastereomers; HPLC separation on silica gel

## INTRODUCTION

It is well recognized that most biologically active compounds controlling physiological functions of living organisms are chiral. Furthermore, studies on chiral molecular devices and molecular machines, such as the light-powered chiral molecular motors developed in our laboratory, have been rapidly progressing in recent years. The biological and molecular functions of these compounds are closely related to the chirality of molecules, i.e., absolute configuration of molecules. Therefore, in the field of biomolecular and molecular material sciences, the unambiguous determination of the absolute configuration of chiral compounds becomes the first major issue. The second issue is the chiral synthesis of target compounds and how efficiently the desired enantiomers can be synthesized with 100% enantiopurity or enantiomeric excess (%ee).

We have developed some chiral carboxylic acids as novel molecular tools useful for both enantioresolution of various alcohols and simultaneous determination of their absolute configurations (see Fig. 1). These chiral molecular tools are very powerful for the facile preparation of chiral compounds with 100% ee and also for the absolute configurational assignment. The methods using these chiral tools have been successfully applied to various com-

pounds, and their methodologies and applications are explained in this review.

## METHODOLOGIES FOR DETERMINING ABSOLUTE CONFIGURATIONS

### *Nonempirical Methods for Determining Absolute Configurations of Chiral Compounds (Table 1)*

It is well known that the absolute configuration of chiral compounds was first determined by the X-ray crystallography Bijvoet method using heavy atom effects.<sup>1</sup> In X-ray crystallography, as the anomalous dispersion effect of heavy atoms can be measured accurately under proper conditions, absolute stereostructures have been clearly determined by the use of the Flack parameter,<sup>2</sup> instead of

Contract grant sponsors: Ministry of Education, Science, Sports, Culture, and Technology, Japan; Japan Society for the Promotion of Science.

\*Correspondence to: Nobuyuki Harada, Department of Chemistry, Columbia University, 3000 Broadway, MC3152, New York, NY 10027, USA. E-mail: nh2212@columbia.edu, n\_harada@ma.mni.ne.jp

Received for publication 12 June 2007; Accepted 10 August 2007

DOI: 10.1002/chir.20478

Published online 8 October 2007 in Wiley InterScience (www.interscience.wiley.com).

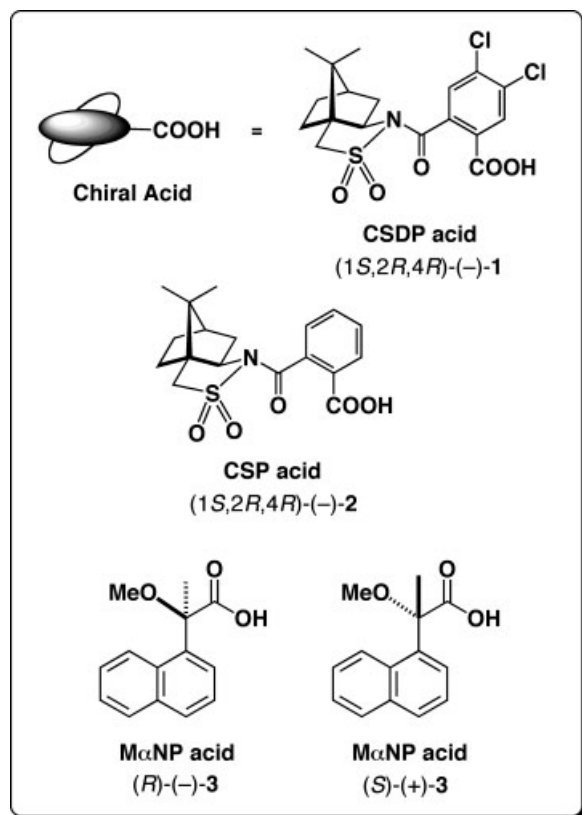


Fig. 1. Chiral carboxylic acids useful for enantioresolution and determination of absolute configuration of alcohols.

the measurement of Bijvoet pairs. The obtained results are unambiguous and reliable. In addition, the molecule can be projected as a three-dimensional structure, and therefore, the method has been extensively employed. However, the X-ray method needs single crystals of a large size suitable for X-ray diffraction experiments, and so the critical problem is how to obtain such large single crystals.

The CD (circular dichroism) exciton chirality method<sup>3-6</sup> is also useful because the absolute configuration can be determined in a nonempirical manner, and it does not require crystallization. Furthermore, chiral chemical and biological reactions are traceable by CD, and even the absolute configurations and conformations of unstable compounds can be obtained by this method. However, since some compounds are not ideal targets for this method, the results must be carefully interpreted. In addition, the CD spectra of chiral compounds with a strongly twisted  $\pi$ -electron chromophore can be calculated by the  $\pi$ -electron SCF-CI-DV MO (self-consistent field/configuration interaction/dipole velocity molecular orbital) method.<sup>7</sup> The method has been successfully applied to various natural and synthetic chiral compounds to determine their absolute configurations.<sup>8,9</sup> The absolute configurations theoretically determined have been established by total syntheses of those chiral compounds.

Recently the ab initio calculation method of vibrational circular dichroism (VCD), Raman optical activity, optical rotatory dispersion, and CD, has been developed as the

TABLE 1. Methods for determining the absolute configurations of chiral compounds

Method	Phenomena, key points, and/or reagents	Refs.
<b>Nonempirical methods</b>		
X-ray crystallography	Heavy atom effect	1
		2
CD spectroscopy	Coupled oscillator	3
	Exciton coupling	4,5
		6
	Twisted $\pi$ -electron system	7
CD, VCD, ROA, and/or ORD	Ab initio calculation	8,9
		10
		11
		12
		13
<b>Relative and/or empirical methods</b>		
X-ray crystallography	Internal reference of absolute configuration: recent examples	
	CSDP acid and HPLC	14-20
	MαNP acid and HPLC	21,22
	Inclusion complex	23-25
	Part of systems	26-28
<sup>1</sup> H NMR spectroscopy	Diamagnetic anisotropy effect	
	MTPA acid	39
	MPA acid	40
	MTPA, 1NMA, 2NMA, 2ATMA acids	41-43
	MTPA, 1NMA, 2NMA, 9AMA acids	44-48
	CFTA acid	49,50
	HPLC and diamagnetic anisotropy effect	
	MαNP acid	19-22, 51-60
	M9PP acid	61,62
Comparison of CD spectra		
Chemical correlation		

third nonempirical method.<sup>10-13</sup> By comparison of the observed spectra with calculated ones, one can determine the absolute configurations. The method is applicable to compounds having no chromophore, and so it should be more widely used in the near future.

#### Relative and/or Empirical Methods for Determining Absolute Configuration Using an Internal Reference of Known Absolute Configuration (Table 1)

**X-ray crystallography.** Absolute configuration can be obtained by determining the relative configuration at the position of interest against a reference compound or substituent with known absolute configuration. A typical example is the X-ray crystallography performed after the introduction of a chiral X-ray internal reference (CXR) with known absolute configuration (see Fig. 2).<sup>14-28</sup> In this case, the absolute configuration of the point in question can be automatically determined using the chirality of the



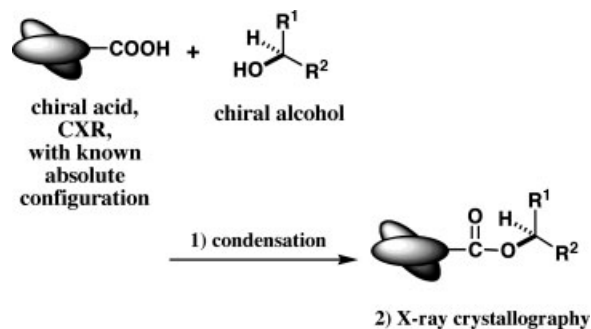


Fig. 2. A general scheme for determining the absolute configuration by X-ray crystallography using a CXR, where the case of ester formation is shown.

auxiliary introduced as an internal reference. Consequently, samples do not need to contain heavy atoms for anomalous dispersion effect.

An example of this method is shown in Figure 3, where alcohol (–)-5 has a heavy bromine atom, but no single crystals suitable for X-ray analysis were obtained.<sup>29</sup> Therefore, alcohol (–)-5 was esterified with (1*S*)-(–)-camphanic acid 4 (CXR), yielding ester 6 as single crystals. From the X-ray stereostructure of ester 6, the absolute configuration of (–)-5 was unambiguously determined to be *R*.

The results obtained by this internal reference method are very clear and reliable, even when the final *R*-value is not small enough due to poor quality of the single crystal, as exemplified by the recent determination of the absolute configurations of chiral C<sub>60</sub> fullerene *cis*-3 bisadducts by X-ray crystallography (see Fig. 4).<sup>26</sup> For the absolute configuration of chiral C<sub>60</sub> fullerene *cis*-3 bisadducts, there had been many controversies among research groups.<sup>30–33</sup> They had synthesized *cis*-3 bisadducts with different chiral tethers, and had calculated the molecular energies of possible diastereomers by the molecular mechanics force field method, because they had assumed that the product obtained should be the most stable diastereomer. From the calculation results, they had determined the absolute configurations of *cis*-3 bisadducts. However, their reported assignments were inconsistent with one another.<sup>30–35</sup>

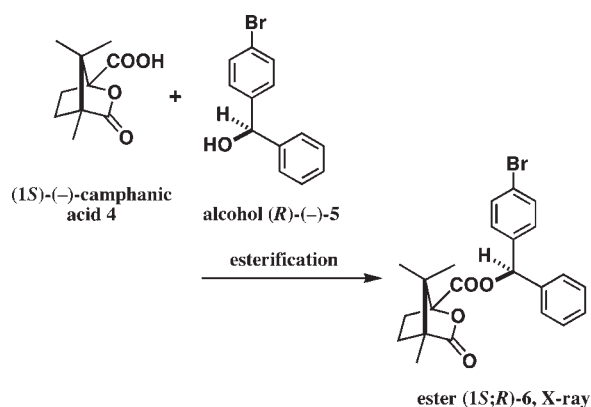


Fig. 3. An example of the determination of absolute configuration by the use of CXR.

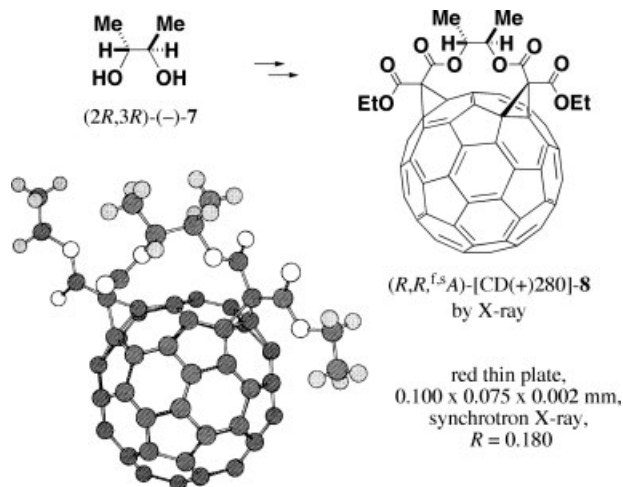


Fig. 4. Absolute configuration of chiral C<sub>60</sub>-fullerene *cis*-3 bisadduct 8 by X-ray internal reference method.<sup>26</sup>

We had calculated the CD spectra of *cis*-3 bisadducts by the  $\pi$ -electron SCF–CI–DV MO method, because the  $\pi$ -electron system of *cis*-3 bisadducts can be treated as a twisted chromophore. From the CD calculation results, the absolute configuration of *cis*-3 bisadduct was determined.<sup>36</sup> The Diederich group had applied the CD exciton chirality method to derivatives to determine their absolute configurations.<sup>37</sup> Later we had synthesized two possible diastereomeric *cis*-3 bisadducts with a pertinent chiral tether, and carefully analyzed the  $^1\text{H}$  NMR (nuclear magnetic resonance) chemical shift and coupling constant data. From the  $^1\text{H}$  NMR studies, we had come to the same absolute configurations, which had been previously determined by the CD calculation.<sup>38</sup> The absolute configurations of *cis*-3 bisadducts determined by us have been finally established by X-ray crystallography as follows.

Starting from (2*R*,3*R*)-(–)-2,3-butanediol 7, chiral C<sub>60</sub> fullerene *cis*-3 bisadduct [CD(+)-280]-8 was synthesized (see Fig. 4), and the product was recrystallized from chloroform/hexane (1:1) giving extremely thin plate single crystals, which had a thickness of 1–2  $\mu\text{m}$ . Those crystals are too thin for conventional X-ray diffractometers, and therefore the synchrotron X-ray radiation at the SPring-8 in Hyogo, Japan, was used for the X-ray analysis. Although the final *R*-value remained large (*R* = 0.180), the absolute configuration of bisadduct [CD(+)-280]-8 was clearly determined as <sup>f,s</sup>*A* (= <sup>f</sup>*C*) by using the (2*R*,3*R*) absolute configuration of the tether moiety as an internal reference. On the basis of this X-ray analysis and comparison of CD spectra, the absolute configurations of C<sub>60</sub> fullerene *cis*-3 bisadducts have been conclusively determined.<sup>26</sup>

A variety of methods to link an internal reference to the target molecule have been developed. For example, there are ionic bonds such as conventional acid–base salts, covalent bonds such as esters or amides, and the recently developed inclusion complexes.<sup>23–25</sup> Very recently, structure analyses have become possible also by X-ray diffraction of crystalline powder. Therefore, the X-ray crystallography using an internal reference is expected to find widespread applications.

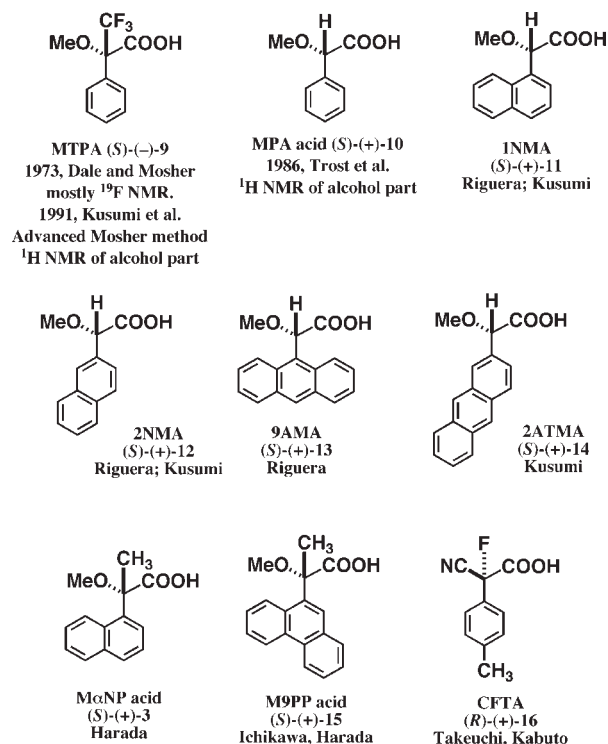


Fig. 5. Chiral acids useful for the advanced Mosher method.

**$^1\text{H}$  NMR advanced Mosher method.** Recently, the proton nuclear magnetic resonance ( $^1\text{H}$  NMR) anisotropy method has often been used as a relative and empirical method, and it is useful for the study of the absolute configurations of natural products and chiral synthetic compounds.<sup>39–63</sup> In particular, the absolute configurations of secondary alcohols have been successfully determined by the Trost's method using  $\alpha$ -methoxyphenylacetic acid (MPA, (S)-(+)-10)<sup>40</sup> or by the advanced Mosher method developed by Kusumi and coworkers.<sup>41</sup> In the advanced Mosher method, the absolute configuration of a chiral auxiliary, the Mosher's reagent [ $\alpha$ -methoxy- $\alpha$ -(trifluoromethyl)phenylacetic acid (MTPA, (S)-(-)-9)]<sup>39</sup> is known, and the preferred conformations of the esters formed with a chiral secondary alcohol and MTPA have been rationalized. The  $^1\text{H}$  NMR chemical shift of alcoholic part protons are affected by the diamagnetic anisotropy effect generated by the phenyl group of MTPA. From  $\Delta\delta$  values reflecting anisotropy effects, the absolute configuration of alcohol part can be determined. Since then, various chiral acids suitable for this method have been developed mostly by the Kusumi group<sup>41–43</sup> and the Riguera group,<sup>44–48</sup> and have been applied to various chiral compounds (Table 1 and Fig. 5).

The outline of the advanced Mosher method is as follows (see Fig. 6). To determine the absolute configuration of a chiral alcohol, a chiral alcohol (X)-17 with unknown absolute configuration X is esterified with MTPA acid (S)-(-)-9 giving ester (S,X)-18A. Alcohol (X)-17 is similarly esterified with MTPA acid (R)-(+)-9 giving ester (R,X)-18B. These MTPA esters take preferred conformations

shown in Figure 6b, where  $\text{CF}_3$  group is synperiplanar to carbonyl oxygen atom, and the methine proton of secondary alcohol moiety is also synperiplanar to carbonyl oxygen atom.<sup>39,41</sup> Therefore, these moieties lie on a single plane, the MTPA plane, in the preferred conformations. In the preferred conformation of ester (S,X)-18A, the alcoholic substituent  $\text{R}^1$  is above of the benzene plane of the MTPA moiety.

In MTPA esters, the aromatic substituent (phenyl group) generates a diamagnetic anisotropy effect due to the ring current induced under the external magnetic field, and so the proton NMR signals of the alcohol moiety, which faces the phenyl group in the preferred conformation, are moved to a higher magnetic field (high field shift). So, in ester (S,X)-18A, the protons of group  $\text{R}^1$  feel a diamagnetic anisotropy effect, and hence their  $^1\text{H}$  NMR signals show high-field shifts. On the other hand, in the ester (R,X)-18B, the alcoholic substituent  $\text{R}^2$  is above of the benzene plane of the MTPA moiety, and hence the protons of group  $\text{R}^2$  show high-field shifts.

The parameter  $\Delta\delta$  reflecting the anisotropy effects is defined as  $\Delta\delta = \delta(\text{S,X}) - \delta(\text{R,X})$  for MTPA esters.<sup>41</sup> By combining the anisotropy effects discussed above and the definition of  $\Delta\delta$  parameter, the empirical rule for determining the absolute configurations of chiral secondary alco-

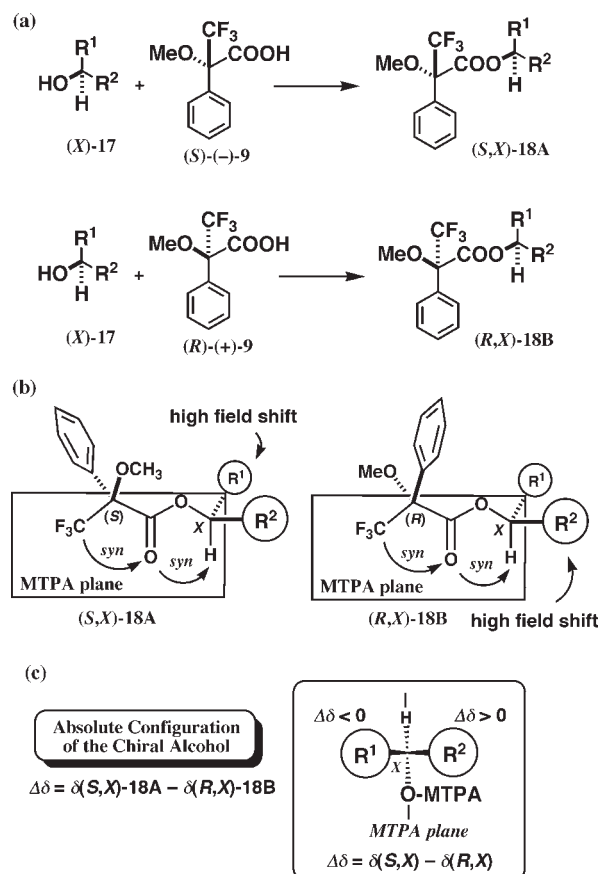


Fig. 6. The advanced Mosher method for determining the absolute configuration of chiral secondary alcohols using both (S)- and (R)-MTPA acids: (a) preparation of MTPA esters, (b) preferred conformations of MTPA esters, and (c) definition of  $\Delta\delta$  value and sector rule.

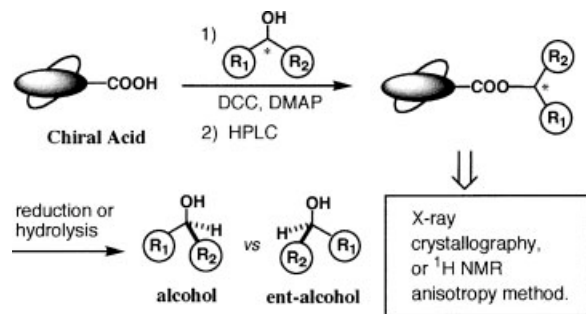


Fig. 7. Enantioresolution and determination of absolute configuration of alcohols using chiral carboxylic acid.

hols was proposed as illustrated in Figure 6c, where the MTPA moiety is placed in the down and rear side, while the methine proton of the secondary alcohol moiety in the up and rear side. The substituent  $\text{R}^2$  showing positive  $\Delta\delta$  values is placed at the right side, while the substituent  $\text{R}^1$  showing negative  $\Delta\delta$  values is at the left side. So, the absolute configuration ( $X$ ) of alcohol **17** can be determined.<sup>41</sup> This method is thus convenient, since it does not require crystallization of compounds.

In the case of the Trost's method using MPA,<sup>40</sup> the methoxyl group is synperiplanar to the ester carbonyl oxygen atom in their preferred conformations, and the parameter reflecting the  $^1\text{H}$  NMR anisotropy effect,  $\Delta\delta$  is defined as  $\Delta\delta = \delta(\text{R}, X) - \delta(\text{S}, X)$ .

One problem of this method is that it is based on the assumption of preferred conformation of molecules in solution. However, it is reliable in most cases since the method itself has a self-diagnostic function.<sup>41–47</sup> Namely, in some exceptional cases of MTPA esters,<sup>48</sup> to which the NMR anisotropy method is not applicable, the observed  $\Delta\delta$  values reflecting the anisotropy effect are small and/or distribute randomly. On the other hand, if the  $\Delta\delta$  values are sufficiently large and show a reasonable distribution pattern, it leads to a reliable assignment. Therefore, the applicability of the  $^1\text{H}$  NMR anisotropy method can be judged from the magnitude and distribution pattern of the observed  $\Delta\delta$  values. Although the method has been widely applied to secondary alcohols, the method could be extended to other kinds of compounds.

#### PREPARATION OF ENANTIOPURE COMPOUNDS AND SIMULTANEOUS DETERMINATION OF THEIR ABSOLUTE CONFIGURATIONS

The author considers that the most reliable and practical method for determining the absolute configuration is the X-ray crystallography by the use of internal reference, as described above. Namely, the absolute configurations of points in question can be unambiguously determined from the X-ray stereoview showing a relative stereochemistry, because the absolute configuration of the chiral auxiliary is already known. Therefore, it is easy to determine the absolute configuration, and there is no possibility of making a mistake in the assignment.

We also consider that a highly efficient method for preparing an appropriate amount of various chiral compounds with 100% enantiopurity in a laboratory scale is the enantioresolution method, as illustrated in Figure 7, although it is called a classical method. In the method, a chiral auxiliary is covalently bonded to racemates, and therefore the obtained diastereomeric mixture can be separated by conventional HPLC on silica gel. If the chromatogram shows a baseline separation and the chiral reagent used is enantiopure, the diastereomers separated are also enantiopure. It is easy to recover enantiopure alcohols from the diastereomeric esters obtained. Therefore, if the absolute configuration of one of diastereomers can be determined by X-ray crystallography and/or by  $^1\text{H}$  NMR anisotropy, enantiopure alcohols with established absolute configurations are obtained.

#### (–)-CSDP Acid, a CXR Useful for the Enantioresolution of Alcohols by HPLC and Simultaneous Determination of their Absolute Configurations by X-ray Crystallography

As a chiral auxiliary useful for preparation of enantiopure alcohols and simultaneous determination of their absolute configurations, we have developed a chiral molecular tool, camphorsultam dichlorophthalic acid (CSDP acid) (–)-**1**<sup>64</sup> connecting (1*S*,2*R*,4*R*)-2,10-camphorsultam and 4,5-dichlorophthalic acid (see Fig. 8), and have applied this chiral tool to various compounds.<sup>14–20</sup> The 2,10-camphorsultam was selected because of its good affinity with silica gel used in HPLC, allowing good separation of two diastereomers. In addition, the sultam amide moiety is effective for providing prismatic single crystals suitable for X-ray diffraction experiment. Furthermore, the (1*S*,2*R*,4*R*) absolute stereochemistry of 2,10-camphorsultam is useful as the internal reference of absolute configuration. To connect alcohols, an ester bond was chosen, because it could be readily formed and cleaved off. Accordingly, 4,5-dichlorophthalic acid was selected as a linker for CSDP acid (–)-**1**, and phthalic acid for CSP (camphorsultam phthalic) acid (–)-**2** (see Fig. 8).<sup>64,65</sup>

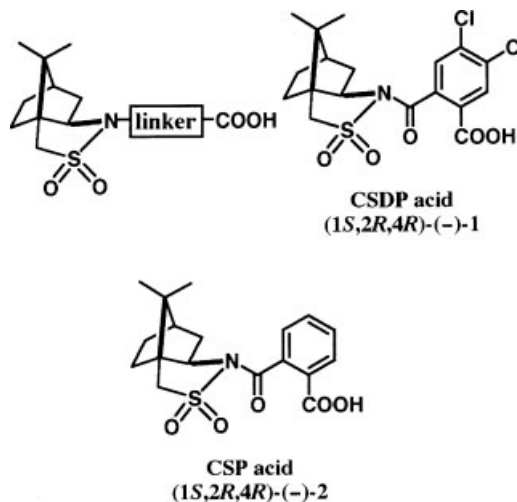


Fig. 8. Design of a chiral molecular tool, CSDP and CSP acids containing 2,10-camphorsultam moiety.

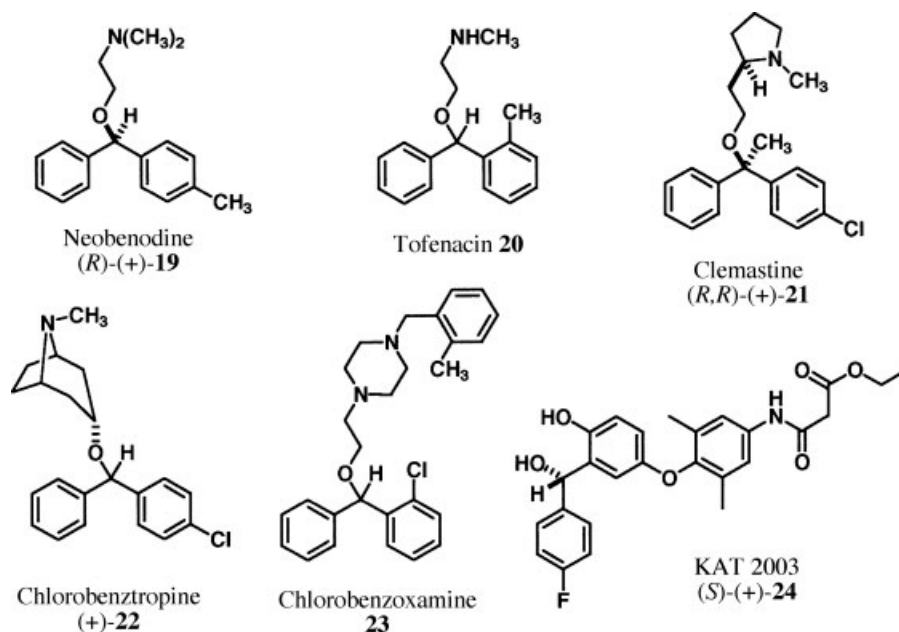


Fig. 9. Chiral drugs with a diarylmethanol skeleton.

The desired molecular tool, CSDP acid (*-*)-**1**, was synthesized by reacting (1*S*,2*R*,4*R*)-(*-*)-2,10-camphorsultam anion with 4,5-dichlorophthalic anhydride: acid (*-*)-**1**, mp 221°C from EtOH;  $[\alpha]_D^{20} -101.1$  (*c* 1.375, MeOH).<sup>64</sup> This carboxylic acid was condensed with alcohol under the conditions of 1,3-dicyclohexylcarbodiimide (DCC) and 4-dimethylaminopyridine (DMAP).

Various chiral drugs with a diphenylmethanol skeleton have been developed as shown in Figure 9. Among them,

the absolute configurations of some drugs have remained undetermined. In addition, those drugs were prepared mostly by means of asymmetric syntheses and/or enzymatic reactions. Therefore, it is hard to obtain enantiopure drugs without purification by recrystallization. How can we determine the absolute configuration of these chiral drugs and also obtain enantiopure compounds? To solve these problems, we have applied the CSDP acid method to various diphenylmethanols as follows.

To exemplify a general procedure of the CSDP acid method, we show here the results of chiral (2,6-dimethylphenyl)phenylmethanol (**25**). The CSP acid (*-*)-**1** was allowed to react with (*±*)-**25** using DCC and DMAP in CH<sub>2</sub>Cl<sub>2</sub> yielding diastereomeric esters, which were effectively separated by HPLC on silica gel: hexane/EtOAc = 6:1;  $\alpha = 1.25$ ,  $R_s = 1.94$  (Figs. 10 and 11).<sup>66</sup> The first-eluted ester (*-*)-**26a** obtained was recrystallized from EtOH giving prisms. A single crystal of **26a** was subjected to X-ray analysis affording the ORTEP drawing as shown

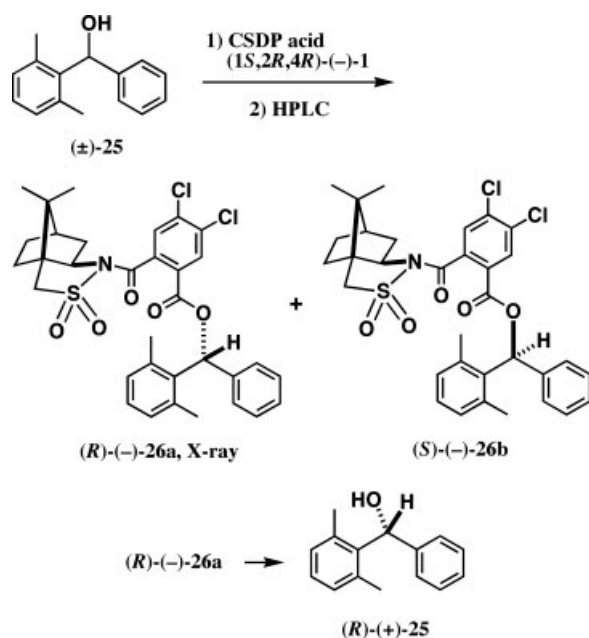


Fig. 10. Preparation of CSDP esters: DCC, DMAP in CH<sub>2</sub>Cl<sub>2</sub> and recovery of enantiopure alcohol (*R*)-(+)-**25**.<sup>66</sup>

Chirality DOI 10.1002/chir

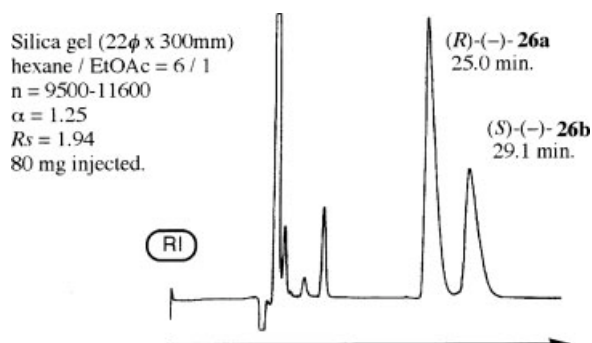


Fig. 11. HPLC separation of CSDP esters **26a** and **26b**.<sup>66</sup>



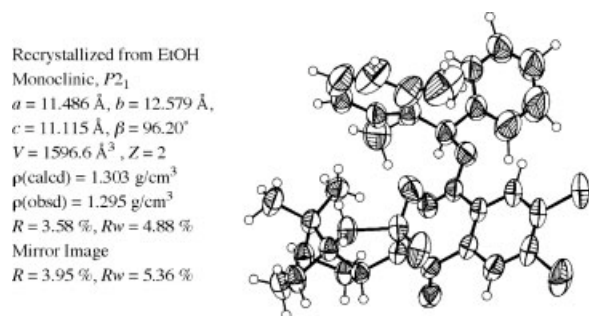


Fig. 12. ORTEP drawing of CSDP ester (*R*)-(-)-**26a**.<sup>66</sup>

in Figure 12, from which the absolute configuration of the alcohol part was clearly determined as *R* based on the absolute configuration of the camphorsultam moiety used as an internal reference. The *R* absolute configuration of **26a** was also confirmed by the heavy atom effect of two chlorine and sulfur atoms contained. The reduction of the first-eluted ester (*R*)-(-)-**26a** with  $\text{LiAlH}_4$  in THF yielded enantiopure alcohol (*R*)-(+)-**25**.<sup>66</sup> Although the reduction with  $\text{LiAlH}_4$  was used here to recover the alcohol, we found later that the solvolysis with  $\text{K}_2\text{CO}_3$  in MeOH as a more mild condition is also applicable to most CSDP esters.

As shown in Table 2, the method using CSDP and/or CSP acids has been successfully applied to various substituted diphenylmethanols **27–33**, **35**, **37–42**, and **51–56** (entries 2–14 and 23–28). Namely the diastereomeric esters prepared from racemic alcohols and CSDP acid (1*S*,2*R*,4*R*)-(-)-**1** were effectively separated by HPLC on silica gel with separation factor  $\alpha = 1.10$ –1.34. It is known that if the separation factor  $\alpha$  is larger than 1.10, the two components are baseline separable, yielding pure compounds. In the case of alcohols **32**, **38**, **40**, **51**, **52**, and **54–56**, the CSDP acid method has been applied in a straightforward manner; the separated CSDP esters were recrystallized giving single crystals, which were subjected to X-ray crystallography (entries 7, 11, 12, 23, 24, and 26–28). The absolute configurations of the alcohol parts were thus explicitly determined.

In the case of alcohols **27** and **28**, those compounds were previously enantioresolved by means of CSP acid (1*S*,2*R*,4*R*)-(-)-**2**, a similar chiral auxiliary developed by us as shown in Figures 1 and 8, and the absolute configurations of their CSP esters were determined by X-ray crystallography (entries 2' and 3'). So, by comparison with the data, the absolute configurations of CSDP acid esters of alcohols **27** and **28** were established by chemical correlation. It should be noted that the CSDP acid esters of **27** and **28** were more effectively separated by HPLC on silica gel than the corresponding CSP acid esters: separation factor  $\alpha = 1.20$ –1.26 vs. 1.1 (entries 2, 2', 3, and 3'). In general, CSP acid esters have low solubility, possibly due to too better crystallinity, resulting in longer elution time and smaller  $\alpha$  value in HPLC on silica gel. In addition, CSP esters were often obtained as fine needles, which were unsuitable for X-ray crystallography. Therefore CSDP acid **1** is more useful in most cases than CSP acid **2**.

In the case of halogenated alcohols **29** and **30**, their diastereomeric CSDP esters were obtained as fine crystals, which were unsuitable for X-ray crystallography. So, as described above, the enantiopure alcohol (-)-**29** recovered was converted to camphanate ester, the absolute configuration of which was determined by X-ray crystallography as *R* (entry 4, Table 2). Alcohol (-)-**30** was treated in the same way, but its camphanate ester was not suitable for X-ray analysis (entry 5). The absolute configuration of (-)-**30** was determined as *R* by the comparison of its CD spectrum with that of (*R*)-(-)-**29**.

Methyl-substituted alcohol **31** could not be enantioresolved by the CSDP acid method, because of the small difference in substituent effects: Me vs. H (entry 6). Therefore, we have adopted the chemical conversion method as follows: racemic alcohol **32** with 4-Me and 4'-Br groups was effectively enantioresolved as CSDP esters, the absolute configuration of which was determined by X-ray crystallography (entry 7). The enantiopure alcohol (*R*)-(-)-**32** obtained was reduced to remove Br atom yielding (*S*)-(-)-**31**.

Alcohols **34** and **36** are very unique chiral compounds, the chirality of which is generated by the substitution of isotopes: in the case of **34**, H vs. D; in the case of **36**,  $^{12}\text{C}$  vs.  $^{13}\text{C}$ . So, it is very difficult to recognize directly such an ultimately small chirality. To synthesize enantiopure alcohols **34** and **36**, and to determine their absolute configurations, the indirect chemical conversion method was employed as follows. For example, deuterium-substituted/4-Br alcohol **35** was similarly enantioresolved as in the case of compound **29** (entry 9). The enantiopure alcohol (*S*)-(-)-**35** obtained was reduced to remove the Br atom yielding  $[\text{CD}(-)270.4]$ -(*S*)-**34**, which exhibits a negative CD Cotton effect at 270.4 nm. In a similar way,  $^{13}\text{C}$ -substituted diphenylmethanol  $[\text{CD}(-)270]$ -**36** was synthesized in an enantiopure form and its absolute configuration was determined as *S* (entry 10).

Although the CSDP acid method was easily applicable to *o*-methoxy-substituted alcohol **38** (entry 11), *o*-methyl-substituted alcohol **39** could not be enantioresolved as the CSDP acid esters. So, the indirect method was adopted as follows: *o*-hydroxymethyl-substituted alcohol **40** was enantioresolved as CSDP esters, where the primary alcohol moiety was esterified (entry 12). Enantiopure alcohol (*R*)-(+)-**40** was then converted to the target compound (*R*)-(-)-**39**. It should be noted that the absolute configuration of alcohol **39** was once estimated on the basis of asymmetric reaction mechanism, but it was revised later by this study. The data of alcohols **41** and **42** indicate that the HPLC separation as CSDP esters is easier for silyl ethers (entries 13 and 14).

The CSDP acid method was applicable to benzyl alcohols **43–46** and naphthalene alcohols **47–49**, the CSDP esters of which were effectively separated by HPLC on silica gel with  $\alpha = 1.11$ –1.38 (entries 15–21). In addition, except the case of **45**, the absolute configurations of their CSDP esters were determined by X-ray crystallography.

Alcohol (3*R*,4*R*)-(+)-**47** is a key compound for the synthesis of a light-powered chiral molecular motor  $[\text{CD}(-)237.2]$ -(+)-**59a**, which rotates in one rotational

TABLE 2. Enantioresolution of alcohols by HPLC on silica gel using (1*S*,2*R*,4*R*)-(-)-CSDP acid 1, and determination of their absolute configurations by X-ray crystallography

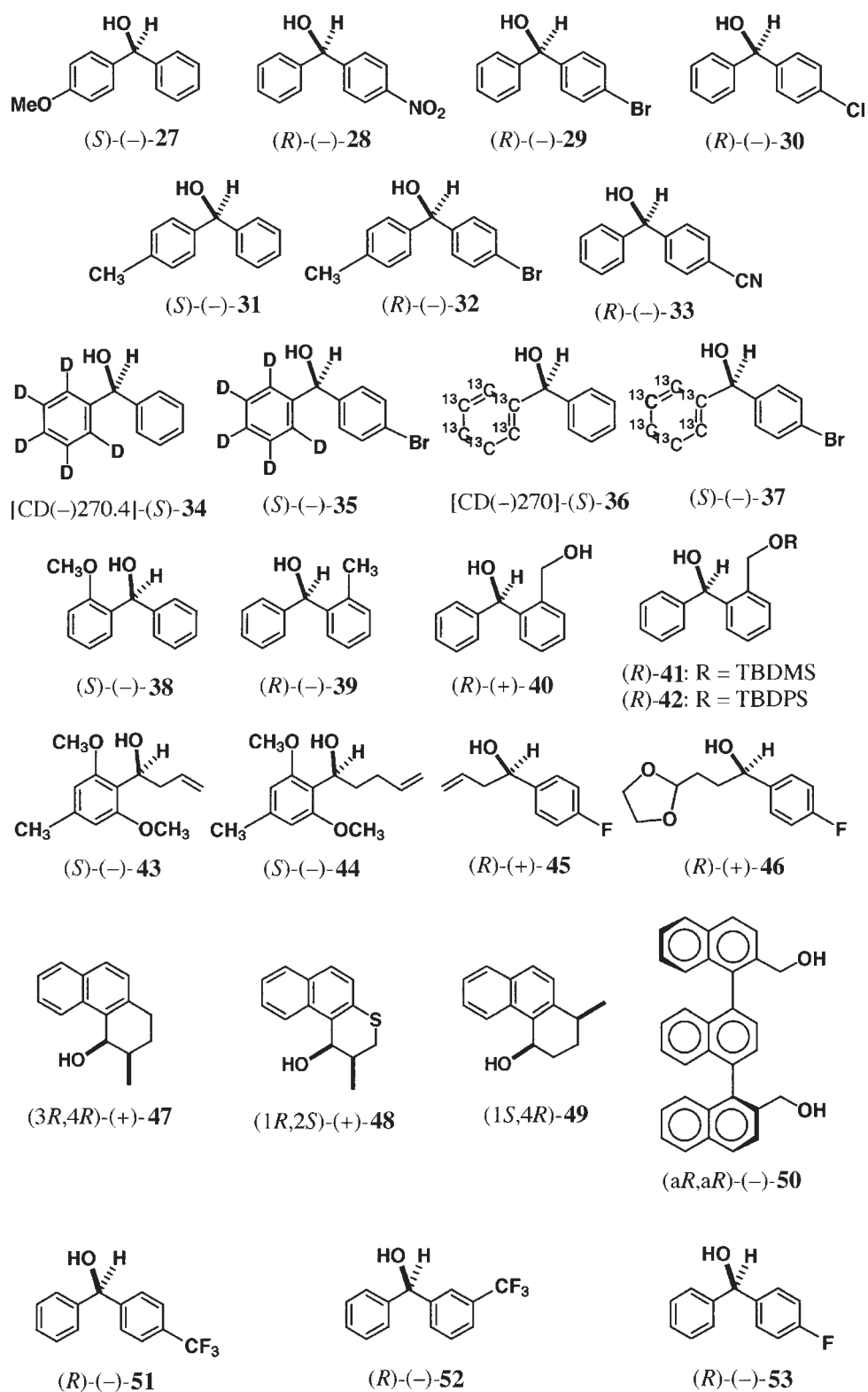
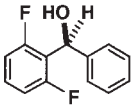
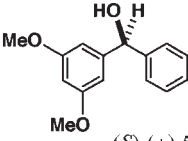
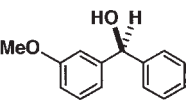
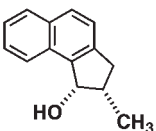
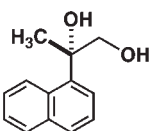


TABLE 2. Continued

<div style="display: flex; justify-content: space-around; align-items: center;"> <div style="text-align: center;">  <p>(<i>S</i>)-(-)-<b>54</b></p> </div> <div style="text-align: center;">  <p>(<i>S</i>)-(+)-<b>55</b></p> </div> <div style="text-align: center;">  <p>(<i>S</i>)-(+)-<b>56</b></p> </div> </div>							
<div style="display: flex; justify-content: space-around; align-items: center;"> <div style="text-align: center;">  <p>(1<i>S</i>,2<i>S</i>)-(+)-<b>57</b></p> </div> <div style="text-align: center;">  <p>(<i>S</i>)-(-)-<b>58</b></p> </div> </div>							
Entry	Alcohol	Solvent <sup>a</sup>	$\alpha^b$	$R_s^c$	X-ray <sup>d</sup>	Abs.Config. First Fr.	Ref.
1	<b>25</b>	H/EA = 6/1	1.25	1.94	<i>y</i> (1st, Fr.)	<i>R</i>	66
2	<b>27</b>	H/EA = 4/1	1.20	0.91	–	<i>S</i>	Fujita K, Harada N. unpublished data.
2 <sup>e</sup>	<b>27</b>	H/EA = 4/1	1.1	1.3	<i>y</i> (1st, Fr.)	<i>S</i>	
3	<b>28</b>	H/EA = 5/1	1.26	1.37	–	<i>R</i>	Fujita K, Harada N. unpublished data.
3 <sup>e</sup>	<b>28</b>	H/EA = 5/1	1.1	1.6	<i>y</i> (1st, Fr.)	<i>R</i>	
4	<b>29</b>	H/EA = 8/1	1.1	1.3	<i>y</i> <sup>f</sup>	<i>R</i>	29
5	<b>30</b>	H/EA = 6/1	1.17	0.95	–	<i>R</i>	Fujita K, Harada N. unpublished data.
6	<b>31</b>	H/EA = 7/1	–	–	–	–	
7	<b>32</b>	H/EA = 8/1	1.18	0.83	<i>y</i> (1st, Fr.)	<i>R</i>	67
8	<b>33</b>	H/EA = 4/1	1.1	1.0	–	<i>R</i>	Fujita K, Harada N. unpublished data.
9	<b>35</b>	H/EA = 8/1	1.21	1.07	<i>y</i> <sup>f</sup>	<i>S</i>	
10	<b>37</b>	H/EA = 4/1	1.27	1.20	<i>y</i> <sup>f</sup>	<i>S</i>	68
11	<b>38</b>	H/EA = 5/1	1.12	1.01	<i>y</i> (1st, Fr.)	<i>S</i>	69
12	<b>40</b>	H/EA = 4/1	1.14	0.91	<i>y</i> (2nd, Fr.) <sup>g</sup>	<i>R</i>	69,70
13	<b>41</b>	H/EA = 10/1	1.26	1.03	–	<i>R</i>	69
14	<b>42</b>	H/EA = 6/1	1.26	1.29	–	<i>R</i>	Taji H, Harada N. unpublished data.
15	<b>43</b>	H/EA = 5/1	1.16	1.11	<i>y</i> (1st, Fr.)	<i>S</i>	
16	<b>44</b>	H/EA = 5/1	1.12	0.87	<i>y</i> (1st, Fr.)	<i>S</i>	71
17	<b>45</b>	H/EA = 2/1	1.11	0.88	–	<i>R</i>	71
18	<b>46</b>	H/EA = 2/1	1.38	1.19	<i>y</i> (1st, Fr.)	<i>R</i>	71
19	<b>47</b>	H/EA = 7/1	1.18	1.06	<i>y</i> (2nd, Fr.)	3 <i>R</i> ,4 <i>R</i>	27,64
20	<b>48</b>	H/EA = 7/1	1.23	1.27	<i>y</i> (1st, Fr.), <i>y</i> (2nd, Fr.)	1 <i>R</i> ,2 <i>S</i>	Koumura N, Harada N. unpublished data.
21	<b>49</b>	H/EA = 10/1	1.30	1.74	<i>y</i> (1st, Fr.)	1 <i>S</i> ,4 <i>R</i>	
22	<b>50</b>	H/EA = 3/1	1.2	1.6	<i>y</i> (2nd, Fr.)	a <i>R</i> ,a <i>R</i>	72,73
23	<b>51</b>	H/EA = 5/1	1.34	2.37	<i>y</i> (1st, Fr.)	<i>R</i>	74
24	<b>52</b>	H/EA = 5/1	1.16	1.22	<i>y</i> (1st, Fr.), <i>y</i> (2nd, Fr.)	<i>R</i>	74
25	<b>53</b>	H/EA = 5/1	1.11	1.33	–	<i>R</i>	74
26	<b>54</b>	H/EA = 4/1	1.21	2.50	<i>y</i> (1st, Fr.)	<i>S</i>	74
27	<b>55</b>	H/EA = 5/1	1.16	1.42	<i>y</i> (1st, Fr.)	<i>S</i>	75
28	<b>56</b>	H/EA = 4/1	1.15	1.34	<i>y</i> (1st, Fr.)	<i>S</i>	75
29	<b>57</b>	H/EA = 10/1	1.17	1.79	<i>y</i> (2nd, Fr.)	1 <i>R</i> ,2 <i>R</i>	28
30	<b>58</b>	H/EA = 4/1	1.27	1.49	<i>y</i> <sup>h</sup>	<i>S</i>	51

<sup>a</sup>H = *n*-hexane, EA = ethyl acetate.<sup>b</sup>Separation factor  $\alpha = (t_2 - t_0)/(t_1 - t_0)$  where  $t_1$  and  $t_2$  are the retention times of the first- and second-eluted fractions, respectively, and  $t_0$  is the retention time of an unretained compound (void volume marker).<sup>c</sup>Resolution factor  $R_s = 2(t_2 - t_1)/(W_1 + W_2)$  where  $W_1$  and  $W_2$  are the band-widths of the first- and second-eluted fractions at the base-line level, respectively.<sup>d</sup>*y*: yes.<sup>e</sup>The case of esters with (1*S*,2*R*,4*R*)-(-)-CSP acid **2**.<sup>f</sup>X-ray analysis of camphanate ester.<sup>g</sup>CSDP ester of the primary alcohol moiety.<sup>h</sup>X-ray analysis of 4-bromobenzoate.

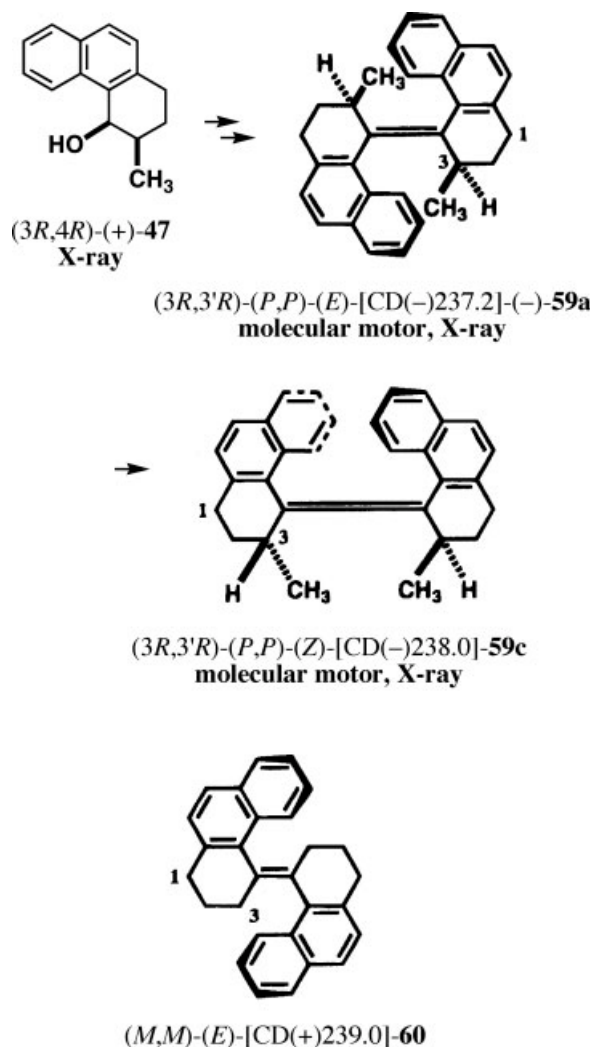


Fig. 13. Synthesis of a light-powered chiral molecular motor **59a** and determination of its absolute configuration.

direction by the use of light energy (see Fig. 13). *cis*-Olefin [CD(-)238.0]-**59c** is one of the motor rotation isomers. The molecular framework of these compounds takes a twisted structure, the absolute configuration of which is defined as (*P,P*) or (*M,M*). Compound [CD(+239.0)]-**60** also takes a similar twisted structure, and therefore it shows a strong positive CD band at 239.0 nm. To determine the absolute configuration of [CD(+239.0)]-**60**, we have adopted the next strategy. Enantiopure alcohol (3*R*,4*R*)-(+)-**47** was prepared by the CSDP acid method, and its absolute configuration was determined by X-ray crystallography. Starting from (3*R*,4*R*)-(+)-**47**, chiral molecular motors [CD(-)237.2]-(-)-**59a** and [CD(-)238.0]-**59c** were synthesized, and a single crystal of (-)-**59a** was subjected to X-ray analysis. As compound (-)-**59a** contains no heavy atoms, X-ray analysis provided the relative stereochemistry, but not the absolute configuration. However, compound (-)-**59a** has two methyl groups at chiral positions, i.e., (3*R*,3'*R*) configuration, which can be used as internal references of absolute configuration. We

have thus determined the absolute sense of helicity of (-)-**59a** as (*P,P*). So, the chirality of the molecular motor is expressed as (3*R*,3'*R*)-(*P,P*)-(E)-[CD(-)237.2]-(-)-**59a**. As the CD spectrum of [CD(+239.0)]-**60** is almost mirror image of (3*R*,3'*R*)-(*P,P*)-(E)-[CD(-)237.2]-(-)-**59a**, the absolute helicity of [CD(+239.0)]-**60** was determined as (*M,M*)-(E). This is another unique example of the use of internal reference in X-ray crystallography.

Ternaphthalene-dimethanol **50** is an interesting compound having three naphthalene chromophores in chiral positions. Therefore, it was expected that it would show intense exciton-coupled CD, from which its absolute configuration could be determined. The CSDP esters of **50** were separable with  $\alpha = 1.2$  (entry 22), and the absolute configuration of the second-eluted fraction was determined by X-ray crystallography. The (*aR,aR*) configuration of (-)-**50** agreed with the assignment by the CD exciton chirality method.

Various fluorinated diphenylmethanols **51**–**54** were also enantioresolved as CSDP esters (entries 23–26). In the case of alcohols **51**, **52**, and **54**, their absolute configurations were determined by X-ray crystallography. Meta-

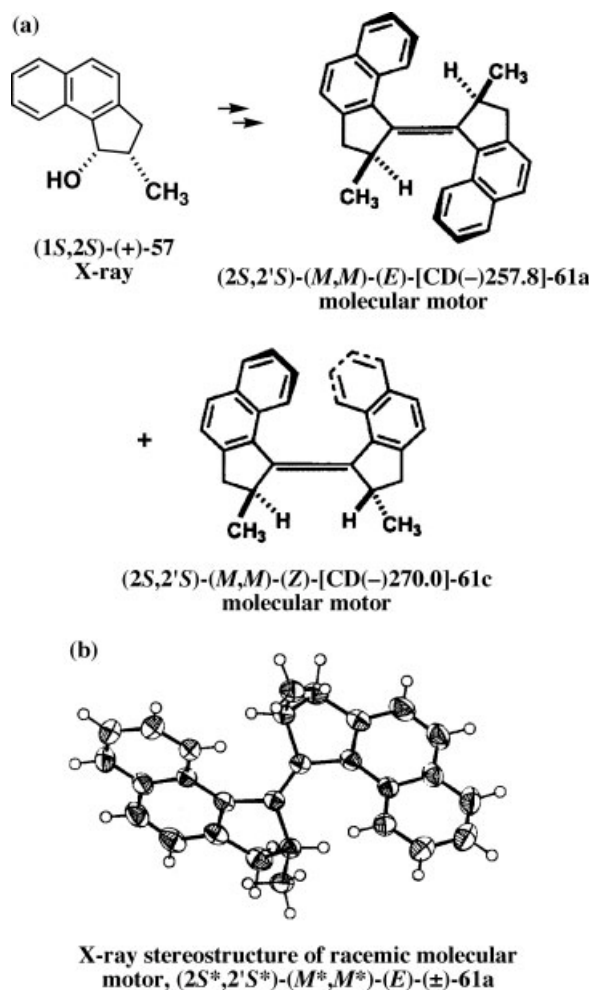
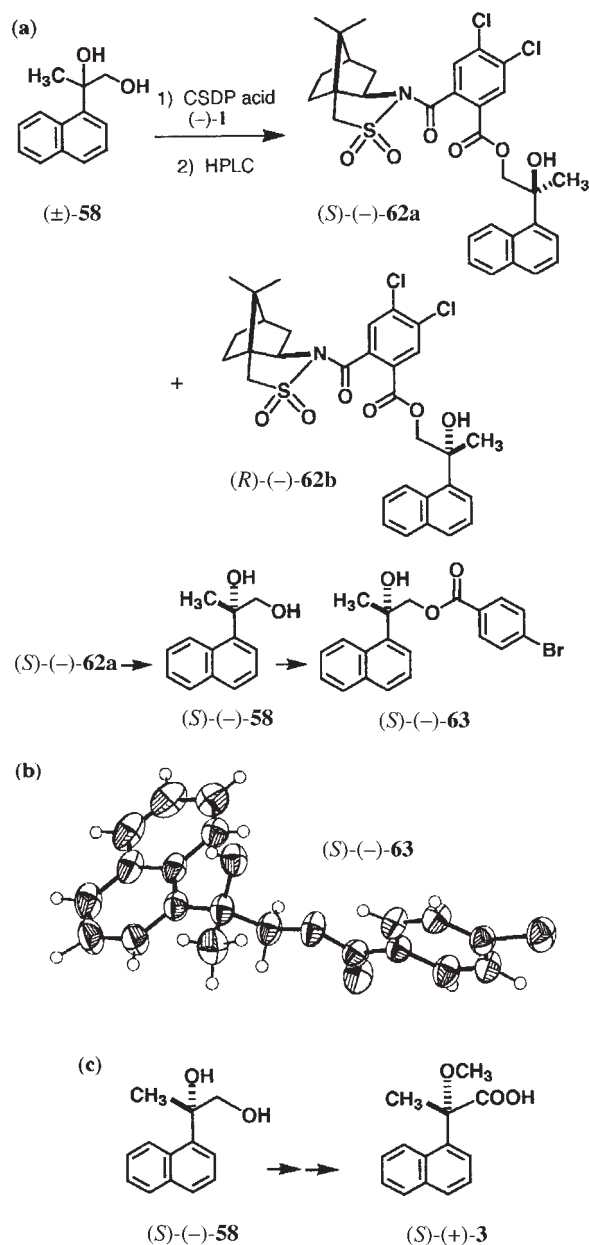


Fig. 14. A new model of light-powered chiral molecular motor **61a**: (a) synthesis and (b) X-ray stereostructure of racemic motor (±)-**61a**.





**Fig. 15.** (a) Enantioresolution and determination of the absolute configuration of 2-(1-naphthyl)propane-1,2-diol (**58**). (b) ORTEP drawing of 4-bromobenzoate (S)-(-)-**63**, whose absolute configuration was determined by the heavy atom effect of bromine atom. (c) Preparation of (S)-(+)-MαNP acid (**3**) from glycol (S)-(-)-**58**.<sup>51</sup>

substituted diphenylmethanols **55** and **56** were enantioresolved by the CSDP acid method yielding enantiopure alcohols, the absolute configurations of which were unambiguously determined by X-ray crystallography (entries 27 and 28).

A new model of molecular motor **61a** with five-membered rings, which rotates faster than the previous molecular motor **59a**, was synthesized (see Fig. 14). *cis*-Alcohol (±)-**57** was similarly enantioresolved as CSDP acid ester, the absolute configuration of which was estab-

lished by X-ray crystallography (entry 29). Starting from *cis*-alcohol (1*S*,2*S*)-(+)-**57**, chiral molecular motor isomers [CD(−)257.8]-**61a** and [CD(−)270.0]-**61c** were synthesized. To determine the helicity of the molecular skeleton by X-ray analysis, we have attempted the crystallization of chiral olefin [CD(−)257.8]-**61a**. However, all attempts were unsuccessful. Instead, we have succeeded in obtaining single crystals of racemic molecular motor (±)-**61a**. As shown in Figure 14b, its relative stereostructure was determined by X-ray analysis to be (2*S*\*,2'*S*\*)-(*M*\*,*M*\*)-(*E*), which means that the crystal contains enantiomers (2*R*,2'*R*)-(*P*,*P*)-(*E*)-**61a** and (2*S*,2'*S*)-(*M*,*M*)-(*E*)-**61a** in 1:1 ratio. Since the absolute configurations of methyl groups at 2- and 2'-positions were already established to be *S* and *S*, respectively, by X-ray analysis of CSDP ester of (+)-**57**, the absolute configuration of molecular motor [CD(−)257.8]-**61a** was unambiguously determined to be (2*S*,2'*S*)-(*M*,*M*)-(*E*). The (2*S*,2'*S*)-(*M*,*M*)-(Z) absolute configuration was assigned to [CD(−)270.0]-**61c**. As exemplified here, in the methods for determining absolute configurations by X-ray crystallography using internal references, the X-ray analyses of racemic compounds are also useful.

For this new model of chiral molecular motor, an opposite absolute configuration had been once assigned.<sup>76</sup> Namely the (2*R*,2'*R*)-(P,P) absolute configuration was assigned to *cis*-olefin [CD(−)270.0]-**61c** by comparison of its CD spectrum with that of six-membered *cis*-olefin (3*R*,3'*R*)-(P,P)-(Z)-[CD(−)238.0]-**59c**. It should be noted that such comparison of CD spectra leads to wrong absolute configurations. Therefore, when determining absolute configurations by comparison of CD spectra, it is of critical importance to judge whether such comparison is reasonable or not.

A very important example is the case of 2-(1-naphthyl)propane-1,2-diol **58**, which was isolated as a chiral metabolite of 1-isopropynaphthalene in rabbits. The metabolite, however, was not enantiopure and its absolute configuration had been only empirically estimated based on the reaction mechanism. To obtain the enantiopure diol **58** and to determine its absolute configuration in an unambiguous way, the method of CSDP acid was applied to (±)-**58** (see Fig. 15).<sup>51</sup> In this case, only the primary alcohol part was esterified, and the diastereomeric mixture obtained was clearly separated by HPLC on silica gel: hexane/EtOAc = 4:1,  $\alpha = 1.27$ ,  $R_s = 1.14$  (entry 30 and Fig. 16). In this HPLC, the presence of a free tertiary hydroxyl group is important, because the protection of the tertiary alcohol group led to poor separation.

Despite repeated recrystallizations, both diastereomers **62a** and **62b** were obtained only as amorphous solids. Therefore, the first-eluted fraction (−)-**62a** was reduced with  $\text{LiAlH}_4$  to yield enantiopure glycol (−)-**58**, which was further converted to 4-bromobenzoate (−)-**63** (Fig. 15a). By recrystallization from EtOH, good single crystals of ester (−)-**63** were obtained and subjected to X-ray analysis. Consequently, its absolute configuration was explicitly determined as *S* by the Bijvoet pair measurement of the anomalous dispersion effect of the bromine atom contained (Fig. 15b).<sup>51</sup>

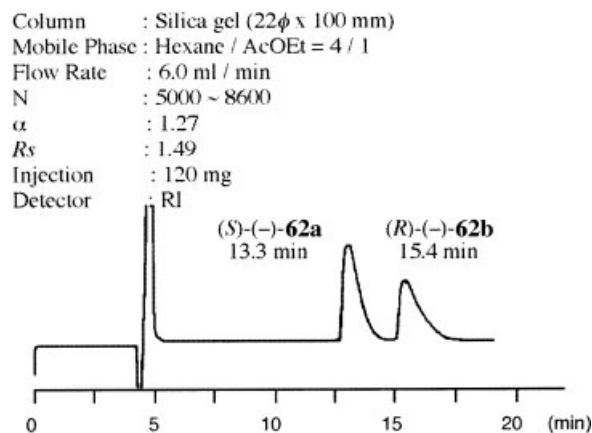


Fig. 16. HPLC separation of esters (S)-(-)-62a and (R)-(-)-62b.

Furthermore, we have obtained enantiopure 2-methoxy-2-(1-naphthyl)propionic acid (M $\alpha$ NP acid) (S)-(+)-**3** via several reactions from diol (S)-(-)-**58** (Fig. 15c).<sup>51</sup> Regarding this carboxylic acid, Goto et al. had first used (-)-**3** for analytical studies of racemic amino acid methyl esters.<sup>77,78</sup> Amino acid methyl esters were condensed with acid (-)-**3** giving diastereomeric amides, which were efficiently separated by HPLC. However, those separated amides had not been used for recovering chiral amino acids or methyl esters. In addition, at that time, the absolute configuration of acid (-)-**3** had not been determined yet. Later, Ichikawa reported the *S* absolute configuration of acid (-)-**3** on the basis of <sup>1</sup>H NMR spectroscopy data.<sup>79</sup> However, this assignment was revised later by our X-ray crystallographic analysis and chemical correlation as shown in Figure 15. Since then, as will be discussed below, the absolute configuration of M $\alpha$ NP acid **3** has been independently determined by X-ray crystallographic studies of 1:1 complex of 9-*O*-(*tert*-butylcarbamoyl)quinine,<sup>80</sup> ester prepared with (-)-menthol,<sup>22</sup> and of amide formed with (S)-(-)-phenylalaninol.<sup>81</sup> All four X-ray studies, of course, are consistent with one another.

We have discovered that this carboxylic acid, M $\alpha$ NP acid **3**, was also effective for enantioresolution and simultaneous determination of the absolute configuration of various secondary alcohols by the <sup>1</sup>H NMR anisotropy method.<sup>19–22,51–60,82–87</sup> The results obtained by the <sup>1</sup>H NMR anisotropy method are consistent with those by the X-ray method. Therefore, the methods of CSDP and M $\alpha$ NP acids are useful as complementary molecular tools, as will be discussed later.

**M $\alpha$ NP Acid, a CAR Powerful for Both Enantioresolution of Alcohols and Simultaneous Determination of Their Absolute Configurations by <sup>1</sup>H NMR Anisotropy**

We have discussed above the design and applications of CSDP acid useful for both the preparation of enantiopure compounds and the unambiguous determination of their absolute configurations by X-ray analysis. The X-ray crystallographic method using the internal reference of absolute configuration thus leads to the unambiguous and reliable determination of absolute configuration. However,

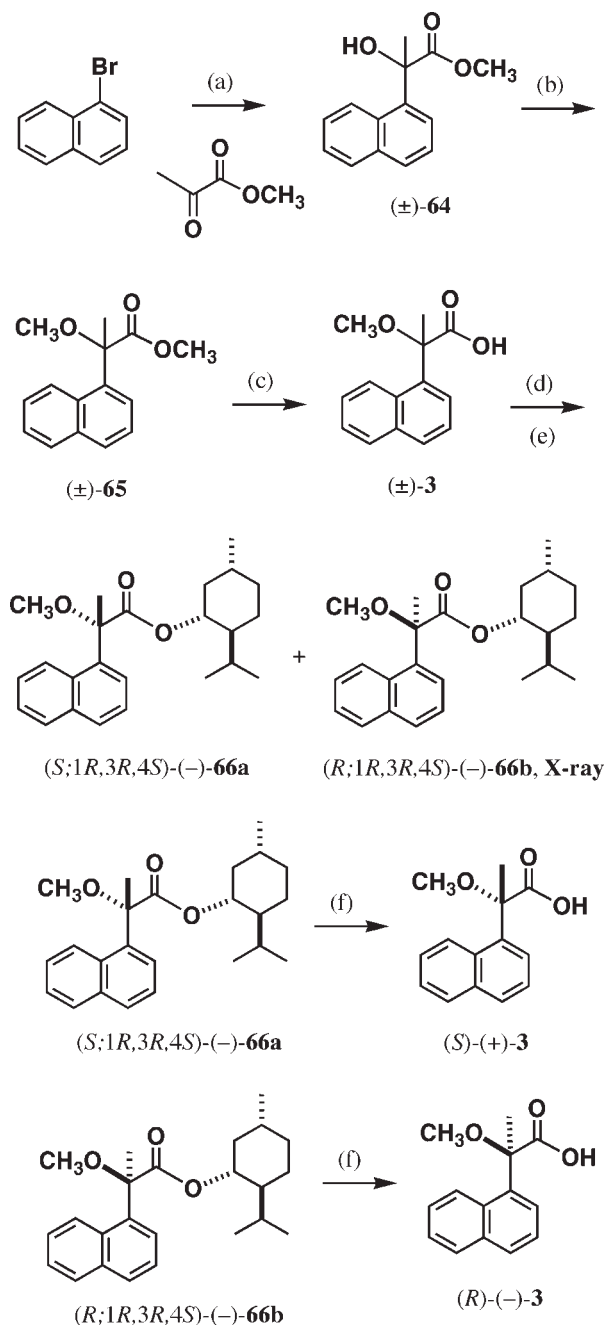
the disadvantage of X-ray crystallography is that the method needs single crystals, and, therefore, it is not applicable to noncrystalline materials. However, in daily experiments, prismatic single crystals suitable for X-ray analysis are not always obtainable. So is there any other method applicable to noncrystalline materials? In addition, the applications of the CSDP acid method have been mostly applied to aromatic compounds as shown in Table 2. So, a powerful method applicable to aliphatic compounds has been required.

As discussed above, the <sup>1</sup>H NMR anisotropy method using  $\alpha$ -methoxy- $\alpha$ -trifluoromethylacetic acid, MTPA acid, (**9**) is also useful as another method for determining absolute configurations. However, MTPA acid **9** is not so useful for enantioresolving racemic alcohols. Namely, it is not easy to separate diastereomeric esters prepared from racemic alcohol and chiral MTPA acid (R)-(+)-**9** by HPLC on silica gel, because of less polar nature of fluoro-derivatives. Are there new chiral <sup>1</sup>H NMR anisotropy reagents (CAR) powerful for both enantioresolution of alcohols and determination of their absolute configurations?

We have discovered that 2-methoxy-2-(1-naphthyl)propionic acid (M $\alpha$ NP acid(**3**) Figs. 1 and 15) is remarkably effective in enantioresolution of aliphatic alcohols, especially acyclic aliphatic alcohols.<sup>19–22,51–60,82–87</sup> In the <sup>1</sup>H NMR spectra of the esters formed from M $\alpha$ NP acid **3** and alcohols, the chemical shifts of the protons in the alcohol moiety are strongly affected by the magnetic anisotropy effect induced by the naphthyl group. Therefore, this M $\alpha$ NP acid **3** can be used as a CAR useful for determining the absolute configuration of secondary alcohols. Another advantage of the M $\alpha$ NP acid **3** is that it does not racemize, because the  $\alpha$ -position of **3** is fully substituted, and therefore, it is easy to prepare enantiopure acid **3**. Furthermore, as will be discussed below, M $\alpha$ NP acid **3** is a very powerful chiral auxiliary, which enables enantioresolution of alcohols. Namely, the M $\alpha$ NP esters prepared from chiral acid **3** and racemic alcohols are easily separable by HPLC on silica gel. From the M $\alpha$ NP esters separated, enantiopure alcohols can be recovered together with chiral acid **3**. Therefore M $\alpha$ NP acid **3** is very useful not only for determination of the absolute configurations of natural products and biologically active synthetic chiral compounds, e.g., chiral drugs, but also for preparation of enantiopure compounds.

In the following sections, the principle and applications of this chiral M $\alpha$ NP acid method are described: (a) synthesis of M $\alpha$ NP acid **3** and its enantioresolution with chiral alcohols, (b) absolute configurational and conformational analyses of M $\alpha$ NP acid esters by NMR and CD spectroscopic methods, (c) enantioresolution of racemic alcohols and determination of their absolute configuration using chiral M $\alpha$ NP acid **3**, (d) recovery of chiral alcohols with 100% enantiopurity from the separated diastereomeric esters.

**Facile synthesis of M $\alpha$ NP acid and its enantioresolution with natural (-)-menthol.**<sup>51,52,56</sup> To synthesize a large amount of enantiopure chiral M $\alpha$ NP acid **3** the facile synthesis and enantioresolution of racemic acid **3** were



(a) Mg/THF, then methyl pyruvate, 86%. (b) NaH,  $\text{CH}_3\text{I}$ /THF, 88%. (c) KOH, aqueous MeOH, ca. 100%.  
 (d) (-)-menthol, DCC, DMAP/ $\text{CH}_2\text{Cl}_2$ .  
 (e) HPLC on silica gel (hexane/EtOAc = 10:1), **66a**, 49%, **66b**, 46%. (f) NaOMe/MeOH,  $\Delta$ , ca. 100%.

Fig. 17. Preparation of enantiopure M $\alpha$ NP acids (S)-(+)-3 and (R)-(-)-3.<sup>56</sup>

carried out as shown in Figure 17. In general, for enantio-resolution of carboxylic acids, chiral synthetic amines or alkaloids have been used. However, we have adopted the following novel strategy to use chiral alcohols; chiral alco-

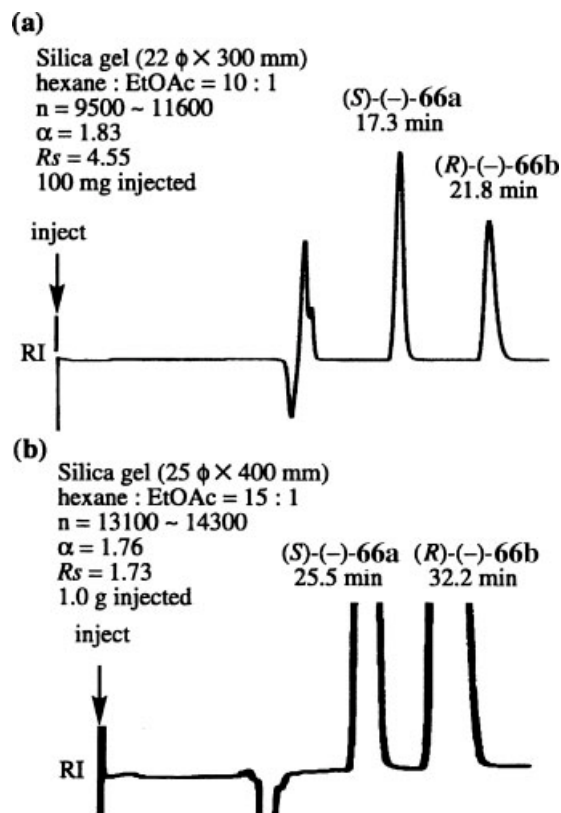


Fig. 18. HPLC separation of M $\alpha$ NP acid menthol esters (S;1R,3R,4S)-(-)-66a and (R;1R,3R,4S)-(-)-66b<sup>56</sup>: (a) analytical HPLC; (b) preparative HPLC.

hols are condensed with racemic acid 3 and the diastereomeric esters formed are separated by HPLC on silica gel. The separated esters are then hydrolyzed to yield both enantiomers of the desired carboxylic acids 3.

As a chiral alcohol, naturally occurring (1R,2S,5R)-(-)-menthol was selected and esterified with racemic acid (±)-3. It was surprising that diastereomeric esters **66a**

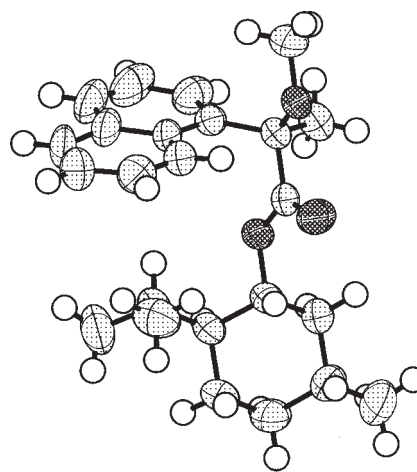


Fig. 19. The X-ray stereostructure of menthol M $\alpha$ NP ester (R;1R,3R,4S)-(-)-66b.<sup>22</sup>

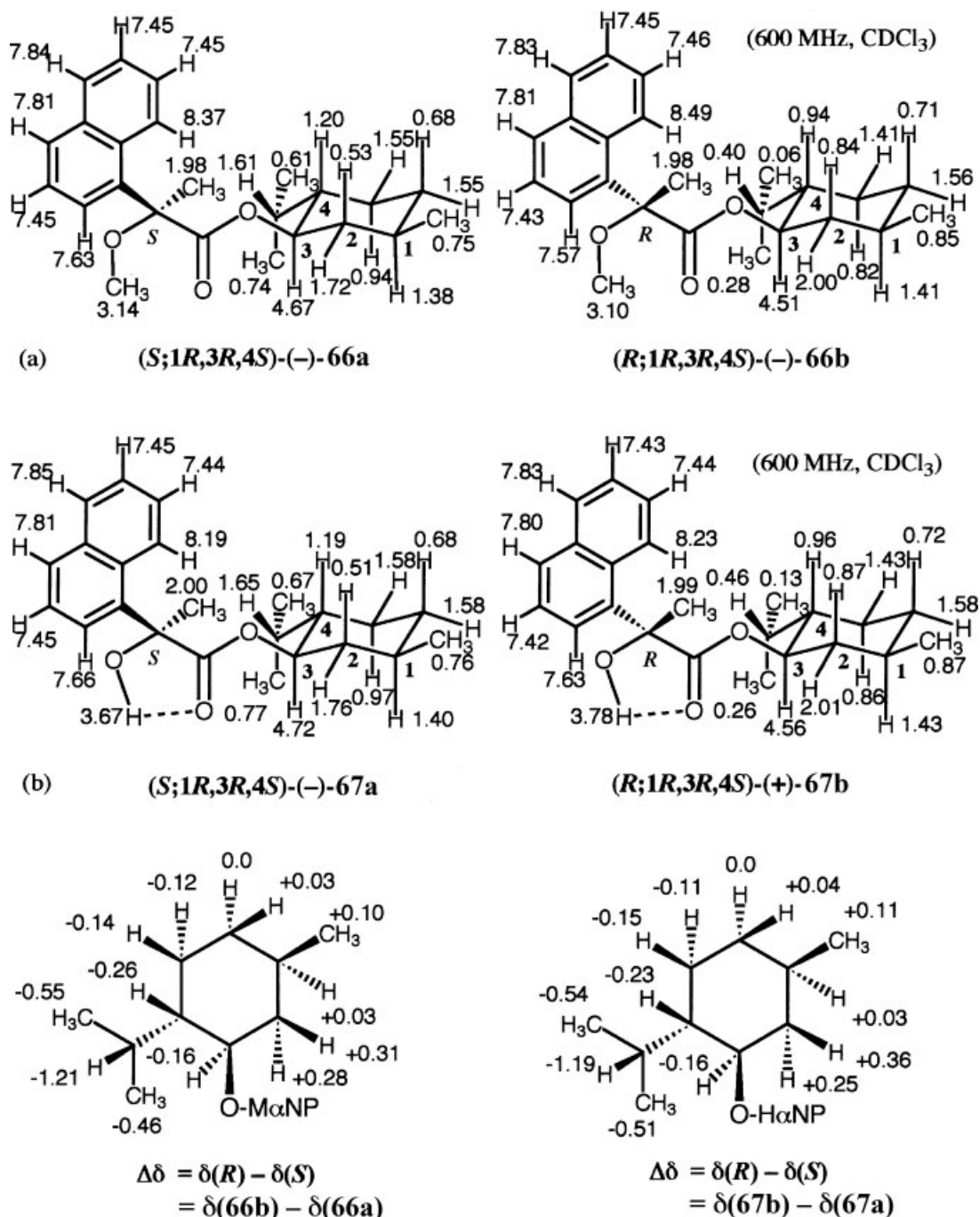


Fig. 20.  $^1\text{H}$  NMR data of  $\text{M}\alpha\text{NP}$  and  $\text{H}\alpha\text{NP}$  acid menthol esters: chemical shift  $\delta$  (ppm) and  $\Delta\delta$  (ppm).<sup>52,56</sup>

and **66b** formed were very easily separated by HPLC on silica gel (hexane/EtOAc = 10:1) as illustrated in Figure 18. The separation and resolution factors were extraordinarily high ( $\alpha = 1.83$ ,  $R_s = 4.55$ ), indicating that  $\text{M}\alpha\text{NP}$  acid **3** has great ability to recognize the chirality of the alcohols. The efficiency in separation enabled the HPLC of a preparative scale: esters **66a**/**66b** (1.0–1.8 g) were separable in one run using a glass column of silica gel (250  $\times$  400 mm). The first-eluted ester **66a** was subjected to solvolysis to yield chiral acid (+)-**3**, while the second-eluted

ester **66b** gave acid (–)-**3**. To confirm the absolute configurations of chiral acids **3** obtained, they were converted to methyl esters, the CD spectra of which were measured. By comparison of those CD spectra with that of the authentic sample with known absolute configuration, which was established by X-ray analysis and chemical correlation (see Figure 15), the absolute configurations of chiral acids **3** were determined as (*S*)-(+)- and (*R*)-(–), respectively. Therefore, the results led to the assignment of (*S*;1*R*,3*R*,4*S*)-(-)-**66a** and (*R*;1*R*,3*R*,4*S*)-(-)-**66b**.<sup>56</sup>



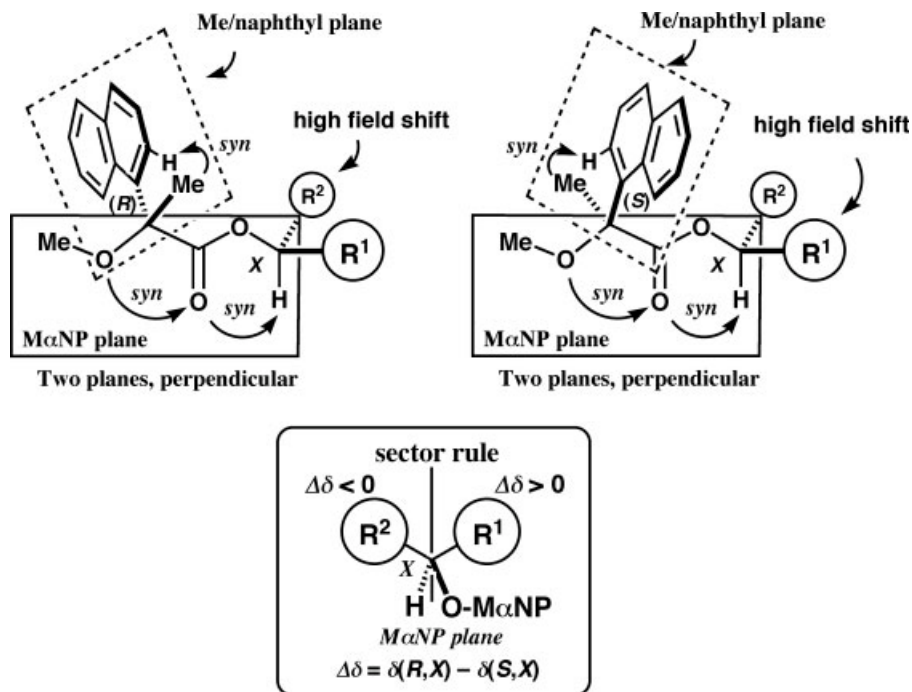


Fig. 21. The preferred conformation of MαNP esters, and the sector rule for determining the absolute configuration of chiral alcohols by the use of  $^1\text{H}$  NMR  $\Delta\delta$  values.<sup>58</sup>

Later we have succeeded in obtaining the single crystals of the second-eluted MαNP ester (–)-**66b**, one of which was subjected to X-ray crystallography. The stereostructure of (–)-**66b** is shown in Figure 19.<sup>22</sup> By reference to the (1*R*,3*R*,4*S*) absolute configuration of menthol moiety, the absolute configuration of acid part was definitely determined to be *R*. The present results are naturally consistent with the previous absolute configurational assignment of MαNP acid (S)-(+)-**3**, carried out by the Bijvoet method. In this case, (1*R*,3*R*,4*S*)-(–)-menthol worked as a CXR.

**The  $^1\text{H}$  NMR anisotropy method for determining the absolute configuration of secondary alcohols: The sector rule and applications.**<sup>52,56</sup> As described above the  $^1\text{H}$  NMR anisotropy method has been frequently used as a relative and empirical method for determining the absolute configurations of chiral organic compounds.<sup>39–50</sup> In the cases of Mosher's MTPA and Trost's MPA acids, the phenyl group exhibits the magnetic anisotropy effect induced by the aromatic ring current, affecting the chemical shift ( $\delta$ ) of protons in the alcohol part. We have found that MαNP acid **3** is superior to Mosher's MTPA and Trost's MPA acids, because the magnetic anisotropy effect of the naphthyl group is much larger than that of a phenyl group and, therefore, larger  $\Delta\delta$  values are obtained. So, the absolute configuration of chiral alcohols can be unambiguously determined, when using MαNP acid **3** as a CAR. Moreover, MαNP acid has another advantage of not racemizing, because the  $\alpha$ -position of **3** is fully substituted. For these reasons, it is advisable to use MαNP acid **3** for determin-

ing the absolute configuration of chiral alcohols including natural and synthetic compounds.

All NMR proton peaks of diastereomeric menthol MαNP esters **66a** and **66b** were fully assigned by various methods including two-dimensional ones ( $^1\text{H}$ ,  $^1\text{H}$ - $^1\text{H}$  COSY,  $^{13}\text{C}$ ,  $^1\text{H}$ - $^{13}\text{C}$  COSY, HMBC, Fig. 20a). The protons of the isopropyl group in ester **66b** appeared at much higher fields than in ester **66a**. On the other hand, the protons in the 2-position in **66a** appeared at higher fields than in ester **66b**. Those high field shifts are obviously due to the diamagnetic anisotropy effect induced by the naphthyl group of the MαNP acid moiety.

To determine the absolute configuration from the  $^1\text{H}$  NMR anisotropy effect, it is required to determine the preferred conformation of each diastereomer. In esters **66a** and **66b**, the absolute configurations of MαNP acid and menthol moieties are established as described above, and so the following stable conformations are proposed to satisfy the anisotropy effects observed in the NMR spectra (Figs. 20 and 21). Namely, MαNP esters adopt the preferred conformations shown in Figure 21, where the terminal methyl group of the propionic acid part is *synperiplanar* to H-2 proton of naphthalene group forming the Me/naphthyl plane as shown with dotted lines. On the other hand, the oxygen atom of the methoxyl group is *synperiplanar* to the ester carbonyl oxygen atom, which is also *synperiplanar* to the methine proton of the alcohol moiety, forming the MαNP plane as shown with solid lines. These two planes are perpendicular to each other because of the tetrahedral configuration of the quaternary stereogenic center.

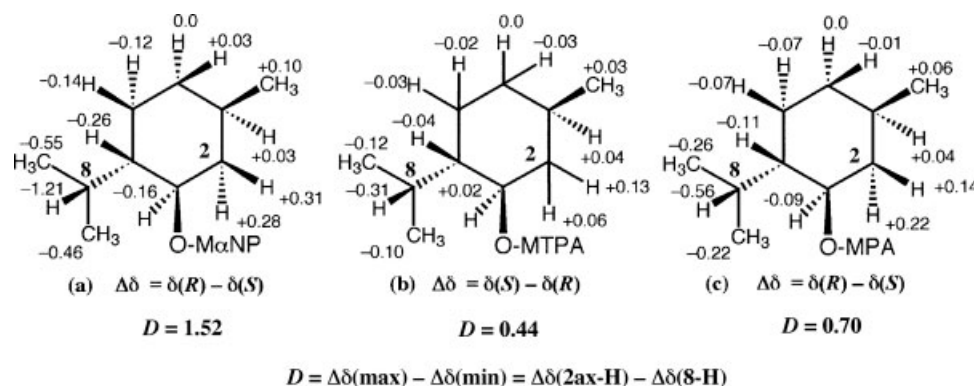


Fig. 22. Comparison of the  $^1\text{H}$  NMR  $\Delta\delta$  (ppm) and  $D$  values (ppm,  $\text{CDCl}_3$ ) of menthol esters formed with chiral carboxylic acids.<sup>52</sup>

In the preferred conformation of ester formed from (*R*)-M $\alpha$ NP acid, the substituent  $\text{R}^2$  is in close proximity to the plane of naphthalene moiety, falling in its field of diamagnetic anisotropy and leading to the high-field shifts of  $\text{R}^2$  protons (see Fig. 21). On the other hand, in the other ester made with (*S*)-M $\alpha$ NP acid, the substituent  $\text{R}^1$  is located above the naphthalene plane, and, therefore, high-field shifts of  $\text{R}^1$  protons are observed.

In menthol ester **66a**, the naphthyl group and H-2 protons are on the same front side of the M $\alpha$ NP plane, and the H-2 protons are located above the naphthyl plane (see Fig. 20). Therefore, the H-2 protons feel the magnetic anisotropy effect of high field shift, and so appear at higher field. In ester **66b**, the naphthyl group is close to the isopropyl group, and the high field shifts of isopropyl protons are observable.

The predominance of the *syn* conformations in esters **66a** and **66b** is also supported by the comparison of the  $^1\text{H}$  NMR data with those of 2-hydroxy-2-(1-naphthyl)propionic acid (H $\alpha$ NP) menthol esters **67a** and **67b** shown in Figure 20b. From the NMR chemical shift and IR data, it is obvious that the tertiary hydroxyl group of H $\alpha$ NP esters is hydrogen-bonded to the oxygen atom of the ester carbonyl group. Namely, the hydroxyl group and the ester carbonyl oxygen atom take a *syn* conformation. We have found a very interesting fact that the  $^1\text{H}$  NMR chemical shift data of M $\alpha$ NP acid menthol ester (*S*;1*R*,3*R*,4*S*)-(-)-**66a**, especially those of the menthol part, are very similar to those of H $\alpha$ NP acid menthol ester (*S*;1*R*,3*R*,4*S*)-(-)-**67a** as shown in Figure 20. The same is true for the pairs of other diastereomers, (*R*;1*R*,3*R*,4*S*)-(-)-**66b** and H $\alpha$ NP

acid menthol ester (*R*;1*R*,3*R*,4*S*)-(-)-**67b** (see Fig. 20). These facts indicate that M $\alpha$ NP acid menthol esters take the *syn* conformation, as H $\alpha$ NP acid menthol esters usually do. This fully explains the observed magnetic anisotropy effects.

By using the NMR anisotropy effect of M $\alpha$ NP esters, the sector rule for determining the absolute configuration of secondary alcohols can be deduced (see Fig. 21). The basic procedure is as follows: (*R*)-M $\alpha$ NP and (*S*)-M $\alpha$ NP acids are separately allowed to react with a chiral alcohol, the unknown absolute configuration of which is defined as *X*. So, the ester prepared from (*R*)-M $\alpha$ NP acid has the (*R,X*) absolute configuration, while the other ester prepared from (*S*)-M $\alpha$ NP acid has the (*S,X*) absolute configuration. All  $^1\text{H}$  NMR proton signals of (*R,X*)- and (*S,X*)-esters are fully assigned by careful analyses. If necessary, the use of two-dimensional spectra is suggested. The  $\Delta\delta$  values ( $\Delta\delta = \delta(\text{R},X) - \delta(\text{S},X)$ ) are calculated for all protons in the alcohol moiety. Figure 21 shows the sector rule for the M $\alpha$ NP ester, where the M $\alpha$ NP group is placed in the down and front side, while the methine proton of the secondary alcohol is in the down and rear side. The group  $\text{R}^1$  with protons exhibiting positive  $\Delta\delta$  values is placed at the right side, while the group  $\text{R}^2$  with protons showing negative  $\Delta\delta$  values on the left side. From this projection, the absolute configuration *X* of chiral alcohol can be determined.

The magnetic anisotropy effect of chiral M $\alpha$ NP acid is much stronger than those of conventional chiral carboxylic acids as shown in Figure 22. We have introduced a new parameter  $D$  representing the strength of the anisotropy

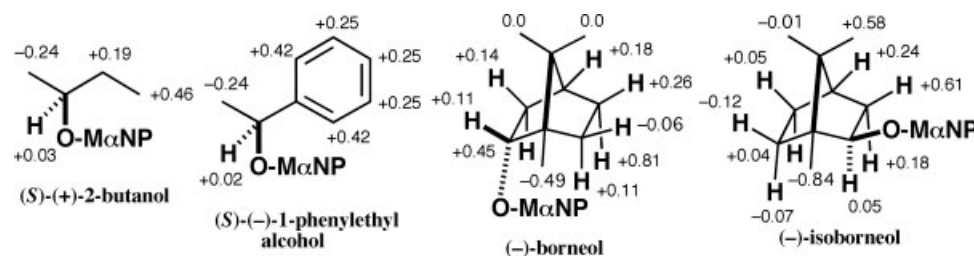


Fig. 23. The  $^1\text{H}$  NMR  $\Delta\delta$  values (ppm,  $\text{CDCl}_3$ ) and absolute configurations determined by the M $\alpha$ NP acid method.<sup>52</sup>

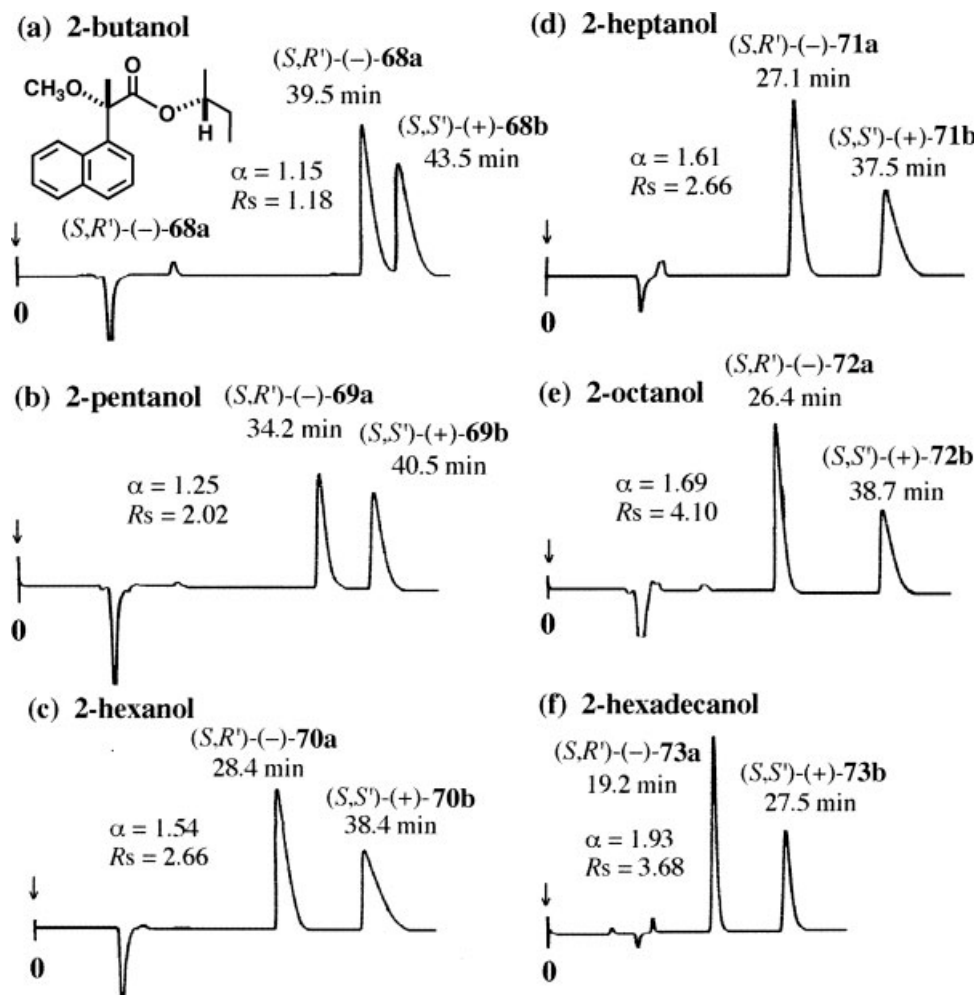


Fig. 24. HPLC separation of diastereomeric esters formed from aliphatic alcohols and (S)-(+)-M $\alpha$ NP acid **3** (silica gel, 220  $\times$  300 mm, hexane/EtOAc = 20:1).<sup>53</sup>

effect, which is defined as  $D = \Delta\delta(\text{max}) - \Delta\delta(\text{min})$ , where  $\Delta\delta(\text{max})$  indicates the maximum value of  $\Delta\delta$  in the alcohol moiety, while  $\Delta\delta(\text{min})$  indicates the minimum value of  $\Delta\delta$  (negative largest one). In the case of menthol esters,  $\Delta\delta(\text{max})$  was determined by the shift of the proton at the 2ax-position, H-2ax, and  $\Delta\delta(\text{min})$  determined by the H-8 proton. Therefore  $D = \Delta\delta(\text{max}) - \Delta\delta(\text{min}) = \Delta\delta(\text{H-2ax}) - \Delta\delta(\text{H-8})$ ; this definition was used for other menthol esters. In the case of menthol M $\alpha$ NP acid esters **66a**/**66b**,  $D = +0.31 - (-1.21) = 1.52$  (ppm); for menthol MTPA esters,  $D = 0.44$  (ppm); for menthol MPA esters,  $D = 0.70$  (ppm). The  $\Delta\delta$  values of the M $\alpha$ NP-menthol ester are approximately four times larger than those of Mosher's MTPA esters (Fig. 22b): twice for Trost's MPA esters (Fig. 22c); comparable to 1-NMA and 2-NMA esters reported by Riguera et al. and Kusumi et al. M $\alpha$ NP acid is thus effective for determining the absolute configurations of chiral secondary alcohols.

Some application examples of this M $\alpha$ NP acid method to chiral alcohols are shown in Figure 23.

**Enantioresolution of various alcohols using M $\alpha$ NP acid and simultaneous determination of their absolute configurations.**<sup>53,56</sup> Another extraordinary quality of M $\alpha$ NP acid is its excellent ability in chiral recognition. For example as discussed earlier, racemic M $\alpha$ NP acid could be successfully enantioresolved as the esters of natural (-)-menthol; the diastereomeric esters formed were largely separated by HPLC on silica gel. M $\alpha$ NP acid could be also enantioresolved with other chiral alcohols. These facts logically indicate that if enantiopure M $\alpha$ NP acid is used, racemic alcohols can be enantioresolved. In fact, we have succeeded in the enantioresolution of various alcohols using enantiopure M $\alpha$ NP acid (S)-(+)-**3** as exemplified in Figure 24.

Chiral M $\alpha$ NP acid (S)-(+)-**3** has thus a remarkable enantioresolving power for alcohols, especially for aliphatic alcohols. For instance, in the case of 2-butanol, the diastereomeric esters **68a**/**68b** can be baseline separated with the separation factor  $\alpha = 1.15$  and resolution factor  $R_s = 1.18$  (see Fig. 24). In this case, it is obvious that the

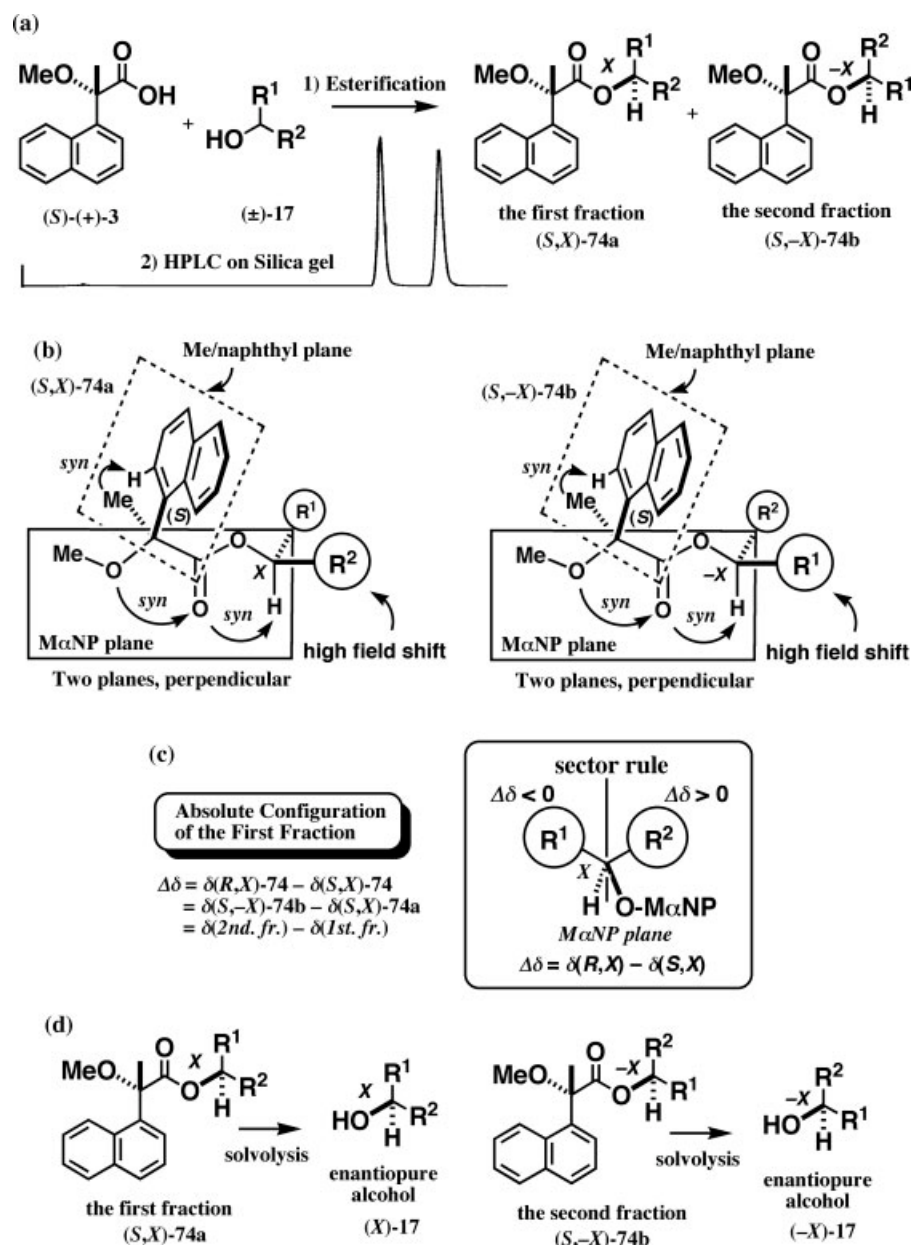


Fig. 25. Enantioresolution of racemic alcohol as (S)-M $\alpha$ NP esters, and determination of the absolute configuration of the first-eluted fraction by the  $^1\text{H}$  NMR anisotropy method.<sup>52,53,56</sup>

chiral carboxylic acid **3** recognizes well the slight difference between methyl and ethyl groups.

Diastereomeric M $\alpha$ NP esters (**69a/69b–73a/73b**) of higher 2-alkanols were more easily separated by HPLC on silica gel, where the separation factor  $\alpha$  ranges from 1.25 to 1.93. This is an excellent practical method for preparing enantiopure aliphatic alcohols, because chiral acid (S)-(+)-**3** exhibits a high resolving power for aliphatic alcohols, to which, in general, asymmetric syntheses are hardly applicable.

The next question is then how the absolute configuration of the alcohol moiety is determined. The absolute configurations of separated diastereomers can be determined

Chirality DOI 10.1002/chir

by applying the  $^1\text{H}$  NMR anisotropy method using chiral M $\alpha$ NP acid described above. A general scheme is illustrated in Figure 25, where racemic alcohol ( $\pm$ )-**17** is esterified with M $\alpha$ NP acid (S)-(+)-**3** yielding a mixture of diastereomeric esters **74a/74b**, which is separated by HPLC on silica gel. The absolute configuration of the first-eluted ester **74a** is defined as (S,X), where S denotes the absolute configuration of the M $\alpha$ NP acid part, while X denotes that of the alcohol part. So, the absolute configuration of the second-eluted ester **74b** is expressed as (S,-X), where -X indicates the opposite absolute configuration of X. As described above, the original definition of  $\Delta\delta$  value is  $\Delta\delta = \delta(R,X) - \delta(S,X)$ , and so the value of



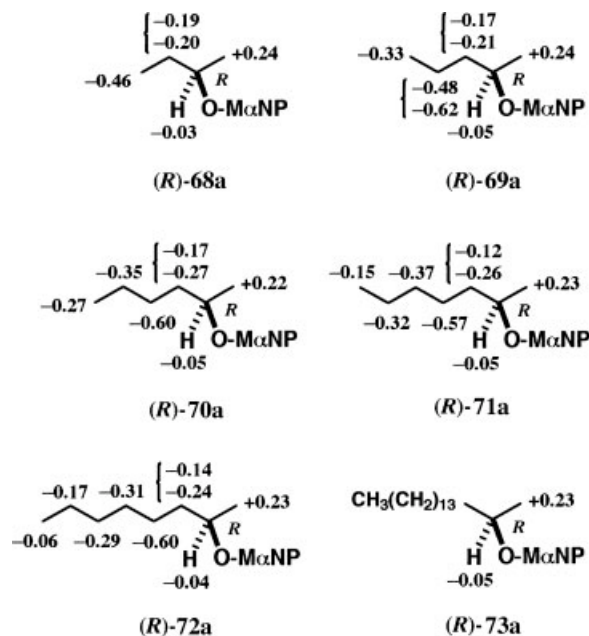


Fig. 26. Determination of the absolute configurations of first-eluted esters shown in Figure 24 by the  $^1\text{H}$  NMR anisotropy method using (S)-(+)-M $\alpha$ NP acid **3** and the observed  $\Delta\delta$  values (ppm,  $\text{CDCl}_3$ ).<sup>53</sup>

$\delta(R,X)$  is required to calculate  $\Delta\delta$  value. However, the enantiomer ( $R,X$ ) does not exist in this scheme, and so the original equation of  $\Delta\delta$  is not useful here.

To solve the above problem, the following conversion of the equation was performed. Since the ester ( $S,-X$ ) is the enantiomer of ester ( $R,X$ ), their NMR data should be identical:  $\delta(R,X) = \delta(S,-X)$ . Therefore,  $\Delta\delta = \delta(R,X) - \delta(S,X) = \delta(S,-X) - \delta(S,X) = \delta(2\text{nd fr.}) - \delta(1\text{st fr.})$ , when M $\alpha$ NP acid (S)-(+)-**3** is used. The absolute configuration  $X$  of the first-eluted fraction can be thus determined from the  $\Delta\delta$  value, which is obtained by subtracting the chemical shift of the first-eluted fraction from that of the second-eluted fraction (see Fig. 25). This method has been applied to the esters shown in Figure 24, giving  $\Delta\delta$  values and the absolute configurations of the first-eluted esters (see Fig. 26). The  $\Delta\delta$  values are reasonably distributed: positive values at the right, and negative value at the left. The absolute configuration of the first-eluted ester can be thus determined, and the opposite absolute configuration is, of course, assigned to the second-eluted ester. It should be noted that when M $\alpha$ NP acid ( $R$ )-(–)-**3** is used, the  $\Delta\delta$  value is defined as  $\Delta\delta = \delta(R,X) - \delta(S,X) = \delta(R,X) - \delta(R,-X) = \delta(1\text{st fr.}) - \delta(2\text{nd fr.})$ , see last subsection.

The next step is the recovery of enantiopure alcohol and chiral M $\alpha$ NP acid **3**. As exemplified in Figure 27, enantiopure alcohol was readily obtained by the solvolysis of the separated ester.<sup>56,60</sup> The chiral M $\alpha$ NP acid **3** was also recovered and could be recycled.

How good is the enantiopurity of the recovered alcohols? In our method, both diastereomeric esters obtained are enantiopure, if M $\alpha$ NP acid **3** used is enantiopure, because they are fully separated in HPLC. The M $\alpha$ NP acid **3** was enantioresolved with natural (–)-

menthol, the enantiopurity of which was confirmed as 100% by gas chromatography using chiral stationary phase.<sup>56</sup>

As described here, M $\alpha$ NP acid has excellent enantioresolving power despite its simple molecular structure and the absence of so-called heteroatoms. Besides, the chiral acid **3** has larger magnetic anisotropy effects than Mosher's MTPA and Trost's MPA acids.

**Recent applications of the M $\alpha$ NP acid method to various alcohols**<sup>53,56,57,74,88</sup>. The M $\alpha$ NP acid method has been successfully applied to various racemic alcohols listed in Table 3 for preparation of enantiopure secondary alcohols and simultaneous determination of their absolute configurations. If the separation factor  $\alpha$  is as large as in the case of 1-octyn-3-ol **76** (entry 2 in Table 3,  $\alpha = 1.88$ ), a large-scale HPLC separation of diastereomeric M $\alpha$ NP esters is feasible. For example, in the case of esters **91a** and **91b** derived from alcohol **76**, 0.85–1.0 g of the mixture was separable in one run by the HPLC (hexane/EtOAc = 20:1) using a silica gel glass column (220  $\times$  300 mm) (Figs. 28 and 29).

The HPLC separation data of diastereomeric esters prepared from other racemic alcohols **77–90** with M $\alpha$ NP acid (S)-(+)-**3** are listed in Table 3. It should be emphasized that in the cases of most alcohols, their diastereomeric M $\alpha$ NP esters are clearly separated with  $\alpha$  values of 1.08–1.93. Phenylacetylene alcohol **77** was separable as M $\alpha$ NP esters **92a/92b** ( $\alpha = 1.30$ , entry 3). Substituted cyclohexanols **78** and **79** were also effectively separated as M $\alpha$ NP esters (entries 4 and 5). Significantly, the  $\alpha$  value of *trans*-2-isopropylcyclohexanol M $\alpha$ NP esters **93a/93b** is as large as 1.88, which is comparable to that of the menthol case. On the other hand, in the case of *trans*-2-methylcyclohexanol M $\alpha$ NP esters **94a/94b**, the  $\alpha$  value is relatively small,  $\alpha = 1.21$ . These results indicate that the combination of a longer and larger alkyl group on one side and a smaller alkyl group on the other side leads to better separation of the two diastereomers, as seen for 2-hexadecanol esters **73a/73b** (entry 1, Fig. 24) and *trans*-2-isopropylcyclohexanol M $\alpha$ NP esters **93a/93b**.

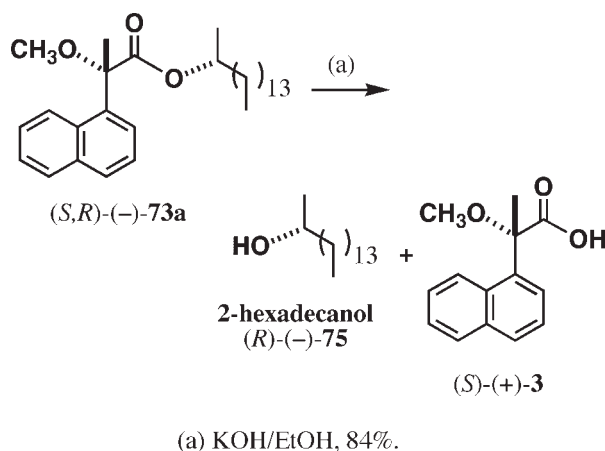
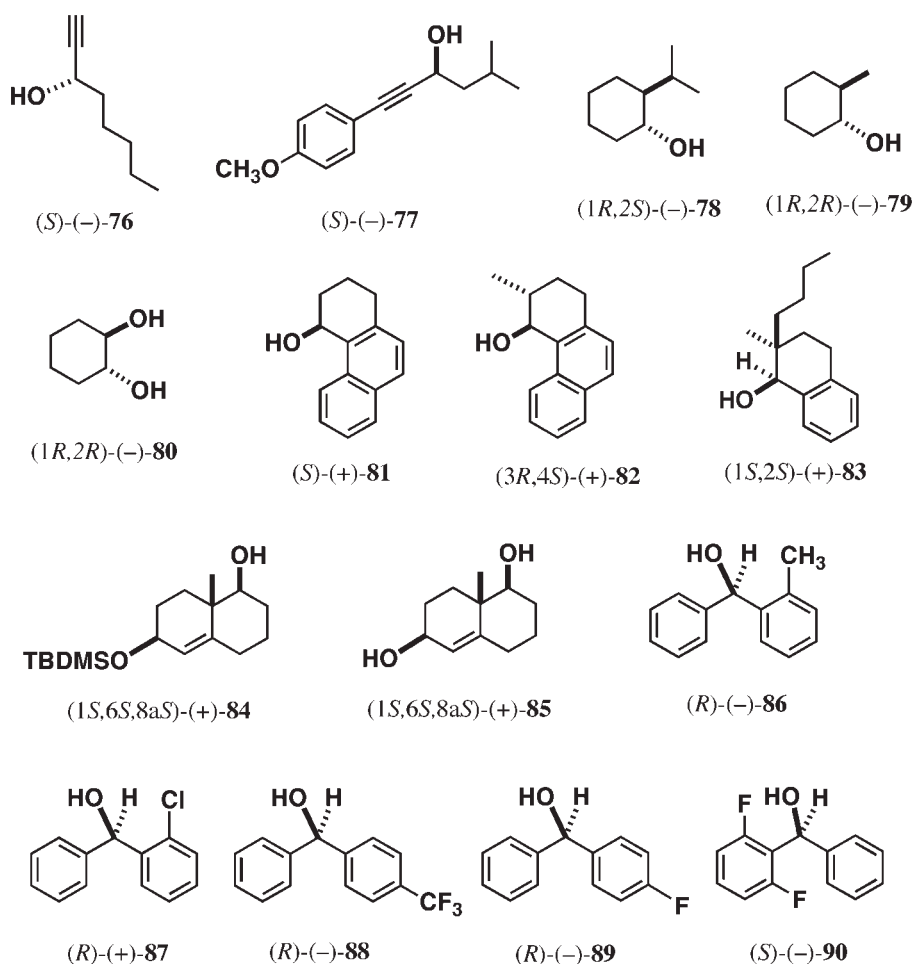


Fig. 27. Recovery of enantiopure alcohol and M $\alpha$ NP acid.

**TABLE 3.** HPLC<sup>a</sup> separation of diastereomeric esters formed from alcohols with M $\alpha$ NP acid (*S*)-(+)-3, determination of their absolute configurations by the <sup>1</sup>H NMR anisotropy method, and absolute configurations of recovered chiral alcohols



Entry	Alcohol	Solvent <sup>b</sup>	$\alpha^c$	$R_s^d$	Ester (1st Fr.)	Chiral Alcohol (from 1st Fr.)	Ref.
1	( $\pm$ )- <b>75</b>	H/EA = 20/1	1.93	3.68	( <i>S</i> ; <i>R</i> )-(-)- <b>73a</b>	( <i>R</i> )-(-)- <b>75</b>	53, 56
2	( $\pm$ )- <b>76</b>	H/EA = 20/1	1.88	4.67	( <i>S</i> ; <i>S</i> )-(-)- <b>91a</b>	( <i>S</i> )-(-)- <b>76</b>	53, 56
3	( $\pm$ )- <b>77</b>	H/EA = 10/1	1.30	2.38	( <i>S</i> ; <i>S</i> )-(-)- <b>92a</b>	( <i>S</i> )-(-)- <b>77</b>	56
4	( $\pm$ )- <b>78</b>	H/EA = 20/1	1.88	4.97	( <i>S</i> ;1 <i>R</i> ,2 <i>S</i> )-(-)- <b>93a</b>	(1 <i>R</i> ,2 <i>S</i> )-(-)- <b>78</b>	56
5	( $\pm$ )- <b>79</b>	H/EA = 20/1	1.21	1.54	( <i>S</i> ;1 <i>R</i> ,2 <i>R</i> )-(-)- <b>94a</b>	(1 <i>R</i> ,2 <i>R</i> )-(-)- <b>79</b>	56
6	( $\pm$ )- <b>80</b>	H/EA = 2/1	1.35	1.82	( <i>S</i> ;1 <i>R</i> ,2 <i>R</i> )-(-)- <b>95a</b> <sup>e</sup>	(1 <i>R</i> ,2 <i>R</i> )-(-)- <b>80</b>	56
7	( $\pm$ )- <b>81</b>	H/EA = 10/1	1.22	1.54	( <i>S</i> ; <i>S</i> )-(+)- <b>96a</b>	( <i>S</i> )-(+)- <b>81</b>	56
8	( $\pm$ )- <b>82</b>	H/EA = 15/1	1.46	2.77	( <i>S</i> ;3 <i>R</i> ,4 <i>S</i> )-(+)- <b>97a</b>	(3 <i>R</i> ,4 <i>S</i> )-(+)- <b>82</b>	56
9	( $\pm$ )- <b>83</b>	H/EA = 15/1	1.81	5.97	( <i>S</i> ;1 <i>S</i> ,2 <i>S</i> )-(-)- <b>98a</b>	(1 <i>S</i> ,2 <i>S</i> )-(+)- <b>83</b>	88
10	( $\pm$ )- <b>84</b>	H/EA = 10/1	1.80	1.30	( <i>S</i> ;1 <i>R</i> ,6 <i>R</i> ,8 <i>aR</i> )-(-)- <b>99a</b>	(1 <i>R</i> ,6 <i>R</i> ,8 <i>aR</i> )-(-)- <b>84</b>	57
11	( $\pm$ )- <b>85</b>	H/EA = 1/1	1.27	1.83	( <i>S</i> ;1 <i>S</i> ,6 <i>S</i> ,8 <i>aS</i> )-(+)- <b>100a</b>	(1 <i>S</i> ,6 <i>S</i> ,8 <i>aS</i> )-(+)- <b>85</b>	57
12	( $\pm$ )- <b>86</b>	H/EA = 15/1	1.12	1.45	( <i>S</i> ; <i>R</i> )-(-)- <b>101a</b>	( <i>R</i> )-(-)- <b>86</b>	56
13	( $\pm$ )- <b>87</b>	H/EA = 15/1	1.10	1.40	( <i>S</i> ; <i>R</i> )-(-)- <b>102a</b>	( <i>R</i> )-(+)- <b>87</b>	56
14	( $\pm$ )- <b>88</b>	H/EA = 8/1	1.39	4.84	( <i>S</i> ; <i>R</i> )-(-)- <b>103a</b>	( <i>R</i> )-(-)- <b>88</b>	74
15	( $\pm$ )- <b>89</b>	H/EA = 10/1	1.18	2.55	( <i>S</i> ; <i>R</i> )-(-)- <b>104a</b>	( <i>R</i> )-(-)- <b>89</b>	74
16	( $\pm$ )- <b>90</b>	H/EA = 8/1	1.08	1.28	( <i>S</i> ; <i>S</i> )-(-)- <b>105a</b>	( <i>S</i> )-(-)- <b>90</b>	74

<sup>a</sup>Glass column (220  $\times$  300 mm, or 250  $\times$  400 mm) of silica gel (particle size 5–10  $\mu$ m).

<sup>b</sup>H = *n*-hexane, EA = ethyl acetate.

<sup>c</sup>Separation factor  $\alpha = (t_2 - t_0)/(t_1 - t_0)$  where  $t_1$  and  $t_2$  are the retention times of the first- and second-eluted fractions, respectively, and  $t_0$  is the retention time of an unretained compound (void volume marker).

<sup>d</sup>Resolution factor  $R_s = 2(t_2 - t_1)/(W_1 + W_2)$  where  $W_1$  and  $W_2$  are the band-widths of the first- and second-eluted fractions at the base-line level, respectively.

<sup>e</sup>Mono-M $\alpha$ NP ester.

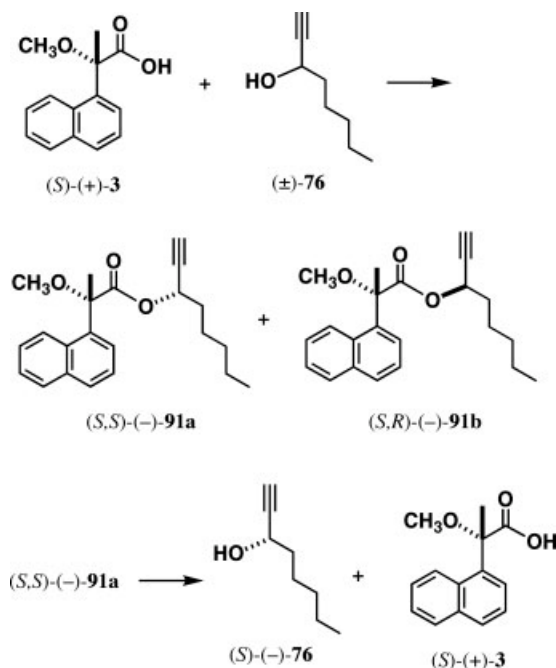


Fig. 28. Preparation of enantiopure 1-octyn-3-ol  $(S)\text{-}(-)\text{-}76$ .<sup>56</sup>

Entry 6 is an interesting case, where mono-M $\alpha$ NP esters **95a/95b** of *trans*-1,2-cyclohexanediol **80** were sufficiently separated, despite the existence of a polar hydroxyl group ( $\alpha = 1.35$ ). In the case of cyclic naphthalene alcohols **81** and **82**, their M $\alpha$ NP esters were separated well, but the values depend on the neighboring substituent. Namely, the M $\alpha$ NP esters **97a/97b** of *trans*-alcohol **82** were more efficiently separated ( $\alpha = 1.46$ ) than those of unsubstituted alcohol **81** (esters **96a/96b**,  $\alpha = 1.22$ ) (entries 7 and 8).

Tetralol derivative **83** was similarly enantioresolved by this method as M $\alpha$ NP esters **98a/98b**, which were separated well by HPLC on silica gel ( $\alpha = 1.81$ ) (entry 9). The absolute configuration of the first-eluted ester  $(-)\text{-}98a$  was determined to be  $(S;1S,2S)$  by  $^1\text{H}$  NMR and X-ray methods. Ester  $(-)\text{-}98a$  was used as a key compound for

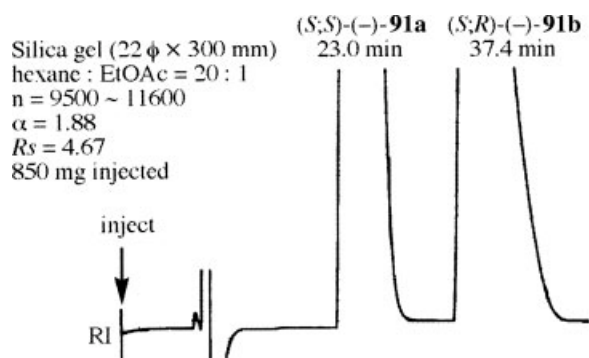


Fig. 29. A large-scale HPLC separation of diastereomeric esters  $(S,S)\text{-}(-)\text{-}91a$  and  $(S,R)\text{-}(-)\text{-}91b$ .<sup>56</sup>

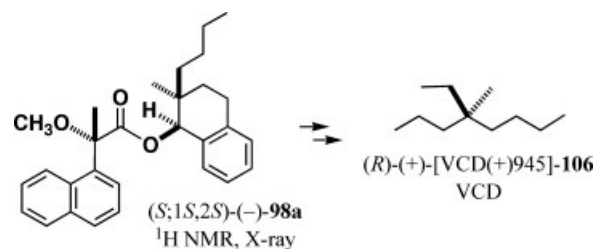


Fig. 30. Synthesis of  $(R)\text{-}(+)\text{-}[\text{VCD}(+945)]\text{-}4\text{-ethyl-4-methyloctane}$  **106**.

the synthesis of  $(R)\text{-}(+)\text{-}[\text{VCD}(+945)]\text{-}4\text{-ethyl-4-methyloctane}$  **106**, the simplest chiral saturated hydrocarbon with a quaternary stereogenic center (see Fig. 30). Namely, alcohol  $(1S,2S)\text{-}(+)\text{-}83$  recovered from ester  $(-)\text{-}98a$  was converted to enantiopure hydrocarbon  $(R)\text{-}(+)\text{-}106$ . This is the first synthesis of enantiopure hydrocarbon **106** and the first determination of its absolute configuration.<sup>88</sup> The absolute configuration of  $(+)\text{-}[\text{VCD}(+945)]\text{-}106$ , which shows a positive VCD band at  $945\text{ cm}^{-1}$ , was also determined to be  $R$  by the ab initio calculation of VCD.<sup>88</sup>

Chiral Wieland–Miescher ketone (W–M ketone,  $(8aS)\text{-}(+)\text{-}107$ ) has a long history as a key synthon useful for the total syntheses of various chiral natural products (see Fig. 31).<sup>57</sup> To prepare W–M ketone **107** of high enantiopurity, many efforts have been devoted to develop efficient preparation methods. However, it was still difficult to obtain enantiopure W–M ketone **107** in an efficient way. So, we have applied the M $\alpha$ NP acid method to enantioresolve W–M ketone derivatives and also to determine their absolute configurations by the  $^1\text{H}$  NMR anisotropy method. We have found a very interesting phenomenon that M $\alpha$ NP acid esters of alcohols with less polar and more bulky substituents were more effectively separated by HPLC on silica gel. Namely, M $\alpha$ NP esters **99a/99b** of *tert*-butyldimethylsilyl (TBDMS) ether–alcohol **84** were excellently separated by HPLC on silica gel with a large  $\alpha$  value ( $\alpha = 1.80$ , entry 10), while mono M $\alpha$ NP esters **100a/100b** at the position 1 of diol **85** were less effectively separated ( $\alpha = 1.27$ , entry 11). This substituent effect found for the HPLC separation would be very useful for future applications of the M $\alpha$ NP acid method. By this

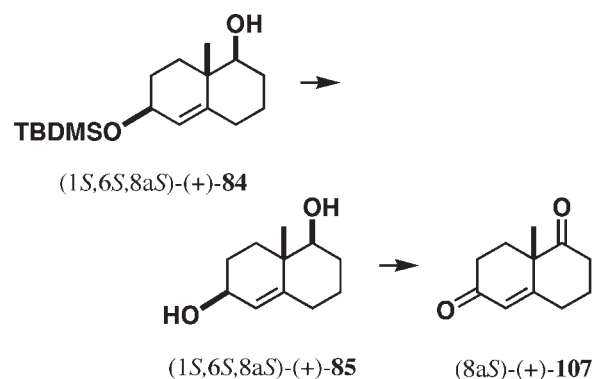


Fig. 31. Preparation of enantiopure W–M ketone by the M $\alpha$ NP acid method.

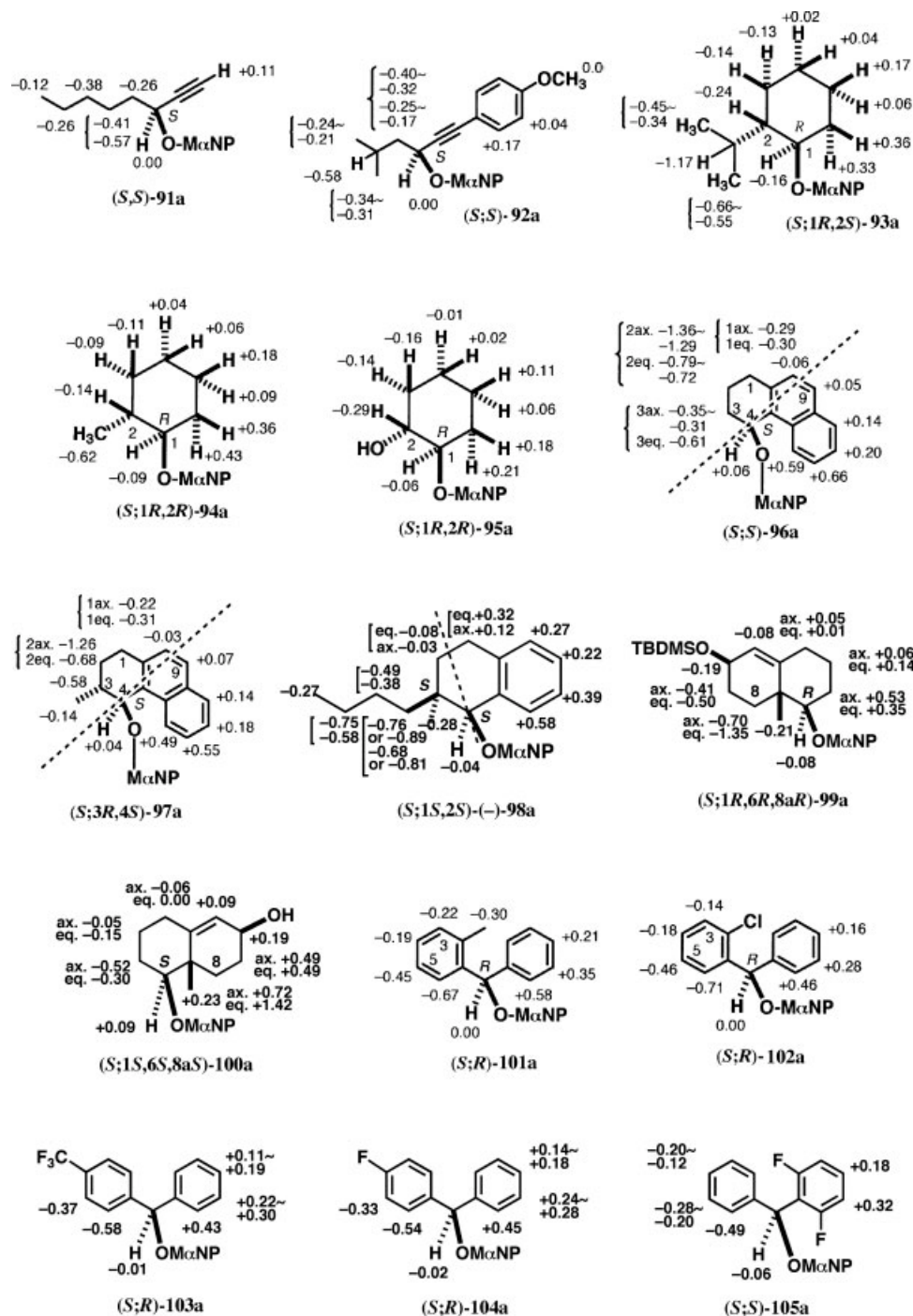


Fig. 32. Determination of absolute configurations by the  $^1\text{H}$  NMR anisotropy method using (*S*)-(+)-M $\alpha$ NP acid 3: observed  $\Delta\delta$  values (ppm,  $\text{CDCl}_3$ ) and the absolute configuration of the first-eluted esters.<sup>56,57,74,88</sup>

method, we have provided another route for the preparation of enantiopure W-M ketone (see Fig. 31).

The enantioresolution of *ortho*-substituted diphenylmethanols **86** and **87** was one of the most difficult cases. We had previously applied the CSDP acid method to these alcohols as described above.<sup>69,70</sup> However, the diastereomeric CSDP esters of **86** appeared as a single peak in Chirality DOI 10.1002/chir

HPLC, indicating no separation at all. However, the M $\alpha$ NP esters **101a**/**101b** of alcohol **86** were baseline separated ( $\alpha = 1.12$ , entry 12). In a similar way, alcohol **87** was also enantioresolved as M $\alpha$ NP esters **102a**/**102b** ( $\alpha = 1.10$ , entry 13).

The M $\alpha$ NP acid method was also applied to racemic fluorinated diphenylmethanols **88**, **89**, and **90** (Table 3). A



diastereomeric mixture of esters **103a/103b** prepared from (4-trifluoromethylphenyl)phenylmethanol **88** was separated well by HPLC on silica gel:  $\alpha = 1.39$ ;  $R_s = 4.84$  (entry 14). Other fluorinated diphenylmethanols were similarly esterified with (*S*)-(+)-**3**, and the diastereomeric mixtures obtained were subjected to HPLC on silica gel. Diastereomeric M $\alpha$ NP esters of (4-fluorophenyl)phenylmethanol **89** were separated well with  $\alpha$ -values of 1.18 (entry 15). On the other hand, the separation of diastereomeric M $\alpha$ NP esters of (2,6-difluorophenyl)phenylmethanol **90** took more time and effort, because of its smaller  $\alpha$ -value:  $\alpha = 1.08$  (entry 16).

By applying the  $^1\text{H}$  NMR anisotropy method, the absolute configurations of the first-eluted M $\alpha$ NP esters **91a–105a** were determined as illustrated in Figure 32. The observed  $\Delta\delta$  values (ppm) are distributed in a reasonable manner; protons near the M $\alpha$ NP group show larger  $\Delta\delta$  values than do remote ones, and the protons at the right side show positive  $\Delta\delta$  values, while ones at the left side show negative  $\Delta\delta$  values. In the 1-octyn-3-ol M $\alpha$ NP esters **91a/91b**, the acetylene proton showing positive  $\Delta\delta$  value (+0.11) is placed on the right side, while the pentyl group having negative  $\Delta\delta$  values is on the left side. So, the absolute configuration of (–)-**91a** was assigned to be *S*. In the phenyl acetylene alcohol esters **92a/92b**, the phenyl protons show clearly positive  $\Delta\delta$  values, despite the long distance from the M $\alpha$ NP group, while the *iso*-butyl group shows large negative  $\Delta\delta$  values. Therefore, the *S* absolute configuration was assigned to (–)-**92a**.

In the cyclic alcohol esters **93a/93b** and **94a/94b**, the observed  $\Delta\delta$  values are similar at the corresponding positions, leading to the (1*R*,2*S*)-absolute configuration of (–)-**93a** and the (1*R*,2*R*)-absolute configuration of (–)-**94a**. The case of vicinal diol mono-M $\alpha$ NP esters **95a/95b** is a unique example; there was some concern that the conformation of the M $\alpha$ NP group might be deviated from the ideal *syn*-conformation by the effect of the adjacent polar hydroxyl group. However, the distribution pattern of observed  $\Delta\delta$  values is similar to that of esters **94a/94b**, although their absolute values are different. So, the (1*R*,2*R*) absolute configuration was assigned to (–)-**95a**.

The naphthalene–cyclic alcohol esters **96a/96b** are also interesting cases; the naphthalene moiety contained in the alcohol skeleton also works as a strong  $^1\text{H}$  NMR anisotropy-inducing group. Therefore, it was considered that the  $^1\text{H}$  NMR anisotropy effect of M $\alpha$ NP esters **96a/96b** might become confusing because of the two naphthalene groups. However,  $\Delta\delta$  values observed are reasonably distributed even in the naphthalene region. Furthermore it should be emphasized that the 2-axial proton exhibits a very large negative  $\Delta\delta$  value (–1.36 to –1.29) as shown in Figure 32. This phenomenon is interpreted as follows; the M $\alpha$ NP ester group takes an axial orientation in both **96a** and **96b** because of the *peri*-position of the naphthalene group, and, therefore, in the *syn*-conformation of **96b**, the 2-axial proton is located just below the naphthalene ring of the M $\alpha$ NP moiety, falling in the area of high field shift. From the observed  $\Delta\delta$  data, the *S* absolute configuration was unambiguously assigned to the first-eluted ester (+)-**96a**.

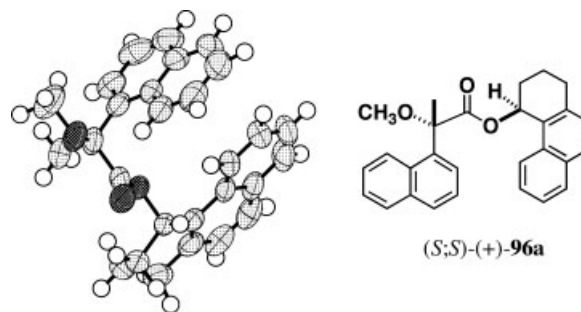


Fig. 33. Crystalline state conformation of M $\alpha$ NP ester (*S,S*)-(+)-**96a**, where methoxyl oxygen and ester carbonyl oxygen atoms are in the syn-periplanar (*syn*) relation.<sup>21</sup>

It should be also noted that the boundary line of  $\Delta\delta$  values is tilted to the right side as indicated by the dotted line in **96a** (see Fig. 32). Namely, the M $\alpha$ NP plane dividing the space into two sectors of  $\Delta\delta$  is moved from the regular position of the C4–C1 line to that of C4–C10. This phenomenon implies that the M $\alpha$ NP ester moiety declines toward the aliphatic side of C-3, not toward the aromatic side of C-4a, because of steric hindrance. This conformation was in fact proved by the X-ray crystallographic analysis of ester **96a**, which indicated that the ester plane was tilted from the alcohol methine proton plane by  $41.7^\circ$  to the methylene side at the C-3 position (see Fig. 33).<sup>21</sup> The absolute configuration (+)-**96a** determined here by the  $^1\text{H}$  NMR anisotropy method was established by X-ray analysis. The  $\Delta\delta$  data of *trans*-methyl alcohol esters **97a/97b** are similar to those of esters **96a/96b** except that of the methyl group, leading to the (3*R*,4*S*) absolute configuration of (+)-**97a**.

In the case of esters **98a/98b**, the boundary line of  $\Delta\delta$  values is tilted to the left side (see Fig. 32), which implies that the M $\alpha$ NP ester moiety declines toward the aromatic side, because of steric hindrance of a quaternary carbon at the C-2 position. Despite such a phenomenon, the absolute configuration of the first-eluted ester (–)-**98a** was clearly determined to be (1*S*,2*S*).

The  $^1\text{H}$  NMR anisotropy method has been similarly applied to the W–M ketone derivatives **99a/99b** and **100a/100b**. It should be noted that the 8-equatorial proton of **99a/99b** exhibits an extremely large anisotropy effect,  $\Delta\delta = -1.35$  (see Fig. 32). This phenomenon indicates that in the preferred conformation of **99b**, the 8-equatorial proton is located above the naphthalene plane, falling in the section of high-field shift and therefore appearing at  $\delta = 0.07$  ppm. On the other hand, in ester **99a**, the 8-equatorial proton appears at  $\delta = 1.42$  ppm, because it is remote from the naphthalene plane. The anomalously large anisotropy effect of the 8-equatorial proton is thus explicable by the preferred conformation of M $\alpha$ NP esters. From the projection with  $\Delta\delta$  values, the absolute configuration of ester (–)-**99a** was determined to be (*S*;1*R*,6*R*,8*aR*).

The anomalously large anisotropy effect of the 8-equatorial proton is also observed in esters **100a/100b** (see Fig. 32), indicating that the preferred conformations of

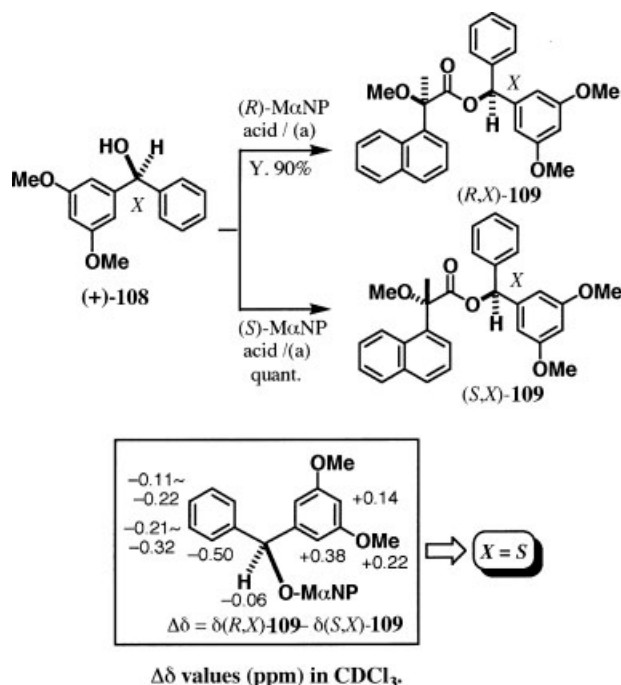


Fig. 34. The *S* absolute configuration of alcohol (+)-108 as determined by the  $^1\text{H}$  NMR anisotropy method using MαNP acid: (a) DCC, DMAP, CSA/ $\text{CH}_2\text{Cl}_2$ , r.t.<sup>75</sup>

esters **100a/100b** are similar to those of **99a/99b**. The distribution pattern of  $\Delta\delta$  values led to the (S;1*S*,6*S*,8*aS*) absolute configuration of ester (+)-**100a**. It should be noted that the absolute configuration of ester (+)-**100a** is opposite to that of ester (-)-**99a**. Namely, the elution order in HPLC is reversed, when the less polar group, OTBDMS, is converted to a polar free hydroxyl group. This is a pertinent example showing that the absolute configuration cannot be determined by the elution order of HPLC.

In the case of (2-methylphenyl)phenylmethanol MαNP esters **101a/101b**, it was easy to assign the proton signals of two phenyl groups, leading to the *R* absolute configuration of (-)-**101a**, which was corroborated by X-ray crystallography. In the 2-methylphenyl group on the left side, the  $\Delta\delta$  value of the H-5 proton (-0.45) is larger than that of the H-3 proton (-0.22), indicating that esters **101a/101b** take a preferred conformation where the H-5 proton is more shielded by the naphthyl group than the H-3 proton. A similar phenomenon was also observed in esters **102a/102b**; the  $\Delta\delta$  value of the H-5 proton (-0.46) is larger than that of the H-3 proton (-0.14). The absolute configuration of **102a** was unambiguously determined as *R*.

In the similar way, the absolute configurations of fluorinated diphenylmethanol MαNP esters **103a–105a** were assigned as shown in Figure 32. In the case of **103a** and **104a**, the phenyl groups have large positive  $\Delta\delta$  values (+0.11 to +0.45 ppm), while the fluorinated phenyl groups show large negative  $\Delta\delta$  values (-0.58 to -0.33 ppm), and therefore *R* absolute configurations were assigned to the

first-eluted esters. On the other hand, in the case of (2,6-difluorophenyl)phenylmethanol **90**, the first-eluted MαNP ester **105a** takes *S* absolute configuration (see Fig. 32). The observed  $\Delta\delta$  values distribute with regularity; *ortho*-protons have the largest  $\Delta\delta$  values (0.49–0.58 ppm), *meta*-protons middle  $\Delta\delta$  values (0.20–0.37 ppm), and *para*-protons smallest  $\Delta\delta$  values (0.11–0.20 ppm). These data indicate that the absolute configurational assignments performed by the  $^1\text{H}$  NMR anisotropy method using MαNP acid are reliable. In the case of alcohols **88** and **90**, the absolute configurations determined by the MαNP acid method agreed with those by X-ray crystallography.

Enantiopure alcohols were recovered from the corresponding diastereomeric MαNP esters: (i) by hydrolysis with KOH in EtOH, or (ii) by solvolysis with  $\text{NaOCH}_3$  in MeOH followed by treatment with water, or (iii) by reduction with  $\text{LiAlH}_4$ , or (iv) by hydrolysis with  $\text{K}_2\text{CO}_3$  in MeOH (Table 3). The MαNP acid method is thus very useful for the preparation of enantiopure alcohols and also for simultaneous determination of their absolute configurations by the  $^1\text{H}$  NMR anisotropy method.

**Absolute configurations of chiral meta-substituted diphenylmethanol and the thyroid hormone analogue KAT-2003 as determined by the  $^1\text{H}$  NMR anisotropy method with MαNP acid.** If the purpose is only to determine the absolute configuration of chiral alcohols, the MαNP acid method is applicable as follows. For example, alcohol (+)-**108** was esterified with (R)-(-)-MαNP acids **3**, yielding ester (R,X)-**109**, where X denotes the absolute configuration of alcohol moiety (see Fig. 34).<sup>75</sup> A similar reaction was repeated using (S)-(+)-MαNP acid **3** affording ester (S,X)-**109**. The  $^1\text{H}$  NMR spectra of both products were fully assigned using the  $^1\text{H}$ ,  $^1\text{H}$ - $^1\text{H}$  COSY,  $^{13}\text{C}$ , HMQC, and HMBC methods. The  $\Delta\delta$  values ( $\Delta\delta = \delta(R,X) - \delta(S,X)$ ) were calculated as shown in Figure 34. Namely the 3,5-dimethoxyphenyl group has positive  $\Delta\delta$  values, while phenyl has negative ones. By applying the MαNP sector rule, the absolute configuration of the alcohol part was determined as  $X = S$ . This result agrees with the *S* absolute configuration as previously determined by the X-ray method (Table 2). It was thus established that the  $^1\text{H}$  NMR anisotropy method using MαNP acid is safely applicable to such chiral alcohols.

It was reported that the chiral thyroid hormone analogue KAT-2003 (+)-**110** (see Fig. 35) showed hypocholesterolemic activities and decreases of hepatic triglyceride contents with low cardiac side effects, while the opposite enantiomer (-)-**110** was less active than (+)-**110**.<sup>55</sup> So

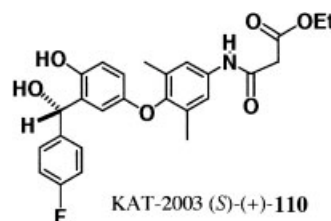


Fig. 35. Absolute configuration of KAT-2003 (+)-**110**.<sup>55</sup>

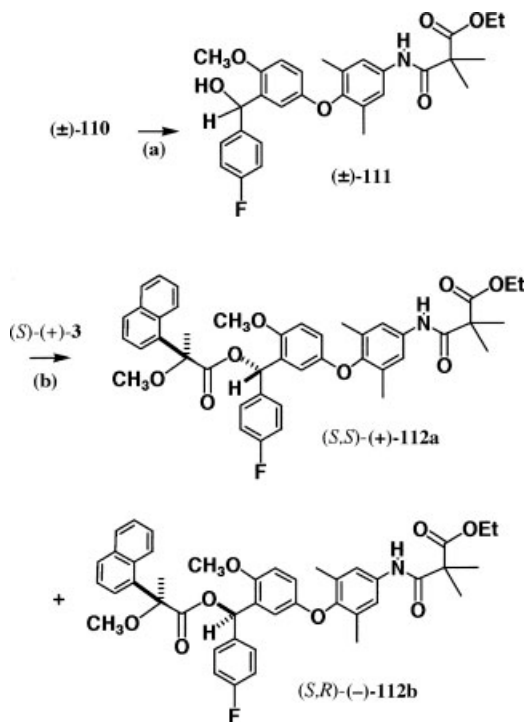


Fig. 36. (a)  $\text{CH}_3\text{I}$ ,  $\text{Cs}_2\text{CO}_3/\text{CH}_3\text{CN}$ : ( $\pm$ )-**111**, 75%. (b) DCC, DMAP,  $\text{CSA}/\text{CH}_2\text{Cl}_2$ , r.t.: (+)-**112a**, 45%; (–)-**112b**, 50%.<sup>55</sup>

the chiral thyroid hormone analogue KAT-2003 (+)-**110** had been developed as a potent medicine. However, its absolute configuration had remained undetermined.

KAT-2003 (+)-**110** having a chiral diphenylmethanol moiety had been prepared by the asymmetric reduction of the corresponding ketone with chiral reagent, (+)-*B*-chlorodiisopinocampheylborane (DIP-chloride<sup>TM</sup>). We have first applied the CSDP acid method to KAT-2003 **110** and its methyl ether derivative. However, we were unable to separate diastereomeric CSDP esters by HPLC. We then applied the method of M $\alpha$ NP acid **3** to chiral KAT-2003 (+)-**110** to determine its absolute configuration.<sup>55</sup>

To apply the M $\alpha$ NP acid method, the phenol group of KAT-2003 has to be protected, e.g., as methyl ether. So, racemic KAT-2003 ( $\pm$ )-**110** was methylated with  $\text{CH}_3\text{I}$  and  $\text{Cs}_2\text{CO}_3$  in acetonitrile yielding trimethylated alcohol ( $\pm$ )-**111** in a good yield (see Fig. 36). Esterification of ( $\pm$ )-**111** with (S)-(+)-M $\alpha$ NP acid **3** gave a diastereomeric mixture of esters, which was easily separated by HPLC on silica gel (see Fig. 37). In general, the M $\alpha$ NP esters of less polar aliphatic alcohols, such as 2-hexadecanol, are more effectively separated by HPLC on silica gel than the M $\alpha$ NP esters of polar alcohols as discussed above. Therefore it was interesting to find that the diastereomeric mixture of M $\alpha$ NP esters **112a/112b** composed of polar groups was clearly separated by HPLC on silica gel (hexane/EtOAc = 5:1): separation factor  $\alpha = 1.72$ ; resolution factor  $R_s = 2.52$ . It should be emphasized that a diastereomeric mixture (50 mg) of esters was separable even with a HPLC silica gel column of 10 cm length. Ester (+)-

**112a** (45%) was eluted first and ester (–)-**112b** (50%) second.

To determine the absolute configuration of the first-eluted ester (+)-**112a** by the  $^1\text{H}$  NMR anisotropy method, all NMR signals of both diastereomeric esters (+)-**112a** and (–)-**112b** were fully assigned by the  $^1\text{H}$ ,  $^1\text{H}$ – $^1\text{H}$  COSY,  $^{13}\text{C}$ , HMQC, and HMBC methods (see Fig. 38). The anisotropy value,  $\Delta\delta = \delta(2\text{nd fr.}) - \delta(1\text{st fr.}) = \delta(\text{112b}) - \delta(\text{112a})$ , was calculated for all protons as shown in Figure 38. According to the sector rule, the 4-fluorophenyl group with negative  $\Delta\delta$  values was placed in the left side, while the remaining group with positive  $\Delta\delta$  values in the right side. From the projection, the absolute configuration of the first-eluted ester was determined as  $X = S$ , leading to the absolute configurations (S,S)-(+)-**112a** and (S,R)-(–)-**112b**.

To assign the absolute configuration of chiral KAT-2003 (+)-**110**, the compound was treated in the same way giving trimethyl derivative (–)-**111** (82%), the spectroscopic data of which agreed with those of racemate ( $\pm$ )-**111** except optical rotation. Alcohol (–)-**111** was esterified with (S)-(+)-M $\alpha$ NP acid **3** to give ester (+)-**112a** which was completely identical with the first-eluted ester (S,S)-(+)-**112a** obtained by HPLC in Figure 37. Therefore the absolute configuration of the chiral thyroid hormone analogue KAT-2003 (+)-**110** was established to be S.

As described here, the M $\alpha$ NP method is very powerful for determining the absolute configurations of chiral synthetic drugs. When single crystals suitable for X-ray analysis are not available, the  $^1\text{H}$  NMR anisotropy method using “M $\alpha$ NP acid” is useful as a complementary technique.

**Other interesting application examples of the M $\alpha$ NP acid method.** Some application examples of the M $\alpha$ NP acid method reported by other research groups are

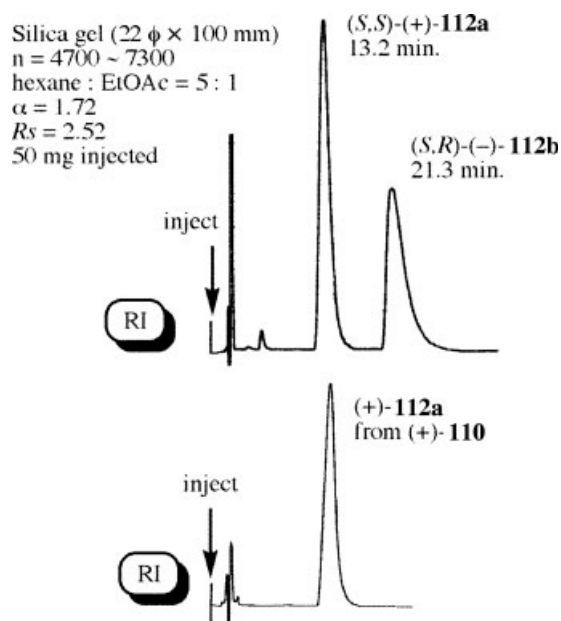


Fig. 37. HPLC separation of diastereomeric esters (S,S)-(+)-**112a** and (S,R)-(–)-**112b**.<sup>55</sup>



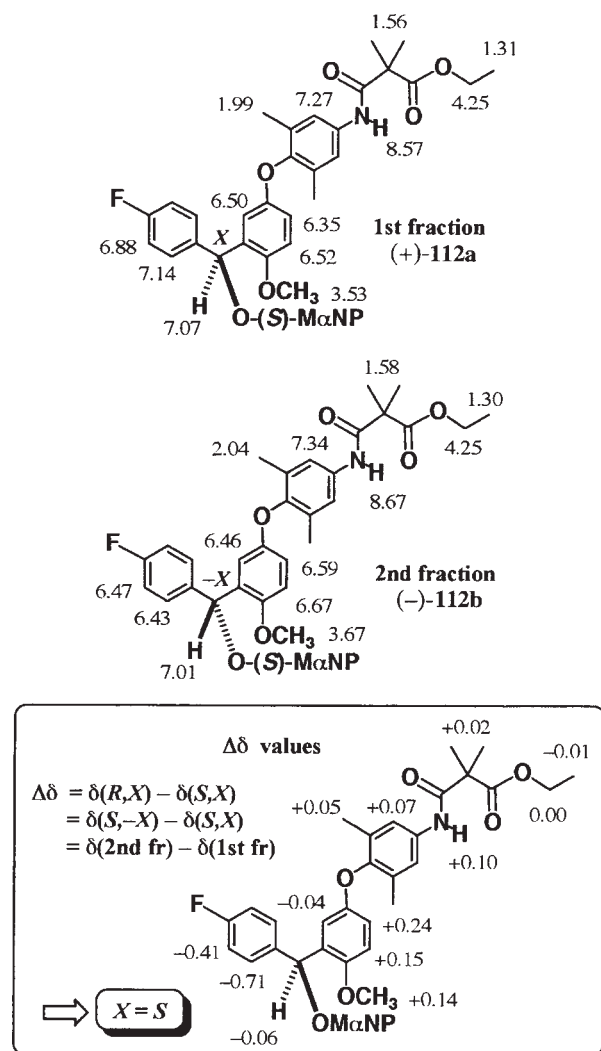


Fig. 38. The  $^1\text{H}$  NMR chemical shift data (600 MHz, ppm,  $\text{CDCl}_3$ ) of esters (+)-112a and (-)-112b and the absolute configuration of the first-eluted ester (+)-112a as determined by the  $^1\text{H}$  NMR anisotropy method using (S)-M $\alpha$ NP acid.<sup>55</sup>

shown in Figure 39. Compound (1*R*,3*S*)-(+)-113 was synthesized as a synthetic precursor of chiral 5-lipoxygenase inhibitors.<sup>89</sup> It is interesting that diastereomeric M $\alpha$ NP esters 115a/115b with two free hydroxyl groups were effectively separated by flash chromatography, while corresponding bis(silyl) ethers 114a/114b were inseparable by chromatography. Namely, M $\alpha$ NP esters with polar substituents were efficiently separable. This substituent effect is opposite to that of W-M ketone derivatives discussed above (Table 3 and Fig. 31). Therefore, to obtain better separation, it is advisable to check the substituent effect in each case. Starting from ester (-)-115a, mispyric acid, an inhibitor of DNA polymerase  $\beta$ , was first synthesized and its absolute configuration was determined.<sup>90</sup>

Enantiopure sulcatol (*R*)-(-)-116<sup>91</sup> and 2-methyl-4-heptanol (*R*)-(-)-117,<sup>92</sup> a pheromone, were synthesized by resolution and their absolute configurations were determined by the  $^1\text{H}$  NMR anisotropy method. A hydroxy metabolite (-)-118 of blonanserine (AD-5423) was synthe-

sized and its absolute configuration was determined to be *S* by X-ray crystallography of HBr salt and also by the  $^1\text{H}$  NMR anisotropy method using M $\alpha$ NP acid.<sup>93</sup>

The case of inherently chiral *anti*-*O*,*O'*-dialkylated calix[4]arene derivative is an interest application example. To enantioresolve *anti*-*O*,*O'*-dibenzylcalix[4]arenes, their (S)-M $\alpha$ NP acid esters were prepared and separated well by HPLC giving all four possible diastereomers. The absolute configuration of one of esters, (-)-119c, was clearly determined by X-ray crystallography as shown by the use of (S)-M $\alpha$ NP acid moiety as an internal reference.<sup>94</sup> From the results of X-ray and CD studies, the absolute configurations of the remaining three derivatives were determined. Compound 120 also shows an interesting example. To determine the absolute configuration of antibiotic PF1140 (-)-120, it was converted to (S)-M $\alpha$ NP acid ester 121, to which the  $^1\text{H}$  NMR anisotropy is not applicable, because of the phenolic ester. Instead, the absolute configuration of 121 was established by X-ray crystallography using an internal reference of M $\alpha$ NP acid moiety.<sup>95</sup>

**A new route for the large-scale preparation of enantiopure M $\alpha$ NP acid by the use of (S)-(-)-phenylalaninol.**<sup>81</sup> As an extension of the M $\alpha$ NP acid method, we have developed the MS spectral method for determining the

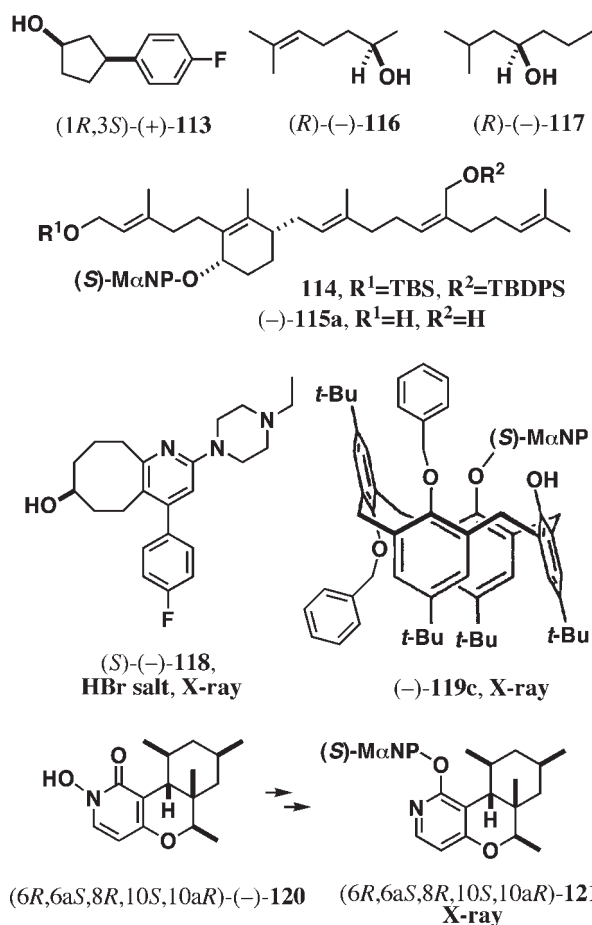


Fig. 39. Some examples of the enantioresolution of alcohols by the M $\alpha$ NP acid method, and determination of absolute configurations by the  $^1\text{H}$  NMR anisotropy method and/or X-ray crystallography.



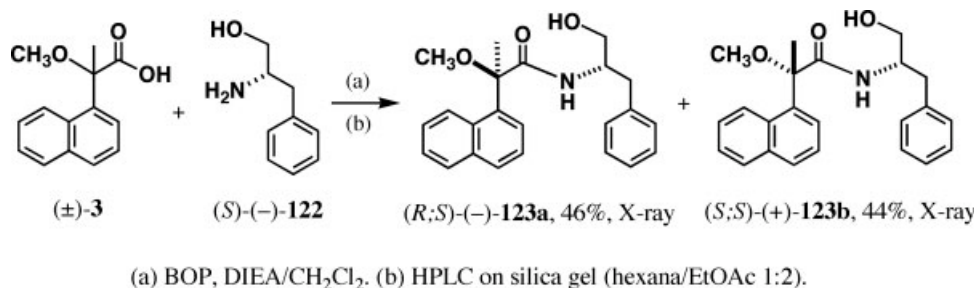


Fig. 40. Preparation of diastereomeric amides from M $\alpha$ NP acid ( $\pm$ )-**3** and phenylalaninol (*S*)-(-)-**122**.

%ee of chiral alcohols.<sup>60</sup> The method has an advantage to be free from the kinetic resolution effect, which is always accompanied by the formation of diastereomers and disturbs the exact %ee determination. The M $\alpha$ NP acid method for determining %ee has been successfully applied to an aliphatic chiral alcohol. To apply this method to the age-determination of fossil materials, we planned to measure the %ee of  $\alpha$ -amino acids, although the HPLC separation of  $\alpha$ -amino acid methyl esters as M $\alpha$ NP amides had been previously reported.<sup>77,78</sup> To avoid the possible partial racemization during the derivatization reaction, we chose to reduce  $\alpha$ -amino acids to  $\alpha$ -amino alcohols, which never racemize.

As a preliminary experiment, (*S*)-(-)-phenylalaninol **122** was condensed with racemic M $\alpha$ NP acid ( $\pm$ )-**3** yielding a diastereomeric mixture of amides **123a** and **123b** (see Fig. 40). It was surprising to find that these diastereomeric amides were separable by HPLC on silica gel with a large separation factor  $\alpha = 4.53$ ,  $R_s = 4.50$  (Fig. 41 and Table 4). As shown in Figure 41, it should be noted that diastereomers **123a**/**123b** were effectively separated even on a short column ( $220 \times 100$  mm). This effective separation of diastereomeric amides is comparable to those reported by Helmchen et al.,<sup>96,97</sup> where (*R*)-(-)-phenylglycinol was used as a chiral amino alcohol.

Such an effective HPLC separation prompted us to develop a new route for the preparation of enantiopure M $\alpha$ NP acid **3** by the use of (*S*)-(-)-phenylalaninol **122**. However, we were soon confronted with the fact that the

recovery of acid **3** from amides **123a** and **123b** by hydrolysis or solvolysis was extremely difficult. We attempted various reactions, but all attempts were unsuccessful. During this period, the preparation of chiral methoxy(1-naphthyl)acetic acid (1NMA) *via* amides with (*S*)-(-)-**122** was reported by Kusumi et al.,<sup>98</sup> where the amides were hydrolyzed under an acidic condition.<sup>97</sup> We also attempted the acidic hydrolysis, but the elimination of methanol occurred together with the hydrolysis of amide bond, and therefore the chirality of the molecule vanished. Since then we have studied the cleavage reaction for a long time, and finally succeeded in solving this problem. This new route enables a large-scale preparation of enantiopure M $\alpha$ NP acid **3** as described below.

The first-eluted amide (-)-**123a** was recrystallized from MeOH affording colorless prisms, one of which was subjected to X-ray crystallography. The structure was solved by the direct method and successive Fourier syntheses:  $R = 0.0403$  and  $R_w = 0.0957$ ; Flack  $\chi = 0.0$  (3). As the *S* absolute configuration of the phenylalaninol part was known, the absolute configuration of the M $\alpha$ NP acid part was automatically determined to be *R* as shown in Figure 42a.

The second-eluted amide (+)-**123b** was obtained initially as amorphous solid. After many attempts, however we found that amide (+)-**123b** crystallized as prisms from toluene, and a single crystal was subjected to X-ray crystallography. One asymmetric unit contains two independent molecules of (+)-**123b** and one molecule of toluene as a crystal solvent, which takes a disordered structure:  $R = 0.0540$  and  $R_w = 0.1323$ ; Flack  $\chi = -0.1$  (2). As the *S* absolute configuration of the phenylalaninol part was known, the absolute configuration of M $\alpha$ NP acid part was determined to be *S* as shown in Figure 42b. The X-ray crystallography using an internal reference gives a clear absolute configurational assignment, even if single crystals are of low quality.

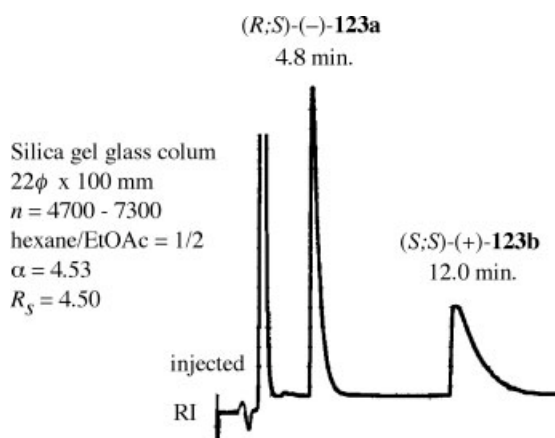


Fig. 41. HPLC separation of M $\alpha$ NP amides (*R,S*)-(-)-**123a** and (*S,S*)-(+)-**123b**.<sup>81</sup>

TABLE 4. HPLC separation of diastereomeric amides and oxazolines

Entry	Diastereomers	Solvent <sup>a</sup>	$\alpha$	$R_s$	1st-eluted Fr.
1 <sup>b</sup>	<b>123a</b> / <b>123b</b>	H/EA = 1/2	4.53	4.50	( <i>R,S</i> )-(-)- <b>123a</b>
2 <sup>c</sup>	<b>124a</b> / <b>124b</b>	H/EA = 5/1	1.25	2.79	( <i>R,S</i> )-(+)- <b>124a</b>

<sup>a</sup>H = hexane, EA = ethyl acetate.

<sup>b</sup>Glass column ( $220 \times 100$  mm) of silica gel (particle size 5–10  $\mu\text{m}$ ).

<sup>c</sup>Glass column ( $220 \times 300$  mm) of silica gel (particle size 5–10  $\mu\text{m}$ ).

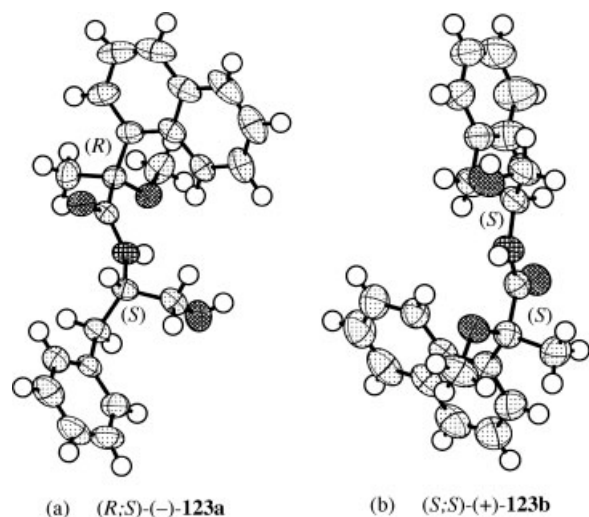


Fig. 42. X-ray stereostructures of M $\alpha$ NP amides  $(R,S)-(-)-123a$  and  $(S,S)-(+)-123b$ . In the case of  $(S,S)-(+)-123b$ , the second independent molecule of  $(+)-123b$  and crystal solvent of toluene are omitted.<sup>81</sup>

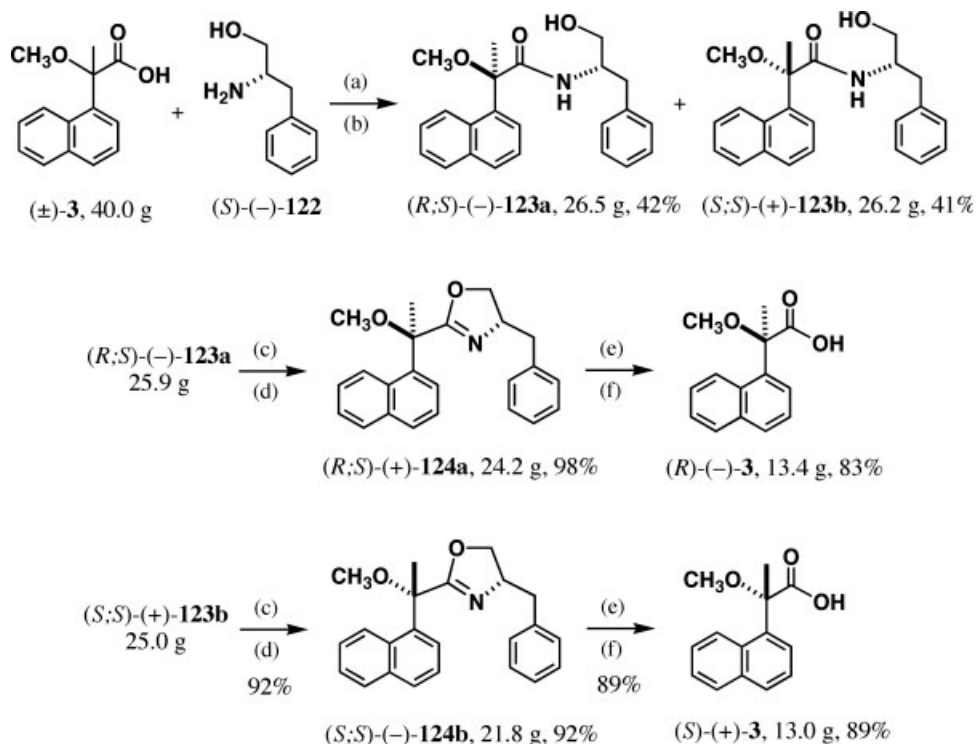
As the method of a large-scale preparation of enantiopure M $\alpha$ NP acids  $(R)-(-)-3$  and  $(S)-(+)-3$ , we have developed a procedure shown in Figure 43. The condensation of M $\alpha$ NP acid  $(\pm)-3$  (40 g) and phenylalaninol  $(S)-(-)-122$  with DCC, HOBT, 10-camphorsulfonic acid (CSA), DIEA in  $CH_2Cl_2$  provided amides  $123a/123b$  in good

yields. The separation of diastereomeric amides  $123a/123b$  was carried out by combining fractional crystallizations and HPLC: total yield of enantiopure  $123a$ , 42%;  $123b$ , 41% after removal of crystal solvent.

To recover enantiopure M $\alpha$ NP acid  $(R)-(-)-3$  from amide  $(R,S)-(-)-123a$ , we have adopted the route via oxazoline  $(R,S)-(+)-124a$ , as shown in Figure 43. Amide  $(R,S)-(-)-123a$  was treated with  $SOCl_2$ , and the crude product obtained was successively treated with NaOMe yielding oxazoline  $(R,S)-(+)-124a$ . The product  $(+)-124a$  was treated with iodomethane, and the crude product was hydrolyzed with NaOH giving enantiopure M $\alpha$ NP acid  $(R)-(-)-3$  (13.4 g). From amide  $(S,S)-(+)-123b$ , enantiopure M $\alpha$ NP acid  $(S)-(+)-3$  (13.0 g) was similarly prepared via oxazoline  $(S,S)-(-)-124b$ .

There may be an alternative strategy to separate diastereomers at the stage of oxazolines  $124a/124b$ . So we checked the HPLC separation of diastereomers  $124a/124b$  on silica gel, which were baseline separated ( $\alpha = 1.25$ ) as listed in Table 4, where  $124a$  was eluted first. However, the separation factor  $\alpha$  is much smaller than that of amides  $123a/123b$  ( $\alpha = 4.53$ ). Therefore, the separation of diastereomers at the stage of the amides described above is much better.

To check the enantiopurity of M $\alpha$ NP acids  $(R)-(-)-3$  and  $(S)-(+)-3$ , we have studied the enantioseparation of racemic M $\alpha$ NP acid  $(\pm)-3$  using HPLC columns with chiral stationary phases. It was found that when a column of



(a) DCC, HOBT, CSA, DIEA/ $CH_2Cl_2$ . (b) fractional recrystallization and HPLC. (c)  $SOCl_2$ /toluene,  $\Delta$ . (d) 28% NaOMe/MeOH,  $\Delta$ . (e)  $CH_3I$ ,  $\Delta$ . (f) NaOH/MeOH, water,  $\Delta$ .

Fig. 43. A large-scale preparation of enantiopure M $\alpha$ NP acids  $(R)-(-)-3$  and  $(S)-(+)-3$  by the enantioresolution with phenylalaninol  $(S)-(-)-122$ .  
 Chirality DOI 10.1002/chir

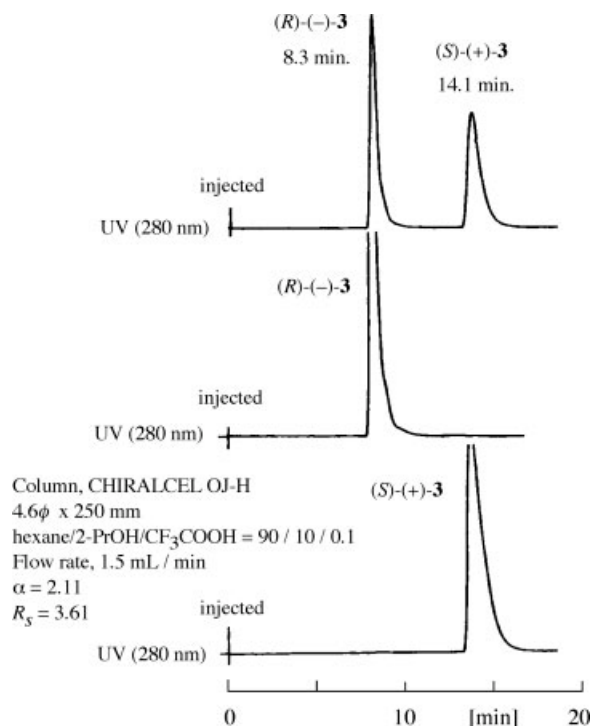


Fig. 44. HPLC check of the enantiopurity of M $\alpha$ NP acids (R)-(-)-3 and (S)-(+)-3.<sup>81</sup>

CHIRALCEL OJ-H (Daicel Co., Ltd., Tokyo) was used, the enantiomers were effectively separated ( $\alpha = 2.11$ ,  $R_s = 3.61$ ) as shown in Figure 44a. Under the same HPLC conditions, M $\alpha$ NP acids (R)-(-)-3 and (S)-(+)-3 prepared above were injected into the column, respectively, revealing that each acid was enantiopure as illustrated in Figures 44b and 44c.

Phenylalaninol (S)-(-)-122 works well as a CXR with resolving power for the enantioresolution of M $\alpha$ NP acid. Namely, amino alcohol (S)-(-)-122 has the following advantages: (i) diastereomeric amides are easily separable by HPLC on silica gel; (ii) separated amides have high probability of crystallizing as single crystals suitable for X-ray analysis; (iii) enantiopure M $\alpha$ NP acids are recovered via the oxazoline derivative. Therefore, the present method should be useful for the enantioresolution of carboxylic acids having nonracemizable structures, and the simultaneous determination of their absolute configurations by X-ray crystallography as shown in Figure 45.

**Short remarks for the use of (R)-(-)-M $\alpha$ NP acid as a CAR.** In our studies, we have used only M $\alpha$ NP acid (S)-(+)-3 as a CAR, which was recovered from the first-eluted menthol ester (S;1*R*,3*R*,4*S*)-(-)-66a (Figs. 17 and 18). In HPLC, it is easier to collect the first-eluted fraction in an enantiopure form than the second-eluted one. So, M $\alpha$ NP acid (S)-(+)-3 was selected. Another reason why we have used only M $\alpha$ NP acid (S)-(+)-3 is to prevent a careless mistake in the determination of absolute configuration. If the absolute configuration of a CAR is mistaken, the results obtained by the  $^1\text{H}$  NMR anisotropy method are, of

course, wrong. So, researchers should always mind which enantiomer of chiral reagents is used in their experiments.

In the enantioresolution of M $\alpha$ NP acid with phenylalaninol (S)-(-)-122 discussed above, M $\alpha$ NP acid (R)-(-)-3 was obtained from the first-eluted amide (R;S)-(-)-123a, which was easily recrystallized from MeOH affording colorless prisms. Therefore it is easier to prepare enantiopure M $\alpha$ NP acid (R)-(-)-3 than (S)-(+)-3. Figure 46 shows the procedure for determining absolute configurations by the  $^1\text{H}$  NMR anisotropy method using M $\alpha$ NP acid (R)-(-)-3. The principle is the same as in the case of M $\alpha$ NP acid (S)-(+)-3. One important point to be noted is that the definition of anisotropy factor  $\Delta\delta$  is different from the case of M $\alpha$ NP acid (S)-(+)-3. Namely, parameter  $\Delta\delta$  is logically transformed as shown below (see Fig. 46).

The absolute configurations of the first-eluted ester 128a and the second-eluted ester 128b are defined as (R,X) and (R,-X), respectively. Since ester (R,-X) is the enantiomer of ester (S,X), their NMR data should be identical:  $\delta(R,-X) = \delta(S,X)$ . So, the original definition of  $\Delta\delta$  is transformed as  $\Delta\delta = \delta(R,X) - \delta(S,X) = \delta(R,X) - \delta(R,-X) = \delta(128a) - \delta(128b) = \delta(1\text{st fr.}) - \delta(2\text{nd fr.})$ . Namely,  $\Delta\delta$  values are obtained by subtraction of the chemical shift data of the second-eluted ester from those of the first-eluted ester. This is an important point to

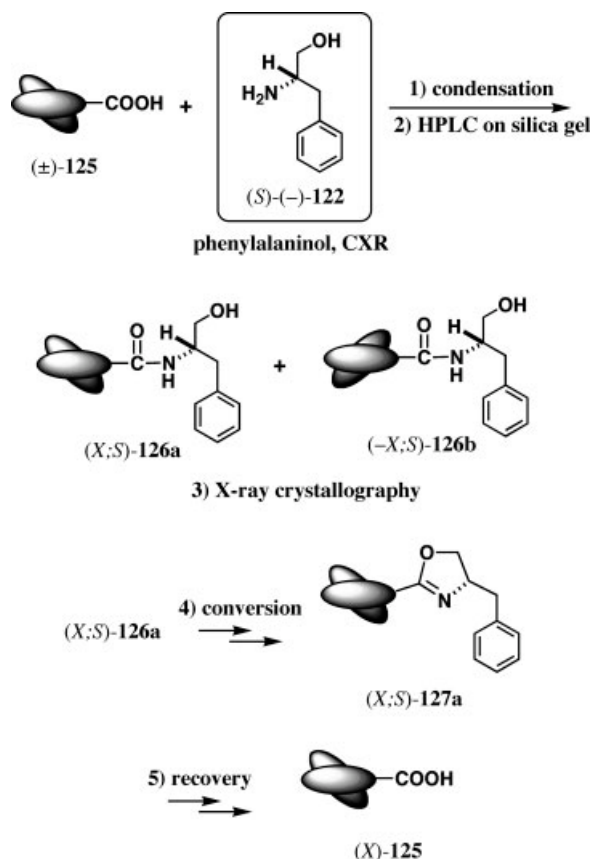
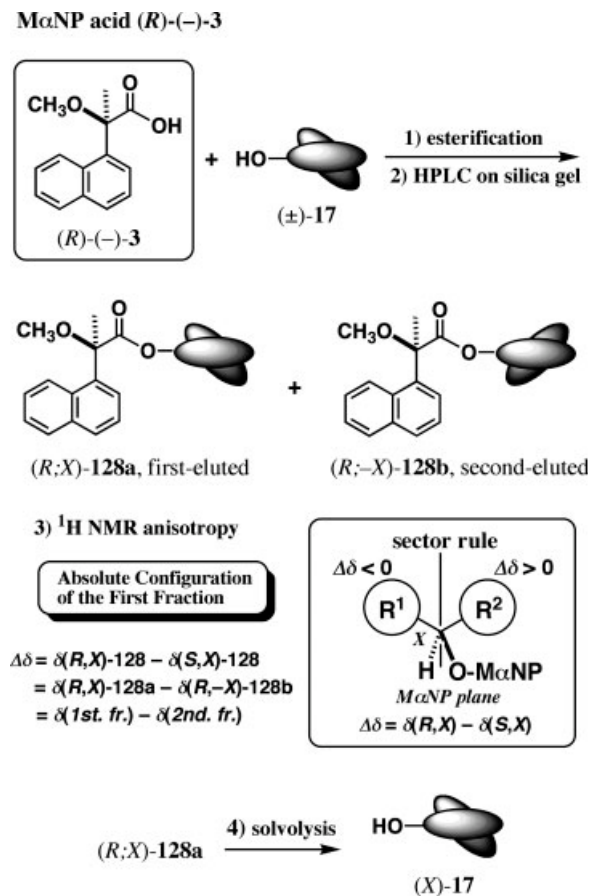


Fig. 45. A general scheme of the enantioresolution of carboxylic acids having nonracemizable structures, and the determination of their absolute configurations by X-ray crystallography by the use of (S)-(-)-phenylalaninol, a CXR with resolving power.





**Fig. 46.** Enantioresolution of alcohols and determination of their absolute configurations by the use of M $\alpha$ NP acid (*R*)-(-)-3, a CAR with resolving power.

notice, when M $\alpha$ NP acid (*R*)-(-)-3 is used. From the distribution of  $\Delta\delta$  values in the sector rule, the absolute configuration *X* of the first-eluted ester can be determined.

## CONCLUSION

In this review, the principles and applications of methods for determining absolute configurations of chiral compounds by X-ray crystallography with an internal reference and  $^1\text{H}$  NMR anisotropy are explained using mostly our own data. In order to facilitate understanding by beginners or graduate students, attempts have been made to explain clearly. Thus this is not a comprehensive review covering all reported data and literatures.

CSDP acid, a CXR, is useful for preparation of enantiopure alcohols by resolution and simultaneous determination of their absolute configuration by X-ray analysis. The X-ray crystallographic method using an internal reference is, of course, the best for determining absolute configuration. However, ideal single crystals are not always obtainable. In such a case, the NMR method using M $\alpha$ NP acid, a CAR, is effective, because it requires no crystallization. In addition, M $\alpha$ NP acid has an excellent ability to enantioresolve alcohols. Chiral CSDP acid and M $\alpha$ NP acid are

*Chirality* DOI 10.1002/chir

thus useful as complementary. If the resolution with one reagent is unsuccessful, the use of the other is suggested. Phenylalaninol is also useful as a CXR for enantioresolving carboxylic acids having nonracemizable structures. The methods using such CXRs and CARs with resolving power are thus useful for preparation of enantiopure compounds and also for simultaneous determination of their absolute configurations.

We have recently reported the conformational analyses of M $\alpha$ NP esters, aromatic geometry and solvent effects on  $\Delta\delta$  values, and crystalline state conformational analyses of various M $\alpha$ NP esters studied by X-ray crystallography.<sup>22,58</sup> However, those will be explained elsewhere, because of limited space and time. Chiral (1*S*,2*R*,4*R*)-(-)-CSDP, (*R*)-(-)-M $\alpha$ NP, and (*S*)-(+)-M $\alpha$ NP acids are commercially available from TCI (Tokyo Chemical Industry; <http://www.tciamerica.com/> or <http://www.tcieurope.eu/>).

## ACKNOWLEDGMENTS

The author thanks all the coworkers, whose names are listed in references cited, for their efforts and cooperation. He also thanks Drs. George A. Ellestad and Koji Nakanishi, Department of Chemistry, Columbia University, for their valuable suggestions.

## REFERENCES

- Bijvoet JM, Peerdeman AF, van Bommel AJ. Determination of the absolute configuration of optically active compounds by means of X-rays. *Nature* 1951;168:271–272.
- Flack HD. On enantiomorph-polarity estimation. *Acta Crystallogr A* 1983;39:876–881.
- Mason SF. The absolute configuration of calcanthine. *Proc Chem Soc* 1962;362–363.
- Harada N, Nakanishi K. A method for determining the chiralities of optically active glycols. *J Am Chem Soc* 1969;91:3989–3991.
- Harada N, Nakanishi K. Circular dichroic spectroscopy—exciton coupling in organic stereochemistry. Mill Valley, CA: University Science Books; 1983.
- Berova N, Nakanishi K. Exciton chirality method: principles and applications. In: Berova N, Nakanishi K, Woody RW, editors. *Circular dichroism, principles and applications*. New York: Wiley-VCH; 2000. Chapter 12.
- Kemp C, Mason SF. The absorption and circular dichroism spectra and the absolute configuration of (+)-1-fluoro-12-methylbenzo[*c*]phenanthrene. *Tetrahedron* 1966;22:629–635.
- Harada N. Circular dichroism spectroscopy and absolute stereochemistry of biologically active compounds. In: Cooper R, Snyder JK, editors. *The biology-chemistry interface*. New York: Marcel Dekker; 1999. Chapter 6, p 139–190.
- Harada N. Circular dichroism of twisted  $\pi$ -electron systems: theoretical determination of the absolute stereochemistry of natural products and chiral synthetic organic compounds. In: Berova N, Nakanishi K, Woody RW, editors. *Circular dichroism, principles and applications*. New York: Wiley-VCH; 2000. Chapter 15.
- Cheeseman JR, Frisch MJ, Devlin FJ, Stephens PJ. Ab initio calculation of atomic axial tensors and vibrational rotational strengths using density functional theory. *Chem Phys Lett* 1996;252:211–220.
- Polavarapu PL. *Vibrational spectra: Principles and applications with emphasis on optical activity*. Amsterdam: Elsevier; 1998.
- Freedman TB, Cao X, Dukor RK, Nafie LA. Absolute configuration determination of chiral molecules in the solution state using vibrational circular dichroism. *Chirality* 2003;15:743–758.
- Barron LD. *Molecular light scattering and optical activity*, 2nd ed. Cambridge: Cambridge University Press; 2004.



14. Harada N, Soutome T, Murai S, Uda H. A chiral probe useful for optical resolution and X-ray crystallographic determination of the absolute stereochemistry of carboxylic acids. *Tetrahedron: Asymmetry* 1993;4:1755–1758.
15. Harada N, Soutome T, Nehira T, Uda H, Oi S, Okamura A, Miyano S. Revision of the absolute configurations of [8]paracyclophane-10-carboxylic and 15-methyl[10]paracyclophane-12-carboxylic acids. *J Am Chem Soc* 1993;115:7547–7548.
16. Harada N, Hattori T, Suzuki T, Okamura A, Ono H, Miyano S, Uda H. Absolute stereochemistry of 1-(9-phenanthryl)-2-naphthoic acid as determined by CD and X-ray methods. *Tetrahedron: Asymmetry* 1993;4:1789–1792.
17. Hattori T, Harada N, Oi S, Abe H, Miyano S. 1,12-Dioxo[12](1,4)naphthalenophane-14-carboxylic acid: practical synthesis, resolution and absolute configuration of the enantiomers. *Tetrahedron: Asymmetry* 1995;6:1043–1046.
18. Harada N. Chiral auxiliaries powerful for both enantiomer resolution and determination of absolute configuration by X-ray crystallography. In: Denmark SE, Siegel JS, editors. *Topics in stereochemistry*, Vol 25. New Jersey: John Wiley; 2000. Chapter 6, p 177–203.
19. Harada N. Powerful chiral molecular tools for preparation of enantiopure alcohols and simultaneous determination of their absolute configurations by X-ray crystallography and/or  $^1\text{H}$  NMR anisotropy methods. In: Francotte E, Lindner W, editors. *Chirality in drug research*. Weinheim, Germany: Wiley-VCH; 2006. Chapter 9, p 283–321.
20. Harada N, Watanabe M, Kuwahara S. Novel chiral derivatizing agents powerful for enantioresolution and determination of absolute stereochemistry by X-ray crystallographic and  $^1\text{H}$  NMR anisotropy methods. In: Busch KW, Busch MA, editors. *Chiral analysis*. Amsterdam: Elsevier; 2006. Chapter 18.
21. Fujita T, Kuwahara S, Watanabe M, Harada N. Crystalline state conformation of 2-methoxy-2-(1-naphthyl)propionic acid ester. *Enantiomer* 2002;7:219–224.
22. Kuwahara S, Naito J, Yamamoto Y, Kasai Y, Fujita T, Noro K, Shimamuki K, Akagi M, Watanabe M, Matsumoto T, Watanabe M, Ichikawa A, Harada N. Crystalline state conformational analysis of  $\text{M}\alpha\text{NP}$  esters, powerful resolution and chiral  $^1\text{H}$  NMR anisotropy tools. *Eur J Org Chem* 2007;1827–1840.
23. Toda F. Isolation and optical resolution of materials utilizing inclusion crystallization. *Top Curr Chem* 1987;140:43–69.
24. Toda F, Tanaka K, Miyahara I, Akutsu S, Hirotsu K. Role of methanol in chiral combinations of host–guest molecules in the inclusion crystal: structure determination by X-ray crystallography. *J Chem Soc Chem Commun* 1994;1795–1796.
25. Toda F, Tanaka K, Watanabe M, Abe T, Harada N. Enantiomer resolution by crystallization with chiral hosts: application to monoterpenes, verbenone and apoverbenone. *Tetrahedron: Asymmetry* 1995;6:1495–1498.
26. Kuwahara S, Obata K, Yoshida K, Matsumoto T, Harada N, Yasuda N, Ozawa Y, Toriumi K. Conclusive determination of the absolute stereochemistry of chiral  $\text{C}_{60}$  fullerene *cis*-3 bisadducts by X-ray crystallography and circular dichroism. *Angew Chem Int Ed* 2005;44:2262–2265.
27. Harada N, Koumura N, Feringa BL. Chemistry of unique chiral olefins. 3. Synthesis and absolute stereochemistry of *trans*- and *cis*-1,1',2,2',3,3',4,4'-octahydro-3,3'-dimethyl-4,4'-biphenanthrylidenes. *J Am Chem Soc* 1997;119:7256–7264.
28. Fujita T, Kuwahara S, Harada N. A new model of light powered chiral molecular motor with higher speed of rotation. 1. Synthesis and absolute stereostructure. *Eur J Org Chem* 2005;4533–4543.
29. Harada N, Fujita K, Watanabe M. Molecular chirality by isotopic substitution. Synthesis, absolute configuration, and CD spectra of chiral diphenylmethanols. *Enantiomer* 1998;3:64–70.
30. Nakamura E, Isobe H, Tokuyama H, Sawamura M. Regio- and diastereo-controlled double cycloaddition to [60]fullerene: one-step synthesis of  $\text{C}_s$  and  $\text{C}_2$  chiral organofullerenes with new tris-annulating reagent. *Chem Commun* 1996;1747–1748.
31. Taki M, Sugita S, Nakamura Y, Kawashima E, Yashima E, Okamoto Y, Nishimura J. Selective functionalization on [60]fullerene governed by tether length. *J Am Chem Soc* 1997;119:926–932.
32. Nierengarten JF, Habicher T, Kessinger R, Cardullo F, Diederich F, Gramlich V, Gisselbrecht JP, Boudon C, Gross M. Macrocyclization on the fullerene core: direct regio- and diastereoselective multi-functionalization of [60]fullerene, and synthesis of fullerene-dendrimer derivatives. *Helv Chim Acta* 1997;80:2238–2276.
33. Taki N, Nakamura Y, Uehara H, Sato M, Nishimura J. [60]Fullerene ( $\text{A}_1, \text{D}_1$ )-bisadducts: CD spectra of enantiomers and diastereospecific synthesis. *Enantiomer* 1998;3:231–239.
34. Ishi-i T, Nakashima K, Shinkai S, Ikeda A. Saccharide libraries as potential templates for regio- and chiroselective introduction of two functional groups into [60]fullerene. *J Org Chem* 1999;64:984–990.
35. Nakamura Y, O-kawa K, Nishimura J. Biscycloaddition to [60]fullerene: regioselectivity and its control with templates. *Bull Chem Soc Jpn* 2003;76:865–882.
36. Goto H, Harada N, Crassous J, Diederich F. Absolute configuration of chiral fullerenes and covalent derivatives from their calculated circular dichroism. *J Chem Soc Perkin Trans 2* 1998:1719–1723.
37. Kessinger R, Thilgen C, Mordasini T, Diederich F. Optically active macrocyclic *cis*-3-bis-adducts of  $\text{C}_{60}$ : regio- and stereoselective synthesis, exciton chirality coupling, and determination of the absolute configuration, and first observation of exciton coupling between fullerene chromophores in a chiral environment. *Helv Chim Acta* 2000;83:3069–3096.
38. Yoshida K, Osawa S, Monde K, Watanabe M, Harada N. Absolute stereochemistry of chiral  $\text{C}_{60}$  fullerene bis-adducts. *Enantiomer* 2002;7:23–32.
39. Dale JA, Mosher HS. Nuclear magnetic resonance enantiomer reagents. Configurational correlations via nuclear magnetic resonance chemical shifts of diastereomeric mandelate, *O*-methylmandelate, and  $\alpha$ -methoxy- $\alpha$ -trifluoromethylphenylacetate (MTPA) esters. *J Am Chem Soc* 1973;95:512–519.
40. Trost BM, Belletire JL, Godleski S, McDougal PG, Balkovec JM, Baldwin JJ, Christy ME, Ponticello GS, Varga SL, Springer JP. On the use of the *O*-methylmandelate ester for establishment of absolute configuration of secondary alcohols. *J Org Chem* 1986;51:2370–2374.
41. Ohtani I, Kusumi T, Kashman Y, Kakisawa H. High-field FT NMR application of Mosher's method. The absolute configurations of marine terpenoids. *J Am Chem Soc* 1991;113:4092–4096.
42. Kusumi T, Takahashi H, Hashimoto T, Kan Y, Asakawa Y. Determination of the absolute configuration of ginnol, a long-chain aliphatic alcohol, by use of a new chiral anisotropic reagent. *Chem Lett* 1994;1093–1094.
43. Yamase H, Ooi T, Kusumi T. Determination of the absolute configuration of linear secondary alcohols adopting one enantiomer of the chiral anisotropic reagents, methoxy(1- and 2-naphthyl)acetic acids. *Tetrahedron Lett* 1998;39:8113–8116.
44. Seco JM, Latypov Sh, Quinoa E, Riguera R. New chirality recognizing reagents for the determination of absolute stereochemistry and enantiomeric purity by NMR. *Tetrahedron Lett* 1994;35:2921–2924.
45. Seco JM, Latypov Sh, Quinoa E, Riguera R. Determining factors in the assignment of the absolute configuration of alcohols by NMR. The use of anisotropic effects on remote positions. *Tetrahedron* 1997;53:8541–8564.
46. Seco JM, Tseng LH, Godejohann M, Quinoa E, Riguera R. Simultaneous enantioresolution and assignment of absolute configuration of secondary alcohols by directly coupled HPLC-NMR of 9-AMA esters. *Tetrahedron: Asymmetry* 2002;13:2149–2153.
47. Seco JM, Quinoa E, Riguera R. The assignment of absolute configuration by NMR. *Chem Rev* 2004;104:17–117.
48. Seco JM, Quinoa E, Riguera R. The assignment of absolute configurations by NMR of arylmethoxyacetate derivatives: is this methodology being correctly used? *Tetrahedron: Asymmetry* 2000;11:2781–2791.
49. Takahashi T, Fukuishima A, Tanaka Y, Takeuchi Y, Kabuto K, Kabuto C. CFTA, a new efficient agent for determination of absolute configurations of chiral secondary alcohols. *Chem Commun* 2000;787–788.
50. Fujiwara T, Sasaki M, Omata K, Kabuto C, Kabuto K, Takeuchi Y. An efficient procedure for the resolution of  $\alpha$ -cyano- $\alpha$ -fluoro-*p*-tolylacetic acid (CFTA) via the diastereomeric *N*-carbobenzyloxy-*cis*-1-amino-2-indanol esters. *Tetrahedron: Asymmetry* 2004;15:555–563.

51. Kuwahara S, Fujita K, Watanabe M, Harada N, Ishida T. Enantioresolution and absolute stereochemistry of 2-(1-naphthyl)propane-1,2-diol and related compounds. *Enantiomer* 1999;4:141–145.
52. Harada N, Watanabe M, Kuwahara S, Sugio A, Kasai Y, Ichikawa A. 2-Methoxy-2-(1-naphthyl)propionic acid, a powerful chiral auxiliary for enantioresolution of alcohols and determination of their absolute configurations by the  $^1\text{H}$  NMR anisotropy method. *Tetrahedron: Asymmetry* 2000;11:1249–1253.
53. Tajiri H, Kasai Y, Sugio A, Kuwahara S, Watanabe M, Harada N, Ichikawa A. Practical enantioresolution of alcohols with 2-methoxy-2-(1-naphthyl)propionic acid and determination of their absolute configurations by the  $^1\text{H}$  NMR anisotropy method. *Chirality* 2002;14:81–84.
54. Kasai Y, Watanabe M, Harada N. Convenient method for determining the absolute configuration of chiral alcohols with racemic  $^1\text{H}$  NMR shift reagent,  $\text{M}\alpha\text{NP}$  acid. Use of HPLC–CD detector. *Chirality* 2003;15:295–299.
55. Nishimura T, Tajiri H, Harada N. Absolute configuration of the thyroid hormone analogue KAT-2003 as determined by the  $^1\text{H}$  NMR anisotropy method with a novel chiral auxiliary,  $\text{M}\alpha\text{NP}$  acid. *Chirality* 2004;16:13–21.
56. Kasai Y, Tajiri H, Fujita T, Yamamoto Y, Akagi M, Sugio A, Kuwahara S, Watanabe M, Harada N, Ichikawa A, Schurig V.  $\text{M}\alpha\text{NP}$  acid, a powerful chiral molecular tool for preparation of enantiopure alcohols by resolution and determination of their absolute configurations by the  $^1\text{H}$  NMR anisotropy method. *Chirality* 2004;16:569–585.
57. Kasai Y, Shimanuki K, Kuwahara S, Watanabe M, Harada N. Preparation of enantiopure Wieland-Miescher ketone and derivatives by the  $\text{M}\alpha\text{NP}$  acid method. Substituent effect on the HPLC separation. *Chirality* 2006;18:177–187.
58. Kasai Y, Sugio A, Sekiguchi S, Kuwahara S, Matsumoto M, Watanabe M, Ichikawa A, Harada N. Conformational analysis of  $\text{M}\alpha\text{NP}$  esters, powerful chiral resolution and  $^1\text{H}$  NMR anisotropy tools. Aromatic geometry and solvent effects on  $\Delta\delta$  values. *Eur J Org Chem* 2006;1811–1826.
59. Kasai Y, Naito J, Kuwahara S, Watanabe M, Ichikawa A, Harada N. Novel chiral molecular tools for preparation of enantiopure alcohols by resolution and simultaneous determination of their absolute configurations by the  $^1\text{H}$  NMR anisotropy method. *J Synth Org Chem* 2004;62:1114–1127.
60. Tajiri H, Watanabe M, Harada N, Naoki H, Ueda Y. Diastereomer method for determining  $[\text{M}]_D$  by  $^1\text{H}$  NMR and/or MS spectrometry with complete removal of the kinetic resolution effect. *Org Lett* 2002;4:2699–2702.
61. Ichikawa A, Ono H, Harada N. Synthesis and analytical properties of (S)-(+)-2-methoxy-2-(9-phenanthryl)propionic acid. *Tetrahedron: Asymmetry* 2003;14:1593–1597.
62. Ichikawa A, Ono H, Harada N. Stereochemical studies of chiral resolving agents, M9PP and H9PP acids. *Chirality* 2004;16:559–567.
63. Wenzel TJ. Discrimination of chiral compounds using NMR spectroscopy. USA: John Wiley; 2007.
64. Harada N, Koumura N, Robillard M. Chiral dichlorophthalic acid amide: an improved chiral auxiliary useful for enantioresolution and X-ray crystallographic determination of absolute stereochemistry. *Enantiomer* 1997;2:303–309.
65. Harada N, Nehira T, Soutome T, Hiyoshi N, Kido F. Chiral phthalic acid amide, a chiral auxiliary useful for enantiomer resolution and X-ray crystallographic determination of the absolute stereochemistry of alcohols. *Enantiomer* 1996;1:35–39.
66. Kosaka M, Kuwahara S, Watanabe M, Harada N, Job GE, Pirkle WH. Comparison of CD spectra of (2-methylphenyl)- and (2,6-dimethylphenyl)-phenylmethanols leads to erroneous absolute configurations. *Enantiomer* 2002;7:213–218.
67. Harada N, Fujita K, Watanabe M. Enantioresolution and absolute stereochemistry of diarylmethanols. *Enantiomer* 1997;2:359–366.
68. Harada N, Fujita K, Watanabe M. Molecular chirality by isotopic substitution. Synthesis, absolute configuration, and CD spectra of  $^{13}\text{C}$  substituted chiral diphenylmethanol. *J Phys Org Chem* 2000;13:422–425.
69. Kuwahara S, Watanabe M, Harada N, Koizumi M, Ohkuma T. Enantioresolution and absolute stereochemistry of *o*-substituted diphenylmethanols. *Enantiomer* 2000;5:109–114.
70. Watanabe M, Kuwahara S, Harada N, Koizumi M, Ohkuma T. Enantioresolution by the chiral phthalic acid method: absolute configurations of (2-methylphenyl)phenylmethanol and related compounds. *Tetrahedron: Asymmetry* 1999;10:2075–2078.
71. Kosaka M, Watanabe M, Harada N. Enantioresolution by the chiral phthalic acid method: Absolute configurations of substituted benzylic alcohols. *Chirality* 2000;12:362–365.
72. Harada N, Hiyoshi N, Vassilev VP, Hayashi T. Synthesis, circular dichroism, and absolute stereochemistry of 1,1':4',1''-ternaphthalene compounds. *Chirality* 1997;9:623–625.
73. Harada N, Vassilev VP, Hiyoshi N. Absolute configuration and conformation of 1,1':4',1''-ternaphthalene compounds as determined by X-ray crystallography. *Enantiomer* 1997;2:123–126.
74. Naito J, Kosaka M, Sugito T, Watanabe M, Harada N, Pirkle WH. Enantioresolution of fluorinated diphenylmethanols and determination of their absolute configurations by X-ray crystallographic and  $^1\text{H}$  NMR anisotropy methods. *Chirality* 2004;16:22–35.
75. Kosaka M, Sugito T, Kasai Y, Kuwahara S, Watanabe M, Harada N, Job GE, Shvet A, Pirkle WH. Enantioresolution and absolute configurations of chiral meta-substituted diphenylmethanols as determined by the X-ray crystallographic and  $^1\text{H}$  NMR anisotropy methods. *Chirality* 2003;15:324–328.
76. ter Wiel MKJ, van Delden RA, Meetsma A, Feringa BL. Increased speed of rotation for the smallest light-driven molecular motor. *J Am Chem Soc* 2003;125:15076–15086.
77. Goto J, Hasegawa M, Nakamura S, Shimada K, Nambara T. New derivatization for liquid chromatographic resolution of amino acid enantiomers. *Chem Pharm Bull* 1977;25:847–849.
78. Goto J, Hasegawa M, Nakamura S, Shimada K, Nambara T. New derivatization reagents for the resolution of amino acid enantiomers by high-performance liquid chromatography. *J Chromatogr* 1978;152:413–419.
79. Ichikawa A. Application of  $\alpha\text{MNPA}$  to stereochemical studies of monoterpene alcohol. *Chirality* 1999;11:70–74.
80. Akasaka K, Gyimesi-Forras K, Lammerhofer M, Fujita T, Watanabe M, Harada N, Lindner W. Investigations of molecular recognition aspects related to the enantiomer separation of 2-methoxy-2-(1-naphthyl)propionic acid using quinine carbamate as chiral selector: an NMR and FT-IR spectroscopic as well as X-ray crystallographic study. *Chirality* 2005;17:544–555.
81. Naito J, Tajiri H, Sekiguchi S, Watanabe M, Kuwahara S, Watanabe M, Harada N. A new route to enantiopure  $\text{M}\alpha\text{NP}$  acid, a powerful resolution and chiral  $^1\text{H}$  NMR anisotropy reagent. *Chirality* 2007; 19: 335–343.
82. Ichikawa A, Hiradate S, Sugio A, Kuwahara S, Watanabe M, Harada N. Absolute stereochemistry of 2-hydroxy-2-(1-naphthyl)propionic acid as determined by the  $^1\text{H}$  NMR anisotropy method. *Tetrahedron: Asymmetry* 1999;10:4075–4078.
83. Ichikawa A, Hiradate S, Sugio A, Kuwahara S, Watanabe M, Harada N. Absolute configuration of 2-methoxy-2-(2-naphthyl)propionic acid, as determined by the  $^1\text{H}$  NMR anisotropy method. *Tetrahedron: Asymmetry* 2000;11:2669–2675.
84. Ichikawa A, Ono H, Hiradate S, Watanabe M, Harada N. Absolute configuration of 2-methoxy-2-(1-naphthyl)propionic and 2-methoxy-2-(2-naphthyl)propionic acids as determined by the phenylglycine methyl ester (PGME) method. *Tetrahedron: Asymmetry* 2002;13:1167–1172.
85. Gyimesi-Forras K, Akasaka K, Lammerhofer M, Fujita T, Tajiri H, Watanabe M, Harada N, Lindner W. Enantiomer separation of a powerful chiral auxiliary, 2-methoxy-2-(1-naphthyl)propionic acid by liquid chromatography using chiral anion exchanger type stationary phases in polar-organic mode; Investigation of molecular recognition aspects. *Chirality* 2005;17:S134–S142.
86. Naito J, Yamamoto Y, Akagi M, Sekiguchi S, Watanabe M, Harada N. Unambiguous determination of the absolute configurations of acetylene alcohols by combination of the Sonogashira reaction and the CD exciton chirality method—Exciton coupling between phenylacetylene and benzoate chromophores. *Monatsh Chem* 2005;136:411–445.
87. Kosaka M, Sekiguchi S, Naito J, Kuwahara S, Watanabe M, Harada N, Hiroi K. Synthesis of enantiopure phthalides including 3-butyl-

- phthalide, a fragrance component of celery oil, and determination of their absolute configurations. *Chirality* 2005;17:218–232.
88. Fujita T, Obata K, Kuwahara S, Miura M, Nakahashi A, Monde K, Decatur J, Harada N. (*R*)-(+)-[VCD(+)]945]-4-Ethyl-4-methyloctane, the simplest chiral saturated hydrocarbon with a quaternary stereogenic center. *Tetrahedron Lett* 2007;48:4219–4222.
89. Okumura Y, Ando A, William Stevens R, Shimizu M. Efficient and practical synthesis of both enantiomers of 3-phenylcyclopentanol derivatives. *Tetrahedron* 2002;58:8729–8736.
90. Imamura Y, Takikawa H, Sasaki M, Mori K. Triterpenoid total synthesis. Synthesis and absolute configuration of mispyric acid. *Org Biomol Chem* 2004;2:2236–2244.
91. Ichikawa A, Ono H. Preparation of single-enantiomer semiochemicals using 2-methoxy-2-(1-naphthyl)propionic acid and 2-methoxy-2-(9-phenanthryl)propionic acid. *Tetrahedron: Asymmetry* 2005; 16:2559–2568.
92. Ichikawa A, Ono H. Preparation of single-enantiomer 2-methyl-4-heptanol, a pheromone of *Metamasius hemipterus*, using (*S*)-2-methoxy-2-(1-naphthyl)propionic acid. *J Chromatog A* 2006;1117:38–46.
93. Ochi T, Sakamoto M, Minamida A, Suzuki K, Ueda T, Une T, Toda H, Matsumoto K, Terauchi Y. Syntheses and properties of the major hydroxy metabolites in humans of blonanserin AD-5423, a novel antipsychotic agent. *Bioorg Med Chem Lett* 2005; 15:1055–1059.
94. Narumi F, Hattori T, Yamabuki W, Kabuto C, Kameyama H. Resolution of inherently chiral *anti-O,O'*-dialkylated calix[4]arenes and determination of their absolute stereochemistries by CD and X-ray methods. *Tetrahedron: Asymmetry* 2005;16:793–800.
95. Fujita Y, Oguri H, Oikawa H. The relative and absolute configuration of PF1140. *J Antibiot* 2005;58:425–427.
96. Helmchen G, Nill G, Flockerzi D, Schule W, Youssef MSK. Extreme liquid chromatographic separation effects in the case of diastereomeric amides containing polar substituents. *Angew Chem Int Ed Engl* 1979;18:62–63.
97. Helmchen G, Nill G, Flockerzi D, Youssef MSK. Preparative scale directed resolution of enantiomeric carboxylic acids and lactones via liquid chromatography and neighboring-group assisted hydrolysis of diastereomeric amides. *Angew Chem Int Ed Engl* 1979;18:63–65.
98. Arita S, Yabuuchi T, Kusumi T. Resolution of 1- and 2-naphthyl-methoxyacetic acids, NMR reagents for absolute configuration determination, by use of L-phenylalaninol. *Chirality* 2003;15:609–614.



## Review Article

# Determination of Absolute Configuration of Secondary Alcohols Using Lipase-Catalyzed Kinetic Resolutions

QING JING AND ROMAS J. KAZLAUSKAS\*

*Department of Biochemistry, Molecular Biology, and Biophysics and the Biotechnology Institute, University of Minnesota, Saint Paul, Minnesota*

**ABSTRACT** Lipases show high enantioselectivity toward a wide range of secondary alcohols. An empirical rule based on the relative sizes of the substituents predicts which enantiomer reacts faster. X-ray structures of lipases provide a molecular basis for this empirical rule: their alcohol-binding pocket contains large hydrophobic pocket open to solvent and another smaller pocket. This predictable enantiopreference of lipases allows the determination of the absolute configuration of secondary alcohols using lipase-catalyzed kinetic resolution. Researchers have used this relative method to determine the configuration of ~50 secondary alcohols either as the only method or in combination with other methods. *Chirality* 20:724–735, 2008. © 2008 Wiley-Liss, Inc.

**KEY WORDS:** kinetic resolution; lipases; secondary alcohol; absolute configuration; empirical rule; enantioselectivity

## INTRODUCTION

Determining the absolute configuration of a molecule by kinetic resolution is a relative, not an absolute, method for determining configuration. It is not based on first principles of molecular structure, but on a similarity to molecule with already established absolute configuration. If the two behave similarly, the configurations are the same; if the two behave differently, then their configuration is opposite. The reliability of the method rests on the similarity of the unknown molecule and the molecule with established absolute configuration in the kinetic resolution. The focus of this reviews the determination of absolute configuration of secondary alcohols using lipase-catalyzed kinetic resolution. In most cases the primary goal of these kinetic resolutions is the preparation of enantiopure secondary alcohol and the determination of absolute configuration is a secondary goal.

Ziffer's group was the first to propose using enantioselective hydrolysis of esters to determine absolute configuration of secondary alcohols in the early 1980s.<sup>1–3</sup> They used cultures of *Rhizopus nigricans* (a common bread mold) that contained a secreted enantioselective esterase. They tested 22 acyclic secondary alcohols<sup>2</sup> and 26 cyclic secondary alcohols<sup>3</sup> with known absolute configuration and confirmed that a simple rule can predict which enantiomer reacts faster based on the relative sizes of the two substituents in the secondary alcohol.

Later many groups reported that this rule also applies to commercial enzymes, Table 1. This shift from cultures of microorganisms, which are unfamiliar and inconvenient for most organic chemists, to commercial enzymes, which can be stored and handled like chemical reagents, greatly

expanded the synthetic usefulness of these kinetic resolutions. Researchers found that lipases show high enantioselectivity toward a wide range of secondary alcohols and have resolved hundreds of secondary alcohols. These examples, together with the X-ray structures of lipases (see below) have increased confidence in this rule and now permit researchers to use it as a method to determine absolute configuration.

The empirical rule only applies to secondary alcohols. Although lipases also catalyze the enantioselective hydrolysis of primary alcohols, lactones, carboxylic acids, and others, the empirical rule above does not apply to them. Researchers have not yet found reliable and general empirical rules for these other classes of molecules because apparently minor changes in substituents can reverse the enantiopreference.<sup>18</sup> An example of the difficulties is the proposal of two opposite empirical rules to predict the enantiopreference of porcine pancreatic lipase toward primary alcohols.<sup>19</sup> Clearly, neither proposed rule for primary alcohols is reliable.

## General Procedure for Determination of Absolute Configuration

The determination of absolute configuration correlates the predicted structure of the fast-reacting enantiomer in

\*Correspondence to: Romas Kazlauskas, Department of Biochemistry, Molecular Biology, and Biophysics and the Biotechnology Institute, University of Minnesota, Saint Paul, MN 55106-6104. E-mail: rjk@umn.edu.

Received for publication 12 October 2007; Accepted 6 December 2007

DOI: 10.1002/chir.20543

Published online 15 February 2008 in Wiley InterScience (www.interscience.wiley.com).



TABLE 1. Sized-based rules similar to those in Figure 1 proposed for commercially available lipases

Lipase	Comments	Reference
<i>Candida antarctica</i> lipase B, CAL-B <sup>a</sup>		4
<i>Burkholderia cepacia</i> lipase, BCL, lipase PS <sup>b</sup>		5–9
<i>Candida rugosa</i> lipase, CRL <sup>c</sup>	86 Substrates; reliable for cyclic, but not acyclic, substrates	7
<i>Pseudomonas aeruginosa</i> lipase, PAL <sup>c</sup>	28 Substrates	10
<i>Pseudomonas fluorescens</i> lipase, PFL, lipase AK <sup>b</sup>	31 Substrates	11
<i>Pseudomonas fluorescens</i> lipase, PFL, lipase YS <sup>b</sup>	27 Substrates	12, 13
Porcine pancreatic lipase, PPL <sup>c</sup>		14, 15
<i>Rhizomucor miehei</i> lipase, RML <sup>c</sup>	6 Substrates	16
Bovine cholesterol esterase, CE <sup>c</sup>	15 Substrates	7
<i>Alcaligenes</i> sp. lipase, lipase QL <sup>b</sup>	27 Substrates	17

<sup>a</sup>Manufactured by Novozymes, available from Sigma or Fluka.

<sup>b</sup>Manufactured by Amano Pharmaceutical Company, Nagoya, Japan. The Amano trade name for these lipase is also indicated. Amano PS was previously known as *Pseudomonas cepacia* lipase.

<sup>c</sup>Multiple commercial sources; for example, Sigma or Fluka.

Figure 1 with an experimentally measured property of the actual fast-reacting enantiomer. The steps below outline a recommended procedure.

1. For a reliable determination, the structure of the alcohol should have a large difference in the sizes of the two substituents (large and medium in Fig. 1). For increased reliability choose a lipase or esterase that shows good enantioselectivity ( $E \geq 20$ , preferably  $>50$ ) toward a structurally similar secondary alcohol with established absolute configuration. The closer is the similarity in structure the more reliable is the assignment.
2. Resolve the racemic sample with this lipase: For example, combine equal weights of lipase powder and racemic secondary alcohol in vinyl acetate with or without added organic solvent. Monitor the reaction by a convenient method (e.g., thin layer chromatography, gas, or liquid chromatography) and stop the reaction at ~40% conversion. Separate the product acetate and unreacted alcohol by an appropriate method.
3. Measure the enantiomeric purity of the product acetate, including some property of the favored enantiomer. For example, separation of enantiomers by chromatography on a chiral stationary phase establishes whether the favored enantiomer elutes first or second, NMR measurement with a chiral shift reagent establishes an upfield or downfield shift for the favored enantiomer, or optical rotation establishes whether the favored enantiomer has a (+) or (–) rotation.
4. Calculate the enantioselectivity of the kinetic resolution from the enantiomeric purity of the product ester and percent conversion of the reaction.<sup>20</sup> If the percent conversion is difficult to measure, alternatively, one can measure the enantiomeric purity of the remaining starting material and use this value in the calculation. The enantioselectivity should be  $\geq 20$ , preferably  $>50$  for a reliable determination of absolute configuration. If the enantioselectivity is too low, try several other lipases to find one with higher enantioselectivity. The enantioselectivity,  $E$ , refers to the relative rates of formation of the fast-reacting enantiomer vs. the slow-reacting enantiomer.

5. The predicted configuration of the product alcohol acetate is in Figure 1. Thus, depending on the measurement made in Step 4, one can match some easily measured behavior of the enantiomer with its absolute configuration. For example, one could conclude that the fast-eluting peak corresponds to the (*R*)-enantiomer, that the upfield shift in the presence of the shift reagent corresponds to the (*R*)-enantiomer or something similar.
6. [optional] Measure the optical rotation of the favored product enantiomer to correlate the sign of rotation to the absolute configuration.

The key factors for high reliability are (1) a large difference in the size of the two substituents so that the rule in Figure 1 can be applied unambiguously, (2) high enantioselectivity in the kinetic resolution showing that the lipase strongly favors one enantiomer, and (3) known enantio-preference of the chosen lipase with similar secondary alcohols.

Variations in this general procedure are possible. For example, instead of resolving by acylation in an organic solvent, one can prepare the racemic acetate or butyrate ester of the secondary alcohol and resolve it by lipase-catalyzed hydrolysis in aqueous buffer at pH 6–8.

A similar empirical rule predicts the fast reacting enantiomer for primary amines of the type  $\text{NH}_2\text{CHR}^1\text{R}^2$  where  $\text{R}^1$  and  $\text{R}^2$  are large and medium substituents. These amines are isosteric with secondary alcohols. Lipases are very slow catalyst for the hydrolysis of amides, but are

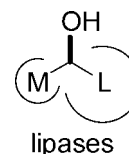


**Fig. 1.** An empirical rule to predict which enantiomer of a secondary alcohol reacts faster in lipase-catalyzed reactions. M, medium-sized substituent, e.g., methyl. L, large substituent, e.g., phenyl. In acylation reactions, the enantiomer shown reacts faster; in hydrolysis reactions, the ester of the enantiomer shown reacts faster. This rule suggests that lipases distinguish between enantiomeric secondary alcohols primarily by comparing the sizes of the two substituents.

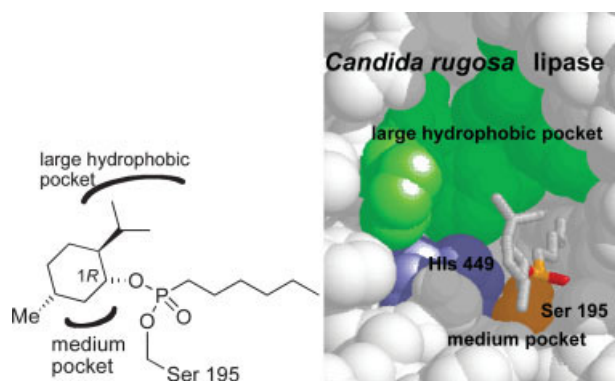


**Fig. 2.** Proposed binding site for secondary alcohols in lipase from *Candida rugosa*. Schematic of the phosphonate analog of a tetrahedral intermediate in the hydrolysis of (1*R*)-menthyl heptanoate (fast-reacting enantiomer). X-ray structure of this phosphonate analog (sticks representation) in the active site lipase from *Candida rugosa* (space-filling representation). Colors indicate the large hydrophobic pocket (green) and the catalytic residues Ser 209 (orange), His 449 (purple). The large substituent of the menthyl moiety (top half of cyclohexyl ring including the isopropyl substituent) binds in the large hydrophobic pocket, while the medium substituent (bottom part of the cyclohexyl ring including the methyl substituent) binds in the medium pocket.

good catalysts for the acylation of amines. No one has yet used a lipase catalyzed kinetic resolution to determine the absolute configuration of an amine, mostly likely because these resolutions are less common than for secondary alcohols.

This determination of absolute configuration by lipase-catalyzed kinetic resolution, like other kinetic resolution methods, is a relative, not an absolute method. It relies on the similar behavior of the secondary alcohol with unknown configuration and known configuration. Like all relative methods for determination of absolute configuration, it is less reliable than absolute methods such as chemical correlation, anomalous scattering of X-rays or excitation chirality.

### Theoretical Justification

X-ray structures of transition state analogs containing a secondary alcohol, menthol, bound to CRL identified the alcohol binding pocket, Figure 2.<sup>21</sup> Crude CRL is moderately enantioselective toward (1*R*)-enantiomer of menthyl esters ( $E \sim 15$ ), but the purified isozyme shown in the structure below is highly enantioselective ( $E > 100$ ).<sup>22</sup> The alcohol-binding pocket indeed resembles the empirical rule: a large hydrophobic pocket and a smaller pocket for the medium-sized substituent, Figure 2.

The structures of several other lipases also show alcohol-binding regions with one large hydrophobic pocket and a medium pocket, consistent with the notion that the empirical rule in Figure 1 applies to all lipase and esterases. Lipases and esterases all adopt the same protein fold and this fold likely causes this similarity in the alcohol-binding region. Lipases and esterases all adopt the  $\alpha/\beta$ -hydrolase fold and have similar catalytic machinery. As the protein folds to orient the catalytic machinery, it also creates the medium-substituent pocket. A loop that positions

the catalytic histidine forms the left side of the pocket (left refers to the orientation in Fig. 2 above), a loop that positions the catalytic serine forms the bottom of the pocket and finally a loop that positions one of the oxyanion-hole residues forms the right side of the medium binding pocket. Several helices common to the  $\alpha/\beta$ -hydrolase fold similarly create the large hydrophobic pocket. Other experimental support for the empirical rule are the ability to increase the enantioselectivity of lipase-catalyzed reactions by modifying the substrate to increase the size of the large substituent (for examples see: Refs. 7, 23–26) or even reverse the enantioselectivity by converting the medium substituent into the larger one.<sup>27</sup>

The most common lipases used for determination of absolute configuration are lipase from *Burkholderia cepacia* (BCL) and lipase B from *Candida antarctica* (CAL-B). These lipases show high enantioselectivity toward a wide range of secondary alcohols<sup>28</sup> and reliably follow the empirical rule for both cyclic and acyclic secondary alcohols. In contrast, only cyclic secondary alcohols reliably follow the empirical rule for lipase from *Candida rugosa*, possibly because its active site is wider. X-ray structures of BCL containing a transition state analog for hydrolysis of the fast-reacting enantiomer of secondary alcohol acetate<sup>29</sup> show large- and medium-sized pockets in the same orientation as discussed above for CRL. X-ray structures of CAL-B also show similar pockets<sup>30</sup> and molecular modeling suggest a similar catalytically productive orientation for the fast-reacting enantiomer.<sup>31</sup>

### Examples

We found 35 examples where lipase-catalyzed kinetic resolution was the primary method to assign the absolute configuration of a secondary alcohol, Table 2. The majority of the resolutions use either *Burkholderia cepacia* lipase (BCL) or lipase B from *Candida antarctica* (CAL-B). Approximately half of the examples are acyclic secondary alcohols, usually with an aromatic group as the large substituent. The other half contains cyclic secondary alcohols on five- or six-membered rings. In most cases, the resolution was highly enantioselective ( $E > 20$ ). Further, in approximately half of the examples, researcher refer to a reference compound, that is, a secondary alcohol whose absolute configuration has been established by other methods, whose structure is similar to the alcohol with unknown configuration, and which behaves similarly in the lipase-catalyzed resolutions. In some other cases (e.g., Entry 1) such a reference compound exists (1-phenylethanol), but was not specifically mentioned by the authors.

In most cases, the resolution involved acetylation of the racemic secondary alcohol with vinyl acetate. For example, Franssen and coworkers determined the absolute configuration of 1-(4-hydroxyphenyl)ethanol using a BCL-catalyzed acetylation,<sup>32</sup> Scheme 1. Injecting this reaction mixture onto a gas chromatography column with a chiral stationary phase ( $\beta$ -cyclodextrin) allowed the researchers to assign the (*R*)-configuration to the first eluting peak because it was the peak that corresponded to fast-reacting enantiomer. Injecting the unknown sample onto the same column identified whether it had the (*R*)- or (*S*)-configuration.

TABLE 2. Examples of secondary alcohols whose absolute configuration was assigned by lipase-catalyzed resolution

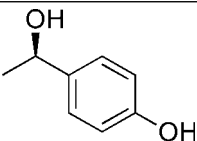
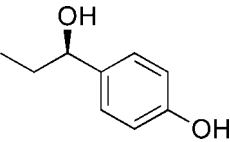
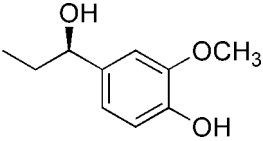
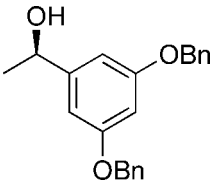
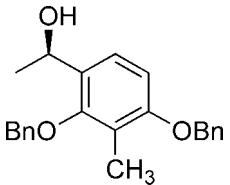
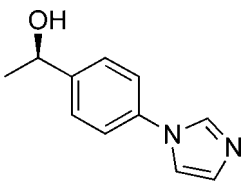
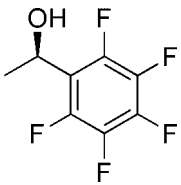
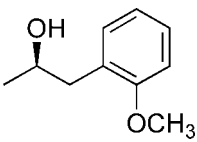
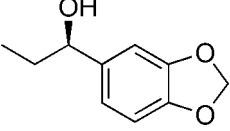
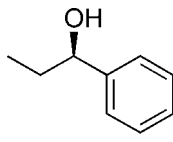
Entry	alcohol	Reagents and conditions	Reference compounds	Ref.
1		BCL, vinyl acetate, <i>E</i> high		32
2		BCL, vinyl acetate, <i>E</i> high		32
3		BCL, vinyl acetate, <i>E</i> high		32
4		BCL, vinyl acetate, <i>E</i> > 200		33
5		BCL, vinyl acetate, <i>E</i> = 29		33
6		BCL, vinyl acetate, <i>E</i> > 200		33
7		BCL, vinyl acetate, <i>E</i> > 200		33
8		BCL, vinyl acetate, <i>E</i> = 62		33
9		CAL-B, vinyl acetate, <i>E</i> > 200		34

TABLE 2. Continued

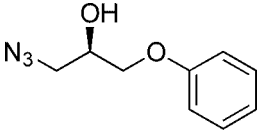
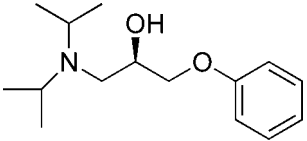
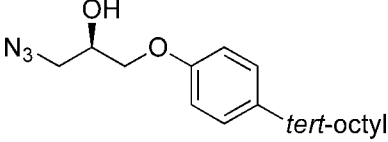
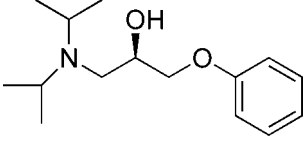
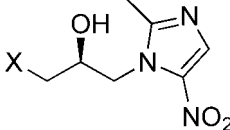
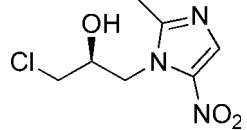
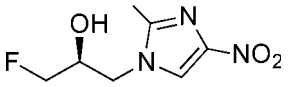
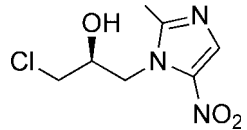
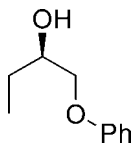
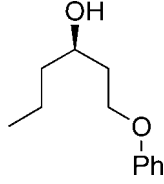
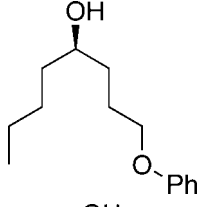
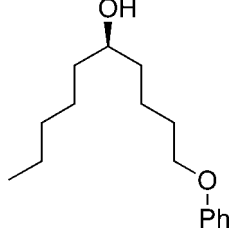
Entry	alcohol	Reagents and conditions	Reference compounds	Ref.
10 <sup>b</sup>		BCL, vinyl acetate, $E = 17$		9
11		BCL, vinyl acetate, $E = 29$		9
12	 X = F X = Br	BCL, vinyl acetate,  $E > 200$ $E = 29$		35
13		BCL, vinyl acetate, $E = 134$		35
14		PFL, vinyl acetate, $E = 50$		36
15 <sup>a</sup>		CRL, vinyl acetate, $E = 5$		36
16 <sup>a</sup>		CRL, vinyl acetate, $E = 20$		36
17 <sup>a</sup>		GCL, vinyl acetate, $E = 50$		36



TABLE 2. Continued

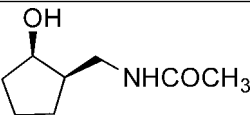
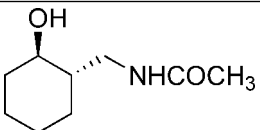
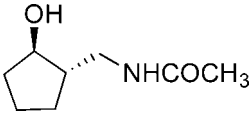
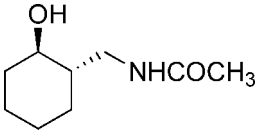
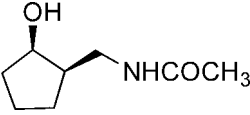
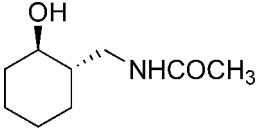
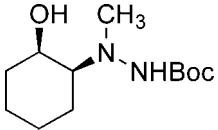
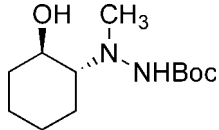
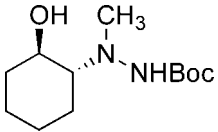
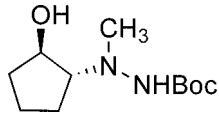
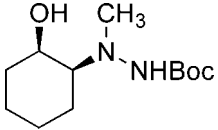
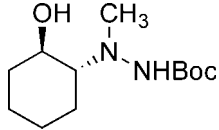
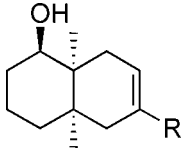
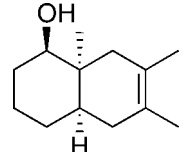
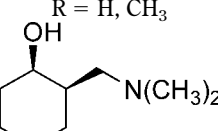
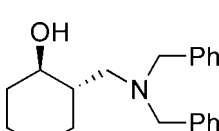
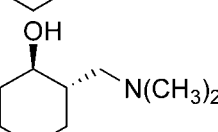
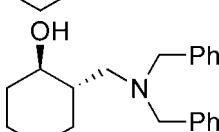
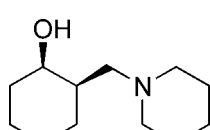
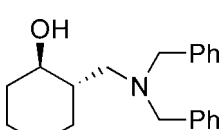
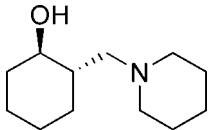
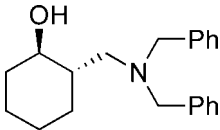
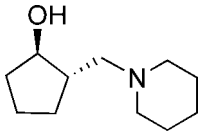
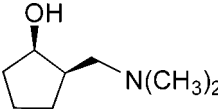
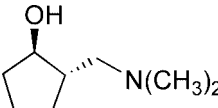
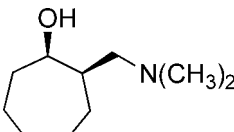
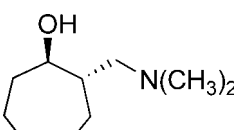
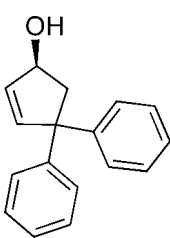
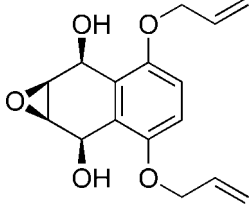
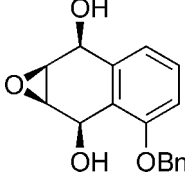
Entry	alcohol	Reagents and conditions	Reference compounds	Ref.
18		CAL-B, ethanolysis of acetate, $E > 200$		37
19 <sup>b</sup>		CAL-B, ethanolysis of acetate, $E = 17$		37
20		CAL-B, ethanolysis of acetate, $E = 78$		37
21		BCL, vinyl butyrate, $E > 200$		38
22 <sup>b</sup>		CAL-B, vinyl acetate, $E = 11$		38
23		BCL, vinyl acetate, $E > 200$		38
24		CAL-B, vinyl acetate, $E > 200$		39
25		BCL, vinyl acetate, $E > 200$		40
26		CAL-B, vinyl acetate, $E > 200$		40
27		BCL, vinyl acetate, $E > 200$		40

TABLE 2. Continued

Entry	alcohol	Reagents and conditions	Reference compounds	Ref.
28		CAL-B, vinyl acetate, $E > 200$		40
29		BCL, vinyl acetate, $E > 200$		41
30		CAL-B, vinyl acetate, $E > 200$		41
31		CAL-B, vinyl acetate, $E > 200$		41
32		BCL, vinyl acetate, $E > 200$		42
33		BCL, vinyl acetate, $E > 200$		42
34 <sup>c</sup>		BCL, isopropenyl acetate, $E = 8$		42
35		CAL-B, isopropenyl acetate, $E \sim 100$		43

<sup>a</sup>These assignments are questionable. See text for details. GCL: *Geotrichum candidum* lipase.

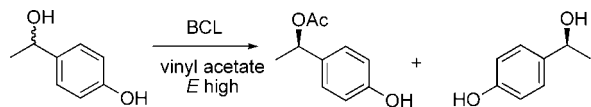
<sup>b</sup>Enantioselectivity is below 20, but the comparison with a closely related compound with known absolute configuration adds confidence to the assignment.

<sup>c</sup>The original paper incorrectly applied the empirical rule (see caution 1 in text). The structure shown is the corrected assignment.

In other cases, researchers used alcoholysis of the racemic acetate,<sup>37</sup> Scheme 2.

In one case, researchers used not a resolution, but a desymmetrization of a mesocompound, Entry 35, Scheme 3. CAL-B-catalyzed the acetylation of the meso diol with

high selectivity. The configuration of the fast-reacting alcohol group was assigned as (*S*) because the structure of the (*S*)-alcohol fits the empirical rule. Mosher ester derivative analysis by NMR confirmed the high stereoselectivity.<sup>43</sup>



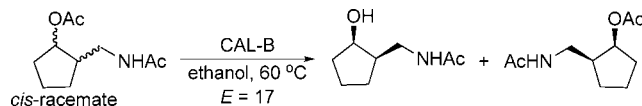
**Scheme 1.** Kinetic resolution of a secondary alcohol by BCL-catalyzed acetylation.

The assignments of absolute configuration for Entries 15 and 16 are questionable for four reasons. First, the lipase chosen for the resolution—lipase from *Candida rugosa* (CRL)—follows the empirical rule in Figure 1 only for cyclic secondary alcohols, but is not reliable for acyclic secondary alcohols such as those in the example.<sup>7</sup> The molecular basis for this lack of reliability is likely the larger active site pocket for CRL as compared with the other lipases. Second, the substrates in Entries 15 and 16 have similar sizes for the three or four atoms closest to the secondary alcohol. These atoms interact with the active site most closely and lead to the largest discrimination between enantiomers. Their similarity lowers the confidence with which one can apply the empirical rule to these substrates. Third, the enantioselectivity for the resolution in Entry 15 is only moderate ( $E = 5$ ), which also lowers the confidence in the assignment. Fourth, there is no reference compound—a compound with the similar structure, but known absolute configuration that behaves similarly in this resolution.

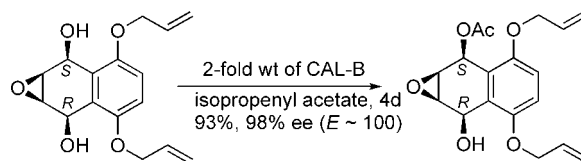
The assignment of absolute configuration for Entry 17 is also questionable. Only limited data are available for lipase from *Geotrichum candidum*, but its structure is similar to that for lipase from *Candida rugosa*. It is uncertain if GCL reliably follows the empirical rule for both cyclic and acyclic secondary alcohols. Although the enantioselectivity in this example is high ( $E > 50$ ), the two substituents are identical for four methylene units from the stereocenter and are highly flexible. It is unusual to see such high enantioselectivity when the differences between substituents occur so far from the stereocenter.

In ~20 other cases, researchers combined lipase-catalyzed kinetic resolution with other methods to assign absolute configuration, Table 3. We did not include examples where researchers combined lipase-catalyzed resolution with a definitive method like X-ray crystallography, chemical correlation or even comparison to samples of known configuration. In these cases, the lipase-catalyzed resolution did not help to assign the absolute configuration. The examples in Table 3 are those where the kinetic resolution confirmed or verified another method.

Adam et al. resolved a series of  $\alpha$ -hydroxy acids by lipase-catalyzed acetylation (Entry 1, Table 3).<sup>44</sup> The absolute configurations of the  $\alpha$ -hydroxy acids were established by the exciton chirality method. This method, based



**Scheme 2.** Kinetic resolution of an ester by CAL-B-catalyzed ethanolysis.



**Scheme 3.** Desymmetrization of *meso*-diol by CAL-B-catalyzed acetylation. The (*S*)-alcohol fits the empirical rule.

on the through-space interaction between two chromophores, correlates the sign of the lower energy band in the circular dichroism spectrum with the relative orientation of the chromophores. With rigid structures and well-understood chromophores, the exciton chirality method is unambiguous and is considered an absolute method comparable with the anomalous dispersion in X-ray crystallography. To apply the exciton chirality method, Adam et al. converted the enantioenriched  $\alpha$ -hydroxy acids to the bichromophoric 2-naphthoate 9-anthrylmethyl derivatives, Scheme 4. The relative orientation between these chromophores depends not only on the absolute configuration, but also on the conformation of the bonds connecting them. In previous work, Adam et al. showed that the exciton chirality method could assign the absolute configuration of  $\alpha$ -hydroxy acids, thus suggesting that the conformation along the bonds connecting the chromophores was predictable. It is likely that these new  $\alpha$ -hydroxy acids behave similarly, but the agreement of the assigned absolute configuration with the empirical rule in Figure 1 increased the level of confidence.

In similar manner, Cuiper et al. assigned the absolute configuration of pyrrolinones by the using exciton chirality (Entries 4–6), but since the chromophores were unusual for this technique, they confirmed the assignment with the empirical rule for lipase-catalyzed resolutions.<sup>47</sup>

Gotor's group assigned the absolute configuration of pyridyl alcohols by a combination of the sign of optical rotation, elution order in HPLC and the empirical rule for lipase-catalyzed resolutions (Entry 7). The derivatives where R = Me or Et have established absolute configurations and served as the reference compounds. The configuration of the unknown compounds (R = Pr and Bu) was established by their similar behavior in three tests mentioned.<sup>48</sup>

Zacchino resolved the threo diastereomer of 2-bromo-1-(3,4-dimethoxyphenyl)propan-1-ol by hydrolysis of the corresponding acetate using a culture of *Rhizopus nigricans*, Scheme 5. They assigned the absolute configuration of the fast-reacting enantiomer as (1*S*,2*S*) by both <sup>1</sup>H NMR of  $\alpha$ -methoxy- $\alpha$ -(trifluoromethyl)phenylacetate (MTPA) derivative and the empirical rule, Scheme 5.<sup>50</sup> This case required a combination of methods because the enantioselectivity of the hydrolysis was too low to make a reliable assignment on the empirical rule alone.

### Cautions

1. Substituent size, not the *R,S* nomenclature, predicts the fast-reacting enantiomer. In most cases the Cahn-Ingold-Prelog priority of L is higher than that of M, so

**TABLE 3. Examples of absolute configuration of secondary alcohols assigned by lipase-catalyzed resolution combined with other methods**

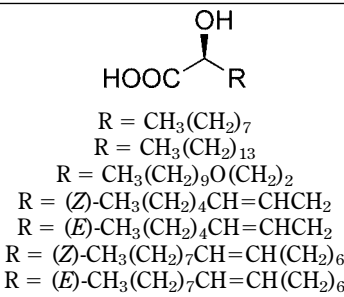
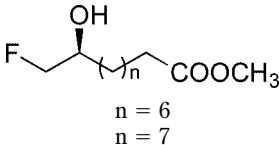
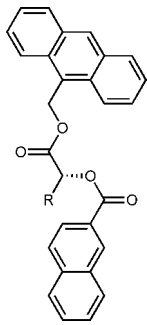
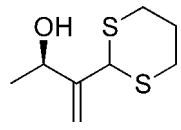
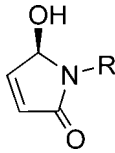
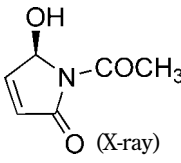
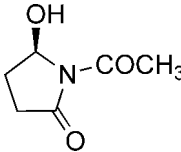
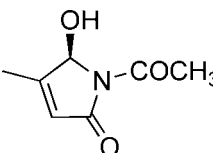
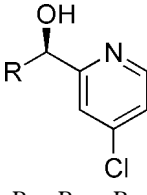
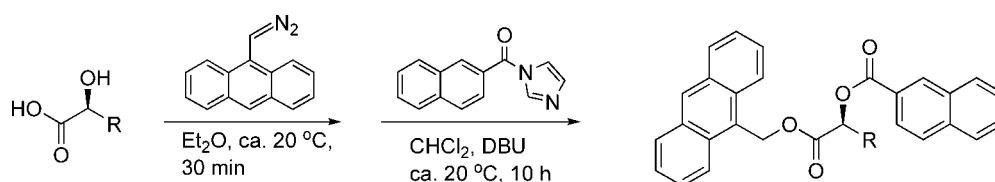
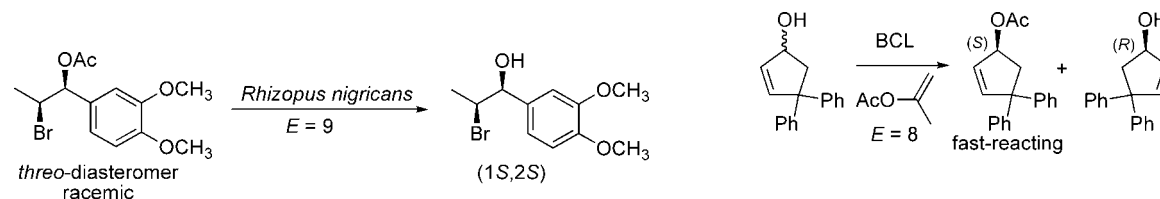
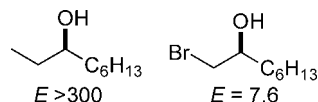
Entry	alcohol	Reagents and conditions	Other methods applied <sup>a</sup>	Ref.
1		CAL-B or BCL, vinyl acetate	Exciton chirality	44
2		BCL, Ac <sub>2</sub> O  <i>E</i> = 91 <i>E</i> = 33	 [α] <sub>D</sub> , CD	45
3		CAL-B, vinyl acetate, <i>E</i> > 200	Elution order on GC column with chiral stationary phase	46
4	 R = COC <sub>2</sub> H <sub>5</sub> R = CH <sub>3</sub> R = Ph R = COCH <sub>2</sub> SCH <sub>3</sub>	CAL-B, alcoholysis of acetate with <i>n</i> -BuOH  <i>E</i> > 200 <i>E</i> > 200 <i>E</i> > 61 <i>E</i> > 200	CD, [α] <sub>D</sub>   (X-ray)	47
5		CAL-B, alcoholysis of acetate with <i>n</i> -BuOH, <i>E</i> > 200	[α] <sub>D</sub>	47
6		CAL-B, alcoholysis of acetate with <i>n</i> -BuOH, <i>E</i> = 38	[α] <sub>D</sub>	47
7 <sup>b</sup>	 R = Pr or Bu	BCL, vinyl acetate, <i>E</i> > 200	HPLC, [α] <sub>D</sub>	48



TABLE 3. Continued

Entry	alcohol	Reagents and conditions	Other methods applied <sup>a</sup>	Ref.
8 <sup>c</sup>		HLL, vinyl acetate, $E = 17^b$	$[\alpha]_D$	49
9 <sup>c</sup>		HLL, vinyl acetate, $E = 56$	$[\alpha]_D$	49
10 <sup>c</sup>		HLL, vinyl acetate, $E = 68$	$[\alpha]_D$	49
11 <sup>c</sup>		HLL, vinyl acetate, $E = 56$	$[\alpha]_D$	49
12 <sup>c</sup>		HLL, vinyl acetate, $E = 14^b$	$[\alpha]_D$	49
13		<i>Rhizopus nigricans</i> , hydrolysis of acetate ester, $E = 9^b$	NMR of S-MTPA <sup>d</sup> ester	50

<sup>a</sup>See discussion in text.<sup>b</sup>Enantioselectivity is lower than 20, lowering the reliability of the assignment.<sup>c</sup>HLL: *Humicola lanuginosa* lipase.<sup>d</sup> $\alpha$ -methoxy- $\alpha$ -(trifluoromethyl)phenylacetate.**Scheme 4.** Functionalization of the  $\alpha$ -hydroxy acids to the corresponding bichromophoric diester to apply the exciton chirality method of determining absolute configuration.**Scheme 5.** Kinetic resolution of the threo diastereomer of 2-bromo-1-(3,4-dimethoxyphenyl)propan-1-ol by hydrolysis of its acetate ester. Because the enantioselectivity is low, the assignment of absolute configuration was confirmed by  $^1\text{H}$  NMR of the MTPA derivative.**Scheme 6.** The empirical rule in Figure 1 predicts which enantiomer of a secondary alcohol reacts faster based on the relative sizes of the substituents, not  $R,S$ -nomenclature. Either the ( $R$ )- or ( $S$ )-alcohol can be the fast-reacting one. In most cases it is the ( $R$ )-alcohol, but in this case the empirical rule predicts that the ( $S$ )-enantiomer reacts faster.



**Scheme 7.** Electronic effects can influence enantioselectivity, but steric effects remain more important and determine the enantiopreference. Although no one yet reported an example of electronic effects overwhelming steric effects, it remains a possibility and thus reference structures should not differ significantly in polarity from the unknown structures.

the fast-reacting enantiomer has the (*R*)-configuration. But in other cases, the priority is reversed and the rule predicts that the (*S*)-enantiomer reacts faster. For example, in Entries 12–13 and 35, Table 2 and entries 1, 2, and 13, Table 3 the (*S*)-enantiomer is the fast reacting one. In one case, researchers made an incorrect tentative assignment because they assumed the fast-reacting enantiomer would have the (*R*)-configuration.<sup>42</sup> Scheme 6 and Table 2, Entry 34 show the correct assignment. The enantioselectivity is low, so this assignment still needs confirmation by another method.

2. Steric effects are the most important determinant of lipase enantioselectivity, but electronic effects also influence enantioselectivity. For example, the CAL-B shows high enantioselectivity toward 3-nonanol ( $E > 300$ ), but low enantioselectivity toward 1-bromo-2-octanol ( $E = 7.6$ ) under the same conditions, Scheme 7.<sup>4,26</sup> Both an ethyl and a  $-\text{CH}_2\text{Br}$  group are similar in size, indicating that electronic effects lowers the enantioselectivity for the bromo-substituted compound. The best reference structures will be those that also match the polarity of the unknown.
3. Subtilisin-catalyzed kinetic resolutions of secondary alcohols should not be used to assign absolute configurations because the enantiopreference is less reliable. Lipases have a deep hydrophobic pocket for the large substituent of a secondary alcohol, while subtilisins have a shallow binding site and leave the large substituent in the solvent. For this reason, both the reaction solvent and substituent polarity strongly affect the enantiopreference of subtilisin.<sup>51</sup>
4. The empirical rule only predicts the configuration of secondary alcohols. It does not apply to primary alcohols, lactones, carboxylic acids, or other compounds even though lipases can catalyze enantioselective reactions of these other classes of compounds.

## CONCLUSION

An empirical rule based on the relative sized of the substituents reliably predicts which enantiomeric secondary alcohol reacts faster in lipase- and esterase-catalyzed kinetic resolutions. The X-ray structures of lipases and esterase revealed that the shape of the alcohol-binding pocket matches the empirical rule, thus providing a molecular basis for this rule. Absolute configurations can be assigned using this rule and are most reliable when the substituents clearly differ in size, the lipase show high enantioselectivity

and a closely related secondary alcohol with known absolute configuration behaves similarly.

## LITERATURE CITED

1. Kawai K, Imuta M, Ziffer H. Microbially mediated enantioselective hydrolysis of racemic acetates. *Tetrahedron Lett* 1981;22:2527–2530.
2. Ziffer H, Kawai K, Kasai M, Imuta M, Froussios C. Microbially mediated enantioselective ester hydrolyses utilizing *Rhizopus nigricans*. A new method of assigning the absolute stereochemistry of acyclic 1-arylalkanol. *J Org Chem* 1983;48:3017–3021.
3. Kasai M, Kawai K, Imuta M, Ziffer H. Enantioselective ester hydrolyses employing *Rhizopus nigricans*. A method of preparing and assigning the absolute stereochemistry of cyclic alcohols. *J Org Chem* 1984;49:675–679.
4. Orrenius C, Öhrner N, Rotticci D, Mattson A, Hult K, Norin T. Candida antarctica lipase B catalysed kinetic resolutions: substrate structure requirements for the preparation of enantiomerically enriched secondary alcohols. *Tetrahedron: Asymmetry* 1995;6:1217–1220.
5. Laumen KE. Esterhydrolasen—anwendung in der organischen Synthese: chirale Bausteine aus Estern prochiraler und racemischer Alkohole. Ph.D. Thesis, Bergische Universität Wuppertal, Germany, 1987.
6. Xie ZF, Suemune H, Sakai K. Stereochemical observation on the enantioselective hydrolysis using *Pseudomonas fluorescens* lipase. *Tetrahedron: Asymmetry* 1990;1:395–402.
7. Kazlauskas RJ, Weissfloch ANE, Rappaport AT, Cuccia LA. A rule to predict which enantiomer of a secondary alcohol reacts faster in reactions catalyzed by cholesterol esterase, lipase from *Pseudomonas cepacia*, and lipase from *Candida rugosa*. *J Org Chem* 1991;56:2656–2665.
8. Lemke K, Lemke M, Theil F. A three-dimensional predictive active site model for lipase from *Pseudomonas cepacia*. *J Org Chem* 1997;62:6268–6273.
9. Theil F, Lemke K, Ballschuh S, Kunath A, Schick H. Lipase-catalysed resolution of 3-(aryloxy)-1,2-propanediol derivatives—towards an Improved active site model of *Pseudomonas cepacia* lipase (Amano PS). *Tetrahedron: Asymmetry* 1995;6:1323–1344.
10. Kim MJ, Cho H. *Pseudomonas* lipases as catalysts in organic synthesis: specificity of lipoprotein lipase. *J Chem Soc Chem Commun* 1992;1411–1413.
11. Burgess K, Jennings LD. Enantioselective esterifications of unsaturated alcohols mediated by a lipase prepared from *Pseudomonas* sp. *J Am Chem Soc* 1991;113:6129–6139.
12. Naemura K, Ida H, Fukuda R. Lipase YS-catalyzed enantioselective transesterification of alcohols of bicarbocyclic compounds. *Bull Chem Soc Jpn* 1993;66:573–577.
13. Naemura K, Fukuda R, Murata M, Konishi M, Hirose K, Tobe Y. Lipase-catalyzed enantioselective acylation of alcohols: a predictive active site model for lipase YS to identify which enantiomer of an alcohol reacts faster in this acylation. *Tetrahedron: Asymmetry* 1995;6:2385–2394.
14. Janssen AJM, Klunder AJH, Zwanenburg B. Resolution of secondary alcohols by enzyme-catalyzed transesterification in alkyl carboxylates as the solvent. *Tetrahedron* 1991;47:7645–7662.
15. Lutz D, Huffer M, Gerlach D, Schreier P. Carboxylester-lipase-mediated reactions: a versatile route to chiral molecules. In: Teranishi R, Takeoka GR, Guentert M, editors. *Flavor precursors: thermal and enzymatic conversions*. Washington, DC: American Chemical Society; 1992. p 32–45.
16. Roberts SM. Use of enzymes as catalysts to promote key transformations in organic synthesis. *Philos Trans R Soc Lond B* 1989;324:577–587.
17. Naemura K, Murata M, Tanaka R, Yano M, Hirose K, Tobe Y. Enantioselective acylation of primary and secondary alcohols catalyzed by lipase QL from *Alcaligenes* sp.: a predictive active site model for lipase QL to identify which enantiomer of an alcohol reacts faster in this acylation. *Tetrahedron: Asymmetry* 1996;7:3285–3294.
18. Hultin PG, Mueseler FJ, Jones JB. Enzymes in organic synthesis. 48. Pig liver esterase and porcine pancreatic lipase catalyzed hydrolyses

- of 3,4-(isopropylidenedioxy)-2,5-tetrahydrofuran-yl diesters. *J Org Chem* 1991;56:5375–5380.
19. Wimmer Z. A suggestion to the PPL active site model dilemma. *Tetrahedron* 1992;48:8431–8436.
20. Chen CS, Fujimoto Y, Girdaukas G, Sih CJ. Quantitative analyses of biochemical kinetic resolutions of enantiomers. *J Am Chem Soc* 1982;104:7294–7299.
21. Cygler M, Grochulski P, Kazlauskas RJ, Schrag JD, Bouthillier F, Rubin B, Serregei AN, Gupta AK. Molecular basis for the chiral preference of lipases. *J Am Chem Soc* 1994;116:3180–3186.
22. Vorlova S, Bornscheuer UT, Gattfield I, Hilmer JM, Bertram HJ, Schmid RD. Enantioselective hydrolysis of D,L-menthyl benzoate to L-(–)-menthol by recombinant *Candida rugosa* lipase LIP1. *Adv Synth Catal* 2002;344:1152–1155.
23. Adam W, Mock-Knoblach C, Saha-Möller CR. Kinetic resolution of hydroxy vinylsilanes by lipase-catalyzed enantioselective acetylation. *Tetrahedron: Asymmetry* 1997;8:1441–1444.
24. Gupta AK, Kazlauskas RJ. Substrate modification to increase the enantioselectivity of hydrolases. A route to optically-active cyclic allylic alcohols. *Tetrahedron: Asymmetry* 1993;4:879–888.
25. Kim MJ, Choi YK. Lipase-catalyzed enantioselective transesterification of *O*-trityl 1,2-diols. Practical synthesis of (*R*)-tritylglycidol. *J Org Chem* 1992;57:1605–1607.
26. Rotticci D, Orrenius C, Hult K, Norin T. Enantiomerically enriched bifunctional sec-alcohols prepared by *Candida antarctica* lipase B catalysis. Evidence of non-steric interactions. *Tetrahedron: Asymmetry* 1997;8:359–362.
27. Shimizu M, Kawanami H, Fujisawa T. A lipase mediated asymmetric hydrolysis of 3-acyloxy-1-octynes and 3-(*E*)-acyloxy-1-octenes. *Chem Lett* 1992;21:107–110.
28. Bornscheuer UT, Kazlauskas RJ. Hydrolases in organic synthesis. Regio- and stereoselective biotransformations, 2nd ed. Weinheim: Wiley-VCH; 2005. Chapter 5.
29. Luić M, Tomić S, Lešćić I, Ljubović E, Šepac D, Šunjić V, Vitale L, Saenger W, Kojić-Prodić B. Complex of *Burkholderia cepacia* lipase with transition state analogue of 1-phenoxy-2-acetoxybutane. *Eur J Biochem* 2001;268:3964–3973.
30. Uppenberg J, Öhrner N, Norin M, Hult K, Kleywegt GJ, Patkar S, Waagen V, Anthonsen T, Jones TA. Crystallographic and molecular modelling studies of lipase B from *Candida antarctica* reveal a stereospecificity pocket for secondary alcohols. *Biochemistry* 1995;34:16838–16851.
31. Rotticci D, Haeffner F, Orrenius C, Norin T, Hult K. Molecular recognition of sec-alcohol enantiomers by *Candida antarctica* lipase B. *J Mol Catal B Enzyme* 1998;5:267–272.
32. Drijfhout FP, Fraaije MW, Jongejan H, van Berkel WJH, Franssen MCR. Enantioselective hydroxylation of 4-alkylphenols by vanillyl alcohol oxidase. *Biotechnol Bioeng* 1998;59:171–177.
33. Ema T, Yoshii M, Korenaga T, Sakai T. Mechanism-based enzymatic method for reliable determination of absolute configuration of chiral 1-substituted ethanols: combination with NMR method. *Tetrahedron: Asymmetry* 2002;13:1223–1229.
34. Reigada JB, Tcacenco CM, Andrade LH, Kato MJ, Porto ALM, Lago JHG. Chemical constituents from *Piper marginatum* Jacq. (Piperaceae)—antifungal activities and kinetic resolution of (*RS*)-marginatamol by *Candida antarctica* (Novozym 435). *Tetrahedron: Asymmetry* 2007;18:1054–1058.
35. Skupin R, Cooper TG, Fröhlich R, Prigge J, Haufe G. Lipase-catalyzed resolution of both enantiomers of ornidazole and some analogues. *Tetrahedron: Asymmetry* 1997;8:2453–2464.
36. Ljubović E, Šunjić V. Correlation between distance of the perturbing groups and enantioselectivity of the lipase catalyzed acetylation of acyclic sec alcohols. *Tetrahedron: Asymmetry* 1997;8:1–4.
37. Kámán J, Forró E, Fülöp F. Enzyme-catalysed kinetic resolution of *N,O*-diacetyl derivatives of cyclic 1,3-amino alcohols. *Tetrahedron: Asymmetry* 2001;12:1881–1886.
38. Forró E, Szakonyi Z, Fülöp F. Enzymatic resolution of (±)-2-(*N*β-t-butoxycarbonyl-*N*α-methylhydrazino)cycloalkanols. *Tetrahedron: Asymmetry* 1999;10:4619–4626.
39. Vieira TO, Ferraz HMC, Andrade LH, Porto ALM. Highly enantioselective enzymatic resolution of cis-fused octalols mediated by *Candida antarctica* lipase (Novozym 435). *Tetrahedron: Asymmetry* 2006;17:1990–1994.
40. Forró E, Kanerva LT, Fülöp F. Lipase-catalyzed resolution of 2-dialkylaminomethylcyclohexanols. *Tetrahedron: Asymmetry* 1998;9:513–520.
41. Forró E, Fülöp F. Enzymatic resolution of 2 dialkylaminomethylcyclopentanols and cycloheptanols. *Tetrahedron: Asymmetry* 1999;10:1985–1993.
42. Take K, Okumura K, Tsubaki K, Taniguchi K, Shiokawa Y. Asymmetric synthesis and determination of the absolute configuration of FK584, an agent for the treatment of overactive detrusor. *Chem Pharm Bull* 2000;48:1903–1907.
43. Betts RL, Murphy ST, Johnson CR. Enzymatic desymmetrization/resolution of epoxydiols derived from 1,4-naphthoquinone, 5-hydroxy-1,4-naphthoquinone and 5,8-dihydroxy-1,4-naphthoquinone. *Tetrahedron: Asymmetry* 2004;15:2853–2860.
44. Adam W, Lazarus M, Schmerder A, Humpf H-U, Saha-Möller CR, Schreier P. Synthesis of optically active α-hydroxy acids by kinetic resolution through lipase-catalyzed enantioselective acetylation. *Eur J Org Chem* 1998;2013–2018.
45. Sattler A, Haufe G. Synthesis of (9*R*)- and (9*S*)-10-fluorodecan-9-olide (fluoro-Phoracantholide I). First lipase-catalyzed enantioselective esterification of β-fluoroalcohols. *Tetrahedron: Asymmetry* 1995;6:2841–2848.
46. Anthonsen T, Hoff BH, Hofsløkken NU, Skattebøl L, Sundby E. Synthesis of 1,3-dithianes and 1,3-dithiolanes. Bakers' yeast reduction and lipase-catalyzed resolution for synthesis of enantiopure derivatives. *Acta Chem Scand* 1999;53:360–365.
47. Cuiper AD, Brzostowska M, Gawronski JK, Smeets WJJ, Spek AL, Hiemstra H, Kellogg RM, Feringa BL. Determination of the absolute configuration of 3-pyrrolin-2-ones. *J Org Chem* 1999;64:2567–2570.
48. Busto E, Gotor-Fernández V, Gotor V. Chemoenzymatic synthesis of chiral 4-(*N,N*-dimethylamino)pyridine derivatives. *Tetrahedron: Asymmetry* 2005;16:3427–3435.
49. Chimni SS, Singh S, Kumar S, Mahajan S. Kinetic resolution of heteroaryl β-hydroxy sulfides catalyzed by *Humicola lanuginosa* lipase. *Tetrahedron: Asymmetry* 2002;13:511–517.
50. Zacchino SA. Enantioselective route to threo 8.0.4'-type neolignans: synthesis of (–)-Virolin. *J Nat Prod* 1994;57:446–451.
51. Savile CK, Kazlauskas RJ. How substrate solvation contributes to the enantioselectivity of subtilisin toward secondary alcohols. *J Am Chem Soc* 2005;127:12228–12229.

## Review Article

# Direct Assignment of the Absolute Configuration of Molecules from Crystal Morphology

ISABELLE WEISSBUCH, LESLIE LEISEROWITZ, AND MEIR LAHAV\*

*Department of Materials and Interfaces, The Weizmann Institute of Science, Rehovot, Israel*

**ABSTRACT** A method for direct assignment of the absolute configuration of molecules and the absolute structures of polar crystals, independent to that of Bijvoet, is described. The method correlates between the two-dimensional packing arrangement of specific faces, that delineate crystals during their growth and dissolution, with molecules present in the environment. The structural information stored in these faces is transferred to “tailor-made” molecules added to the solvent by controlled morphological changes induced to the growing crystals and by the creation of etch pits at specific crystal faces during their dissolution. In addition, the “tailor-made” molecules are occluded enantioselectively as guests within specific sectors of the host crystals. The method is illustrated for a variety of molecules and crystals including the assignment of the absolute configuration of several  $\alpha$ -amino acids as “tailor-made” additives in centrosymmetric crystals of glycine and serine, for the absolute structure of polar crystals of sugars and  $\alpha$ -amino acids and consequently the absolute configuration of molecules packed in such crystals. *Chirality* 20:736–748, 2008. © 2008 Wiley-Liss, Inc.

**KEY WORDS:** absolute configuration; crystal morphology; polar crystals; centrosymmetric crystals; “tailor made”; auxiliaries; hemihedral faces; etch pits; amino acids; sugars; contact angle

## INTRODUCTION

Louis Pasteur,<sup>1</sup> in his remarkable experiment of the manual separation of the sodium ammonium tartrate enantiomorphous crystals in 1848, laid the foundations of modern stereochemistry. He demonstrated, for the first time, that certain classes of molecules display enantiomerism even when dissolved in a solvent. The success of his findings depended on two central but not commonly encountered properties of racemates, spontaneous resolution into enantiomorphous crystals and the expression of hemihedral faces that make the crystals nonsuperimposable to one another. These results paved the way for the inspired suggestion of the tetrahedral arrangements of bonds around the carbon atom, made by van't Hoff<sup>2</sup> and Le Bel<sup>3</sup> two decades later.

During an entire century, stereochemistry was manipulated on a relative basis. Fisher<sup>4</sup> and Rosanoff<sup>5</sup> introduced an arbitrary convention for the absolute configuration of (L)- and (D)-glyceraldehyde from which the configuration of stereogenic carbon atoms of other molecules, such as sugars,  $\alpha$ -amino acids, steroids, and alkaloids, was assigned after they were converted to glyceraldehyde following laborious chemical degradations.

Crystals have played an important role in the assignment of absolute configuration on a relative basis. For example, Fredga<sup>6,7</sup> introduced the method of quasi-racemates by comparing the phase diagrams of co-

crystals composed from homochiral and heterochiral molecules.

Attempts to assign the absolute configuration of chiral molecules on the basis of the enantiomorphous shape of the host crystal were unsuccessful, even if the crystal structure was known via a conventional X-ray diffraction determination. The reason for this deficiency was a result of the assumption of Friedel's law, according to which the X-ray diffraction intensities  $I(h,k,l)$  and  $I(-h,-k,-l)$  of an enantiomorphous crystal are the same, as if arising from a centrosymmetric crystal. It was only in 1951, when Bijvoet, by applying the method of anomalous scattering of X-rays, assigned the absolute configuration of crystalline sodium rubidium tartrate.<sup>8</sup>

In the course of our studies on crystal and morphology engineering with “tailor-made” auxiliary molecules, it became possible to manipulate the morphology of crystals in a rational manner and correlate directly between molecular enantiomerism and crystal enantiomorphism, thus providing a method independent from that of Bijvoet for

Contract grant sponsor: Israel Science Foundation

\*Correspondence to: Meir Lahav, Department of Materials and Interfaces, The Weizmann Institute of Science, Rehovot 76100, Israel.

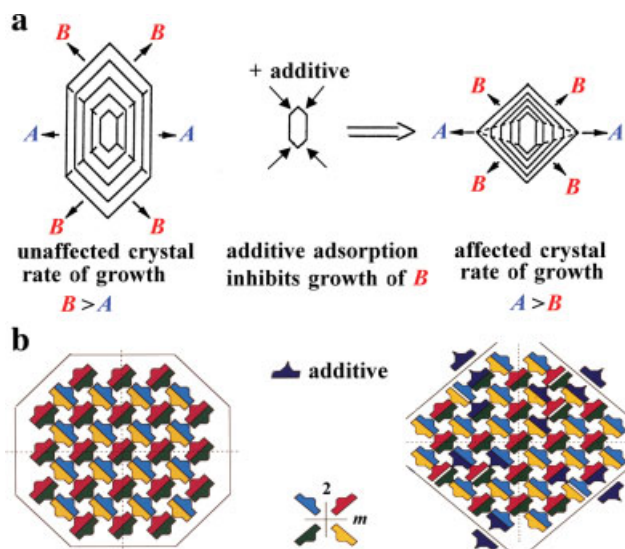
E-mail: meir.lahav@weizmann.ac.il

Received for publication 3 July 2007; Accepted 13 October 2007

DOI: 10.1002/chir.20498

Published online 16 January 2008 in Wiley InterScience (www.interscience.wiley.com).





Scheme 1.

the direct assignment of the absolute configuration of chiral molecules and the absolute structure of polar crystals.<sup>9</sup>

#### A BRIDGE BETWEEN CRYSTAL STRUCTURE, CRYSTAL MORPHOLOGY AND MOLECULAR CHIRALITY

Pasteur recognized in his experiments on resolution of enantiomers that macroscopic chirality of a crystal implies chirality of its constituent molecules. Hence, it would seem possible to deduce the absolute configuration of chiral molecules from the asymmetric morphology of crystals. Since asymmetry in crystal morphology results from a difference in the relative rates of growth of opposite  $(h,k,l)$  and  $(-h,-k,-l)$  crystal faces (determined on a single-crystal X-ray diffractometer), the assignment of the absolute handedness of a molecule requires, in principle, knowledge of the molecular packing arrangement of the crystal

and an understanding of the mechanism of its growth. However, growth and dissolution, and the development of the crystal faces depend not only on the two-dimensional structures of these crystal surfaces but also upon their different interactions with solvent molecules. Therefore, bridging between morphological and molecular chirality requires an understanding of these interactions on the molecular level. Such correlation became possible with the application of the method of "tailor-made" auxiliaries in crystallization processes.<sup>9-12</sup>

#### Modification of the Pasteur Method of Conglomerates Resolution by Entrainment

The habit of a crystal is defined by the relative rates of its growth in different directions; the faster the growth in a given direction the smaller the surface area of the face developed perpendicular thereto. Consequently, when growth is inhibited in a direction perpendicular to a given face, the area of this face is expected to increase relative to the areas of other faces of the same crystal. Differences in the relative surface areas of the various faces can therefore be directly correlated to the rate of impediment induced by stereospecific inhibition in different growth directions. Dramatic morphological changes observed during growth of organic crystals in the presence of "tailor-made" additives revealed a high degree of specificity in the interaction of the foreign molecules with the different structures of surfaces of the crystalline substrate. Such a change in crystal morphology is depicted in Schemes 1a and 1b, highlighting in (a) the general effect of additive bound to the diagonal faces and how this process is manifested at the molecular level in (b).

From a systematic study of a variety of organic compounds crystallized in the presence of auxiliary molecules with structures similar to those of the corresponding substrate molecules and so labeled "tailor-made" additives, it was possible to deduce a stereochemical correlation between the structures of the affected crystal surfaces and the molecular structure of the additives. We inferred and experimentally demonstrated that "tailor-made" additives

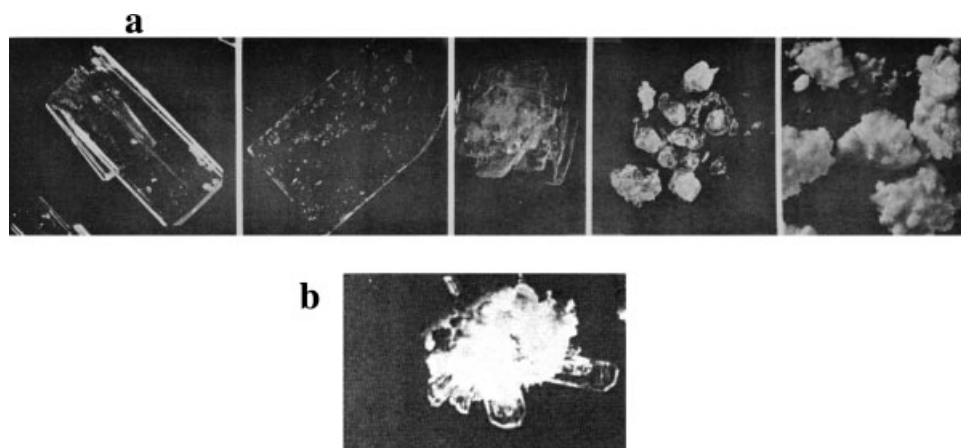


**Fig. 1.** (a) From left-to-right (S)-Glu-HCl crystals grown in the absence and in the presence of increasing amounts of S-lysine additive. (b) Racemate grown in the presence of S-lysine; the plates are the (R)-crystals whereas the powder is the (S) enantiomorph.

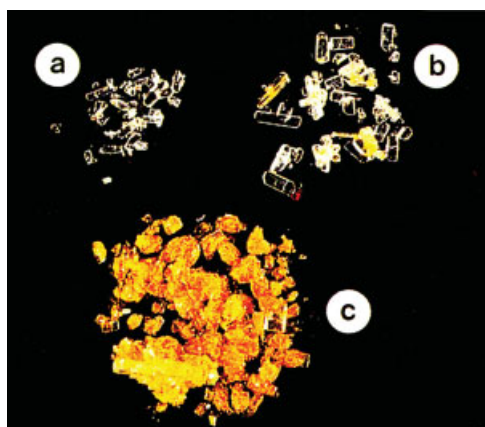
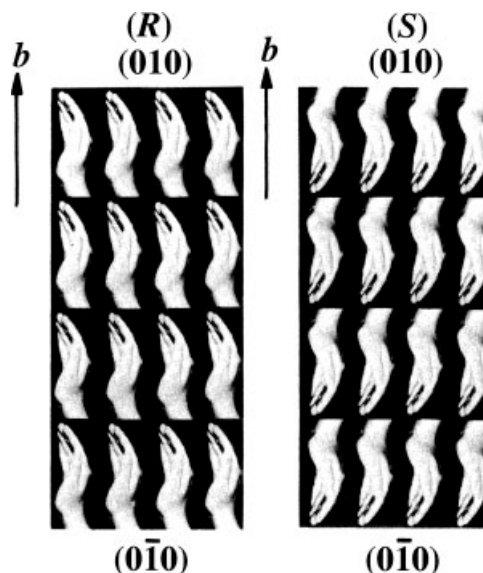


**Fig. 2.** Crystallization of (*R,S*)-Glu-HCl in the presence of *N*<sup>c</sup>-(2,4-dinitrophenyl)-*S*-lysine. (a) First crop, colorless (*R*)-Glu-HCl; (b) Second crop, mixture of colorless (*R*)-Glu-HCl and yellow (*S*)-Glu-HCl crystals; (c) Third crop primarily contains small, yellow crystals of (*S*)-Glu-HCl.

are adsorbed on the growing crystals, but only at certain surfaces and with the part of the adsorbate that differs from the substrate emerging from the crystal.<sup>9–12</sup> The role of the “tailor-made” additives is first described here with the extension of the Pasteur method for separation of enantiomorphous crystals by manual sorting.

Enantiomorphous crystals behave alike in their interactions towards external achiral molecules. However, if one can select an enantiopure additive that can interact enantioselectively with the faces of the chiral crystals, it should affect the growing faces of the two enantiomorphs differently. Consequently, a enantiomerically pure inhibitor, *S'* consisting of a slightly modified *S* molecule will be, in general, adsorbed only at the crystal surface of the (*S*)-enantiomorph and not at the surfaces of the (*R*)-crystal. This stereoselective adsorption causes the (*S*)-crystals to undergo drastic morphological changes that allow visual identification and manual separation of the two enantiomorphs.<sup>13,14</sup> This principle is illustrated with the racemic glutamic acid-HCl (Glu-HCl) that undergoes spontaneous separation to yield a conglomerate mixture of (*R*)- and (*S*)-



**Scheme 2.**

plate-like crystals; however, the crystals do not express hemihedral faces.<sup>15</sup> Figure 1 shows how adsorption of *S*-lysine (Lys) additive causes (*S*)-Glu-HCl crystals to grow as thinner and thinner plates and finally as powder at higher inhibitor concentrations, while the (*R*)-Glu-HCl preserve their original morphology. Moreover, upon addition to the crystallizing racemate solution of *S*-Lys together with the yellow *N*<sup>c</sup>-(2,4-dinitrophenyl)-*S*-Lys dye, the (*R*)-Glu-HCl crystals precipitate first as colorless plates whereas the (*S*)-Glu-HCl crystals precipitate later as yellow thin plates due to the occlusion of the dye, (Fig. 2).

Analogous behavior was observed with conglomerate racemates of asparagine-H<sub>2</sub>O and threonine crystals.<sup>13</sup> Racemic threonine (Thr) crystallizes as a conglomerate of plate-like needles. When another enantiomerically pure  $\alpha$ -amino acid e.g. 2–5% w/w of (*S*)-glutamic acid (Glu) is added to the crystallization solution, there is a delay in the precipitation of the (*S*)-Thr as compared to (*R*)-Thr crystals. Furthermore, the morphology of the (*S*)-Thr crystals is altered depending on the concentration of *S*-Glu. At 10% (w/w of Thr) *S*-Glu additive, (*S*)-Thr crystals precipitate as a powder whereas the (*R*)-Thr crystals remain unaffected (Fig. 3).

High-performance liquid chromatography (HPLC) enantiomeric analysis using a chiral mobile phase confirmed for all the conglomerate crystal systems that *S'*-inhibitors were selectively occluded only in the bulk of substrate (*S*)-crystals, typically in amounts of 0.5–1% w/w (and by symmetry, occlusion of *R'* occurred only in the (*R*)-crystals). The presence of a “tailor-made” inhibitor causes a drastic decrease in the growth and nucleation rates of the affected enantiomer, leading to an efficient kinetic resolution on the basis of which various racemates have been resolved.<sup>15–18</sup> This correlation between the crystal and the additive can be applied as a method for the assignment of the configuration of chiral molecules on a relative basis, in a manner similar to the quasi-racemate method of Fredga.<sup>7</sup>

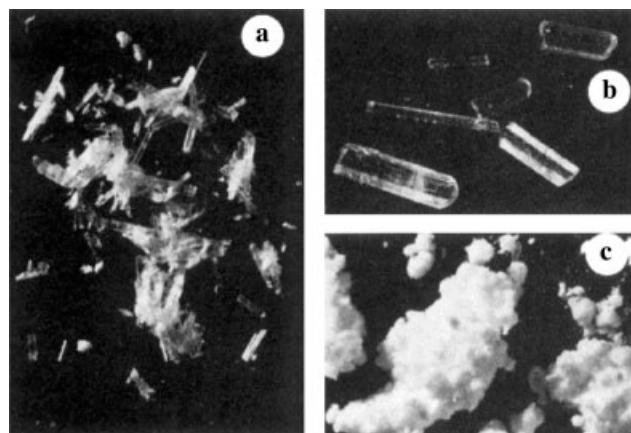


**Fig. 3.** Threonine crystallized in the presence of glutamic acid: (a) *R,S*-Thr + 5% (w/w of Thr) *S*-Glu: the powder is (*S*)-Thr and the needles are (*R*)-Thr; (b) (*S*)-Thr + 10% *R*-Glu; (c) (*S*)-Thr + 10% *S*-Glu.

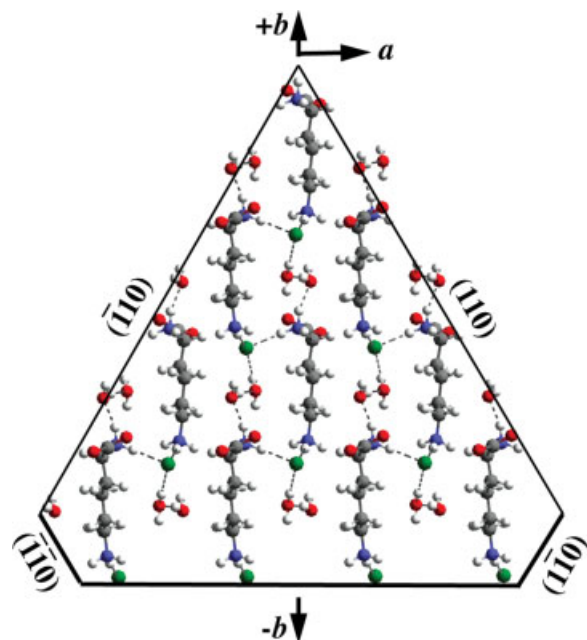


Fig. 4. Packing arrangement of (S)-lysine-HCl·2H<sub>2</sub>O crystal delineated by the observed (hk0) crystal faces, viewed along the *c* axis.

#### A Direct Correlation Between Molecular Enantiomerism and Crystal Enantiomorphism

Having established the basic mechanism of interaction between “tailor-made” additives and crystal surfaces, we

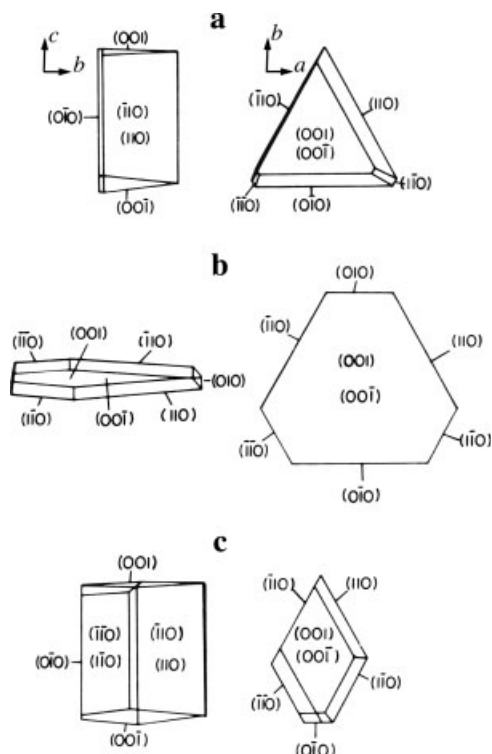


Fig. 5. Morphology of the experimentally obtained (S)-Lysine-HCl·2H<sub>2</sub>O crystals viewed along *a* and *c* axes: (a) pure; (b, c) grown in the presence of *S*-lysine-methyl ester and *S*-norleucine, respectively.

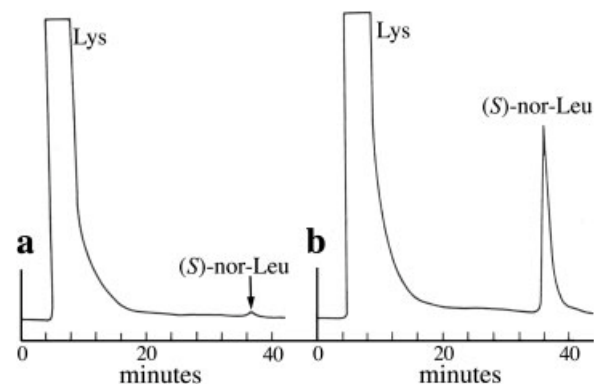


Fig. 6. HPLC analysis of *S*-norleucine occluded in the (S)-Lysine-HCl·2H<sub>2</sub>O crystals. Materials taken from (a) *+b* side of the crystal, (b) the *-b* side of the crystal.

return now to the original problem of direct assignment of the absolute configuration of a chiral molecule. We shall first examine how to establish by such means the orientation of a chiral molecule in a chiral crystal. As a result of Friedel's law, the orientation of the molecules vis-à-vis a polar axis or polar direction in an enantiomorphous crystal cannot be determined by conventional X-ray analysis. The absolute configuration of a molecule can be assigned provided its orientation is fixed either by the application of the Bijvoet method of anomalous X-ray scattering or by use of “tailor-made” auxiliaries, described later. To demonstrate the method, we first focus on polar crystals composed of enantiopure molecules. Scheme 2 shows two enantiomorphous sets of hands arranged in a lattice, right hands forming an (*R*)-crystal and left hands forming an (*S*)-crystal.

The fingers of the hands are exposed at the (010) face of the right-handed “molecules” and, by symmetry, at the

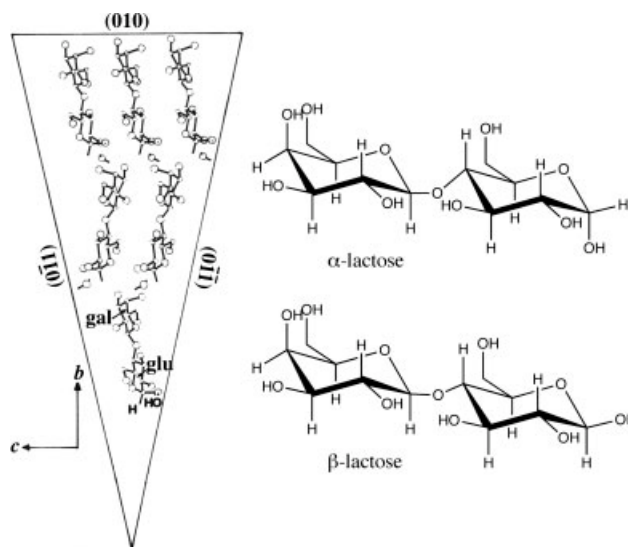
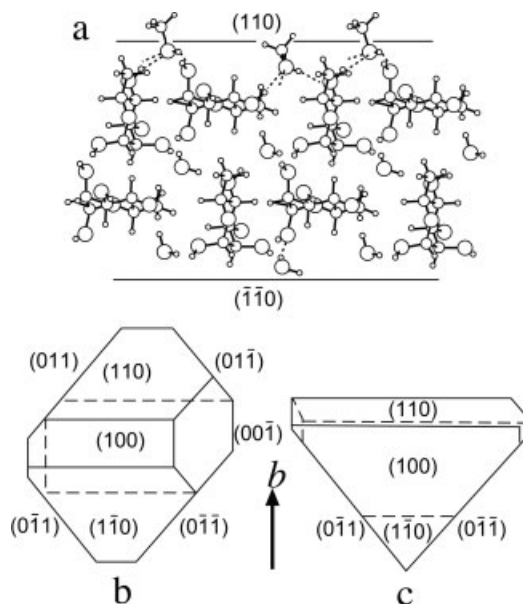


Fig. 7. (Left) Packing arrangement of  $\alpha$ -lactose monohydrate delineated by the observed crystal faces, as viewed along the *a* axis. (Right) The  $\alpha$ - and  $\beta$ -lactose formulae.





**Fig. 8.** (a) Packing arrangement of  $\alpha$ -rhamnose monohydrate crystal viewed along the  $a$  axis; the OH bonds of the hydrate water molecules point towards the  $+b$ , but not the  $-b$ , direction; replacement of water by methanol on the  $\{110\}$  faces is depicted; (b, c) Morphology of  $\alpha$ -rhamnose monohydrate crystals grown from aqueous solution and 9:1 methanol:water solution, respectively, as viewed along the  $a$  axis.

(0–10) face for the left-handed “molecules.” Thus, by determining at which face of the crystal specimen the fingers or wrists are exposed, the handedness of the constituent molecules may be assigned, by applying the two-step adsorption-inhibition mechanism described earlier with appropriate “tailor-made” additives.

We illustrate this approach with (S)-Lysine-HCl·2H<sub>2</sub>O crystal, space group  $P2_1$ , with the packing arrangement shown in Figure 4 and morphology of the pure crystals in Figure 5a.<sup>19</sup>

Lysine molecules are aligned parallel to the  $b$  axis, with the  $^+H_3N-C^*H-COO^-$  moiety emerging from the  $+b$  end of the crystal. The  $\varepsilon-NH_3^+$  points toward  $-b$  end and are hydrogen bonded to a molecule in a direction perpendicular to the  $\{1-10\}$  faces. Additives with a modified carboxylate or  $\alpha$ -amino group, such as lysine-methyl ester, inhibited growth in the  $+b$  direction, inducing development of the (010) face (Fig. 5b). Conversely, additives that

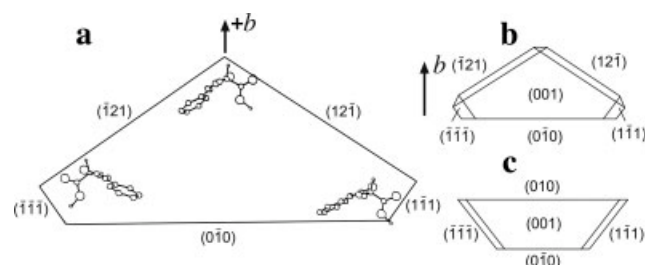
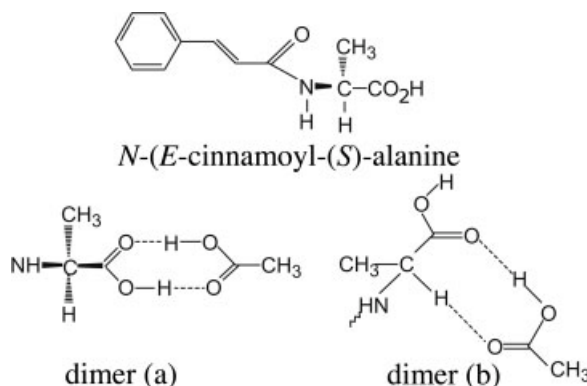


**Fig. 9.** Packing arrangement of  $N$ -( $E$ -cinnamoyl)-( $S$ )-alanine delineated by the faces observed when grown from methanol; (b, c) Morphology of the crystals grown from methanol and acetic acid, respectively.

Chirality DOI 10.1002/chir



**Scheme 3.** Chemical formulae of  $N$ -( $E$ -cinnamoyl)-( $S$ )-alanine and of the two possible hydrogen bonded dimmers with acetic acid.

bear a modified side chain such as norleucine or norvaline inhibited growth along the  $-b$  direction, with a concomitant pronounced increase in the area of the  $\{1-10\}$  faces (Fig. 5c).

Assuming growth of the crystals in the opposite polar directions from a nucleation center, the selective adsorption of additive molecules at one end of the polar axis implies that the additive must be occluded only in that part of the crystal that had exposed the adsorbing face to solution during growth. Therefore, the analysis of the occluded additive at the crystal extremities along the polar  $b$  axis must reveal an anisotropic distribution. This expectation was experimentally confirmed for the growth of (S)-Lysine-HCl·2H<sub>2</sub>O in the presence of  $S$ -norleucine. According to HPLC analysis of material taken from the  $+b$  and  $-b$  ends of the crystal, the additive was occluded preferentially at the  $-b$  side, (Fig. 6).<sup>9</sup>

The anisotropic distribution of the occluded additive provides a second independent method of confirming the absolute configuration assigned by means of morphological changes, once the adsorption mechanism is known.

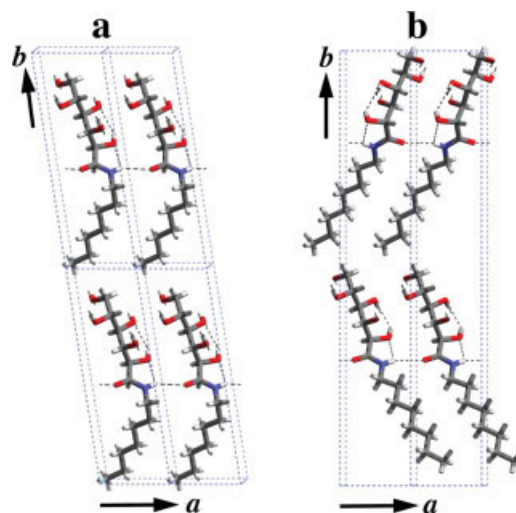


**Fig. 10.** Packing arrangements of  $n$ -heptyl and  $n$ -octyl gluconamides viewed along their  $c$  axes.



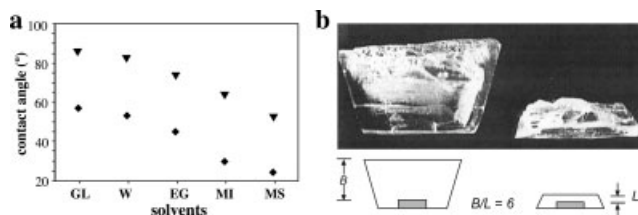


**Fig. 11.** (a) Contact angle measurements on the hemihedral faces *N*-*n*-octylgluconamide crystals grown in methanol: GL, glycerol; W, water; EG, ethylene glycol; MI, methylene iodide; MS, mother solution (methanol). (◆) hydrophilic (010) face; (▼) hydrophobic (0–10) face. (b) Morphology of crystals grown from seeds that can be observed as an opaque shadow at the bottom. Thickness of added material on the hydrophobic surface is denoted as *B* and that added on the hydrophilic surface is denoted as *L*. The *B/L* ratio has an average value of about 5.

The influence of  $\beta$ -lactose on the growth of  $\alpha$ -lactose crystals is an additional example.<sup>20</sup> The  $\alpha$ - and  $\beta$ -lactoses (Fig. 7) are disaccharides composed of a galactose and an  $\alpha$ - or  $\beta$ -glucose moiety linked through a glycoside bond. They are anomers that interconvert spontaneously in solution.  $\alpha$ -Lactose crystallizes from water as a monohydrate in space group  $P2_1$ , packing in a polar arrangement (Fig. 7), the crystals displaying a characteristic tomahawk morphology,<sup>21</sup> with the apex at the  $-b$  end. The crystals were observed to grow only along the  $+b$  direction, which has been interpreted by Michaelis and van Kreveld<sup>22</sup> as an inhibition of growth along  $-b$  by the  $\beta$ -lactose anomer. These authors predicted, on this basis, the orientation of the disaccharide with respect to the polar axis, although the crystal structure<sup>23,24</sup> had not been determined at that time. In fact, from the crystal structure it is obvious that  $\beta$ -lactose can be adsorbed only at the  $-b$  end of the crystal by virtue of the unmodified galactose moiety. Once adsorbed, the modified  $\beta$ -glucose inhibits growth perpendicular to the  $\{0-11\}$  faces. Therefore, by fixing the absolute polarity of the molecule inside the crystal, its absolute configuration is assigned.

By applying similar considerations, it was possible on the basis of the growth of sucrose crystals in the presence of raffinose and kestose to determine the absolute configuration of sucrose.<sup>9</sup>

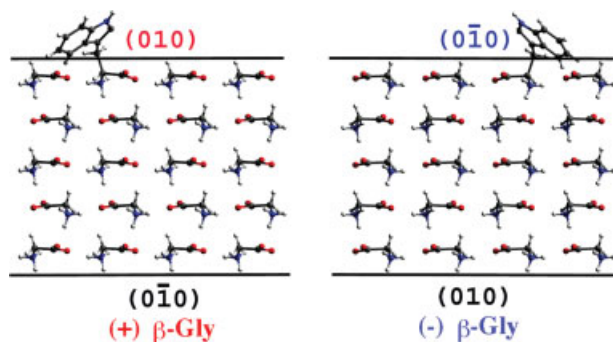


**Fig. 12.** (a, b) Packing arrangements of the (+)- and (-)- $\beta$ -polymorphs of Gly delineated by the  $\{010\}$  crystal faces and showing the adsorption of *R*- and *S*-Trp molecules, respectively.

### Solvent as a “Tailor-Made” Additive

Solvent has a strong influence on the habit of crystalline materials; however, the role played by solvent–surface interactions in enhancing or inhibiting crystal growth is still a matter of debate. Till about the 1980’s, there had been two different approaches to help clarify this point. In one approach, favorable interactions between solute and solvent on specific faces leads to reduced interfacial tension, causing a transition from a smooth to a rough interface and a concomitant faster surface growth.<sup>25–27</sup> Alternatively, it has been proposed that preferential adsorption at specific faces will inhibit their growth as removal of bound solvent poses an additional energy barrier for continued growth. Our studies on the role played by “tailor-made” additives are in keeping with the latter approach. Therefore, solvents may act in a manner similar to “tailor-made” additives.<sup>12</sup> This effect is illustrated with the use of solvent for the determination of the absolute configuration of molecules packing in polar crystals that are crystalline solvates and where the solvent of crystallization plays the dual role of solvent and solute. Such crystals were grown in the added presence of “tailor-made” solvent, which is a slightly modified version of the solvate solvent. When crystalline hydrates were grown from aqueous solution in the added presence of methanol (the “tailor-made” solvent), it was found that the change in morphology was interpretable<sup>12,28</sup> in a manner akin to the effect of a “tailor-made” inhibitor. For this purpose, we made use of the crystal structure of  $\alpha$ -rhamnose monohydrate, which embodies a polar arrangement (Fig. 8a) in space group  $P2_1$  and, when grown from pure aqueous solution, displays a bipyramidal morphology (Fig. 8b).

The two O–H bonds of the hydrate water molecules are oriented exclusively towards the  $+b$  direction of the crystal. A methanol molecule may replace a water molecule at the (110) face of the crystal by virtue of a hydrogen bond of the OH group such that the methyl group protrudes from the surface and perturbs the regular growth along the  $+b$  direction but not towards the  $-b$  direction of the crystal. Consequently, the addition of methanol as cosolvent changes the bipyramidal crystal morphology into pyramidal (Fig. 8c). A similar change in crystal morphology was accomplished on growing crystals of aspara-

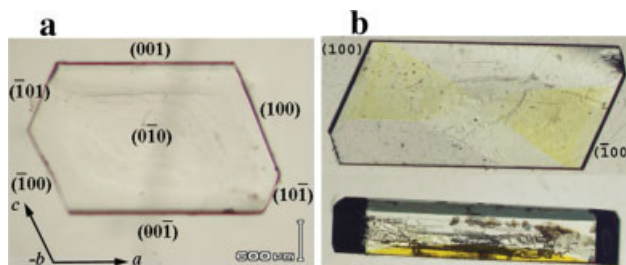
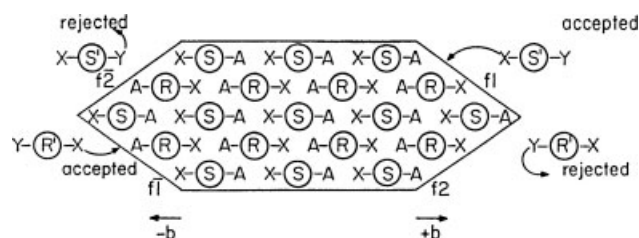


**Fig. 13.** Crystals of  $\beta$ -Gly grown from aqueous solutions in the presence of a mixture of 2% *R,S*-Trp and (a) 0.1% *S*-DNPLys or (b) *R*-DNPLys. Note in (b) two views of the same yellow colored crystal; bottom, view along *c* direction showing the color at only one side, and top, view along *b* direction showing coloring in the (100) and  $(-100)$  sectors.



**Scheme 4.** Scheme showing the adsorption of enantiopure additives onto enantiotopic faces of a centrosymmetric crystal.

gine monohydrate, which does not exhibit polar axes, in the presence of methanol.<sup>29</sup>

A second example is that of *N*-(*E*-cinnamoyl)-(*S*)-alanine which crystallizes as a polar crystal in space group  $P2_1$ .<sup>19</sup> The orientation of the molecules vis-à-vis the various faces that delineate the crystals grown in methanol are shown in Figure 9a. It was found that the solvent may act in a manner similar to the tailor-made additives, for example, by growing the crystal from acetic acid instead of methanol.<sup>12</sup> The crystals grown in glacial acetic acid display well expressed (010) and {1-11} faces, (Fig. 9c). This change in morphology could be easily explained by a selective binding of the acetic acid at the exposed carboxylic acid groups of the two (1-11) and (-1-1-1) faces of the crystal forming a hydrogen-bonded dimer (a), as in Scheme 3. In addition, acetic acid can also bind to the  $\text{CHCO}_2\text{H}$  moiety of cinnamoyl-alanine via a cyclic dimer (b) on the (010) face.

The absolute configuration of glucose molecules could be also determined by differences in the wetting properties of hydrophobic and hydrophilic crystal faces in the class of enantiopure alkyl gluconamides  $\text{C}_n\text{H}_{2n+1}\text{—NHCO(CHOH)}_4\text{CHOH}$  where  $n = 7\text{--}10$ .<sup>30</sup> These molecules crystallize as plates in a head-to-tail packing arrangement, shown in Figure 10.<sup>31</sup> Thus, one face of the plate is hydrophobic and the opposite hemihedral face is hydrophilic.

Measurements of contact angle with a variety of polar solvents deposited on the opposite plate-like faces of specimen crystals could establish which face is hydrophobic and which is hydrophilic, Figure 11a.<sup>32</sup>

This information fixes the orientation of the constituent molecules along the polar  $b$  axis of the crystal specimen and consequently their chirality. These wettability experiments also led to crystal growth experiments on these systems to help determine the role of the solvent on crystal growth. Since polar solvents are expected to interact more firmly with the hydrophilic faces of the crystal, they should impede the growth of these faces. When these crystals were grown in methanol at the hydrophilic face, methanol can form  $\text{O—H}\cdots\text{O}$  hydrogen bonds interlinking the terminal hydroxyl groups of two neighboring chains, since the translation distance between them is about 5 Å. Figure 11b shows the growth of two identical seeds exposing either the hydrophilic or the hydrophobic face towards the methanol solution. The crystals exposing the hydrophobic face grew four to five times faster in comparison to those that exposed the hydrophilic face to the same solution.<sup>32</sup>

An attempt to assign the sense of polarity of glycine  $\beta$ -polymorph ( $\beta$ -Gly) specimen crystals, space group  $P2_1$ , via the Bijvoet method was unsuccessful because the atoms are weak anomalous X-ray scatterers and the molecular arrangement, when only the relevant O, N, C atoms need be considered, is nearly centrosymmetric (space group pseudo- $P2_1/m$ ). Growth kinetic measurements of single  $\beta$ -Gly crystals in 1:1 ethanol-water solutions revealed a fast growth at one end of the needle-like crystal (the polar  $b$ -axis is along the needle direction) and a very slow growth at the opposite end.<sup>33</sup> The method of “tailor-made” additives was more appropriate for the assignment of the crystal sense of polarity, employing in this case tryptophan (Trp).<sup>33</sup> For convenience, we define the two enantiomorphous crystals of  $\beta$ -Gly as follows: the enantiomorph in which the Gly C—H bonds point along the  $+b$  direction, and thus would emerge from the (010) face, is defined as

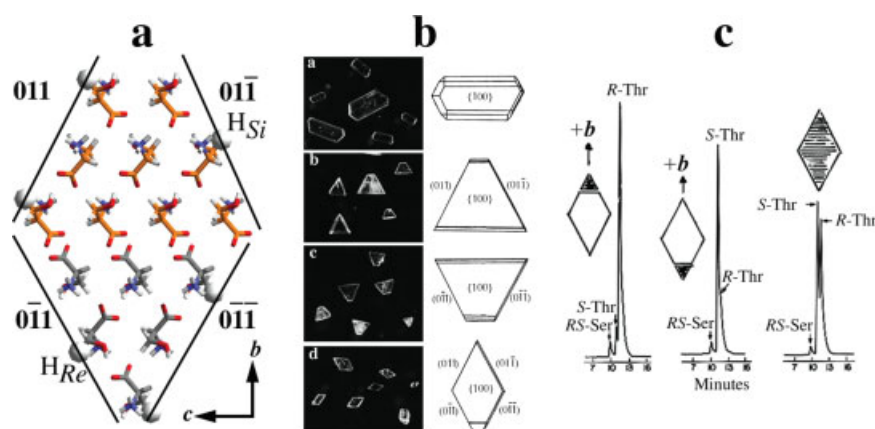
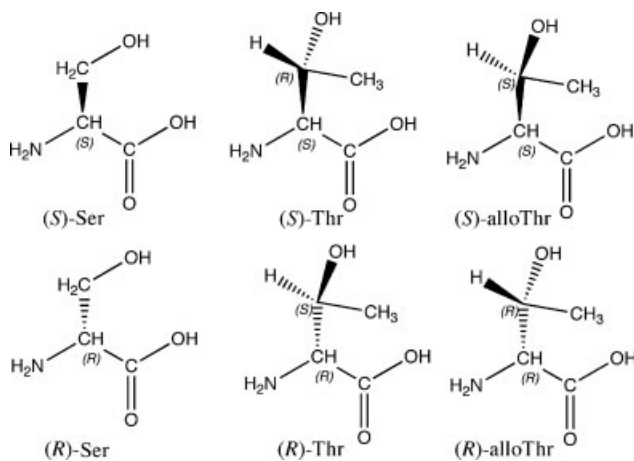


**Fig. 14.** (a) The packing of (*R,S*)-serine crystal viewed along the  $a$  axis. Each  $bc$  layer is composed of *R* or *S* molecules only. For clarity only half of each *R* (orange) and *S* (gray) layer is shown. The positions of the four {011} faces are shown with respect to the crystal structure. Threonine additive molecules have been stereospecifically inserted, with the  $\beta$ -methyl groups indicated by large circles. (b) Photographs of (*R,S*)-serine crystals, from top to bottom: pure and grown in the presence of *R*-Thr, *S*-Thr, and *RS*-S-Thr, accompanied by the computer-drawn morphology specifying the relevant crystal faces. (c) HPLC enantiomeric analysis of Thr occluded at the  $-b$  tip,  $+b$  tip and whole crystal of (*R,S*)-serine grown in the presence of *R,S*-Thr.



Scheme 5.

(+) (Fig. 12 left). Hypothetical replacement of these H atoms by deuterium (to form a C–D bond) would yield Gly molecules of “*R*-configuration.” By symmetry, the opposite (–) enantiomorph containing Gly molecules whose C–H bond vectors emerge from the (0–10) face would be of “*S*-configuration” (Fig. 12 right). Thus, on crystal growth, any *R*-amino acid additives are expected to bind selectively to the (010) face of (+)  $\beta$ -Gly and *S*-amino acids onto the (0–10) face of (–)  $\beta$ -Gly.

Crystallization of  $\beta$ -Gly in 1:1 ethanol:water solutions in the presence of racemic Trp yielded, as expected, the formation of short prismatic crystals due to enantioselective binding of the additive followed by retardation of crystal growth at either (010) or (0–10) face of the (+) and (–)  $\beta$ -enantiomorphs, respectively. Therefore, we concluded that  $\beta$ -Gly grows faster at the C–H exposed side than at the opposite N–H exposed side.

To differentiate between the (+) and (–)  $\beta$ -enantiomorphs, we colored them enantioselectively by growing

the  $\beta$ -Gly crystals in aqueous solutions in the presence of mixtures of 2% *R,S*-Trp and 0.1% of either *R*- or *S*-*N*-(2,4-dinitro-phenyl)lysine (DNPLys).<sup>34</sup> The  $\beta$ -Gly plate-like crystals grown in the presence of *S*-DNPLys appeared as a mixture of colorless (+)-enantiomorphs (Fig. 13a) and (–)-enantiomorphs colored only at the (0–10) face (Fig. 13b). Furthermore, an enantiomeric analysis, by chiral HPLC, of the Trp occluded in the  $\beta$ -Gly plates revealed an excess of *R*-Trp (enantiomeric excess, ee ~ 65–88%) in the colorless (+) crystals and (*S*)-Trp in the colored (–) crystals. These results also prove that *S*-Trp and *S*-DNPLys are occluded in the colored (–) crystals by replacing the C–H bond of a glycine host molecule with the side group of the additive. By symmetry, *R*-Trp and *R*-DNPLys are occluded in the same manner but in the (+) crystals.<sup>34</sup>

An attempt to apply the same method for the elucidation of the absolute configuration of glycine molecules in specimen crystals of the  $\gamma$ -polymorph was only partially successful.  $\gamma$ -glycine crystallizes in the polar  $P3_1$  or  $P3_2$  space groups. The application of “tailor-made” auxiliary method allowed us to determine the absolute sense of polarity of the crystal but not the sense of chirality of the glycine molecules.

#### ASSIGNMENT OF ABSOLUTE CONFIGURATION OF MOLECULES USING CENTROSYMMETRIC CRYSTALS

In contrast to the situation for chiral crystals, it had not been generally appreciated that in centrosymmetric crystals the orientations of the constituent enantiomeric molecules are unambiguously assigned with respect to the crystal axes, from a conventional structure determination. Thus, the known orientation of the two enantiomeric molecules in a centrosymmetric crystal can be exploited for the direct assignment of absolute configuration of chiral resolved molecules, provided the structural information embedded in the racemic crystal can be transferred to chiral additive molecules. The direct assignment of the abso-

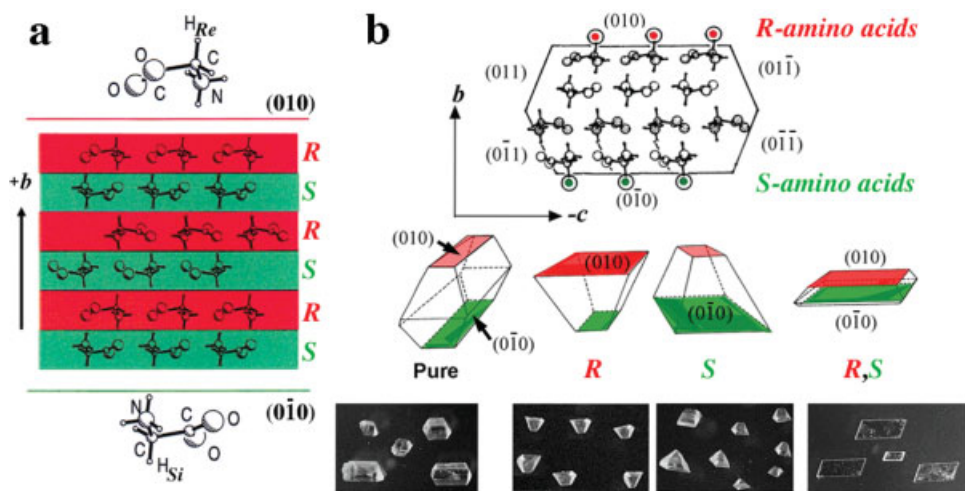
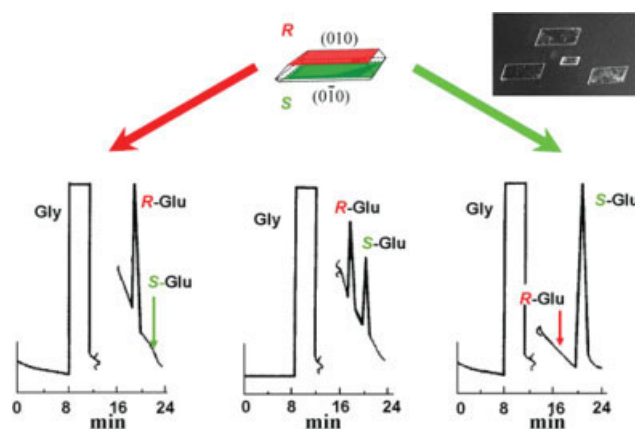


Fig. 15. (a) Packing arrangement of  $\alpha$ -Gly with the crystal heterochiral layers of chiral Gly molecules colored in red and green; (b) Morphology and photographs of the crystals of pure  $\alpha$ -Gly as well as (c–e) grown in the presence of (*R*)-, (*S*)-, and (*R,S*)- $\alpha$ -amino acid additives.





**Fig. 16.** Enantiomeric HPLC analyses of the occluded additives in plate-like crystals of glycine grown in the presence of (*RS*)-glutamic acid; (left to right) sample taken from the  $+b$  pole, sample from a whole crystal and sample taken from the  $-b$  pole.

lute configuration of such chiral resolved additives may thus be determined through the morphological changes they induce selectively on one set of enantiotopic faces of centrosymmetric crystals with appropriate packing features.

It is convenient to regard a racemic centrosymmetric crystal consisting of a mixture of enantiopure chiral molecules as enantiopolar with respect to each enantiomer, namely to consider the racemic crystals as though it were composed of two mutually enantiomorphous chiral crystal structures, related to each other through an inversion center. A prerequisite for application of this method is that within the centrosymmetric racemic crystal a specific functional group attached to a (*R*)-molecule points toward the face *f*1 but not toward the opposite face *f*-1 (Scheme 4). By symmetry, the same functional group attached to a (*S*) molecule will emerge at the enantiotopic face *f*-1, but not *f*1. Crystallization of a centrosymmetric crystal in the presence of a chiral additive *R'* designed so that it will fit in the site of a (*R*) molecule on the growing crystal faces *f*-1 or *f*-2 but not on the enantiotopic faces *f*1 or *f*2, will hinder

growth in the  $-b$  direction but not in the  $+b$  direction (Scheme 4).

By virtue of symmetry, the enantiomeric additive *S'* will inhibit growth perpendicular to faces *f*1 and *f*2, while racemic additives *R',S'* will inhibit growth in both directions,  $+b$  and  $-b$ .

We illustrate this method for the assignment of the absolute configuration of the threonine from the morphology changes induced by this molecule in the centrosymmetric crystals of racemic (*R,S*)-serine.

### Serine-Threonine System

Racemic serine (Ser) crystallizes in centrosymmetric space group  $P2_1/a$ . Within the structure (Fig. 14a) the  $C_\beta \rightarrow H_{Si}$  bond vector of the rigid methylene group of *R*-Ser molecule has a major component along  $+b$  and, by symmetry, the  $C_\beta \rightarrow H_{Re}$  bond vector of the *S*-Ser has a major component along  $-b$ . Thus, their replacement by a methyl, as in threonine (Thr), will inhibit growth in the *b* direction. That is, an *R*-Thr molecule with a side-chain  $\beta$ -carbon of *S*-chirality (Scheme 5) will inhibit growth along  $+b$ , while the  $-\text{CH}_3$  group of *S*-Thr will replace the  $H_{Re}$  hydrogen of *S*-Ser and hence inhibit growth along  $-b$ . (*R,S*)-Ser forms tabular crystals with point symmetry  $2/m$  (Fig. 14b); the crystals affected by either *R*- or *S*-Thr exhibit reduced morphological point symmetry 2 (the mirror plane is lost) and are enantiomorphous (Fig. 14b).<sup>35,36</sup>

When *R,S*-Thr is used as the additive, the morphological point symmetry  $2/m$  is left unchanged because the effects induced by each additive separately combine. The crystals turn into rhombs, with a clear increase in the areas of the {011} side faces relative to those of the pure form (Fig. 14b). The changes in morphology observed with the additives (Fig. 14b), with respect to that of the pure crystals, can be interpreted only in terms of selective adsorption of the *R*-Thr at faces (011) and (0 $\bar{1}$ -1), and of *S*-Thr at (0-11) and (0-1-1), in agreement with the calculated enantioselective surface binding energies<sup>36</sup> of the additive molecules on the corresponding crystal faces. These results fix the absolute chirality of the chiral resolved Thr additive.

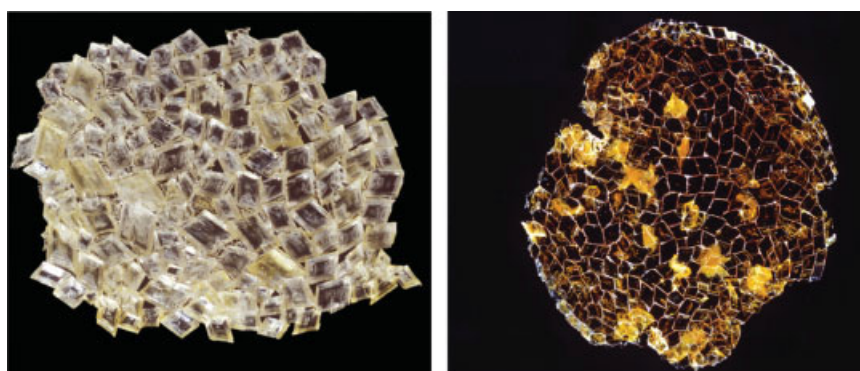


**Fig. 17.** Photographs of white crusts and yellow crusts of glycine crystals grown at the air/aqueous solution interface in the presence of *N*<sup>ε</sup>-(2,4-dinitrophenyl)-*S*-lysine and leucine in a ratio *S/R* > 1 and *S/R* < 1, respectively. The white crystals exposed their (010) face towards the solution whereas the yellow crystals exposed their (0-10) face.



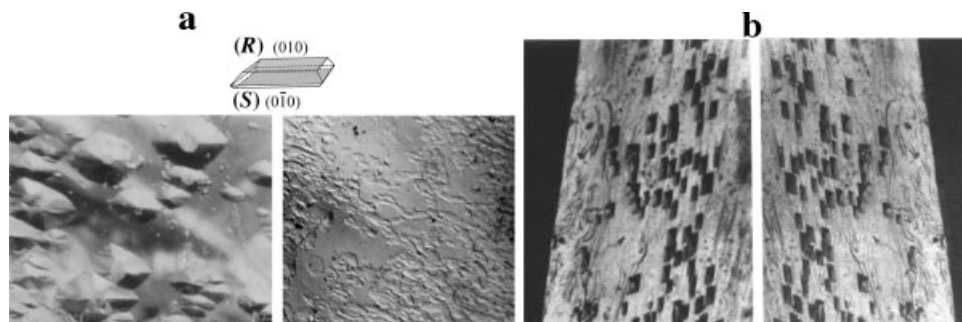


**Fig. 18.** (a) Photographs of the (010) and (0–10) faces of a plate-like  $\alpha$ -Gly crystals after etching in the presence of *R*-alanine; (b) The (010) and (0–10) faces of a cleaved  $\alpha$ -Gly crystal subsequently etched in the presence of *R,S*-alanine.

This assignment was further supported by enantioselective dissolution/etching experiments.<sup>36</sup>

The morphological changes and our interpretation thereof, imply that in the (*R,S*)-serine crystals grown in the presence of *R,S*-Thr the occluded additive molecules must segregate along the *b* axis during crystal growth; *R*-Thr, being occluded through the symmetry-related (011) and (01–1) faces, will predominate at the  $+b$  half of the crystal whereas *S*-Thr will predominate at the  $-b$  half, as confirmed experimentally by HPLC enantiomeric analysis, (Fig 14c).

By contrast, the (*R,S*)-Ser crystal is not appropriate for the assignment of the absolute configuration of allo-threonine (Scheme 5) since enantiopure allo-Thr molecules of either handedness can each be adsorbed onto the homotopic {100} faces, as experimentally observed.<sup>36</sup>

#### $\alpha$ -Glycine- $\alpha$ -Amino Acids System<sup>12,37,38</sup>

When grown from aqueous solutions, Gly crystallizes in its centrosymmetric  $\alpha$ -polymorph (space group  $P2_1/n$ ). The achiral molecules of Gly in solution become chiral in the crystalline environment because they assume a chiral conformation. In the crystal, the C–H<sub>Re</sub> vector of Gly molecules in *R*-layers points towards the  $+b$  direction emerging perpendicular to the (010) face (Fig. 15a) whereas the C–H<sub>Si</sub> vector of Gly molecules in *S*-layers points towards the  $-b$  direction emerging perpendicular to the (0–10) face, the two H-atoms being diastereotopic. The other two H-atoms are within the molecular planes. Thus, the centro-

symmetric  $\alpha$ -Gly crystal is composed from chiral layers of Gly molecules, colored in red and in green (Fig. 15a). When  $\alpha$ -Gly crystals are grown in aqueous solutions in the presence of racemic mixtures of amino acids they display a plate-like morphology with two well-expressed chiral enantiotopic (010) and (0–10) faces, Figure 15b. During growth, the *R*-amino acids interact enantioselectively with the (010) face by virtue of their  $\alpha$ -amino acid moieties and thus replace “red” glycine host molecules so that their side chains emerge from the crystal surface and thus do not interfere with the intralayer binding process. A minor fraction of these amino acid guest molecules would be occluded within the bulk of the  $\alpha$ -Gly crystal on growth. By symmetry, the *S*-amino acids would be occluded into the bulk of the  $\alpha$ -Gly crystal through the (0–10) face. As a result of this process, racemic  $\alpha$ -amino acids can undergo segregation into enantiomers upon occlusion within  $\alpha$ -Gly crystals, Figure 16.

Furthermore, if  $\alpha$ -Gly crystals are grown at an interface that blocks growth at one of the enantiotopic faces, say (010), then only the *S*-enantiomer of the racemic  $\alpha$ -amino acids will be occluded within the crystals through their (0–10) face exposed to solution thus “converting” the achiral host  $\alpha$ -Gly crystal into a homochiral mixed crystal of single handedness. This transformation can be illustrated with  $\alpha$ -Gly crystals grown in the presence of *N*<sup>ε</sup>-(2,4-dinitrophenyl)-*S*-lysine. Crystals that exposed only their (010) face to solution during growth had not occluded the yellow dye and therefore are white whereas the crystals

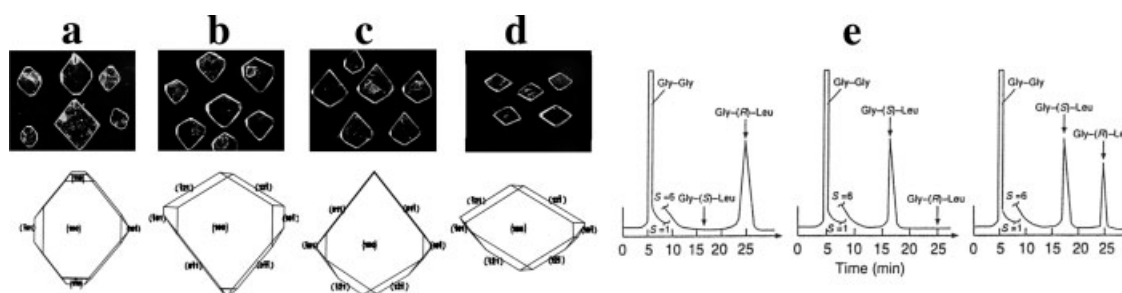
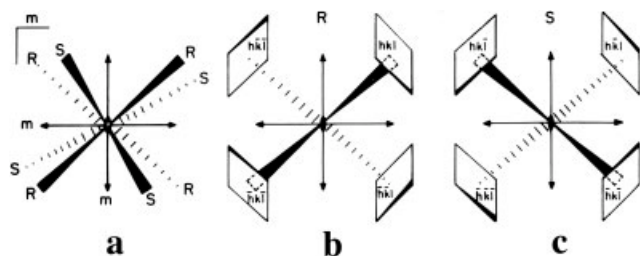


**Fig. 19.** (a–d) Photographs and computer-drawn morphology of glycyl-glycine crystals grown in aqueous solutions (a) pure and (b–d) in the presence of *R*-, *S*-, and *R,S*-glycyl-leucine. (e) Enantiomeric HPLC analyses of samples taken from single crystals as in (d) cut at the  $+b$  and  $-b$  poles and sample from the whole crystal (left to right).



Scheme 6.

exposing to the solution the (0–10) face during growth are yellow, (Fig. 17).

One may envisage that such conglomerates of crusts of glycine crystals might be spread to yield enantio-enriched environments as in the mechanism proposed by Welch.<sup>39</sup>

The diastereisomeric interactions between chiral surfaces of nonchiral crystals and chiral molecules present in solution become manifest by the formation of etch pits. Etch pits were formed only on the (010) face of an  $\alpha$ -Gly crystal partially dissolved in an undersaturated solution containing *R*-alanine, whereas the (0–10) face does not exhibit etch pits, (Fig. 18a). When  $\alpha$ -Gly crystals were cleaved at the {010} plane exposing (010) and (0–10) surfaces that were subsequently etched in a solution containing *R,S*-alanine, they revealed mirror-symmetry related etching patterns, as clearly seen in Figure 18b.

By applying the same principles, we have assigned the absolute configuration of the dipeptide glycyl-leucine that induced a change in the morphology and underwent segregation upon enantioselective occlusion within glycyl-glycine crystals (Fig. 19).<sup>40,41</sup>

In the above systems, all the host crystals belong to the monoclinic space group of point symmetry  $2/m$ . In principle, the present method of the assignment of absolute configuration may also be applied to orthorhombic crystals of point symmetry  $2/m2/m2/m$ , provided that the modified functional groups tend to be directed towards the body diagonal of the crystal (Scheme 6a). In this case, the two enantiomers form two enantiopolar sets (of point symme-

try 222) represented separately in Schemes 6b and 6c. An *R'* additive would affect the faces shown in Scheme 6b and an *S'* additive the enantiopolar set Scheme 6c.

### "Absolute" Asymmetric Synthesis in Centrosymmetric Crystals

In the previous examples, either both the host and the guest were chiral molecules or only the guest was chiral. These studies were extended to centrosymmetric crystals where both the host and guest components are achiral molecules, to yield in a photoreaction a product that is homochiral, where the absolute sense of chirality of the product can be assigned from the structure of the crystal surfaces. Thus, additive *E*-cinnamic acid  $\text{C}_6\text{H}_5\text{—CH=CH—CO}_2\text{H}$  induces a loss of the center of inversion in the crystal of *E*-cinnamamide  $\text{C}_6\text{H}_5\text{—CH=CH—CONH}_2$  which, in pure form, appears in a centrosymmetric monoclinic arrangement, space group  $P2_1/c$ . The crystal structure (Fig. 20a) is composed of hydrogen-bonded dimers interlinked by  $\text{N—H}\cdots\text{O}$  bonds to form a ribbon-like motif that runs parallel to the *b* axis. *E*-cinnamic acid is preferentially occluded through half of the {011} surface sites of the crystal at the opposite ends of these ribbons, resulting in a change in crystal morphology, (Figs. 20b and 20c), the affected crystal composed of two enantiomorphous halves of at most  $P2_1$  symmetry. This reduced symmetry was proven photochemically.<sup>42</sup> Ultraviolet irradiation of *E*-cinnamamide yields centrosymmetric photodimers, by virtue of a cyclobutane ring formation involving pairs of close packed  $>\text{C}=\text{C}<$  bonds across centers of inversion (Fig. 21). Replacement of one of such a pair by *E*-cinnamic acid results in the formation of asymmetric cinnamamide–cinnamic acid photodimers of opposite chirality at the two enantiomorphous halves of the mixed crystal, with an enantiomeric ratio of 60:40 at each opposite half, Figure 20c. This absolute configuration of the C4 rings follows directly from the mode the acid is inserted in the growing crystal. The four C-atoms of the C4 ring formed by insertion of the acid at the  $+b$  pole of the crystal are of *R*-absolute configuration, whereas that formed at  $-b$  side are of *S*-

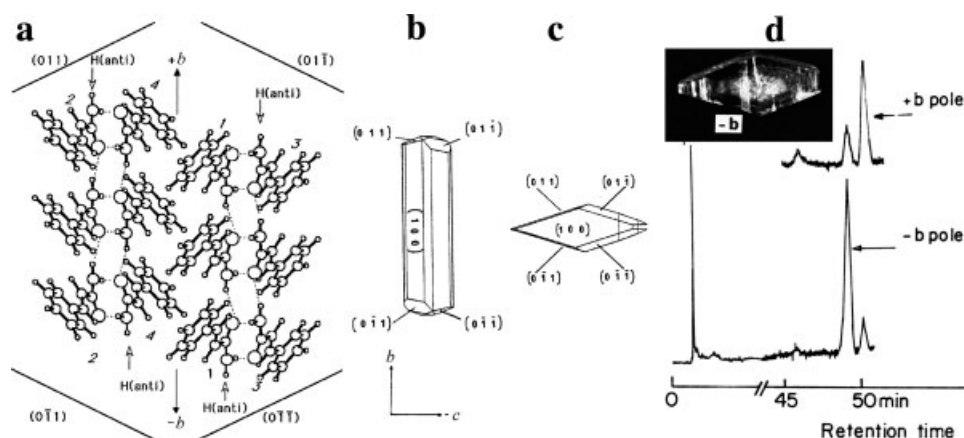
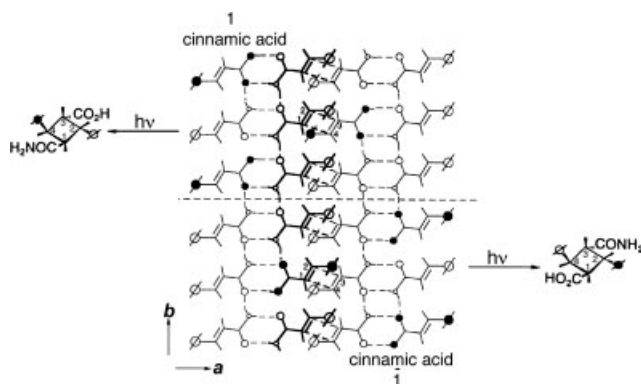


Fig. 20. Packing arrangement of *E*-cinnamamide viewed along the *a* axis delineated by the {011} faces; (b, c) morphology of *E*-cinnamamide crystals, pure and grown in the presence of cinnamic acid; (d) HPLC analysis of the products obtained at the  $+b$  and  $-b$  poles of the host crystal.



**Fig. 21.** Ribbons, along the *b* axis, of hydrogen-bonded molecules composed of *E*-cinnamamide (open circles) and occluded guest *E*-cinnamic acid molecules (full circles). The latter were adsorbed through site 1 at the  $+b$  end and site  $-1$  at the  $-b$  end, leading to two enantiomorphous domains joined at the central dotted line. Shown also are the ribbons related by translation along the *a* axis so depicting the close 4 Å contact between C=C double bonds related by a center of inversion. Also shown are two enantiomorphous cyclobutane photodimers between the host and occluded guest from the top and bottom halves of the crystal.

configuration.<sup>42</sup> The predicted configuration was confirmed by an independent Bijvoet analysis.

## CONCLUSIONS

The use of “tailor-made” additives on crystallization and dissolution processes provide two methods for the assignment of absolute configuration of chiral molecules, independent of the Bijvoet method that involves the use of anomalous X-ray scattering. For the process of crystallization, the methods involving “tailor-made” additives exploit the change in crystal morphology and possible detection of additives enantioselectively occluded within the crystal for the assignment of absolute molecular configuration. The first method comprises for crystals possessing a polar axis, determination of its direction vis-à-vis the crystal structure, leading directly to the assignment of the absolute configuration of the constituent molecules. The second method involves the direct assignment of the absolute configuration of chiral molecules as additives by their effect on the morphology of centrosymmetric crystals and by their anisotropic distribution within the host crystal on enantioselective occlusion. For the process of partial dissolution, the selective etching of crystal faces has been useful for the assignment of absolute configuration of chiral molecules and fixation of crystal polarity. Although these methods do not compete with the general method involving anomalous X-ray scattering developed by Bijvoet and fine-tuned by Flack,<sup>43</sup> it may have advantages in specific cases such as the assignment of the absolute configuration of the  $\beta$ -polymorph of glycine, the chiral crystal structure of which is close to  $2/m$  symmetry. Furthermore, this method, by virtue of its experimental and conceptual simplicity, is useful for demonstrating to chemistry students the assignment of the absolute configuration of chiral molecules.

## ACKNOWLEDGMENTS

This research was made possible in part by the historic generosity of the Harold Perlman family.

## LITERATURE CITED

1. Pasteur L. Sur les relations qui peuvent exister entre la forme cristalline, la composition chimique et le sens de la polarisation rotatoire. *Ann Chim Phys* 1848;24:442–459.
2. Van't Hoff JH. Sur les formules de structure dans l'espace. *Arch Neerl Sci Exactes Nat* 1874;9:445–454.
3. Le Bel JA. *Bull Soc Chim France* 1874;22:337–347.
4. Fischer E. Ueber die Configuration des Traubenzuckers und seiner Isomeren. II. *Chem Ber* 1891;24:2683–2687.
5. Rosanoff MA. On Fischer's classification of stereo-isomers. *J Am Chem Soc* 1906;28:114–121.
6. Fredga A. *The Svedberg 1844–1944 Uppsala and Stockholm* 1944;261.
7. Fredga A. Steric correlations by the *quasi-racemate* method. *Tetrahedron* 1960;8:126–144.
8. Bijvoet JM, Peerdeman AF, vanBommel AJ. Determination of the absolute configuration of optically active compounds by means of X-rays. *Nature* 1951;168:271–272.
9. Addadi L, Berkovitch-Yellin Z, Weissbuch I, Lahav M, Leiserowitz L. A link between macroscopic phenomena and molecular chirality: crystals as probes for the direct assignment of absolute configuration of chiral molecules. In: Eliel EL, Willen SH, Allinger NL, editors. *Topics in stereochemistry*, Vol. 16. New York: Wiley; 1986. p 1.
10. Addadi L, Berkovitch-Yellin Z, Weissbuch I, van Mil J, Shimon LJW, Lahav M, Leiserowitz L. Growth and dissolution of organic crystals with tailor-made inhibitors—implications in stereochemistry and material science. *Angew Chem Int Ed* 1985;24:466–485.
11. Weissbuch I, Addadi L, Lahav M, Leiserowitz L. Molecular recognition at crystal interfaces. *Science* 1991;253:637–645.
12. Weissbuch I, Popovitz-Biro R, Lahav M, Leiserowitz L. Understanding and control of nucleation, growth, habit, dissolution and structure of two and three-dimensional crystals using “tailor-made” auxiliaries. *Acta Crystallogr B* 1995;51:115–148.
13. Addadi L, Gati E, Lahav M. Useful impurities for optical resolutions. III. An improved pasteur-type resolution of conglomerates and a new empirical method for assignment of absolute configuration. *J Am Chem Soc* 1981;103:1251–1252.
14. Addadi L, Berkovitch-Yellin Z, Domb N, Gati E, Lahav M, Leiserowitz L. Resolution of conglomerates by stereoselective habit modification. *Nature* 1982;296:21–26.
15. Addadi L, Weinstein S, Gati E, Weissbuch I, Lahav M. Resolution of conglomerates with the assistance of tailor-made impurities. Generality and mechanistic aspects of the “rule of reversal”. A new method for assignment of absolute configuration. *J Am Chem Soc* 1982;104:4610–4617.
16. Zbaida D, Weissbuch I, Shavit-Gati E, Addadi L, Leiserowitz L, Lahav M. Design of chiral polymers for the kinetic resolution of racemic conglomerates. *React Polym* 1987;6:241–253.
17. Zbaida D, Lahav M, Drauz K, Knaup G, Kottenhahn M. A cyclic continuous process for converting conglomerates into optically pure enantiomers by crystallization and dissolution with the assistance of “tailor-made” polymers. *Tetrahedron* 2000;56:6645–6649.
18. Kondepudi DK, Crook KE. Theory of conglomerate crystallization in the presence of chiral impurities. *Cryst Growth Des* 2005;5:2173–2179.
19. Berkovitch-Yellin Z, Addadi L, Idelson M, Leiserowitz L, Lahav M. Absolute-configuration of chiral polar crystals. *Nature* 1982;296:27–34.
20. Visser RA, Bennema P. Interpretation of the morphology of  $\alpha$ -lactose hydrate. *Neth Milk Dairy* 1983;37:109–116.
21. Traube N. *Neues Jahrb Min Geol* 1891; USW Beilage Bd. 7:S43.
22. Michaelis AS, vanKreveld A. Influences of additives on growth rates in lactose crystals. *Neth Milk Dairy* 1966;20:163–181.

23. Fries PC, Rao ST, Sundaralingam M. Structural chemistry of carbohydrates. III. Crystal and molecular structure of 4-*O*- $\beta$ -D-galactopyranosyl- $\alpha$ -D-glucopyranose monohydrate ( $\alpha$ -lactose monohydrate). *Acta Crystallogr B* 1971;27:994–1005.
24. Beevers CA, Hansen HN. The structure of  $\alpha$ -lactose monohydrate. *Acta Crystallogr B* 1971;27:1323–1325.
25. Bennema P, Gilmer G. In: Hartman P, editor. *Kinetics of crystal growth*. Amsterdam: North-Holland; 1973. p 263.
26. Bourne JR, Davey RJ. The role of solvent–solute interactions in determining crystal growth mechanisms from solution. I. The surface entropy factor. *J Cryst Growth* 1976;36:278–286.
27. Elwenspock M, Bennema P, vanderEerden JP. Orientational order in naphthalene crystal-solution interfaces. *J Cryst Growth* 1987;83:297–305.
28. Shimon LJW, Vaida M, Addadi L, Lahav M, Leiserowitz L. Molecular recognition at the solid-solution interface: a relay mechanism for the effect of solvent on crystal growth and dissolution. *J Am Chem Soc* 1990;112:6215–6220.
29. Shimon LJW, Lahav M, Leiserowitz L. Stereoselective etchants for molecular crystals. Resolution of enantiomorphs and assignment of absolute structure of chiral molecules and polar crystals. *Nouv J Chem* 1986;10:723–737.
30. Wang J-L, Lahav M, Leiserowitz L. Direct assignment of absolute configuration of chiral alkyl gluconamides by wettability measurements. *Angew Chem Int Ed* 1991;30:696–698.
31. Zabel V, Müller-Fahrnow A, Hilgenfeld R, Saenger W, Pfannemüller B, Enkelmann V, Welte W. Amphiphilic properties of synthetic glycolipids based on amide linkages. II. Crystal and molecular structure of *N*-(*n*-octyl)-D-gluconamide, an amphiphilic molecule in head-to-tail packing mode. *Chem Phys Lipids* 1986;39:313–327.
32. Wang J-L, Leiserowitz L, Lahav M. A correlation between surface wettability and solvent effect on crystal growth. The *N*-Octyl-gluconamide/methanol System. *J Phys Chem* 1992;96:15–16.
33. Weissbuch I, Torbeev VY, Leiserowitz L, Lahav M. Solvent effect in crystal polymorphism: why addition of methanol or ethanol to aqueous solutions induces the precipitation of the least stable <sup>®</sup> form of glycine. *Angew Chem Int Ed* 2005;44:3226–3229.
34. Torbeev VY, Shavit E, Weissbuch I, Leiserowitz L, Lahav M. Control of crystal polymorphism by tuning the structure of auxiliary molecules as nucleation inhibitors. The  $\beta$ -polymorph of glycine grown in aqueous solutions. *Cryst Growth Des* 2005;5:2190–2196.
35. Addadi L, Berkovitch-Yellin Z, Weissbuch I, Lahav M, Leiserowitz L. The use of “enantiopolar directions in centrosymmetric crystals for direct assignment of absolute configuration of chiral molecules: application to the serine/threonine. *J Am Chem Soc* 1982;104:2075–2077.
36. Weissbuch I, Shimon LJW, Addadi L, Berkovitch-Yellin Z, Weinstein S, Lahav M, Leiserowitz L. Stereochemical discrimination at organic crystal surfaces: the systems serine/threonine and serine/allo-threonine. *Isr J Chem* 1985;25:353–361.
37. Weissbuch I, Addadi L, Berkovitch-Yellin Z, Gati E, Weinstein S, Lahav M, Leiserowitz L. Centrosymmetric crystals for the direct assignment of the absolute configuration of chiral molecules—application to the  $\alpha$ -amino acids by their effect on glycine crystals. *J Am Chem Soc* 1983;105:6615–6621.
38. Weissbuch I, Lahav M, Leiserowitz L. Toward stereochemical control, monitoring and understanding of crystal nucleation. *Cryst Growth Des* 2003;3:125–150.
39. Welch C. Formation of highly enantioenriched microenvironments by stochastic sorting of conglomerate crystals: a plausible mechanism for generation of enantioenrichment on the prebiotic earth. *Chirality* 2001;13:425–427.
40. Weissbuch I, Berkovitch-Yellin Z, Leiserowitz L, Lahav M. Stereochemical discrimination at organic crystal surfaces: the effect of the molecular structure and conformation of dipeptide additives on the morphology of glycyl-glycine crystals. *Isr J Chem* 1985;25:362–372.
41. Weissbuch I, Leiserowitz L, Lahav M. Stochastic “mirror symmetry breaking” via self-assembly, reactivity and amplification of chirality: relevance to abiotic conditions. In: Walde P, editor. *Topics in Current Chemistry*, Vol. 259. Berlin: Springer-Verlag; 2005. p 123–165.
42. Vaida M, Shimon LJW, van Mil J, Ernst-Cabrera K, Addadi L, Leiserowitz L, Lahav M. Absolute asymmetric photochemistry using centrosymmetric single crystals. The host/guest system (*E*)-cinnamamide/(*E*)-cinnamic acid. *J Am Chem Soc* 1989;111:1029–1034.
43. Flack HD, Bernardinelli G. Absolute structure and absolute configuration. *Acta Crystallogr A* 1999;55:908–915.



## Review Article

# Chiral Doping of Nematic Phases and Its Application to the Determination of Absolute Configuration

SILVIA PIERACCINI,<sup>1</sup> ALBERTA FERRARINI,<sup>2\*</sup> AND GIAN PIERO SPADA<sup>1\*</sup>

<sup>1</sup>*Alma Mater Studiorum–Università di Bologna, Dipartimento di Chimica Organica “A. Mangini”, via San Giacomo 11, I-40126 Bologna, Italy*

<sup>2</sup>*Università di Padova, Dipartimento di Scienze Chimiche, via F. Marzolo 1, I-35131 Padova, Italy*

**ABSTRACT** Doping nematic liquid crystals with nonracemic chiral compounds induces a twisted nematic (cholesteric) phase. The ability of solutes to twist the nematic phase may be related to the overall shape of the chiral dopant and consequently to its absolute configuration. The cholesteric induction is therefore a powerful tool complementary to chiroptical techniques to obtain stereochemical information on chiral molecules. *Chirality* 20:749–759, 2008. © 2007 Wiley-Liss, Inc.

**KEY WORDS:** cholesteric induction; absolute configuration; liquid crystal; nematic; helical twisting power

## INTRODUCTION

In 1888 an Austrian botanist, Friedrich Reinitzer, while working on cholesteryl benzoate discovered a novel state of matter, which was later called liquid crystalline.<sup>1</sup> Although liquid crystals have been known for more than a century, only in the past 30 years their unusual properties have found technological applications, especially in displays and other electronic devices.<sup>2</sup>

Liquid crystalline phases (LCs), or mesophases, are intermediate between the crystal and the ordinary liquid phases (For general books on LC, see for example Refs. 3–6). Their range of existence in temperature is between those typical of liquids and crystals. Intermediate is also the order of the systems: they are characterized by long-range orientational order, which is anyway lower than in crystals.

Although liquid crystals exhibit certain properties of solids (e.g., birefringence) and liquids (e.g., fluidity), they also possess properties that are not found in either liquids or solids. The orientation of the optical axis, for example, can be controlled by magnetic or electric fields; in some liquid crystals the optical activity is one order of magnitude higher than in liquids; certain liquid crystals change their color as a result of the sensitivity of their structure to temperature. These are some of the properties on which the practical applications of liquid crystals are based.

A variety of liquid crystal phases have been found, which are characterized by a different organization. The common nematic LCs have one-dimensional order; the molecules forming the phase are anisometric (usually elongated) and tend to align along a common direction (the director). From a stereochemical point of view, the most important phase is the cholesteric phase (or chiral nematic phase) that may occur when the system is com-

posed by chiral molecules. The cholesteric phase can be considered a twisted nematic, with a nematic-like order of molecules with respect to the local director, which rotates in space in helical way (see Fig. 1). The cholesteric helix is characterized by the pitch length (the distance along the helix axis for a rotation of 360° of the director) and its handedness.

## The Cholesteric Induction

More than 80 years ago G. Friedel, a French physicist, described the close relationship between the nematic and the cholesteric phase.<sup>7</sup> He showed that a small amount of a chiral nonracemic compound, dissolved in a nematic phase, transforms it into a cholesteric phase. This discovery remained unappreciated for almost 50 years: the next papers on this topic appeared during the 1960s.<sup>8</sup>

The key property for the configuration assignment of chiral molecules is the induction of oppositely-handed cholesterics by enantiomers; however, the relation between absolute configuration of the dopant and sense of the induced cholesteric is neither simple nor obvious.

Contract grant sponsor: MiUR/PRIN (Modelling and characterization of liquid crystals for nano-organized structures); Contract grant number: 2005035119

\*Correspondence to: Prof. Gian Piero Spada, Alma Mater Studiorum–Università di Bologna, Dipartimento di Chimica Organica “A. Mangini,” Via San Giacomo 11, I-40126 Bologna (Italy). E-mail: gianpiero.spada@unibo.it or Prof. Alberta Ferrarini, Università di Padova, Dipartimento di Scienze Chimiche, Via F. Marzolo 1, I-35131 Padova (Italy).

Received for publication 31 May 2007; Accepted 16 August 2007

DOI: 10.1002/chir.20482

Published online 12 October 2007 in Wiley InterScience (www.interscience.wiley.com).

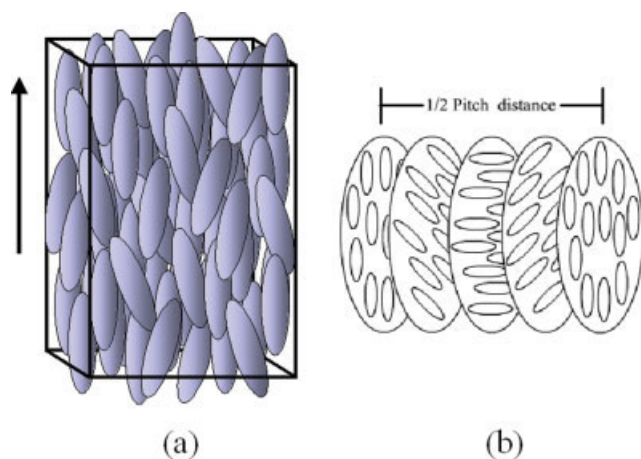


**Fig. 1.** Schematic representation of a nematic (a) and a cholesteric phase (b). The mean alignment axis in the nematic phase (the director) is shown by the arrow. The director rotates around the helical axis, remaining perpendicular to it, in the cholesteric phase.

A quantitative study of the cholesteric induction has required the definition of the concept of “helical twisting power”, i.e., the ability of a chiral dopant to twist a nematic phase<sup>9</sup>:

$$\beta = (pcr)^{-1} \quad (1)$$

where  $p$  is the cholesteric pitch,  $c$  the dopant molar fraction, and  $r$  its enantiomeric excess. The sign of  $\beta$  is taken positive for a right-handed cholesteric ( $P$ ) and negative for a left-handed one ( $M$ ). This inverse proportionality relation between pitch and dopant concentration is experimentally observed for molar fraction lower than about 0.01–0.05. The twisting ability is characteristic of a given dopant, with some dependence on temperature and solvent. From a stereochemical point of view, one can notice that  $\beta$  characterizes a chiral dopant in a way similar to the classical rotatory power. Nevertheless the origin of the two properties is different. The optical rotation is a consequence of the interaction between light and matter, while the cholesteric induction originates from solute–solvent interactions. Reasonably, we can expect to obtain different information from the two techniques: the LC technique should be more sensitive to the molecular shape and less to the electronic characteristics of the molecules.

The quantification of  $\beta$  requires the determination of the magnitude and sense of the cholesteric pitch.<sup>10</sup> This can be obtained with spectroscopic or nonspectroscopic methods.<sup>11,12</sup> The former techniques are based on typical optical properties of the cholesterics. In particular,<sup>13</sup> in their planar texture (i.e., with the cholesteric axis parallel to the light propagation direction) the cholesteric helix reflects circular polarized light of the same handedness and transmits circular polarized light of the opposite handedness, when the wavelength is close to  $\lambda_0 = np$  (where  $n$  is the mean refractive index); as a result, a  $P$ -cholesteric displays an intense negative CD at  $\lambda_0$ . Hence, this spectro-

scopic technique allows the simultaneous determination of pitch and sign of the induced cholesteric. The nonspectroscopic methods are usually based on the observation of the cholesteric phase with an optical microscope in linearly polarized light. Some of these are modification of the Grandjean–Cano method<sup>14–17</sup> based on the observation of the disclination lines that appear when a cholesteric is inserted in a variable-pathlength cell whose windows are appropriately rubbed to obtain the necessary alignment. The lens version is illustrated in Figure 2. From the distance between these lines one can obtain the cholesteric pitch. The sense of the cholesteric can be obtained either modifying the geometry of the cell (e.g., modifying the rubbing directions of the windows surfaces or rotating one window—the lens—with respect to the other—the plate), or from the observation of the rotatory power originated by the helicoidal molecular order.<sup>13</sup>

Another technique widely used to measure the cholesteric pitch is based on the Bragg scattering of monochromatic light obtained with a He-Ne laser: its angular dependence is strictly related to the cholesteric pitch.<sup>18</sup>

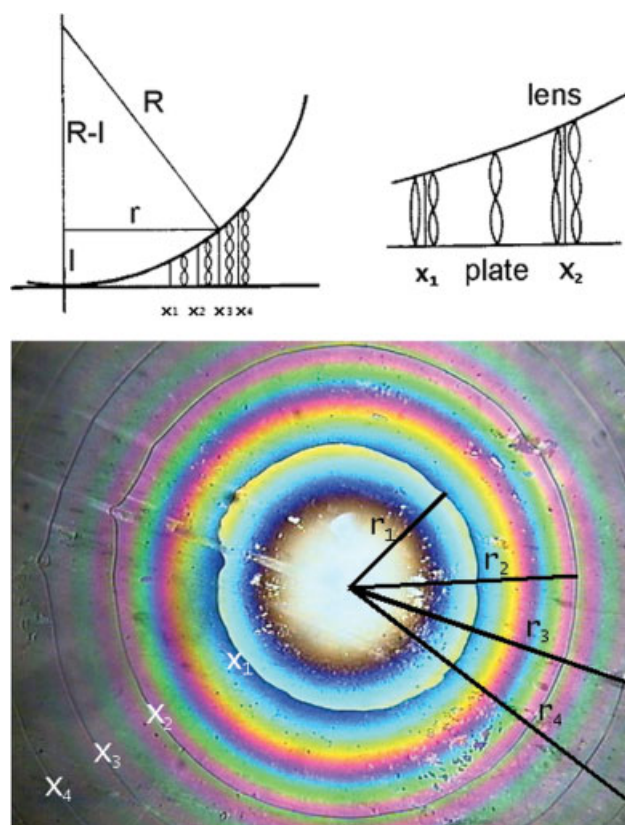


**Fig. 2.** A schematic representation of the origin of the Grandjean–Cano disclination lines which form when a cholesteric is inserted between a plano-convex lens and a glass plate (a) and a typical texture (b). The surfaces of both lens and plate are rubbed to produce grooves along which the director is aligned; the rubbing directions of the top and bottom surfaces lie parallel to each other. In correspondence of the  $x$ 's, the number of half-turns changes by one and this causes defects which are visible as sharp lines of circular shape. The radii  $r$  of the circular Grandjean–Cano disclinations are a function of only the curvature radius  $R$  of the lens and of the pitch of the cholesteric phase.

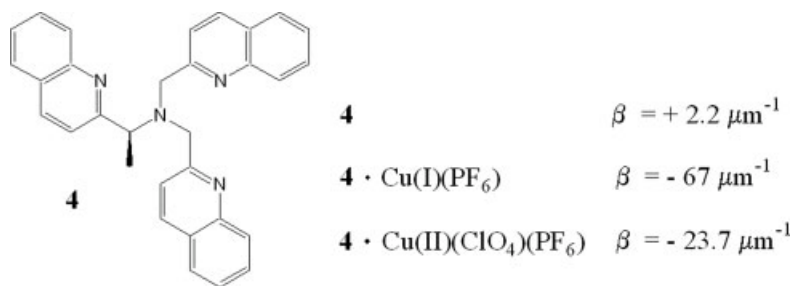
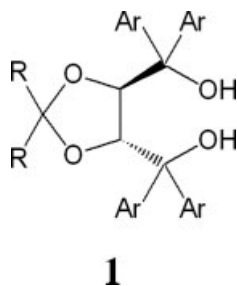


Fig. 3. Enhancement of helical twisting power by metal coordination (solvent: MBBA).

### The Amplification of Chirality\*

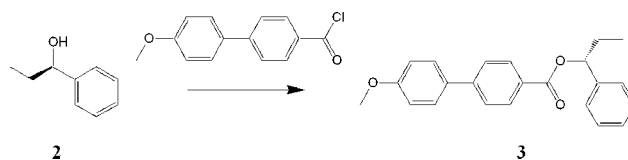
On passing from molecular to mesophase chirality, the molecular dissymmetry is amplified in the supramolecular helix structure.<sup>21,25,26</sup> This allows one to detect even traces of chiral dopants. Jean Jacques was the first in 1968 to use the cholesteric induction to detect the spontaneous resolution of racemates when the single crystals were too small to allow optical rotation measurements.<sup>27</sup> Later, several papers described the use of the cholesteric induction for detecting traces of chiral dopants<sup>9,28</sup> or to detect compounds with very low optical rotation.<sup>29</sup>

Chiral dopants can exhibit a different ability to twist the nematic phase spanning from weak inducers ( $\beta < 1 \mu\text{m}^{-1}$ ) to strong inducers ( $\beta > 20 \mu\text{m}^{-1}$ ); to our knowledge, the strongest chiral dopants investigated are TADDOL derivatives **1** typically showing twisting powers in the range 300–400  $\mu\text{m}^{-1}$ .<sup>30</sup> A record of 534  $\mu\text{m}^{-1}$  was achieved with TADDOL where Ar =  $\beta$ -naphthyl and R,R = 2,2'-biphenyldien in the nematic phase 4'-pentyl-4-cyanobiphenyl.<sup>31</sup>



\*Chiral doping of nematic phases has been investigated over the last 30 years along two major directions. The first focuses on the investigation of the chirality transfer between a "shape persistent" dopant and a nematic solvent: the aim is "reading" the stereochemical information of the solute (e.g., its absolute configuration) by means the solvent and will be reviewed in the next sections. A second line is dedicated to the development of switchable dopants able to modify their shape (and hence their chiral transfer to the solvent) as a function of external stimuli (usually light or heat). A remarkable example has been reported on recently by Feringa and coworkers.<sup>19,20</sup> They described the rotational reorganization of cholesteric liquid crystalline films as the result of the conversion of a chiral molecular motor dopant to an isomer with a different helical twisting power, leading to a change in the cholesteric pitch. The direction of this reorganization is correlated to the sign of the change in helical twisting power of the dopant. The rotational reorganization of the liquid crystalline film was used to rotate microscopic objects 4 orders of magnitude larger than the bistable dopants in the film, which shows that molecular motors and switches can perform work. This field of the cholesteric induction by switchable dopants (whose emphasis points mainly to applications, material chemistry, ...) is beyond the scope of the present review and has been reviewed elsewhere.<sup>21–24</sup>

When the helical twisting power is very low (as often observed for molecules whose chirality is due to stereogenic centres, vide infra), different approaches have been used to improve the ability of the molecule to express its chirality at the mesophase level. One possibility is to adopt a "mesogenic functionalization" of the chiral dopant. The introduction of a group resembling the structure of the nematic host enhances the solubility and the solute–solvent interactions and this yields an enhancement of the dopant twisting ability. Feringa and coworkers adopted this approach for simple amines and alcohols: while the parent compounds show very low  $\beta$ s (e.g. for **2** it is negligible), the functionalized compounds exhibit twisting powers sufficiently high (e.g. 36.7  $\mu\text{m}^{-1}$  for **3**) to allow the generation of colored LC films.<sup>32–34†</sup>



Scheme. Mesogenic functionalization of chiral alcohol **2**.

The interaction of a chiral dopant with a nematic host may be improved also by metal coordination.<sup>35</sup> Tris(pyridyl)amine-based ligands (e.g. **4**, see Fig. 3) show negligible to small helical twisting powers in the most common nematic solvents, whereas complexation with Cu(I) or Cu(II) greatly increases  $\beta$  as a consequence of the reduced conformational flexibility and of the (more or less) propeller-like shape of the complexes. Furthermore, changes in overall shape of the complexes induced by different metals and counterions are transferred to the supramolecular level and proportionate changes of the helical twisting powers are observed.<sup>36,37</sup> C<sub>2</sub> or C<sub>3</sub>-symmetry, propeller-shaped tris(diketonate) metal complexes are reported to show high twisting power<sup>36,37</sup> (see below for the discussion on the importance of these elements in determining the  $\beta$ -values).

A third approach to enhance the chirality employs a cosolute that binds to the low- $\beta$  dopant. Eelkema and Fer-

†As the color of these films is dependent on the enantiomeric excess of the dopants, this method allowed the evaluation of the enantiomeric excess of simple chiral compounds by inspection of the color after mesogenic derivatization and doping in a nematic LC.



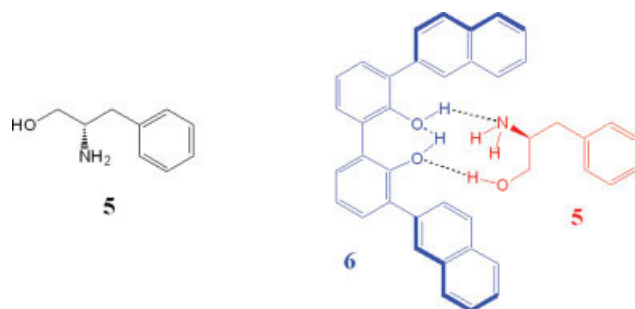


**Fig. 4.** Dynamically chiral biphenyl-based receptor **6** for the enhancement of the cholesteric induction by the chiral aminoalcohol **5**.

inga proposed a “double amplification” approach which employs a dynamically chiral biphenol or biphenyl phosphoric acid receptors for amplifying the chirality of simple amines and aminoalcohols. The binding between the dopant (e.g. **5**, see Fig. 4) and the receptor (e.g. **6**) through H-bonding, induces a chiral conformation of the biphenyl receptor which, in turn, induces more efficiently a cholesteric in a commercial nematic LC (see below the importance of the conformation of biaryl units in the cholesteric induction).<sup>38,39</sup>

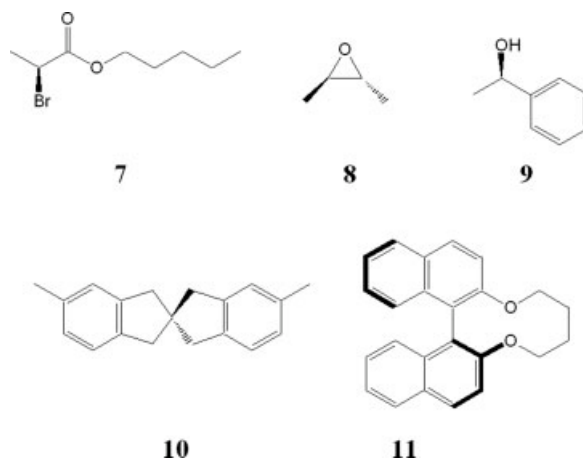
#### EMPIRICAL APPROACHES FOR THE CONFIGURATION ASSIGNMENT

In cholesteric induction experiments the molecular chirality is mapped onto an achiral (nematic) phase to yield a superstructural phase chirality which can be measured. With a model that relates the molecular chirality to the mesophase chirality one could infer stereochemical information about the dopant (e.g., the absolute configuration, the preferred conformation). In 1984 Solladié published the first review summarising the state of the art at that time.<sup>10</sup> Later on, several review articles updated this subject.<sup>40–42</sup>

The first empirical correlation between the cholesteric handedness and the solute configuration was described by Gottarelli et al. in 1975.<sup>43</sup> They reported that a series of homochiral benzyl alcohols in MBBA induces cholesterics of the same handedness. A few years later, Korte et al. reported<sup>44–46</sup> the first attempt to find a general correlation between the configuration of a stereocenter and the handedness of the induced cholesteric. He related the handedness of the cholesteric to a stereochemical descriptor of the dopant based on the effective volume of the substituents. This relation is followed by more than 100 compounds, as claimed by Korte, but also exceptions were reported.<sup>47</sup> Furthermore, this approach does not account for the structure of the nematic solvent molecules; it may happen that the same compound induces cholesterics of opposite handedness in different nematics.<sup>48,49</sup>

At the beginning of the 1980s an empirical approach, based on the analysis of many systems, was followed to identify the structural features of dopant and solvent associated to high values of  $\beta$ . The results, summarized in Refs. 40–42, indicated that most dopants with high twisting power are characterized by the presence of two (or more)

(quasi-)planar moieties twisted one with respect to the other(s). For example, while aliphatic compounds with one or two stereocenters **7** and **8**, derivative **9** with one aromatic ring and spiro-compound **10** with two almost perpendicular benzene rings have helical twisting powers not exceeding  $1 \mu\text{m}^{-1}$ , biaryl **11** has  $\beta$  around  $60 \mu\text{m}^{-1}$  in the same (or similar) solvent (see Table 1).



The recognition that this molecular feature is connected to a highly efficient transfer of chirality does not allow the prediction of the sense of the induced cholesteric: a molecular model is required to this purpose. In the first empirical approach proposed,<sup>53</sup> the solvent molecules are considered as achiral rigid rods and the role of the chiral dopant is to prevent their parallel alignment, leading to the helical arrangement. This model, which has been used to assign the configuration of a few series of compounds,<sup>43,53</sup> cannot account for the dependence of the value of  $\beta$  (and sometimes its sign)<sup>48,49</sup> on the nature of the solvent and its increase when the chemical structure of the solute and solvent molecules are similar.<sup>54</sup> As a general finding, biaryl dopants show the highest value of  $\beta$  in biaryl solvents (e.g., cyanobiphenyl nematics),<sup>55</sup> while *trans*-diaryl oxiranes (and related molecules) exhibit the highest  $\beta$ s in MBBA<sup>50</sup> (see Fig. 5). Furthermore, the ability to twist the nematic also depends on the conformational mobility of the host, and in a rigid core solvent the values of  $\beta$  are generally smaller.<sup>56</sup>

These results allowed the proposal, at the beginning of the 1980s, of a different molecular model for cholesteric induction.<sup>54,55</sup> This model is sketched in Figure 6 in the case when both nematic host and chiral guest have a

**TABLE 1.** Helical twisting powers of compounds **7–11** measured at room temperature

	$\beta$	Solvent	Ref.
<b>7</b>	+0.5	MBBA/EBBA	46
<b>8</b>	+0.5	MBBA	50
<b>9</b>	−1.0	MBBA	51
<b>10</b>	−1.0	MBBA/EBBA	46
<b>11</b>	+79	PCB	52



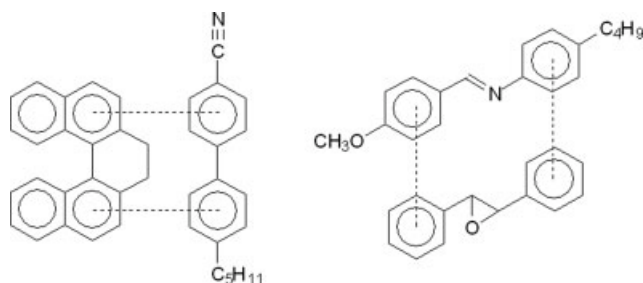
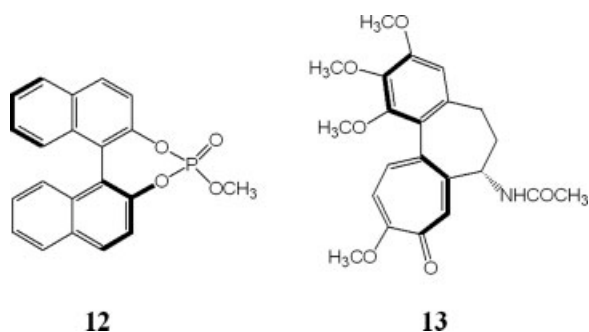


Fig. 5. Structural similarity between a biaryl derivative and the nematic phase K15, and between *trans*-stilbene oxide and the nematic MBBA.

biaryl structure. Typical nematogenic molecules are flexible and can exist in chiral enantiomorphic conformations of opposite helicity in fast interconversion. The chiral dopant has a well defined molecular helicity (*M* in Fig. 6)<sup>‡</sup> and stabilizes the homochiral conformation of the solvent: in this way, the *M*-chirality is transferred from the dopant to the near molecule of the solvent and from this to the next-near one and so on. This leads to a deracemization of the nematic solvent and its transformation into a *M*-cholesteric.<sup>57</sup>

The mechanism of Figure 6 has been supported by rotatory power measurements in isotropic solutions.<sup>58</sup> The rotatory power in dynamically chiral nonmesogenic solvents (e.g. biphenyls) is increased or decreased in comparison with ordinary solvents (e.g. acetonitrile) in relation to the sign of twisting power of the solute. Binaphthyl **12**, a compound with positive twisting power ( $\beta = +73 \mu\text{m}^{-1}$  in E7, a mixture of biaryl derivatives), in nonmesogenic biphenyl solvents displays a rotatory power ( $+762^\circ$ , in 4-pentylbiphenyl) which is much more positive than in acetonitrile ( $+469^\circ$ ); cholchicine (**13**) has a positive  $\beta$  ( $+54 \mu\text{m}^{-1}$  in E7) and is laevorotatory in acetonitrile ( $-162^\circ$ ), while in biphenyl solvents it displays a small negative rotation ( $-9^\circ$ ). These data can be interpreted assuming that the right-handed twisting compounds **12** and **13** in biaryl solvents induce an excess of solvent molecules in the *P*-conformation; their contribution to the rotatory power is positive. Molecular statistical calculations support this chirality transfer.<sup>58</sup>



<sup>‡</sup>In this context, the *P*, *M* descriptors do not refer to the configuration of chirality axes, planes or helices according to IUPAC, but simply to the handedness of the twist between the two planes. For example, biphenyl is designed as *P* when the two phenyl rings are arranged in such a way that a clockwise rotation of the ring closer to the observer is required to obtain the coplanarity of the two aromatic planes.

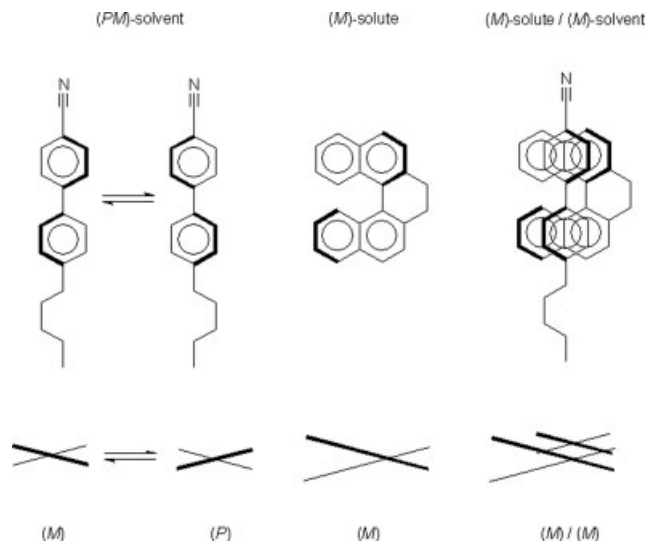


Fig. 6. The chirality transfer from the dopant to the solvent. A chiral inducer with an (*M*)-helicity<sup>‡</sup> aligned with its biaryl axis parallel to the biphenyl axis of the solvent can have close contact only with molecules of the solvent having the same helicity: the chirality is therefore transferred from the dopant to the near solvent molecule and from this to the next-near one and so on, via chiral conformations.

Several stereochemical applications of cholesteric induction have been described;<sup>10,40–42</sup> reliable results are obtained especially when the dopant has a high twisting power. One of the molecular fragments associated to a high value of twisting power is, as anticipated earlier, the biaryl unit; therefore many experiments have been done on compounds containing this unit.

The main factor in determining the handedness of the cholesterics induced by bridged 1,1'-binaphthyls is the helicity (*P* or *M*) of the solute and this observation is the basis of many configurational studies of chiral binaphthyls. All the homochiral (*aR*)-binaphthyls **14–18** have an *M*-helicity of the core, and all induce, in biphenyl nematics, *M*-cholesterics.<sup>54,59</sup> By systematic structural variations of the covalent bridge, it is possible to obtain 1,1'-binaphthalenes with dihedral angles ranging from 60 to 96° (see series **19–23**); the handedness of the cholesteric phase always matches the helicity of the binaphthyl unit (see Table 1).<sup>48</sup> It should be noticed that derivatives **22** and **23** have helicity (*P*, *s-trans*) opposite to all the other derivatives, hence they induce opposite-handed cholesterics (see Table 2).

	X	Y	Z
<b>14</b>	CH <sub>2</sub>	H	H
<b>15</b>	CH <sub>2</sub>	H	Br
<b>16</b>	CH <sub>2</sub>	H	BzO
<b>17</b>	(CH <sub>2</sub> ) <sub>3</sub>	H	H
<b>18</b>	(CH <sub>2</sub> ) <sub>4</sub>	H	H
<b>19</b>	CH <sub>2</sub>	6-acetamido-2-Py	BzO
<b>20</b>	(CH <sub>2</sub> ) <sub>2</sub> N(CO <sub>2</sub> C <sub>2</sub> H <sub>5</sub> )(CH <sub>2</sub> ) <sub>2</sub>	6-acetamido-2-Py	BzO
<b>21</b>	(CH <sub>2</sub> ) <sub>2</sub> N(CH <sub>3</sub> )(CH <sub>2</sub> ) <sub>2</sub>	6-acetamido-2-Py	BzO
<b>22</b>	CH <sub>2</sub> CCCH <sub>2</sub>	6-acetamido-2-Py	BzO
<b>23</b>	CH <sub>2</sub> ( <i>m</i> -C <sub>6</sub> H <sub>4</sub> )CH <sub>2</sub>	6-acetamido-2-Py	BzO

**TABLE 2. Helical twisting powers of compounds 14–23 measured at room temperature in biphenyl-type nematics<sup>48,55,59</sup>**

	$\beta$	C1-C1' conformation	Core helicity <sup>a</sup>
<b>14</b>	−85	<i>s-cis</i>	<i>M</i>
<b>15</b>	−68	<i>s-cis</i>	<i>M</i>
<b>16</b>	−80	<i>s-cis</i>	<i>M</i>
<b>17</b>	−80	<i>s-cis</i>	<i>M</i>
<b>18</b>	−79	<i>s-cis</i>	<i>M</i>
<b>19</b>	−33.6	<i>s-cis</i>	<i>M</i>
<b>20</b>	−65.6	<i>s-cis</i>	<i>M</i>
<b>21</b>	−2.5	<i>s-cis/s-trans</i>	–
<b>22</b>	+40.0	<i>s-trans</i>	<i>P</i>
<b>23</b>	+95.2	<i>s-trans</i>	<i>P</i>

Also the conformations around the C1-C1' binaphthyl bond and the biaryl core helicities are reported.

<sup>a</sup>See page footnote<sup>‡</sup>.

This finding allows one to obtain useful information also on the conformation of nonbridged binaphthyls in solution.<sup>59–62</sup> In the case of (aS)-binaphthyls, *s-cis*, and *s-trans* conformations are characterized by opposite helicities along the biaryl axis. Therefore one may expect the induction of left-handed or right-handed cholesterics depending on the dominant conformation in solution. In fact, binaphthyls with substituents able to stabilize the *s-cis* conformation exhibit oppositely-signed  $\beta$  values with respect to binaphthyls with the bulkiest substituents stabilizing the *s-trans* conformation.

### THEORETICAL APPROACHES FOR THE CONFIGURATION ASSIGNMENT

The earlier reported examples clearly show the difficulty in associating the measured cholesteric handedness to the dopant configuration. This difficulty is strictly related to the origin of the cholesteric organization, i.e., the interplay of anisotropy (i.e., deviation from spherical symmetry) and chirality (i.e., nonidentity of mirror images) of intermolecular interactions. The former is necessary for the onset of orientational order in liquid crystals, whereas the latter is responsible for the helical arrangement of the director in the case of cholesterics. Chiral interactions are washed out by the orientational disorder in liquids; in nematics on the contrary, by virtue of the orientational anisotropy, they are averaged to a non-zero value and originate a torque, which tends to twist the director. At equilibrium, the twisted configuration is the result of a compromise between the chiral strength and the elastic restoring forces which oppose director deformations.

Important issues, which have to be considered when dealing with theoretical models of chiral induction, are on one side the fluid nature of liquid crystals, which requires interactions to be averaged over all dopant orientations, and on the other side the weakness of the chiral contribution to the intermolecular interactions and its subtle dependence on the molecular structure, which call for detailed modeling. Statistical mechanics treatments have

Chirality DOI 10.1002/chir

been proposed to connect atomic and meso-scale levels, using simplified representation of molecules and suitable approximations to derive a molecular form of the free energy;<sup>63–67</sup> simple expressions for the twisting power have been obtained in the case of toy models. These approaches have played an important role to explain the mechanism of chiral induction, but they can be of limited usefulness if the link between dopant configuration and cholesteric handedness is concerned. Also Monte Carlo techniques have been used to evaluate the helical twisting power of solutes<sup>57,68,69</sup>; atomistic force fields allow a detailed account of the structure of the dopant, but long trajectories are needed for an exhaustive sampling of chiral properties, and the high computational demand of simulations is certainly a limit for practical purposes. Phenomenological models, able to account for the molecular structure with a modest computational cost, seem to provide more suitable tools for the assessment of the absolute configuration. An example is provided by the so called “surface chirality” method, which was presented about a decade ago,<sup>70,71</sup> and since then has been successfully applied to different classes of dopants. It relies on a physically sound model of cholesteric induction, based on a molecular expression of the free energy of the twisted nematic phase, comprising a chiral and an elastic restoring contribution; the helical twisting power is then obtained by minimization of the free energy. A simple form is used for the molecular field: renouncing a detailed representation of the solvent, which is approximated as an elastic continuum, the structure of the solute is explicitly taken into account by parameterizing the chirality and anisotropy of intermolecular interactions according to the molecular surface. Phenomenological expressions scaling with the surface are widely used in other contexts, e.g., within models for implicit solvation,<sup>72–75</sup> with the underlying reason that short range interactions can be related to the amount of surface of a solute accessible to the surrounding molecules. The surface chirality model leads to a linear relationship between the helical twisting power  $\beta$  and the so called “surface chirality parameter”  $Q$ <sup>70,71</sup>:

$$\beta = AQ \quad (2)$$

where  $A$  is a quantity which only depends on the nematic solvent; it is defined as  $A = N_A \xi / 2\pi K_{22} v_m$ , with  $N_A$  being the Avogadro number,  $K_{22}$  and  $v_m$  the twist elastic constant and the molecular volume of the liquid crystal solvent, respectively, and the parameter  $\xi$  the orienting strength, which is related to the degree of order of the solvent. It follows from the definition that the value of  $A$  for a given solvent is a function of temperature; it bears a dependence on the structure of the solvent, mainly through the twist elastic constant, which generally increases with the rigidity of the constituent molecules.<sup>3–6</sup> As far as the application of LC to the determination of configuration is concerned,  $A$  can be taken as a scaling factor, identical for different dopants in the same nematic solvent; usual values are of the order of a few  $\mu\text{m}^{-1} \text{\AA}^{-3}$ .

The surface chirality parameter  $Q$  is the key property, specific of each chiral dopant; it is proportional to the aver-

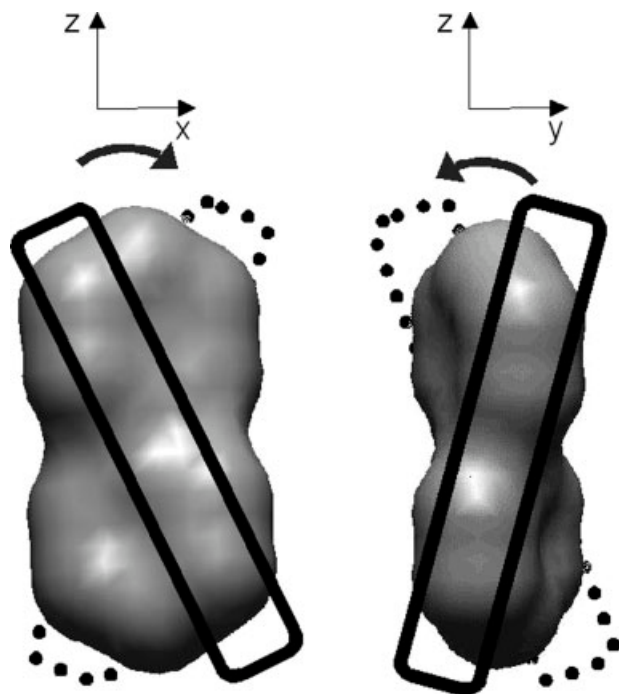


**Fig. 7.** Molecular surface of biphenyl with a twist angle equal to  $\phi = +\pi/4$ , viewed along the  $x$  and  $y$  axes, which tend to lie perpendicular to the helical axis in the LC phase. The  $x$  axis is parallel to the bisector of the twist angle.

age helicity of the molecular surface in the nematic environment, according to the relation<sup>70,71</sup>:

$$Q = -6^{1/2}(Q_{xx} + Q_{yy})S_{\perp} + 6^{-1/2}(Q_{yy} - Q_{xx})\Delta S_{\perp} \quad (3)$$

where  $Q_{ii}$  is the helicity of the molecular surface along the  $i$ th axis and  $S_{\perp} = (S_{xx} + S_{yy})/2$  and  $\Delta S_{\perp} = (S_{xx} - S_{yy})$ , with  $S_{ii}$  being the order parameters, which specify the degree of alignment to the director of the  $i$ th axis. Let us chose  $x$  and  $y$  as the molecular directions, which tend to lie perpendicular to the local director; then, the sign of  $S_{\perp}$  is negative, and the first contribution to the helical twisting power in eq. 3 has the same sign as the average of the helicities of the molecular surface along  $x$  and  $y$ . The second term in eq. 3 accounts for the different contribution of the  $x$  and  $y$  helicities, which derives from the different degree

of order of the corresponding axes. If  $\Delta S_{\perp} \sim 0$ ,  $Q$  is simply proportional to the mean helicity of the molecular surface along the  $x, y$  axes. The surface chirality parameter of a given molecular structure can be easily calculated,<sup>70,71,76</sup> on the basis of the molecular surface which can be generated if the nuclear positions are available.<sup>77,78</sup>

Other approaches for the prediction of the helical twisting power on the basis of the molecular structure have been proposed over the years,<sup>79–83</sup> which however in most cases do not care about the physical origin of the phenomenon, but rather focus on the search of descriptors of the intrinsic chirality of the dopant, assuming that this is linearly related to  $\beta$ , as in eq. 2. The quality of the model is then evaluated from the correlation between calculated and experimental values for sets of solutes. One of the earliest methods in this class is due to Osipov et al., who proposed a chirality tensor, calculated from of the nuclear coordinates, in a form derived from the theory of optical activity.<sup>79</sup> From this tensor two chirality indices were obtained, describing respectively the isotropic and the anisotropic parts of the chirality of the nuclear distribution. Also other chirality indices, defined on the basis of the nuclear positions or the molecular surface of the dopant, have been proposed.<sup>80–84</sup> Calculations for dopants of different structure have shown a general agreement between the various chirality parameters, at least in the sign.

In the following, the surface chirality method will be reviewed in some more detail, considering a few significant examples, which will highlight how the interplay of order and chirality determines the helical twisting ability of a chiral dopant. Biphenyl, whose structure is chiral for twist angles  $\phi \neq n\pi/2$ , with  $n$  integer, is a simple case, yet sufficient to illustrate some important issues. Two different views of the molecular surface of biphenyl for  $\phi = +\pi/4$  (*P*-twisted enantiomer) are shown in Figure 7, together with the corresponding helicities. Order parameters and surface chirality components of biphenyl change as a function of the twist angle; accordingly, also the chirality parameter  $Q$  changes, as shown in Figure 8. For *P*-helicity of biphenyl ( $\phi < \pi/2$ ) a positive helical twisting power is predicted, as a result of the strong tendency of the  $y$  axis, characterized by high positive helicity, to lie perpendicular to the director.

Indeed, a highly positive twisting power has been measured for the homochiral (*P*) biphenyl derivatives **24**–

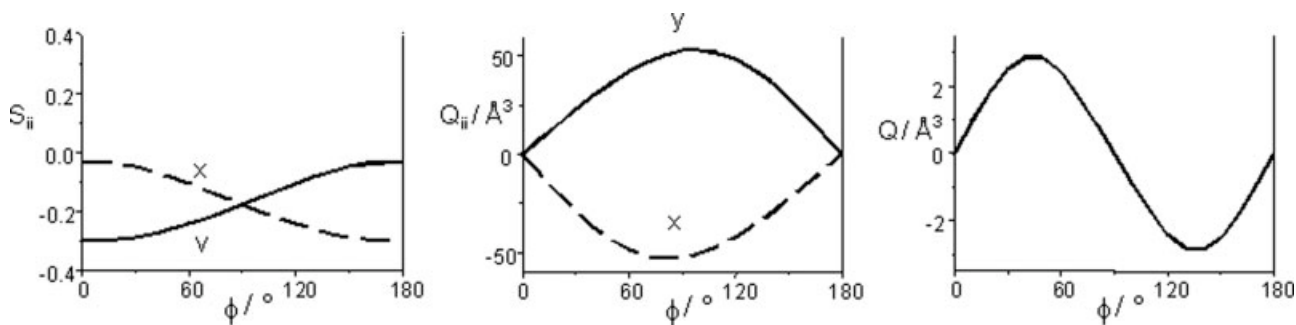


**Fig. 8.** Order parameters, surface chirality components and of biphenyl and chirality parameter  $Q$ , calculated for biphenyl as a function of the twist angle between the aromatic rings.

**TABLE 3. Helical twisting powers of compounds 24–31 measured at room temperature in biphenyl-type nematics<sup>10,82–84</sup>**

	$\beta$	Molecular shape (see text)	Core helicity <sup>a</sup>
<b>24</b>	+21	disk-like	<i>P</i>
<b>25</b>	+20	disk-like	<i>P</i>
<b>26</b>	+15	disk-like	<i>P</i>
<b>27</b>	−1.5	disk-like	<i>P</i>
<b>28</b>	−11.4	rod-like	<i>P</i>
<b>29</b>	−17.2	rod-like	<i>P</i>
<b>30</b>	−19.3	rod-like	<i>P</i>
<b>31</b>	−20.3	rod-like	<i>P</i>

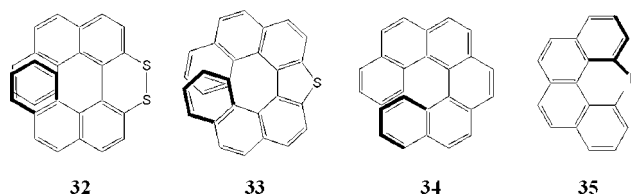
Also the molecular shape derived from the calculation of their orientational behaviour (see text) is reported.

<sup>a</sup>See page 5 footnote<sup>3</sup>.

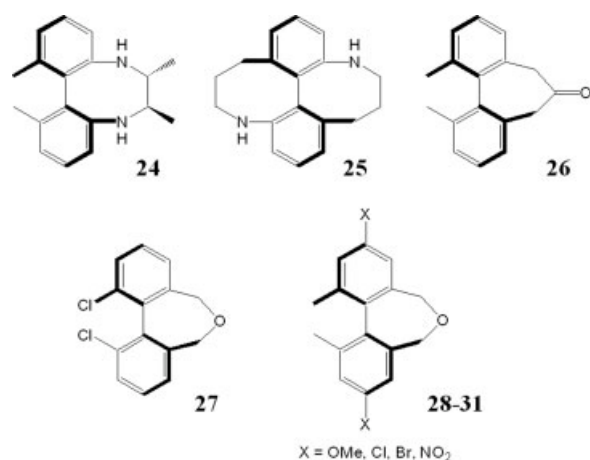
**26**,<sup>10,85–87</sup> which are constrained in a geometry with a twist angle comprised between 20 and 60° and are characterized by *P*-helicity along the biphenyl axis.<sup>‡</sup> However, there are counter examples, like the derivatives **27–31** which, although sharing the same *P*-helicity at the molecular level, have twisting powers spanning from highly negative to negligible values (see Table 3).<sup>10,85–87</sup> Calculations performed with the surface chirality method show that these differences between the dopants can be mainly traced back to their different orientational behavior, induced by the substitution in the central biphenyl core. Whereas the compounds **24–26**, like biphenyl, have a definite preference for keep what we have denoted as the *y* axis perpendicular to the director, the compounds **28–31**, which are more elongated, behave more as rods, with a small difference in the degree of alignment between the *x* and *y* axes. It follows that in the first case the *y*-helicity (right-handed) is imparted to the nematic host, whereas in the latter there is a significant contribution of the left-handed *x* helicity.<sup>87</sup> It is worth singling out the difference from binaphthyl, in which case the propensity of the *y* axis to lie perpendicular to the director is significantly higher than that of the *x* axis, irrespectively of the presence of substituents, so that right-handed cholesterics are induced by *P*-enantiomers.

The simultaneous presence of different helicities in the same molecule clearly appears in heptalene, as shown in Figure 9. A small helical twisting power has been predicted for this molecule, as the result of the competition between oppositely handed contributions. The presence of substituents, depending on their locations, can enhance the one or the other contribution, leading to induced cholesterics of opposite handedness for heptalene derivatives with the same absolute configuration.<sup>71,88</sup>

Another interesting example is represented by helicenes and related molecules. Compounds very different spectroscopically, such as **32–35**, and hence hardly comparable with chiroptical techniques, are very similar in shape and give helical twisting powers of the same sign and of comparable intensity;<sup>89,90</sup> the twisting powers of helicenes can be easily explained by the surface chirality model.



The opposite behavior, i.e., similarity of the chiroptical properties and dramatic differences in the helical twisting power despite a clear molecular helicity, has been found for series of oligonaphthalene derivatives linked at the 1,4-position.<sup>91</sup> Configurationally homogeneous derivatives with a different number of monomers have molecular structures corresponding to helices of the same handedness. Surprisingly, it has been observed that relatively small changes in the substituents can have dramatic effects on their twisting ability. For some derivatives (e.g., **36**), cholesterics of the same handedness are induced by oligomers of different length. However, series of derivatives have been found (e.g., **37**), which display and unexpected sign alternation of  $\beta$  with length. Calculations with the surface chirality model have shown the importance of local contributions, strongly dependent upon the substitution pattern,



X = OMe, Cl, Br, NO<sub>2</sub>

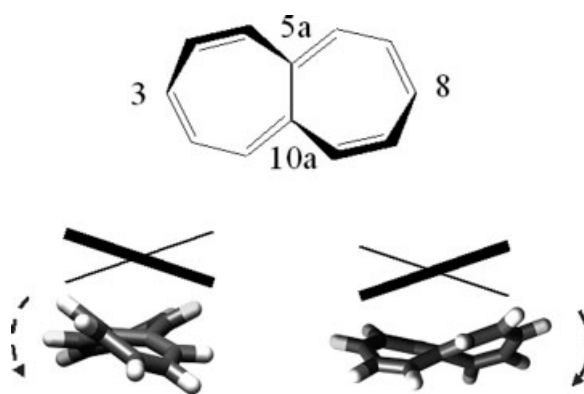
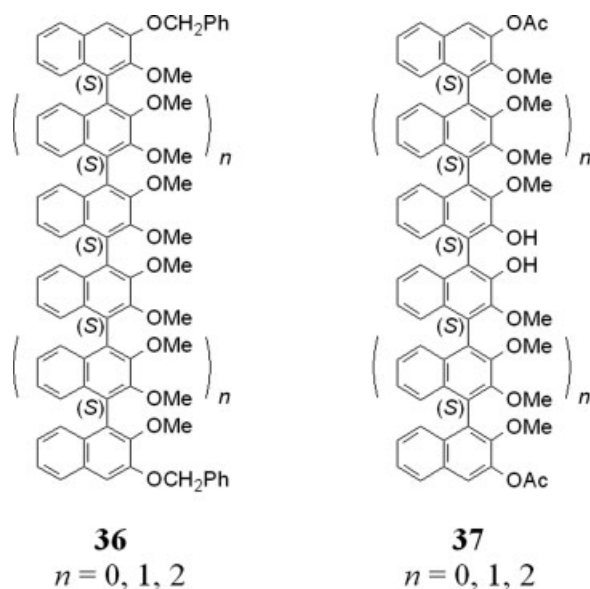


**Fig. 9.** Opposite helicities of (*P*)-heptalene along the C(3)–C(8) direction (left) and the C(5a)–C(10a) bond (right).



and the scarce meaning of global stereochemical descriptors for the phenomenon of cholesteric induction.



On the basis of the considerations presented earlier it is not difficult to understand that bulky molecules, in which chirality results in a sizeable shape distortion and a well-defined orientational behavior can be devised, generally have a strong twisting ability, not dramatically affected by substituents. Moreover, a significant role of the molecular flexibility can be expected, because different conformers can have different order parameters and different chirality. The  $Q$  value for a flexible dopant is obtained by averaging over all the conformers<sup>92</sup>:

$$Q = \sum_{\alpha} p_{\alpha} Q_{\alpha} \quad (4)$$

where  $p_{\alpha}$  and  $Q_{\alpha}$  are the probability and the chirality parameter of the  $\alpha$  conformer. As calculations show, different conformers can have opposite twisting ability, and this makes even more difficult to associate absolute configuration and cholesteric handedness, even for dopants with the same chiral core. As a general rule, with increasing flexibility the possibility of chiral conformers with high twisting ability of opposite handedness is predicted, which however results in a significantly lower net twisting power after averaging over the whole ensemble.<sup>92,93</sup>

In most cases, the handedness of the induced cholesteric phase is characteristic of a given dopant, and is maintained irrespectively of the chemical structure of the nematic solvent and of the temperature. These have the only effect of scaling the magnitude of the pitch, according to eq. 2. However, in some cases changes of handedness with solvent and temperature have been observed, mostly for solutes with a modest twisting ability. They can be explained as a result of a change in the orientational behavior<sup>67,71</sup> and/or in the conformational distribution of the dopant. The effects of the nematic solvent on the tor-

sional potential, and then on the molecular alignment and the helical twisting power, have been thoroughly investigated in the case of arylalkylsulfoxides.<sup>94,95</sup>

## CONCLUDING REMARKS

The results reported in this article show the extreme sensitivity of the LC technique to the molecular chirality. This methodology, which has the valuable features of experimental simplicity and low cost, affords a powerful tool to obtain stereochemical information about configuration and conformation. The origin of chirality amplification in LC is independent of that of the traditional chiroptical techniques: whereas the former is determined by the interplay of anisotropy and chirality of solute-solvent interactions, the latter relies on the chirality of the electron distribution in the chromophoric groups. It follows that the LC technique is sensitive to the whole molecular shape of the molecule, and is strongly affected by the presence of substituents. The cholesteric helicity bears a nontrivial relation with the molecular chirality, and sometimes apparently conflicting results can be found. However, as appears from several examples reported earlier, some useful guidelines can be found, at least for rigid dopants with relatively high twisting power (larger than about  $10 \mu\text{m}^{-1}$ ), without groups involved in strong specific interactions. In these cases the handedness of the induced cholesteric phase is mostly independent of the nature of the LC host and can be taken as a signature of the configuration of the dopant. Simple empirical correlations between configuration and handedness can be found for homologous series of rigid molecules, with a clear shape chirality such as that deriving from the presence of twisted planes, and a well defined orientational behavior, which are hardly affected by substituents. In general, for dopants, which do not satisfy such requirements, or in the presence of bulky substituents and/or molecular flexibility, modeling can give a significant contribution; the surface chirality method, thanks to its capacity to take into account the molecular details and the low computational cost, has been shown to be a reliable tool for this purpose.

## ACKNOWLEDGMENTS

We thank all people who contributed to this work and in particular the coworkers who are individually recognized in the cited references. A special thank to Prof. G. Gottarelli for his pioneering study on cholesteric induction.

## LITERATURE CITED

- Reinitzer F. Beiträge zur Kenntniss des Cholesterins für Chemie. *Monatsh Chem* 1888;9:421-441.
- Bahadur B, editor. *Liquid crystals—Applications and uses*. Singapore: World Scientific; 1990.
- Collins PJ, Hird M. *Introduction to liquid crystals—Chemistry and physics*. London: Taylor and Francis; 1997.
- Dierking I. *Textures of liquid crystals*. Weinheim: Wiley-VCH; 2003.
- Demus D, Goodby J, Gray GW, Spiess HW, Vill V, editors. *Handbook of liquid crystals*. Weinheim: Wiley-VCH; 1998.
- Kitzerow HS, Bahr C, editors. *Chirality in liquid crystals*. New York: Springer-Verlag; 2001.

7. Friedel G. The mesomorphic states of matter. *Ann Phys* 1922;18:273–474.
8. Buckingham AD, Ceasar GP, Dunn MB. The addition of optically active compounds to nematic liquid crystals. *Chem Phys Lett* 1969; 3:540–541.
9. Korte EH. Discrimination of enantiomers at microgram level using liquid crystalline solutions. *Appl Spectrosc* 1978;32:568–572.
10. Solladié G, Zimmermann R. Liquid crystals: A tool for studies on chirality. *Angew Chem Int Ed Eng* 1984;23:348–362.
11. Hakemi H, Varanasi PP. The determination of cholesteric pitch from the diffusion profile a new experimental approach. *Liq Cryst* 1986;1: 63–71.
12. Chilaya GS, Lisetski LN. Cholesteric liquid crystals: Physical properties and molecular-statistical theories. *Mol Cryst Liq Cryst* 1986;140: 243–286.
13. De Vries H. Rotatory power and other optical properties of certain liquid crystals. *Acta Crystallog* 1951;4:219–226.
14. Grandjean F. The existence of equidistant layers normal to the optic axis in anisotropic liquids (liquid crystals). *Compt Rend* 1921;172:71–74.
15. Cano R. An explanation of Grandjean discontinuities. *Bull Soc Fr Mineral* 1968;91:20–27.
16. Heppke G, Oestreicher F. Determination of the helical sense of cholesteric liquid crystals using the Grandjean-Cano method. *Z Naturforsch (A)* 1977;32:899–901.
17. Heppke G, Oestreicher F. Determination of the cholesteric screw sense. *Mol Cryst Liq Cryst* 1978;41:245–249.
18. Kahn FJ. Electric-field-induced color changes and pitch dilation in cholesteric liquid crystals. *Phys Rev Lett* 1970;24:209–212.
19. Eelkema R, Pollard MM, Katsonis N, Vicario J, Broer DJ, Feringa BL. Rotational reorganization of doped cholesteric liquid crystalline films. *J Am Chem Soc* 2006;128:14397–14407.
20. Eelkema R, Pollard MM, Vicario J, Katsonis N, Ramon BS, Bastiaansen CWM, Broer DJ, Feringa BL. Nanomotors rotates microscale objects. *Nature* 2006;440:163.
21. Eelkema R, Feringa BL. Amplification of chirality in liquid crystals. *Org Biomol Chem* 2006;4:3729–3745.
22. Ichimura K. Photoalignment of liquid-crystal systems. *Chem Rev* 2000;100:1847–1873.
23. Ikeda T, Kanazawa A. In: Feringa BL, editor. *Molecular switches*. Weinheim: Wiley-VCH; 2001. p 363–397.
24. Ikeda T. Photomodulation of liquid crystal orientations for photonic applications. *J Mater Chem* 2003;13:2037–2057.
25. Proni G, Spada GP. Doped nematic phases: A tool for amplifying and detecting chirality. *Enantiomer* 2001;6:171–179.
26. Kuball HG, Höfer B. From a chiral molecule to a chiral anisotropic phase. In: Bahr CH, Kitzerow HS, editors. *Chirality in liquid crystals*. New York: Springer-Verlag; 2001. p 67–100.
27. Penot JP, Jacques J, Billard J. Reducing the part of chance in research on spontaneous resolution. II. A microdiagnostic technique for optical activity and its application. *Tetrahedron Lett* 1968;37:4013–4016.
28. Bertocchi G, Gottarelli G, Prati R. Determination of heroin by means of the pitch of induced cholesteric mesophases. *Talanta* 1984;31:138–140.
29. Gottarelli G, Samori B, Fuganti C, Grasselli C. Liquid crystal characterization of compounds chiral by deuterium substitution. *J Am Chem Soc* 1981;103:471–472.
30. Kuball HG, Weiß B, Beck AK, Seebach D. TADDOLs with unprecedented helical twisting power in liquid crystals. Preliminary communication. *Helv Chim Acta* 1997;80:2507–2514.
31. Seebach D, Beck AK, Heckel A. TADDOLs, their Derivatives, and TADDOL analogues: Versatile chiral auxiliaries. *Angew Chem Int Ed* 2001;40:92–138.
32. Van Delden RA, Feringa BL. Color indicators of molecular chirality based on doped liquid crystals. *Angew Chem Int Ed* 2001;40:3198–3200.
33. Van Delden RA, Feringa BL. Colour indicator for enantiomeric excess and assignment of the configuration of the major enantiomer of an amino acid ester. *Chem Commun* 2002;174–175.
34. Eelkema R, van Delden RA, Feringa BL. Direct visual detection of the stereoselectivity of a catalytic reaction. *Angew Chem Int Ed* 2004;43: 5013–5016.
35. Zahn S, Proni G, Spada GP, Canary JW. Supramolecular detection of metal ion binding: ligand conformational control of cholesteric induction in nematic liquid crystalline phases. *Chem Eur J* 2001;7: 88.
36. Yoshida J, Sato H, Yamagishi A, Hoshino N. On the parity in helical twisting power of Ru(III) 1,3-diketones of C<sub>2</sub> symmetry in nematic liquid crystals. *J Am Chem Soc* 2005;127:8453–8456.
37. Drake AF, Gottarelli G, Spada GP. The twisting power of some chiral tris(pentane-2,4-dionate)metal(III) complexes in nematic liquid crystals. *Chem Phys Lett* 1984;110:630–633.
38. Eelkema R, Feringa BL. Macroscopic expression of the chirality of amino alcohols by a double amplification mechanism in liquid crystalline media. *J Am Chem Soc* 2005;127:13480–13481.
39. Eelkema R, Feringa BL. Phosphoric acids as amplifiers of molecular chirality in liquid crystalline media. *Org Lett* 2006;8:1331–1334.
40. Gottarelli G, Spada GP. Induced cholesteric mesophases: origin and applications. *Mol Cryst Liq Cryst* 1985;123:377–388.
41. Gottarelli G, Spada GP, Solladié G. Some stereochemical applications of induced cholesteric liquid crystals. *Nouv J Chim* 1986;10:691–696.
42. Spada GP, Proni G. The nematic liquid crystal phase as a probe of the molecular shape helicity. *Enantiomer* 1998;3:301–314.
43. Gottarelli G, Samori B, Marzocchi S, Stremmenos C. Induction of a cholesteric mesophase in a nematic liquid crystal by some optically active alcohols. Possible method for the correlation of configurations. *Tetrahedron Lett* 1975;24:1981–1984.
44. Krabbe HJ, Heggemeier H, Schrader B, Korte EH. Relationship between the infrared rotatory dispersion of liquid-crystalline solutions of chiral molecules and their absolute configuration. *Angew Chem Int Ed Eng* 1977;16:791–792.
45. Krabbe HJ, Heggemeier H, Schrader B, Korte EH. Determination of the absolute configuration of chiral molecules from the infrared rotatory dispersion of their liquid-crystalline solutions. *J Chem Res (S)* 1978;238. *J Chem Res (M)* 1978;3023–3040.
46. Korte EH, Schrader B, Bualek S. A new method for the study of molecular chirality: Infrared rotatory dispersion of induced cholesteric solutions. *J Chem Res (S)* 1978;236–237. *J Chem Res (M)* 1978;3001–3022.
47. Gottarelli G, Samori B, Folli U, Torre G. Induction of cholesteric mesophases in nematic liquid crystals by some optically active sulfoxides: Relationship between the absolute configurations, the dimensions of the substituents and the handedness of the induced mesophases. *J Phys (C)* 1979;40:25–26.
48. Proni G, Spada GP, Lustenberger P, Welti R, Diederich F. Conformational analysis in solution of C<sub>2</sub>-symmetric 1,1'-binaphthyl derivatives by circular dichroism spectroscopy and cholesteric induction in nematic mesophases. *J Org Chem* 2000;65:5522–5527.
49. Superchi S, Donnoli MI, Proni G, Spada GP, Rosini C. Induction of cholesteric mesophases by simple cyclic derivatives of *p,p'*-disubstituted 1,2-diphenylethane-1,2-diols: Importance of shape and electronic factors. *J Org Chem* 1999;64:4762–4767.
50. Gottarelli G, Mariani P, Spada GP, Samori B, Forni A, Solladié G, Hibert M. Induction of cholesteric mesophases in nematic liquid crystals and correlation of absolute configurations of some chiral oxiranes and thiiranes. *Tetrahedron* 1983;39:1337–1344.
51. Gottarelli G, Samori B, Stremmenos C, Torre G. Induction of cholesteric mesophases in nematic liquid crystals by some chiral aryl alkyl carbinols. *Tetrahedron* 1981;37:395–399.
52. Suchod B, Renault A, Lajzerowicz J, Spada GP. A study of the conformation of some chiral binaphthyl and bithienyl derivatives in the solid state and in solution. An approach by X-ray diffraction, circular dichroism spectroscopy and induced cholesteric mesophase analysis. *J Chem Soc Perkin Trans 2* 1992;1839–1844.
53. Rinaldi PL, Wilk M. Use of liquid crystal induced circular dichroism for absolute configurational assignments of  $\beta$ -amino alcohols. *J Org Chem* 1983;48:2141–2146.

54. Mioskowski C, Bourguignon J, Candau S, Solladié G. Photochemically induced cholesteric-nematic transition in liquid crystals. *Chem Phys Lett* 1976;38:456–459.
55. Gottarelli G, Hibert M, Samori B, Solladié G, Spada GP, Zimmermann R. Induction of the cholesteric mesophase in nematic liquid crystals: Mechanism and application to the determination of bridged biaryl configuration. *J Am Chem Soc* 1983;105:7318–7321.
56. Gottarelli G, Spada GP, Varche D, Jacques J. All-*trans* 2,7-dialkylperhydrophenanthrene as a solvent for measurements of helical twisting power and linear dichroism. *Liq Cryst* 1986;1:29–35.
57. Memmer R, Kuball HG, Schönhöfer A. Computer simulation of chiral liquid crystal phases. III. A cholesteric phase formed by chiral Gay-Berne atropisomers. *Mol Phys* 1996;89:1633–1649.
58. Gottarelli G, Osipov MA, Spada GP. A study of solvent effect on the optical rotation of chiral biaryls. *J Phys Chem* 1991;95:3879–3884.
59. Bandini M, Casolari S, Cozzi PG, Proni G, Schmohel E, Spada GP, Tagliavini E, Umani Ronchi A. Synthesis and characterization of new enantiopure 7,7'-disubstituted 2,2'-dihydroxy-1,1'-binaphthyls: Useful ligands for the asymmetric allylation reaction of aldehydes. *Eur J Org Chem* 2000;491–497.
60. Gottarelli G, Spada GP, Bartsch R, Solladié G, Zimmermann R. Induction of the cholesteric mesophase in nematic liquid crystals: correlation between the conformation of open-chain chiral 1,1'-binaphthyls and their twisting powers. *J Org Chem* 1986;51:589–592.
61. Rosini C, Rosati I, Spada GP. A conformational analysis of mono and dialkyl ethers of 2,2'-dihydroxy-1,1'-binaphthalene by circular dichroism spectroscopy and cholesteric induction in nematic liquid crystals. *Chirality* 1995;7:353–358.
62. Deussen HJ, Shibaev PV, Vinokur R, Bjørnholm T, Schaumburg K, Bechgaard K, Shibaev VP. New 6,6'-disubstituted-binaphthol derivatives as chiral dopants: Synthesis and temperature dependence of molecular conformations. *Liq Cryst* 1996;21:327–340.
63. Goossens WJA. Molecular theory of the cholesteric phase and of the twisting power of optically active molecules in a nematic liquid crystal. *Mol Cryst Liq Cryst* 1971;12:237–244.
64. Stegemeyer H, Finkelmann H. Temperature dependence of helical pitch of induced cholesteric mesophases. *Naturwiss* 1975;62:436–437.
65. Van der Meer BW, Vertogen G. The helix inversion in cholesteric-nematic mixtures. *Phys Lett (A)* 1979;74:242–244.
66. Allen MP. Calculating the helical twisting power of dopants in a liquid crystal by computer simulation. *Phys Rev (E)* 1993;47:4611–4614.
67. Emelyanenko AV, Osipov MA, Dunmur DA. Molecular theory of helical sense inversions in chiral nematic liquid crystals. *Phys Rev (E)* 2000;62:2340–2352.
68. Berardi R, Kuball HK, Memmer R, Zannoni C. Chiral induction in nematics. A computer simulation study. *J Chem Soc Farad Trans* 1998;94:1229–1234.
69. Cook MJ, Wilson MR. Calculation of helical twisting power for liquid crystal chiral dopants. *J Chem Phys* 2000;112:1560–1564.
70. Ferrarini A, Moro GJ, Nordio PL. Simple molecular model for induced cholesteric phases. *Phys Rev (E)* 1996;53:681–688.
71. Ferrarini A, Moro GJ, Nordio PL. Shape model for ordering properties of molecular dopants inducing chiral mesophases. *Mol Phys* 1996;87:485–499.
72. Eisenberg D, McLachlan A. Solvation energy in protein folding and binding. *Nature* 1986;319:199–203.
73. Ooi T, Oobatake M, Nemethy G, Scheraga HA. Accessible surface areas as a measure of the thermodynamic parameters of hydration of peptides. *Proc Natl Acad Sci USA* 1987;84:3086–3090.
74. Still WC, Tempczyk A, Hawley RC, Hendrickson T. Semianalytical treatment of solvation for molecular mechanics and dynamics. *J Am Chem Soc* 1990;112:6127–6129.
75. Cramer CJ, Truhlar DG. Implicit solvation models: equilibria, structure, spectra, and dynamics. *Chem Rev* 1999;99:2161–2200.
76. Ferrarini A, Janssen F, Moro GJ, Nordio PL. Molecular surface and order parameters in liquid crystals. *Liq Cryst* 1999;26:201–210.
77. Richards FM. Areas, volumes, packing and protein structure. *Ann Rev Biophys Bioeng* 1997;151–176.
78. Connolly ML. Analytical molecular surface calculation. *J Appl Cryst* 1983;548–558.
79. Osipov MA, Pickup BT, Dunmur DA. A new twist on molecular chirality: Intrinsic chirality indices. *Mol Phys* 1995;84:1193–1206.
80. Solymosi M, Low RJ, Grayson M, Neal MP. A generalized scaling of chiral indices for molecules. *J Chem Phys* 2002;116:9875–9881.
81. Neal MP, Solymosi M, Wilson MR, Earl DJ. Helical twisting power and scaled chiral indices. *J Chem Phys* 2003;119:3567–3573.
82. Kamberaj H, Osipov MA, Low RJ, Neal MP. Helical twisting power and chirality indices. *Mol Phys* 2004;102:431–446.
83. Kamberaj H, Low RJ, Neal MP. Correlation between molecular chirality and helical twisting power: a computer simulation study. *Mol Phys* 2006;104:335–357.
84. Ferrarini A, Nordio PL. On the assessment of molecular chirality. *J Chem Soc Perkin Trans 2* 1998;455–460.
85. Gottarelli G, Spada GP, Seno K, Hagishita S, Kuriyama K. Induced cholesteric mesophases as a probe for the stereochemistry of chiral biphenyls. *Bull Chem Soc Jpn* 1986;56:1607–1608.
86. Williams VE, Lemieux RP. Substituent effects in the induction of a cholesteric liquid crystal phase by atropisomeric dibenzoxepins: A study of arene–arene interactions. *Chem Commun* 1996;2259–2260.
87. Di Matteo A, Todd SM, Gottarelli G, Solladié G, Williams VE, Lemieux RP, Ferrarini A, Spada GP. Correlation between molecular structure and helicity of induced chiral nematics in terms of short-range and electrostatic-induction interactions. *J Am Chem Soc* 2001;123:7842–7851.
88. Gottarelli G, Hansen H-J, Spada GP, Weber RH. A liquid crystal study of heptalene. *Helv Chim Acta* 1987;70:430–435.
89. Gottarelli G, Proni G, Spada GP, Fabbri D, Gladiali S, Rosini C. Conformational and configurational analysis of 4,4'-biphenanthryl derivatives and related helicenes by circular dichroism spectroscopy and cholesteric induction in nematic mesophases. *J Org Chem* 1996;61:2013–2019.
90. Ferrarini A, Gottarelli G, Nordio PL, Spada GP. Determination of the absolute configuration of helicenes and related biaryls from calculation of helical twisting powers by the surface chirality model. *J Chem Soc Perkin Trans 2* 1999;411–417.
91. Pieraccini S, Ferrarini A, Kaoro F, Gottarelli G, Lena S, Tsubaki K, Spada GP. Homochiral helices inducing opposite-handed cholesteric phases. *Chem Eur J* 2006;12:1121–1126.
92. Ferrarini A, Nordio PL, Shibaev PV, Shibaev VP. Twisting power of bridged binaphthol derivatives: Comparison of theory and experiment. *Liq Cryst* 1998;24:219–227.
93. Earl DJ, Wilson MR. Predictions of molecular chirality and helical twisting powers: A theoretical study. *J Chem Phys* 2003;119:10280–10288.
94. Pieraccini S, Donnoli MI, Ferrarini A, Gottarelli G, Licini G, Rosini C, Superchi S, Spada GP. A correlation between the absolute configuration of alkyl aryl sulfoxides and their helical twisting power in nematic liquid crystals. *J Org Chem* 2003;68:519–526.
95. Celebre G, de Luca G, Maiorino M, Iemma F, Ferrarini A, Pieraccini S, Spada GP. Solute-solvent interactions and chiral induction in liquid crystals. *J Am Chem Soc* 2005;127:11736–11744.